TRANSACTIONS
OF THE ASME
Series E

Journal of APPLIED MECHANICS

September 1960

DYNAMICS • VIBRATIONS • ELASTICITY • LUBRICATION AND WEAR
RHEOLOGY • FRACTURES • STRUCTURES • HYDRAULICS • AERODYNAMICS
INTERNAL FLOW • MECHANICAL PROPERTIES OF METALS • THERMODYNAMICS
TURBULENCE • HEAT TRANSFER • COMPUTING DEVICES AND METHODS
BOUNDARY LAYERS • AEROELASTICITY • EXPERIMENTAL STRESS ANALYSIS

Published Quarterly by
THE AMERICAN SOCIETY OF MECHANICAL ENGINEERS

TRANSACTIONS
OF THE ASME
Series E

EDITORIAL DEPARTMENT

APPLIED MECHANICS DIVISION

OFFICERS OF THE ASME

PUBLICATIONS COMMITTEE

REGIONAL ADVISORY BOARD

Journal of
APPLIED MECHANICS
VOLUME 27 • SERIES E • NUMBER 3
September 1960

CONTENTS

TECHNICAL PAPERS

381 **On Three and Two-Dimensional Disturbances of Pipe Flow** (60—APM-12)
Kurt Spielberg and Hans Timan

390 **On the Indeterminateness of the Boundary Conditions for the Mixing of Two Parallel Streams** (59—A-68)
K. T. Yen

393 **Thermal Transfer in Turbulent Gas Streams. Effect of Turbulence on Local Transport From Spheres** (60—APM-30)
W. W. Short, R. A. S. Brown, and B. H. Sage

403 **Hydrodynamic Entrance Lengths for Incompressible Laminar Flow in Rectangular Ducts** (59—A-82)
L. S. Han

410 **Stability of a Turbine-Generator Rotor Including the Effects of Certain Types of Steam and Bearing Excitations** (60—APM-9)
A. H. Landzberg

417 **On Saint Venant's Principle: Elastic Shells and Plates** (60—APM-11)
P. M. Naghdi

423 **On the Airy Stress Functions of Plane Dislocation Problems** (60—APM-14)
F. D. Ju

429 **Effect of Pressure on Bending Characteristics of Actuator System** (60—APM-16)
Paul Seide

438 **The Contact Problem for Viscoelastic Bodies** (59—A-83)
E. H. Lee and J. R. M. Radok

445 **Stresses in Curved Beams of Noncircular Center Line** (60—APM-21)
M. M. Abbassi

455 **Shear Buckling of Bars** (59—A-91)
G. Herrmann and A. E. Armenàkas

458 **Buckling of Circular Cones Under Axial Compression** (60—APM-17)
Leslie Lackman and Joseph Penzien

461 **Additional Deflection of a Cantilever Due to Elasticity of Support** (60—APMW-3)
W. J. O'Donnell

465 **Thermoelastic Stresses in Beams** (60—APM-28)
E. S. Barrekette

474 **Elastic Instability of Rectangular Sandwich Panel of Orthotropic Core With Different Face Thicknesses and Materials** (60—APM-26)
C. C. Chang and I. K. Ebcioglu

481 **Transient and Residual Thermal Stresses in an Elastic-Plastic Cylinder** (60—APM-4)
H. G. Landau and E. E. Zwicky, Jr.

489 **On Strain-Hardened Circular Cylindrical Shells** (60—APM-20)
Nicholas Perrone and P. G. Hodge, Jr.

496 **The Elastoplastic Thick-Walled Sphere Subjected to a Radial Temperature Gradient** (60—APM-22)
G. R. Cowper

501 **Rupture Instability of Plane Membranes and Solids** (60—APM-1)
S. F. Borg

505 **Expansion of Thick-Walled Cylinders Fabricated From Cold Bent Plates** (60—APMW-2)
Irwin Berman

CONTENTS

513 **Dispersion of Flexural Waves in an Elastic, Circular Cylinder** (59—A-84)
Yih-Hsing Pao and R. D. Mindlin

521 **Modeling of Large Transient Elastic and Plastic Deformations of Structures Subjected to Blast Loading** (60—APM-18)
W. E. Baker

528 **Shock Spectra of a Nonlinear System** (60—APM-23)
W. T. Thomson

535 **Forced Flexural Vibrations of Sandwich Plates in Plane Strain**
Yi-Yuan Yu

541 **Extensional Vibrations and Waves in a Circular Disk and a Semi-Infinite Plate** (60—APM-3)
D. C. Gazis and R. D. Mindlin

548 **Effect of Small Hub-Radius Change on Bending Frequencies of a Rotating Beam** (60—APMW-5)
Hsu Lo, J. E. Goldberg, and J. L. Bogdanoff

551 **Forced Lateral Vibration of a Uniform Cantilever Beam With Internal and External Damping** (60—APM-15)
Ho Chong Lee

557 **A Method for Investigating Certain Eigenvalue Problems of the Buckling and Vibration of Plates** (60—APM-25)
H. D. Conway and A. W. Leissa

559 **Dynamical Response of an Elastic Half-Space to Tangential Surface Loadings** (60—APM-29)
Chi-Chang Chao

568 **On a Special Class of Self-Sustained Oscillations**
K. Klotter and E. Kreyszig

575 **Random Excitation of a Loaded Nonlinear String** (60—APMW-1)
T. K. Caughey

579 **On the Use of Nonsinusoidal Approximating Functions for Nonlinear Oscillation Problems**
K. Klotter and P. R. Cobb

BRIEF NOTES

584 Stress-Displacement Relations for Shell Membranes in Oblique Co-Ordinates — *G. D. Galletly*

586 A Note on the Stability Problem of Shallow Translational Shells — *Kristoffer Apeland*

589 Transient Response of Linear Viscoelastic Plates — *G. E. Mase*

590 A Note on the Hydrodynamic Pocket Bearing — *C. F. Kettleborough*

DISCUSSION

593 Discussion of previously published papers by *S. A. Hovanessian; V. L. Salerno and M. A. Goldberg; M. A. Goldberg and Michael Sadowsky; Wen-Hsiung Li; T. R. Goodman and J. J. Shea; L. N. Tao*

BOOK REVIEWS

TRANSACTIONS OF THE ASME Series A

Journal of
ENGINEERING FOR POWER

Volume 82 • Series A • Number 3

CONTENTS FOR JULY, 1960

169 An Experimental Investigation of Fuel Additives in a Supercharged Boiler, by R. J. Zoschak and R. W. Bryers. (59—A-160)

181 External Corrosion of Superheaters in Boilers Firing High-Alkali Coals, by P. Sedor, E. K. Diehl, and D. H. Barnhart. (59—A-76)

194 Corrosion of Superheaters and Reheaters of Pulverized-Coal-Fired Boilers, by Wharton Nelson and Carl Cain, Jr. (59—A-89)

205 Considerations for the Reduction of Noise in Ship Installations of Gas Turbines, by E. M. Herrmann. (59—A-238)

215 A Torsional Vibration Problem as Associated With Synchronous Motor Driven Machines, by R. N. Brown. (59—A-141)

221 Design Control of Overcompression in Rotary-Vane Compressors, by E. O. Bransford and R. A. Stein. (59—A-109)

227 Operation of Steam Turbines to Minimize Shell Cracking, by S. B. Coulter and R. L. Jackson. (59—Pwr-10)

TRANSACTIONS OF THE ASME Series B

Journal of
ENGINEERING FOR INDUSTRY

Volume 82 • Series B • Number 3

CONTENTS FOR AUGUST, 1960

173 Synthesis of Epicyclic Gear Trains Using the Velocity Ratio Spectrum, by R. C. Brewer. (59—A-22)

179 Helixform Bevel and Hypoid Gears, by G. M. Spear, C. B. King, and M. L. Baxter, Jr. (59—A-90)

191 The Twinworm Drive—A Self-Locking Worm-Gear Transmission of High Efficiency, by B. Popper and D. W. Pessen. (59—A-75)

200 Determination of Cutter Trajectories for Contoured Turbine Buckets, by R. G. DeBiase. (59—A-111)

205 An Analysis of Factors Used for Strength Rating Helical Gears, by E. J. Wellauer. (59—A-121)

213 Bending Strength of Gear Teeth by Cantilever-Plate Theory, by E. J. Wellauer and A. Seireg. (59—A-50)

223 Rocket Motor Gear Tooth Analysis (Hertzian Contact Stresses and Times), E. K. Gatcombe and R. W. Prowell. (59—A-256)

231 Analysis of Power Spinning of Cones, by B. Avitzur and C. T. Yang. (59—A-173)

246 Some Problems of Press Forging Lead and Aluminum, by A. G. MacDonald, S. Kobayashi, and E. G. Thomsen. (59—A-164)

253 The Deformation Process in Metal-Cutting, by W. J. McDonald and B. F. Murphey. (59—A-165)

259 Influence Coefficients and Pressure Vessel Analysis, by G. D. Galletly. (59—A-163)

270 Tube Metal Temperatures for Structural Design, by E. E. Ungar and L. A. Mekler. (59—A-166)

277 Supersonic-Wind-Tunnel Air-Drying-System Design, by T. W. Macios. (59—A-161)

TRANSACTIONS
Series C

Journal of
HEAT TRANSFER
Vol. 82 • Series C • No. 3

CONTENTS FOR AUGUST, 1960

155 Rocket Heat-Transfer Literature

170 Unsteady Turbulent Heat Transfer in Tubes, by E. M. Sparrow and R. Siegel. (59—HT-16)

181 Improved Lumped Parameter Method for Transient Heat Conduction Calculations, by H. G. Elrod, Jr. (59—HT-28)

189 Local and Average Heat Transfer and Pressure Drop for Refrigerants Evaporating in Horizontal Tubes, by M. Altman, R. H. Norris, and F. W. Staub. (59—A-278)

199 Heat-Transfer and Flow-Friction Characteristics of Crossed-Rod Matrices, by A. L. London, J. W Mitchell, and W. A. Sutherland. (59—A-168)

214 Experiments on Heat Transfer From Spheres Including Combined Natural and Forced Convection, by T. Yuge. (59—A-123)

221 Heat Transfer to Freon 12 Near the Critical State in a Natural-Circulation Loop, by J. P. Holman and J. H. Boggs. (59—A-142)

227 Combined Free and Forced-Convection Heat-Generating Laminar Flow Inside Vertical Pipes With Circular Sector Cross Sections, by Pau-Chang Lu. (59—A-145)

233 On Combined Free and Forced Convection in Channels, by L. N. Tao. (59—A-77)

239 The Role of the Skin in Heat Transfer, by A. M. Stoll. (59—A-138)

243 The Prediction of Human Thermal Tolerance When Using a Ventilating Garment With An Anti-exposure Suit, by J. W. Mc Cutchan. (59—A-114)

252 Heat Transfer by Laminar Flow From a Rotating Cone, by C. L. Tien.

253 Apparent Emissivity and Heat Transfer in a Long Cylindrical Hole, by E. M. Sparrow and L. U. Albers.

255 On the Variable-Density Single-Fluid Model for Two-Phase Flow, by Novak Zuber.

258 Nearly Quasi-Steady Free Convection Heat Transfer in Gases, by E. M. Sparrow and J. L Gregg.

260 The Effect of Mass Transfer on Free Convection, by R. Eichhorn.

263 An Interferometric Method of Studying Boundary Layer Oscillations, by J. P. Holman, H. E. Gartrell and E. E. Soehngen.

TRANSACTIONS
Series D

Journal of
BASIC ENGINEERING
Vol. 82 • Series D • No. 3

CONTENTS FOR SEPTEMBER, 1960

505 Theoretical and Experimental Analysis of Hydrostatic Thrust Bearings, by R. C. Elwell and B. Sternlicht. (59—A-152)

513 Precise Measurement of Clothes Insulation During Controlled Operation of the Human, by A. S. Iberall. (59—A-197)

528 Radial Distributions of Temporal-Mean Peripheral Velocity and Pressure for Fully Developed Turbulent Flow in Curved Channels, by A. W. Marris. (59—A-51)

539 Flow Phenomena of Partially Enclosed Rotating Disks, by L. A. Maroti, G. Deak, and F. Kreith. (59—A-49)

553 Roughness Effects on Frictional Resistance of Enclosed Rotating Disks, by R. E. Nece and J. W. Daily. (59—A-55)

563 Rotating Wakes in Vaneless Diffusers, by R. C. Dean, Jr., and Y. Senoo. (59—A-104)

575 Incidence and Deviation-Angle Correlations for Compressor Cascades, by Seymour Lieblein. (59—A-171)

588 A Study of Boundary-Layer Characteristics of Turbomachine Blade Rows and Their Relation to Over-All Blade Loss, by W. L. Stewart, W. J. Whitney, and R. Y. Wong. (59—A-23)

593 Laminar Boundary Layers in Oscillatory Flow, by P. G. Hill and A. H. Stenning. (59—A-265)

609 Experimental Determination of Statistical Properties of Two-Phase Turbulent Motion, by S. L. Soo, H. K. Ihrig, Jr., and A. F. El Kouh. (59—A-59)

622 The Turbulent Boundary Layer at a Plane of Symmetry in a Three-Dimensional Flow, by J. P. Johnston. (59—A-72)

629 Heat-Transfer Characteristics of Hot-Film Sensing Element Used in Flow Measurement, by S. C. Ling. (59—A-172)

635 The Adiabatic Bulk Modulus of Normal Paraffin Hydrocarbons From Hexane to Hexadecane, by R. E. Rolling and C. J. Vogt. (59—A-169)

645 Variable Flow Resistance With Adjustable Multihole Orifice Plates in Series, by J. Sherman, F. A. Grochowski, and J. E. Sharbaugh. (59—A-182)

654 Cycle-Dependent Stress Relaxation of A-286 Alloy, by A. S. Ross and JoDean Morrow. (59—A-116)

661 Low-Cycle Fatigue of Two Nickel-Base Alloys by Thermal-Stress Cycling, by F. J. Mehringer and R. P. Felgar. (59—A-58)

671 The Stability of Metals Under Cyclic Plastic Strain, by L. F. Coffin, Jr. (59—A-100)

683 Roll-Force and Torque Coefficients for Hot-Strip Steel Mill, by B. N. Garudachar and H. A. Peterson. (59—A-153)

689 Steady-State Creep of a Thick-Walled Cylinder Under Combined Axial Load and Internal Pressure, by Iain Finnie. (59—A-57)

695 Burst Strengths and Deformations of Welded Composite Turbine Wheels as Related to Weld Quality and Plasticity Calculations, by A. G. Holms and A. J. Repko. (59—A-28)

710 The Twin Throat Venturi: A New Fluid-Flow Measuring Device, by A. A. Kalinske. (59—A-154)

717 A Study of Viscosity Effect and Its Compensation on Turbine-Type Flowmeters, by W. F. Z. Lee and Henning Karlby. (59—A-105)

729 The Quadrant Edge Orifice—A Fluid Meter for Low Reynolds Numbers, by M. Bogema and P. L. Monkmeyer. (59—A-140)

735 Small-Diameter-Orifice Metering, by T. J. Filban and W. A. Griffin. (59—A-101)

741 Analysis of Axially Loaded Annual Shells With Applications to Welded Bellows, by M. Hetényi and R. J. Timms. (59—A-175)

TECHNICAL BRIEFS

756 Cavitation Problems in Cryogenics, by R. B. Jacobs and K. B. Martin.

KURT SPIELBERG
Instructor,
Department of Physics,
The City College,
New York, N. Y.[1]

HANS TIMAN
Institute of Theoretical Physics,
University of Vienna,
Vienna, Austria[2]

On Three and Two-Dimensional Disturbances of Pipe Flow

A system of ordinary, coupled differential equations is set up for three-dimensional disturbances of Poiseuille flow in a straight pipe of circular cross section. The commonly treated equations are shown to be special cases arising from particular assumptions. It is shown that in the nonviscous, and therefore also in the general case, there exists, in contrast to the analogous problem in Cartesian co-ordinates, no transformation reducing the given problem to a two-dimensional one. A fourth-order differential equation is derived for disturbances independent of the direction of the main flow. The solutions, which are obtained, show that those two-dimensional disturbances, termed cross disturbances, decay with time and do therefore not disturb the stability of the main flow. Explicit expressions for the cross disturbances are obtained and a discussion of their nature is given.

Introduction

THE transition of laminar to turbulent flow of a viscous, incompressible fluid has for a long time attracted attention. In particular, the effect of small, incidental disturbances on the main flow has been studied. A review of the methods and results can be found in the books of C. C. Lin and H. Schlichting [1, 2].[3] Notable results have been achieved mainly in the case of two-dimensional disturbances of Couette flow and to a lesser extent of Poiseuille flow. Occasionally one has attempted to extend results established for plane flows to the cylindrical configuration without sufficient justification.

The present paper should establish that in the case of pipe flow a proof of stability against two-dimensional disturbances allows no final conclusion about the sensitivity against three-dimensional ones. This contrasts with the problem of three-dimensional disturbances of plane Poiseuille flow, which allows the reduction discussed in the following text. Investigations of the stability character of cylindrical Poiseuille flow will have to be based on a system of coupled differential equations to be presented in the sequel.

In his paper [3] H. B. Squire was able to show that an ordinary differential equation

$$\frac{d^4v}{dy^4} - 2(\alpha^2+\beta^2)\frac{d^2v}{dy^2} + (\alpha^2+\beta^2)^2 v = i\alpha R\left\{(W-c)\left[\frac{d^2v}{dy^2} - (\alpha^2+\beta^2)v\right] - W''v\right\} \quad (1)$$

governing a three-dimensional disturbance of plane Poiseuille-flow $W(y)$ can be easily transformed by means of the substitution

$$\tilde{\alpha}^2 = \alpha^2+\beta^2; \quad \tilde{c} = c$$
$$\tilde{R}\tilde{\alpha} = R\alpha; \qquad \tilde{\beta} = 0 \quad (2)$$

to the well-known equation for two-dimensional disturbances;

$$\frac{d^4v}{dy^4} - 2\tilde{\alpha}^2\frac{d^2v}{dy^2} + \tilde{\alpha}^4 v = i\tilde{\alpha}\tilde{R}\left\{(W-c)\left[\frac{d^2v}{dy^2} - \tilde{\alpha}^2 v\right] - W''v\right\} \quad (3)$$

That means that a stability proof of equation (3) holds good also for a three-dimensional disturbance, determined by (1). We will show now that there is no such possibility in the case of Poiseuille flow in a circular pipe.

The Three-Dimensional Problem in Cylindrical Co-ordinates

Starting with the Stokes-Navier differential equations, we obtain four equations governing the behavior of disturbances $\bar{\mathfrak{q}}(\bar{u}, \bar{v}, \bar{w})$ superimposed on a main-flow in the z-direction, $W = 1 - r^2$

$$\frac{\partial\bar{u}}{\partial t} + W\frac{\partial\bar{u}}{\partial z} - \frac{1}{R}\left[\nabla^2\bar{u} - \frac{\bar{u}}{r^2} - \frac{2}{r^2}\frac{\partial\bar{v}}{\partial\varphi}\right] = -\frac{\partial p}{\partial r} \quad (4a)$$

$$\frac{\partial\bar{v}}{\partial t} + W\frac{\partial\bar{v}}{\partial z} - \frac{1}{R}\left[\nabla^2\bar{v} - \frac{\bar{v}}{r^2} + \frac{2}{r^2}\frac{\partial\bar{u}}{\partial\varphi}\right] = -\frac{1}{r}\frac{\partial p}{\partial\varphi} \quad (4b)$$

$$\frac{\partial\bar{w}}{\partial t} + W\frac{\partial\bar{w}}{\partial z} - \frac{1}{R}\left[\nabla^2\bar{w} + W'' + \frac{1}{r}W'\right] + \bar{u}W' = -\frac{\partial p}{\partial z} \quad (4c)$$

$$\frac{1}{r}\bar{u} + \frac{\partial\bar{u}}{\partial r} + \frac{1}{r}\frac{\partial\bar{v}}{\partial\varphi} + \frac{\partial\bar{w}}{\partial z} = 0 \text{ (equation of continuity)} \quad (4d)$$

with

$$\nabla^2 \equiv \frac{\partial^2}{\partial r^2} + \frac{1}{r}\frac{\partial}{\partial r} + \frac{1}{r^2}\frac{\partial^2}{\partial\varphi^2} + \frac{\partial^2}{\partial z^2}$$

Elimination of the pressure p and introduction of the conventional expressions for the disturbances,

---

[1] Also, International Business Machines Corporation, New York, N. Y.

[2] Also, Allen B. Dumont Laboratories, Clifton, N. J.

[3] Numbers in brackets designate References at end of paper.

Presented at the Summer Conference of the Applied Mechanics Division, University Park, Pa., June 20–22, 1960, of THE AMERICAN SOCIETY OF MECHANICAL ENGINEERS.

Discussion of this paper should be addressed to the Secretary, ASME, 29 West 39th Street, New York, N. Y., and will be accepted until October 10, 1960, for publication at a later date. Discussion received after the closing date will be returned.

NOTE: Statements and opinions advanced in papers are to be understood as individual expressions of their authors and not those of the Society. Manuscript received by ASME Applied Mechanics Division, August 27, 1958. Paper No. 60—APM-12.

$$\mathbf{q}_i(\bar{u}, \bar{v}, \bar{w}) = \mathbf{q}_i(u, v, w) \exp\{i(\alpha z + \beta\varphi - \alpha c t)\} \quad (5)$$

leads after some calculation to the basic system of ordinary, but coupled, differential equations:

$$i\alpha R(W - c)(i\alpha u - w') - 2i\beta R v = \left(\Delta - \frac{1}{r^2}\right)(i\alpha u - w') - \frac{2\beta^2}{r^2} w + \frac{2\alpha\beta}{r^2} v \quad (6a)$$

$$i\alpha R(W - c)(\alpha v - \beta w) + 2\beta R r u = \Delta(\alpha v - \beta w) - \frac{2}{r}(\alpha v - i\alpha\beta u) - 2\alpha v' \quad (6b)$$

$$i\alpha R(W - c)(i\beta u - r v') + i\alpha R v(3r^2 - 1 + c) = \left(\Delta - \frac{2}{r}\frac{\partial}{\partial r} + \frac{1}{r^2}\right)(i\beta u - v) - r\Delta v' \quad (6c)$$

$$\frac{u}{r} + u' + \frac{i\beta}{r} v + i\alpha w = 0$$

with

$$\Delta \equiv \frac{\partial^2}{\partial r^2} + \frac{1}{r}\frac{\partial}{\partial r} - \frac{\beta^2}{r^2} - \alpha^2$$

$$W \equiv 1 - r^2$$

As becomes clear from the derivation, only two of the first three equations are independent. For purposes of specialization, however, it is useful to establish all four equations of system (6).

The boundary conditions for system (6) are that the velocity components $\mathbf{q}_i$ vanish at the pipe walls and remain finite in the center:

$$u(1) = v(1) = w(1) = 0, \qquad u(0), v(0), w(0) \ldots \text{finite}. \quad (7)$$

While in the Cartesian case it is easily possible to eliminate two of the three unknown velocity components, this system does not seem to lend itself to further simplification without additional assumptions. Yet it is instructive to see how the commonly treated equations arise as special cases of (6).

In the first place, one can make the assumption of rotational symmetry, $\frac{\partial}{\partial\varphi} = 0$, or $\beta = 0$, with $v(r) \not\equiv 0$. [$v(r) = 0$ would be the case of axial symmetry.] Then equation (6*b*) reduces to the ordinary differential equation for $G(r) = rv(r)$:

$$i\alpha R(W - c)G = G'' - \frac{1}{r} G' - \alpha^2 G \quad (8)$$

which was treated by Sexl [4] and Pekeris [5].

It admits of simple solutions, satisfying the boundary conditions for $Im(\alpha c) < 0$ only. The inference is that the case of rotational symmetry is no more subject to turbulence than that of axial symmetry.

Equations (6*a*) and (6*d*) lead to the well-known Orr-Sommerfeld equation, the starting point of a number of investigations of axial flow. One need merely satisfy the equation of continuity by the substitution:

$$u = -\frac{i\alpha}{r} f, \qquad w = \frac{1}{r} f' \quad (9)$$

Then $i\alpha u - w' = -1/r\left(f'' - \frac{1}{r} f' - \alpha^2 f\right)$ and one obtains:

$$i\alpha R(W - c)g(r) = g'' - \frac{1}{r} g' - \alpha^2 g \quad (10a)$$

$$g(r) \equiv f'' - \frac{1}{r} f' - \alpha^2 f \quad (10b)$$

It should be noted that only in the special cases of plane Couette and of pipe flow the fourth-order differential equation reduces to a system of two equations. The case of Couette flow was treated first by L. Hopf [6], that of Poiseuille flow by Sexl [4, 7]. More recent discussions are given by Pekeris [5], Synge [8], Wasow [9], Pai [10], Thomas [11], Sexl and Spielberg [12]. All papers give stability of pipe flow against disturbances of the special type investigated. These investigations, however, have not exhausted the manifold of possible two-dimensional disturbances. To complete the picture we will have to investigate "cross disturbances" in later sections.

Associated Two-Dimensional Disturbances for Nonviscous Flow

Whereas system (6) in its most general form seems hardly tractable, a reduction to separate equations in u, v, and w is possible for the limiting case of nonviscous fluids. $1/R$ can then be considered as vanishing, so that system (6) is modified to:

$$i\alpha(W - c)(i\alpha u - w') = 2i\beta v \quad (11a)$$

$$i\alpha(W - c)(\alpha v - \beta w) = -2\beta r u \quad (11b)$$

$$i\beta v + (ur)' + i\alpha r w = 0 \quad (11c)$$

Elimination of v and w leads now to an equation of the second order for the velocity component u, first arrived at in a different manner by Sexl [7].

$$u'' + u' \frac{3\beta^2 + \alpha^2 r^2}{r(\beta^2 + \alpha^2 r^2)} + u \frac{\frac{4\beta^2 r^2}{W - c} + \beta^2 - \beta^4 - 2\alpha^2\beta^2 r^2 - \alpha^2 r^2 - \alpha^4 r^4}{r^2(\beta^2 + \alpha^2 r^2)} = 0 \quad (12)$$

It is clear that the two integrals of (12) cannot by themselves do justice to the system and the boundary conditions

$$u(1) = u'(1) = 0 \quad u(0), \quad u'(0) \ldots \text{finite} \quad (13)$$

They can, however, be expected to represent asymptotically (for large R) two solutions of a fourth-order differential equation, not explicitly derivable from (6). (Compare the analogous problem in Cartesian co-ordinates treated by Squire [3].) If a complete solution for u, involving four particular integrals, could be found and adjusted to the boundary conditions, v and w would follow from lower-order equations of system (6).

At this stage it is quite natural to consider whether it is not feasible to circumvent such an elaborate procedure by an analogon to Squire's theorem. In other words, following Squire, we ask, can one, quite generally, associate with each three-dimensional disturbance, given by the variables and parameters $(q_i, \alpha, \beta, c, R)$ a two-dimensional one $(\bar{q}_i, \bar{\alpha}, \bar{c}, \bar{R})$, which satisfies the same differential equations and boundary conditions. For in that case the stability of all two-dimensional disturbances, encompassing all associated three-dimensional disturbances, would establish stability for the three-dimensional case as well.

Unfortunately the answer must here be negative, even though in the Cartesian case it turns out to be positive. An affirmative reply would mean, for instance, that a three-dimensional disturbance $[u(r), \alpha, \beta, c]$ of the nonviscous flow, governed by (12), could be accounted for by the equation for two-dimensional perturbations following from system (11) or from equation (12) for $\beta = 0$.

$$\bar{u}'' + \frac{1}{r}\,\bar{u}' + \bar{u}\left(-\frac{1}{r^2} - \bar{\alpha}^2\right) = 0 \qquad (14)$$

$$\bar{u}(0) \ldots \text{finite};\ \bar{u}(1) = 0$$

A condition necessary for this possibility would be that for any three-dimensional disturbance $[u(r),\ \alpha,\ \beta]$ there existed a transformation

$$\bar{u} = \bar{u}[u(r),\ \alpha, \beta, c, r];\quad \bar{\alpha} = \bar{\alpha}(\alpha, \beta, c) \qquad (15)$$

which, substituted in (14), lead identically to equation (12). Such a transformation can be written, on account of the assumed smallness of $u(r)$, e.g. by Taylor's theorem, as:

$$\bar{u} = f(\alpha, \beta, c;\ r) + g(\alpha, \beta, c;\ r)u(r)$$

$$f(\alpha, 0, c, r) = f(\alpha, \beta, c, 1) = 0, \qquad g(\alpha, 0, c;\ r) = 1 \qquad (16)$$

Substituting of (16) in (14) then leads to the relation

$$u'' + u'[2g'/g + 1/r] + u\left[g''/g + \frac{1}{r}\,g'/g - 1/r^2 - \bar{\alpha}^2\right] + \left[\frac{f''}{g} + \frac{1}{r}\,\frac{f'}{g} + \frac{f}{g}\left(-\frac{1}{r^2} - \bar{\alpha}^2\right)\right] = 0 \qquad (17)$$

which should be identical with (12). Equating the first coefficients leads to $g(r) = \dfrac{\alpha r}{(\beta^2 + \alpha^2 r^2)^{1/2}}$. Equating the second coefficients and comparing equal powers of r results in the relations:

$$\left.\begin{aligned} \alpha^6 - \bar{\alpha}^2\alpha^4 = 0; \qquad (1 - c)(\beta^4 - \beta^2) = 0 \\ 3\alpha^4\beta^2 + (1 - c)(\bar{\alpha}^2\alpha^4 - \alpha^6) - 2\alpha^2\bar{\alpha}^2\beta^2 = 0 \\ 3\alpha^2\beta^4 - \bar{\alpha}^2\beta^4 + (1 - c)(2\alpha^2\bar{\alpha}^2\beta^2 - 3\alpha^4\beta^2) = 0 \\ 3\beta^6 + \beta^4 + (1 - c)(\bar{\alpha}^2\beta^4 + 4\alpha^2\beta^2 - 3\alpha^4\beta^4) = 0 \end{aligned}\right\} \qquad (18)$$

Obviously there is no way of satisfying this system except the trivial one, $\alpha^2 = \bar{\alpha}^2, \beta = 0$. We can conclude that the much more complicated nonviscous problem, formulated in the system (6), will, if anything, be even less amenable to a reduction to two-dimensional equations.

Disturbances Independent of z ("cross disturbances")

As shown above, any real solution of the stability problem for pipe-flow will have to take into account the full system (6). Nevertheless it has always been of interest to consider special cases, such as that of axial symmetry ($v = 0$) and that of rotational symmetry $\left(\dfrac{\partial}{\partial\varphi} = 0, v \neq 0\right)$. The corresponding investigations point to stability in each case.

It is interesting, however, that so far there exists no treatment of disturbances which are independent of the direction of the main-flow, z.

This assumption, hardly more artificial than the others, is characterized by $\dfrac{\partial}{\partial z} = 0$ or $\alpha = 0$. To obtain equations in the perturbation components u, v, w we have to take equations (6b), (6c), (6d) with $\alpha = 0$, since equations (6a) and (6b) would now be interdependent.

$$iR\delta w + 2Rru + \Delta w = 0 \qquad (19a)$$

$$iR\delta(rv' - i\beta u) + iR\delta v = \left[\Delta - \frac{2}{r}\,\frac{\partial}{\partial r} + \frac{1}{r^2}\right](i\beta u - v) - r\Delta v' \qquad (19b)$$

$$u' + u/r + \frac{i\beta}{r}\,v = 0, \qquad \delta \equiv \alpha c \equiv \delta_r + i\delta_i \qquad (19c)$$

The disturbances governed by system (19) might for convenience be termed "cross disturbances," since they are identical for each cross section of the pipe. They evidently correspond to perturbations created uniformly along parallels to the cylinder axis. The parameter $\delta = \alpha c$ is the coefficient of t in the expressions (5) and of course does not vanish with α. Its imaginary part δ_i is the determining factor of the stability problem, positive values indicating growth, negative values pointing to decay of cross-disturbances with time. It should also be noted that equations 19 are not independent of the main stream $W = 1 - r^2$, even though the latter does not explicitly appear in the system (19). System (6) and its consequences have been derived specifically for Poiseuille flow, $W = 1 - r^2$.

To satisfy the equation of continuity, we introduce the stream function $\psi(r)$:

$$u(r) = \psi(r)/r;\quad v(r) = \frac{i}{\beta}\,\psi' \qquad (20)$$

The governing differential equation for the amplitude functions $u(r)$ and $v(r)$ is now:

$$\psi'''' + 2/r\psi''' + \psi''/r^2(-2\beta^2 - 1) + \psi'/r^3(2\beta^2 + 1) + \frac{\psi}{r^4}\,\beta^2(\beta^2 - 4) = iR\delta\left(\frac{\beta^2}{r^2}\,\psi - \psi'/r - \psi''\right) \qquad (21)$$

The z-component is determined by equation (19a). Consequently the first step must be to solve the fourth-order differential equation (21).

It should be noted here that the parameter β is restricted to positive integral values to insure uniqueness of the perturbations.

Solution of the Differential Equation (21) and Computation of the Eigenvalues

Introducing the operator $\Theta = \partial^2/\partial r^2 + 1/r\ \partial/\partial r - \beta^2/r^2$, we can rewrite equation (21) as follows:

$$\Theta\cdot\left(\psi'' + \frac{1}{r}\,\psi' - \frac{\beta^2}{r^2}\,\psi\right) = -iR\delta\quad \Theta\cdot\psi$$

It is seen easily that the operator-equation $\Theta\cdot f = 0$ has the solutions r^β and $r^{-\beta}$. The remaining differential equation

$$\psi'' + 1/r\psi' - \frac{\beta^2}{r^2}\,\psi + iR\delta\psi = 0 \qquad (22)$$

can be solved by means of the Bessel functions

$$Z_\beta(kr) = c_2 J_\beta(kr) + c_4 Y_\beta(kr) \qquad (23a)$$

with

$$k = \sqrt{iR\delta}; \qquad k^2 = -R\delta_i + iR\delta_r \qquad (23b)$$

Now we have the general solution of the differential equation (21).

$$\psi = c_1 r^\beta + c_2 J_\beta(kr) + c_3 r^{-\beta} + c_4 Y_{-\beta}(kr) \qquad (24)$$

However, in view of the boundary conditions (7), the coefficients c_3 and c_4 must vanish. The remaining conditions are

$$\psi(1) = 0;\ \psi'(1) = 0 \qquad (25)$$

Replacing the derivative in accordance with the recursion formula

$$J_\beta'(z) = -\beta/zJ_\beta(z) + J_{\beta-1}(z) \qquad (26)$$

we obtain the equations

$$c_1 + c_2 J_\beta(k) = 0; \qquad c_1\beta + c_2[\beta J_\beta(k) - kJ_{\beta+1}(k)] = 0 \qquad (27)$$

The existence of nontrivial solutions for c_1 and c_2 demands that

the determinant of the system (27) vanishes. That leads to the simple boundary condition:

$$J_{\beta+1}(k) = 0 \tag{28}$$

The boundary problem has therefore been reduced to the problem of determining and investigating the zeros of a Bessel function of order $\beta + 1$ and complex argument k. The manifold of all k_m satisfying (28) gives immediately all possible values for δ_i and δ_r. It is possible to show that equation (28) admits real solutions k_0 only [13, p. 482].

Based on this fact, we can demonstrate the stability of Poiseuille flow with respect to cross disturbances. For the relation (23*b*) then implies $k_m^2 = -R\delta_{im} + iR\delta_{rm}$

$$\delta_{rm} = 0; \qquad \delta_{im} = -k_m^2/R \tag{29}$$

It follows that for any β and R the imaginary part of the "time-parameter" is negative.

The conclusion is that Poiseuille flow is indeed stable against any two-dimensional perturbances.

Corresponding to the zeros of $J_{\beta+1}$ there exist an infinite number of eigenvalues δ_{i1}, δ_{i2}, δ_{i3} . . . . They can quite easily be calculated for the special cases of small and very large values of β. In the instance of small β we can limit ourselves to the Bessel functions of second and third order.

Their first zeros are given by:

$\beta = 1$	$k_1 \approx 5.13$	$\beta = 2$	$k_1 \approx 6.38$
$\beta + 1 = 2$	$k_2 \approx 8.42$	$\beta + 1 = 3$	$k_2 \approx 9.76$
	$k_3 \approx 11.62$		$k_3 \approx 13.02$
	. . . . .		. . . . .

For large β we have (compare [2, p. 143]):

$$k_1 = \beta + 1 + 1.856\sqrt[3]{\beta+1} + \dots$$

$$k_2 = \beta + 1 + 3.245\sqrt[3]{\beta+1} + \dots$$

$$k_3 = \beta + 1 + 4.382\sqrt[3]{\beta+1} + \dots \text{ etc.}$$

The corresponding eigenvalues can be easily established, for instance:

$$\beta = 1; \quad \delta_{i1} = -26.32/R; \quad \beta = 2; \quad \delta_{i1} = -40.70/R$$

Large β: $k_1^2 \cong (\beta + 1 + 1.85\sqrt[3]{\beta+1})^2 \simeq \beta^2 + 2\beta + 3.7\beta^{4/3} + 3.24\beta^{2/3} + 4.8\beta^{1/3}$

$$\delta_{i1} = -\beta^2/R - \beta/R(3.7\beta^{1/3} + 2 + \dots) \text{ etc.}$$

The boundary condition $\psi(1) = 0$ leads to $c_1 + c_2 J_\beta(k_m) = 0$; $c_1 = -c_2 J_\beta(k_m)$, so that the stream function for the eigenvalue k_m becomes:

$$\psi_m = c\{J_\beta(k_m r) - J_\beta(k_m) r^\beta\} \tag{30}$$

This equation and its derivative allows to determine the amplitude functions for a representative eigenvalue k_m as:

$$u = c/r\{J_\beta(k_m r) - J_\beta(k_m) r^\beta\} \tag{31a}$$

$$v = ic/r\left\{J_\beta(k_m r) - \frac{k_m}{\beta} r J_{\beta+1}(k_m r) - J_\beta(k_m) r^\beta\right\} \tag{31b}$$

Now we are in the position to compute the z component $w(r)$.

The Final Expressions for the Velocity Components

With $iR\delta = -k_m^2$ and $ru = \psi$ the equation (19*a*) becomes

$$w'' + \frac{w'}{r} + (k_m^2 - \beta^2/r^2)w = -2R\psi \tag{32}$$

This differential equation is solved by the method of variation of constants; we bring the lengthy calculation in the Appendix. Omitting the argument $k_m r$ in the sequel, we obtain the solution:

$$w = C\frac{2R}{k_m^2}\left[r^\beta J_\beta(k_m) - J_\beta - \frac{k_m r}{2} J_{\beta+1}\right] \tag{33}$$

The equations (31*a*), (31*b*), (33) represent the amplitude functions u, v, w. To get the actual disturbance we need only multiply u and w with the real, v with the imaginary part of the exponential term.

$$\bar{u} = Ce^{-(k_m^2/R)t}\cos(\beta\varphi)\cdot\frac{1}{r}\{J_\beta - r^\beta J_\beta(k_m)\} \tag{34a}$$

$$\bar{v} = Ce^{-(k_m^2/R)t}\sin(\beta\varphi)\cdot\frac{1}{r}\{r^\beta J_\beta(k_m) - J_\beta + (k_m/\beta) r J_{\beta+1}\} \tag{34b}$$

$$\bar{w} = Ce^{-(k_m^2/R)t}\cos(\beta\varphi)\cdot\frac{2R}{k_m^2}\left\{r^\beta J_\beta(k_m) - J_\beta - \frac{k_m r}{2} J_{\beta+1}\right\} \tag{34c}$$

The velocity distribution in the circular pipe is given by

$$v_r = \bar{u}; \quad v_\varphi = \bar{v}; \quad v_z = W(r) + \bar{w} \tag{35}$$

Physical Discussion

For any given β a consultation of tables of Bessel functions will allow an evaluation of the flow distribution. In the following we will discuss the extremes: β small (e.g., 1 or 2), β large ($\beta \gg 1$). Constant factors will be deleted for simplicity.

First eigenvalues: k_1 (fundamental).

(a) $\beta = 1$, $\quad k_1 = 5.135$, $\quad r = \dfrac{z}{5.135}$:

The boundary condition becomes $J_z(k_1) = 0$ and the argument z takes on values between 0 and 5.135 as r varies from 0 to 1.

$$u = J_1/r - J_1(k_1), \qquad J_1(k_1) = -0.339$$

$u = J_1/r + 0.339$, $u' = -k_1/r \cdot J_2$ and the extremes are at $r = 0$ and $r = 1$. At $r = 0$ we have $J_1/r = k_1/2 = 2.567$. For $z = z_0 = 3.832$ we have $J_1(z_0) = 0$. As $J_2 > 0$ throughout the interval, u decreases monotonically.

The actual behavior of u, v, and w is best established from a set of tables [14]:

r	z	$J_1(z)$	$J_1(z)/r$	$u(r)$
0	0.0	0.0	2.567	2.906
0.1	0.513	0.247	2.47	2.809
0.2	1.026	0.448	2.24	2.579
0.3	1.539	0.563	1.876	2.215
0.4	2.052	0.573	1.432	1.771
0.6	3.078	0.309	0.515	0.854
0.7	3.591	0.099	0.141	0.480
0.8	4.104	−0.103	−0.129	0.210
0.9	4.617	−0.259	−0.288	0.051
1.0	5.13	−0.339	−0.339	0.0

$$v(r) = k_1 J_2 + J_1(k_m) - \frac{J_1}{r} = k_1 J_2 - u(r)$$

$$v'(r) = k_1(k_1 J_1 - J_2/r) \qquad v'(0) = 0,\ v'(1) < 0$$

As can be seen, the extremes of v must lie in the interval $0 < z < z_0$, where $J_1 > 0$.

r	$J_3(z)$	$k_1 J_2$	v
0.0	0.0	0.0	−2.906
0.1	0.032	0.164	−2.645
0.2	0.119	0.610	−1.968
0.3	0.242	1.242	−0.973
0.4	0.364	1.867	0.096
0.6	0.486	2.493	1.639
0.7	0.444	2.278	1.798
0.8	0.338	1.734	1.524
0.9	0.184	0.944	0.893
1.0	0.0	0.0	0.0

$$w(r) = rJ_1(k_m) - J_1 - \frac{k_1}{2} rJ_2$$

$$w'(r) = J_1(k_m) - k_1 J_1 - \frac{k_1^2}{2} rJ_2 - \frac{k_1}{2} J_2$$

$$= {}^3/_2 k_1 J_2 + J_1(k_m) - J_1/r - \frac{k_1^2}{2} rJ_1$$

$$w'(0) < 0; \quad w'(z_0) > 0; \quad w'(1) = -\frac{k_1^2}{2} J_1(k_1) > 0$$

$w(r)$ reaches its maximal value in the neighborhood of J_2 max. For the numerical calculation we use $w/r = -u - \frac{k_1}{2} J_2$.

$w(0) = 0.0$; $w(1/10) = -0.289$; $w(2/10) = -0.576$; $w(3/10) = -0.850$;

$w({}^1/_2) = -1.230$; $w({}^6/_{10}) = -1.260$; $w({}^9/_{10}) = -0.471$; $w(1) = 0.0$

We skip the analogous calculations and tabulations for the second parameter value $\beta = 2$ and represent the results in the form of graphs which show the behavior of the perturbations as functions of r. As we shall presently see, the curves for $\beta = 2$ exhibit already the features that are characteristic for large parameter values, Figs. 1, 2.

(b) $\beta \gg 1$; $k_1 = \beta + 1 + 1.86\sqrt[3]{\beta + 1} + \ldots$ (the first positive zero of $J_{\beta+1}$):

As our approximations in the appendix show, nearly the whole main flow remains undisturbed. Only near the walls we have to expect perturbations. The larger β is, the smaller is the region where the disturbances are noticeable, the nearer are the extremes of the amplitude functions to the walls.

As an example, we examine the amplitude functions for $\beta = 22$.

$$k_1 = 23 + 1.856\sqrt[3]{23} = 28.28$$

We obtain the following expressions for the amplitude functions:

$$u(r) = J_{22}/r - J_{22}(k_1) r^{21} = J_{22}/r + 0.083(r^{21})$$

$$v(r) = -u + \frac{k_1}{\beta} J_{21} = -u + 1.27 J_{22}$$

$$w(r) = -ru - \frac{k_1}{2} rJ_{22} = -ru - 14.14 rJ_{22}$$

We omit the calculations and show the behavior of the three amplitudes in the following sketches (Fig. 3).

Eigenvalues of higher order.

We can extend the above considerations to eigenvalues of higher order in an appropriately modified manner.

Suppose k_2 is the second zero of $J_{\beta+1}$. The argument z will now vary between 0 and k_2. The corresponding zeros of J_β are z_1 and z_2.

$u = 1/r[J_\beta(k_2 r) - J_\beta(k_2) r^\beta]$ and $J_\beta(k_2) > 0$. Hence u, which is positive around 0, will be negative at $r = z_1/k_2$. It follows that there is a zero of $u(r)$ to the left of z_1. All together u has 3 zeros

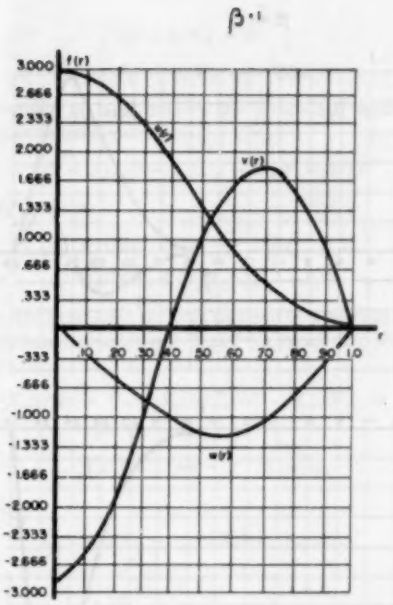

Fig. 1 Perturbation amplitudes as functions of radius, $\beta = 1$

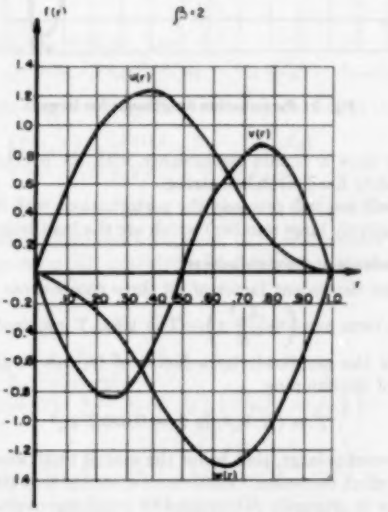

Fig. 2 Perturbation amplitudes as functions of radius, $\beta = 2$

and 2 extremes (one positive, one negative), the latter of which practically coincide with the extremes of the Bessel functions J_β.

$v(r) \simeq -\psi' \simeq -u'$. For large values of β we have a coincidence of extrema of u and zeros of v. As similar calculations show, v has 4 zeros and 3 extremes. The z-component $w(r)$, being initially (around $r = 0$) negative, becomes zero in the neighborhood of z_1. Again, as in the case of u, there are 3 zeros and one positive as well as one negative maximum. The higher zeros of $J_{\beta+1}$ give rise to amplitude functions whose behavior is quite analogous. For a zero of index n the functions u and w have $n + 1$ zeros and n extrema of alternating signs, v has $n + 2$ zeros and $n + 1$ maxima.

If the order of zeros is not too large, nearly the whole main flow remains undisturbed. In the peripheral region the feasible dis-

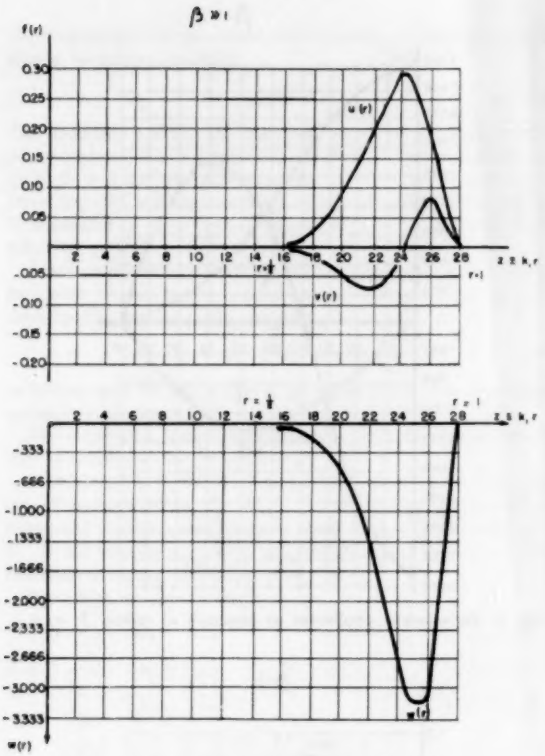

Fig. 3 Perturbation amplitudes for large β

turbances have a certain resemblance with the overtones of an appropriately fixed stretched string.

As we will see, it is precisely the perturbations with large index m (k_m relatively large number) which are the least important.

Time dependence of the disturbances.

The time dependent factor of all three components is the exponential term $\exp\left(-\frac{k_m^2}{R}t\right)$. The time T required for a reduction of the amplitude by a factor of $^1/_2$ can be taken as a measure of the damping.

$$T = (R/k_m^2)\ln 2 = 0.693R/k_m^2$$

As R becomes large, that is, for the case of small viscosity, the damping effect decreases. Furthermore, we see that the stability of the flow is primarily determined by small eigenvalues, damping increasing very strongly for larger values of k_m. At any rate the damping decreases for increasing R, a result which agrees with the experimental fact, that increasing R usually means inclination toward turbulence.

Discussion of the velocity vector.

The velocity vector of a disturbance $\mathbf{v}$ consists of a component in the plane of a cross-section q and a component in the z-direction, perpendicular to the first one. According to our basic assumption the vector $\mathbf{v}$ is the same for every cross-section q (independent of z).

$$\mathbf{v} = \mathbf{v}_q + \mathbf{v}_z = (\bar{u}\mathbf{e}_r + \bar{v}\mathbf{e}_\varphi) + \bar{w}\mathbf{e}_z \qquad |\mathbf{e}_i| = 1$$

We again consider the "basic oscillation" corresponding to the first zero k_1. Neglecting the time-dependent and constant factors we get

$$\mathbf{v}_q^2 = u^2 + \sin^2(\beta\varphi)\left[-\frac{2k_1}{\beta}uJ_{\beta+1} + \frac{k_1^2}{\beta^2}J^2_{\beta+1}\right]$$

$u(r)$ and $v(r)$ are constant on every circle $r = r_0$. In the following we count the angle φ from an arbitrarily taken diameter $\varphi = 0$.

From the equations (34a) and (34b) we obtain:

For

$$\beta\varphi = m\pi: \qquad v(r) = 0$$

$$\beta\varphi = 2n\pi: \qquad \mathbf{v}_q = u\mathbf{e}_r$$

$$\beta\varphi = (2n+1)\pi: \qquad \mathbf{v}_q = -u\mathbf{e}_r$$

For

$$\beta\varphi = (2n+1)\pi/2: \qquad u(r) = 0$$

$$\beta\varphi = (4n+1)\pi/2: \qquad \mathbf{v}_q = v\mathbf{e}_\varphi$$

$$\beta\varphi = (4n+3)\pi/2: \qquad \mathbf{v}_q = -v\mathbf{e}_\varphi$$

Between the special directions for which $\mathbf{v}_q$ is entirely radial or transverse we have to consider both respective components (of magnitude $\bar{u}$ and $\bar{v}$). Denoting the angle between $\mathbf{v}_q$ and the radial direction by α we have the relation $\tan\alpha = \bar{v}/\bar{u} = v/u \cdot \tan(\beta\varphi)$. This means, v/u being constant for any specific value of r, that the angle $\beta\varphi$ is also a measure of the deviation of the component $\mathbf{v}_q$ from the radial direction. The component u has no zero within the pipe, but v vanishes where u attains its maximum value.

For such a special value of r there exist 2β points where both u and v vanish. As the following diagrams (Figs. 4, 5, 6) show, these points constitute centers of rotational motion for the fluid. We see furthermore that the disturbances corresponding to large values of β qualitatively duplicate the behavior obtained for the case $\beta = 1$. We then simply have to consider 2β identical sectors which in their peripheral part exhibit the appropriately modified rotational motion.

The z-component, $w(r)$, which is superposed on the main flow, behaves similar to u, but is distinguished by a relatively quite large amplitude. On account of its dependence on the trigonometric function $\cos(\beta\varphi)$, the velocity distribution in the z-direction has a lamellar structure with β-directions of maximal ac-

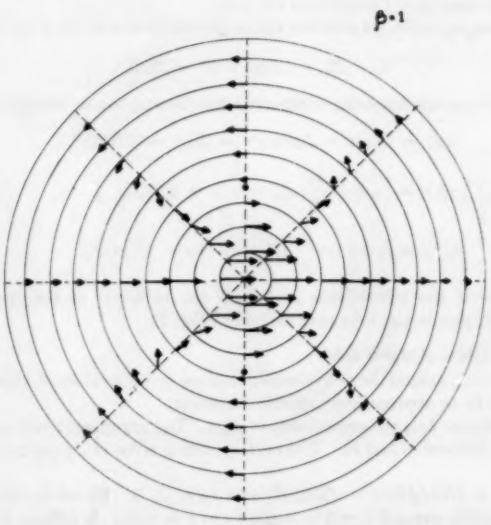

Fig. 4 Perturbation vector $\mathbf{v}_q$ in an arbitrary cross section, $\beta = 1$

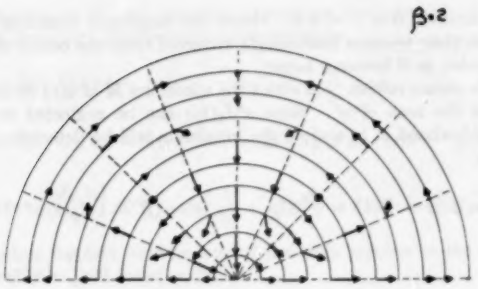

Fig. 5 Perturbation vector v_0 for $\beta = 2$

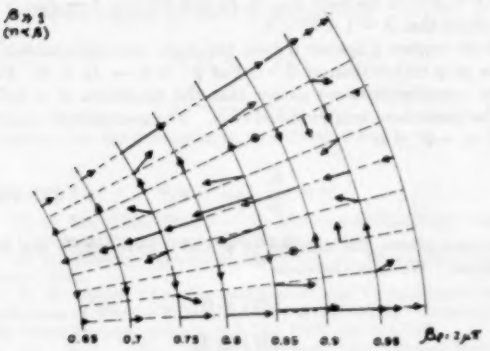

Fig. 6 Perturbation vector v_0 for large β

celeration and β-directions of maximal retardation of the main flow in alternating sequence.

It is clear that the azimuthal orientation of the flow pattern is physically determined by the nature of the initial excitation. Of course, the actual perturbation is a superposition of all Fourier components, with smaller values of β being predominant.

Acknowledgment

The authors would like to express their appreciation to Professor Th. Sexl, University of Vienna, for his continuous advice and encouragement.

APPENDIX 1

Solution of the Differential Equation (32).

$$w'' + \frac{1}{r}\,w' + (k_m^2 - \beta^2/r^2)w = -2R\psi \qquad (32)$$

To solve this equation we must deal with the homogeneous equation

$$w_H'' + \frac{1}{r}\,w_H' + (k_m^2 - \beta^2/r^2)w_H = 0 \qquad (36)$$

It is of the Bessel type and has the solution:

$$w_H = Z_\beta(k_m r) = c_1 J_\beta(k_m r) + c_2 Y_\beta(k_m r) \qquad (37)$$

In the following we will omit the argument $k_m r$. Differentiation with respect to r is indicated by a prime ($'$), differentiation with respect to the argument $z = k_m r$ of the Bessel function by a dot ($\cdot$). These derivatives are related by $k_m \dot{J}_p = J_p'$.

Varying the constants of solution (37) we arrive at the system:

$$c_1' J_\beta + c_2' Y_\beta = 0$$

$$c_1' J_\beta' + c_2' Y_\beta' = -2R\psi$$

Its determinant is, if W denotes the Wronskian determinant of the Bessel functions, given by:

$$\Delta = J_\beta Y_\beta' - J_\beta' Y_\beta = k_m W = 2/\pi r$$

and the c_i' become:

$$c_1' = CR\pi[rJ_\beta Y_\beta - r^{\beta+1} J_\beta(k_m) Y_\beta]$$

$$c_2' = CR\pi[r^{\beta+1} J_\beta(k_m) J_\beta - rJ_\beta^2]$$

To obtain the expression for $w(r)$ we have to make use of the following relations for arbitrary Bessel functions X_ν, $\bar{X}_\nu$ [13, pp. 133–135]:

$$\int z X_\nu(lz)\bar{X}_\nu(lz)dz = {}^1/_{2l^2}[2X_\nu(lz)\bar{X}_\nu(lz) - X_{\nu-1}\bar{X}_{\nu+1} - X_{\nu+1}\bar{X}_{\nu-1}] \qquad (38)$$

$$\int z^{\nu+1} X_\nu(z)dz = z^{\nu+1} X_{\nu+1}(z) \qquad (39)$$

In particular

$$\int z X_\nu^2(lz)dz = {}^1/_{2l^2}\{X_\nu^2 - X_{\nu-1}X_{\nu+1}\}$$

and we get

$$\int (rJ_\beta Y_\beta - r^{\beta+1} J_\beta(k_m) Y_\beta)dr = {}^1/_{2l^2}(2J_\beta Y_\beta - J_{\beta-1}Y_{\beta+1} - J_{\beta+1}Y_{\beta-1}) - \frac{1}{k_m} r^{\beta+1} J_\beta(k_m) Y_{\beta+1} + K_1 \qquad (40)$$

$$\int [r^{\beta+1} J_\beta(k_m) J_\beta - rJ_\beta(k_m)]dr = 1/k_m J_\beta(k_m) r^{\beta+1} J_{\beta+1} - {}^1/_{2l^2}(J_\beta^2 - J_{\beta-1}J_{\beta+1}) + K_2$$

Thus we obtain the third perturbation component in the form

$$w = CR\pi \left\{ \begin{matrix} 1/k_m J_\beta(k_m) r^{\beta+1}[J_{\beta+1}Y_\beta - Y_{\beta+1}J_\beta] \\ + {}^1/_{2l^2}[2J_{\beta-1}J_{\beta+1}Y_\beta - J_\beta(J_{\beta-1}Y_{\beta+1} + J_{\beta+1}Y_{\beta-1})] \end{matrix} \right\} + K_1 J_\beta + K_2 Y_\beta \qquad (41)$$

The boundary conditions $w(0)$ finite, $w(1) = 0$ require K_2 to be zero. Expression (41) can be simplified by means of the recursion formulas:

$$J_{\beta+1}Y_\beta - Y_{\beta+1}J_\beta = 2/\pi z$$

$$2J_{\beta-1}J_{\beta+1}Y_\beta - J_\beta(J_{\beta-1}Y_{\beta+1} + J_{\beta+1}Y_{\beta-1}) = Y_\beta\left[\left(\frac{\beta}{z}J_\beta + \dot{J}_\beta\right)\left(\frac{\beta}{z}J_\beta - \dot{J}_\beta\right)\right] - J_\beta\left[\left(\frac{\beta}{z}J_\beta + \dot{J}_\beta\right)\left(\frac{\beta}{z}Y_\beta - \dot{Y}_\beta\right) + \left(\frac{\beta}{z}J_\beta - \dot{J}_\beta\right)\left(\frac{\beta}{z}Y_\beta + \dot{Y}_\beta\right)\right]$$

$$= 2\dot{J}_\beta(-Y_\beta\dot{J}_\beta + J_\beta\dot{Y}_\beta) = \frac{4}{\pi z}\dot{J}_\beta = \frac{4}{\pi k_m r}\left(\frac{\beta}{k_m r}J_\beta - J_{\beta+1}\right)$$

Thus we arrive at:

$$w = CR/k_m^2[2r^\beta J_\beta(k_m) + \beta J_\beta - zJ_{\beta+1}] + K_1 J_\beta \qquad (42)$$

The second boundary condition allows us to eliminate one constant

$$w(1) = 0 \rightarrow K_1 = -\frac{\beta+2}{k_m^2}RC$$

so that we get formula (33) of the text.

APPENDIX 2

Discussion of the Behavior of the Amplitude Functions for Large β

If $\beta \gg 1$, the first positive zero of $J_{\beta+1}$ is

$$k_1 = \beta + 1 + 1.86\sqrt[3]{\beta+1} + \dots$$

The first maximum of $J_{\beta+1}$ is given by

$$\bar{m} = \beta + 1 + 0.81\sqrt[3]{\beta+1}$$

The argument z again takes on values between 0 and k_1; corresponding r-values are given by

$$r \equiv z/k_1$$

Similarly we obtain the first zero z_0 of J_β

$$z_0 = \beta + 1.86\sqrt[3]{\beta} + \dots$$

and the first maximum m:

$$m = \beta + 0.81\sqrt[3]{\beta}$$

From the theory of Bessel functions we know that J_β and $J_{\beta+1}$ will increase monotonically up to their first maxima, decreasing monotonically afterward.

Now

$$\bar{m} - m = 1 + 0.81(\sqrt[3]{\beta+1} - \sqrt[3]{\beta}) \approx 1;\ k_1 - z_0 \approx 1$$

so that the respective r-values are approximately $\Delta r \simeq 1/k_1$. The Bessel recursion formula becomes:

$$z = m:\ J_{\beta+1} = \frac{\beta}{z} J \to J_{\beta+1}(m) < J_\beta(m)$$

$$z = \bar{m}:\ J_\beta = \frac{\beta+1}{z} J_{\beta+1} \to J_{\beta+1}(\bar{m}) > J_\beta(\bar{m})$$

Thus we obtain:

$$z = z_0:\ J_{\beta+1} = -J_\beta > 0$$

$$z = k_1:\ J_\beta = J_{\beta+1} < 0$$

$$0 < z \leqq m:\ J_\beta > J_{\beta+1}$$

$$\bar{m} \leqq z \leqq k_1:\ J_{\beta+1} > J_\beta$$

Furthermore, we know from the theory of Bessel functions that

$$J_{\beta+1}(\bar{m}) < J_\beta(m)$$

There must exist a point $m < \bar{z} < \bar{m}$ where $J_{\beta+1}(\bar{z}) = J_\beta(\bar{z})$.

In the following we assume that $|r^\beta J_\beta(k_1)| \ll J_\beta(m), J_{\beta+1}(\bar{m})$ in the neighborhood of m, $\bar{m}$. Here $r < 1$ and $r^\beta \ll 1$ for large values of β.

We infer from a Taylor expansion:

$$J_\beta(k_1) = J_\beta(z_0 + 1) = J_\beta(z_0) + \dot{J}_\beta(z_0) + {}^1/_2\ddot{J}_\beta(z_0)$$

$$= -J_{\beta+1}(z_0) + \frac{1}{2z_0} J_{\beta+1}(z_0) = \frac{1-2z_0}{2z_0} J_{\beta+1}(z_0) \to$$

$$|J_\beta(k_1)| < J_{\beta+1}(\bar{m}) < J_\beta(m)$$

We can now proceed to approximate the extrema and zeros of the amplitude functions, to get an insight in the general behavior of these functions.

From the theory of Bessel functions we know that $J_p(p/n)$ is monotonically decreasing with increasing $n (n > 1)$. Furthermore we can discard the numerical values of $J_p(p/2)$ e.g., $J_{20}(10) = 17 \times 10^{-7}$. Practically we can also neglect $|r^\beta J_\beta(k_1)|$ in, at least, the interval $0 < r < 0.8$. Hence the amplitude functions will reach their maxima increasingly removed from the center of the cylinder, as β becomes larger.

To obtain information about the maximum M of $u(r)$ we determine the zero of u'. Since $r^\beta J_\beta(k_1)$ can be neglected in the neighborhood of m and $\bar{m}$, the maximum will be determined by J_β/r.

$$u' = \psi'/r - \psi/r^2 = \frac{k_1}{r} J_\beta - J_\beta/r^2 - (\beta-1)J_\beta(k_1)r^{\beta-2}$$

$$\approx \frac{k_1}{r} J_\beta - J_\beta/r^2$$

$$u' = 0 \to zJ_\beta = J_\beta \to J_\beta > 0 \quad \text{or} \quad (\beta-1)J_\beta = zJ_{\beta+1}$$

For $z < \beta - 1$ we have $J_{\beta+1} < J_\beta$ and for $z > \bar{z} \to J_{\beta+1} > J_\beta$. It follows that $\beta - 1 < M < \bar{z}$.

If we neglect 1 against β from the start, one can establish the zeros of ψ rather than of ψ/r. For $\psi' = 0 \to J_\beta < 0$. From these considerations we gather that the maximum of u will lie in the immediate neighborhood of m. The φ-amplitude function $v(r) = -\psi'/\beta$ is

$$v = \frac{k_1}{\beta} J_{\beta+1} - \psi/r$$

As shown above, the maxima of ψ and u have nearly the same position. We have therefore

$$v(0) = 0$$

$$v(M) \cong 0$$

$$v(1) = 0$$

that means at least 2 extremes.

With $\beta \gg 1$ we can approximate v' as follows:

$$v' = \frac{k_1^2}{\beta} J_{\beta+1} + \frac{1}{r^2}\psi - \psi'/r$$

$$\approx 1/r^2\left[zJ_{\beta+1} - \frac{z^2}{\beta}\frac{\beta}{z} J_{\beta+1} + \frac{z^2}{\beta} J_\beta - \beta\psi\right]$$

$$\approx \frac{1}{r^2}\left[\frac{z^2}{\beta} J_\beta - \beta\psi\right]$$

$$v' = 0 \to (z^2 - \beta^2)J_\beta + \beta^2 J_\beta(k_1)r^\beta = 0$$

We infer that for

$$z < \beta \to J_\beta > 0$$

and for

$$z > z_0 \to \begin{matrix} J_\beta < 0 \\ z^2 - \beta^2 > 0 \end{matrix}$$

so we can have no extremes in these intervals.

Furthermore we have

$$v = -\frac{k_1}{\beta} J_\beta + J_\beta(k_1)r^{\beta-1}$$

for all positive values of $J_\beta \to v < 0$, especially for $z = m$, $v < 0$.

For $z = z_0$ is $v' < 0$, as shown above.

v has a negative maximum in $\beta < z < M$; then it takes on positive values and has a positive maximum in $M < z < z_0$, as can be seen from our approximations.

All factors of $w(r)$ are monotonically increasing in the interval $0 < z < m$

$$w = -ru - \frac{z}{2} J_{\beta+1}$$

The maximum W_m can therefore be only on the right side of m.

The derivative gives a better approximation

$$w' = \beta r^{\beta-1} J_\beta(k_1) - k_1 J_\beta - \frac{z}{2} k_1 J_{\beta+1} - \frac{k_1}{2} J_{\beta+1}$$

$$= \beta r^{\beta-1} J_\beta(k_1) - \beta k_1 \left(\frac{1}{z} + z/2\beta\right) J_\beta + \beta k_1 (1/\beta + 1/2) J_{\beta+1}$$

$$w'/\beta k_1 = \frac{J_\beta(k_1)}{k_1} r^{\beta-1} - J_\beta\left(\frac{1}{z} + z/2\beta\right) + (1/\beta + 1/2) J_{\beta+1}$$

Neglecting the first term because of the large number in the denominator we have for $w' = 0$:

$$J_\beta\left(\frac{1}{z} + \frac{z}{2\beta}\right) = (1/\beta + 1/2) J_{\beta+1} \rightarrow W_m < z_0$$

If $z > m$ we can neglect $1/z$ and $1/\beta$, respectively;

$$\rightarrow J_\beta \approx \frac{\beta}{z} J_{\beta+1}$$

$$\rightarrow J_{\beta+1} > J_\beta$$

that means that the maximum w_m is between z and z_0.

The sketches of Fig. 3 and the following tables for the numerical values of the amplitude functions for $\beta = 22$ as a model show that our approximations are in excellent agreement with the calculated results.

$\beta = 22$: $k_1 = 28.28$ $z_0 = 27.57$

$\bar{m} = 25.28$

$m = 24.25$

$r = \frac{z}{28.28}$	$u(r)$	$v(r)$	$w(r)$
0–0.5	≈0.0	≈0.0	<−0.0005
0.64	0.029	−0.018	−0.099
0.75	0.147	−0.062	−0.813
0.79	0.204	−0.066	−1.276
0.87	0.277	−0.019	−2.67
0.9	0.255	0.038	−3.135
0.93	0.197	0.086	−3.083
0.96	0.107	0.045	−1.723
1	0.0	0.0	0.0
	$u'(1) = 0$	$v'(1) < 0$	$w'(1) > 0$

References

1 C. C. Lin, "The Theory of Hydrodynamic Stability," Cambridge University Press, Cambridge, England, 1955.

2 H. Schlichting, "Grenzschichttheorie," G. Braun, Karlsruhe, Germany, 1951.

3 H. B. Squire, "On the Stability of the Three-Dimensional Disturbances of Viscous Flow Between Parallel Walls," Proceedings of The Royal Society, series A, vol. 142, 1933, pp. 612–628.

4 Th. Sexl, "Zur Stabilitaetsfrage der Poiseuilleschen Stroemung," *Annalen der Physik*, vol. 83, 1927, pp. 835–848.

5 C. L. Pekeris, "Stability of the Laminar Flow Through a Straight Pipe of Circular Cross-Section to Infinitesimal Disturbances Which are Symmetrical About the Axis of the Pipe," Proceedings, National Academy of Science, Washington, D. C., vol. 34, 1948, pp. 285–295.

6 L. Hopf, "Der Verlauf kleiner Schwingungen auf einer Stroemung reibender Flüssigkeit," *Annalen der Physik*, vol. 44, 1914, pp. 1–60.

7 Th. Sexl, "Ueber dreidimensionale Stoerungen der Poiseuilleschen Stroemung," *Annalen der Physik*, vol. 84, 1927, pp. 835–848.

8 J. L. Synge, "Hydrodynamic Stability," Semi-Centennial Publications of American Mathematical Society, 1942, pp. 227–269.

9 W. Wasow, "On Small Disturbances of Plane Couette-Flow," Journal of Research, National Bureau of Standards, Washington, D. C., vol. 51, 1953, pp. 195–202.

10 S. I. Pai, "On the Stability of Parallel Flows with Respect to Periodic Disturbances," *Journal of The Franklin Institute*, vol. 259, 1955, pp. 197–208.

11 T. Y. Thomas, "Qualitative Analysis of the Flow of Fluids in Pipes," *American Journal of Mathematics*, vol. 64, 1942, pp. 754–767.

12 Th. Sexl and K. Spielberg, "Zum Stabilitaetsproblem der Poiseuille-Stroemung," *Acta Physica Austriaca*, vol. 12, 1958, pp. 9–28.

13 G. N. Watson, "Theory of Bessel Functions," Cambridge University Press, Cambridge, England, 1945.

14 E. Jahnke and F. Emde, "Tables of Functions," Dover Publications, Inc., New York, N. Y., 1945.

15 E. Kamke, "Differentialgleichungen," Band 1, Akademische Verlagsgesillschaft Geest & Portig KG, Leipzig, Germany, 1942.

16 H. Timan, "Ueber allgemeine und spezielle Stoerungen der Poiseuille Stroemung," Thesis, University of Vienna, 1958.

On the Indeterminateness of the Boundary Conditions for the Mixing of Two Parallel Streams

K. T. YEN
Professor,
Department of Aeronautical Engineering,
Rensselaer Polytechnic Institute,
Troy, N. Y.

Results obtained from a study of the indeterminateness of the boundary conditions for laminar "free" mixing of two parallel streams under constant pressure are presented in this paper. A method is given for the determination of the interface velocity, the location of the interface in the mixing region, and the transverse force acting on the dividing wall as a consequence of the mixing. Based on available numerical data, calculations have been made for two free-stream velocity ratios, 0.5 and 0. It is shown that values of interface velocity obtained here differ appreciably from those obtained using other proposed boundary conditions (the third condition). In addition, for a free-stream velocity ratio of 0.5 the interface deflects toward the higher velocity stream, while for a zero free-stream velocity ratio it deflects toward the zero (lower) velocity stream.

THE two-dimensional problem of laminar mixing of two parallel streams under constant pressure, Fig. 1, has been considered by many workers [1].[1] The equations of motion for the flow in the mixing region take the form of boundary-layer equations, but the boundary conditions differ from those for the boundary-layer problem. If the stream function is assumed to be of the form

$$\psi(x, y) = (\nu U x)^{1/2} F\{y(U/\nu x)^{1/2}\} = (\nu U x)^{1/2} F(\eta), \qquad (1)$$

where $U = (U_1 + U_2)/2$, an ordinary differential equation of the third order for $F(\eta)$ is obtained. However, there are only two boundary conditions apparent. They are $u \to U_1$ and U_2 as $y \to +\infty$ and $-\infty$, respectively.

For the third boundary condition, necessary for a unique solution, several proposals have been made. The simplest one is $F'(0) = 1$ [1], which implies that the x-component of the velocity along the interface is the mean of the two stream velocities.

Kuethe [2] applied the following boundary condition proposed by von Karman:

$$U_1 V_1 + U_2 V_2 = 0 \qquad (2)$$

to the turbulent mixing case, which has the same indeterminateness of boundary conditions. In Equation (2), V_1 and V_2 are the y-components of the velocity at the upper and lower "edges" of the mixing region, respectively.

In a recent paper [3], Crane proposed that this third boundary condition be taken as

$$\psi(\eta_0) = 0$$

with η_0 to be determined experimentally or by some other means.

It is clear that this additional boundary condition depends on

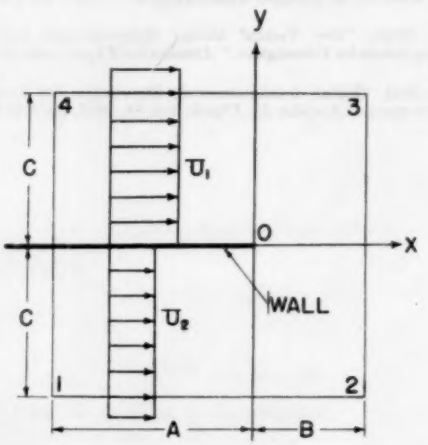

Fig. 1

[1] Numbers in brackets designate References at end of paper.

Contributed by the Applied Mechanics Division and presented at the Annual Meeting, Atlantic City, N. J., November 29–December 4, 1959, of THE AMERICAN SOCIETY OF MECHANICAL ENGINEERS.

Discussion of this paper should be addressed to the Secretary, ASME, 29 West 39th Street, New York, N. Y., and will be accepted until October 10, 1960, for publication at a later date. Discussion received after the closing date will be returned.

NOTE: Statements and opinions advanced in papers are to be understood as individual expressions of their authors and not those of the Society. Manuscript received by ASME Applied Mechanics Division, May 6, 1959. Paper No. 59—A-68.

Nomenclature

L = transverse force exerted on dividing wall by fluid
U = $(U_1 + U_2)/2$
U_1, U_2 = x-components of free-stream velocity of upper and lower streams, respectively
(U_2/U_1) = free-stream velocity ratio
u, v = x and y-components of velocity, respectively
V_1, V_2 = y-components of velocity at upper and lower edges of mixing zone, respectively
x, y = Cartesian co-ordinates
η = $y(U/\nu x)^{1/2}$
η_0 = value of η at which $\psi = 0$
η_* = $\eta - \eta_0$
λ = $(U_1 - U_2)/(U_1 + U_2)$
μ = coefficient of viscosity ($\mu = \rho\nu$)
ψ = stream function
ρ = density

the kinematic conditions actually imposed on the streams. For example, one stream may be free and the other stream restricted in some manner (such as by a rigid wall). In a limiting case, the "free" mixing of two streams may be considered. In this case, the two streams would extend to infinity with no solid boundary restraint (except that of the dividing wall).

In this paper, the free mixing of two streams is considered in some detail. Von Karman's condition, Equation (2), is shown to be the correct one for this problem. A method is given to determine the location of the interface of the two streams in the mixing region. Based on the numerical results of reference [5], two examples are presented to illustrate the use of this method.

Basic Relations

The equations of motion governing the laminar mixing of two streams of incompressible fluid under constant pressure, Fig. 1, are [1]

$$u\frac{\partial u}{\partial x} + v\frac{\partial u}{\partial y} = \nu\frac{\partial^2 u}{\partial y^2}, \tag{3}$$

$$\frac{\partial u}{\partial x} + \frac{\partial v}{\partial y} = 0 \tag{4}$$

Let a stream function $\psi(x, y)$ be introduced such that

$$u = \frac{\partial \psi}{\partial y}, \quad v = -\frac{\partial \psi}{\partial x}, \tag{5}$$

and $\psi = 0$ at the interface of the two streams. It is convenient to express the stream function in the following form:

$$\psi(x, y) = (\nu U x)^{1/2} F(\eta - \eta_0) = (\nu U x)^{1/2} F(\eta_*), \tag{6}$$

where

$$U = (U_1 + U_2)/2, \quad \eta = y(U/\nu x)^{1/2},$$

and η_0 is a constant to be determined such that $F(\eta_*) = 0$, at $\eta_* = 0$. From Equation (3), the equation for $F(\eta_*)$ is

$$2F'''(\eta_*) + F(\eta_*)F''(\eta_*) = 0 \tag{7}$$

The boundary conditions are

$$F'(\eta_*) = (1 + \lambda), \quad \eta_* = \infty, \tag{8}$$

$$F'(\eta_*) = (1 - \lambda), \quad \eta_* = -\infty, \tag{9}$$

$$F(\eta_*) = 0, \quad \eta_* = 0, \tag{10}$$

where $\lambda = (U_1 - U_2)/(U_1 + U_2)$. Some solutions of this problem have been given by Lock [4]. In reference [4], the case $\rho\mu = 1$ corresponds to the problem considered here. The asymptotic behavior of the solution is

$$F(\eta_*) \to (1 + \lambda)\eta_* - \alpha, \quad \eta_* \to \infty, \tag{11}$$

$$F(\eta_*) \to (1 - \lambda)\eta_* - \beta, \quad \eta_* \to -\infty \tag{12}$$

From Equation (5)

$$v = -\tfrac{1}{2}(\nu U/x)^{1/2}\{F(\eta_*) - \eta F'(\eta_*)\} \tag{13}$$

Hence the asymptotic behavior of v is

$$v \to \tfrac{1}{2}(\nu U/x)^{1/2}\{\alpha + \eta_0(1 + \lambda)\}, \quad \eta_* \to \infty, \tag{14}$$

$$v \to \tfrac{1}{2}(\nu U/x)^{1/2}\{\beta + \eta_0(1 - \lambda)\}, \quad \eta_* \to -\infty \tag{15}$$

Thus the value of η_0 will have direct bearing on the velocity component v at the edges of the mixing region. The problem now is to determine η_0 according to the condition of free mixing of the two streams. This is considered in the next section.

Free Mixing—Consideration of the Third Boundary Condition

Free mixing of two parallel streams occurs when no restraint (except that of the straight dividing wall ahead of the mixing region) is imposed on the streams. At infinity, it is expected that all disturbances should vanish.

Consider the momentum equilibrium in the y-direction for fluid within the control surface shown in Fig. 1. Both A and C are chosen to be large, while B is chosen such that boundary 2–3 is sufficiently far away from the singular point 0. The result is that the following equation must be satisfied for any choice of B and C:

$$\rho\int_1^2 v^2 dx + \rho\int_3^4 v^2 dx + \rho\int_2^3 uv dy - \int_2^3 \tau_{xy} dy + L = 0, \tag{16}$$

where L is the transverse force in the y-direction exerted on the dividing wall by the fluid. It will be assumed for the present purpose that, as A and C approach infinity, the contribution from the first two integrals in Equation (16) vanishes. In order to justify this point, an improved solution of the mixing problem must be obtained. Such an analysis by using parabolic co-ordinates is given in reference [5]. It also will be evident from the analysis in reference [5] that the transverse force L is due to the change in the static pressure over the wall as a result of the mixing.

If the functions u, v, and τ_{xy}, obtained from the solutions of Equations (6) to (10) are substituted into Equation (16), the following equation is obtained:

$$\frac{1}{2}\mu U\int_{-\infty}^{\infty} F''(\eta_*)\{\eta F'(\eta_*) - F(\eta_*)\}d\eta = \mu(U_1 - U_2) - L \tag{17}$$

Upon integration by parts and by using Equation (7), the integral in the foregoing equation reduces to

$$\int_{-\infty}^{\infty} F'(\eta_*)\{\eta F'(\eta_*) - F(\eta_*)\}d\eta = -4\lambda + \{(1 + \lambda)[\alpha + \eta_0(1 + \lambda)] - (1 - \lambda)[\beta + \eta_0(1 - \lambda)]\}\eta\Big|_{\eta=-\infty}^{\infty} - \{\alpha + \eta_0(1 + \lambda)\}^2 - \{\beta + \eta_0(1 - \lambda)\}^2$$

Hence in order to insure convergence for the integral in Equation (17) the following condition must be satisfied:

$$\frac{1 + \lambda}{1 - \lambda} = \frac{\beta + \eta_0(1 - \lambda)}{\alpha + \eta_0(1 + \lambda)} \tag{18}$$

For a given λ, relation (18) can be used to determine η_0.

In the foregoing analysis, only the first-order solution of the mixing problem is considered. If the stream function is assumed to have the form

$$\psi(x, y) = (\nu U x)^{1/2}\{F(\eta_*) + x^{-1/2}F_1(\eta_*) + x^{-1}F_2(\eta_*) + \ldots\}, \tag{19}$$

it is evident that in order to have $\psi = 0$ at $\eta_* = 0$,

$$F_1(0) = F_2(0) = \ldots = 0 \tag{20}$$

In addition, $F_1' = F_2' = \ldots = 0$, as $\eta_* \to \infty$ and $-\infty$. Thus each of the functions F, F_1, F_2, etc., in Equation (19) has three required boundary conditions and the problem is made determinate.

From Equations (8), (9), (14), and (15), it is evident that the boundary condition as represented by Equation (18) is equivalent to von Karman's proposed condition, Equation (2).

Equation (17) now becomes

$$2L = \mu U\{8\lambda + (2\eta_0 + \alpha + \beta)(2\lambda\eta_0 + \alpha - \beta)\} \quad (21)$$

Numerical Examples

Because of limited available data as given in reference [4], only two numerical examples can be given at this time.

I $U_2/U_1 = 0.501$; i.e., $\lambda = (1/3)$

From the results of [4], $\alpha = 0.2829$, $\beta = 3.4$ (estimated) and from Equation (18) the value of η_0 is found to be approximately 1.42. This gives a velocity at the interface of approximately 0.9063 as compared with the mean value of U_1 and U_2 of 0.75 assumed by Görtler, and the value of 0.7657 obtained by Lock [4]. From Equation (21), $L = -5.74\mu U$.

II $U_2 = 0$; i.e., $\lambda = 1$

In this case, Equation (18) becomes $\alpha + 2\eta_0 = 0$. From [4], $\alpha = 0.5289$ and $\beta = 1.2386$. Thus $\eta_0 = -0.2645$, approximately. Hence the velocity at the interface is 0.65 as compared with Görtler's value of 0.5 and Lock's value of 0.5873. From Equation (21), $L = 3.233\mu U_1$.

Conclusions

It has been shown that the solution of laminar free mixing of two streams under constant pressure can be made determinate by considering the condition of conservation of momentum in the y-direction. The main results thus obtained are given by Equations (18) and (21). Equation (18) is equivalent to von Karman's proposed condition, Equation (2), and serves to determine the value of η_0, at which $\psi = 0$. Thus the location of the interface is obtained. Based on available numerical results, two examples have been calculated for $(U_2/U_1) = 0.5$ and 0. The values of interface velocity obtained here are found to differ appreciably from previous results based on other third boundary condition.

The fact that the interface velocity varies appreciably with the choice of the third boundary condition indicates the importance of this boundary condition. It appears that the choice of the third boundary condition cannot be made in an arbitary manner without introducing some first-order errors.

Equation (21) gives the transverse force L acting on the dividing wall as a result of the mixing. It is of interest to note that for $(U_2/U_1) = 0.5$, this force is negative and the interface of the two streams in the mixing region deflects toward the higher velocity stream. On the other hand, for $(U_2/U_1) = 0$, the force acting on the wall is positive and the interface deflects to the side of the stationary fluid.

In practice, free mixing may be difficult to achieve. The technique given here, however, can be modified readily to yield the third boundary condition and the location of the interface for other practical cases. If the upper stream is bounded by a rigid wall, for example, the third boundary condition is simply $(1 + \lambda)\eta_0 + \alpha = 0$, from which η_0 can be determined immediately.

Acknowledgment

This research was supported by the United States Air Force through the Air Force Office of Scientific Research of the Air Research and Development Command, under Contract No. AF 49(638)-23. Reproduction in whole or in part is permitted for any purpose of the United States Government.

The author wishes to express his thanks to Prof. John R. Crawford, Rensselaer Polytechnic Institute, for his help in preparing this paper, and to Mr. John B. Watson, Graduate Fellow of the Department of Aeronautical Engineering, Rensselaer Polytechnic Institute, for his help in checking some of the results and carrying out the numerical computations.

References

1 S. I. Pai, "Fluid Dynamics of Jets," Van Nostrand and Company, New York, N. Y., 1954, p. 80.

2 A. M. Kuethe, "Investigations of the Turbulent Mixing Regions Formed by Jets," JOURNAL OF APPLIED MECHANICS, vol. 2, TRANS. ASME, vol. 57, 1935, p. A-87.

3 L. J. Crane, "The Laminar and Turbulent Mixing of Jets of Compressible Fluid—Part II, The Mixing of Two Semi-Infinite Streams," *Journal of Fluid Mechanics*, vol. 3, 1957, p. 81.

4 R. S. Lock, "The Velocity Distribution in the Laminar Boundary Layer Between Parallel Streams," *Quarterly Journal of Mechanics and Applied Mathematics*, vol. 4, 1951, p. 42.

5 K. T. Yen, "On the Indeterminateness of the Boundary Conditions for a Mixing Problem," TR AE5710, Rensselaer Polytechnic Institute, 1957 (AFOSR TN 58-449, AD-158-255).

Thermal Transfer in Turbulent Gas Streams. Effect of Turbulence on Local Transport From Spheres

W. W. SHORT
Physics Section,
Convair, San Diego, Calif.

R. A. S. BROWN
University of Alberta,
Edmonton, Canada

B. H. SAGE
Professor,
California Institute of Technology,
Pasadena, Calif.

The present investigation was undertaken because of the paucity of data concerning the effect of level of turbulence upon local thermal transport from spheres in a free stream. A series of measurements was made of the local thermal transport in the forward hemisphere and a part of the after hemisphere of a silver sphere 0.5 in. diam. The measurements were made in an undisturbed air stream and at several positions in the wake of a grid inserted in the air stream. The apparent level of longitudinal turbulence was varied between 0.013 and 0.15 for Reynolds numbers up to 3600. At an apparent level of turbulence of 0.013 and a Reynolds number of 3600, the local thermal transfer varied by a factor of eight around the sphere. Increasing the apparent level of turbulence to 0.15 increased the over-all thermal transfer 20 per cent. The local thermal transfer varied by a factor of five at the latter level of turbulence.

MANY experimental measurements have been made of the gross convective thermal transport from spheres, and these have been well correlated by McAdams [1][1] for conditions of turbulent flow. The predictions of Johnstone [2] and measurements of Tang [3] show a divergence from the correlation of McAdams which may be in part the result of differences in levels of turbulence in the stream.

Studies of local thermal transport from spheres are limited. Cary [4] investigated local thermal transport from a 5-in. iron sphere in an air stream at Reynolds numbers between 0.44×10^5 and 1.5×10^5. Similar information was obtained by Lautman and Droege [5] for a 9-in. copper sphere in air at Reynolds numbers between 1.3×10^5 and 10×10^5. The work of Lautman and Droege was repeated by Xenakis and co-workers [6] with a 9-in. sphere and with 6 and 12-in. spheres in air at Reynolds numbers between 0.87×10^5 and 1.8×10^5. More recent work by Wadsworth [7] gave information on the local transport to a copper sphere in a relatively narrow duct for Reynolds numbers between 0.15×10^5 and 3.5×10^5. Hsu [8] studied the local thermal transport from spheres under conditions of thermal transport and combined thermal and material transport. His work was carried out with two 0.5-in. spheres for Reynolds numbers between 1500 and 4200, based on properties at the interface, and at a turbulence level in the stream of 0.054 root-mean-square longitudinal fluctuation.

The status of the mathematical analysis of heat transfer in the three-dimensional boundary flow encountered at the surface of spheres was recently reviewed by Hsu [8]. All of the theoretical predictions of local transport available to the authors appear to be subject to limiting assumptions and to represent only an approximation of the behavior in the boundary flow about a sphere.

Sibulkin developed an exact solution of the thermal transfer at the stagnation point of a sphere [9] and also calculated the local thermal transfer associated with the forward half of the sphere by integral methods [10]. Korobkin [11] applied the Karman-Pohlhausen integral method [12] to the prediction of the local thermal transfer. Frössling [13] developed both an exact and an integral method to predict the local transport. Eckert [14] and Drake [15] submitted approximate methods for determining the local thermal transfer on a surface of revolution.

The present experimental investigation was concerned with

[1] Numbers in brackets designate References at end of paper.

Presented at the Summer Conference of the Applied Mechanics Division, University Park, Pa., June 20–22, 1960, of THE AMERICAN SOCIETY OF MECHANICAL ENGINEERS.

Discussion of this paper should be addressed to the Secretary, ASME, 29 West 39th Street, New York, N. Y., and will be accepted until October 10, 1960, for publication at a later date. Discussion received after the closing date will be returned. First draft of manuscript received by ASME Applied Mechanics Division, May 19, 1959; final draft received, January 18, 1960. Paper No. 60—APM-30.

Nomenclature

A = area, sq ft
d = diameter of sphere, in. or ft
d = differential operator
h = thermal transfer coefficient, Btu/(sq ft)(sec)(deg F)
k = thermal conductivity, Btu/(sq ft)(sec)(deg F/ft)
Nu = Nusselt number, hd/k
$\dot{Q}$ = local thermal flux from surface, Btu/(sec)(sq ft)
$\dot{Q}$ = total thermal flux from surface, Btu/sec
Re = Reynolds number, dU/ν
r = radius, in. or ft
r_0 = radius of sphere, in. or ft
t = temperature, deg F
U_∞ = gross or free-stream velocity, fps
x, z = co-ordinate axes with origin at center of sphere, in.
α_T = apparent turbulence level (fractional)
δ_t = thermal boundary-layer thickness, ft
ν = kinematic viscosity, sq ft/sec
T = normalized temperature
ψ = polar angle from stagnation point, deg
∂ = partial differential operator

Subscripts

a = air
i = solid-gas interface
w = thermocouple wire
ψ = polar angle
∞ = free stream

Superscript

$*$ = space average

rates of local thermal transport from a silver sphere 0.5 in. in diam. Measurements were made at Reynolds numbers between 900 and 3600. Local transport was determined from the radial temperature gradients encountered within the boundary flow. This investigation constitutes a portion of a study of the effects of the level and scale of turbulence in the stream upon thermal and material transport at relatively low Reynolds numbers.

Methods and Equipment

The temperature distribution in a turbulent air stream near an electrically heated, silver sphere 0.5 in. in diam was determined experimentally at a free-stream temperature of 100 deg F and at gross velocities between 4 and 16 fps. For each of the velocities investigated, the apparent level of turbulence was varied between 0.013 and approximately 0.15 root-mean-square longitudinal fluctuation.

The equipment which furnished the air supply has been described in detail [16]. The air stream approached the working section in a 12-in. × 12-in. steel duct and was reduced, within a distance of approximately 2 ft, to a 12-in. × 3-in. jet in which the sphere was suspended. The undisturbed vertical stream emerging upward from the constricted section yielded an apparent level of transverse turbulence of 0.013 [17]. The temperature of the undisturbed air stream was known within 0.1 deg F relative to the international platinum scale [16]. The velocity of the stream was established [8] within 0.5 per cent and did not vary more than 0.2 per cent during any one investigation. The velocity of flow was substantially constant throughout the greater part of the cross section of the emerging jet.

In order to increase the level of turbulence, a steel plate 0.1875 in. thick with 0.875-in. holes on 1-in. centers was inserted in the air stream at the exit of the jet. Sections of steel duct 3 in. × 12 in. in cross section, in lengths varying between 3 and 12 in., were added on the downstream side of the perforated plate in order to permit investigation at several distances downstream from the plate. Davis [18, 19] made an extensive investigation of the characteristics of the longitudinal and transverse fluctuating velocities downstream from a grid of the same dimensions. His data were employed in the present study to estimate the character of the turbulence as a function of longitudinal position along the axis of the jet. The parameter employed in this discussion was the longitudinal level of turbulence expressed as the ratio of the root-mean-square of the longitudinal component of the fluctuating velocity to the average velocity.

From an experimental standpoint, the results presented here are in reality an evaluation of local thermal transport as a function of polar angle for several different longitudinal positions in the wake of a grid constructed with 0.875-in. holes drilled on 1-in. centers. Results, based upon measurements of Davis [19], on the longitudinal and transverse levels of turbulence as a function of position downstream from such a grid, are shown in Fig. 1. The downstream distance reported here is measured from the downstream face of the grid to the stagnation point of the sphere.

It should be recognized that, for distances closer than 5 in. to the grid, marked inhomogeneities [20] in the flow field existed. Furthermore, there were significant variations in the mean speed from point to point in the wake of the grid. The turbulence levels based upon Davis' data, which are set forth in Fig. 1, are for the conditions of flow existing along the axis of the wake. Davis' measurements clearly indicate that at distances up to 12 in. no influence of the wall penetrated more than 0.5 in. into the stream. For this reason, it is believed that the data shown in Fig. 1, which are based directly upon the measurements of Davis [19], are a reasonable approximation of the conditions of flow existing. The authors' choice of root-mean-square longitudinal fluctuating velocity as a single parameter to describe the conditions of flow in the wake of the grid is open to discussion. For this reason, it has been called the apparent level of turbulence, and corresponding scales of the downstream position are included on the figures. The molecular properties for air used in this work were based upon a set of critically chosen values [21].

The 0.5-in. silver sphere employed in this investigation was described by Hsu [8]. It was provided with a resistance heater which uniformly covered the surface of an inner core. Four 0.005-in-diam thermocouples were imbedded in the surface of the sphere to measure the surface temperature. The sphere was supported by two horizontal stainless-steel tubes 0.096 in. in diam through which the leads for the heater and thermocouples were introduced. Guard heaters were provided to avoid thermal losses along the supporting tubes.

The supporting tubes produced a turbulent wake which added to the difficulties when making measurements at angles greater than 150 deg. The effect of the supporting tubes upon the boundary layer of the sphere at 90 deg was estimated by computing from potential theory the increase in velocity at 0.25 in. from the center of a 0.096-in. cylinder. This increase was 0.64 fps for a free-stream velocity of 16 fps. In addition, studies with a 0.5-in. porous sphere [8] and a 1-in. silver sphere supported from a single tube at the axis of the wake gave no noticeable difference in boundary flow from that encountered in these studies at polar angles measured from stagnation to at least 150 deg.

A 0.0003-in. platinum, platinum-rhodium thermocouple mounted upon a probe [8] was used to measure the temperature of the air in the boundary flow. The thermocouple was parallel to the supporting tubes and the junction was in the plane of the great circle on the sphere perpendicular to the tubes. The probe tips to which the thermocouple wires were attached were $^3/_4$ in. apart, so that the wake of the probe did not interesect the sphere. The position of the thermocouple relative to the surface of the sphere was known within 0.001 in. The temperature of the thermocouple was determined within 0.02 deg F relative to the international platinum scale. Fluctuations in air temperature in the boundary flows were of the order of 0.05 deg F, except in the wake where fluctuations of as much as 0.2 deg F were encountered as a result of vortex rings being shed by the sphere. Traverses were made in the horizontal direction at all polar angles, measured

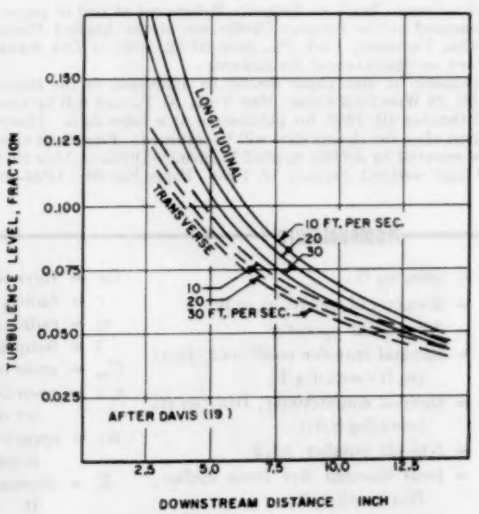

Fig. 1 Transverse and longitudinal level of turbulence as a function of downstream position

from stagnation, except at the stagnation point where a vertical traverse was made.

Analysis

In order to compare the temperature distribution about a sphere under several conditions of forced convection it is convenient to consider a normalized temperature distribution in the boundary flow [8]. Such a normalized temperature is particularly helpful when measurements at several different surface temperatures, as in the present case, are to be compared. This quantity was defined for present purposes as

$$\mathrm{T} = \frac{t - t_\infty}{t_i^* - t_\infty} \tag{1}$$

In cases in which the temperature t refers to a particular temperature, subscripts are used to indicate the particular temperature. For example, the temperature of the thermocouple wire at the junction is represented by t_w, and the temperature at the interface between the sphere and the boundary flows by t_i. The normalized temperature is marked with the same subscript as the temperature T_w or T_i. Equation (1) is only one simple means of making a first-order correlation of the temperature distribution in the boundary flows about a sphere.

The space-average surface temperature t_i^* presented in equation (1) was evaluated as follows:

$$t_i^* = \frac{1}{A} \oint_0^A t_i \, dA \tag{2}$$

In earlier work [22] it was found that the local temperature variation from point to point on the sphere was less than 1.0 deg F at a temperature difference, $t_i^* - t_\infty$, of about 60 deg F. It has since been found to be, with but one exception, less than 0.3 deg F. Thus for present purposes, the sphere may be treated as an isothermal body with but small error.

In the present study the Reynolds number was based upon properties of the free stream, as indicated in the following equation:

$$\mathrm{Re}_\infty = \frac{dU_\infty}{\nu_\infty} \tag{3}$$

Local thermal flux at the surface of the sphere was established from

$$\dot{Q} = -k_i \left(\frac{\partial t}{\partial r} \right)_{i,\psi} \tag{4}$$

The quantity $(\partial t/\partial r)_{i,\psi}$ represents the radial temperature gradient at the interface for a constant polar angle. In dealing with macroscopic quantities, a knowledge of the total thermal flux from the sphere is necessary. This was established from the measurements of the electrical power required to keep the sphere under steady conditions. Appropriate correction for the areas of the supporting tubes was made [22]. In addition, for comparison with the local transport, the total thermal flux from the sphere may be obtained from:

$$\dot{\mathrm{Q}} = \oint_0^A \dot{Q} dA = - \oint_0^A k_i \left(\frac{\partial t}{\partial r} \right)_{i,\psi} dA \tag{5}$$

A local Nusselt number based upon the molecular characteristics of the fluid at the interface was defined by:

$$\mathrm{Nu}_i = \frac{\dot{Q}d}{k_i(t_i - t_\infty)} = \frac{(\partial t/\partial r)_{i,\psi} d}{t_i - t_\infty} \tag{6}$$

Similarly, a macroscopic or space-average Nusselt number was evaluated from

$$\mathrm{Nu}_i^* = \frac{\dot{\mathrm{Q}}d}{(t_i^* - t_\infty)k_i^* A} = - \frac{\left[\oint_0^A k_i (\partial t/\partial r)_{i,\psi} \, dA \right] d}{(t_i^* - t_\infty) k_i A} = - \frac{\left[\oint_0^A (\partial t/\partial r)_{i,\psi} \, dA \right] d}{\oint_0^A (t_i - t_\infty) dA} \tag{7}$$

The second equalities in equations (6) and (7) result directly from the substitution of equations (4) and (5), respectively, into the definitions of the local and space-average Nusselt number. The last equality in equation (7) is established by the evaluation of the space-average temperature from equation (2) and the assumption that thermal conductivity at all points around the sphere is equal.

For the purposes of portraying the distribution of the local thermal transport around the sphere under a variety of conditions of flow, a relative local transport defined as the ratio of the local Nusselt number to the space-average Nusselt number at the same level of turbulence and Reynolds number was employed. The expression for this ratio given in equation (8) follows directly from the last equalities of equations (6) and (7):

$$\frac{\mathrm{Nu}_i}{\mathrm{Nu}_i^*} = \frac{(\partial t/\partial r)_{i,\psi} \oint_0^A (t_i - t_\infty) dA}{(t_i - t_\infty) \oint_0^A (\partial t/\partial r)_{i,\psi} \, dA} \tag{8}$$

It is apparent from equation (8) that a knowledge of the radial temperature gradient about the sphere and of the surface temperature is all that is required for the evaluation of this relative local transport. The ratio compares the transport at a point on the sphere directly to the space-average thermal transport for the entire sphere under the same conditions of flow. The use of equation (8) to evaluate directly the quotient $\mathrm{Nu}_i/\mathrm{Nu}_i^*$ avoids any systematic bias which might result from the independent evaluation of Nu_i from the second equality of equation (6) and of Nu_i^* from the first equality of equation (7). The actual local thermal transport, Nu_i, was evaluated as the product of the relative

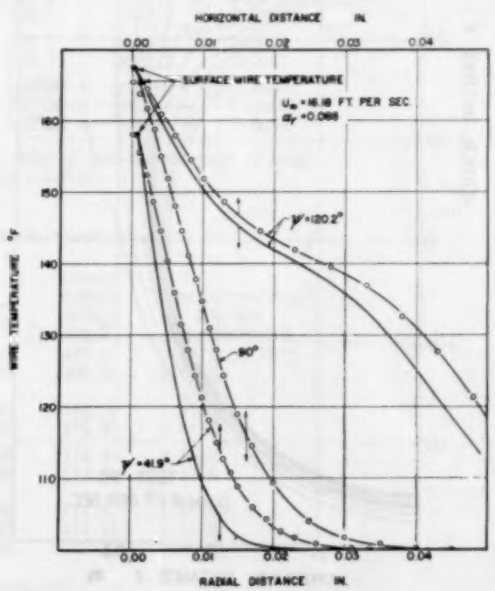

Fig. 2 Comparison of horizontal and radial temperature distributions

local transport, Nu_i/Nu_i^*, as determined from equation (8), and the macroscopic transport, Nu_i^*, established from the first equality of equation (7).

In Fig. 2 typical experimental measurements at three polar angles are illustrated. The traverses are shown with the experimental points and are associated with the horizontal distance from the surface of the sphere. By suitable graphical manipulation, these traverse data were converted directly to corresponding radial temperature distributions and are shown by the full curves in Fig. 2. At the equator, which corresponds to a polar angle of 90 deg, the radial distribution and the horizontal traverse are coincident. It should be recognized that the data of Fig. 2 represent the distribution of the temperatures recorded directly from the thermocouple readings which are called "wire" temperatures. The solid points in Fig. 2 correspond to the extrapolated values of the wire temperature at the surface of the sphere. The distribution of wire temperatures around the sphere at a gross velocity of 16.18 fps is shown in Fig. 3. Information such as shown in Figs. 2 and 3 was obtained for each set of experimental conditions investigated.

As a result of large temperature gradients along the axis of the wire, significant thermal transfer from the thermocouple junction was encountered by conduction along the wire. For this reason there existed a significant difference between the wire temperature and the air temperature. A direct measure of the magnitude of this difference can be obtained by comparison between the surface temperature of the silver sphere as measured by a thermocouple mounted within the surface of the sphere, designated t_i, and the surface temperature as measured with a traversing thermocouple immediately adjacent to, but not touching, the sphere, t_{wi}.

Fig. 4 illustrates typical experimental wire-temperature data obtained at the equator for a velocity of 16.18 fps. The corresponding temperature as determined by a thermocouple mounted within the surface of the sphere is indicated. It is apparent that it is necessary to apply a correction to the wire temperatures in order to obtain the temperature of the air. Efforts to compute a correction based upon available information concerning boundary flows around spheres [13] and thermal transfer to small wires [23] did not yield corrections as large as those shown in Fig. 4 for conditions near the sphere.

One method of making appropriate microscopic corrections is available [24]. However, the detailed experimental measurements required for such corrections to the thermocouple readings were not available in this case nor was there available information concerning the coefficient of thermal transfer from the air in the boundary flow to the thermocouple wire as a function of polar angle and distance from the sphere. For these reasons, an approximate correction in the wire-temperature gradient at the surface was made by use of the thermal boundary-layer thickness:

$$\delta_t = \int_0^\infty \frac{t_w - t_\infty}{t_{w,i} - t_\infty}\, dr \qquad (9)$$

It was found, as would be expected, that the thermal boundary-layer thickness as evaluated from equation (9) was a function of polar angle, Reynolds number, and apparent level of turbulence.

The thermal boundary-layer thickness is equal to the thickness of a layer of gas at temperature t_i containing the same total internal energy above that of the free stream as the actual

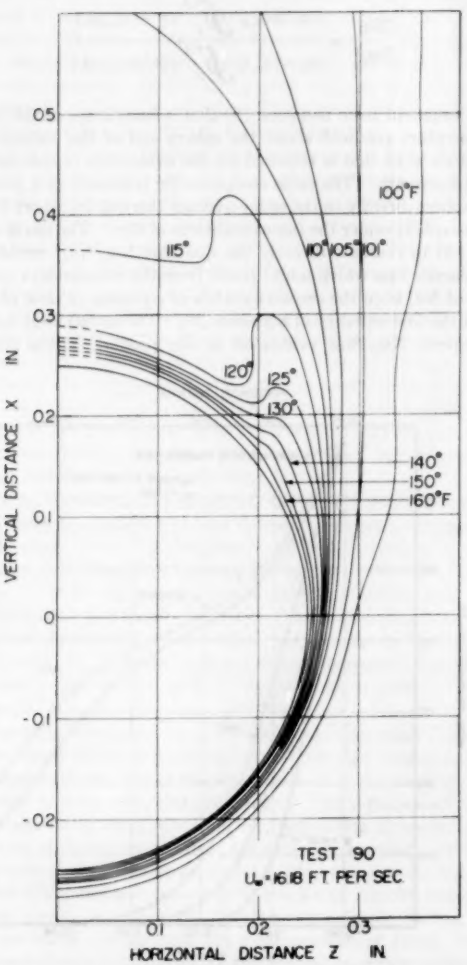

Fig. 3 Wire temperature distribution around a 0.5-in. heated sphere

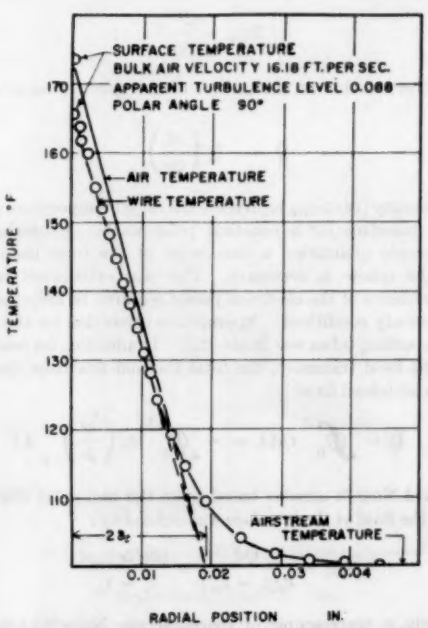

Fig. 4 Comparison of air and wire temperatures

boundary flow. It follows that this energy can be distributed over a linear temperature gradient in a thickness twice the thermal boundary layer. As indicated in Fig. 4, the correction to the wire-temperature gradient may be evaluated on the basis of the foregoing approximation. Under these circumstances the radial air-temperature gradient may be related to the corresponding radial wire-temperature gradient by the following expression:

$$\left(\frac{\partial t_a}{\partial r}\right)_{i,\phi} = \left(\frac{\partial t_w}{\partial r}\right)_{i,\phi} + \left(\frac{t_i - t_{w,i}}{2\delta_t}\right)_{\phi} = \left(\frac{\partial t_w}{\partial r}\right)_{i,\phi} + \left[\frac{T_i - T_{w,i}}{2\delta_t}(t_i^* - t_\infty)\right]_{\phi} \quad (10)$$

The difference between the surface temperature of the sphere and the wire temperature at the surface ($t_i - t_{w,i}$) is a systematic function of polar angle, Reynolds number, and apparent level of turbulence. The standard error of estimate of the experimental measurements from the smoothed data is less than 1 deg F. However, corrections to the wire-temperature gradients vary systematically from 2 per cent at the equator to as much as 20 per cent at stagnation. It should be emphasized that although the existence of a difference between the wire temperature and the temperature of the air introduces some degradation in the accuracy of the results, it does not interfere with the precision of measurement. It was not possible to employ smaller thermocouples because of breakage and the difficulty in construction of a junction to yield a uniform section of the thermocouple. Comparison with microscopic corrections [24] indicates that the uncertainty in the evaluation of the air-temperature gradient at the surface of the sphere from the wire-temperature gradient at the surface was not more than 2 per cent.

Experimental Results

The experimental conditions in the air stream for the investigations reported here are set forth in Table 1. The test numbers are used in subsequent discussion to identify each set of conditions. The velocity given in the table is the gross velocity of the stream approaching the sphere. The apparent turbulence level was evaluated from the downstream distance from the grid, as already described. The temperature, pressure, and weight fraction water represent the total temperature, static pressure, and humidity of the air stream. Table 2 presents the thermal transport from the 0.5-in. heated silver sphere for the conditions listed in Table 1. Values of macroscopic Nusselt number, determined directly from the first equality of equation (7), are reported for both free-stream and surface conditions. These data are based upon direct measurements of the energy addition to the sphere and measurements of its average surface temperature and are not related to the measurements of the temperature in the boundary flows about the sphere.

Typical experimental values of wire temperature as a function of horizontal and vertical distance from the surface are given in Table 4 in the Appendix. Table 5 in the Appendix gives the normalized surface temperatures based upon measurements made with the internal thermocouples, the ratio of the thermal boundary-layer thickness established from equation (9) to the diameter of the sphere, and the ratio of the local Nusselt number at the interface to the space-average Nusselt number at the interface as

Table 1 Experimental conditions in air stream

Test no.	Velocity, fps	Downstream distance from grid, in.	Apparent turbulence level,* fraction	Temp, deg F	Pressure, psfa	Weight fraction water
161	4.03	no grid	0.013	100.1	2068.6	0.0122
160	16.14	no grid	0.013	100.1	2066.1	0.0091
110	8.06	13.04	0.054	100.1	2055.9	0.0048
109	16.13	13.04	0.051	100.1	2069.2	0.0035
89	8.03	7.09	0.094	100.1	2064.1	0.0052
90	16.15	7.08	0.088	100.1	2067.2	0.0053
92	7.97	4.06	0.146	100.1	2080.8	0.0060
93	8.00	4.06	0.146	100.0	2073.6	0.0060
91	16.07	4.07	0.135	100.1	2077.8	0.0051

* Longitudinal level of turbulence expressed as ratio of root-mean-square of longitudinal component of fluctuating velocity to average velocity.

Table 2 Thermal transport from a 0.5-in. heated sphere

Test no.	Reynolds no., free stream	Macroscopic Nusselt no.* Free stream, Nu_∞	Surface, Nu_i	$Nu_i / Re_\infty^{1/2}$	Average surface temp, deg F	Total thermal flux,† Btu/sec (experimental)
161	909	18.23	16.26	0.5393	177.0	0.7972×10^{-3}
160	3643	36.98	30.00	0.4970	206.6	2.1247
110	1807	25.99	23.30	0.5481	175.5	1.1146
109	3638	36.53	32.67	0.5416	175.2	1.5617
89	1806	26.01	23.17	0.5452	175.4	1.1146
90	3640	37.44	33.35	0.5528	173.4	1.5616
92	1807	27.44	24.68	0.5806	171.5	1.1146
93	1808	27.59	24.82	0.5837	171.1	1.1148
91	3641	40.94	36.95	0.6124	167.1	1.5621

* Determined directly from first equality in equation (7).
† Total observed energy addition was corrected for area of supporting tubes.

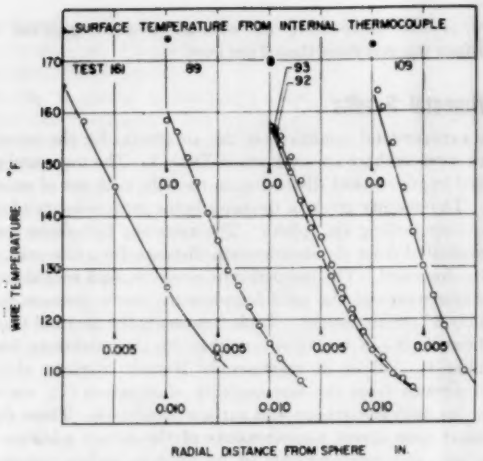

Fig. 5 Wire temperature distribution at stagnation

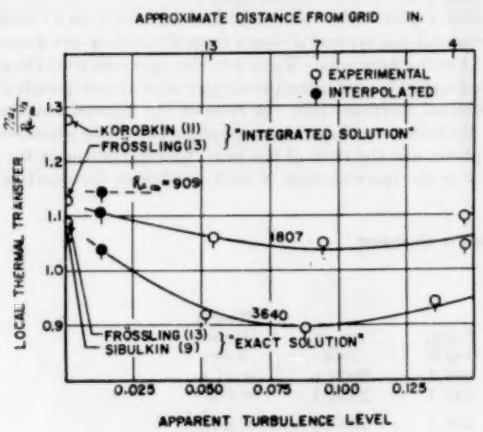

Fig. 6 Local thermal transfer at stagnation

determined directly from equation (8). The main body of the table presents the normalized wire temperatures as obtained by application of equation (1).

The vertical temperature distribution at stagnation for several different conditions of flow is shown in Fig. 5. These data are based upon wire-temperature measurements. The corresponding values of surface temperature measured with the internal thermocouples are indicated. The local thermal transfer at stagnation is presented in Fig. 6 as a function of the apparent level of turbulence for the experimental conditions investigated. It was necessary to interpolate the experimental data to the Reynolds numbers indicated in the case of a level of turbulence corresponding to the free stream.

The experimental data are compared with the thermal transfer at stagnation predicted by Sibulkin [9], Korobkin [11], and Frössling [13]. These latter values were reported for the molecular properties of the fluid at the average of the temperatures existing at the interface and in the free stream. All the data in Fig. 6 are expressed in terms of the quotient of the local Nusselt number and the square root of the free-stream Reynolds number. The agreement of the experimental values for the several levels of turbulence is satisfactory, whereas the difference between several of the theoretical evaluations is significant.

It should be recognized that the decrease in the local Nusselt

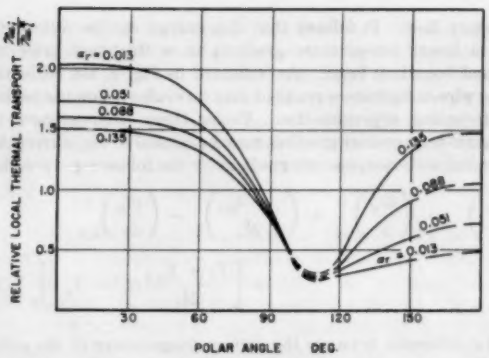

Fig. 7 Effect of polar angle upon relative local thermal transport

number at stagnation with an increase in the apparent level of turbulence is at variance with earlier experimental results for cylinders [25]. However, other measurements on cylinders [26] indicate a progressive decrease in the effect of level of turbulence upon thermal transfer with a decrease in Reynolds number. The measurements of Giedt upon cylinders [25] were made at much higher Reynolds numbers than were covered in this investigation, and it is not surprising that somewhat different trends are found. Furthermore, there is no assurance that the effect of turbulence level is the same for cylinders and spheres.

The influence of polar angle upon the relative local thermal transport, as determined from equation (8), is illustrated in Fig. 7. These data show the differences induced by various apparent levels of turbulence for a Reynolds number of 3640, corresponding to a gross velocity of 16 fps. The standard error of estimate of the experimental values shown from the smooth curves drawn is 0.074. It is improbable that the variation in local transport with respect to polar angle is as simple near separation as shown in Fig. 7. However, the experimental data did not permit the details of behavior in this region to be established with certainty. Similar behavior was encountered at other gross velocities. It is of interest to note that in the forward hemisphere an increase in the apparent level of turbulence decreases the relative local thermal transport, whereas in the after hemisphere it increases the transport.

The direct influence of apparent level of turbulence upon local thermal transport is shown in Fig. 8 for a Reynolds number of 3640. It is apparent that an increase in the level of turbulence causes an increase in the average Nusselt number for all the conditions covered in this investigation. However, as was also shown in Fig. 6, the local transport near stagnation first decreases, reaches a minimum, and then increases again as the apparent level of turbulence is increased. In the after hemisphere an increase in the apparent level of turbulence causes a rapid increase in the local thermal transport.

The experimentally determined local thermal transport for levels of turbulence of zero and 0.15 is presented in Fig. 9 as a function of polar angle. These data are for a Reynolds number of 3640, corresponding to a velocity of 16 fps. The theoretical evaluations of Eckert [14], Drake [15], and Sibulkin [10] and the experimental data available from the work of Cary [4], Lautman [5], Xenakis [6], and Wadsworth [7] are included. As in Fig. 6, the theoretical values were reported for the molecular properties of the fluid at the average of the temperature existing at the interface and in the free stream. The function $Nu_i^*/Re_\infty^{1/2}$ was not even approximately independent of Reynolds number beyond the separation point, and for that reason only limited data aside from those of the authors are shown for this region.

As a matter of convenience to the reader there are recorded in Table 3 values of the local Nusselt number as a function of ap-

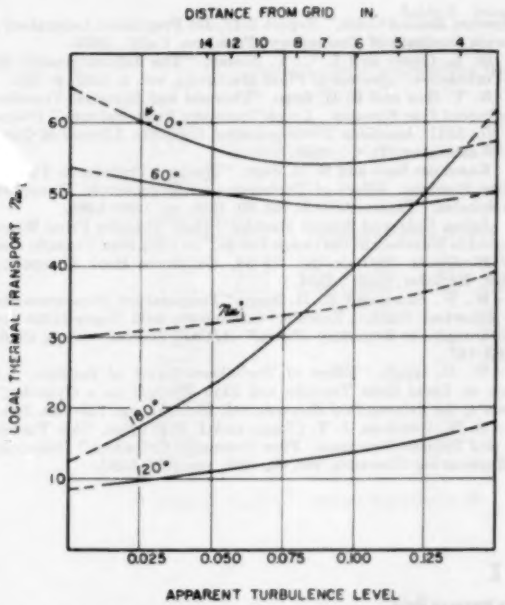

Fig. 8 Influence of apparent turbulence level upon local thermal transport

Table 3 Local thermal transport from spheres

Polar angle, deg	Apparent Turbulence Level 0	0.05	0.10	0.15
	Gross air velocity, 8 fps			
	$Re_\infty = 1807$			
	(23.0)[a,b]	23.3	23.8	25.0
0	(48.4)[c]	45.3	44.2	45.0
30	(47.3)	44.2	44.0	44.0
60	(39.0)	37.4	37.1	37.1
90	(22.2)	21.7	21.8	21.8
120	(3.9)	5.4	7.8	7.8
150	(2.5)	(10.6)	(30.4)	30.4
180	(2.9)	(12.2)	(38.2)	38.2
	Gross air velocity, 16 fps			
	$Re_\infty = 3640$			
	(30.1)[a]	32.2	34.0	(38.5)
0	(65.1)[c]	56.2	54.4	(57.3)
30	(63.2)	55.0	53.4	(56.2)
60	(53.7)	50.4	48.2	(50.5)
90	(26.1)	26.4	27.0	(29.2)
120	(8.5)	10.9	13.5	(17.8)
150	(11.0)	19.4	(35.1)	(55.8)
180	(12.4)	23.0	(39.8)	(61.4)

[a] Space-average Nusselt number Nu_t^* obtained from first equality of equation (7).

[b] All values in parentheses are extrapolated values.

[c] Local thermal transport Nu_t computed from Nu_t/Nu_t^* and the values of Nu_t^* recorded.

parent level of turbulence and polar angle. In addition, values of gross Nusselt number for each value of apparent level of turbulence are included. These data serve to illustrate clearly the marked effect of apparent level of turbulence upon the local transport. It should again be emphasized that the apparent levels of turbulence are, in so far as the experimental work is concerned, only a chosen single-valued parameter which is directly related to the downstream distance from the grid used in this experimental work. The corresponding values of downstream distance from the grid are included on all diagrams in which the level of turbulence is an independent variable.

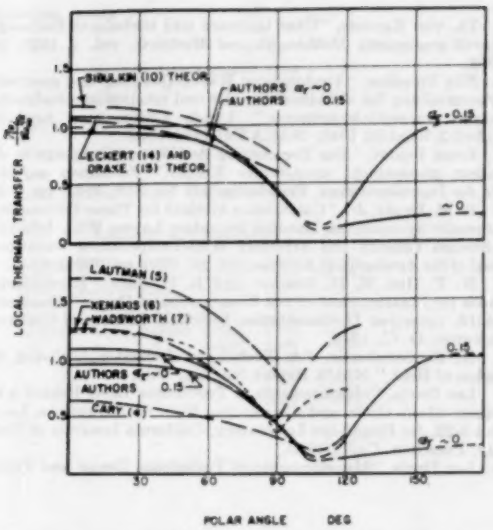

Fig. 9 Comparison of local thermal transfer from several sources

Acknowledgment

The Fluor Corporation contributed to support of the experimental program, and the senior author was the recipient of the Peter E. Fluor Fellowship. The assistance of N. T. Hsu and Kazuhiko Sato in the accumulation of the experimental data is acknowledged. Emilio Venezian contributed to the technical appraisal of the results. Lorine Faris carried out many of the calculations associated with reduction of the experimental data, and Ann Taylor contributed to preparation of the manuscript.

References

1 W. H. McAdams, "Heat Transmission," McGraw-Hill Book Company, Inc., New York, N. Y., third edition, 1954.

2 H. F. Johnstone, R. L. Pigford, and J. H. Chapin, "Heat Transfer to Clouds of Falling Particles," *Trans. AIChE*, vol. 37, 1941, pp. 95–133.

3 Y. S. Tang, J. M. Duncan, and H. E. Schweyer, "Heat and Momentum Transfer Between a Spherical Particle and Air Streams," NACA TN 2867, March, 1953.

4 J. R. Cary, "The Determination of Local Forced-Convection Coefficients for Spheres," TRANS. ASME, vol. 75, 1953, pp. 483–487.

5 L. G. Lautman and W. C. Droege, "Thermal Conductances About a Sphere Subjected to Forced Convection," Report No. AIRL A 6118 50-15-3, U. S. Air Force, Air Materiel Command, Willow Run Airport, Ypsilanti, Mich., August, 1950.

6 G. Xenakis, A. E. Amerman, and R. W. Michelson, "An Investigation of the Heat-Transfer Characteristics of Spheres in Forced Convection," Technical Report 53-117, Wright Air Development Center, Dayton, Ohio, April, 1953.

7 J. Wadsworth, "The Experimental Examination of the Local Heat Transfer on the Surface of a Sphere When Subjected to Forced Convective Cooling," Report No. MT-39, National Research Council of Canada, Division of Mechanical Engineering, September 12, 1958.

8 N. T. Hsu and B. H. Sage, "Thermal and Material Transfer in Turbulent Gas Streams. Local Transport From Spheres," *AIChE Journal*, vol. 3, 1957, pp. 405–410.

9 Merwin Sibulkin, "Heat Transfer Near the Forward Stagnation Point of a Body of Revolution," *Journal of the Aeronautical Sciences*, vol. 19, 1952, pp. 570–572.

10 Merwin Sibulkin, "Theoretical Solutions for Heat Transfer on a Sphere," unpublished, 1952; reported in reference [11].

11 Irving Korobkin, "Discussion of Local Laminar Heat Transfer Coefficients for Spheres and Cylinders in Incompressible Flow," Paper No. 54—F-18-Revised, contributed by the Heat Transfer Division and presented at the ASME Fall Meeting, Milwaukee, Wis., September 8–10, 1954.

12 Th. von Karman, "Über laminare und turbulente Reibung," *Zeitschrift angewandte Mathematik und Mechanik*, vol. 1, 1921, pp. 233–252.

13 Nils Frössling, "Verdunstung Wärmeübergang und geschwindigkeitsverteilung bei zweidimensionaler und rotationssymmetrischer laminarer grenzschichtströmung," Lunds Universitets Arsskrift, N. F. Avd 2, band 36, 1940, NACA TM 1432, 1958

14 Ernst Eckert, "Die Berechnung des Wärmeüberganga in der laminaren grenzschicht umströmter Körper," *Forschung auf dem gebiete des Ingenieurwesens*, Forschungsheft No. 416, 1942, pp. 1–24.

15 R. M. Drake, Jr., "Calculation Method for Three-Dimensional Rotationally Symmetrical Laminar Boundary Layers With Arbitrary Free-Stream Velocity and Arbitrary Wall-Temperature Variation," *Journal of the Aeronautical Sciences*, vol. 20, 1953, pp. 309–316.

16 N. T. Hsu, H. H. Reamer, and B. H. Sage, "Experimental Methods for Measurement of the Evaporation of Drops," Document No. 4219, American Documentation Institute, Library of Congress, Washington, D. C., 1954.

17 G. B. Schubauer, "A Turbulence Indicator Utilizing the Diffusion of Heat," NACA Report No. 524, 1935.

18 Leo Davis, "Measurements of Turbulence Level Behind a Set of Square-Mesh Grids and Correlation With Grid Pressure Loss," Report 3-22, Jet Propulsion Laboratory, California Institute of Technology, Pasadena, Calif., 1950.

19 Leo Davis, "Measurements of Turbulence Decay and Turbulent Spectra Behind Grids," Report 3-17, Jet Propulsion Laboratory, California Institute of Technology, Pasedena, Calif., 1952.

20 H. L. Grant and I. C. T. Nisbet, "The Inhomogeneity of Grid-Turbulence," *Journal of Fluid Mechanics*, vol. 2, 1957, p. 263.

21 N. T. Hsu and B. H. Sage, "Thermal and Material Transfer in Turbulent Gas Streams. Local Transport From Spheres," Document No. 5311, American Documentation Institute, Library of Congress, Washington, D. C., 1957.

22 Kazuhiko Sato and B. H. Sage, "Thermal Transfer in Turbulent Gas Streams. Effect of Turbulence on Macroscopic Transport From Spheres," TRANS. ASME, vol. 80, 1958, pp. 1380–1388.

23 Julian Cole and Anatol Roshko, "Heat Transfer From Wires at Reynolds Numbers in the Oseen Range," in *1954 Heat Transfer and Fluid Mechanics Institute*, pp. 12–23, California Book Company, Limited, Berkeley, Calif., 1954.

24 W. W. Short and B. H. Sage, "Temperature Measurements in a Spherical Field. Transfer Coefficients and Corrections for Thermocouples in Boundary Flows," *AIChE Journal*, vol. 6, 1960, pp. 163–167.

25 W. H. Giedt, "Effect of Turbulence Level of Incident Air Stream on Local Heat Transfer and Skin Friction on a Cylinder," *Journal of the Aeronautical Sciences*, vol. 18, 1951, pp. 725–730, 766.

26 E. W. Comings, J. T. Clapp, and J. F. Taylor, "Air Turbulence and Transfer Processes. Flow Normal to Cylinders," *Industrial and Engineering Chemistry*, vol. 40, 1948, pp. 1076–1082.

APPENDIX

Table 4 Typical temperature traverse data

Horizontal Traverse[a] at x = -0.186 inch (φ = 41.9°)

Horizontal Distance from Surface in.	Radial Distance from Surface in.	Wire Temperature °F.
0	0	158.37
0.001	0.0006	155.72
0.002	0.0013	152.52
0.003	0.0020	148.76
0.004	0.0027	144.72
0.005	0.0033	140.38
0.006	0.0040	136.01
0.007	0.0046	131.61
0.008	0.0053	128.02
0.009	0.0060	124.41
0.010	0.0067	121.34
0.011	0.0074	118.25
0.012	0.0081	115.16
0.013	0.0088	112.90
0.014	0.0095	110.92
0.015	0.0102	108.92
0.017	0.0116	106.07
0.019	0.0130	104.36
0.021	0.0145	102.64
0.023	0.0157	101.78
0.026	0.0180	100.92
0.031	0.0217	100.35
0.036	0.0253	100.06

Horizontal Traverse[a] at x = 0.001 inch (φ = 90.2°)

Horizontal Distance from Surface in.	Radial Distance from Surface in.	Wire Temperature °F.
0	0	165.49
0.001	0.001	163.91
0.002	0.002	161.81
0.003	0.003	158.90
0.004	0.004	155.18
0.005	0.005	151.98
0.006	0.006	148.22
0.007	0.007	144.72
0.008	0.008	141.20
0.009	0.009	137.92
0.010	0.010	135.64
0.011	0.011	131.06
0.012	0.012	128.02
0.013	0.013	124.41
0.015	0.015	119.10
0.017	0.017	114.60
0.020	0.020	109.49
0.025	0.025	104.08
0.030	0.030	101.78
0.035	0.035	100.92
0.040	0.040	100.35
0.045	0.045	100.06

Horizontal Traverse[a] at x = 0.126 inch (φ = 120.2°)

Horizontal Distance from Surface in.	Radial Distance from Surface in.	Wire Temperature °F.
0	0.0001	167.58
0.002	0.0018	164.70
0.004	0.0035	161.52
0.006	0.0053	158.11
0.008	0.0070	154.92
0.010	0.0088	151.98
0.013	0.0114	148.76
0.018	0.0158	144.72
0.023	0.0202	142.01
0.028	0.0246	139.56
0.033	0.0291	137.10
0.038	0.0335	132.71
0.043	0.0380	127.74
0.048	0.0425	121.34
0.053	0.0471	116.00
0.058	0.0516	110.92
0.063	0.0561	107.21
0.068	0.0607	104.08
0.078	0.0699	101.21
0.093	0.0837	100.35
0.123	0.1069	100.06

Vertical Traverse[b] below Sphere at x = 0.002 inch (φ = 0.5°)

Vertical Distance from Surface in.	Radial Distance from Surface in.	Wire Temperature °F.
0	0	158.37
0.001	0.001	155.98
0.002	0.002	151.18
0.003	0.003	146.34
0.004	0.004	140.38
0.005	0.005	135.18
0.006	0.006	129.68
0.007	0.007	126.35
0.008	0.008	122.18
0.009	0.009	118.82
0.010	0.010	115.44
0.011	0.011	112.34
0.013	0.013	108.07
0.015	0.015	104.65
0.017	0.017	102.64
0.027	0.027	100.06

[a] Test 90
[b] Test 89

Table 5 Local conditions around sphere

Test 161

	Polar Angle from Stagnation Point					
	0°	30°	60°	90°	120°	150°
$\pi_{a_i}/\pi_{a_i}^*$	2.13*	2.07	1.66	0.76	0.21	0.23
δ_t/d	0.01910	0.01927	0.02347	0.03259	-	-
Normalized Surface Temp.	0.987	0.989	0.994	1.000	1.004	1.006
Radial Distance from Surface, in.	Normalized Wire Temperature					
0	0.845	0.854	0.882	0.922	0.951	-
0.005	0.607	0.760	0.713	0.818	0.900	-
0.010	0.362	0.397	0.542	0.716	0.854	-
0.015	0.181	-	0.369	-	0.818	-
0.020	-	-	0.195	-	0.786	-
0.025	-	-	-	-	0.755	-
0.030	-	-	-	-	0.723	-
0.040	-	-	-	-	0.653	-
0.050	-	-	-	-	0.553	-
0.060	-	-	-	-	-	-
0.080	-	-	-	-	-	-
0.100	-	-	-	-	-	-
0.150	-	-	-	-	-	-
0.200	-	-	-	-	-	-
0.250	-	-	-	-	-	-
0.300	-	-	-	-	-	-

Test 110

	Polar Angle from Stagnation Point					
	0°	30°	60°	90°	120°	150°
$\pi_{a_i}/\pi_{a_i}^*$	1.95	1.90	1.60	0.92	0.23	0.48
δ_t/d	0.01330	0.01361	0.01584	0.02683	-	-
Normalized Surface Temp.	0.983	0.985	0.992	1.001	1.006	1.007
Radial Distance from Surface, in.	Normalized Wire Temperature					
0	0.814	0.829	0.862	0.903	0.927	0.937
0.005	0.525	0.548	0.588	0.736	0.880	0.844
0.010	0.240	0.260	0.312	0.570	0.831	0.751
0.015	0.0829	0.0643	0.133	0.401	0.783	0.661
0.020	0.0218	0.00610	0.0371	0.233	0.734	0.586
0.025	0.00398	0	0.00663	0.130	0.682	0.519
0.030	0	-	0	0.0497	0.625	0.476
0.040	-	-	-	0.00530	0.486	0.442
0.050	-	-	-	0	0.345	0.430
0.060	-	-	-	-	0.208	0.423
0.080	-	-	-	-	0.478	0.424
0.100	-	-	-	-	0.00265	0.434
0.150	-	-	-	-	0	0.369
0.200	-	-	-	-	-	0.167
0.250	-	-	-	-	-	0.424
0.300	-	-	-	-	-	0.00597

* Values of $\pi_{a_i}/\pi_{a_i}^*$ obtained from Equation (8).

Test 89

	Polar Angle from Stagnation Point					
	0°	30°	60°	90°	120°	150°
$\pi_{a_i}/\pi_{a_i}^*$	1.87	1.82	1.55	0.90	0.27	0.78
δ_t/d	0.01358	0.01392	0.01603	0.02686	-	-
Normalized Surface Temp.	0.983	0.985	0.992	1.001	1.006	1.007
Radial Distance from Surface, in.	Normalized Wire Temperature					
0	0.758	0.783	0.835	0.881	0.901	0.909
0.005	0.470	0.459	0.531	0.707	0.838	0.816
0.010	0.214	0.164	0.254	0.536	0.775	0.723
0.015	0.0750	0.0531	0.173	0.360	0.713	0.634
0.020	0.0226	0.0106	0.0438	0.218	0.651	0.545
0.025	0.00318	0	0.0133	0.114	0.589	0.476
0.030	0	-	0.0265	0.0617	0.527	0.435
0.040	-	-	0	0.0154	0.403	0.388
0.050	-	-	-	0.00133	0.289	0.358
0.060	-	-	-	0	0.186	0.339
0.080	-	-	-	-	0.0541	0.330
0.100	-	-	-	-	0.00796	0.340
0.150	-	-	-	-	0	0.301
0.200	-	-	-	-	-	0.177
0.250	-	-	-	-	-	0.0727
0.300	-	-	-	-	-	0.0252

Test 92

	Polar Angle from Stagnation Point					
	0°	30°	60°	90°	120°	150°
$\pi_{a_i}/\pi_{a_i}^*$	1.81	1.76	1.51	0.88	0.31	1.18
δ_t/d	0.01409	0.01447	0.01675	0.02772	-	-
Normalized Surface Temp.	0.983	0.985	0.992	1.001	1.006	1.007
Radial Distance from Surface, in.	Normalized Wire Temperature					
0	0.805	0.824	0.856	0.887	0.908	0.914
0.005	0.506	0.560	0.610	0.707	0.845	0.802
0.010	0.210	0.293	0.364	0.528	0.780	0.651
0.015	0.0693	0.105	0.161	0.342	0.715	0.515
0.020	0.0136	0.0483	0.0791	0.210	0.649	0.374
0.025	0.0168	0.021	0.0468	0.128	0.587	0.300
0.030	0.00770	0.00770	0.0258	0.0833	0.522	0.277
0.040	0	0.00148	0.0154	0.0385	0.405	0.252
0.050	-	0	0.00210	0.0175	0.309	0.237
0.060	-	-	0	0.0060	0.235	0.228
0.080	-	-	-	0.00252	0.118	0.214
0.100	-	-	-	0	0.0280	0.206
0.150	-	-	-	-	0.00770	0.188
0.200	-	-	-	-	0	0.156
0.250	-	-	-	-	-	0.104
0.300	-	-	-	-	-	0.0630

Test 93

	Polar Angle from Stagnation Point					
	0°	30°	60°	90°	120°	150°
$\pi_{a_i}/\pi_{a_i}^*$	1.81	1.76	1.51	0.88	0.31	1.18
δ_t/d	0.01409	0.01447	0.01675	0.02772	-	-
Normalized Surface Temp.	0.983	0.985	0.992	1.001	1.006	1.007
Radial Distance from Surface, in.	Normalized Wire Temperature					
0	0.805	0.824	0.856	0.887	0.908	0.914
0.005	0.476	0.563	0.590	0.711	0.847	0.759
0.010	0.170	0.305	0.331	0.540	0.783	0.598
0.015	0.0704	0.101	0.120	0.369	0.719	0.436
0.020	0.0345	0.0450	0.0633	0.200	0.656	0.322
0.025	0.016	0.0211	0.0373	0.115	0.591	0.289
0.030	0.00591	0.00844	0.0239	0.0753	0.527	0.269
0.040	0	0.00141	0.0095	0.0373	0.407	0.247
0.050	-	0	0.0281	0.0194	0.308	0.240
0.060	-	-	0	0.0101	0.231	0.236
0.080	-	-	-	0.00310	0.115	0.231
0.100	-	-	-	0	0.0549	0.228
0.150	-	-	-	-	0.00732	0.209
0.200	-	-	-	-	0	0.158
0.250	-	-	-	-	-	0.103
0.300	-	-	-	-	-	0.0640

Test 160

	Polar Angle from Stagnation Point					
	0°	30°	60°	90°	120°	150°
$\pi_{a_i}/\pi_{a_i}^*$	2.04	2.00	1.73	0.86	0.30	0.42
δ_t/d	0.00917	0.00960	0.01128	0.01990	-	-
Normalized Surface Temp.	0.986	0.988	0.993	1.002	1.007	1.008
Radial Distance from Surface, in.	Normalized Wire Temperature					
0	0.934	0.927	0.918	0.843	0.976	-
0.005	0.831	0.585	0.499	-	0.839	-
0.010	0.727	0.237	0.174	-	0.778	-
0.015	0.624	0.053	0.0366	-	0.737	-
0.020	0.521	-	-	-	0.698	-
0.025	0.417	-	-	-	0.663	-
0.030	-	-	-	-	0.627	-
0.040	-	-	-	-	0.548	-
0.050	-	-	-	-	0.420	-
0.060	-	-	-	-	0.164	-
0.080	-	-	-	-	0.0479	-
0.100	-	-	-	-	0.0103	-
0.150	-	-	-	-	-	-
0.200	-	-	-	-	-	-
0.250	-	-	-	-	-	-
0.300	-	-	-	-	-	-

Table 5 (*Continued*)

	Test 109						Test 90					
	Polar Angle from Stagnation Point						Polar Angle from Stagnation Point					
	0°	30°	60°	90°	120°	150°	0°	30°	60°	90°	120°	150°
$r_{a_i}/r_{a_i}^*$	1.74	1.70	1.55	0.82	0.34	0.61	1.60	1.57	1.43	0.78	0.38	0.91
δ_i/d	0.00965	0.01006	0.01178	0.02004	-	-	0.01010	0.01061	0.01241	0.02054	-	-
Normalized Surface Temp.	0.986	0.988	0.993	1.002	1.007	1.008	0.986	0.988	0.993	1.002	1.007	1.008
Radial Distance from Surface, in.	Normalized Wire Temperature						Normalized Wire Temperature					
0	0.837	0.851	0.880	0.917	0.939	0.956	0.767	0.791	0.846	0.887	0.914	0.930
0.005	0.432	0.389	0.496	0.677	0.844	0.778	0.439	0.438	0.490	0.690	0.896	0.832
0.010	0.0891	0.0652	0.162	0.441	0.760	0.605	0.130	0.106	0.146	0.495	0.795	0.730
0.015	0.0193	0.00825	0.0279	0.214	0.713	0.455	0.0320	0.0252	0.0402	0.303	0.639	0.623
0.020	0.00293	0	0.00466	0.0805	0.678	0.391	0.00682	0.00341	0.0102	0.136	0.574	0.518
0.025	0	-	0	0.0239	0.644	0.353	0	0.00136	0.00204	0.0689	0.520	0.410
0.030	-	-	-	0.00466	0.607	0.326	-	0	0	0.0344	0.466	0.303
0.040	-	-	-	0	0.521	0.287	-	-	-	0.0136	0.385	0.261
0.050	-	-	-	-	0.356	0.263	-	-	-	0	0.293	0.246
0.060	-	-	-	-	0.174	0.252	-	-	-	-	0.200	0.238
0.080	-	-	-	-	0.0705	0.234	-	-	-	-	0.0552	0.228
0.100	-	-	-	-	0.0220	0.238	-	-	-	-	0.0286	0.224
0.150	-	-	-	-	0.0479	0.291	-	-	-	-	0.0136	0.218
0.200	-	-	-	-	0	0.183	-	-	-	-	0	0.0777
0.250	-	-	-	-	-	0.0479	-	-	-	-	-	0.0348
0.300	-	-	-	-	-	0.00825	-	-	-	-	-	-

	Test 91					
	Polar Angle from Stagnation Point					
	0°	30°	60°	90°	120°	150°
$r_{a_i}/r_{a_i}^*$	1.51	1.48	1.32	0.76	0.44	1.33
δ_i/d	0.01193	0.01135	0.01332	0.02093	-	-
Normalized Surface Temp.	0.986	0.988	0.993	1.002	1.007	1.008
Radial Distance from Surface, in.	Normalized Wire Temperature					
0	0.761	0.781	0.822	0.861	0.895	0.907
0.005	0.473	0.487	0.542	0.602	0.767	0.754
0.010	0.160	0.197	0.271	0.359	0.661	0.581
0.015	0.0529	0.0686	0.0902	0.230	0.583	0.402
0.020	0.0218	0.0343	0.0423	0.111	0.517	0.257
0.025	0.00745	0.0164	0.0171	0.0641	0.458	0.224
0.030	0	0.00596	0.00745	0.0388	0.406	0.203
0.040	-	0	0	0.0171	0.315	0.184
0.050	-	-	-	0.00820	0.238	0.174
0.060	-	-	-	0.00298	0.175	0.168
0.080	-	-	-	0	0.0868	0.161
0.100	-	-	-	-	0.0343	0.158
0.150	-	-	-	-	0.00596	0.146
0.200	-	-	-	-	0	0.116
0.250	-	-	-	-	-	0.0812
0.300	-	-	-	-	-	0.0522

Hydrodynamic Entrance Lengths for Incompressible Laminar Flow in Rectangular Ducts

L. S. HAN
Associate Professor,
Department of Mechanical Engineering,
The Ohio State University,
Robinson Laboratory,
Columbus, Ohio

The problem of determining the hydrodynamic entrance length in a rectangular channel is solved by the method of linearizing the Navier-Stokes equation. The resulting equation is regarded as an equation to generate a mathematical expression for the axial velocity in the entire region, making smooth transition from a uniform profile to the fully developed one. From this expression, the entrance length, defined as where 99 per cent of the fully developed center-line velocity is attained, is calculated for channels of six aspect ratios. The pressure drops are also calculated and presented herein. A comparison is made with the limited amount of experimental and theoretical data.

When a viscous fluid enters a duct with a uniform velocity distribution, it will ultimately, at a certain axial distance downstream, assume a velocity profile which is invariant with respect to the axial-flow co-ordinate. Theoretically, the required distance to attain that velocity profile, commonly referred to as the fully developed profile, is infinitely large; however, for engineering calculations, the axial distance required for the center-line velocity to attain say 99 per cent of the fully established velocity is defined as the entrance length. A knowledge of the entrance length is of importance in many engineering applications; e.g., in the estimates of pressure-drop and heat-transfer parameters in ducts of finite lengths, or in any flow-intake devices.

While the problem is of engineering significance and of academic interest, there are few available solutions; namely, circular and between parallel plates. The solution for a circular pipe was solved by Atkinson-Goldstein [1][1] starting with the boundary-layer equations and by Schiller [2] using an integral equation and an assumed transition profile. More recently, the problem for a circular pipe has been solved by Langhaar [3] and by Shapiro, et al. [4]. The latter paper concluded that the solution given by Langhaar [3] yielded the most accurate result when the axial distance parameter $(z/D_e\text{Re})$ is more than 0.01. For flow between a pair of parallel and infinite plates, a solution was obained by Schlichting [5]. His method consists of smoothly joining two asymptotic series solutions, one based on Blasius' solution of the boundary-layer development, expanded in a series toward the downstream direction, and the other based on the Hagen-Poiseuille solution of a parabolic velocity distribution, expanded in a series form toward the upstream direction. An approximate

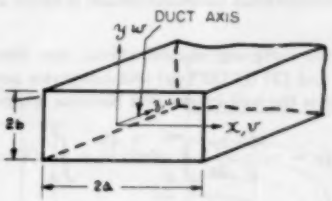

Fig. 1 Duct configuration

[1] Numbers in brackets designate References at end of paper.

Contributed by the Applied Mechanics Division and presented at the Annual Meeting, Atlantic City, N. J., November 29-December 4, 1959, of The American Society of Mechanical Engineers.

Discussion of this paper should be addressed to the Secretary, ASME, 29 West 39th Street, New York, N. Y., and will be accepted until October 10, 1960, for publication at a later date. Discussion received after the closing date will be returned.

Note: Statements and opinions advanced in papers are to be understood as individual expressions of their authors and not those of the Society. Manuscript received by ASME Applied Mechanics Division, May 22, 1959. Paper No. 59—A-82.

Nomenclature

A = area
a, b = side dimensions, one half of
C = coefficients
D = diameter (D_e = 4 × area/perimeter)
f = friction factor
I_1, I_2 = functions of (βa) as defined by equations (15) and (16)
K = correction factor in equation (22)
L = length
p = static pressure of fluid
Re = Reynolds number ($D_e U/\nu$)
m, n = dummy indexes
u, v, w = velocities of fluid in z, x, and y-directions, Fig. 1
x, y, z = co-ordinates, Fig. 1
U = average velocity
β = parameter
γ = aspect ratio (a/b)
∇^2 = Laplacian operator $\left(\frac{\partial^2}{\partial x^2} + \frac{\partial^2}{\partial y^2}\right)$
μ = absolute viscosity
ν = kinematic viscosity
ρ = density
Φ = dimensionless entrance length ($L_e/D_e\text{Re}$), equation (1)

Subscripts

ap = apparent
e = equivalent
fd = fully developed
0 = center line, ($x = y = 0$)
∞ = for $z = \infty$, $x = y = 0$

solution similar to Schiller's integral analysis was recently given by Sparrow [6]. The results of these analyses can be summarized by the following equation for the entrance length L_e to attain the fully established center-line velocity:

$$L_e = \Phi(D_e \mathrm{Re}) \tag{1}$$

For circular pipes:	Φ
Langhaar [3][2]	0.0570
Schiller [2]	0.0288
For parallel plates:	
Schlichting [5][2]	0.0100
Sparrow [6]	0.0065

The purpose of this paper is to report a solution to the entrance problem for a rectangular duct based essentially on Langhaar's method.

Analysis

Assuming the fluid incompressible having constant physical properties, the boundary-layer equation of motion in the axial direction is

$$u\frac{\partial u}{\partial z} + v\frac{\partial u}{\partial x} + w\frac{\partial u}{\partial y} = -\frac{1}{\rho}\frac{\partial p}{\partial z} + \nu\left(\frac{\partial^2 u}{\partial x^2} + \frac{\partial^2 u}{\partial y^2}\right) \tag{2}$$

and the equation of continuity is

$$\frac{\partial u}{\partial z} + \frac{\partial v}{\partial x} + \frac{\partial w}{\partial y} = 0 \tag{3}$$

referring to Fig. 1 for configuration details.

The usual boundary-layer analysis which assumes a small region close to the duct wall in which the shearing stress is large, leads to the following conclusions:

(*a*) That $(\partial^2 u/\partial z^2)$ may be dropped in comparison with $(\partial^2 u/\partial x^2, \partial^2 u/\partial y^2)$.

(*b*) That, within the duct, the transverse velocities v and w are small compared to u.

(*c*) Consequently the pressure gradient term $\partial p/\partial z$ is independent of cross-sectional co-ordinates and is hence a function of z only.

Observing the foregoing simplifications, one then multiplies equations (2) and (3) by $(dx)(dy)$ and integrates across the section; the result is the well-known von Karman integral equation:

$$\frac{\partial}{\partial z}\int_A u^2 dx\,dy = -\frac{1}{\rho}\frac{\partial p}{\partial z}\int_A dx dy + \nu\int_A (\nabla^2 u) dx dy \tag{4a}$$

$$\int_A u dx\,dy = 4abU \tag{4b}$$

It is well established that a solution to equations (4) constitutes at least a first approximation to the solution to equation (2). The actual work in obtaining a solution to equation (4) as has been done by Schiller and Sparrow is to assume the flow as divided into a friction region and a potential core. For the friction region, the velocity varies from zero at the boundary to the core velocity at the border line making a smooth connection; for the potential core the velocity is constant with respect to the cross-sectional co-ordinate, while for the circular and parallel-plates configurations, the division of flow region is easily accomplished; i.e., the dividing lines are a circle and straight lines, respectively.

For cross sections other than those, this preliminary step, i.e., division of flow regions, is difficult and we shall take advantage of a technique introduced in reference [3] which consists of linearizing equation (2) by replacing the left-hand side convective terms by $(\nu\beta^2 u)$. The resulting equation is

$$\frac{\partial^2 u}{\partial x^2} + \frac{\partial^2 u}{\partial y^2} = \beta^2 u + \frac{1}{\mu}\frac{\partial p}{\partial z} \tag{5}$$

where β^2 is a function of z only.

The justifications for the substitution by $\nu\beta^2 u$ are discussed in reference [3]. The nature of equation (4) is such that the solution, as can be easily examined, assumes the form of a fully developed velocity profile when $\beta = 0$ and assumes a uniform velocity profile at $\beta = \infty$, thus providing a smooth transition.

We shall therefore regard equation (5) as a velocity function-generating equation.

The use of equation (5) to generate a transition-velocity profile is seen to have the advantage that it does not require the use of a finite "boundary-layer thickness" in treating this type of problem. In general, the solution to equation (5) is not obtainable in closed forms. Where this is the case, it is best to treat equation (5) as an analogous membrane equation and using the Rayleigh-Ritz approximation procedure. It must be noted further that the present analysis is only an approximate one, because of the fact that in the entrance region the vorticity along z-axis is ignored. This is also the case of Carrier's [9] analysis of flow distribution along a corner, composed of two mutually perpendicular planes.

Velocity Profiles

Referring to Fig. 1, the equation used to generate a continuous velocity profile is equation (5). In order to bring out the essential features of the solution to equation (5), we first write

$$\frac{1}{\rho}\frac{\partial p}{\partial z} = \left(\frac{16}{\pi^2}\right)\left(\frac{1}{\rho}\frac{\partial p}{\partial z}\right)\sum_{m,\,n=1,3,5\ldots}^{\infty\ \infty}\left(\frac{1}{mn}\right)(-1)^{\frac{m+n}{2}-1}\cos(m\pi x/2a)\cos(n\pi y/2b) \tag{6}$$

valid for $|x| < a$, $|y| < b$.

Since the velocity u is to satisfy the conditions of zero velocity on $|x| = a$, $|y| = b$, the following Fourier series development for u will obviously meet the requirements:

$$u = \sum_{m,\,n\ \text{odd integers}}^{\infty\ \infty} C_{mn}\cos(m\pi x/2a)\cos(n\pi y/2b) \tag{7}$$

in which C_{mn} are to be determined.

Substitution of equations (6) and (7) into equation (5) yields the coefficients C_{mn}; and the velocity expression u in equation (7) becomes

$$U = -\left(\frac{16}{\pi^2}\right)\left(\frac{1}{\rho}\frac{\partial p}{\partial z}\right)\times \sum_{m,\,n=1,3,5\ldots}^{\infty}\frac{(-1)^{\frac{m+n}{2}-1}\cos(m\pi x/2a)\cos(n\pi y/2b)}{mn\left[\left(\frac{m\pi}{2a}\right)^2 + \left(\frac{n\pi}{2b}\right)^2 + \beta^2\right]} \tag{8}$$

The pressure-drop term is eliminated by the continuity relation, equation (4*b*); thus integrating u over the section one obtains

$$\left(\frac{u}{U}\right) = \left(\frac{\pi^2}{4}\right)\left\{\sum_{m,\,n=1,3,5\ldots}^{\infty}\frac{(-1)^{\frac{m+n}{2}-1}\cos(m\pi x/2a)\cos(n\pi y/2b)}{mn[m^2 + n^2\gamma^2 + (2\beta a/\pi)^2]}\right\}\Big/$$

[2] When the center-line velocity is 99 per cent of the fully developed value.

$$\left\{\sum_{m,n=1,3,5\ldots}^{\infty}\frac{1}{m^2n^2[m^2+n^2\gamma^2+(2\beta a/\pi)^2]}\right\} \quad (9)$$

This expression would approach a uniform profile as $\beta a \to \infty$, i.e.,

$$\lim_{\beta\to\infty}\left(\frac{u}{U}\right) = \lim_{\beta\to\infty}\frac{\pi^2}{4}$$

$$\left\{\sum_{m,n=1,3,5\ldots}^{\infty}\frac{(-1)^{\frac{m+n}{2}}\cos(m\pi x/2a)\cos(m\pi y/2b)}{mn\left[1+\left((m^2+n^2\gamma^2)\Big/\left(\frac{2\beta a}{\pi}\right)^2\right)\right]}\right\}\Bigg/$$

$$\left\{\sum_{m,n=1,3,5\ldots}^{\infty}\frac{1}{m^2n^2\left[1+\left((m^2+n^2\gamma^2)\Big/\left(\frac{2\beta a}{\pi}\right)^2\right)\right]}\right\}$$

$$= \frac{\pi^2}{4}\left\{\sum_{m,n=1,3,5\ldots}^{\infty}\frac{(-1)^{\frac{m+n}{2}-1}}{mn}\cos(m\pi x/2a)\cos(n\pi y/2b)\right\}\Bigg/\left\{\sum_{m,n=1,3,5\ldots}^{\infty}\frac{1}{m^2n^2}\right\} = 1$$

for $|x| < a$ and $|y| < b$.

The velocity at the fully established section is obtained directly by letting $\beta = 0$ in equations (8) and (9) which of course satisfy the corresponding equation (5) with $\beta = 0$.

From the foregoing, it is seen that the velocity u expressed by equation (9) satisfies the following conditions

(*a*) Continuity.
(*b*) Zero velocity on the boundary.
(*c*) Assuming a uniform velocity profile at $\beta = \infty$.
(*d*) Becoming fully developed velocity at $\beta = 0$.
(*e*) Having a smooth transition from (*c*) to (*d*).

Fig. 2 contains the velocity contours, as computed from equation (18), an alternate of equation (8) in a duct of aspect ratio 0.5, and for three different (βa)-values 6.0, 2.0, and 0.80. These contours are for distances of $(z/D_e\,\mathrm{Re}) = 0.00172$, 0.0156, and 0.0460 as can be seen from data in Table 1, discussed later.

Variation of β-Values With Z

The remaining problem is then to determine how β is to vary with z. It is apparent from a physical consideration that, at the entrance,

$$z = 0, \quad (u/U) = 1 \quad \text{or} \quad \beta = \infty \quad (10)$$

and for fully developed flow,

$$z = \infty, \quad (u/U) \to (u/U)_{est} \quad \text{or} \quad \beta = 0 \quad (11)$$

If one takes the Navier-Stokes equation (2) and sets $x = y = 0$, i.e., at the center line of the duct, the equation becomes

$$u_0\frac{\partial u_0}{\partial z} = -\frac{1}{\rho}\frac{\partial p}{\partial z} + \nu(\nabla^2 u)_0 \quad (12)$$

where u_0 denotes the center-line velocity.

Now multiply equation (12) by $dx\,dy$ and integrate across; the result is

$$\frac{\partial}{\partial z}\int_A\left(\frac{u_0^2}{2}\right)dxdy = -\frac{1}{\rho}\frac{\partial p}{\partial z}\int_A dxdy + \nu\int_A(\nabla^2 u)_0 dxdy \quad (13)$$

Subtracting equation (13) from equation (4*a*), the following is obtained:

$$\frac{\partial}{\partial z}\int_A(u^2 - u_0^2/2)dxdy = \nu\int_A[\nabla^2 u - (\nabla^2 u)_0]dxdy \quad (14)$$

It is to be noted that both integrands in equation (14) are now functions of β only. Using the following notations:

$$I_1(\beta) = \int_A[u^2 - u_0^2/2]dxdy \quad (15)$$

$$I_2(\beta) = \left\{\nu\int_A[\nabla^2 u - (\nabla^2 u)_0]dxdy\right\}^{-1} \quad (16)$$

equation (14) may be put in the following form:

$$\frac{d}{dz}(I_1) = 1/I_2$$

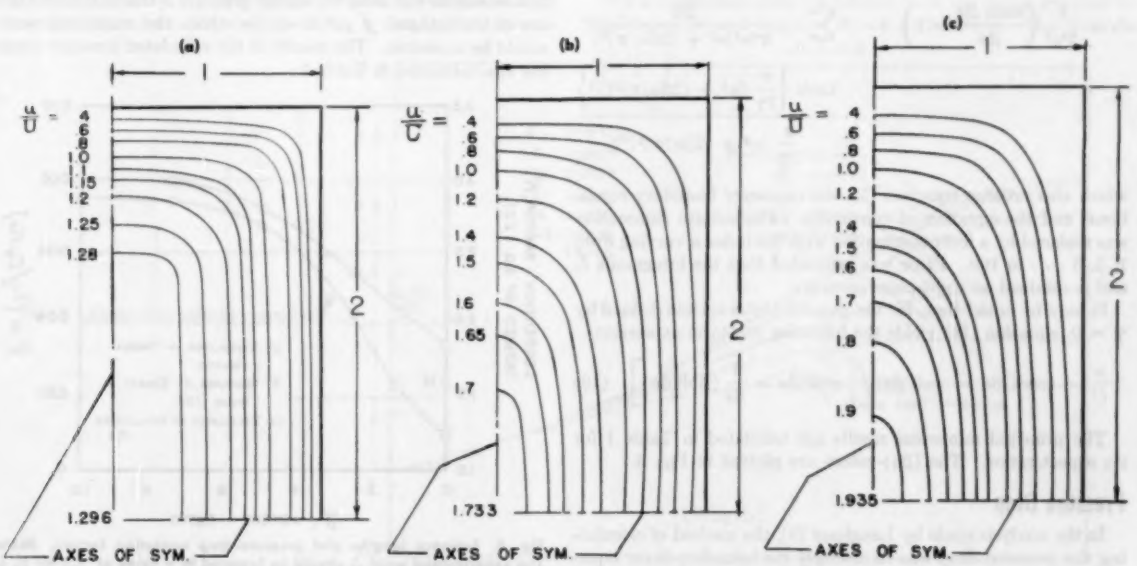

Fig. 2 Velocity contours in a duct of 2:1 aspect ratio

or

$$z = \int_{\beta=-\infty}^{\beta} I_2 d(I_1) \tag{17}$$

Equation (17) thus provides the necessary relationship between z and β. This numerical work consists, for a fixed value of γ, of the following steps:

(a) Assign a series of β-values to equation (9).
(b) Calculate the integrands I_1 and I_2.
(c) Plot I_2 against I_1 with β as a parametric value.
(d) Numerically integrate $\int_{\beta=-\infty}^{\beta} I_2 dI_1$; i.e., calculate the area underneath the $I_2 \sim I_1$ curve. The area then represents a z-value corresponding to the β-value at the end of the integration process.

The β-value in turn defines the ratio of the center-line velocity to that at the entrance. In this way, the relationships between β, $(u/U)_0$, and z are determined.

In carrying out the procedures as outlined, all numerical work was accomplished by an IBM 650 at the Numerical Computation Laboratory of the Ohio State University Research Foundation. All together, six aspect ratios were used, and for each, 36 β-values were selected for evaluating the integrands I_1 and I_2. In actual computational work, the double-summation expression as indicated by equation (9) is reduced to a single-summation expression in equation (18):

$$\frac{u}{U} = \frac{F_1}{F_2} \tag{18}$$

where

$$F_1 = \frac{1}{\beta^2 a^2}\left(\frac{\cosh \beta x}{\cosh \beta a} - 1\right) + \sum_{n=1,3,5\ldots}^{\infty} \frac{16(-1)^{\frac{n-1}{2}} \cos\left(\frac{n\pi x}{2a}\right)}{\pi^2 n[n^2 + (2\beta a/\pi)^2]} \frac{\cosh\left\{\frac{\pi}{2\gamma}[n^2 + (2\beta a/\pi)^2]^{1/2} \frac{y}{b}\right\}}{\cosh\left\{\frac{\pi}{2\gamma}[n^2 + (2\beta a/\pi)^2]^{1/2}\right\}}$$

$$F_2 = \frac{1}{\beta^2 a^2}\left(\frac{\tanh \beta a}{\beta a} - 1\right) + \sum_{n=1,3,5\ldots}^{\infty} \frac{32}{\pi^4 n^2[n^2 + (2\beta a/\pi)^2]} \frac{\tanh\left\{\frac{\pi}{2\gamma}[n^2 + (2\beta a/\pi)^2]^{1/2}\right\}}{\frac{\pi}{2\gamma}[n^2 + (2\beta a/\pi)^2]^{1/2}}$$

which also satisfies equation (5), the necessary boundary conditions, and the equation of continuity. The infinite summation was replaced by a finite summation with the index n varying from 1, 3, 5 . . . to 199. Error was estimated that the integrands I_1 and I_2 retained an eight-place accuracy.

It may be noted that, for the parallel-plates system defined by $\gamma = 0$, equation (18) yields the following one-term expression:

$$\frac{u}{U} = (\cosh \beta a - \cosh \beta z) \Big/ \left[\cosh \beta a - \frac{1}{\beta a}(\sinh \beta a)\right] \tag{19}$$

The principal numerical results are tabulated in Table 1 for six aspect ratios. The (βa)-values are plotted in Fig. 3.

Pressure Drop

In the analysis made by Langhaar [3], the method of calculating the pressure drop was to multiply the boundary-layer equation (2) by $u\,dx\,dy$ and then integrate across the section. From a physical viewpoint, this method amounts to an energy balance taking into account the energy dissipation as heat. An equally valid procedure is to integrate the boundary-layer equation directly, and calculate the pressure-drop term. The latter procedure is based on the momentum principle. When the boundary-layer equation is solved exactly, these two procedures lead to identical results. Since equation (5) from which the velocity profile is obtained is a linearized form of the Navier-Stokes equation, it can be regarded as a function-generating device. The solution represented by equation (9) or (18) with the βa-values tabulated in Table 1 satisfies the momentum principle, equation ($4a$), exactly and the boundary-layer equation (2) only partially. It is therefore natural to expect different pressure-drop results when calculated according to these two methods.

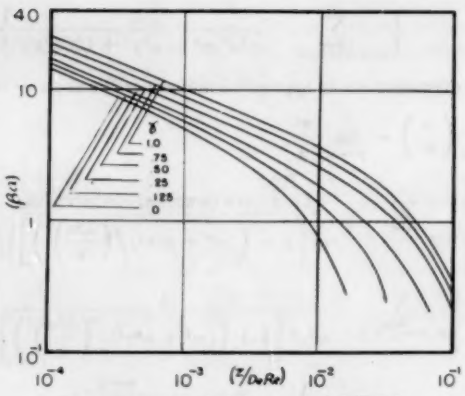

Fig. 3 Variation of (βa)-value with $(z/D_e Re)$

In the present analysis, the pressure drop is directly calculated from equation (12); i.e., based on the momentum principle, hence

$$(p_{z=0} - p_z)/(\rho U^2/2) = \left[\left(\frac{u_0}{U}\right)^2 - 1\right] + \frac{2\nu}{U^2}\int_0^z (-\nabla^2 u)_0 dz \tag{20}$$

The reason for not using the energy principle is that it involves the use of the integral $\int_A u^3\,dx\,dy$ for which the numerical work would be excessive. The results of the calculated pressure drops are also tabulated in Table 1.

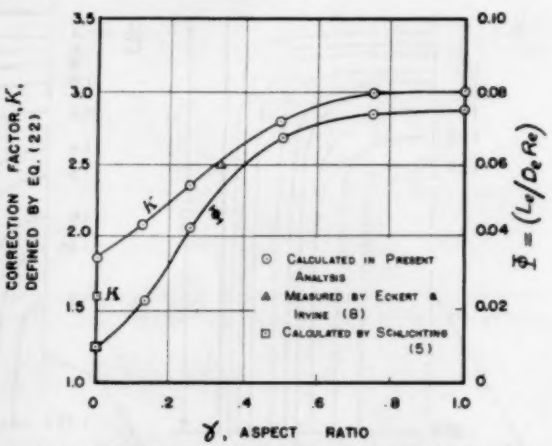

Fig. 4 Entrance lengths and pressure-drop correction factors. (Note: The experimental point △ should be lowered to a value of 2.3 for K, as the authors of [8] have so informed.)

Table 1 Dimensionless velocity, pressure-drop, and axial distance relationships

$F_2 = \left(\frac{u_0}{U}\right)$, $F_4 = (z/D_e\mathrm{Re}) \times 10^{-3}$, $F_5 = (p_{z=0} - p_z)/(^1/_{2\rho}U^2)$

	$\gamma = 1.0$			$\gamma = 0.75$			$\gamma = 0.50$			$\gamma = 0.25$			$\gamma = 0.125$			$\gamma = 0$		
(βa)	F_2	F_4	F_5	F_2	F_4	F_5	F_2	F_4	F_5	F_2	F_4	F_5	F_2	F_4	F_5	F_2	F_4	F_5
∞	1.0000	0	0	1.0000	0	0	1.0000	0	0	1.0000	0	0	1.0000	0	0	1.0000	0	0
20	1.1072	18	0.2422	1.0930	14	0.1948	1.0792	10	0.1681	1.0658	7	0.1344	1.0592	6	0.1219	1.0526	4	0.1079
10	1.2302	98	0.5135	1.1981	71	0.4356	1.1676	50	0.3634	1.1386	34	0.2965	1.1246	27	0.2649	1.1110	21	0.2343
8	1.2972	172	0.6831	1.2551	124	0.5756	1.2151	86	0.4766	1.1774	57	0.3866	1.1595	45	0.3446	1.1421	35	0.3046
6	1.4108	348	0.9952	1.3533	251	0.8337	1.2961	172	0.6820	1.2430	112	0.5468	1.2180	89	0.4853	1.1941	69	0.4274
5	1.4974	532	1.2576	1.4304	388	1.0545	1.3597	263	0.8554	1.2934	168	0.6784	1.2625	132	0.5993	...	...	...
4	1.6113	857	1.6482	1.5368	638	1.3923	1.4483	431	1.1202	1.3616	269	0.8726	1.3218	208	0.7642	1.2842	159	0.6636
3.5	1.6793	1110	1.9148	1.6033	840	1.6293	1.5049	569	1.3081	1.4040	349	1.0057	1.3578	267	0.8746	.....	...	...
3.0	1.7537	1459	2.2477	1.6790	1129	1.9325	1.5713	771	1.5526	1.4526	462	1.1742	1.3982	348	1.0112	1.3477	260	0.8649
2.75	1.7926	1681	2.4451	1.7200	1317	2.1158	1.6084	907	1.7036	1.4794	538	1.2762	1.4199	400	1.0919	...	...	...
2.50	1.8321	1946	2.6676	1.7626	1546	2.3253	1.6479	1076	1.8793	1.5076	630	1.3937	1.4424	464	1.1829	1.3825	338	1.0121
2.25	1.8716	2262	2.9198	1.8063	1825	2.5659	1.6898	1286	2.0856	1.5375	745	1.5306	1.4656	541	1.2866	...	...	...
2.00	1.9105	2642	3.2077	1.8503	2167	2.8442	1.7335	1555	2.3303	1.5688	893	1.6929	1.4893	636	1.4060	1.4174	448	1.1611
1.80	1.9407	3003	3.4688	1.8853	2497	3.0996	1.7693	1822	2.5605	1.5947	1041	1.8465	1.5084	729	1.5160	1.4308	529	1.2369
1.60	1.9694	3428	3.7640	1.9193	2893	3.3908	1.8054	2151	2.8295	1.6211	1226	2.0282	1.5274	842	1.6426	1.4436	567	1.3207
1.40	1.9964	3934	4.1016	1.9518	3370	3.7267	1.8409	2560	3.1474	1.6479	1463	2.2472	1.5461	984	1.7911	1.4556	644	1.4143
1.20	2.0210	4544	4.4945	1.9819	3955	4.1203	1.8751	3077	3.5292	1.6743	1771	2.5176	1.5641	1162	1.9694	1.4665	733	1.5191
1.00	2.0429	5297	4.9630	2.0091	4685	4.5926	1.9070	3740	3.9981	1.6998	2182	2.8616	1.5810	1395	2.1902	1.4763	845	1.6429
0.90	2.0526	5737	5.2315	2.0214	5116	4.8647	1.9217	4140	4.2730	1.7119	2437	3.0681	1.5890	1537	2.3210	1.4806	910	1.7126
0.80	2.0615	6236	5.5324	2.0326	5607	5.1702	1.9354	4602	4.5848	1.7234	2738	3.3077	1.5964	1708	2.4710	1.4845	983	1.7900
0.70	2.0694	6812	5.8745	2.0428	6176	5.5181	1.9479	5142	4.9433	1.7341	3098	3.5884	1.6033	1901	2.6454	1.4881	1067	1.8769
0.65	2.0730	7132	6.0635	2.0474	6493	5.7104	1.9536	5446	5.1428	1.7391	3303	3.7468	1.6065	2013	2.7433	1.4897	1114	1.9248
0.60	2.0764	7480	6.2679	2.0517	6838	5.9185	1.9590	5778	5.3593	1.7439	3530	3.9205	1.6095	2137	2.8502	1.4912	1165	1.9765
0.55	2.0795	7854	6.4868	2.0557	7213	6.1433	1.9641	6143	5.5950	1.7483	3781	4.1112	1.6123	2273	2.9672	1.4926	1221	2.0324
0.50	2.0824	8266	6.7271	2.0594	7628	6.3900	1.9688	6546	5.8545	1.7525	4061	4.3230	1.6150	2425	3.0968	1.4938	1283	2.0938
0.45	2.0850	8712	6.9860	2.0628	8082	6.6598	1.9730	6994	6.1410	1.7564	4376	4.5588	1.6174	2594	3.2405	1.4950	1352	2.1623
0.40	2.0873	9209	7.2737	2.0658	8591	6.9610	1.9769	7500	6.4623	1.7599	4733	4.8254	1.6196	2786	3.4025	1.4960	1427	2.2359
0.375	2.0884	9563	7.4768	2.0672	8912	7.1480	1.9787	7797	6.6502	1.7615	4942	4.9803	1.6206	2902	3.4994	...	...	...
0.350	2.0894	9851	7.6426	2.0685	9209	7.3225	1.9803	8093	6.8375	1.7630	5153	5.1372	1.6216	3015	3.5944	1.4970	1518	2.3249
0.325	2.0903	10084	7.7773	2.0697	9492	7.4890	1.9819	8394	7.0276	1.7645	5371	5.2983	1.6225	3128	3.6893	...	...	...
0.300	2.0912	10333	7.9211	2.0708	9559	7.5321	1.9833	8600	7.1597	1.7658	5536	5.4219	1.6233	3192	3.7438	1.4978	1611	2.4154
0.275	2.0920	10646	8.1011	2.0718	9912	7.7389	1.9846	8967	7.3900	1.7670	5801	5.6178	1.6241	3333	3.8609	...	...	...
0.250	2.0927	11987	8.8621	2.0728	10771	8.2394	1.9859	9608	7.7902	1.7682	6235	5.9353	1.6248	3604	4.0852	1.4984	1695	2.4979
0.225	2.0934	13020	9.4495	2.0737	11519	8.6695	1.9870	10211	8.1667	1.7692	6652	6.2409	1.6255	3852	4.2901	...	...	...
0.200	2.0939	17977	12.2597	2.0744	13600	9.8702	1.9880	10992	8.6523	1.7701	7043	6.5273	1.6260	4288	4.6487	1.4990	2059	2.8472
0	2.0971	∞	∞	2.0777	∞	∞	1.9909	∞	∞	1.7728	∞	∞	1.6280	∞	∞	1.5000	∞	∞

Table 2 Characteristic values for $(u_0/u_\infty) = 0.99$

γ	Φ	(βa)	K	C_{fRe}
1.0	0.0752	0.590	3.02	56.85
0.75	0.0735	0.533	3.00	57.83
0.50	0.0660	0.485	2.80	62.10
0.25	0.0427	0.470	2.36	72.83
0.125	0.0227	0.550	2.10	82.25
0	0.0099	0.793	1.85	96.00

Results and Discussion

Entrance Length. Since, in the present analysis, the velocity profile as expressed by equation (9) or (18), changes from a uniform profile to that of the fully developed flow gradually, the entrance length L_e is therefore defined, as is conventionally done, as that length where the center-line velocity u_0 is 99 per cent of the fully established velocity u_∞. The latter is given by equation (18) with $x = y = \beta = 0$. Data contained in Table 1 are used for determining the entrance lengths and the results are shown in Table 2.

The values shown in Table 2 are also plotted in Fig. 4 for the purpose of interpolation. The variations of the center-line velocities (u_0/U) for different aspect ratios are shown graphically as function of the dimensionless distance $(z/D_e\mathrm{Re})$ in Fig. 5.

For a comparison with the existing data, the values reported by Schlichting [5] and Sparrow [6] are recited here. The entrance

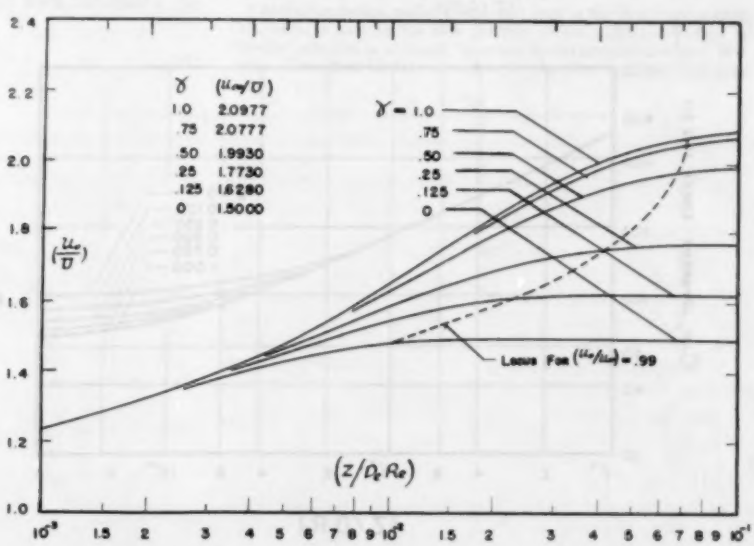

Fig. 5 Center-line velocity variations

lengths are 0.0100 and 0.0065 for $\gamma = 0$, according to these sources. Hahnemann and Ehret's [7] value is 0.0064.[3] Comparison with Sparrow's data is not made because of the different approaches used between his analysis and that herein employed; while the value indicated by Schlichting [5] is in complete agreement with the present result. A further comparison is made in Fig. 6 in which the center-line velocities for $\gamma = 0$ from Schlichting [5] and computed from equation (19) are shown. The agreement in values is quite satisfactory, noting that a log-scale has been used for the dimensionless distance $(z/D_e\mathrm{Re})$, thereby magnifying possible discrepancies.

Pressure Drops. The pressure drops as expressed in equation (20) and tabulated in Table 1 are not convenient for engineering use. For this purpose, the following two equations are used to express the pressure-loss terms:

$$(p_{z=0} - p_z)/(\rho U^2/2) = (C_{ap}/\mathrm{Re})(z/D_e) \qquad (21)$$

and

$$(p_{z=(-)} - p_z)/(\rho U^2/2) = (C_{ast}/\mathrm{Re})(z/D_e) + K \qquad (22)$$

In equation (21), the ratio (C_{ap}/Re) is the ordinary friction factor f. For large z, $C_{ap} \to C_{ast}$. The value of C_{ast} is, in the case of a circular tube, 64; and, in the case of a pair of parallel plates, 96. The values of C_{ap} are obtained from Table 1 and plotted in Fig. 7 for different aspect ratios with the dimensionless distance as abscissa. In equation (22), the symbol $p_{z=(-)}$ is used to denote the pressure of a fluid upstream of the duct entrance. Thus the difference between $p_{z=(-)}$ and $p_{z=0}$ is one velocity head $(\rho U^2/2)$. The use of equation (22) is convenient when the duct length is greater than the entrance length L_e. It treats the entire duct length as if in the region of the fully developed flow and the pressure drop so calculated is modified by a correction factor K. The K-factors are reduced from Table 1 and shown in Table 2 and Fig. 4 for interpolation.

Eckert and Irvine [8] reported an experimentally measured value of 2.3 (average of 8 measurements) in a duct of aspect ratio (1/3); Schlichting [5] and Goldstein [1] give values of 1.601 and 1.614 for $\gamma = 0$. These latter values as noted in Fig. 4, are lower than the values of 1.850 as obtained in the present analysis.

The discrepancy between the present value for $\gamma = 0$, of $K = 1.850$ and $K = 1.601$ given by Schlichting [5] can be traced back to the different asymptotic friction factors obtained from these two analyses:

Since in the present analysis, the pressure drop is evaluated directly from equation (12). For $\gamma = 0$, the equation reads

[3] The nature of their analysis is unknown as their paper is unavailable to the author.

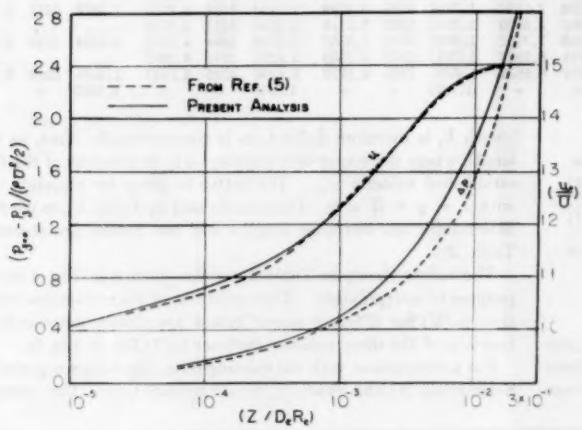

Fig. 6 Comparison with Schlichting's [5] data for $\gamma = 0$

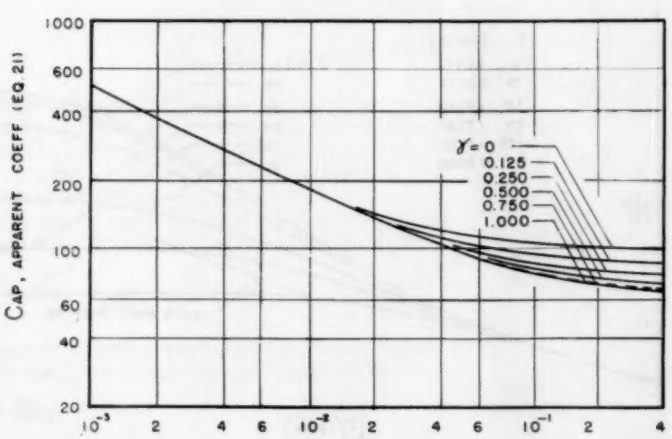

Fig. 7 Apparent coefficient C_{ap}

$$u_0 \frac{\partial u_0}{\partial z} = -\frac{1}{\rho}\frac{\partial p}{\partial z} + \nu\left(\frac{\partial^2 u}{\partial x^2}\right)_0 \tag{23}$$

and the center-line velocity is given by equation (19) with $x = 0$.

For large βa-values, i.e., small z, it can be seen from Fig. 3 that

$$(\beta a)^2 \approx [1.72 \times 10^{-2}/(z/D_e\mathrm{Re})] \tag{24}$$

Now

$$\frac{\partial u_0}{\partial z} = \frac{\partial u_0}{\partial(\beta a)}\frac{\partial(\beta a)}{\partial z} \tag{25}$$

equations (19) and (24) give, for large (βa),

$$\frac{\partial u_0}{\partial(\beta a)} = -\frac{U}{(\beta a)^2}$$

and

$$\frac{\partial(\beta a)}{\partial z} = -[(1.72 \times 10^{-2})^{1/2}]/[2z(z/D_e\mathrm{Re})^{1/2}]$$

Hence,

$$\frac{\partial u_0}{\partial z} \approx \frac{U}{2}\,[1/(1.72 \times 10^{-2})]^{1/2}(z/D_e\mathrm{Re})^{1/2}(1/z) \tag{26}$$

from which the following is obtained:

$$u_0 \doteq U[1 + 7.61(z/D_e\mathrm{Re})^{1/2}] \tag{27}$$

In equation (23), the term $(\partial^2 u/\partial x^2)_0$ vanishes faster than $\partial u_0/\partial z$ as given by equation (26), and can be ignored. Therefore

$$\frac{\partial p}{\partial z} = -\left(\frac{\rho U^2}{2}\right)[1 + 7.61(z/D_e\mathrm{Re})^{1/2}][7.61(z/D_e\mathrm{Re})]^{1/2}(1/z) \tag{28}$$

Accordingly,

$$(p_{z=0} - p_z)/(\tfrac{1}{2}\rho U^2) \approx 15.2(z/D_e\mathrm{Re})^{1/2} \tag{29}$$

valid for small z.

The apparent coefficient of friction as defined by equation (21) is therefore

$$C_{ap}(z/D_e\mathrm{Re})^{1/2} \to 15.2 \tag{30}$$

On the other hand, Schlichting's solution gives, for small z, the center-line velocity as

$$u_0 = U[1 + 6.91(z/D_e\mathrm{Re})^{1/2} + \ldots] \tag{31}$$

for which the apparent coefficient is given by

$$C_{ap}(z/D_e\mathrm{Re})^{1/2} \to 13.8 \tag{32}$$

which is in agreement with the value determined by Shapiro [4] for circular pipes.

It is to be noted that although Schlichting's work[4] was based on Blasius' solution, his solution as well as that of the present analysis are both invalidated as z approaches zero. The relative merits of both sets of data cannot be ascertained in the absence of experimental data.

Acknowledgment

The author wishes to thank Professor S. M. Marco, chairman, Department of Mechanical Engineering, for his interest and his effort in obtaining a grant from the Engineering Experiment Station, The Ohio State University. The work reported herein was supported in part by the said grant.

References

1 S. Goldstein, editor, "Modern Developments in Fluid Dynamics," Oxford University Press, London, England, vol. 1, 1938, p. 304.

2 L. Schiller, "Die Entwicklung der laminaren Geschwindigkeitverteilung under ihre Bedentung für Zahigkeitmessungen," *Zeitschrift für angewandte Mathematik und Mechanik*, vol. 2, 1922, p. 96.

3 H. L. Langhaar, "Steady Flow in the Transition Length of a Straight Tube," JOURNAL OF APPLIED MECHANICS, vol. 9, TRANS. ASME, vol. 64, 1942, p. A-55.

4 A. H. Shapiro, et al., "Friction Factor in the Laminar Entry Region of a Round Tube," Proceedings of the Second U. S. National Congress of Applied Mechanics, ASME, 1954, p. 733.

5 H. Schlichting, "Boundary Layer Theory," McGraw Hill Book Company, Inc., New York, N. Y., 1955, p. 146; also, "Laminare Kanaleinlaufstromung," *Zeitschrift für angewandte Mathematik und Mechanik*, vol. 14, 1934, p. 368.

6 E. M. Sparrow, "Analysis of Laminar Forced Convection Heat Transfer in Entrance Region of Flat Rectangular Ducts," NACA TN 3331, 1955.

7 H. Hahnemann and L. Ehret, "Der Druckverlust der laminaren Stromung in der Anlaufstrecke von geraden, eben Spalten," *Jahrbuch der deutschen Luftfahrtforschung*, 1941, p. 21.

8 E. R. G. Eckert and T. F. Irvine, Jr., "Incompressible Friction Factor, Transition and Hydrodynamic Entrance Length Studies of Ducts With Triangular and Rectangular Cross-Sections," WADC Technical Report 58-85, ASTIA D. N. AD-151027, 1957.

9 G. F. Carrier, "The Boundary Layer in a Corner," *Quarterly of Applied Mathematics*, vol. 4, 1946-1947, p. 367.

[4] Attention is also called to the fact that in the Schlichting analysis $(\partial^2\mu/\partial x^2)_0$ is zero in the fore portion of the entrance region where Blasius' solution is utilized; whereas in the present analysis, it is not zero. This then further accounts for the increased pressure drop.

Stability of a Turbine-Generator Rotor Including the Effects of Certain Types of Steam and Bearing Excitations[1]

A. H. LANDZBERG
IBM Research Center,
Mohansic Laboratory,
Yorktown Heights, N. Y.
Assoc. Mem. ASME

The effects of certain steam forces and bearing oil-film forces on vibration stability of a turbine-generator rotor are considered. A matrix method for systematically calculating the characteristic equation of a real rotor is developed with the aid of complex notation. The matrices are 4 × 4 in size. Pedestal effects are not included. A simple example is worked out and the results are compared to those obtained by another author. Complete agreement is obtained in the determination of the characteristic equation.

Introduction

THE problem of rotor instability has been a troublesome one for many years in the design of steam turbine-generator rotors. There have been many instances in which rotors have been found to vibrate with large amplitudes at or near the so-called "first turbine critical speed," while the rotation velocity was considerably higher. This behavior is in contrast to the usual type of shaft resonance in which both the vibration and rotation frequencies are known to be the same. It is really a problem of vibration instability, and in the past it has been solved in a practical way by making design and operating modifications which usually result in a change in critical speed and/or in an increase in bearing damping.

As to basic information, many investigations have been made in an attempt to understand better the fundamentals of rotor instability. This includes both laboratory investigations and analytical studies. Most of these have been concerned with "oil whip," both the critical-speed type, and the half running-speed type. From an analytical viewpoint, even if one or more of the available methods [1, 2, 3, 4, 7, 9, 11][2] for dealing with the oil-whip problem were precisely correct, it would still be impossible to apply them *per se* to the calculation of vibration stability of a large turbine-generator rotor. This is due to the complexity of such a system, with its multiple rotors and bearings, and dynamic behavior which is considerably more involved than that of the rather simple one and two-bearing configurations that have been studied in the past. This paper is concerned, therefore, with the extension of previous work on oil whip to include the actual dynamic characteristics of an entire turbine-generator rotor.

Owczarek [8] has described the possible harmful effects of a certain type of steam force (at right angles to the shaft displacement) which can feed energy into a whirling shaft. It is postulated that this force, when acting together with oil-whip forces, may produce a more substantial instability than oil whip alone, and cut down even further the speed range in which smooth operation can be obtained. The form of this steam-force term is such that it is readily included in this analysis along with all the other dynamic forces. In fact, the method described herein is

[1] The work described in this paper was carried out while the author was employed by the Large Steam Turbine-Generator Department, General Electric Company, Schenectady, N. Y.

Presented at the Summer Conference of the Applied Mechanics Division, University Park, Pa., June 20–22, 1960, of THE AMERICAN SOCIETY OF MECHANICAL ENGINEERS.

Discussion of this paper should be addressed to the Secretary, ASME, 29 West 39th Street, New York, N. Y., and will be accepted until October 10, 1960, for publication at a later date. Discussion received after the closing date will be returned.

NOTE: Statements and opinions advanced in papers are to be understood as individual expressions of their authors and not those of the Society. Manuscript received by ASME Applied Mechanics Division, July 9, 1959. Paper No. 60—APM-9.

[2] Numbers in brackets designate References at end of paper.

Nomenclature

A = recurrence matrix relating adjacent station vectors on shaft, given in Equation (20), mixed units
a = steam-force constant, lb per in.
B = matrix of shaft properties given in Equation (22), mixed units
b = constant defined in Equation (14), lb per in.
C = matrix of shaft properties given in Equation (23), mixed units
D = matrix defined in Equation (25), mixed units
E = modulus of elasticity, psi
$F(\lambda)$ = imaginary part of characteristic equation, defined in Equation (45), in. lb^2
$f(\lambda)$ = real part of frequency function g, given in Equation (14), lb per in.
$G(\lambda)$ = real part of characteristic equation, defined in Equation (45), in. lb^2
$g(\lambda)$ = complex frequency function given in Equation (14), lb per in.
I = area moment of inertia of shaft cross section, in.^{4}
i = denotes imaginary part, $\sqrt{-1}$
k = oil-film constant, lb per in.
k' = oil-film constant, lb per in.
M = complex shaft moment, in. lb
m = mass, lb sec^2/in.
$P(\lambda)$ = real part of characteristic equation in sample problem, lb
$Q(\lambda)$ = imaginary part of characteristic equation in sample problem, lb
R = complex station vector defined in Equation (18), mixed units

(Continued on next page)

such, that any force in a rotating system can be included with equal facility, provided it is linear with the shaft displacement or its derivatives.

The bearing-force terms used herein are based on the work of Poritsky [9] and Boeker and Sternlicht [1]. This representation is the most satisfactory one available although, as has been pointed out in [1], it is primarily suited to vertical shafts with axisymmetric bearings. In this analysis the displacements, velocities, and accelerations are measured from a steady-state operating point (the position that the shaft would have if there were no lateral oscillations) rather than the bearing center as with a vertical shaft. This bearing formulation is best suited for lightly loaded bearings, and it is fortuitous indeed that such bearings are the critical ones (it is known from many years of operating experience that lightly loaded bearings are those which are most prone to vibration instability). It should be noted that Schnittger [12] has successfully used a modification of this bearing-force representation in his paper concerning instability of a double-spool gas-turbine rotor.

Analysis

The analysis developed in this paper is one in which the characteristic equation of the vibrating rotor is systematically generated in a method which is somewhat similar to the Myklestadt-Prohl technique [10]. This equation may then be studied by known methods for its stability characteristics [9]. Alternately, it may be examined in greater detail by actually solving for its roots with the aid of existing digital-computer programs.

In this analysis the bearing pedestals are regarded as being rigid; flexibility exists only in the oil films that support the shaft. This permits a comparatively simple formulation of the governing equations, and it enables one to generate the characteristic equation in a rather straightforward manner. Pedestal effects such as elasticity, damping, and mass could also be included; however, this would lead to a considerable increase in complexity. Prior practical experience both with respect to turbine operation and also with similar computational problems indicates that it is not warranted at this time.

The analysis is concerned with the onset of instability. Thus the motion of the rotor is assumed to be of small amplitude, allowing for a linearization of an otherwise nonlinear system of equations.

The method is developed with the aid of complex notation, as originally employed by Poritsky [9]. This allows for a concise statement of the governing equations, in spite of the fact that the rotor motion has components along two mutually perpendicular axes. The only instances in which complex notation will not be used are in those places where improved clarity can be achieved by writing out the real relations.

Forces Acting on Shaft. The forces considered in this section result from oil-film behavior, steam flow, and rotor inertia.

Bearing Forces. Using a notation similar to that of Boeker and Sternlicht [1] the components of bearing force V^B in the x and y-directions are

$$V_x^B = -\frac{2k}{\omega}\dot{x} - k'x - ky \tag{1}$$

$$V_y^B = -\frac{2k}{\omega}\dot{y} - k'y + kx$$

in which k and k' are constants and ω is the speed of rotation. The quantities x and y are shaft-displacement components measured from the steady-state equilibrium position and the dot notation indicates the time derivative. Even for a steady-state whirl it can be seen that the first two terms represent conventional dashpot and spring-restoring forces while the third term is a coupling term which is capable of feeding energy into the shaft. It is precisely this term, and a similar one that appears for the steam forces, which lead to the present instability problem.

By introducing the complex displacement z,

$$z = x + iy \tag{2}$$

where i is the $\sqrt{-1}$, and defining a complex force V_z,

$$V_z = V_x + iV_y \tag{3}$$

one may consolidate Equations (1)

$$V_z^B = -\frac{2k}{\omega}\dot{z} - k'z + ikz \tag{4}$$

Now, it is assumed that the motion of the shaft is of an exponential form

$$z = \bar{z}e^{\lambda t} \tag{5}$$

in which $\bar{z}$ is the amplitude, and λ is the complex frequency of the motion. Equation (5) leads to the velocity and acceleration expressions:

$$\dot{z} = \lambda z, \quad \ddot{z} = \lambda^2 z \tag{6}$$

Substituting the first of Equations (6) in Equation (4) gives

$$V_z^B = \left[-\left(\frac{2k}{\omega}\lambda + k'\right) + ik\right]z \tag{7}$$

the desired expression for the bearing force.

Nomenclature

u = complex vector associated with a particular power of frequency, λ, defined in Equation (26), mixed units
V = complex shear force, lb
x, y = displacements of shaft center from steady-state equilibrium position, in.
z = complex displacement, $x + iy$, in.
β = shaft constant given in Equation (16), 1/in. lb
Δ = length of shaft element, in.
$\Delta(\lambda)$ = characteristic equation
θ = slope of shaft, radians
λ = complex frequency, radians per sec (rps)
ω = rotation frequency, radians per sec (rps)

Subscripts

i = defines degree of λ-term with which u-vector is associated
l = last station on shaft
n = index of station numbers on shaft
r = root of characteristic equation
x, y = real components of complex vector
z = complex shear force
0 = left-end values

Superscripts

B = bearing forces
I = inertia force
S = steam force
I, II, III, IV = calculated quantities associated with starting vectors given in Equation (33)
., dot notation indicating time derivative
—, bar notation indicating amplitude of z or conjugate of a quantity

It should be noted that the constants k and k' can be determined in a variety of ways. The most convenient are (a) steady-state pure journal rotation under a static load, and (b) whirl motion as with unbalance. Many papers giving calculated and experimental data on steady-state behavior of bearings can provide data for the first technique. For method (b) the data of Hagg and Sankey [5, 6] are quite useful. The calculations of Sternlicht [13] provide yet another source of information for the evaluation of these constants. All that is required for method (a) is the slope of the load-eccentricity curve in the vicinity of the steady-state operating point.

Steam Force. The components of steam force V^s, which have been recognized as potentially harmful [8], are represented mathematically in the form:

$$V_x^s = -ay \qquad V_y^s = ax \tag{8}$$

in which a is a constant. These components stem from a whirl displacement of the shaft. Such a displacement increases steam-leakage area along one half the periphery of a given turbine wheel and decreases the area on the other half. These area variations are accompanied by perturbations in leakage flow, and hence in the main stream flow also. The latter results in a net force on the shaft at right angles to the whirl displacement and in the direction of the whirl. As such, this force is capable of feeding energy into the whirling motion, and may be an important factor in determination of shaft instability. As with the bearing-force components, Equations (8) may be written in complex notation

$$V_z^s = iaz \tag{9}$$

Inertial Force. Using the principle of d'Alembert, the components of the inertia force V^I acting on the shaft may be written:

$$V_x^I = -m\ddot{x} \tag{10}$$

$$V_y^I = -m\ddot{y} \tag{11}$$

On combination, using the second of Equations (6), V_z^I is obtained

$$V_z^I = -m\lambda^2 z \tag{12}$$

All Forces. At a given station on the shaft, say the nth station, one or more of the foregoing forces may be acting. Hence, it is convenient to add up all the forces, yielding V_m

$$V_m = g_n(\lambda) z_n \tag{13}$$

where

$$g_n(\lambda) = f_n(\lambda) + ib_n$$

$$f_n(\lambda) = -\left(m_n\lambda^2 + \frac{2k_s}{\omega}\lambda + k_n'\right) \tag{14}$$

$$b_n = k_n + a_n$$

and the meaning of the subscript, n, is obvious. Henceforth, the subscript z will be dropped as it leads to no ambiguity.

Recurrence Relations for Shaft. The recurrence relations to be used, in satisfying the equilibrium and compatibility conditions for the shaft, are those given by Prohl [10]. A typical section of the shaft is shown in Fig. 1. The recurrence relations are:

$$V_{n+1} = V_n + g_n z_n$$

$$M_{n+1} = M_n + V_{n+1}\Delta_{n+1}$$

$$\theta_{n+1} = \frac{\beta_{n+1}}{2}(M_n + M_{n+1}) + \theta_n \tag{15}$$

$$z_{n+1} = \frac{\beta_{n+1}}{3}\left(M_n + \frac{M_{n+1}}{2}\right)\Delta_{n+1} + \theta_n\Delta_{n+1} + z_n \tag{15 cont.}$$

in which Δ denotes length of shaft, M denotes the complex moment, and θ denotes the complex slope. The constant β_{n+1} is short for

$$\beta_{n+1} = \frac{\Delta_{n+1}}{E_{n+1}I_{n+1}} \tag{16}$$

Now, Equations (15) may be put into a more suitable form by elimination of V_{n+1} and M_{n+1} on the right-hand side. This results in the equations:

$$\begin{aligned}
V_{n+1} &= V_n + g_n z_n \\
M_{n+1} &= \Delta_{n+1}V_n + M_n + g_n\Delta_{n+1}z_n \\
\theta_{n+1} &= \frac{\beta_{n+1}\Delta_{n+1}}{2}V_n + \beta_{n+1}M_n + \theta_n + \frac{g_n\beta_{n+1}\Delta_{n+1}}{2}z_n \\
z_{n+1} &= \frac{\beta_{n+1}\Delta_{n+1}^2}{6}V_n + \frac{\beta_{n+1}\Delta_{n+1}}{2}M_n + \Delta_{n+1}\theta_n \\
&\quad + \left(\frac{\beta_{n+1}g_n\Delta_{n+1}^2}{6} + 1\right)z_n
\end{aligned} \tag{17}$$

which can easily be put in matrix form.

Matrix Representation of Recurrence Relations. If a complex vector R is defined

$$R = \begin{bmatrix} V \\ M \\ \theta \\ z \end{bmatrix} \tag{18}$$

then Equation (17) can be written

$$R_{n+1} = A_n R_n \tag{19}$$

where A_n is the square, 4×4, matrix

$$A_n = \begin{bmatrix} 1 & 0 & 0 & g_n \\ \Delta_{n+1} & 1 & 0 & g_n\Delta_{n+1} \\ \dfrac{\beta_{n+1}\Delta_{n+1}}{2} & \beta_{n+1} & 1 & \dfrac{g_n\beta_{n+1}\Delta_{n+1}}{2} \\ \dfrac{\beta_{n+1}\Delta_{n+1}^2}{6} & \dfrac{\beta_{n+1}\Delta_{n+1}}{2} & \Delta_{n+1} & \left(\dfrac{\beta_{n+1}g_n\Delta_{n+1}^2}{6} + 1\right) \end{bmatrix} \tag{20}$$

Furthermore, A_n can be split into two parts for the purpose of separating out the frequency-dependent parts:

$$A_n = B_n + g_n(\lambda)C_n \tag{21}$$

in which $g_n(\lambda)$ is the same g that was defined in Equation (14) and B_n and C_n are real square matrices.

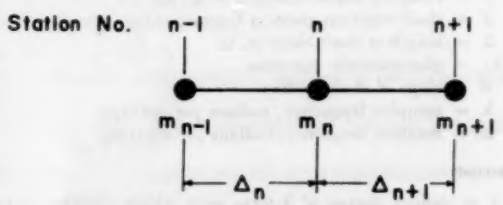

Fig. 1 Notation for stations on shaft

$$B_n = \begin{bmatrix} 1 & 0 & 0 & 0 \\ \Delta_{n+1} & 1 & 0 & 0 \\ \dfrac{\beta_{n+1}\Delta_{n+1}}{2} & \beta_{n+1} & 1 & 0 \\ \dfrac{\beta_{n+1}\Delta_{n+1}^2}{6} & \dfrac{\beta_{n+1}\Delta_{n+1}}{2} & \Delta_{n+1} & 1 \end{bmatrix} \tag{22}$$

$$C_n = \begin{bmatrix} 0 & 0 & 0 & 1 \\ 0 & 0 & 0 & \Delta_{n+1} \\ 0 & 0 & 0 & \dfrac{\beta_{n+1}\Delta_{n+1}}{2} \\ 0 & 0 & 0 & \dfrac{\beta_{n+1}\Delta_{n+1}^2}{6} \end{bmatrix} \tag{23}$$

To better show the frequency dependence of A_n, Equation (14) is now substituted in Equation (21), yielding

$$A_n = -m_n C_n \lambda^2 - \frac{2k_n}{\omega} C_n \lambda + D_n \tag{24}$$

in which D_n is

$$D_n = (B_n - k_n' C_n) + i b_n C_n \tag{25}$$

A_n, given in Equation (24), is now in a form convenient for the development of the characteristic equation.

At any station along the shaft the R-vector can be expressed as a polynomial in the frequency, λ. At the nth station, we have a polynomial, the degree of which is at most $2n$:

$$R_n = \sum_{i=0}^{2n} \lambda^i u_{n,i} \tag{26}$$

The maximum possible degree is $2n$ because of the quadratic form of A_n. The $u_{n,i}$ are complex vectors multiplying the powers of λ. The station numbers are taken to increase from left to right, with the left end (at a bearing) denoted as shown in Fig. 2. By substituting Equation (26) in Equation (19), and making use of Equation (24), it is possible to find a recurrence relation for the u-vectors. One obtains first

$$R_{n+1} = -m_n C_n \sum_{i=0}^{2n} \lambda^{i+2} u_{n,i} - \frac{2k_n}{\omega} C_n \sum_{i=0}^{2n} \lambda^{i+1} u_{n,i} + D_n \sum_{i=0}^{2n} \lambda^i u_{n,i} \tag{27}$$

But R_{n+1}, by analogy with Equation (26), can also be expressed with u-vectors having $n + 1$ in the subscript:

$$R_{n+1} = \sum_{i=0}^{2n+2} \lambda^i u_{n+1,i} \tag{28}$$

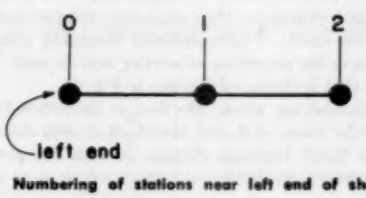

Fig. 2 Numbering of stations near left end of shaft

Since Equations (27) and (28) must be equivalent, one is led to equate the vector coefficients of the same powers of λ. This gives the desired recurrence relation for $u_{n+1,i}$

$$u_{n+1,i} = -m_n C_n u_{n,i-2} - \frac{2k_n}{\omega} C_n u_{n,i-1} + D_n u_{n,i} \qquad 0 \leq i \leq 2n+2 \tag{29}$$

Thus, $u_{n+1,i}$ may be easily generated from the u_n-vectors at the previous station. Equation (29) may be used very generally, except for the terminating vectors where one must use the special relations:

$$\begin{aligned} u_{n,-1} &= 0, \qquad u_{n,-2} = 0 \\ u_{n,2n+1} &= 0, \qquad u_{n,2n+2} = 0 \end{aligned} \tag{30}$$

which can be shown by expanding Equations (27) and (28).

Having the recurrence relation for the u-vectors, the R-vectors which are polynomials in λ may be successively generated by advancing, station by station, from the left end of the shaft to the right end. The final R-vector is obtained for the end station which is placed a distance, $\Delta = 0$, from the next-to-last station located at the right-end bearing. This simple trick is used to provide for the proper inclusion of the right-end bearing force.

Boundary Conditions and Characteristic Equation. The boundary conditions on the shaft are those which give free ends just beyond the terminal bearings. This requires vanishing shear forces and moments:

$$\begin{aligned} V &= V_x + iV_y = 0 \\ M &= M_x + iM_y = 0 \end{aligned} \tag{31}$$

at the ends of the shaft. It can thus be concluded that the x and y-components must separately be zero:

$$V_x = V_y = M_x = M_y = 0 \tag{32}$$

To meet the boundary conditions at both the left and right ends, the Myklestadt-Prohl method of superimposing linear solutions is employed [10]. In this case, one starts with four different left-end vectors:

$$R_0^{\mathrm{I}} = \begin{bmatrix} 0 \\ 0 \\ 1 \\ 0 \end{bmatrix}, \quad R_0^{\mathrm{II}} = i \begin{bmatrix} 0 \\ 0 \\ 1 \\ 0 \end{bmatrix}, \quad R_0^{\mathrm{III}} = \begin{bmatrix} 0 \\ 0 \\ 0 \\ 1 \end{bmatrix}, \quad R_0^{\mathrm{IV}} = i \begin{bmatrix} 0 \\ 0 \\ 0 \\ 1 \end{bmatrix} \tag{33}$$

The first two provide for unit slopes in the x and y-directions, respectively, and the last two for unit deflections. It can be seen from these that the appropriate free-end boundary conditions, at the left side of the shaft, are already built into the calculations. Starting with each of the foregoing, a vector polynomial can be calculated at the right end of the shaft. Denoting the last station by $n = l$, it is clear that the complete polynomial at this station (and other stations as well) consists of a linear sum of contributions from each of the four parts in (33); that is,

$$R_l = \theta_{x_0} R_l^{\mathrm{I}} + \theta_{y_0} R_l^{\mathrm{II}} + x_0 R_l^{\mathrm{III}} + y_0 R_l^{\mathrm{IV}} \tag{34}$$

where θ_{x_0}, θ_{y_0}, x_0, and y_0 are the left-end slopes and deflections. Using Equation (34), the right-end boundary equations may now be expressed:

$$\theta_{x0}V_l^{\mathrm{I}} + \theta_{y0}V_l^{\mathrm{II}} + x_0V_l^{\mathrm{III}} + y_0V_l^{\mathrm{IV}} = 0$$
$$\theta_{x0}M_l^{\mathrm{I}} + \theta_{y0}M_l^{\mathrm{II}} + x_0M_l^{\mathrm{III}} + y_0M_l^{\mathrm{IV}} = 0 \tag{35}$$

where the shear forces and moments are complex elements (polynomials in λ) taken from the R_l-vectors.

A considerable simplification can be made by observing that the R-vectors associated with R_0^{II} can be obtained by multiplying the corresponding vectors associated with R_0^{I} by i. This results from the fact that

$$R_0^{\mathrm{II}} = iR_0^{\mathrm{I}} \tag{36}$$

Since R_n^{I} and R_n^{II} are obtained by multiplication of R_0^{I} and R_0^{II}, respectively, by the same matrix product it follows also that

$$R_n^{\mathrm{II}} = iR_n^{\mathrm{I}} \tag{37}$$

and, in particular, that

$$R_l^{\mathrm{II}} = iR_l^{\mathrm{I}} \tag{38}$$

The same result is obviously true for R_l^{III} and R_l^{IV} as well, namely, that

$$R_l^{\mathrm{IV}} = iR_l^{\mathrm{III}} \tag{39}$$

One can immediately take advantage of Equations (38) and (39) to obtain, by inspection, the following relations:

$$V_l^{\mathrm{II}} = iV_l^{\mathrm{I}}, \qquad V_l^{\mathrm{IV}} = iV_l^{\mathrm{III}}$$
$$M_l^{\mathrm{II}} = iM_l^{\mathrm{I}}, \qquad M_l^{\mathrm{IV}} = iM_l^{\mathrm{III}} \tag{40}$$

Substituting Equations (40) in Equations (35) one obtains:

$$\theta_0V_l^{\mathrm{I}} + z_0V_l^{\mathrm{III}} = 0$$
$$\theta_0M_l^{\mathrm{I}} + z_0M_l^{\mathrm{III}} = 0 \tag{41}$$

two homogeneous equations in the two complex unknowns θ_0 and z_0 ($\theta_0 = \theta_{x0} + i\theta_{y0}$, $z_0 = x_0 + iy_0$). For a nontrivial solution to exist, Cramer's rule requires that the determinant of the coefficients must vanish. This leads to the equation

$$\Delta(\lambda) = V_l^{\mathrm{I}}M_l^{\mathrm{III}} - V_l^{\mathrm{III}}M_l^{\mathrm{I}} = 0 \tag{42}$$

which can be separated into its real and imaginary parts by using the notation:

$$V_l = V_{xl} + iV_{yl}$$
$$M_l = M_{xl} + iM_{yl} \tag{43}$$

This yields the characteristic equation, a polynomial in λ, with complex coefficients

$$\Delta(\lambda) = G(\lambda) + iF(\lambda) = 0 \tag{44}$$

in which

$$G(\lambda) = V_{xl}^{\mathrm{I}}M_{xl}^{\mathrm{III}} - V_{yl}^{\mathrm{I}}M_{yl}^{\mathrm{III}} - V_{xl}^{\mathrm{III}}M_{xl}^{\mathrm{I}} + V_{yl}^{\mathrm{III}}M_{yl}^{\mathrm{I}}$$
$$F(\lambda) = V_{xl}^{\mathrm{I}}M_{yl}^{\mathrm{III}} + V_{yl}^{\mathrm{I}}M_{xl}^{\mathrm{III}} - V_{xl}^{\mathrm{III}}M_{yl}^{\mathrm{I}} - V_{yl}^{\mathrm{III}}M_{xl}^{\mathrm{I}} \tag{45}$$

If one or more roots, λ_r, of Equation (44) have positive real parts, an exponentially increasing motion will occur; i.e., instability. The behavior of Equation (44) can be studied with the aid of the stability criterion given in [9], or alternately one may do a more complete job by solving for its roots with the aid of existing digital-computer programs.

An important point to note about Equation (45) is that only the I and III superscripts appear. Thus the actual numerical calculations are made with only two different starting vectors; the other two, used in the problem formulation, do not enter explicitly into the computations.

Equation (44) admits of another form which may be of some usefulness. By multiplying by $G(\lambda) - iF(\lambda)$, one obtains the real equation of double degree

$$G^2 + F^2 = 0 \tag{46}$$

Equation (46) has the same roots as does Equation (44), hence one can choose whichever equation is most convenient in computation. Multiplication of Equation (44) by $G(\lambda) - iF(\lambda)$ implies that Equation (46) contains not only the roots of Equation (44), but also the roots of

$$G(\lambda) - iF(\lambda) = 0 \tag{47}$$

The roots of this equation are extraneous to the stability problem. Two interesting characteristics of the foregoing equations will now be mentioned:

1 If Equation (46) has any purely real roots, they must occur in pairs. This follows from the fact that real roots require that both

$$F(\lambda_{\mathrm{real}}) = 0, \qquad G(\lambda_{\mathrm{real}}) = 0 \tag{48}$$

be satisfied simultaneously. Such roots would satisfy Equation (44), and also Equation (47), thus indicating their multiple nature.

2 The complex roots of Equation (46) must occur in conjugate pairs, since its coefficients are real. It can be shown rather simply that one of the pair is a root of Equation (44) and the other is a root of Equation (47). This follows when one takes the conjugate (denoted by bar notation) of Equation (44)

$$\overline{F(\lambda)} - i\overline{G(\lambda)} = 0 \tag{49}$$

and makes use of the properties

$$\overline{F(\lambda)} = F(\bar{\lambda}), \qquad \overline{G(\lambda)} = G(\bar{\lambda}) \tag{50}$$

to give

$$F(\bar{\lambda}) - iG(\bar{\lambda}) = 0 \tag{51}$$

Comparing Equations (47) and Equation (51) it is clear that if λ_r is a root of Equation (44), then $\bar{\lambda}_r$ is a root of Equation (47).

The utility of having an algebraic equation with real coefficients, Equation (46), is considerably offset by its increased degree.

Sample Problem—Simple Shaft With Symmetrical Vibrations

In this sample problem, the dynamical behavior of the simplest possible system will be examined—the symmetric vibrations of a single mass on a massless shaft with symmetric bearings. This example will allow comparison with results obtained by Poritsky [9]. A sketch of the system is shown in Fig. 3.

Formulation of the characteristic equation will be carried out by the method described in the analysis, modified slightly to permit introduction of the symmetry condition. Because of the simplicity of the problem, it will be worked out literally rather than for a specific numerical case. For a more complicated example this would obviously be impractical. To bring symmetry into the shaft vibrations, the calculation will proceed only to the center of the shaft. There, different boundary conditions from those given in the preceding subsection will be used. A sketch of the model that is employed is given in Fig. 4.

Three stations are taken; the first at the left-end bearing, the second at the mass, $m/2$, and the third at zero distance beyond $m/2$. The latter fictitious station, as with the previously discussed boundary conditions, is introduced so as to allow one to

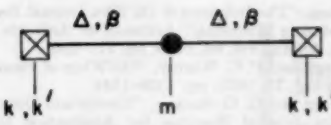

Fig. 3 Notation, simple shaft with lumped mass and symmetrical bearings

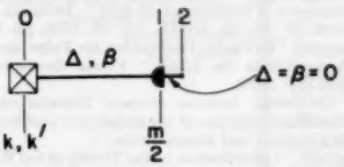

Fig. 4 Numbering of stations for simple shaft, termination at center

meet symmetry requirements. The system constants and matrices are:

First Section

$$m_0 = 0, \quad k_0 = k, \quad k_0' = k', \quad a_0 = 0, \quad \Delta_1 = \Delta, \quad \beta_1 = \beta$$

$$C_0 = \begin{bmatrix} 0 & 0 & 0 & 0 \\ 0 & 0 & 0 & \Delta \\ 0 & 0 & 0 & \frac{\beta\Delta}{2} \\ 0 & 0 & 0 & \frac{\beta\Delta^2}{6} \end{bmatrix} \tag{52}$$

$$D_0 = \begin{bmatrix} 1 & 0 & 0 & 0 \\ \Delta & 1 & 0 & 0 \\ \frac{\beta\Delta}{2} & \beta & 1 & 0 \\ \frac{\beta\Delta^2}{6} & \frac{\beta\Delta}{2} & \Delta & 1 \end{bmatrix} - (k' - ik) \begin{bmatrix} 0 & 0 & 0 & 1 \\ 0 & 0 & 0 & \Delta \\ 0 & 0 & 0 & \frac{\beta\Delta}{2} \\ 0 & 0 & 0 & \frac{\beta\Delta^2}{6} \end{bmatrix}$$

Second Section

$$m_1 = \frac{m}{2}, \quad k_1 = 0, \quad k_1' = 0, \quad a_1 = 0, \quad \Delta_2 = 0, \quad \beta_2 = 0$$

$$C_1 = \begin{bmatrix} 0 & 0 & 0 & 1 \\ 0 & 0 & 0 & 0 \\ 0 & 0 & 0 & 0 \\ 0 & 0 & 0 & 0 \end{bmatrix} \tag{53}$$

$$D_1 = \begin{bmatrix} 1 & 0 & 0 & 0 \\ 0 & 1 & 0 & 0 \\ 0 & 0 & 1 & 0 \\ 0 & 0 & 0 & 1 \end{bmatrix}$$

With these the final R-vector for Case I can be obtained easily. The result is

$$R_2^{\mathrm{I}} = -\frac{m}{2}\lambda^2 \begin{bmatrix} \Delta \\ 0 \\ 0 \\ 0 \end{bmatrix} + \begin{bmatrix} 0 \\ 0 \\ 1 \\ \Delta \end{bmatrix} \tag{54}$$

and for Case III the final R vector is

$$R_2^{\mathrm{III}} = \frac{mk}{\omega}\lambda^2 \begin{bmatrix} \frac{\beta\Delta^2}{6} \\ 0 \\ 0 \\ 0 \end{bmatrix} + \left\{ -\frac{m}{2} \begin{bmatrix} 1 \\ 0 \\ 0 \\ 0 \end{bmatrix} + \frac{m}{2}(k' - ik) \begin{bmatrix} \frac{\beta\Delta^2}{6} \\ 0 \\ 0 \\ 0 \end{bmatrix} \right\} \lambda^2 - \frac{2k}{\omega}\lambda \begin{bmatrix} 1 \\ \Delta \\ \frac{\beta\Delta}{2} \\ \frac{\beta\Delta^2}{6} \end{bmatrix} + \left\{ \begin{bmatrix} 0 \\ 0 \\ 0 \\ 1 \end{bmatrix} - (k' - ik) \begin{bmatrix} 1 \\ \Delta \\ \frac{\beta\Delta}{2} \\ \frac{\beta\Delta^2}{6} \end{bmatrix} \right\} \tag{55}$$

The symmetry requirements which are used as boundary conditions at $n = 2$ are for vanishing slope and shear force. Thus, in lieu of Equation (42), one obtains

$$\Delta(\lambda) = V_l^{\mathrm{I}}\theta_l^{\mathrm{III}} - V_l^{\mathrm{III}}\theta_l^{\mathrm{I}} = 0 \tag{56}$$

with the notation:

$$\begin{aligned} V_l &= V_{xl} + iV_{yl} \\ \theta_l &= \theta_{xl} + i\theta_{yl} \end{aligned} \tag{57}$$

Equation (56) yields the modified characteristic equation

$$\Delta(\lambda) = P(\lambda) + iQ(\lambda) = 0 \tag{58}$$

where now:

$$\begin{aligned} P(\lambda) &= V_{xl}^{\mathrm{I}}\theta_{xl}^{\mathrm{III}} - V_{yl}^{\mathrm{I}}\theta_{yl}^{\mathrm{III}} - V_{xl}^{\mathrm{III}}\theta_{xl}^{\mathrm{I}} + V_{yl}^{\mathrm{III}}\theta_{yl}^{\mathrm{I}} \\ Q(\lambda) &= V_{xl}^{\mathrm{I}}\theta_{yl}^{\mathrm{III}} + V_{xl}^{\mathrm{I}}\theta_{xl}^{\mathrm{III}} - V_{xl}^{\mathrm{III}}\theta_{yl}^{\mathrm{I}} - V_{yl}^{\mathrm{III}}\theta_{xl}^{\mathrm{I}} \end{aligned} \tag{59}$$

To obtain the final expression for $\Delta(\lambda)$ the elements $V_{xl}^{\mathrm{I}} \ldots$. $V_{xl}^{\mathrm{III}} \ldots$. are now extracted from Equations (54) and (55)

$$\begin{aligned} V_x^{\mathrm{I}} &= -\frac{m\Delta}{2}\lambda^2, \qquad \theta_x^{\mathrm{I}} = 1 \\ V_y^{\mathrm{I}} &= 0, \qquad \theta_y^{\mathrm{I}} = 0 \end{aligned} \tag{60}$$

and

$$\begin{aligned} V_x^{\mathrm{III}} &= \frac{mk\beta\Delta^2}{6\omega}\lambda^3 + \frac{m}{2}\left(\frac{k'\beta\Delta^2}{6} - 1\right)\lambda^2 - \frac{2k}{\omega}\lambda - k' \\ V_y^{\mathrm{III}} &= -\frac{mk\beta\Delta^2}{12}\lambda^2 + k \\ \theta_x^{\mathrm{III}} &= -\frac{k\beta\Delta}{\omega}\lambda - \frac{k'\beta\Delta}{2} \\ \theta_y^{\mathrm{III}} &= \frac{k\beta\Delta}{2} \end{aligned} \tag{61}$$

Substituting Equations (60) and (61) in Equation (59) gives

$$\begin{aligned} P(\lambda) &= \frac{mk\beta\Delta^2}{3\omega}\lambda^3 + \frac{m}{2}\left(\frac{k'\beta\Delta^2}{3} + 1\right)\lambda^2 + \frac{2k}{\omega}\lambda + k' \\ Q(\lambda) &= -\frac{mk\beta\Delta^2}{6}\lambda^2 - k \end{aligned} \tag{62}$$

which yields an equation of third degree with complex coefficients:

$$\frac{mk\beta\Delta^2}{3\omega}\lambda^3 + \frac{m}{2}\left[\left(\frac{k'\beta\Delta^2}{3}+1\right) - i\frac{k\beta\Delta^2}{3}\right]\lambda^2 + \frac{2k}{\omega}\lambda + (k' - ik) = 0 \quad (63)$$

Allowing for differences in notation, this is the same characteristic equation as that given in Equation (4.3) of Poritsky's paper [9].[3]

Acknowledgments

The author is indebted to Mr. E. E. Zwicky, Jr., for his many helpful suggestions, especially in establishing recurrence relations for the u-vectors. Also, the aid of Dr. H. Poritsky is acknowledged in connection with symmetry conditions in the sample problem.

References

1 G. F. Boeker and B. Sternlicht, "Investigation of Translatory Fluid Whirl in Vertical Machines," TRANS. ASME, vol. 78, 1956, pp. 13–19.

2 A. Cameron, "Oil Whirl in Bearings," *Engineering*, vol. 179, 1955, pp. 237–239.

3 A. C. Hagg, "The Influence of Oil Film Journal Bearings on the Stability of Rotating Machines," JOURNAL OF APPLIED MECHANICS, vol. 13, TRANS. ASME, vol. 68, 1946, pp. 211–220.

4 A. C. Hagg and P. C. Warner, "Oil-Whip of Flexible Rotors," TRANS. ASME, vol. 75, 1953, pp. 1339–1344.

5 A. C. Hagg and G. O. Sankey, "Elastic and Damping Properties of Oil-Film Journal Bearings for Application to Unbalance Vibration Calculations," JOURNAL OF APPLIED MECHANICS, vol. 25, TRANS. ASME, vol. 80, 1958, pp. 141–143.

6 A. C. Hagg and G. O. Sankey, "Oil Film Properties With Reference to Unbalance Vibration of Rotors," JOURNAL OF APPLIED MECHANICS, vol. 23, TRANS. ASME, vol. 78, 1956, pp. 302–306.

7 C. Hummel, "Kritische Drehzahlen als Folge der Nachgiebigkeit des Schmiermittels im Lager," *Verein Deutscher Ingenieure Forschung*, Heft 287, 1926.

8 J. A. Owczarek, Internal General Electric communication giving a mathematical solution of the instability problem for a simple shaft, including bearing and steam forces.

9 H. Poritsky, "Contribution to the Theory of Oil Whip," TRANS ASME, vol. 75, 1953, pp. 1153–1158.

10 M. A. Prohl, "A General Method for Calculating Critical Speeds of Turbine Generator Rotors," JOURNAL OF APPLIED MECHANICS, vol. 12, TRANS. ASME, vol. 67, 1945, pp. 142–148.

11 D. Robertson, "Whirling of a Journal in a Sleeve Bearing," *Philosophical Magazine*, vol. 15, 1933, pp., 113–130.

12 J. R. Schnittger, "Development of a Smooth Running, Double-Spool, Gas-Turbine Rotor System," JOURNAL OF ENGINEERING FOR POWER, vol. 81, TRANS. ASME, Series A, April, 1959, p. 151.

13 B. Sternlicht, "Elastic and Damping Properties of Cylindrical Journal Bearings," *Journal of Basic Engineering*—TRANS. ASME, vol. 81, Series D, 1959, pp. 101–108.

[3] A typographical error occurs in Equation (4.3) of [9]; the linear term should be $2\lambda k/M$, rather than $2\lambda k/K$.

On Saint Venant's Principle: Elastic Shells and Plates[1]

P. M. NAGHDI
Professor of Engineering Science,
University of California,
Berkeley, Calif.
Mem. ASME

This investigation is concerned with an examination of the validity of Saint Venant's principle in the theory of thin elastic shells and plates. With the aid of an integral formula derived for the displacements and their relevant partial derivatives of all orders at a fixed point of the shell middle surface, the conclusions reached may be roughly stated as follows: If the loads acting on the shell maintained in equilibrium are purely edge loads, then the orders of magnitude of the displacements and stresses are in accord with the traditional statement of Saint Venant's principle. On the other hand, if the loads on the shell are purely surface loads, then the conclusions concerning the orders of magnitude of the displacements and stresses are the same as those of the modified Saint Venant principle.

Introduction

THE main objective of the present investigation is an examination of the validity of Saint Venant's principle in the linear theory of thin elastic shells and plates. Before describing the scope of the paper, however, we turn to an account of the previous developments concerning the principle which was enunciated by Saint Venant [1][2] in connection with the problem of extension, torsion, and flexure of elastic cylinders. As has been remarked by von Mises [2] and again by Sternberg [3], what Saint Venant undoubtedly had in mind was the application of the principle to long cylinders with infinite ratio of length to diameter.

The first universal statement of the principle attributed to Boussinesq [4] has since become traditional. This version of the principle which, with slight variation, may be found in books on elasticity, e.g., Love [5, p. 132], infers a comparison of the effects of certain changes in the tractions on the boundary upon the solution, i.e., the displacements, stresses, and strains in the interior of the body. Since its inception over a century ago, numerous authors, starting with Boussinesq himself [4], have by various means aimed either to justify the principle or to point out its limitations; e.g. [6-7], [8, pp. 102, 138], [9, p. 150], and [10].[3]

In his illuminating paper [3], von Mises recognized that the earlier forms of the statement of the principle, which refer to (at least) a dual comparison of the effects on the solution in the interior of the body due to the changes in the tractions on the boundary, are vague. He further pointed out that the customary statement of the principle becomes meaningful provided the "dual comparison" just mentioned is made explicit. For future reference, we recall here von Mises' interpretation of the traditional statement of Saint Venant's principle which, according to Sternberg [3], may be roughly stated as follows:

If the forces acting on an elastic body are confined to several distinct portions of its surface, each lying within a sphere of radius ϵ, then the stresses and strains at a fixed interior point of the body are of a smaller order of magnitude in ϵ, as $\epsilon \to 0$ when the forces on each of the portions are self-equilibrated than when they are not. (1)

With the aid of two counterexamples, namely, the (three-dimensional) problem of the half-space and the (two-dimensional) problem of the circular disk, both under tangential as well as normal surface loads, von Mises in [2] demonstrated that in general the principle in the form (1) is not valid. Thus, amending the traditional statement, he proposed a modified principle.

A detailed formulation and the general proof of the modified Saint Venant principle were supplied by Sternberg [3]. The proof of this theorem, which is remarkable for its generality, rests essentially on the use of Betti's formula for the dilatation, together with Lauricella's and Somigliana's representations for the strain and the displacement fields, respectively, in the three-dimensional theory of isotropic elasticity. As was subsequently pointed out by Sternberg [11], the theorem established in [3] is also valid for anisotropic elastic media. It is pertinent to recall here the remarks made by von Mises [2] and Sternberg [3] to the effect that the proof of the modified Saint Venant principle does not preclude the possibility of a stronger theorem for a special class of bodies, such as thin plates and shells.

More recently, it has been shown by Boley [12] that theorems analogous to that in [3] may be established for other boundary-value problems characterized by elliptic partial differential equations. In order to provide estimates of errors in stresses due to load changes on the boundary, Boley in [12] has suggested a scheme which requires knowledge of Green's functions appropriate to the boundary-value problem in question. In this connection, mention should be made of Horvay's effort [13] in discussing the rate of decay of stresses due to self-equilibrated loads applied to an edge of rectangular regions.

Although the analysis of the present paper is carried out in conjunction with the theory of thin elastic shells, known as Love's first approximation (hereafter often referred to merely as Love's theory), the essential results are equally valid and, in fact, may be carried out for any of the consistent classical theories of shells, such as the theory known as Flügge-Byrne, as well

[1] The results presented in this paper were obtained in the course of research sponsored by the Office of Naval Research under Contract Nonr-222(69), Project NR-064-436, with the University of California at Berkeley.

[2] Numbers in brackets designate References at end of paper.

[3] The complete bibliography on the subject is too long to be included here. For other references, see [3], [11], and [12].

Presented at the Summer Conference of the Applied Mechanics Division, University Park, Pa., June 20–22, 1960, of THE AMERICAN SOCIETY OF MECHANICAL ENGINEERS.

Discussion of this paper should be addressed to the Secretary, ASME, 29 West 39th Street, New York, N. Y., and will be accepted until October 10, 1960, for publication at a later date. Discussion received after the closing date will be returned.

NOTE: Statements and opinions advanced in papers are to be understood as individual expressions of their authors and not those of the Society. Manuscript received by ASME Applied Mechanics Division, April 27, 1959. Paper No. 60—APM-11.

as the theories of shells which include the effects of transverse shear deformation. Thus, following some preliminaries which include a brief discussion of the validity of the reciprocity theorem for Love's theory, an integral formula is established for the displacements and their partial derivatives at an arbitrary fixed point of the shell middle surface. This representation formula, derived here for thin elastic shells (and plates), though not the same may be regarded as the combined counterparts of Lauricella's and Somigliana's representations for the strain and the displacement fields in the three-dimensional theory of elasticity. Further, utilizing the foregoing representation formula, the validity of Saint Venant's principle for elastic shells (and plates) is examined in a manner similar to that in [3]. The main results of the theorem may be stated roughly as follows: If the loads acting on the shell maintained in equilibrium are purely edge loads, then the orders of magnitude of the displacements and stresses are in support of the traditional statement of the principle cited in (1). On the other hand, if the loads on the shell are purely surface loads, then the conclusions concerning the orders of magnitude of the displacements and stresses are the same as those of the modified principle [3]; only in the special case of the flat plate, where the surface loads are parallel and along the normal to the middle plane of the plate, the conclusions are again in accord with (1).

General Background

Let S be a regular surface[4] occupied by the middle surface of an elastic shell whose boundary is a closed regular curve C. Let ξ_α ($\alpha = 1, 2$), be the co-ordinates of a point on the middle surface of the shell and ζ be the distance measured along the unit normal $\mathbf{n}$ to the middle surface. Then the position vector of a generic point of the shell space is defined by

$$\mathbf{R}(\xi_1, \xi_2, \zeta) = \mathbf{r}(\xi_1, \xi_2) + \zeta\mathbf{n} \tag{2}$$

where $\mathbf{r}$ denotes the position vector to the point on S ($\zeta = 0$). Further, let[5] $\mathbf{t}_\alpha$ be the unit tangent vectors to the ξ_α-parametric curves which, for simplicity's sake, will be referred to the lines of curvature on S ($\mathbf{t}_1$, $\mathbf{t}_2$, and $\mathbf{n}$ form a right-handed system). Thus the square of the linear element of the triply orthogonal co-ordinate system (ξ_α, ζ) is given by

$$d\mathbf{R}\cdot d\mathbf{R} = a_1^2\left(1 + \frac{\zeta}{R_1}\right)^2 d\xi_1^2 + a_2^2\left(1 + \frac{\zeta}{R_2}\right)^2 d\xi_2^2 + d\zeta^2 \tag{3}$$

where R_α and a_α refer, respectively, to the principal radii of curvature and the nonvanishing metric coefficients of the middle surface.

Let $\mathbf{U}$ be a displacement field, and $\mathbf{N}_\alpha$ and $\mathbf{M}_\alpha$ the forces and couples per unit length along the parametric curves which, in the absence of body forces, satisfy the differential equations of the linear theory of thin elastic shells within the space defined by S and $-h/2 \leq \zeta \leq h/2$, h being the thickness of the shell. In the theory of Love's first approximation,[6] where, as in all classical theories of shells the effects of both transverse shear deformation and normal stress are neglected, the displacements are assumed in the form

$$\mathbf{U}(\xi_1, \xi_2, \zeta) = \mathbf{u}(\xi_1, \xi_2) + \zeta\boldsymbol{\beta}(\xi_1, \xi_2) \tag{4a}$$

$$\mathbf{u} = u_\alpha\mathbf{t}_\alpha + w\mathbf{n} \tag{4b}$$

$$\boldsymbol{\beta} = \beta_\alpha\mathbf{t}_\alpha = \left(-\frac{1}{a_1}\frac{\partial w}{\partial \xi_1} + \frac{u_1}{R_1}\right)\mathbf{t}_1 + \left(-\frac{1}{a_2}\frac{\partial w}{\partial \xi_2} + \frac{u_2}{R_2}\right)\mathbf{t}_2 \tag{4c}$$

and $\mathbf{N}_\alpha$ and $\mathbf{M}_\alpha$ are defined by[7]

$$\begin{aligned}\mathbf{N}_\alpha &= N_{\alpha\gamma}\mathbf{t}_\gamma + V_\alpha\mathbf{n}\\ \mathbf{M}_\alpha &= M_{\alpha\gamma}\mathbf{n}\times\mathbf{t}_\gamma\end{aligned} \tag{5}$$

where $N_{\alpha\gamma}$, $M_{\alpha\gamma}$, and V_α are the stress resultants, the stress couples, and the shear stress resultants, respectively. The stress resultants and the stress couples are in turn given by the stress-strain relations

$$\begin{aligned}N_{\alpha\gamma} &= \frac{Eh}{1-\nu^2}\left[\nu\epsilon_{\beta\beta}\delta_{\alpha\gamma} + (1-\nu)\epsilon_{\alpha\gamma}\right]\\ M_{\alpha\gamma} &= \frac{Eh^3}{12(1-\nu^2)}\left[\nu\kappa_{\beta\beta}\delta_{\alpha\gamma} + (1-\nu)\kappa_{\alpha\gamma}\right]\end{aligned} \tag{6a}$$

and

$$\begin{aligned}2\epsilon_{\alpha\gamma} &= \frac{\mathbf{u}_{,\alpha}\cdot\mathbf{r}_{,\gamma}}{a_{(\alpha)}a_{(\gamma)}} + \frac{\mathbf{u}_{,\gamma}\cdot\mathbf{r}_{,\alpha}}{a_{(\gamma)}a_{(\alpha)}}\\ 2\kappa_{\alpha\gamma} &= \frac{\boldsymbol{\beta}_{,\alpha}\cdot\mathbf{r}_{,\gamma}}{a_{(\alpha)}a_{(\gamma)}} + \frac{\boldsymbol{\beta}_{,\gamma}\cdot\mathbf{r}_{,\alpha}}{a_{(\gamma)}a_{(\alpha)}}\end{aligned} \tag{6b}$$

and the shear stress resultants V_α, which are determined from the equilibrium equations, may be expressed in terms of partial derivatives of the middle surface displacements u_α and w. In (6), $(\ )_{,\alpha} \equiv \partial(\ )/\partial\xi_\alpha$; $\delta_{\alpha\gamma}$ is the Kronecker delta; $\mathbf{u}$ and $\boldsymbol{\beta}$ are defined by (4); and E and ν are Young's modulus and Poisson's ratio, respectively.

Let

$$\mathbf{p} = p_\alpha\mathbf{t}_\alpha + p_3\mathbf{n} \tag{7}$$

be a piecewise continuous surface load on[8] S, and let F_j, ($j = 1, 2, 3, 4$), refer to piecewise continuous edge loads (such as stress couple, shear-stress resultant, etc.) acting on the boundary C which produce the displacement $\mathbf{U}$. Further, let $\mathbf{U}'$ be another admissible displacement field which gives rise to a piecewise continuous surface load $\mathbf{p}'$ and piecewise continuous edge loads F_j'. Then the reciprocity theorem for a shell space, whose behavior is characterized by (4), (5), (6), and the resultant equations of equilibrium, may be written as

$$\int_S [p_\alpha' u_\alpha + p_3' w]d\sigma + \int_C\left[\sum_{j=1}^{4} F_j' d_j\right]ds = \int_S [p_\alpha u_\alpha' + p_3 w']d\sigma + \int_C\left[\sum_{j=1}^{4} F_j d_j'\right]ds \tag{8}$$

where $d\sigma = a_1a_2d\xi_1d\xi_2$, $ds = a_jd\xi_j$, and the notation

$$\sum_{j=1}^{4} F_j d_j',$$

introduced here for future convenience, stands for

[4] The definition of "regular surface" as used here is intended in the sense of Kellog [14], pp. 105–106.

[5] In this paper, all Greek indexes have the range $\alpha, \beta, \gamma = 1, 2$, and only the repeated Greek indexes imply the summation convention. Whenever one of the repeated Greek indexes is placed in parentheses, the summation convention is suspended for that index.

[6] A comprehensive account of the theory of Love's first approximation may be found in [15, 16] or [17, chap. 10].

[7] While the assumptions (4) differ from one theory of shells to another, the expressions (5), representing merely the resolution of forces and couples per unit length, hold for all theories of shells.

[8] Recall that within the approximations introduced in Love's theory, similar to those in the classical theory of bending of plates, the surface load is regarded as acting on the middle surface.

$$\sum_{j=1}^{4} F_j d_j' = N_{nn} u_n' + \left(N_{nt} + \frac{M_{nt}}{R_t} \right) u_t' + M_{nn} \beta_n' + \left(V_n + \frac{1}{a_t} \frac{\partial M_{nt}}{\partial \xi_t} \right) w' \quad (9)$$

and the subscripts n and t, respectively, refer to the normal and tangential directions on C. It is clear that when the boundary conditions on the entire curve C are the *natural* boundary conditions (appropriate to Love's theory), with $F_j = 0$, then the line integrals in (8), representing the work done by the edge forces, vanish.

A Remark on Validity of Reciprocal Theorem for Love's Theory

In order to show that the theory of Love's first approximation admits the reciprocity relation (8), we recall here the resultant equations of equilibrium, which, in the absence of body forces, read

$$(a_2 \mathbf{N}_1)_{,1} + (a_1 \mathbf{N}_2)_{,2} + a_1 a_2 \mathbf{p} = 0$$

$$(a_2 \mathbf{M}_1)_{,1} + (a_1 \mathbf{M}_2)_{,2} + a_2 \mathbf{N}_1 \times \mathbf{t}_1 + a_1 \mathbf{N}_2 \times \mathbf{t}_2 = 0 \quad (10)$$

Introduction of (10), (5), and (6) into the right-hand side of (8), followed by appropriate transformations and integration by parts, yields

$$\int_S [p_\alpha u_\alpha' + p_3 w'] d\sigma + \int_C \left[\sum_{j=1}^{4} F_j d_j' \right] ds = \int_S \left\{ \frac{Eh}{1-\nu^2} [(1-\nu) \varepsilon_{\alpha\gamma} \varepsilon_{\alpha\gamma}' + \nu \varepsilon_{\alpha\alpha} \varepsilon_{\gamma\gamma}'] + \frac{Eh^3}{12(1-\nu^2)} [(1-\nu) \kappa_{\alpha\gamma} \kappa_{\alpha\gamma}' + \nu \kappa_{\alpha\alpha} \kappa_{\gamma\gamma}'] \right\} d\sigma \quad (11)$$

In view of (11), the right-hand side of (8) is obviously symmetric in the primed and unprimed variables. It is clear, therefore, that the reciprocity theorem (8) holds for the theory of Love's first approximation whose differential equations are characterized by (10), (5), (4), and (6).

It should be emphasized that the expression for $\kappa_{\alpha\gamma}$ (and therefore $M_{\alpha\gamma}$), as recorded and utilized by many investigators, is at variance with those given by (6) which is in accord with the corresponding expressions in [15], [16], [17, chap. 10], and [18]. Specifically, the variation just referred to occurs in κ_{12} which, if adopted, would result in the violation of the reciprocity theorem.[9] Evidently, it is due to this difference in κ_{12} that some authors, e.g., Novozhilov [19, p. 50] and Goldenveiser [20, p. 80], have stated that Love's theory does not admit the reciprocity relation (8).

An Integral Representation for Displacements and Their Partial Derivatives

As a preliminary to our main objective, we need to establish a representation formula for the determination of $\mathbf{u}$, $\boldsymbol{\beta}$, and their partial derivatives at a fixed point Q on S which may be stated as follows: Let S^* be a closed subregion of S subjected to the surface load $\mathbf{p}$; let C^* be an arc of C subjected to the edge loads F_j; and let the shell be supported in such a manner that the natural boundary conditions are satisfied on the entire boundary C. Furthermore, let Q with position vector $\mathbf{r}(\xi_1^\circ, \xi_2^\circ)$ be a point on S at a finite distance from the origin, but otherwise arbitrary; and

[9] It should be noted here that while the theory characterized by the differential equations (10), (5), (4), and (6) is attributed to Love, the expressions for κ_{12} as given in [5, chap. 24] differs from that in (6). In this connection, see also footnote 9 in [18].

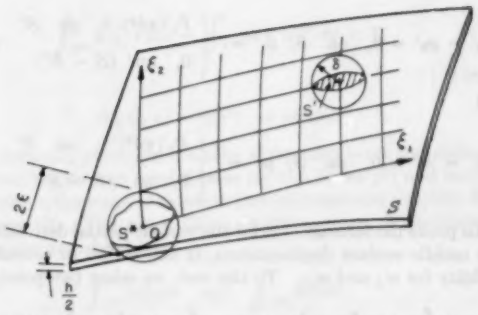

Fig. 1 Shell middle surface, parametric curves ξ_α, sphere of radius δ with center at Q, and load region S^*

let $S'(\delta)$, subjected to the surface load $\mathbf{p}'$, denote the subregion of S enclosed within a sphere of radius $0 < \delta \leq \delta_0$ with center at Q, Fig. 1. If the M-variables Δ_m, $(m = 1, 2, \ldots M)$, stand for the displacements u_1, u_2, w, as well as their partial derivatives $u_{1,1}$, $w_{,1}$, $w_{,12}$, etc., which occur in $N_{\alpha\gamma}$, V_α, and $M_{\alpha\gamma}$, and if $(\mathbf{p}')_m$ designates the mth set of the auxiliary surface load $\mathbf{p}'$, then for each m $(m = 1, 2, \ldots M)$, Δ_m at Q corresponding to $(\mathbf{p}')_m$ is given by

$$\Delta_m(Q) = \int_{S^*} \{p_\alpha u_\alpha'[(\mathbf{p}')_m] + p_3 w'[(\mathbf{p}')_m]\} d\sigma + \int_{C^*} \left\{ \sum_{j=1}^{4} F_j d_j'[(\mathbf{p}')_m] \right\} ds \quad (12)$$

In order to establish the truth of (12), use will be made of the reciprocity relation (8) with $F_j' = 0$, and $\mathbf{p}'$ assigned a set of $(\mathbf{p}')_m$ corresponding to the particular Δ_m in question. Thus, when Δ_m is identified with w, let the components of $(\mathbf{p}')_m$ be specified by the following distributed tractions on S:

$$p_\alpha' = 0, \quad \text{on} \quad S; \quad p_3' = \begin{cases} P_3'(\pi\delta^2)^{-1}, & \text{on} \quad S' \\ 0, & \text{on} \quad (S - S') \end{cases} \quad (13)$$

where P_3' is the resultant of p_3' over S', such that as $\delta \to 0$, p_3' tends to a concentrated load of intensity P_3' at Q. Substitution of (13) into the left-hand side of (8) results in

$$\int_{S'} \frac{P_3'}{\pi\delta^2} w d\sigma = \int_{S^*} [p_\alpha u_\alpha' + p_3 w'] d\sigma + \int_{C^*} \left[\sum_{j=1}^{4} F_j d_j' \right] ds \quad (14)$$

Since the displacement w is regular at Q, and since

$$\lim_{\delta \to 0} \int_{S'} d\sigma \to \pi\delta^2,$$

it follows that in the limit as $\delta \to 0$, the left-hand side of (14) after setting $P_3' = 1$ reduces simply to the value of w at Q, or

$$w(Q) = \int_{S^*} [p_\alpha u_\alpha'(\mathbf{p}') + p_3 w'(\mathbf{p}')] d\sigma + \int_{C^*} \left[\sum_{j=1}^{4} F_j d_j'(\mathbf{p}') \right] ds \quad (15)$$

where the argument $\mathbf{p}'$ of u_α', w', and d_j' refers to the surface load in (13).

By repetition of the process which led to (15), similar expressions may be obtained for the displacements $u_1(Q)$ and $u_2(Q)$ except that instead of (13), the following choices, respectively, should be made for the components of $(\mathbf{p}')_m$:

$$p_2' = p_3' = 0, \quad \text{on} \quad S; \; p_1' = \begin{cases} P_1'(\pi\delta^2)^{-1}, & \text{on} \quad S' \\ 0, & \text{on} \quad (S - S') \end{cases} \tag{16a}$$

and

$$p_1' = p_3' = 0, \quad \text{on} \quad S; \; p_2' = \begin{cases} P_2'(\pi\delta^2)^{-1}, & \text{on} \quad S' \\ 0, & \text{on} \quad (S - S') \end{cases} \tag{16b}$$

To prove the formula (12) for the various partial derivatives of the middle surface displacements, it will suffice to consider its validity for $w_{,1}$ and $w_{,12}$. To this end, we select two points

$$Q_1\left(\xi_1^\circ - \frac{b}{2}, \xi_2^\circ\right) \quad \text{and} \quad Q_2\left(\xi_1^\circ + \frac{b}{2}, \xi_2^\circ\right) \quad \text{on} \quad S$$

and construct two spheres, each of radius $0 < \delta \leq \frac{b}{2} \leq \delta_0$ with centers at Q_1 and Q_2, and designate the subregions of S enclosed within the two spheres by S_1' and S_2', respectively. With the components of $\mathbf{p}'$ prescribed as

$$p_\alpha' = 0, \quad \text{on} \quad S; \; p_3' = \begin{cases} P_4'(\pi b\delta^2)^{-1}, & \text{on} \quad S_2' \\ -P_4'(\pi b\delta^2)^{-1}, & \text{on} \quad S_1' \\ 0, & \text{on} \quad (S - S_1' - S_2') \end{cases} \tag{17}$$

Equation (8) yields

$$\int_{S_2'} \frac{P_4'}{\pi b\delta^2} w d\sigma - \int_{S_1'} \frac{P_4'}{\pi b\delta^2} w d\sigma = \int_{S^*} [p_\alpha u_\alpha' + p_3 w'] d\sigma + \int_{C^*} \left[\sum_{j=1}^{4} F_j d_j'\right] ds \tag{18}$$

Again, since the displacements are regular at Q_1 and Q_2, it follows that in the limit as $\delta \to 0$ and after setting $P_4' = 1$, (18) becomes

$$\frac{w(Q_2) - w(Q_1)}{b} = \int_{S^*} [p_\alpha u_\alpha' + p_3 w'] d\sigma + \int_{C^*} \left[\sum_{j=1}^{4} F_j d_j'\right] ds \tag{19}$$

If on the left-hand side of the last equation we again pass to the limit such that as $b \to 0$, Q_1-and-$Q_2 \to Q$, then the left-hand side of (19) becomes precisely $\partial w/\partial\xi_1$ at Q, and we have

$$w_{,1}(Q) = \int_{S^*} [p_\alpha u_\alpha'(\mathbf{p}') + p_3 w'(\mathbf{p}')] d\sigma + \int_{C^*} \left[\sum_{j=1}^{4} F_j d_j'(\mathbf{p}')\right] ds \tag{20}$$

where the argument of u_α', w', and d_j' refers to (17).

To establish (12) for $\Delta_m \equiv w_{,12}$ we select four points

$$Q_1\left(\xi_1^0 - \frac{b}{2}, \xi_2^0 + \frac{c}{2}\right), \quad Q_2\left(\xi_1^0 + \frac{b}{2}, \xi_2^0 + \frac{c}{2}\right),$$

$$Q_3\left(\xi_1^0 + \frac{b}{2}, \xi_2^0 - \frac{c}{2}\right)$$

and

$$Q_4\left(\xi_1^0 - \frac{b}{2}, \xi_2^0 - \frac{c}{2}\right),$$

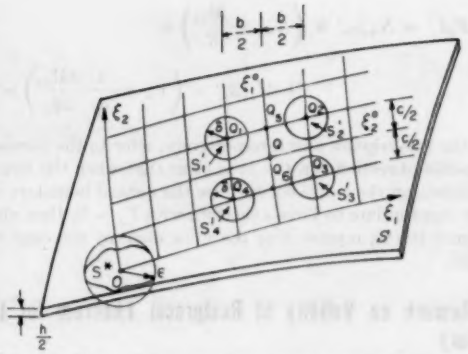

Fig. 2 Shell middle surface, points Q_1 to Q_4 as centers of spheres which are indicated by circles, points Q, Q_5, and Q_6, and load region S^*

and let S_k', $(k = 1, 2, 3, 4)$, refer to subregions of S each enclosed within a sphere of radius

$$0 < \delta \leq \frac{b}{2} \leq \frac{c}{2} \leq \delta_0,$$

as shown in Fig. 2. With $\mathbf{p}'$ specified by

$$p_\alpha' = 0, \quad \text{on} \quad S; \; p_3' = \begin{cases} -P_3'(bc\pi\delta^2)^{-1}, & \text{on} \quad S_2' \text{ and } S_3' \\ +P_3'(bc\pi\delta^2)^{-1}, & \text{on} \quad S_1' \text{ and } S_4' \\ 0, & \text{on} \quad \left[S - \sum_{k=1}^{4} S_k'\right] \end{cases} \tag{21}$$

the left-hand side of the reciprocity relation (8), in the limit as $\delta \to 0$ and after setting $P_k' = 1$, yields

$$\frac{1}{c}\left[\frac{w(Q_4) - w(Q_3)}{b} - \frac{w(Q_2) - w(Q_1)}{b}\right] \tag{22a}$$

Taking the limit of the foregoing expression such that as $b \to 0$, Q_1-and-$Q_2 \to Q_5\left(\xi_1^0, \xi_2^0 + \frac{c}{2}\right)$ and Q_3-and-$Q_4 \to Q_6\left(\xi_1^0, \xi_2^0 - \frac{c}{2}\right)$, (22a) becomes

$$\frac{1}{c}\left[\frac{\partial w}{\partial \xi_1}(Q_5) - \frac{\partial w}{\partial \xi_1}(Q_6)\right] \tag{22b}$$

Imposing a second limit process such that as $c \to 0$, Q_5-and-$Q_6 \to Q(\xi_1^0, \xi_2^0)$, then (22b) becomes precisely $\partial^2 w/\partial\xi_1\partial\xi_2$ at Q and we have

$$w_{,12}(Q) = \int_{S^*} [p_\alpha u_\alpha'(\mathbf{p}') + p_3 w'(\mathbf{p}')] d\sigma + \int_{C^*} \left[\sum_{j=1}^{4} F_j d_j'(\mathbf{p}')\right] ds \tag{23}$$

where in (23) the argument of u_α', w', and d_j' refers to (21).

It is now clear that for all other partial derivatives of the middle surface displacements, the truth of (12) may be established in a similar manner, and by iteration.

As may be seen from (4), (6), and the expressions for the shear-stress resultants, $\epsilon_{\alpha\gamma}$ and $\kappa_{\alpha\gamma}$, as well as $N_{\alpha\gamma}$, V_α, and $M_{\alpha\gamma}$, contain terms of the type Δ_m. Hence, by virtue of the principle of superposition and by application of the general formula (12), the stress resultants and the stress couples, and therefore, the stresses may be determined at a fixed point of the middle surface S.

Saint Venant's Principle for Thin Shells

Let S, a regular surface with boundary C, again occupy the middle surface of an elastic shell whose small displacements, due to appropriate surface and edge loads, are characterized by the differential equations of shell theory which here are taken as those of Love. In what follows, it is expedient to consider two cases: (A) One in which the load on the shell is only a surface load and (B) the other when the load consists of purely an edge load.

(A) The edge load $F_j = 0$ $(j = 1, 2, 3, 4)$: In this case, let S^* (load-region), a monotone increasing function of the parameter ϵ be a closed subregion of S containing the origin such that for every ϵ in $0 < \epsilon \leq \epsilon_0$, $S^*(\epsilon)$ is enclosed within a sphere of minimum radius ϵ, Fig. 1. Let $\mathbf{U}(\xi, \epsilon)$, $\mathbf{N}_\alpha(\xi, \epsilon)$, $\mathbf{M}_\alpha(\xi, \epsilon)$ be a one-parameter family of solutions to the differential equations of Love's theory which satisfy the natural boundary conditions with $F_j = 0$, on the entire C and give rise to a piecewise continuous surface load $\mathbf{p}(\xi, \epsilon)$ which vanishes outside $S^*(\epsilon)$, and remains bounded as $\epsilon \to 0$. This manner of introducing the parameter ϵ through which the notion of "order of magnitude" becomes precise is essential here, and was also employed in [3]. Thus $f(\epsilon)$ is said to be of $0(\epsilon^p)$, if as $\epsilon \to 0$, $|f(\epsilon)/\epsilon^p| < M$ (M independent of ϵ).

We now return to the integral representation for $\Delta_m(Q)$, set $F_j = 0$, and consider its Taylor expansion about the origin. Since u_α' and w' are independent of ϵ and are regular at the origin, we write[10]

$$\Delta_m(Q, \epsilon) = \{u_\alpha'[(\mathbf{p}')_m]\}^0 \int_{S^*} p_\alpha(\xi, \epsilon)d\sigma + \{w'[(\mathbf{p}')_m]\}^0 \int_{S^*} p_3(\xi, \epsilon)d\sigma + \{u_{\alpha,\gamma}'[(\mathbf{p}')_m]\}^0 \int_{S^*} p_\alpha(\xi, \epsilon)\xi_\gamma d\sigma + \{w_{,\gamma}'[(\mathbf{p}')_m]\}^0 \int_{S^*} p_3(\xi, \epsilon)\xi_\gamma d\sigma + \ldots \quad (24)$$

and recall that $\Delta_m(Q, \epsilon)$ depending on the auxiliary surface load $(\mathbf{p}')_m$, $(m = 1, 2, \ldots M)$ stands for the M quantities $u_\alpha(Q, \epsilon)$, $w(Q, \epsilon)$ and their partial derivatives which occur in

$$N_{\alpha\gamma}(Q, \epsilon), \quad V_\alpha(Q, \epsilon), \quad \text{and} \quad M_{\alpha\gamma}(Q, \epsilon)$$

It follows directly from (24) that for fixed (ξ_1, ξ_2) on S, $\Delta_m(Q, \epsilon)$ and therefore the solution

$$\mathbf{U}(Q, \epsilon), \quad \mathbf{N}_\alpha(Q, \epsilon), \quad \text{and} \quad \mathbf{M}_\alpha(Q, \epsilon)$$

due to the surface load $\mathbf{p}(\xi, \epsilon)$ have the following order of magnitude as $\epsilon \to 0$:

(a) If the resultant load does not vanish, i.e., if

$$\int_{S^*} \mathbf{p}(\xi, \epsilon)d\sigma \neq 0,$$

then (25a)

$$\Delta_m(Q, \epsilon) = 0(\epsilon^2) \quad \textit{or smaller}$$

(b) If the resultant load vanishes, i.e., if

$$\int_{S^*} \mathbf{p}(\xi, \epsilon)d\sigma = 0,$$

then (25b)

$$\Delta_m(Q, \epsilon) = 0(\epsilon^3) \quad \textit{or smaller}$$

(c) If the surface load is in astatic equilibrium,[11] i.e., if

$$\int_{S^*} \mathbf{p}(\xi, \epsilon)d\sigma = \int_{S^*} \mathbf{p}(\xi, \epsilon)\xi_\gamma d\sigma = 0,$$

then (25c)

$$\Delta_m(Q, \epsilon) = 0(\epsilon^4) \quad \textit{or smaller}$$

The foregoing estimates of orders of magnitude are the same as those reached for two special cases by von Mises [2] and established within the scope of classical three-dimensional elasticity by Sternberg [3]. The result (25c) stipulates more requirements, namely, the vanishing of

$$\int_{S^*} p_1\xi_1 d\sigma \quad \text{and} \quad \int_{S^*} p_3\delta_\beta d\sigma,$$

than are necessary in order for $\mathbf{p}$ to be self-equilibrated on S^* This contradicts the interpretation of the traditional statement of Saint Venant's principle cited in (1).

(B) The surface load $\mathbf{p} = 0$: In this case, let C^* (load region) a monotone increasing function of ϵ, be an arc of C containing the origin such that for every ϵ in $0 < \epsilon \leq \epsilon_0$, $C^*(\epsilon)$ is enclosed within a circle of minimum radius ϵ. Again, let $\mathbf{U}(Q, \epsilon)$, $\mathbf{N}_\alpha(Q, \epsilon)$, $\mathbf{M}_\alpha(Q, \epsilon)$ be the family of solutions to the differential equations of Love's theory which satisfy the natural boundary conditions on C, and give rise to piecewise continuous edge loads $F_j(s, \epsilon)$, which vanish on $[C - C^*(\epsilon)]$, and remain bounded as $\epsilon \to 0$.

Setting $\mathbf{p} = 0$ in (12), and expanding d_j' (which are independent of ϵ and regular at the origin) in Taylor series about $s = 0$, we have for each j (say $j = 1$),

$$\Delta_m(Q, \epsilon) = \{d_1'[(\mathbf{p}')_m]\}^0 \int_{C^*} F_1(s, \epsilon)ds + \left\{\frac{d}{ds} d_1'[(\mathbf{p}')_m]\right\}^0 \int_{C^*} F_1(s, \epsilon)s\, ds + \ldots \quad (26)$$

We conclude from (26) that for fixed (ξ_1, ξ_2) on S, $\Delta_m(Q, \epsilon)$ and therefore $\mathbf{U}(Q, \epsilon)$, $\mathbf{N}_\alpha(Q, \epsilon)$, and $\mathbf{M}_\alpha(Q, \epsilon)$, due to the edge load $F_j(s, \epsilon)$ on $C^*(\epsilon)$, have the following order of magnitude as $\epsilon \to 0$:

(a) If the resultant edge load does not vanish, i.e., if

$$\int_{C^*} F_j ds \neq 0,$$

then (27a)

$$\Delta_m(Q, \epsilon) = 0(\epsilon) \quad \textit{or smaller}$$

(b) If the resultant edge load vanishes, i.e., if

$$\int_{C^*} F_j ds = 0,$$

then (27b)

$$\Delta_m(Q, \epsilon) = 0(\epsilon^2) \quad \textit{or smaller}$$

(c) If the distribution of the edge loads is such that

$$\int_{C^*} F_j ds = \int_{C^*} F_j s ds = 0,$$

then (27c)

$$\Delta_m(Q, \epsilon) = 0(\epsilon^3) \quad \textit{or smaller}$$

Comparison of the results of the two cases A and B reveals that, for the latter, the order of magnitude of $\Delta_m(Q, \epsilon)$ for each of the three requirements imposed on the resultant load is reduced by ϵ. Moreover, in case B, the conclusions (27) support the traditional statement of the principle cited in (1).

The foregoing theorem established for distributed surface loads and for distributed edge loads may easily be extended to concentrated loads on S and to concentrated edge loads on C. The

[10] The superscript zero attached to a function refers to its value at the origin.

[11] The term "astatic equilibrium" was employed by von Mises [2]. Thus two systems of forces are said to be in astatic equilibrium, if they are parallel to a fixed direction, and remain in equilibrium when rotated through an arbitrary angle.

extension to the case of concentrated surface loads follows along the same lines as those given by Sternberg [3]. Thus, let S^* consist of N nonintersecting closed subregions $S^{(n)}$, $(n = 1, 2, \ldots N)$, and let $\mathbf{p}^{(n)}$ be the surface load on $S^{(n)}$. Then by repetition of the previous argument and proceeding to the limit, as in [3], we find that the results in Case A remain valid for concentrated surface loads provided the integrals in (25) are replaced with the corresponding finite sums, and provided the order of magnitude of $\Delta_m(Q, \epsilon)$ in (25a, b, c) is replaced, respectively, by $0(1)$, $0(\epsilon)$, and $0(\epsilon^2)$. It may be easily shown that these same conclusions for concentrated surface loads hold also for concentrated edge loads.

Discussion

In the classical theory of bending of flat plates where $\mathbf{p} = p_3\mathbf{n}$, S^* refers to the middle plane of the plate, and $p_\alpha = 0$, the integrals in (25c) reduce to

$$\int_{S^*} p_3 d\sigma = \int_{S^*} p_3 \xi_\gamma d\sigma = 0 \tag{28}$$

which are the conditions for a self-equilibrated surface load. Hence, in the theory of bending of plates where the loads consist of edge loads as well as surface loads which are normal to the middle plane of the plate, the traditional statement of the principle is valid.

It should be emphasized that the results (25) and (27) pertain to relative orders of magnitude as the maximum radius of the load-region $\epsilon \to 0$. This requirement of vanishing ϵ, in the case of infinite bodies (e.g., an infinite plate), may be regarded as equivalent to holding the area (or the arc length) of the load region fixed when the distance R from the origin (either on S or on C), tends to infinity. While this latter interpretation is admittedly rough, it does illustrate the meaning of the principle as intended by Saint Venant [1]. Thus, it is clear that Saint Venant's principle as stated and interpreted in [2], [3], as well as the present paper, does not permit a rigorous comparison of the values of $\Delta_m(Q)$ at a finite distance R, due to nonvanishing and bounded surface and edge loads. For such comparisons, it is necessary to resort to other means; e.g., [12] and [13]. These methods, however, essentially require the knowledge of the exact solution to a specific problem, by means of which one may inquire as to the rate of decay of $\Delta_m(Q)$ with increasing R "sufficiently" far from the load-region. Of course, considerations of this type, though very useful, must necessarily be coupled with the magnitude of the load intensities (rather than the load resultants), as well as the admissible error on $\Delta_m(Q)$.

Finally, it may be noted that the results of the preceding section concerning the orders of magnitude of $\Delta_m(Q, \epsilon)$ include the conclusions appropriate to the special cases of beams and rods.

References

1 B. de Saint-Venant, "Mémoire sur la torsion des prismes," *Mem. Savants étrangers*, Académie des Sciences, Paris, France, 1855.

2 R. von Mises, "On Saint-Venant's Principles," *Bulletin of The American Mathematical Society*, vol. 51, 1945, pp. 555–562.

3 E. Sternberg, "On Saint-Venant's Principle," *Quarterly of Applied Mathematics*, vol. 11, 1954, pp. 393–402.

4 M. J. Boussinesq, "Application des Potentiels," Gauthier-Villars, Paris, France, 1885.

5 A. E. H. Love, "A Treatise on the Mathematical Theory of Elasticity," 4th edition, Dover Publications, Inc., New York, N. Y., 1944.

6 J. N. Goodier, "A General Proof of Saint-Venant's Principle," *Philosophical Magazine*, series 7, vol. 23, 1937, pp. 607–609; Supplementary Note on "A General Proof of Saint-Venant's Principle," *Philosophical Magazine*, series 7, vol. 24, 1937, p. 325.

7 J. N. Goodier, "An Extension of Saint-Venant's Principle, With Applications," *Journal of Applied Physics*, vol. 13 1942, pp. 167–171.

8 C. B. Biezeno and R. Grammel, "Engineering Dynamics," vol. 1, Blackie and Son, Limited, Glasgow, Scotland, 1955.

9 S. Timoshenko and J. N. Goodier, "Theory of Elasticity," 2nd edition, McGraw-Hill Book Company, Inc., New York, N. Y., 1951.

10 N. J. Hoff, "The Applicability of Saint-Venant's Principle to Airplane Structures," *Journal of the Aeronautical Sciences*, vol. 12, 1945, pp. 455–460.

11 E. Sternberg, "On Some Recent Developments in the Linear Theory of Elasticity," Technical Report No. 4, ONR Contract Nonr 562(25), Brown University, 1958; presented at the First Symposium of Naval Structures.

12 B. A. Boley, "Some Observations on Saint-Venant's Principle," Proceedings of the Third U. S. National Congress of Applied Mechanics, ASME, 1958, pp. 259–264.

13 G. Horvay, "Some Aspects of Saint-Venant's Principle," *Journal of the Mechanics and Physics of Solids*, vol. 5, 1957, pp. 77–94.

14 O. D. Kellog, "Foundations of Potential Theory," Frederick Ungar Publishing Company, New York, N. Y., 1929.

15 E. Reissner, "A New Derivation of the Equations for the Deformation of Elastic Shells," *American Journal of Mathematics*, vol. 63, 1941, pp. 177–184.

16 F. B. Hildebrand, E. Reissner, and G. B. Thomas, "Notes on the Foundations of the Theory of Small Displacements of Orthotropic Shells," NACA TN 1833, 1949.

17 A. E. Green and W. Zerna, "Theoretical Elasticity," Oxford University Press, New York, N. Y., 1954.

18 P. M. Naghdi and J. G. Berry, "On the Equations of Motion of Cylindrical Shells," JOURNAL OF APPLIED MECHANICS, vol. 21, TRANS. ASME vol. 76, 1954, pp. 160–166.

19 V. V. Novozhilov, "Theory of Thin Shells" (in Russian), Gosudarstvennoe Izdatel'stvo, Leningrad, Russia, 1951.

20 L. A. Goldenveiser, "Theory of Thin Elastic Shells" (in Russian), Gostekhizdat, Moscow, Russia, 1953.

On the Airy Stress Functions of Plane Dislocation Problems

F. D. JU

Assistant Professor,
Department of Mechanical Engineering,
University of New Mexico,
Albuquerque, N. Mex.
Assoc. Mem. ASME

The present paper explores the Airy stress function for a general class of elastic dislocation problems in a doubly connected region. The basic concept of the elastic theory and the dislocation theory, included, are essential to the derivation of the method. Applications deal with two shapes of dislocation cuts; an arbitrary straight cut and a logarithmic spiral cut. For simplicity and illustrative purpose, only an infinite region with a circular hole has been considered. The discussion deals with the singular point and the uniqueness of the general solution.

Introduction

THE plane theory of elasticity has found wide application in many engineering problems, for which the problem of multiple-valued displacements has attained new significance. Its treatment, found in a number of elasticity textbooks, is based on the concept of the dislocation theory as introduced by Volterra [10].[1] In Volterra's theory, the dislocation cut connects two closed boundary curves. After rigid displacement, the two edges are joined again, resulting in a discontinuous displacement along the dislocation cut, while the stress components are continuous. This type of analysis does not apply to a certain class of problem when there is a dislocation cut which initiates from a boundary and ends in the material. A more recent theory, permitting elastic deformation of both edges before joining, and relaxing the stress-continuity condition across the dislocation cut [2], introduces an elastic-dislocation concept. Thus it overcomes this restriction on the Volterra-type dislocation problem. The present paper, through the use of complex-variable representation, generalizes the application of the elastic-dislocation theory. It explores the Airy stress function of a doubly connected region with an arbitrary dislocation cut, which in the sequel is referred to as the cut.

[1] Numbers in brackets designate References at end of paper.

Presented at the Summer Conference of the Applied Mechanics Division, University Park, Pa., June 20–22, 1960, of THE AMERICAN SOCIETY OF MECHANICAL ENGINEERS.

Discussion of this paper should be addressed to the Secretary, ASME, 29 West 39th Street, New York, N. Y., and will be accepted until October 10, 1960, for publication at a later date. Discussion received after the closing date will be returned.

NOTE: Statements and opinions advanced in papers are to be understood as individual expressions of their authors and not those of the Society. Manuscript received by ASME Applied Mechanics Division, July 2, 1959. Paper No. 60—APM-14.

Preliminary Study of Basic Concepts

Plane Elastic Theory. The differential equation for the complex Airy stress function $U(z, \bar{z})$ is

$$\frac{\partial^4 U}{\partial z^2 \partial \bar{z}^2} = 0 \tag{1}$$

where the complex variable $z = x + iy$, and $\bar{z} = x - iy$ its conjugate. Since the Airy stress function is real, the most general solution of (1) is

$$2U = \bar{z}\varphi_1(z) + z\overline{\varphi_1(z)} + \varphi_2(z) + \overline{\varphi_2(z)} \tag{2}$$

Expression (2) was derived by E. Goursat. For a lengthier but more elegant treatment, one is referred to Muskhelishvili [3]. The Kolosov formulas for the stress and the displacement components are

$$\left.\begin{aligned} \sigma_x + \sigma_y &= 2[\varphi_1'(z) + \overline{\varphi_1'(z)}] = 4\Re[\varphi_1'(z)] \\ \sigma_y - \sigma_x + 2i\tau_{xy} &= 2[\bar{z}\varphi_1''(z) + \varphi_2''(z)] \\ 2\mu(u_x + iu_y) &= \kappa\varphi_1(z) - z\overline{\varphi_1'(z)} - \overline{\varphi_2'(z)} \end{aligned}\right\} \tag{3}$$

where

$$\varphi_1'(z) = \frac{\partial \varphi_1}{\partial z}, \quad \varphi_1''(z) = \frac{\partial^2 \varphi_1}{\partial z^2}, \quad \varphi_2'(z) = \frac{\partial \varphi_2}{\partial z}, \quad \varphi_2'' = \frac{\partial^2 \varphi_2}{\partial z^2}$$

The normal and tangential components of displacement and stress for any direction, plus the polar form of the latter are correspondingly as follows [11, 3]:

$$\left.\begin{aligned} \sigma_n - i\tau_n &= \varphi_1'(z) + \overline{\varphi_1'(z)} + [\bar{z}\varphi_1''(z) + \varphi_2''(z)]e^{i2\alpha} \\ \sigma_r - i\tau_{r\theta} &= \varphi_1'(z) + \overline{\varphi_1'(z)} - [\bar{z}\varphi_1''(z) + \varphi_2''(z)]e^{i2\theta} \\ 2\mu(u_t + iu_n)e^{i\alpha} &= \kappa\varphi_1(z) - z\overline{\varphi_1'(z)} - \overline{\varphi_2'(z)} \end{aligned}\right\} \tag{4}$$

Nomenclature

σ_n = normal stress on plane with normal n
τ_n = shearing stress on plane with normal n
$\sigma_x, \sigma_y, \tau_{xy}$ = stress components in Cartesian co-ordinates
$\sigma_r, \sigma_\theta, \tau_{r\theta}$ = stress components in polar co-ordinates
u_x, u_y = displacement components in Cartesian co-ordinates
u_n, u_t = displacement components normal and tangent to dislocation curve, respectively
$U(z, \bar{z})$ = Airy stress function
$\varphi_1(z), \varphi_2(z)$ = functions of z in Airy stress function
λ, μ = Lamé's constants
δ = constant, dislocation of cut at inner boundary
σ', τ' = stress discontinuity along cut
$u' = u^+ - u^-$ = dislocation, or displacement discontinuity along cut
ν = Poisson's ratio
κ = constant, $\kappa = \dfrac{3 - \nu}{1 + \nu}$ in plane-stress and $\kappa = 3 - 4\nu$ in plane-strain case
α = angle between x-axis and tangent to cut
$z_0 = x_0 + iy_0$ = an arbitrary point on cut
$\Re$ = indicating real part of a function
$\Im$ = indicating imaginary part of a function
$(\ )_{mv}$ = multiple-valued portion of a function
$(\ )_{sv}$ = single-valued portion of a function

Dislocation Theory. To every point on the cut correspond two coincident points belonging to the two faces of the curve. One or both of the components of displacement of the coincident points are allowed to take on different values. In other words, the two coincident points are subject to displacements relative to each other and to be called in the sequel dislocations. At the terminus, the end point of the cut, the dislocation is zero, while at its inner-boundary end, the dislocation could be some arbitrary value. The normal and shearing-stress components on the tangent to the cut must be continuous by Newton's third law. By specifying sides of the cut as positive and negative, the dislocation and stress-continuity conditions may be given the form:

$$\left.\begin{aligned} u_t' &= u_t^+ - u_t^- = 0 \\ u_n' &= u_n^+ - u_n^- = 0 \end{aligned}\right\} \text{ at the terminus } (-c, 0), \tag{5}$$

$$\left.\begin{aligned} u_t' &= \delta_1 \\ u_n' &= \delta_2 \end{aligned}\right\} \text{ at the inner-boundary end,} \tag{6}$$

$$\left.\begin{aligned} \sigma_n' &= \sigma_n^+ - \sigma_n^- = 0 \\ \tau_n' &= \tau_n^+ - \tau_n^- = 0 \end{aligned}\right\} \text{ along the cut} \tag{7}$$

The dislocation condition along the cut can be some function of the radial distance.

Boundary Conditions. The boundary-value problem under consideration is of the mixed type. On both the inner and the outer boundaries the stresses are specified; while along the cut, the displacements are given. Points along the cut are excluded to preserve single-valuedness in the region. To study the effect of the presence of a cut, it is sufficient to discuss the case of no external loading, for which

$$\sigma_n = \tau_n = 0, \text{ on both boundaries} \tag{8}$$

Derivation of Method

Nature of Stress Function. It is sufficient here to consider only one cut in the region, which lies in the complex plane. Let the inner boundary encircle the origin, and the terminus of the cut be the point $(-c, 0)$. The shape of the cut is some arbitrary curve connecting the terminus and a point $ae^{i\theta_1}$ on the inner boundary.

The basic concept of the dislocation theory, by which the displacement components and some stress components take on different values upon approaching a point on the cut from different sides, implies that the displacement components and some stress components are multiple-valued in nature. This type of displacement and stress components can only result from a stress function which is a linear combination of both multiple and single-valued terms. The logarithmic function will be chosen as the form of the multiple-valued term. Again, from physical conditions, the stress and the displacements are discontinuous only along the cut, but single-valued elsewhere. To satisfy this requirement, the multiple-valued terms in the equations have to contain two branch points such that the branch cut, connecting the two, falls along the cut but nowhere else in the region. One of the branch points has to be at the terminus of the cut; the other can be anywhere in the closed region bounded by the inner boundary. For convenience and mathematical simplicity, this branch point will be chosen at the origin. The multiple-valued factor in the term is then $\log (z + c)/z$, and the stress functions, expressed in the linear combination of the multiple-valued and single-valued terms, are, in general, of the form:

$$\varphi_1(z) = A(z) \log \frac{z + c}{z} + C(z) \tag{9}$$

$$\varphi_2(z) = B(z) \log \frac{z + c}{z} + D(z) \tag{10}$$

where $A(z)$, $B(z)$, and $C(z)$ are single-valued and analytic in the region. Recalling the fact that $\varphi_2(z)$ occurs in the displacement and the stress equations only in the form of its derivatives (3), (4), the function $D(z)$ is subjected to a less restrictive condition. For higher derivatives of those functions, complex-variable theory conveniently states that all derivatives of an analytic function are analytic. The singularity introduced by the term $\log (z + c)$ at the point $(-c, 0)$ is removed by the condition

$$A(-c, 0) = B(-c, 0) = 0 \tag{11}$$

Method for Determining Multiple-Valued Terms. Inasmuch as only the multiple-valued terms are affected at the cut, the conditions prevailing at the cut are sufficient to determine the multiple-valued terms of the stress function. The displacement equation in (4), combined with the definition of the tangential and the normal components of dislocation, yield

$$2\mu(u_t' + iu_n')e^{i\alpha} = -2\pi i[\kappa A(z_0) + z_0\overline{A'(z_0)} + \overline{B'(z_0)}], \tag{12}$$

where z_0 is an arbitrary point on the cut. This equation is to be solved subject to the boundary conditions (7) and (8). Equations (4) and (7) yield

$$A'(z_0) - \overline{A'(z_0)} + [\bar{z}_0 A''(z_0) + B''(z_0)]e^{i2\alpha} = 0 \tag{13}$$

The analytic functions $A(z)$ and $B(z)$ in equation (16) may be written in the form of Laurent series, such that

$$A(z) = \sum_{-\infty}^{\infty} (R_n + iS_n)z^n \tag{14}$$

$$B(z) = \sum_{-\infty}^{\infty} (P_n + iQ_n)z^{n+1} \tag{15}$$

Method for Determining Single-Valued Terms. The expressions for $\varphi_1(z)$ and $\varphi_2(z)$ are complete with the determination of the single-valued function $C(z)$ and $D'(z)$. After the solution for $D'(z)$ the function $D(z)$ may be considered known since there is only a constant of integration undetermined in the stress function. As long as the constant does not affect the displacements and stresses, it may well be neglected. Next, the functions $C(z)$ and $D'(z)$ will be written in the form of Laurent series, such that

$$\begin{aligned} C(z) &= \sum_{-\infty}^{\infty} (K_n + iL_n)z^{n+1} \\ D'(z) &= \sum_{-\infty}^{\infty} (M_n + iN_n)z^{n-1} \end{aligned} \tag{16}$$

The single-valued part of the stress equation in (4) can thus be expressed in the form of series. To facilitate the mathematical manipulation, the polar form of the series will be used. Thus by a change of limit, there results:

$$\begin{aligned} (\sigma_r - i\tau_{r\theta})_{sv} &= 2K_0 + r^{-2}M_0 + (2rK_1 + 2r^{-1}M_{-1})\cos\theta \\ &+ \sum_{2}^{\infty} [-(n-2)(n+1)r^n K_n - (n-1)(n+2)r^{-n}K_{-n} \\ &- (n-1)r^{n-2}M_n + (n+1)r^{-(n+2)}M_{-n}]\cos n\theta + (-2rL_1 \\ &+ 2r^{-1}N_{-1})\sin\theta + \sum_{2}^{\infty} [(n+1)(n-2)r^n L_n - (n-1)(n \\ &+ 2)r^{-n}L_{-n} + (n-1)r^{n-2}N_n + (n+1)r^{-(n+2)}N_{-n}]\sin n\theta \\ &+ i\left\{ r^{-2}N_0 + (-2rL_1 + 2r^{-2}N_{-1})\cos\theta + \sum_{2}^{\infty} [-n(n \right. \end{aligned}$$

$$+ 1)r^n L_n - n(n-1)r^{-n}L_{-n} - (n-1)r^{n-2}N_n + (n$$
$$+ 1)r^{-(n+2)}N_{-n}] \cos n\theta + (-2rK_1 - 2r^{-1}M_{-1}) \sin \theta$$
$$+ \sum_2^\infty [-n(n+1)r^n K_n + n(n-1)r^{-n}K_{-n}$$
$$- (n-1)r^{n-2}M_n - (n+1)r^{-(n+2)}M_{-n}] \sin n\theta \Big\} \quad (17)$$

The multiple-valued part of the expressions for the stress must be added to (17). Together with the boundary condition (8) the constants K, L, M, and N can be determined by expanding the multiple-valued terms in Fourier series and comparing corresponding sine and cosine terms.

Application

For the problems by which the foregoing work will be demonstrated, the inner boundary is a circle with center at the origin. The outer boundary is at infinity.

Solution of Multiple-Valued Terms. The two classes of cuts to be illustrated are a straight cut and a logarithmic cut; the governing equations are, respectively,

$$(x_0 + c) \tan \alpha_0 = y_0 \quad (18)$$

$$\theta_0 = \pi + \tan \beta \cdot \log(r_0/c) \quad (19)$$

Case I. A Class of Straight Cuts Joining $(-c, 0)$ and an Arbitrary Given Point on the Inner Circumference: $(a \cos \theta_1, a \sin \theta_1)$ (Fig. 1). It is seen from Fig. 1 the angle α is a constant. If the dislocation relation along the cut is linear, the expressions for $A(z)$ and $B(z)$, obtained from equation (12) are

$$A(z) = (R_0 + iS_0) + (R_1 + iS_1)z$$
$$B(z) = (P_{-1} + iQ_{-1}) + (P_0 + iQ_0)z + (P_1 + iQ_1)z^2 \quad (20)$$

It follows from (11) and (13) that

$$(P_{-1} - P_0 c - S_1 c^2 \sin 2\alpha) + i(Q_{-1} - Q_0 c - S_1 c^2 \cos 2\alpha) = 0,$$
$$A(z) = (R_1 + iS_1)(z + c) \quad (21)$$
$$B(z) = (P_{-1} + iQ_{-1}) + (P_0 + iQ_0)z - (\sin 2\alpha + i \cos 2\alpha)S_1 z^2$$

By (12), these values of $A(z)$ and $B(z)$ lead to

$$u_t' = -\{(\kappa R_1 c + P_0) + [(\kappa + 1)R_1 - 2S_1 \sin 2\alpha]x_0 - (\kappa$$
$$- 1 - 2\cos 2\alpha)S_1 y_0\} \frac{\pi}{\mu} \sin \alpha$$
$$+ \{(\kappa S_1 c - Q_0) + (\kappa - 1 + 2\cos 2\alpha)S_1 x_0$$
$$+ [(\kappa + 1)R_1 + 2S_1 \sin 2\alpha]y_0\} \frac{\pi}{\mu} \cos \alpha, \quad (22)$$

$$u_n' = -\{(\kappa R_1 c + P_0) + [(\kappa + 1)R_1 - 2S_1 \sin 2\alpha]x_0$$
$$- (\kappa - 1 - 2\cos 2\alpha)S_1 y_0\} \frac{\pi}{\mu} \cos \alpha$$
$$- \{(\kappa S_1 c - Q_0) + (\kappa - 1 + 2\cos 2\alpha)S_1 x_0$$
$$+ [(\kappa + 1)R_1 + 2S_1 \sin 2\alpha]y_0\} \frac{\pi}{\mu} \sin \alpha, \quad (23)$$

where x_0 and y_0 are the Cartesian co-ordinates of an arbitrary point z_0 on the cut.

(a) Wedge-Shaped Dislocation Cut (Fig. 2). In this type of problem, the dislocation of coincident points is normal to the cut. The dislocation conditions then are

$$u_t' = 0$$
$$u_n'(-c, 0) = 0$$
$$u_n'(a \cos \theta_1, a \sin \theta_1) = \delta_2 = \text{negative constant}$$

The negative normal dislocation is prescribed to avoid any case of interference. Equations (21), (22), and (23) yield the complete solutions for $A(z)$ and $B(z)$:

$$A(z) = \Delta_1(z + c)$$
$$B(z) = \Delta_1 c(z + c)$$

where

$$\Delta_1 = \mu\delta_2/\pi(\kappa + 1)(c^2 + a^2 + 2ca \cos \theta_1)^{1/2}$$

(b) Faces of Cut Slipped With Respect to One Another (Fig. 3). For this dislocation condition, the relative displacement of coincident points is tangential to the cut. The dislocation conditions thus are

$$u_n' = 0$$

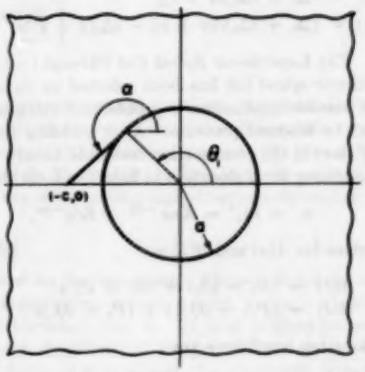

Fig. 1

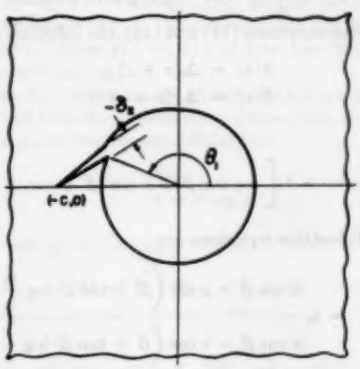

Fig. 2

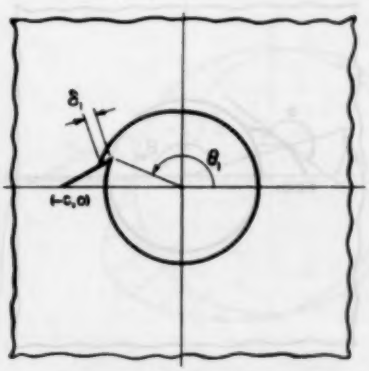

Fig. 3

$$u_i'(-c, 0) = 0$$
$$u_i'(a\cos\theta_1, a\sin\theta_1) = \delta_1$$

Equations (21), (22), and (23) follow the expressions for $A(z)$ and $B(z)$:

$$A(z) = i\Delta_2(z + c)$$
$$B(z) = i\Delta_2 c(z + c) - i\Delta_2(z + c)^2 e^{-i2\alpha},$$

where

$$\Delta_2 = \mu\delta_1/\pi(\kappa + 1)[a\cos(\alpha - \theta_1) + c\cos\alpha]$$

(c) General Linear Dislocation. The solution for this type of dislocation problem will simply be the combination of the two special cases as discussed in (*a*) and (*b*), resulting in

$$A(z) = (\Delta_1 + i\Delta_2)(z + c),$$
$$B(z) = (\Delta_1 + i\Delta_2)c(z + c) - i\Delta_2(z + c)^2 e^{-i2\alpha}$$

Case II. The Logarithmic Spiral Cut Through $(-c, 0)$ (Fig. 4). The logarithmic spiral cut has been selected as an example because of its possible application to problems of thick-walled cylinders subject to internal pressure. After yielding has occurred, the Lüders' lines in the cross section resemble closely logarithmic spirals. Assuming the dislocation to have the form that

$$u_i' + iu_n' = Kr_0 e^{-i\beta} + K' e^{-i\alpha},$$

the expressions for $A(z)$ and $B(z)$ are

$$A(z) = (R_0 + iS_0) + (R_1 + iS_1)z$$
$$B(z) = (P_{-1} + iQ_{-1}) + (P_0 + iQ_0)z$$

The dislocation conditions are

$$u_i'(-c, 0) = u_n'(-c, 0) = 0$$
$$u_n'(r_0 = a) = \delta_2 = \text{a negative constant}$$

Together with equations (11) and (13), the solutions are

$$A(z) = \Delta_3(z + c)$$
$$B(z) = \Delta_3 c(z + c)$$

where

$$\Delta_3 = \mu\delta_2/\pi(\kappa + 1)\left[-a\cos\beta + c\cos\left(\beta + \tan\beta\cdot\log\frac{a}{c}\right)\right],$$

while the dislocation equations are

$$u_i' = \delta_2 \frac{r_0\sin\beta - c\sin\left(\beta + \tan\beta\cdot\log\dfrac{r_0}{c}\right)}{a\cos\beta - c\cos\left(\beta + \tan\beta\cdot\log\dfrac{a}{c}\right)} \tag{24}$$

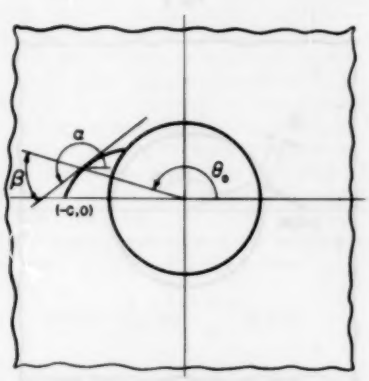

Fig. 4

$$u_n' = \delta_2 \frac{r_0\cos\beta - c\cos\left(\beta + \tan\beta\cdot\log\dfrac{r_0}{c}\right)}{a\cos\beta - c\cos\left(\beta + \tan\beta\cdot\log\dfrac{a}{c}\right)} \tag{25}$$

The foregoing solutions, in a condition closely resembling the Lüders' line of the thick-walled cylinder problem with $\beta = 45$ deg, are expressed as

$$u_i' = \delta_2 \frac{r_0 - \sqrt{2}\,c\sin\left(\dfrac{\pi}{4} + \log\dfrac{r_0}{c}\right)}{a - \sqrt{2}\,c\sin\left(\dfrac{\pi}{4} - \log\dfrac{a}{c}\right)}$$
$$u_n' = \delta_2 \frac{r_0 - \sqrt{2}\,c\sin\left(\dfrac{\pi}{4} - \log\dfrac{r_0}{c}\right)}{a - \sqrt{2}\,c\sin\left(\dfrac{\pi}{4} - \log\dfrac{a}{c}\right)} \tag{26}$$

Single-Valued Terms in the Cases Under Consideration. Let the expressions for $A(z)$ and $B(z)$ be

$$A(z) = (T + iV)(z + c)$$
$$B(z) = (T + iV)c(z + c) - iV(z + c)^2 e^{-i2\alpha_0} \tag{27}$$

where T, V, and α_0 are real constants. α_0 in the second of equations (27) has the value $(\pi + \phi_0)$, where ϕ_0, is the angle included between the $+x$-axis and the line connecting two end points of the cut $(-c, 0)$ and $(a\cos\theta_1, a\sin\theta_1)$. By giving T or V different values, the formulas (27) can be made to call all three of the foregoing problems. The multiple-valued portion of the stress-component equation, by virtue of the expressions for $A(z)$ and $B(z)$ in (27), is as follows:

$$(\sigma_r - i\tau_{r\theta})_{mv} = 2\Re\left[(T + iV)\left(\log\frac{z + c}{z} - \frac{c}{z}\right)\right]$$
$$- (T + iV)c^2\left[\frac{z + ce^{i2\theta}}{z^2(z + c)}\right]$$
$$+ iVe^{-i2(\alpha_0 - \theta)}\left[2\log\frac{z + c}{z} + \frac{c(c - 2z)}{z^2}\right]$$

The complete expression for the stress components is

$$\sigma_r - i\tau_{r\theta} = (\sigma_r - i\tau_{r\theta})_{sv} + (\sigma_r - i\tau_{r\theta})_{mv}$$

The multiple-valued terms can also be expanded into infinite trigonometrical series (in the inner circumference, between the limits $[(\theta_1 - 2\pi) < \theta < \theta_1]$. When the constants in the single-valued portion are determined, the general form of the stress function for the classes of dislocation problems considered is then as follows:

$$\varphi_1(z) = (T + iV)(z + c)\log\frac{z + c}{z} + \sum_{-\infty}^{\infty}(K_n + iL_n)z^{n+1}$$

$$\varphi_2(z) = [(T + iV)c(z + c) - iV(z + c)^2 e^{-i2\alpha_0}]\log\frac{z + c}{z} + \sum_{-\infty}^{\infty}(M_n + iN_n)\int z^{n-1}dz \tag{28}$$

The constants, as solved for a traction-free case, are

$$N_0 = K_0 = K_1 = L_1 = K_2 = L_2 = M_2 = N_2 = K_n = L_n = M_n = N_n = 0$$

$$M_0 = a^2\left\{T\left(\frac{c^2}{a^2} - 1 - 2\log\frac{c}{a}\right) + V\left[2(\pi - \theta_1) - \frac{\left(2ca + \frac{2c^3}{a}\right)\sin\theta_1 + 2c^2\sin 2\theta_1}{a^2 + 2ca\cos\theta_1 + c^2}\right]\right\}$$

$$M_{-1} = a^2\left\{T\left(\frac{c}{a} - \frac{a}{2c}\right) - V\left[\frac{(c^2 + {}^4/_3a^2)\sin\theta_1 + {}^5/_3ca\sin 2\theta_1 + {}^{\frac{2}{3}}/_3c^2\sin 3\theta_1}{a^2 + 2ca\cos\theta + c^2}\right]\right\}$$

$$N_{-1} = a^2V\left[\frac{\frac{a^2}{2c} + {}^5/_2ca + \frac{c^3}{a} + ({}^7/_3a^2 + 3c^2)\cos\theta_1 + {}^5/_3ca\cos 2\theta_1 + {}^1/_3c^2\cos 3\theta_1}{a^2 + 2ca\cos\theta_1 + c^2}\right]$$

$$K_{-2} = a^2\left\{T\left(\frac{a^2}{2c^2} - 1\right) + V\left[\sin 2\theta_1 + \left(2\log\frac{c}{a}\right)\sin 2\alpha_0 - 2(\pi - \theta_1)\cos 2\alpha_0\right]\right\}$$

$$M_{-2} = a^4\left\{T\left(\frac{2a^2}{3c^2} - 1\right) + V\left[{}^2/_3\sin 2\theta_1 + 2\left({}^1/_{12}\cos 4\theta_1 + \log\frac{c}{a}\right)\sin 2\alpha_0 - 2(\pi - \theta_1 + {}^1/_{12}\sin 4\theta_1)\cos 2\alpha_0\right]\right\}$$

$$L_{-2} = a^2V\left[-\cos 2\theta_1 - 2(\pi - \theta_1)\sin 2\alpha_0 - \left(2\log\frac{c}{a}\right)\cos 2\alpha_0 + {}^1/_2 - \frac{a^2}{2c^2}\right]$$

$$N_{-2} = a^4V\left[-{}^2/_3\cos 2\theta_1 - 2(\pi - \theta_1 - {}^1/_{12}\sin 4\theta_1)\sin 2\alpha_0 + 2\left({}^1/_{12}\cos 4\theta_1 - \log\frac{c}{a}\right)\cos 2\alpha_0 + {}^2/_3 - \frac{2a^2}{3c^2}\right]$$

$$K_{-n} = a^n\left\{T\left[\frac{1}{n} - \frac{c^2}{a^2(n-1)}\right]\left(\frac{a}{c}\right)^n(-1)^n + V\left[\frac{2}{(n-1)(n-2)}\sin\overline{(n-2)\theta_1 + 2\alpha_0)} + \frac{2}{n(n-1)}\sin n\theta_1 + (-1)^{n+1}\frac{2\sin 2\alpha_0}{(n-1)(n-2)}\left(\frac{a}{c}\right)^{n-2}\right]\right\}$$

$$M_{-n} = a^{n+2}\left\{T\left(\frac{n}{n+1} - \frac{c^2}{a^2}\right)\left(\frac{a}{c}\right)^n(-1)^n + V\left[\frac{2}{n-2}\sin\overline{(n-2\theta_1 + 2\alpha_0)} - \frac{2}{(n+1)(n+2)}\sin\overline{(n+2\theta_1 - 2\alpha_0)} + \frac{2}{n+1}\sin n\theta_1 + 2(-1)^{n+1}\frac{\sin 2\alpha_0}{n-2}\left(\frac{a}{c}\right)^{n-2}\right]\right\}$$

$$L_{-n} = a^nV\left\{-\frac{2}{(n-1)(n-2)}\cos\overline{(n-2\theta_1 + 2\alpha_0)} - \frac{2}{n(n-1)}\cos n\theta_1 + (-1)^{n+1}\left(\frac{a}{c}\right)^n\left[\frac{1}{n} - \frac{2\cos 2\alpha_0 + n - 2}{(n-1)(n-2)}\frac{c^2}{a^2}\right]\right\}$$

$$N_{-n} = a^{n+2}V\left[-\frac{2}{n-2}\cos\overline{(n-2\theta_1 + 2\alpha_0)} + \frac{2}{(n+1)(n+2)}\cos\overline{(n+2\theta_1 - 2\alpha_0)} - \frac{2}{n+1}\cos n\theta_1 + (-1)^{n+1}\left(\frac{a}{c}\right)^n\left(\frac{n}{n+1} - \frac{2\cos 2\alpha_0 + n - 2}{n-2}\frac{c^2}{a^2}\right)\right]$$

The result is applied for a sliding-face radial cut in an infinite plate. Fig. 5 indicates the distribution of the circumferential stress along the circular hole and the shearing stress along the cut, when the length of cut reaches one radial distance. The maximum circumferential stress is approximately $[9 \times 10^6(\delta/a)]$ psi for steel, where δ/a is the dislocation-radius ratio at the hole end of the cut. The shearing stress at the hole end of the cut is approximately $[7.5 \times 10^6(\delta/a)]$ psi for steel, while at the terminus end it diverges, indicating high stress concentration.

Discussion

Behavior of the Terminus Point. The stress and the displacement-component equations contain a term, $\log(z + c)$, which is singular at the terminus $(-c, 0)$. It is of interest to investigate the nature of the singularity at the particular point $(-c, 0)$. A concentrated force or a couple at the point will introduce a strain energy of some finite magnitude in an arbitrarily small neighborhood of $(-c, 0)$. Consequently, if the strain energy in the ϵ-neighborhood of $(-c, 0)$ approaches an infinitesimal value, the stressed condition at $(-c, 0)$ is at least less than the order of a concentrated loading.

When the expressions in (28) are substituted into equations (4), it is observed that the displacement components are finite, while the stress components become infinite like

$$\lim_{\epsilon \to 0} \log \epsilon$$

The strain energy in the neighborhood of $(-c, 0)$ is

$$2J = \oint_c (\sigma_n u_n + \tau_n u_t)ds,$$

where

$$\max(\sigma_n, \tau_n) = K \lim_{z \to -c} \log(z + c),$$

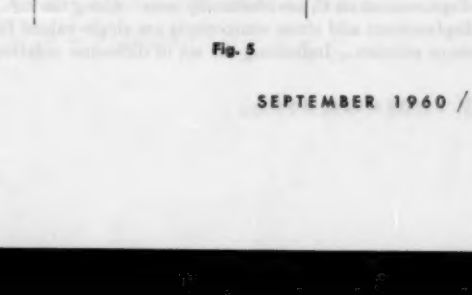

Fig. 5

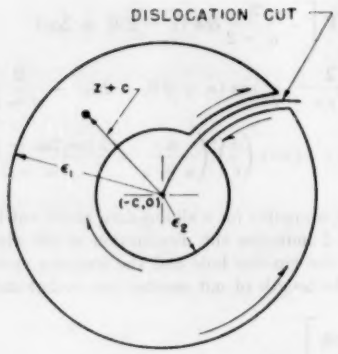

Fig. 6

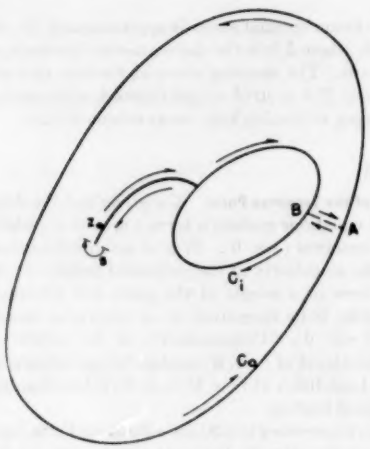

Fig. 7

(u_n, u_t) are finite, and C is the closed path about $(-c, 0)$ shown in Fig. 6. Without loss of generality we may let ϵ_1 be some finite multiple of ϵ_2. Whereupon

$$\lim_{\substack{\epsilon_1 \to 0 \\ \epsilon_2 \to 0}} \left| \oint_c (\sigma_n u_n + \tau_n u_t) ds \right| \leqslant \lim_{\epsilon_2 \to 0} K' \left| \log (z + c) \right| \left| \oint_c ds \right|$$

$$= K' \lim_{\epsilon_2 \to 0} | \epsilon_2 \log \epsilon_2 | = 0$$

The strain energy is infinitesimal in the neighborhood of $(-c, 0)$. Thus the solutions at that point are not the results of any concentrated loading. This type of stress-concentration has been explained by the experimental studies of Lüders' band in the works of Steele and Taira [5, 8].

Uniqueness of Solution. For the proof of uniqueness of solution, the method of mathematical contradiction is employed. Hypothetically it is assumed that there exists a second set of solutions different from the first but satisfying the same differential equation and boundary conditions, in which the stress is prescribed on C_1 while the displacement is given on C_2. C_1 and C_2 together constitute the complete boundary, C, of the region.

The difference of the two solutions should satisfy the same linear homogeneous equation with undisturbed boundary condition. By undisturbed, it means that the prescribed stress on C_1 and displacement on C_2 are identically zero. Along the cut, both the displacement and stress components are single-valued for the difference solution. Indicating the set of difference solutions by a superscript of an asterisk symbol, its strain-energy expression is

$$2J^* = \oint_c (\sigma_n^* u_n^* + \tau_n^* u_t^*) ds$$

With reference to Fig. 7, it is seen that the integrand is zero identically on C_0 and C_i. Single-valuedness of the integrand cancels line integrations along A-B and B-A, as well as along the positive and the negative sides of the cut. Line integration along the semicircular path, s, about the branch point also vanishes, as the radius of the semicircle approaches infinitesimal value. The proof is as follows:

$$\max (\sigma_n^*, \tau_n^*) = K \lim_{\epsilon \to 0} \log \epsilon$$

u_n^* and u_t^* are finite,

thus

$$\left| (\sigma_n^* u_n^* + \tau_n^* u_t^*) \right| \leqslant K' \lim_{\epsilon \to 0} \left| \log \epsilon \right|$$

It follows then

$$\left| \int_s (\sigma_n^* u_n^* + \tau_n^* u_t^*) ds \right| \leqslant \lim_{\epsilon \to 0} K' \left| \log \epsilon \right| \left| \pi \epsilon \right| = 0$$

The strain-energy expression vanishes accordingly. Following the Kirchhoff proof, the difference between two sets of solutions is identically zero. Since it contradicts the hypothesis, there is only one possible solution, which, if it exists, is unique.

By a simple rotation of the complex plane, the terminus can be located at any point z_1. Any number of cuts is permissible through superposition of the multiple-valued terms, provided that there is no cross path of cuts.

Acknowledgment

This paper is a portion of the author's doctorate dissertation under the able supervision of Prof. M. C. Stippes at the Theoretical and Applied Mechanics Department, University of Illinois. Thesis topic was suggested by Dr. M. C. Steele, AiResearch Corp., Phoenix, Arizona.

References

1 K. Knopp, "Elements of the General Theory of Analytic Functions," *Theory of Functions*, Part 1, Dover Publications, Inc., New York, N. Y., 1945.

2 E. H. Mann, "An Elastic Theory of Dislocations," *Proceedings of The Royal Society*, series A, vol. 199, 1949.

3 N. I. Muskhelishvili, "Some Basic Problems of the Mathematical Theory of Elasticity," third edition, P. Noordohoff Limited, Groningen, Holland, 1953.

4 M. C. Steele and L. C. Eichberger, "The Overstraining of Thickwalled Mild Steel Cylinder," T and AM Report No. 79, University of Illinois, Urbana, Ill.

5 M. C. Steele and L. C. Eichberger, "An X-Ray Stress Study of Non-Homogeneous Yielding in Low Carbon Steel Cylinder," T and AM Report No. 111, University of Illinois, Urbana, Ill.

6 M. C. Steele and F. D. Ju, "A Problem in the Elastic Theory of Dislocations," T and AM Report No. 99, University of Illinois, Urbana, Ill.

7 E. Sternberg and R. A. Eubanks, "On the Concept of Concentrated Loads and An Extension of the Uniqueness Theorem in the Linear Theory of Elasticity," *Journal of Rational Mechanics and Analysis*, vol. 4, 1955, pp. 135–168.

8 S. Taira, "Stress Distribution in Partially Yielded Beams of Low Carbon Steel," T and AM Report No. 92, University of Illinois, Urbana, Ill.

9 R. Tiffen, "Uniqueness Theorems of Two-Dimensional Elasticity Theory," *Quarterly of Journal of Mechanics and Applied Mathematics*, vol. 5, 1952, pp. 237–252.

10 V. Volterra, "Sur L'Equilibre des Corps Elastiques Multiplement Connexes," *Annales de L'Ecole Normale Supérieure*, vol. 24, 1907, pp. 401–517.

11 C. T. Wang, "Applied Elasticity," McGraw-Hill Book Company, Inc., New York, N. Y., 1953.

PAUL SEIDE
Member of the Technical Staff,
Space Technology Laboratories, Inc.,
Los Angeles, Calif.
Assoc. Mem. ASME

The Effect of Pressure on the Bending Characteristics of an Actuator System[1]

The effect of internal or external pressure on the bending of a cantilevered bellows, the movable end of which is permitted only to rotate about a fixed point on the longitudinal axis of the beam, is investigated. It is found that the bending characteristics of the system vary considerably with changes in pressure and pivot-point location and that instability of the system may occur. The experimental results given tend to confirm the behavior predicted by the theory.

Introduction

THE fact that internal pressure may under certain circumstances contribute to or be the sole cause of buckling of cylindrical shells has appeared several times in the literature, implicitly or explicitly; but apparently it has not made much of an impression upon workers in the field. A system of equations capable of predicting the effect appeared in 1924 in the book, "Applied Elasticity," by J. Prescott [1][2] and again in 1932 in a paper by K. von Sanden and F. Tölke [2]. The phenomenon was apparently overlooked, however, since the authors were primarily interested in the buckling of shells under external pressure. Specific notice was taken of the phenomenon in 1932 when W. Flügge presented his set of equations for the elastic stability of cylindrical shells [3] and deduced its existence. For the next 20 years or so the phenomenon appears to have been forgotten until the actual occurrence of buckling in various structures stimulated its re-examination [4, 5].

The theoretical results for simply supported circular cylinders presented by the foregoing authors agree when the cylinder is relatively long (length greater than about 30 radii). For this case, buckling occurs when the end-plate reactions are equal to the axial buckling load of the cylinder considered as a simply supported Euler column, provided that the end plates sealing the cylinder are free to rotate but are held against translation in such a way that the cylinder walls are unloaded axially. We may reinterpret this result as implying that internal pressure has little or no effect on the Euler buckling load of the cylinder so that the end result is the same as if the cylinder were closed at the ends and allowed to stretch, then loaded axially with a force equal to the Euler buckling load. The associated mode of buckling is similar to that of a simply supported Euler column, since there is little distortion of the shape of the cross sections, plane sections perpendicular to the neutral axis prior to buckling remain plane and practically perpendicular to the neutral axis after buckling, and the neutral axis assumes the shape of a half-sine wave.

For shorter cylinders the results of references [1–3] do not agree at all. If we neglect higher-order terms in the various stability criteria, which are of little consequence except for extremely short cylinders, we find that Prescott's results indicate no change in the buckling pressure as compared to that predicted on the basis of beam theory, and that von Sanden's and Tölke's results indicate a considerable increase in the buckling pressure, while Flügge's results indicate a considerable decrease in the pressure. Beam theory, which assumes no distortion of the cross sections of the cylinder and thus deals with a stiffer structure, should yield an upper bound to the buckling pressure. We may therefore conclude that von Sanden's and Tölke's results, being higher than beam theory indicates, are incorrect. This is probably due to limitations in their theory. Since Flügge's theory appears to be quite accurate we may further conclude that the decrease in

[1] The paper is a condensation of Report GM-TR-0165-00530 (EM8-25), Space Technology Laboratories, Inc., December 31, 1958.

[2] Numbers in brackets designate References at end of paper.

Presented at the Summer Conference of the Applied Mechanics Division, University Park, Pa., June 20–22, 1960, of THE AMERICAN SOCIETY OF MECHANICAL ENGINEERS.

Discussion of this paper should be addressed to the Secretary, ASME, 29 West 39th Street, New York, N. Y., and will be accepted until October 10, 1960, for publication at a later date. Discussion received after the closing date will be returned.

NOTE: Statements and opinions advanced in papers are to be understood as individual expressions of their authors and not those of the Society. Manuscript received by ASME Applied Mechanics Division, January 26, 1959. Paper No. 60—APM-16.

Nomenclature

A = cross-sectional area of equivalent beam, sq in.
A_1, B_1, C_1, D_1 = constants in deflection function
f_1, f_2, f_3, f_4 = functions of u or $\bar{u}$ defining relationship between actuator moment and angular rotation of actuator arm
k_δ = ratio of applied axial load and axial movement of one end of unpressurized bellows with respect to the other, lb/in.
k_θ = ratio of applied end moment and rotation of one end of unpressurized bellows with respect to the other, in-lb/radian
L = length of bellows, in.
M = moment in equivalent beam, in-lb
M_a = actuator moment, in-lb
P = axial force induced by beam bending, lb
q = pressure, assumed positive when internal, psi
q_E = buckling pressure of clamped bellows ($4\pi^2 k_\delta / AL$), psi
R = mean radius of bellows cross sections, in.
u = $(qA + P)L/k_\theta$, used when $qA + P$ is positive
$\bar{u}$ = $-(qA + P)L/k_\theta$, used when $qA + P$ is negative
V = shear force in equivalent beam, lb
x = distance along bellows, in.
x_p = distance of pivot point from movable end of bellows, in.
y = deflection of equivalent beam, in.
θ = rotation of actuator arm, radians
$\bar{\theta}$ = $[1/4(k\delta/k\theta)]^{1/4} L \dfrac{\theta}{2\pi} \approx \dfrac{L}{R}\dfrac{\theta}{2\pi}$

buckling pressure due to short cylinder length may be significant.

It is not surprising that the phenomenon has escaped attention for so long, since large lengths and/or high pressures are required for buckling to occur. Flügge shows that, for the stresses to remain elastic, the length must be at least 50 cylinder radii, and cylinders of these dimensions are rare.[3] With cylinders of more usual dimensions, it is likely that bursting would occur rather than buckling. There are other structures, however, for which buckling and increase in deflections due to internal pressure may be serious problems. Haringx [6] has shown that, for bellows subjected to internal pressure, buckling can take place with reasonable lengths and pressures, even when the ends are clamped rather than simply supported. This is directly attributable to the decreased flexural stiffness of the bellows as compared to a circular cylinder having the same average radius, length, and material thickness. Furthermore, Haringx's experimental result indicates that an analysis of the buckling of the bellows based on beam theory may be adequate for length-radius ratios considerably lower than the validity limit for a cylinder (the ratio for the test was 9.5). Since the circumferential flexural and extensional stiffnesses of a bellows are much larger than the corresponding meridional stiffnesses, it seems reasonable to expect the beam-theory assumption of undistorted cross sections to be more accurate for short bellows than for short cylinders.

In view of the possibility of bellows buckling in an Euler column mode under internal pressure, it is evident that the effect of pressurization should be taken into account in any application in which the bellows is completely or partially unloaded in the axial direction. In the present paper we deal with a cantilevered bellows, the movable end of which is clamped to a rigid plate constrained by a rigid arm to rotate about a fixed point on the longitudinal axis of the bellows, Fig. 1(*a*). The effect of pressure and pivot-point location of the spring characteristics of the system is investigated. Variations in the pressure and pivot location are shown to cause significant changes in the characteristics of the system which affect the bellows design to a considerable extent. It is found that under internal pressure the system can become unstable for any location of the pivot point and under external pressure when the pivot point lies between the ends of the bellows.

Experimental results are given for two bellows, one internally pressurized and the other under external pressure. The comparison between theory and experiment is quite good for the bellows under external pressure, but poor for the other. A possible explanation of the poor agreement is given and the need for further testing is pointed out.

Theory

Although the particular bellows to which the following theory is to be applied are relatively short, on the basis of the preceding discussion we shall assume that they are adequately represented by uniform cylindrical beams of rigid circular cross section. The equivalent cross-section radius is assumed to be given by the mean of the inner and outer radii of the convolutions of the bellows. The axial stiffness of the beam is denoted by $k_\delta L$, where k_δ is the ratio of an axial load and the resulting axial movement of one end with respect to the other; the bending stiffness is denoted by $k_\theta L$, where k_θ is the ratio of an applied end moment and the resulting rotation of one end with respect to the other. The calculation of k_δ and/or k_θ is beyond the scope of the present paper; it is assumed that these quantities are obtained for the unpressurized beam either by some method of calculation or by direct measurement. Shear deformations are neglected, since

[3] Haringx [4] mentions that in March, 1951, the buckling of drill pipes under internal pressure was discussed at the Spring Meeting of the Southwestern District, Division of Production, American Petroleum Institute.

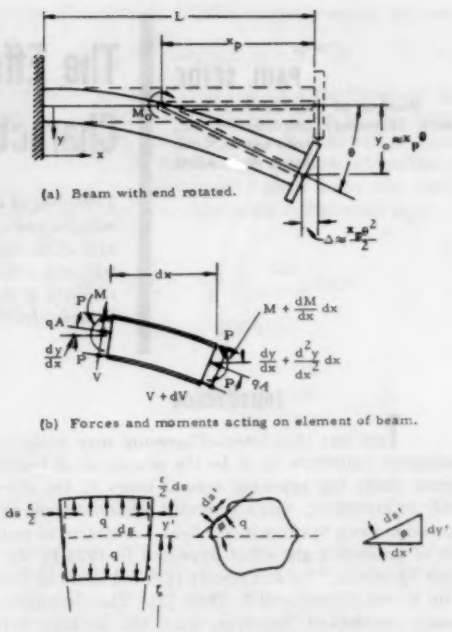

(a) Beam with end rotated.

(b) Forces and moments acting on element of beam.

(c) Pressure force acting on beam element.

Fig. 1 Notation for bellows-actuator problem

the shear stiffness is usually quite large compared to the bending stiffness.

It is assumed that pressure does not induce any axial force in the beam walls. When the actuator arm is rotated, however, the rigid end plate transmits a bending moment, a shear force, and a normal force to the beam. We shall assume that the force P normal to any cross section in the beam remains constant along the length of the beam. With the notation as shown in Fig. 1(*b*), the equations of equilibrium for an element for small deformations, are

$$V = \frac{dM}{dx} \tag{1a}$$

$$\frac{dV}{dx} - (qA + P)\frac{d^2y}{dx^2} = 0 \tag{1b}$$[4]

and the moment-curvature relationship is given by

$$M = -k_\theta L \frac{d^2y}{dx^2} \tag{1c}$$

These can be combined to yield a single equation for the beam deflection,

$$\frac{d^4y}{dx^4} + \frac{qA + P}{k_\theta L}\frac{d^2y}{dx^2} = 0 \tag{2}$$

[4] Since the pressure q has been shown in Fig. 1(*b*) to be acting on the entire cross-sectional area of the beam, it might be thought that the presence of some longitudinal core within the bellows would reduce the area to be used in deriving equation (1*b*). However, the derivation has been based on the pressure forces shown in Fig. 1(*b*) only for convenience; the resultant normal pressure force acting on the beam element actually comes from expansion and contraction of the beam fibers when bending occurs and can be derived as follows, Fig. 1(*c*):

Net Pressure Force in y-direction $= q\,ds \int ds' \cos\varphi$

$$= \frac{q}{\rho}\,ds \int y'\,dx' = \frac{qA}{\rho}\,ds \approx -qA\frac{d^2y}{dx^2}\,dx$$

Thus equation (1*b*) is valid as long as the bellows walls are directly acted upon by fluid pressure.

which is readily solved to yield

$$y = A_1 + B_1 \frac{x}{L} + C_1 \sin \frac{ux}{L} + D_1 \cos \frac{ux}{L} \tag{3}$$

The boundary conditions to be satisfied are as follows:

$$\begin{aligned} y = \frac{dy}{dx} &= 0 \quad \text{at} \quad x = 0 \\ y = x_p\theta, \quad \frac{dy}{dx} &= \theta \quad \text{at} \quad x = L \end{aligned} \tag{4}$$

Substitution of equation (3a) into equations (4) and solution for the constants then yields the following expression for the deflection function:

$$\frac{y}{L\theta} = \frac{\left\{\frac{x_p}{L}\left[(1-\cos u)\left(1-\cos\frac{ux}{L}\right) - \sin u\left(\frac{ux}{L} - \sin\frac{ux}{L}\right)\right] + \frac{1-\cos u}{u}\left(\frac{ux}{L} - \sin\frac{ux}{L}\right) - \left(1-\frac{\sin u}{u}\right)\left(1-\cos\frac{ux}{L}\right)\right\}}{2(1-\cos u) - u\sin u} \tag{5}$$

There are, as yet, two unknown quantities to be determined; i.e., the axial force P (or the parameter u) and the actuating moment required to produce the rotation. The former can be determined from the condition that the end of the beam moves horizontally an amount

$$\Delta \approx {}^1/_2 x_p\theta^2 \approx \frac{P}{k_\theta} + {}^1/_2 \int_0^L \left(\frac{dy}{dx}\right)^2 dx \tag{6}$$

On substituting equation (5) into equation (6), we obtain the following relationship for u as a function of q, x_p/L, and the angular rotation θ of the actuator arm:

$$\bar{\theta}^2 = \frac{\left(\frac{u}{2\pi}\right)^2 - \frac{q}{q_E}}{f_1(u) - \left(\frac{x_p}{L} - {}^1/_2\right)^2 f_2(u)} \tag{7}$$

where

$$f_1(u) = \frac{{}^1/_4\left[\frac{\sin u}{u}(1+5\cos u) - \cos u(1+\cos u)\right] - \frac{1-\cos u}{u^2}\left(1 - \frac{\sin u}{u} + 2\cos u\right)}{\left(2\frac{1-\cos u}{u} - \sin u\right)^2} \tag{8a}$$

$$f_2(u) = \frac{(1-\cos u)\left(2 + \cos u - 3\frac{\sin u}{u}\right)}{\left(2\frac{1-\cos u}{u} - \sin u\right)^2} \tag{8b}$$

The moment required to be applied at the pivot point to obtain the desired angular deflection is given by

$$M_0 = (Vx_p - M)_{x=L} \tag{9}$$

the force P and the pressure q are normal to the end of the beam and thus produce no moment about the pivot point. On substituting equations (1) and (5) into equation (9), we obtain

$$\frac{M_0}{k_\theta\theta} = f_3(u) + \left(\frac{x_p}{L} - {}^1/_2\right)^2 f_4(u) \tag{10}$$

where

$$f_3(u) = \frac{1 - {}^1/_4u^2 - u\cot u}{\frac{\tan\frac{u}{2}}{\frac{u}{2}} - 1} \tag{11a}$$

$$f_4(u) = \frac{u^2}{\frac{\tan\frac{u}{2}}{\frac{u}{2}} - 1} \tag{11b}$$

Equations (7) and (10) thus define the bending characteristics of the bellows-actuator system, and yield a generally nonlinear relationship between the actuating moment and the resulting angular deflection when the parameter u is eliminated.

It has been taken for granted in the preceding deviations that the quantity $qA + P$ corresponds to a compressive force in the beam. For external pressure or for internal pressure when, for certain values of the pivot-point location the quantity $\bar{\theta}$ is large, the quantity $qA + P$ may correspond to a tensile force and thus be negative. For this case we replace u in the pertinent equations by

$$u = i\bar{u} \tag{12}$$

to obtain in real form

$$\frac{y}{L\theta} = \frac{\left\{\frac{x_p}{L}\left[(\cosh\bar{u}-1)\left(\cosh\frac{\bar{u}x}{L} - 1\right) - \sinh\bar{u}\left(\sinh\frac{\bar{u}x}{L} - \frac{\bar{u}x}{L}\right)\right] + \frac{\cosh\bar{u}-1}{\bar{u}}\left(\sinh\frac{\bar{u}x}{L} - \frac{\bar{u}x}{L}\right) - \left(\frac{\sinh\bar{u}}{\bar{u}} - 1\right)\left(\cosh\frac{\bar{u}x}{L} - 1\right)\right\}}{\bar{u}\sinh\bar{u} - 2(\cosh\bar{u} - 1)} \tag{13a}$$

$$\bar{\theta}^2 = -\frac{\left(\frac{\bar{u}}{2\pi}\right)^2 + \frac{q}{q_E}}{f_1(\bar{u}) - \left(\frac{x_p}{L} - {}^1/_2\right)^2 f_2(\bar{u})} \tag{13b}$$

$$\frac{M}{k_\theta\theta} = f_3(\bar{u}) + \left(\frac{x_p}{L} - {}^1/_2\right)^2 f_4(\bar{u}) \tag{13c}$$

where

$$f_1(\bar{u}) = \frac{\frac{1}{4}\left[\cosh \bar{u}(\cosh \bar{u} + 1) - \frac{\sinh \bar{u}}{\bar{u}}(5\cosh \bar{u} + 1)\right] + \frac{\cosh \bar{u} - 1}{\bar{u}^2}\left(2\cosh \bar{u} + 1 - \frac{\sinh \bar{u}}{\bar{u}}\right)}{\left(\sinh \bar{u} - 2\frac{\cosh \bar{u} - 1}{\bar{u}}\right)^2} \tag{14a}$$

$$f_2(\bar{u}) = \frac{(\cosh \bar{u} - 1)\left(\cosh \bar{u} + 2 - 3\frac{\sinh \bar{u}}{\bar{u}}\right)}{\left(\sinh \bar{u} - 2\frac{\cosh \bar{u} - 1}{\bar{u}}\right)^2} \tag{14b}$$

$$f_3(\bar{u}) = -\frac{1 + \frac{1}{4}\bar{u}^2 - \bar{u}\coth \bar{u}}{1 - \frac{\tanh \frac{\bar{u}}{2}}{\frac{\bar{u}}{2}}} \tag{14c}$$

$$f_4(\bar{u}) = \frac{\bar{u}^2}{1 - \frac{\tanh \frac{\bar{u}}{2}}{\frac{\bar{u}}{2}}} \tag{14d}$$

Results and Discussion

It will be noted that the moment-angular rotation relationship given by equations (7) and (10) or (13*b*) and (13*c*) is identical for beams with pivot points located the same distance on either side of the center of the beam. Instead of the problem presently under consideration, Fig. 1(*a*), let us consider the equivalent problem of a beam with two rigid end plates connected by rigid arms to a fixed pivot point. It is then obvious that it is immaterial whether we hold the shorter arm and rotate the longer arm or hold the longer arm and rotate the shorter arm since the same actuator moment will be required to yield a given angular rotation of one end plate with respect to the other. The deflections of the one case will differ from the mirror image of the deflections of the other only by a rigid-body rotation. Indeed, from equation (5), it can be shown that

$$y\left(1 - \frac{x_p}{L},\ 1 - \frac{x}{L},\ u \text{ or } \bar{u}\right) = y\left(\frac{x_p}{L},\ \frac{x}{L},\ u \text{ or } \bar{u}\right) + (L - x_p - x)\theta \tag{15}$$

It is therefore necessary only to treat values of x_p/L from $-\infty$ to 0.5 from 0.5 to $+\infty$ to cover the whole range from $-\infty$ to $+\infty$.

The functions f_1, f_2, f_3, and f_4 which define the moment-angular rotation characteristics are tabulated in Tables 1(*a*), (*b*) for u varying from 0 to 2π and $\bar{u}$ varying from 0 to ∞. It can be shown that the following relationships exist between the functions:

$$\frac{df_3(u)}{du} = 2uf_1(\bar{u}) \tag{16a}$$

$$\frac{df_4(u)}{du} = -2uf_2(u) \tag{16b}$$

$$\frac{df_3(\bar{u})}{d\bar{u}} = -2\bar{u}f_1(\bar{u}) \tag{16c}$$

$$\frac{df_4(\bar{u})}{d\bar{u}} = 2\bar{u}f_2(\bar{u}) \tag{16d}$$

The tabulated values of the functions f_1 to f_4 were used to obtain the curves of Figs. 2 and 3. In Fig. 2 are shown typical graphs of $\bar{\theta}$ versus $u/2\pi$ and $\bar{u}/2\pi$ for various values of the pressure ratio q/q_B and for the pivot location ratio x_p/L equal to 0.5, 1.0 (or 0.0), and 1.5 (or −0.5). In Fig. 3 the variation of the "secant modulus" parameter $M_0/k_\theta\theta$ of the M_0 versus $\bar{\theta}$-curves is

Table 1(*a*) Values of the functions $f_1(u)$, $f_2(u)$, $f_3(u)$, $f_4(u)$

$\frac{u}{2\pi}$	$f_1(u)$	$f_2(u)$	$f_3(u)$	$f_4(u)$	$\frac{u}{2\pi}$	$f_1(u)$	$f_2(u)$	$f_3(u)$	$f_4(u)$
0.00	0.167	1.200	1.000	12.00	0.65	0.061	1.265	3.134	- 8.51
0.05	0.167	1.200	1.016	11.93	0.66	0.054	1.268	-	-
0.10	0.166	1.201	1.066	11.53	0.68	0.038	1.274	-	-
0.15	0.165	1.203	1.147	10.93	0.70	0.018	1.281	3.239	-11.90
0.20	0.162	1.205	1.260	10.10	0.72	- 0.006	1.288	-	-
0.25	0.159	1.207	1.402	9.03	0.74	- 0.036	1.296	-	-
0.30	0.155	1.211	1.573	7.72	0.75	- 0.053	1.300	3.195	-15.59
0.35	0.151	1.215	1.769	6.16	0.76	- 0.073	1.303	-	-
0.40	0.144	1.220	1.987	4.36	0.78	- 0.119	1.312	-	-
0.42	0.141	1.223	-	-	0.80	- 0.191	1.323	2.857	-19.60
0.44	0.138	1.225	-	-	0.82	- 0.262	1.332	-	-
0.45	0.136	1.226	2.223	2.31	0.84	- 0.387	1.344	-	-
0.46	0.134	1.228	-	-	0.85	- 0.450	1.351	1.890	-23.95
0.48	0.130	1.231	-	-	0.86	- 0.538	1 357	-	-
0.50	0.125	1.234	2.467	0.00	0.88	- 0.788	1.374	-	-
0.52	0.120	1.237	-	-	0.90	- 1.273	1.390	-0.707	-28.68
0.54	0.114	1.242	-	-	0.92	- 1.941	1.407	-	-
0.55	0.110	1.243	2.712	- 2.57	0.94	- 3.535	1.427	-	-
0.56	0.107	1 244	-	-	0.95	- 4.997	1.436	-9.938	-33.83
0.58	0.099	1.248	-	-	0.96	- 8.036	1.447	-	-
0.60	0.090	1.253	2.938	- 5.40	0.98	- 32.08	1.472	-	-
0.62	0.080	1.258	-	-	0.99	-127.9	1.486	-	-
0.64	0.068	1.262	-	-	1.00	-∞	1.500	-∞	-39.48

Table 1(*b*) Values of the functions $f_1(\bar{u})$, $f_2(\bar{u})$, $f_3(\bar{u})$, $f_4(\bar{u})$

$\bar{u}$	$\frac{\bar{u}}{2\pi}$	$f_1(\bar{u})$	$f_2(\bar{u})$	$f_3(\bar{u})$	$f_4(\bar{u})$
0.0	0.0000	0.167	1.200	1.000	12.00
0.5	0.0796	0.168	1.200	0.958	12.30
1.0	0.1592	0.170	1.196	0.832	13.20
1.5	0.2387	0.173	1.193	0.618	14.69
2.0	0.3183	0.176	1.189	0.313	16.78
2.5	0.3979	0.181	1.184	- 0.089	19.45
3.0	0.4775	0.186	1.178	- 0.593	22.70
3.5	0.5570	0.190	1.171	- 1.204	26.51
4.0	0.6366	0.194	1.164	- 1.925	30.89
4.5	0.7162	0.199	1.157	- 2.762	35.82
5.0	0.7958	0.203	1.150	- 3.716	41.30
5.5	0.8754	0.206	1.143	- 4.790	47.32
6.0	0.9549	0.209	1.136	- 5.985	53.87
6.5	1.0345	0.212	1.130	- 7.303	60.95
7.0	1.1141	0.215	1.124	- 8.744	68.55
7.5	1.1937	0.217	1.118	- 10.31	76.67
8.0	1.2732	0.219	1.112	- 12.00	85.31
8.5	1.3528	0.221	1.107	- 13.81	94.47
9.0	1.4324	0.222	1.102	- 15.75	104.1
9.5	1.5120	0.224	1.098	- 17.81	114.3
10.0	1.5915	0.225	1.094	- 20.00	125.0
15.0	2.3873	0.233	1.065	- 48.75	259.6
20.0	3.1831	0.238	1.049	- 90.00	444.4
30.0	4.7746	0.242	1.033	-210.0	964.3
40.0	6.3662	0.244	1.025	-380.0	1684
50.0	7.9577	0.245	1.020	-600.0	2604
60.0	9.5493	0.246	1.017	-870.0	3724
∞	∞	0.250	1.000	-∞	∞

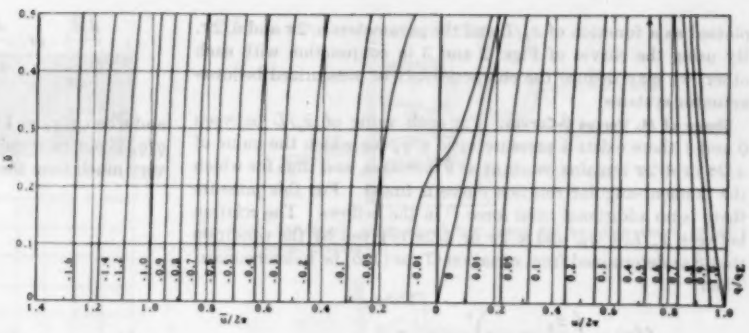

Fig. 2(a) Variation of v and $\bar{v}$ with $\bar{\theta}$ and q/q_E ($x_p/L = 0.5$)

Fig. 2(b) Variation of v and $\bar{v}$ with $\bar{\theta}$ and q/q_E ($x_p/L = 0.0, 1.0$)

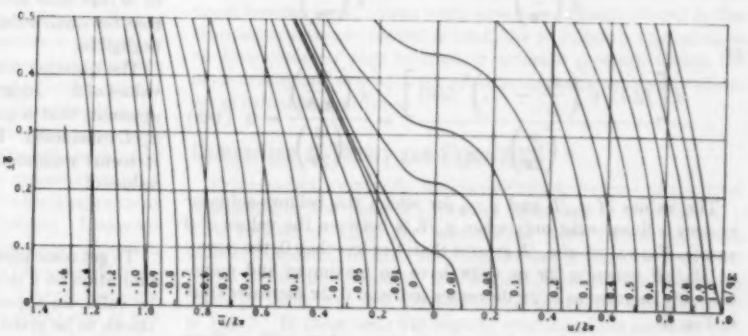

Fig. 2(c) Variation of v and $\bar{v}$ with $\bar{\theta}$ and q/q_E ($x_p/L = -0.5, 1.5$)

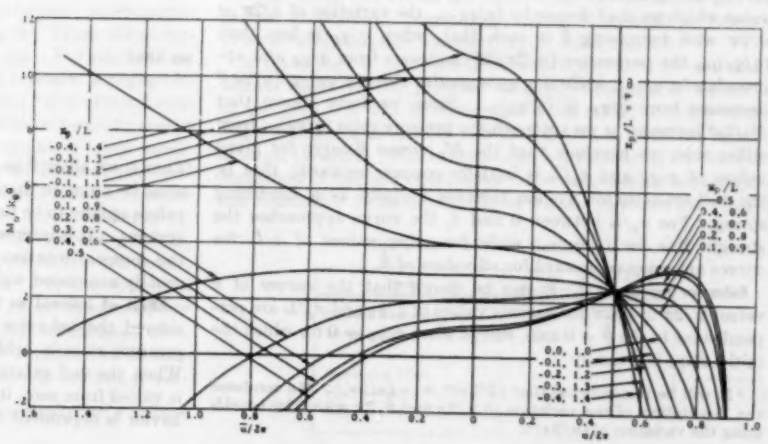

Fig. 3 Variation of equivalent "spring constant" of beam-actuator system with pivot-point location and the parameter v or $\bar{v}$

plotted as a function of x_p/L and the parameters $u/2\pi$ and $\bar{u}/2\pi$. By using the curves of Figs. 2 and 3 in conjunction with each other, we may deduce the characteristics of pressurized bellows-actuator systems.

Shape of M_0 Versus $\bar{\theta}$-Curves. For each value of x_p/L between 0 and 1 there exists a pressure ratio q/q_E for which the value of $u/2\pi$ or $\bar{u}/2\pi$ remains constant as $\bar{\theta}$ increases, and thus for which the moment-angular rotation curve is linear. For this pressure there is no additional axial force P in the bellows. The relation between x_p/L, q/q_E, and $u/2\pi$ or $\bar{u}/2\pi$ is given by the condition that $\bar{\theta}$ as determined from equation (7) or (13*b*) be indeterminate. Then

$$\left.\begin{aligned} f_1(u) - \left(\frac{x_p}{L} - {}^1/_2\right)^2 f_2(u) &= 0 \\ \frac{q}{q_E} &= \left(\frac{u}{2\pi}\right)^2 \end{aligned}\right\} \quad \frac{q}{q_E} > 0 \qquad (17a)$$

$$\left.\begin{aligned} f_1(\bar{u}) - \left(\frac{x_p}{L} - {}^1/_2\right)^2 f_2(\bar{u}) &= 0 \\ \frac{q}{q_E} &= -\left(\frac{\bar{u}}{2\pi}\right)^2 \end{aligned}\right\} \quad \frac{q}{q_E} < 0 \qquad (17b)$$

For the same values of x_p/L and $u/2\pi$ or $\bar{u}/2\pi$, the curves of $M_0/k_\theta\theta$ versus $u/2\pi$ or $\bar{u}/2\pi$ reach their maximum values. From equations (10), (13*c*), and (16), if equations (17*a*) and (17*b*) are satisfied, it follows that

$$\frac{d\left[f_3(u) + \left(\frac{x_p}{L} - {}^1/_2\right)^2 f_4(u)\right]}{d\left(\frac{u}{2\pi}\right)} = \frac{d\left(\frac{M_0}{k_\theta\theta}\right)}{d\left(\frac{u}{2\pi}\right)} = 0 \qquad (18a)$$

or

$$\frac{d\left[f_3(\bar{u}) + \left(\frac{x_p}{L} - {}^1/_2\right)^2 f_4(\bar{u})\right]}{d\left(\frac{u}{2\pi}\right)} = \frac{d\left(\frac{M_0}{k_\theta\theta}\right)}{d\left(\frac{\bar{u}}{2\pi}\right)} = 0 \qquad (18b)$$

The values of x_p/L and q/q_E for which the bellows-actuator system is linear exist only when x_p/L is between the values of 0 and 1. For values of x_p/L greater than 1 or less than 0, the curves of $M_0/k_\theta\theta$ versus $u/2\pi$ or $\bar{u}/2\pi$ have no maximum and monotonically increase as $u/2\pi$ decreases to 0 and $\bar{u}/2\pi$ increases from 0, Fig. 3.

If we now consider a bellows-actuator system with a given pivot-point location and values of q/q_E other than the special value which we shall denote by $(q/q_E)_{\text{lin}}$, the variation of $u/2\pi$ or $\bar{u}/2\pi$ with increasing $\bar{\theta}$ is such that, when q/q_E is less than $(q/q_E)_{\text{lin}}$, the parameter $(u/2\pi)[2]$[1] increases from q/q_E and approaches $(q/q_E)_{\text{lin}}$, while if q/q_E is greater than $(q/q_E)_{\text{lin}}$, $(u/2\pi)^2$ decreases from q/q_E to $(q/q_E)_{\text{lin}}$. Since we have shown that $M_0/k_\theta\theta$ increases as we approach the pressure ratio $(q/q_E)_{\text{lin}}$ from either side, we conclude that the M_0 versus θ-curve for given values of q/q_E and x_p/L is initially concave upward; that is, the bellows-actuator system behaves initially as a hardening spring. For x_p/L between 0 and 1, the curve approaches the straight line for $(q/q_E)_{\text{lin}}$, while for other values of x/L the curves are concave upward for all values of $\bar{\theta}$.

Behavior for Small $\bar{\theta}$. It can be shown that the curves of $\bar{\theta}$ versus $u/2\pi$ or $\bar{u}/2\pi$ for various values of q/q_E and x_p/L are perpendicular to the $\bar{\theta} = 0$ axis, except when $q/q_E = 0$ for which the initial slope is given by

$$\frac{d|\bar{\theta}|}{d\,\frac{u}{2\pi}} \quad \text{or} \quad \frac{d|\bar{\theta}|}{d\,\frac{\bar{u}}{2\pi}} = \frac{1}{\left[\left|{}^1/_6 - {}^4/_5\left(\frac{x_p}{L} - {}^1/_2\right)^2\right|\right]^{1/2}} \qquad (19)$$

and when $q/q_E = 1$ for which the initial slope is 0. Provided that q/q_E is not near unity the quantities $u/2\pi$ and $\bar{u}/2\pi$ do not vary very much from the $\bar{\theta} = 0$ values of

$$\left.\begin{aligned} \frac{u}{2\pi} &= \left(\frac{q}{q_E}\right)^{1/2} \\ \frac{\bar{u}}{2\pi} &= \left(-\frac{q}{q_E}\right)^{1/2} \end{aligned}\right\} \qquad (20)$$

as $\bar{\theta}$ increases within reasonable limits. Thus for small values of $\bar{\theta}$, the M_0 versus θ-curves are linear for most pressure ratios with their slopes given by

$$\frac{M_0}{k_\theta\theta} = f_3\left[2\pi\left(\frac{q}{q_E}\right)^{1/2}\right] + \left(\frac{x_p}{L} - {}^1/_2\right)^2 f_4\left[2\pi\left(\frac{q}{q_E}\right)^{1/2}\right], \quad \frac{q}{q_E} > 0 \qquad (21a)$$

$$\frac{M_0}{k_\theta\theta} = f_3\left[\overline{2\pi\left(-\frac{q}{q_E}\right)^{1/2}}\right] + \left(\frac{x_p}{L} - {}^1/_2\right)^2 f_4\left[\overline{2\pi\left(-\frac{q}{q_E}\right)^{1/2}}\right], \quad \frac{q}{q_E} < 0 \qquad (21b)$$

Pressure ratios near zero may be included in this category since although $u/2\pi$ or $\bar{u}/2\pi$ may vary significantly with $\bar{\theta}$, the value of $M/k_\theta\theta$ does not in the range considered. We may conclude that for small values of $\bar{\theta}$ the additional force P in the bellows is negligible.

The question arises, of course, as to the definition of "small" values of $\bar{\theta}$. Judging from the curves of Fig. 2, it is unfortunately apparent that a general definition must depend on the value of x_p/L considered. However, if we restrict x_p/L to the range 0 to 1, it seems reasonable to restrict the foregoing statements to $\bar{\theta}$-values of

$$|\bar{\theta}| < 0.1 \qquad (22)$$

To get some idea of the angles and bellows lengths to which this limitation on $\bar{\theta}$ refers, we note that, if beam theory is assumed to be valid, an approximate relationship between k_θ and k_δ can be shown to be given by

$$\frac{k_\theta}{k_\delta} \approx {}^1/_2R^2 \qquad (23)$$

so that

$$\bar{\theta} \approx \frac{L}{R}\,\frac{\theta}{2\pi} \qquad (24)$$

Thus if we allow θ to be as much as ± 12 deg, the value of L/R must be no more than about 3 for $|\bar{\theta}|$ to be less than 0.1. These values appear to be reasonable for contemplated bellows-actuator systems. It is interesting to note, however, that for long bellows the moment-rotation curve will be nonlinear at angles more usually associated with small deflections.

Effect of Internal or External Pressure. Heretofore we have considered the behavior of the bellows-actuator system when the pressure ratio is held constant and the end rotation is varied. When the end rotation is held constant and the pressure ratio is varied from zero, it can be seen from Fig. 3 that the initial behavior is dependent on the pivot-point location. When x_p/L is

[1] It will be remembered that $(\bar{u}/2\pi)^2 = -(u/2\pi)^2$. We condense the description of the variation of $u/2\pi$ and $\bar{u}/2\pi$ with θ by considering the variation of $(u/2\pi)^2$.

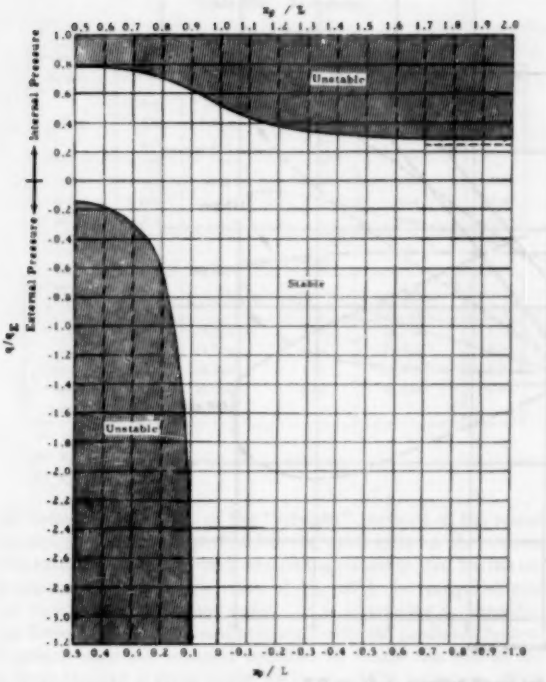

Fig. 4 Variation of minimum critical pressure with pivot point location

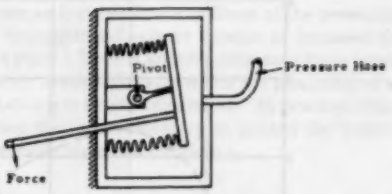

Fig. 5(a) Schematic diagram of test setup for bending small bellows under external pressure

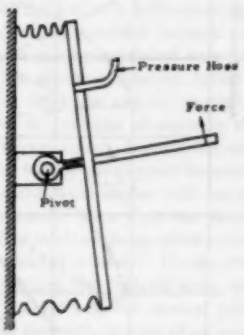

Fig. 5(b) Schematic diagram of test setup for bending large bellows under internal pressure

greater than $^1/_2 - \sqrt{5}/6$ but less than $^1/_2 + \sqrt{5}/6$, the effect of internal pressure is initially to increase the moment exerted on the actuator arm, and the effect of external pressure is to reduce the exerted moment. For x_p/L less than $^1/_2 - \sqrt{5}/6$ or greater than $^1/_2 + \sqrt{5}/6$, the opposite is true. For all values of x_p/L, however, as internal pressure increases, the exerted actuator moment eventually decreases, actually goes through zero, and changes direction. The pressure at which the moment vanishes is highest for $x_p/L = 0.5$ and decreases toward a limiting value as the pivot point moves from the center of the bellows. Under external pressure the exerted actuator moment can change direction only when x_p/L is between the values 0 and 1. The external pressure at which this occurs is lowest for $x_p/L = 0.5$ and increases without limit as the pivot point moves toward either end of the bellows. For all other pivot-point locations, reversal of actuator-moment direction will not occur under external pressure.

Minimum values of the critical pressure beyond which actuator-moment reversal occurs are given in Fig. 4. These values correspond to $\bar{\theta} \approx 0$ and increase as $\bar{\theta}$ increases. For small values of $\bar{\theta}$, however, the variation in the critical pressure is negligible.

Instability of the System. So long as the actuator rotation is controlled, the "critical" pressures in Fig. 4 have no meaning except those at which the exerted actuator moment is very small. Larger internal or external pressures may be imposed provided the bellows strain does not become excessive as a result of changes in deflected shape, and the bellows does not burst because of internal pressure or become unstable due to external pressure. When the moment rather than the angle of rotation is controlled, the significance of critical pressures changes. For this system of control, the bellows-actuator system can rotate spontaneously from a straight position with no exerted actuator moment when these pressures are reached.[6] The angle of rotation can be considerable and might conceivably overstrain the bellows if permitted to occur unrestrained. When moment is applied to the actuator and the pressure is increased to values near the critical value, the rotation of the actuator and the end of the bellows will again become large. Thus when actuator-moment control rather than actuator-angle control is used, the situation is analogous to an Euler column with internal or external pressure taking the place of end load and with the actuator moment acting as a measure of initial imperfection.

[6] This instability has been obtained experimentally for a bellows under external pressure.

Comparison of Theory and Experiment

Experimental results for bellows-actuator systems of the type considered in the present paper are presented in reference [7]. Two bellows of multi-ply construction were tested: A small bellows subjected to external pressure and a large bellows subjected to internal pressure. The dimensions of the specimens are given in Table 2(a) and the test setups are shown schematically in Fig. 5. In these tests the angular rotation of the movable end of the bellows was varied continuously through the range ±8 deg and the force exerted on the lever arms was measured and recorded continuously for various values of internal or external pressure and two pivot locations, $x_p/L = 0.3$ and 0.5.

A typical set of test records is shown in Fig. 6 for the small bellows under external pressure, with the pivot point at the center of the span. It will be noted that each record of force versus angle exhibits a hysteresis loop that increases with the applied external pressure. This is attributed not to bearing friction (the coefficient of friction would have to be considerably higher than can reasonably be assumed) but to friction between the plies of

Table 2(a) Bellows dimensions

Item	Small Bellows	Large Bellows
Outside Diameter, in.	4.75	13.67
Inside Diameter, in.	4.25	12.42
Length, in.	3.13	3.23
Number of Plies	3	12
Ply Thickness, in.	0.006	0.005
Number of Convolutions	27	8

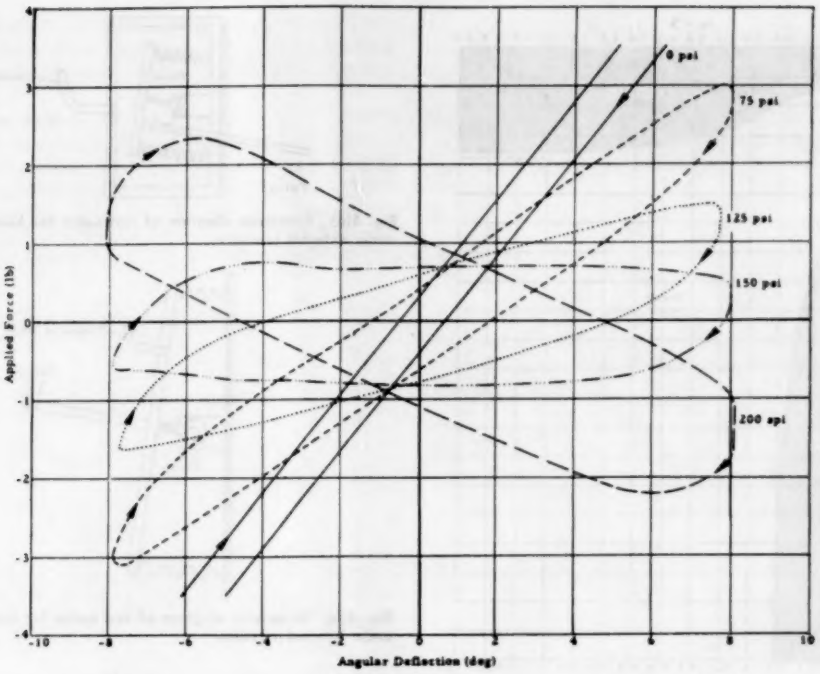

Fig. 6 Force versus angular deflection for small bellows, $x_p/L = 0.5$

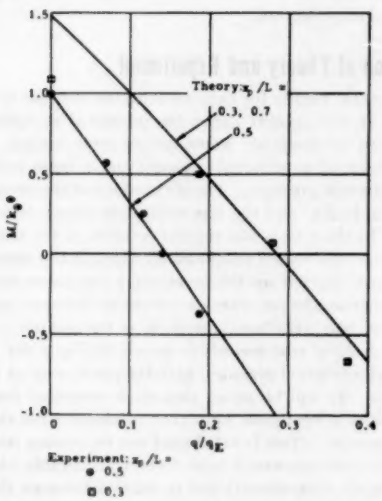

Fig. 7(a) Comparison of theory and experiment for bellows under external pressure

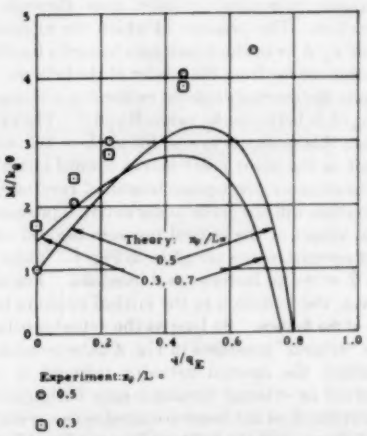

Fig. 7(b) Comparison of theory and experiment for bellows under internal pressure

Table 2(b) Test data

1. Small Bellows

Pressure q, psi	(b) $-q/q_E$	$x_p/L = 0.5$ M/θ $\frac{\text{in.-lb}}{\text{rad}}$	$x_p/L = 0.5$ $M/k_\theta\theta$	$x_p/L = 0.3$ M/θ $\frac{\text{in.-lb}}{\text{rad}}$	$x_p/L = 0.3$ $M/k_\theta\theta$
0	0.000	1355 (a)	1.00	1475	1.09
75	0.070	773	0.57	-	-
125	0.117	332	0.25	-	-
150	0.140	0	0.00	-	-
200	0.187	-512	-0.38	660	0.49
300	0.280	-	-	104	0.07
400	0.373	-	-	-916	-0.68

2. Large Bellows

Pressure q, psi	(c) q/q_E	$x_p/L = 0.5$ M/θ $\frac{\text{in.-lb}}{\text{rad}}$	$x_p/L = 0.5$ $M/k_\theta\theta$	$x_p/L = 0.3$ M/θ $\frac{\text{in.-lb}}{\text{rad}}$	$x_p/L = 0.3$ $M/k_\theta\theta$
0	0.000	9,520 (a)	1.00	16,150	1.70
100	0.115	19,500	2.05	23,300	2.45
200	0.230	28,600	3.01	27,900	2.82
400	0.460	38,700	4.06	36,800	3.87
600	0.690	42,200	4.43		-

(a) k_θ

(b) q_E = 1070 psi

(c) q_E = 870 psi

the bellows. The slope of the "straight" portions of the record for zero pressure is proportional to the value of k_θ for the bellows. The ratio of the slope of each succeeding record to that for the unpressurized bellows is the value of $M_0/k_\theta\theta$[7] to be compared with the theoretically predicted value. It is interesting to note that the force-angle records qualitatively verify the predicted bellows behavior since the moment required to rotate the end of the bellows through a given angle, exclusive of the hysteresis effect, decreases with increasing external pressure and becomes negative after some critical pressure is reached. The buckling phenomenon was also noted during the tests; when the movable end of the bellows was permitted to rotate freely and the external pressure was increased, it was observed that spontaneous deflection would occur when the pressure reached some particular value.

The average values of the force-angle record slopes (converted to M_0/θ-values) for each pressure and pivot-point location are given in Table 2(*b*) for both the small and large bellows and are compared with theory in Figs. 7(*a*) and 7(*b*). The agreement between theory and experiment for the small bellows under external pressure is seen to be relatively good. For the large bellows under internal pressure, however, the agreement between theory and experiment is quite poor. Discrepancies between theory and experiment are believed to be due to the multi-ply construction of the bellows which introduces unknown, and possible varying, amounts of friction into the test results. We may conjecture that for the large bellows the main reason for the poor agreement results from an increase in the stiffness of the pressurized bellows over the unpressurized bellows because of increased friction between the plies. Thus it appears necessary for a conclusive test of the theory to use bellows for which the possibility of extraneous frictional effects is largely eliminated. In practice, this is also desirable since the forces necessary to control the bellows rotation are considerably increased by friction.

[7] The value actually should be increased by an increment due to the weight of the end plate, actuator arm, and force lever arm. However, the effect of this increase would be insignificant; it has been estimated that the additional moment is 2 per cent or less of the moment required to rotate an unpressurized bellows with the pivot point at the center of span.

Conclusion

It has been shown that the moment required to produce a given angular rotation of the end of a bellows-actuator system can be reduced to a small value provided internal or external pressure and bellows stiffness can be regulated accurately. It should be emphasized that the actuator rotation rather than the moment must be controlled, since the angular motion of the actuator is extremely sensitive to pressure changes in the region of small moment-rotation curve slope. Indeed, for certain critical pressures which depend on the pivot-point location, the system may deflect through considerable angles with no applied moment.

The theoretical results show that the sensitivity of moment to pressure near the critical pressures is less pronounced for external pressure than for internal pressure. On the other hand, for pivot points near the center of the bellows span, the external critical pressure is less than the internal critical pressure. Therefore, given some working pressure, the use of an external-pressure system rather than an internal-pressure system would require either a higher bellows stiffness or a shift in the pivot-point location toward the ends of the bellows.

Additional investigation is needed to determine how closely the small-deflection theory predicts results for large values of $\bar{\theta}$ (large L/R, small θ) and to determine the effects of short length for possible deviations from the theory. A major topic for investigation is the prediction of k_δ and k_θ for given bellows convolution shapes, since there is apparently little agreement between the various methods available and insufficient experimental data for choosing between the various methods.

References

1 John Prescott, "Applied Elasticity," first American edition, Dover Publications, New York, N. Y., 1946, pp. 552–554.

2 K. von Sanden and F. Tölke, "Über Stabilitätsprobleme Dünner Kreiszylindrischer Schalen," *Ingenieur-Archiv*, vol. 3, 1932, pp. 24–66.

3 W. Flügge, "Die Stabilität der Kreiszylinderschale," *Ingenieur-Archiv*, vol. 3, 1932, pp. 463–506.

4 J. A. Haringx, "Instability of Thin-Walled Cylinders Subjected to Internal Pressure," Philips Research Reports, vol. 7, 1952, pp. 112–118.

5 F. E. Nagel, "Column Instability of Pressurized Tubes," *Journal of the Aeronautical Sciences*, vol. 23, 1956, pp. 608–609.

6 J. A. Haringx, "Instability of Bellows Subjected to Internal Pressure," Philips Research Reports, vol. 7, 1952, pp. 189–196.

7 D. P. Fitzgibbon, "Experimental Measurements of the Stiffness of a Bellows Systems," Space Technology Laboratories, Report No. EM 8-20, October 1, 1958.

E. H. LEE
Professor,
Division of Applied Mathematics,
Brown University,
Providence, R. I.
Mem. ASME

J. R. M. RADOK
Professor,
Department of Aeronautical Engineering,
Polytechnic Institute of Brooklyn,
Brooklyn, N. Y.

The Contact Problem for Viscoelastic Bodies[1]

The contact problem in viscoelasticity is one in which different types of boundary conditions are prescribed depending on whether boundary points inside or outside the region of contact are considered. Since, in general, the contact region varies with time, this leads to a problem which cannot be treated directly by application of the Laplace transform, which has formed the basis for most published viscoelastic stress-distribution solutions. It is shown that the solution of the viscoelastic counterpart of the Hertz problem in elasticity can, however, be deduced from the elastic solution. A particular example is presented, and the marked effect of viscoelastic behavior on the pressure distribution in the contact region is illustrated. The problem also illustrates the tentative nature of the method of approach and the need for a separate confirmation of the solution. The solution is presented for general linear viscoelastic operators and offers the possibility of determining these from a contact test.

In recent years the development of the theory of linear viscoelasticity has led to the study of stress-distribution problems for viscoelastic materials [1].[2] These are represented mathematically by boundary-value problems which satisfy the following system of equations. The equations of equilibrium

$$\frac{\partial \sigma_{ij}}{\partial x_j} = 0 \tag{1}$$

where x_i are Cartesian co-ordinates, σ_{ij} the stress, and in which the usual summation convention of the tensor suffix notation is assumed. Inertia forces are assumed to be negligible, and the problem is considered as quasistatic. The strain components are given in terms of the displacements by:

$$\epsilon_{ij} = {}^1/_2\left(\frac{\partial u_i}{\partial x_j} + \frac{\partial u_j}{\partial x_i}\right) \tag{2}$$

within the limitation of infinitesimal strain analysis to which the present discussion is confined. The stress-strain relations for linear isotropic viscoelasticity can be expressed in the form:

$$Ps_{ij} = Qe_{ij} \tag{3}$$

$$P'\sigma_{ii} = Q'\epsilon_{ii} \tag{4}$$

where

$$s_{ij} = \sigma_{ij} - {}^1/_3\sigma_{kk}\delta_{ij} \quad \text{and} \quad e_{ij} = \epsilon_{ij} - {}^1/_3\epsilon_{kk}\delta_{ij}$$

are the stress and strain deviators, respectively, and where P, Q and P', Q' are pairs of linear operators in the time variable. They may be the differential operators associated with the common viscoelastic models of springs and dashpots, or the integral operators associated with the hereditary-function approach, or any of the other equivalent means of expressing viscoelastic behavior [2, 3, 4].

Boundary conditions take the form of prescribed surface traction $T_i(x_j, t)$ over the part S_1 of the surface S of the viscoelastic body under consideration, which must be compatible with the stress tensor at the surface according to:

$$T_i = \sigma_{ij}n_j \quad \text{on} \quad S_1 \tag{5}$$

where n_j is the unit outward normal vector. Over the remainder, S_2, of the surface, the displacement $u_i(x_j, t)$ is prescribed. As in elasticity theory, it is also possible to demand certain combinations of traction component and displacement component at surface points, such as zero shear traction and prescribed normal displacement. Appropriate initial conditions are also required throughout the volume V of the viscoelastic body.

A simple method of treatment of this system of equations, which encompasses most published solutions, is available if the regions S_1 and S_2 over which different types of boundary conditions are prescribed do not vary during the time under consideration, although the actual magnitudes of the prescribed quantities may vary arbitrarily. Application of the Laplace transform then removes the variable t, and the problem reduces to an elastic problem in the transformed variables [5]. When S_1 and S_2 vary, this approach fails since the procedure does not determine definite boundary values for the associated elastic problem, since for some fixed points on the surface, neither the traction nor the displacement is known throughout the history of the problem, so that the transform of neither can be determined.

Radok [6] has suggested that a broader range of problems can be treated, which fall outside the scope of the transform method, by taking a one-parameter family of solutions of the elastic problem in the parameter t, the time, with the same boundary conditions as the viscoelastic problem, and by replacing the elastic constants by appropriate viscoelastic operators in the expressions for stress components. These may then comprise tractable mathematical equations for evaluating the stress components for the viscoelastic body. This procedure is open to some question [7] since the manipulation of the elastic constants in the determination of the elastic solution could involve procedures which are not valid for operators, or which lead to the introduction of new functions in the operator case. However, when such a solution has been obtained it is often possible to change the initial formulation so that a direct transform attack is available to check the significance of the result. The contact problem detailed in the text which follows, the analogy to the Hertz problem in elasticity, falls into this category. In this case a valid viscoelastic solution is obtained as long as the contact area does not decrease, but otherwise complications arise which invalidate the viscoelastic solution. Thus the contact problem provides a

[1] The results presented in this paper were obtained in the course of research sponsored by the Office of Naval Research under Contract Nonr-562(10) with Brown University.

[2] Numbers in brackets designate References at end of paper.

Contributed by the Applied Mechanics Division and presented at the Annual Meeting, Atlantic City, N. J. November 29–December 4, 1959, of The American Society of Mechanical Engineers.

Discussion of this paper should be addressed to the Secretary, ASME, 29 West 39th Street, New York, N. Y., and will be accepted until October 10, 1960, for publication at a later date. Discussion received after the closing date will be returned.

Note: Statements and opinions advanced in papers are to be understood as individual expressions of their authors and not those of the Society. Manuscript received by ASME Applied Mechanics Division, May 8, 1959. Paper No. 59—A-83.

cogent example both of the value of this method and of the pitfalls associated with it, in addition to its own intrinsic interest and to its potential value as a vehicle for a simple testing procedure for measuring viscoelastic properties.

The Solution

Fig. 1 shows configurations of a simple example of the contact problem at two instants. A smooth rigid sphere of radius R is pressed against the initially plane surface of a viscoelastic half-space. This particular problem is considered in detail in this paper, but as explained subsequently, the method provides the solution to more general contact problems.

At the time t, the contact region is bounded by a circle of radius $l(t)$. Surface points at a radius from the axis of symmetry equal to $r > l(t)$ are outside the contact area and the boundary condition is zero surface traction. For $r < l(t)$ the normal surface displacement is prescribed by contact with the rigid indenter, and the tangential component of surface traction is zero because the indenter is smooth. As the indentation proceeds and the radius of the contact region increases, a point such as A in Fig. 1 changes from one type of boundary prescription to the other, so that the transform method cannot be used directly to supply either the transform of the normal surface traction or of the normal displacement for the associated elastic problem.

The Hertz solution [8] for a member of the corresponding family of elastic problems as t varies, gives the normal contact pressure, $p(r, t)$, in terms of the shear modulus G and Poisson's ratio ν of the elastic half space according to the relation:

$$p(r, t) = \frac{4}{\pi R} \frac{G}{1 - \nu} \operatorname{Re} [l(t)^2 - r^2]^{1/2} \tag{6}$$

where Re indicates the real part. This solution is based on quasi-static analysis, so that the time t appears only as a parameter prescribing the current radius of contact $l(t)$. Equations (1), (2), (3), and (4) with P, Q, P', and Q' replaced by the corresponding elastic constants do not contain t explicitly, and so the solution at any time t depends on the instantaneous values of the boundary conditions, and not on the history of the process.

Equation (6) appears to be an appropriate form of the elastic solution in which to substitute viscoelastic operators in place of the elastic constants, since the surface traction appears linearly as do stress components in the basic system of equations, nonlinearity occurring only in the geometry of the boundary conditions. For simplicity the case of an incompressible material is considered, $\nu = 1/2$, although this is not a necessary restriction. G is replaced by $Q/2P$ according to (3). Thus a tentative relation for the determination of the pressure distribution associated with the indentation of a smooth rigid sphere on an incompressible viscoelastic half space is

$$P[p(r, t)] = \frac{4}{\pi R} Q[f(r, t)] \tag{7}$$

where

$$f(r, t) = \operatorname{Re}[l(t)^2 - r^2]^{1/2} \tag{8}$$

If the progress of the indentation is prescribed by $l(t)$, (7) permits the evaluation of the surface pressure at each point, with zero initial conditions for the initially undisturbed half space. Depending on the form of the operators P, Q, (7) could be a differential equation, an integral equation, an integral, or some other form of linear operator equation for $p(r, t)$.

The relation (7) was termed tentative since valid algebraic manipulations of the elastic relation (6) could produce a viscoelastic relation not in agreement with (7). For example, removal of the radical in (6) by squaring would determine an operator relation for p^2 which would not be in agreement with (7). This choice is not simply eliminated by demanding that P and Q appear linearly, for when the dilational operators P', Q' are included, rational functions of the operators appear in stress-analysis relations, and powers of the dependent variables in (1), (2), (3), and (4) can also occur as mentioned later in the present example. However, the surface traction $p(r, t)$ determined by (7) can be used to prescribe the problem, which is then amenable to reliable analysis by means of the Laplace-transform procedure.

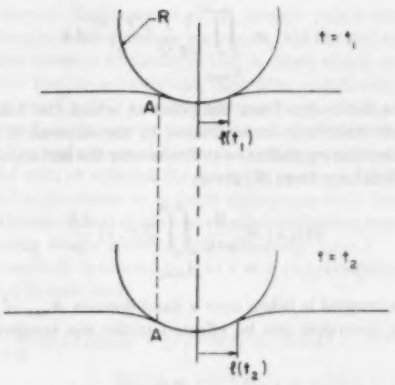

Fig. 1 Indentation configuration

The problem is now set by the prescribed normal surface traction $p(r, t)$, and zero shear traction. Application of the Laplace transform determines an associated elastic problem [5] of prescribed surface pressure $\bar{p}(r, s)$, where the bar indicates the transform, and s is the transform parameter. $\bar{p}(r, s)$ is determined by transforming (7):

$$\bar{p}(r, s) = \frac{4}{\pi R} \frac{\bar{Q}}{\bar{P}} \bar{f}(r, s) \tag{9}$$

$\bar{Q}$ and $\bar{P}$ are the transformed form of the operators [9]. If integral operators are used, the convolution theorem [9] determines the transformed form; for example, the viscoelastic relation in terms of the creep compliance function in shear, $J_c(t)$,

$$e_{ij}(x_k, t) = \int_0^t {}^1/_2 J_c(t - \tau) \frac{\partial s_{ij}(x_k, \tau)}{\partial \tau} \, d\tau \tag{10}$$

becomes

$$\bar{e}_{ij}(x_k, s) = {}^1/_2 \bar{J}_c(s) s \, \bar{s}_{ij}(x_k, s) \tag{11}$$

where the factor $1/2$ appears since $J_c(\tau)$ is based on the usual shear-strain component $\gamma_{ij} = 2e_{ij}$, so that

$$\bar{P} = {}^1/_2 \bar{J}_c(s) s, \qquad \bar{Q} = 1 \tag{12}$$

The surface displacement for the associated elastic problem corresponding to the surface loading (9) can be written down as an integral of the surface pressure distribution in terms of the point load elastic solution [8]. In any physically reasonable contact problem of this type, satisfying the restrictions of the Hertz theory, the region of contact will be limited to a finite area A_{max} of peripheral radius l_{max}. $\bar{p}$ given by (9) is thus nonzero only inside this maximum region of contact corresponding to $r \leq l_{max}$. The shear modulus for the associated elastic problem is given by the transform of (3):

$$\bar{P}\bar{s}_{ij} = \bar{Q}\bar{e}_{ij} \tag{13}$$

The integral for the surface displacement for this associated elastic problem is [8]

$$\bar{w}(r, s) = \iint_{A_{max}} \frac{1}{2\pi} \frac{\bar{P}}{\bar{Q}} \frac{\bar{p}(r', s)}{\rho} dA \tag{14}$$

where ρ is the radius from the point at which the axially symmetric deflection is to be evaluated to the element of area dA, and r' is the running radius co-ordinate over the surface of contact. Substitution for p from (9) gives:

$$\bar{w}(r, s) = \frac{2}{\pi^2 R} \iint_{A_{max}} \bar{f}(r', s) \frac{dA}{\rho} \tag{15}$$

Since the integral is taken over a fixed domain A_{max} of the space variables, inversion can be effected under the integral sign, so that:

$$w(r, t) = \frac{2}{\pi^2 R} \iint_{A_{max}} f(r', t) \frac{dA}{\rho} \tag{16}$$

where the integral need be evaluated only over the current contact area, since the integrand is zero for $r' \geq l(r)$. Equation (16) is the elementary integral which gives the deflection for the elastic solution, and for $r \leq l(r)$ reduces to [8]:

$$w(r, t) = \frac{[l(t)]^2}{R} - \frac{r^2}{2R} \tag{17}$$

This is the condition that within the region of contact, $r < l(t)$, the surface of the half space is in contact with the indenting sphere. Thus the solution given by (7) does satisfy one condition needed for a satisfactory solution of the contact problem for arbitrary choice of the viscoelastic operators P and Q.

If the radius of contact $l(t)$ increases to a maximum and then decreases to zero, (16) shows that the normal deflection of the entire surface reduces to zero, which is contrary to what would be expected for a viscoelastic material in which the delayed elastic and viscous components of strain would be expected to leave a residual indentation after contact had ceased. Such materials can be looked upon as having hereditary properties, and one would expect a residual deformation to be left as a memory of the contact process. The reason for this unexpected paradoxical result is that if $l(t)$ passes through a maximum l_{max} and decreases, $f(r, t)$ in (8) passes through a maximum and returns to zero for $r > l(t)$, but examination of particular cases shows that the corresponding $p(r, t)$ determined by (7) usually passes through zero and takes on negative or tensile values. For example, if P is a differential operator, $p(r, t)$ will be given by its complementary function, and will be nonzero because of the nonzero value of p when $f(r, t)$ first reduces to zero at $r = l(t)$. In the elastic case of course, for which P and Q in (7) are constants, p falls to zero with f. Thus when $l(t)$ decreases a residual tensile surface traction is left in the viscoelastic case at points formerly in the contact region, which violates the contact condition that outside the current region of contact the surface traction should be zero. This difficulty does not arise with nondecreasing $l(t)$, since the zero initial conditions and zero right-hand side of (7) for all earlier times guarantee zero traction outside the region of contact. Thus, although the solution correctly describes a viscoelastic stress and deflection combination, for decreasing $l(t)$ this would require an applied surface traction outside the region of contact, $r = l(t)$, so that it is not the solution which represents the contact situation.

So far, the progress of the indentation has been expressed in terms of the radius of the region of contact $l(t)$, but this would be an inconvenient variable in practice. The central displacement $w(0, t)$ in (17) gives the displacement $\alpha(r)$ of the rigid sphere:

$$\alpha(t) = \frac{[l(t)]^2}{R} \tag{18}$$

so that the previous relations could readily be written in terms of α. For example, (7) gives the pressure distribution in terms of the penetration of the sphere $\alpha(t)$, with $f(r, t)$ defined as:

$$f(r, t) = \mathrm{Re}[R\alpha(t) - r^2]^{1/2} \tag{19}$$

An alternative convenient variable would be the total force of penetration:

$$p_0(t) = \int_0^{l(t)} p(r, t) 2\pi r dr \tag{20}$$

In the circumstances for which the solution is valid the upper limit can be changed to l_{max} to give an invariant region of integration, since $p(r, t)$ is zero for $r > l(t)$. p_0 can then be determined by taking the Laplace transform of (20) and substituting from (9):

$$\bar{p}_0(s) = \frac{4}{\pi R} \frac{\bar{Q}}{\bar{P}} \int_0^{l_{max}} \bar{f}(r, s) 2\pi r dr \tag{21}$$

The inverse transform can be taken directly since the integration limits are invariant; the integral then reduces to the volume of a hemisphere, giving:

$$P[p_0(t)] = \frac{8}{3R} Q[\{l(t)\}^3] \tag{22}$$

or in terms of the penetration of the sphere $\alpha(t)$:

$$P[p_0(t)] = \frac{8}{3R} Q[\{R\alpha(t)\}^{3/2}] \tag{23a}$$

or

$$P[p_0(t)] = \frac{8}{3} \sqrt{R}\, Q[\{\alpha(t)\}^{3/2}] \tag{23b}$$

Thus, given either the variation of the total force or of the motion of the sphere, the contact problem can be solved by means of (23), (18) and (7). Because of the limitation that $l(t)$ must be nondecreasing, (23) is only valid for nondecreasing $\alpha(t)$ by (18).

It is interesting to note that the operator equations (7) [with f defined by (19)] and (23) contain a displacement variable $\alpha(t)$ in a nonlinear manner, even though the original equations (1), (2), (3), and (4) contain displacement components linearly. This fact emphasizes the need for careful choice of the particular expression developed on the basis of elasticity theory from which to generate the viscoelastic solution.

Examples

Because the results developed in the previous section are valid for arbitrary linear viscoelastic operators, interesting particular examples can be obtained readily by selecting appropriate operator representations to provide simple analytical expressions. For example, if the loading history, $p_0(t)$, is given, the viscoelastic representation (10) in terms of the shear creep compliance $J_s(t)$ gives the simplest determination of the variation of contact radius or indentation. With no disturbance for negative t, (22) becomes:

$$\int_0^t {}^1/_2 J_s(t - \tau) \frac{dp_0}{d\tau} d\tau = \frac{8}{3R} [l(t)]^3 = \frac{8}{3} \sqrt{R} [\alpha(t)]^{3/2} \tag{24}$$

If $p_0(t)$ takes the form of a suddenly applied constant force P_0:

$$p_0(t) = P_0 H(t) \tag{25}$$

where $H(t)$ is the Heaviside step function, the derivative in the integrand becomes a delta function, and (24) gives

$$[l(t)]^3 = \frac{3R}{16} J_c(t) P_0 H(t) \tag{26a}$$

$$[\alpha(t)]^{3/2} = \frac{3}{16\sqrt{R}} J_c(t) P_0 H(t) \tag{26b}$$

This expresses a result which one would expect, that materials which flow indefinitely in creep such as the Maxwell material, give a radius of the region of contact and an indentation which would increase without limit for a spherical indenter under constant load. This must of course be interpreted within the constraint of small strain analysis, and the solution be rejected for large indentations on this account. Also, in the justification of the solution which assumed a maximum contact area, A_{max}, the theory applies up to an arbitrary time t_1, and when this is selected the future progress of the solution must be limited to remain within a finite contact area A_{max}. Because of the nature of the Laplace-transform process, and of the operators in the stress-strain law, for which the state of a material is influenced only by its past history, this process will not modify the solution for $t < t_1$. Materials which creep to a limiting strain magnitude, such as the Kelvin delayed elastic material, however, sink in only to a limited extent, after which the viscoelastic material supports the loaded ball. In the steady state the solution coincides with the corresponding elastic solution.

If the total force applied, $p_0(t)$, is reduced to zero at $t = t_1$, then

$$p_0(t) = P_0[H(t) - H(t - t_1)] \tag{27}$$

and (24) gives:

$$[l(t)]^3 = \frac{3R}{16} [J_c(t)H(t) - J_c(t - t_1)H(t - t_1)] \tag{28}$$

This leaves $l(t)$ positive for zero total force, showing that the surface traction is in part tensile which would violate contact conditions. As mentioned previously, however, with decreasing $l(t)$ the force is spread over the maximum range of the contact area, so that for $t > t_1$ contact conditions are also violated otherwise.

To investigate the variation in contact pressure, $p(r, t)$, it is convenient to write (7) in terms of the relaxation modulus in shear [2, 3, 4], $G_R(t)$

$$p(r, t) = \frac{4}{\pi R} \int_0^t 2G_R(t - \tau) \frac{\partial f(r, \tau)}{\partial \tau} d\tau \tag{29}$$

where f is defined in (8) and an initially undisturbed body is assumed. Since $G_R(t)$ is a monotonically decreasing function, it is clear that if $l(t)$ passes through a maximum and then decreases to r, the pressure given by (29) will be negative, showing violation of contact conditions with decreasing $l(t)$.

Consider now some cases of prescribed variation of the radius of the contact area, $l(t)$, or equivalently through (18) of the indentation of the sphere. If

$$l(t) = l_0 H(t), \qquad \alpha(t) = \frac{l_0^3}{R} H(t) \tag{30}$$

(29) determines

$$p(r, t) = \frac{8}{\pi R} G_R(t) \text{ Re } [l_0^2 - r^2]^{1/2} H(t) \tag{31}$$

since the τ derivative gives a delta function. Equation (31) shows that the elastic contact pressure for the instantaneous modulus decays at all points in proportion with the relaxation modulus in shear. For this problem which could be prescribed by a given constant indentation, the radius of the contact region and the normal displacement of all surface points remain constant throughout the pressure relaxation. If the material would relax to zero stress in a relaxation test in shear, which corresponds to indefinite flow in a creep test, then after a sufficient time the pressure given by (31) would approach zero. If the sphere is then removed, a permanent impression of the indentation would be left in the surface, since the zero traction condition would be maintained with or without the sphere in position. If the relaxation modulus decreases to a finite asymptote with increasing t, (31) and the associated stress and strain distribution reduce to the corresponding elastic solution for sufficiently large t.

If l_0 is suddenly increased to l_1 at $t = t_1$ or correspondingly the indentation is increased:

$$p(r, t) = \frac{8}{\pi R} [G_R(t) \text{Re}[l_0^2 - r^2]^{1/2} H(t) + (\text{Re}[l_1^2 - r^2]^{1/2} - \text{Re}[l_0^2 - r^2]^{1/2}) G_R(t - t_1) H(t - t_1)] \tag{32}$$

For $t > t_1$, (32) gives a pressure distribution of the type depicted in Fig. 2. The dip in the pressure distribution B-C-D represents the memory of the viscoelastic material for the early part of the indentation history, $0 < t < t_1$, when the pressure extended over a contact circle of radius l_0, causing an incipient dent over this region.

An effect analogous to the foregoing arises in the case of continuous indentation, but the influence is then smoothed out. Suppose, for example, that indentation at constant velocity v is assumed:

$$\alpha(t) = vt \tag{33}$$

which by (18) corresponds to:

$$[l(t)]^3 = Rvt \tag{34}$$

then (7) gives

$$p(r, t) = \frac{4}{\pi R} \int_0^t 2G_R(t - \tau) \frac{\partial}{\partial \tau} \text{Re } [Rv\tau - r^2]^{1/2} d\tau \tag{35}$$

where for convenience the operator in terms of the relaxation modulus has been used. Simple numerical evaluation is achieved in the case of Maxwell behavior in shear, for which $G_R(t)$ takes the form [2, 3, 4]:

$$G_R(t) = G_0 e^{-t/\tau_0} \tag{36}$$

where τ_0 is the relaxation time. Writing $l_0 = l(\tau_0)$, the radius of the region of contact when the indentation has been continuing for the duration of the relaxation time τ_0, (35) can be expressed in the form:

$$p(r, t) = \frac{8G_0}{\pi R} l_0 e^{-\frac{[l(t)]^2 - r^2}{l_0^2}} \int_0^{\text{Re}\left\{\frac{[l(t)]^2 - r^2}{l_0^2}\right\}^{1/2}} e^{y^2} dy \tag{37}$$

for which tabulated values of the integral are given by Jahnke and Emde [10]. As t/τ_0 approaches zero, this can readily be seen to reduce to the elastic result (6). Fig. 3 shows a dimensionless plot of the contact pressure at several times after first contact, and Fig. 4 shows the same results scaled to a constant radius in order better to compare the shapes of the pressure distributions. The

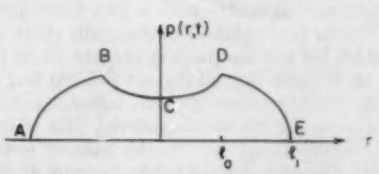

Fig. 2 Contact pressure distribution for stepwise identation

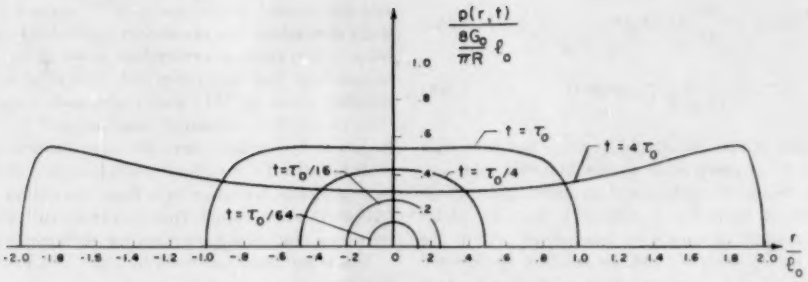

Fig. 3 Contact pressure distribution for continuous indentation of a Maxwell body

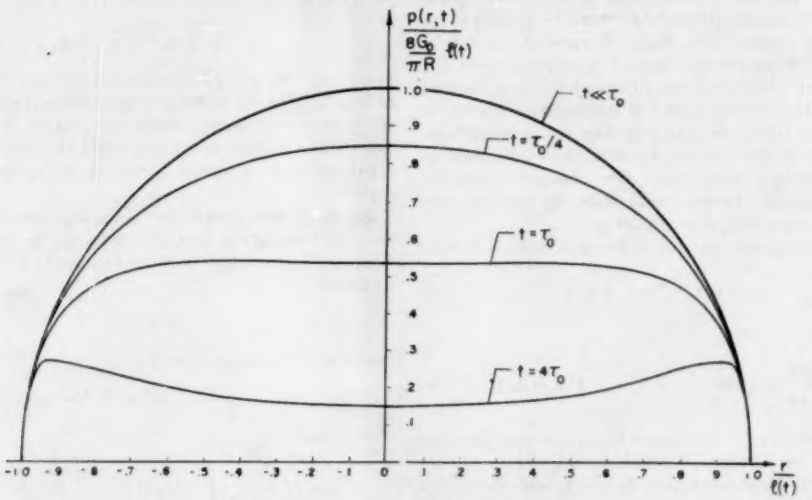

Fig. 4 Comparison of distribution of contact pressure at different times in continuous indentation

dimensionless co-ordinates are chosen so that in both cases the elastic solution (6) would yield semicircular distributions.

Fig. 3 shows that at times much shorter than the relaxation time the behavior is essentially elastic. At the relaxation time the pressure distribution is flattened in the center, and later a central dip occurs. This is due to the influence of the hereditary nature of viscoelastic response and the incipient central dent caused by the more localized pressure during the early history of the contact. After passing through a maximum value the central pressure falls as time increases, and consideration of the limiting value of the integral in (37) as $l(t)/l_0$ approaches infinity shows that the pressure falls toward zero. The central dip in the pressure distribution is analogous to the central decrease in pressure shown in Fig. 2 in the discontinuous loading case.

Fig. 4 shows the gradual departure of the contact pressure distribution from the elastic case as time increases. It also shows the remarkably close approximation to the elastic solution adjacent to the edge of the region of contact. Apparently the local strain caused by the traverse of the boundary of the region of contact, where the material surface is first forced into contact with the indenting sphere, causes an essentially elastic stress distribution which has not been in existence sufficiently long to be affected by the viscoelasticity of the material. At long times this forms a sharp boundary layer of elastic influence just inside the region of contact. For the Kelvin material, with no instantaneous elastic response, and so formally infinite instantaneous modulus, this phenomenon gives infinite pressure at the edge of contact.

It was pointed out previously that the solution for reducing contact area is invalid. However, there is one method of unloading the indenter which is amenable to direct analysis on the basis of the theory given in this paper. If the indenter is removed rapidly, so that after a particular instant the surface tractions can be equated to zero over the whole surface, the transform method based on prescribed surface tractions can be utilized after contact has ceased. Because of the complicated nature of the pressure distribution during indentation, as just detailed in a particular case, the surface formerly in contact will immediately assume a complicated deformation pattern on release of the pressure for a material exhibiting instantaneous elastic response and recovery.

More General Analysis

The problem of indentation by a smooth rigid sphere as just detailed was selected for simplicity of presentation. The method of analysis applies for contact of smooth bodies of arbitrary linear viscoelastic materials, just as the Hertz solution in elasticity applies for arbitrary smooth elastic bodies. The justification follows the treatment detailed in the foregoing by means of the Laplace transformation. An elliptical contact region is determined by semiaxes $a(t)$ and $b(t)$ which depend on the principal radii of curvature of the surfaces, their orientation, and the approach of the bodies. The expression for contact pressure is of the form [8]:

$$p(x, y, t) = \frac{4(A + B)}{\pi m^2 n^2 \left(\frac{1 - \nu_1}{G_1} + \frac{1 - \nu_2}{G_2}\right)} \left\{[a(t)]^2 - x^2 - \frac{m^2}{n^2} y^2\right\}^{1/2} \quad (38)$$

where A and B are geometrical properties of the surfaces to come into contact, m and n are parameters depending on these, and ν_1, G_1, ν_2, G_2 are linear operators representing the viscoelastic properties of the two bodies, the ν corresponding to Poisson's ratios in elasticity, and the G to the shear moduli. Combined operators for particular magnitudes, such as that relating lateral to longitudinal strain in a tensile test, can be obtained for viscoelasticity just as the relations between elastic constants are obtained [11]. Thus the elastic relation:

$$\nu = \frac{3K - 2G}{2(3K + G)}$$

where K is the bulk modulus becomes:

$$\nu = \frac{\frac{Q'}{P'} - \frac{Q}{P}}{2\left(\frac{Q'}{P'} + \frac{Q}{2P}\right)} \quad (39)$$

by replacing the elastic constants by the equivalent viscoelastic operators in (3) and (4). In a particular case, (39) can be represented as a single combined operator pair of the types we have considered for P and Q.

When $p(x, y, t)$ has been determined by (38), the displacement of each surface is given by an integral over the region of contact of the form [8]:

$$w_i(x, y, t) = \int\int \frac{1 - \nu_i}{2\pi G_i} \frac{p(\xi, \eta, t)}{r(x, y, \xi, \eta)} \, d\xi \, d\eta \quad (40)$$

where i takes on the values 1 and 2 for the two bodies. The relative displacement is given by $(w_1 + w_2)$ and with the use of the Laplace transform and fixed space integral over A_{max}, the material operators in (38) and (40) cancel, and the simple geometrical contact condition is achieved of the relative displacement being given as a quadratic form in the surface co-ordinates.

In view of the influence of the viscoelastic properties of the material on the contact pressure distribution presented in the particular case for a Maxwell body, it might be anticipated that difficulty would arise in the theory of contact of dissimilar bodies, since one would call for a different pressure-distribution history than the other. However, in the combined application of (38) and (40) it is the sum of operators for the separate bodies which appears and insures the correct contact condition. The separate operators (40) which determine the surface displacement of each body, with the combined operator appearing in the expression for $p(x, y, t)$ (38), will determine displacement distributions which involve the viscoelastic operators, so that in this case the deformed shape of the surface of contact will be influenced by the viscoelastic operators. This contrasts with the elastic problem for which the deformed region of contact is always spherical in the axially symmetrical case, or represented by a quadratic form in the general case. For contact between bodies of the same material the viscoelastic operators will cancel in the expression for each w_i, (40) and (38), and the deformed region of contact will be given by a quadratic form in the general case, and be spherical in the axially symmetrical case. It will not depend on the material properties but only on the geometry of the contacting surfaces.

Discussion

The contact problem for viscoelastic materials has been previously discussed by Pao [12], who takes the Laplace transform of the approach-force relation (23) to compute some problems of viscoelastic rebound. He states the limitation that viscoelastic effects do not cause the contact area to increase appreciably, and assumes that the pressure distribution remains elliptical as in the elastic case. The present analysis has shown that (23) is valid for large viscoelastic influences which may produce a marked change in the contact pressure distribution as illustrated, for example, in Fig. 3. However, it does not apply for decreasing contact area so that the rebound solutions will be in error. At the "end of rebound" (23) will determine a positive area of contact with a pressure distribution over the maximum area of contact with the compressive components balancing the tensile ones, reducing to zero resultant force.

The earlier work also stated that the theory applied only for the same viscoelastic materials in contact, or if one were rigid. It has been pointed out already that the analysis allowing fully for viscoelastic effects is not subject to this limitation, but that contact between different materials does produce a more complicated deformed shape of the contact surface than arises otherwise or in the Hertz solution.

Experiments on rebound of viscoelastic materials by Tillett [13] show that the assumption of a single equivalent frequency, and so loss factor, gives satisfactory agreement with other methods of measuring viscoelastic response. The present theory indicates that the process is in fact much more complicated than this result would imply, with markedly varying loading history at different surface points. However, this does not rule out the possibility that these smooth out and that the total force-approach relation can be expressed satisfactorily by an equivalent average frequency.

The relation (26), expressing the approach α and the radius of the contact region l for constant force penetration in terms of the viscoelastic compliance function, may form a useful means of measuring material properties. Without the need to prepare specimens it would be possible to determine the creep compliance in shear if measurements of $\alpha(t)$ or $l(t)$ under constant load could be made with sufficient accuracy. The incompressible theory on which (26) is based is probably satisfactory for most plastics in the viscoelastic range, although corresponding relations could be obtained taking into account dilatational response.

Equations (26) also provide a means of testing the linearity of the viscoelastic operators for materials in contact. For linearity, $J_s(t)$ is independent of stress magnitude, so that for different values of total constant force P_0, $[l(t)]^3$ and $[\alpha(t)]^{3/2}$ must be proportional to P_0 for any value of t. The nonlinear power of the approach α arises in the linearity check because of the particular properties of the contact situation, with its increasing contact area.

An alternative testing procedure for checking linearity and measuring viscoelastic properties could be developed on the basis of (31). For suddenly applied constant penetration α_0 corresponding to l_0 through (30), the integral of (31) gives an expression for the total force:

$$p_0(t) = \frac{16\sqrt{R}}{3} G_R(t) \alpha_0^{3/2} \quad (41)$$

which can alternatively be deduced directly from (23). Proportionality of $p_0(t)$ with $\alpha_0^{3/2}$ for any t and different values of α_0 would check linearity, and measurement of the variation of the force needed to maintain constant penetration α_0 would give the relaxation modulus in shear through (41).

Acknowledgment

The authors are indebted to Prof. A. E. Green, of King's College, Newcastle-upon-Tyne, England, for valuable discussions during the formulation of the method of solution presented in this paper.

References

1 E. H. Lee, "Stress Analysis in Viscoelastic Materials," *Journal of Applied Physics*, vol. 27, 1956, pp. 665–672.

2 B. Gross, "Mathematical Structure of the Theories of Viscoelasticity," Hermann and Cie, Paris, France, 1953.

3 H. Leaderman, "Rheology," vol. 2, F. R. Eirich, editor, Academic Press, New York, N. Y., 1958.

4 A. J. Staverman and F. Schwarzl, "Die Physik der Hochpolymeren," H. A. Stuart, editor, Springer-Verlag, Berlin, Germany, 1956.

5 E. H. Lee, "Stress Analysis in Visco-Elastic Bodies," *Quarterly of Applied Mathematics*, vol. 13, 1955, pp. 183–190.

6 J. R. M. Radok, "Visco-Elastic Stress Analysis," *Quarterly of Applied Mathematics*, vol. 15, 1957, pp. 198–202.

7 E. H. Lee and J. R. M. Radok, "Stress Analysis in Linearly Visco-Elastic Materials," Actes of the Ninth Congrès International de Mécanique Appliqué, vol. 5, 1957, pp. 321–329.

8 S. P. Timoshenko, "Theory of Elasticity," McGraw-Hill Book Company, Inc., New York, N. Y., 1934, pp. 339–350.

9 H. S. Carslaw and J. C. Jaeger, "Operational Methods in Applied Mathematics," Oxford University Press, New York, N. Y., 1941.

10 E. Jahnke and F. Emde, "Tables of Functions," Dover Publications, Inc., New York, N. Y., 1945.

11 E. H. Lee, "Viscoelastic Stress Analysis," Proceedings of First Symposium on Naval Structural Mechanics, Pergamon Press, New York, N. Y., 1960, p. 456.

12 Yoh-Han Pao, "Extension of Hertz Theory of Impact to Viscoelastic Case," *Journal of Applied Physics*, vol. 26, 1955, pp. 1083–1088.

13 J. P. A. Tillett, "Study of Impact of Spheres on Plates," Proceedings of The Physical Society, series B, vol. 67, 1954, pp. 677–688.

Stresses in Curved Beams of Noncircular Center Line

M. M. ABBASSI
Assistant Professor of Mathematics,
Faculty of Engineering,
Alexandria University,
Alexandria, Egypt

The paper deals with the general case of a curved beam whose center line is a plane curve not necessarily circular. The body-stress equations and the compatibility equations for stresses in their general form are found for the chosen system of co-ordinates and put in their simplest form. Solutions for the equations with the aim of finding the stresses when the beam is subjected to a torque and to a bending out of its plane of initial curvature are obtained for both elliptic and circular cross sections of the beam. The case of a concentrated load at one end perpendicular to the plane of initial curvature is also considered.

THE problem of determining the stresses in curved beams of circular center line under the action of couples and forces in their plane of initial curvature has been treated by many authors. The problem of stresses in a curved beam of circular center line under the action of forces and couples out of its plane of initial curvature was treated by the author in his first PhD thesis.[1]

However, if the center line of the curved beam is not circular, the problem seems to be a more complicated one. An attempt is made here to simplify the problem by using complex variable and curvilinear co-ordinates.

The center line of the curved beam is a plane curve, the locus of P is the plane $Z = 0$, the normal at P makes an angle θ with Ox, Fig. 1, C is the center of curvature of the center line at P, $PC = \rho$, R is a point on the normal, $PR = r$, unit vectors along the normal $\overrightarrow{CP}$ and tangent to the center line at P are $\hat{r}$ and $\hat{\theta}$, respectively. Q is a point on the cross section normal to $\hat{\theta}$ at P, $QR = Z$; i.e., Q is vertically above R at height Z. If Q' is an adjacent point, not necessarily in the same cross section, we have

$$\overrightarrow{QQ'} = dZ\hat{k} + \overrightarrow{RR'} \tag{1}$$

$$\overrightarrow{QQ'} = dZ\hat{k} + (\rho + r)d\theta\hat{\theta} + dr\hat{r} \tag{2}$$

The triad of unit vectors $\hat{r}$, $\hat{\theta}$, $\hat{k}$ is right-handed in that order, and the co-ordinates r, θ, Z form a set of orthogonal curvilinear co-ordinates, so that

$$\vec{\nabla} = \hat{r}\frac{\partial}{\partial r} + \frac{1}{\rho + r}\hat{\theta}\frac{\partial}{\partial\theta} + \hat{k}\frac{\partial}{\partial Z} \tag{3}$$

$$\vec{\nabla}_1 = \hat{r}\frac{\partial}{\partial r} + \frac{\hat{\theta}}{\rho + r}\frac{\partial}{\partial\theta} = \hat{r}\left(\frac{\partial}{\partial r} + \frac{i}{\rho + r}\frac{\partial}{\partial\theta}\right) \tag{4}$$

since $\hat{\theta} = i\hat{r}$.

Also $\hat{r} = \hat{\imath}e^{i\theta}$, and

$$\vec{\nabla}_1 = \hat{\imath}\frac{\partial}{\partial x} + \hat{\jmath}\frac{\partial}{\partial y} = \hat{\imath}\left(\frac{\partial}{\partial x} + i\frac{\partial}{\partial y}\right) = \hat{\imath}\left(2\frac{\partial}{\partial\bar{z}}\right) \tag{5}$$

where $z = x + iy$, $\bar{z} = x - iy$, so that

$$\hat{\imath}\left(2\frac{\partial}{\partial\bar{z}}\right) = \hat{\imath}e^{i\theta}\left(\frac{\partial}{\partial r} + \frac{i}{\rho + r}\frac{\partial}{\partial\theta}\right) \tag{6}$$

$$\nabla_1^2 = \left(2\frac{\partial}{\partial\bar{z}}\right)\left(2\frac{\partial}{\partial z}\right) = e^{i\theta}\left(\frac{\partial}{\partial r} + \frac{i}{\rho + r}\frac{\partial}{\partial\theta}\right)e^{-i\theta}\left(\frac{\partial}{\partial r} - \frac{i}{\rho + r}\frac{\partial}{\partial\theta}\right)$$

or

$$\nabla_1^2 = \left(\frac{\partial}{\partial r} + \frac{1}{\rho + r} + \frac{i}{\rho + r}\frac{\partial}{\partial\theta}\right)\left(\frac{\partial}{\partial r} - \frac{i}{\rho + r}\frac{\partial}{\partial\theta}\right)$$

so that

$$\nabla^2 = \frac{\partial^2}{\partial r^2} + \frac{1}{\rho + r}\frac{\partial}{\partial r} + \frac{1}{(\rho + r)^2}\frac{\partial^2}{\partial\theta^2} - \frac{\rho'}{(\rho + r)^3}\frac{\partial}{\partial\theta} + \frac{\partial^2}{\partial Z^2} \tag{7}$$

[1] "Stresses in Beams Curved in Plan," submitted to Alexandria University, 1952.

Presented at the Summer Conference of the Applied Mechanics Division, University Park, Pa., June 20–22, 1960, of THE AMERICAN SOCIETY OF MECHANICAL ENGINEERS.

Discussion of this paper should be addressed to the Secretary, ASME, 29 West 39th Street, New York, N. Y., and will be accepted until October 10, 1960, for publication at a later date. Discussion received after the closing date will be returned.

NOTE: Statements and opinions advanced in papers are to be understood as individual expressions of their authors and not those of the Society. Manuscript received by ASME Applied Mechanics Division, December 1, 1958. Paper No. 60—APM-21.

Nomenclature

x, y, Z = rectangular co-ordinates
r, θ, Z = curvilinear co-ordinates
ρ = radius of curvature
$\hat{\imath}, \hat{\jmath}, \hat{k}$, $\hat{r}, \hat{\theta}, \hat{Z}$ = unit vectors
$z = x + iy$
$\bar{z} = x - iy$
$\widehat{xx}, \widehat{yy}, \widehat{ZZ}$ = normal components of stress parallel to x, y, and Z-axes
$\widehat{rr}, \widehat{\theta\theta}, \widehat{ZZ}$ = normal stress components in curvilinear co-ordinates
$\Delta = \widehat{xx} + \widehat{yy} + \widehat{ZZ} = \widehat{rr} + \widehat{\theta\theta} + \widehat{ZZ}$
$\widehat{xy}, \widehat{xZ}, \widehat{yZ}$ = shearing-stress components in rectangular co-ordinates
$\widehat{r\theta}, \widehat{\theta Z}, \widehat{rZ}$ = shearing-stress components in curvilinear co-ordinates
M = bending moment
T = torque
I = moment of inertia of a cross section
η = Poisson's ratio
Φ, Ψ, χ = stress functions

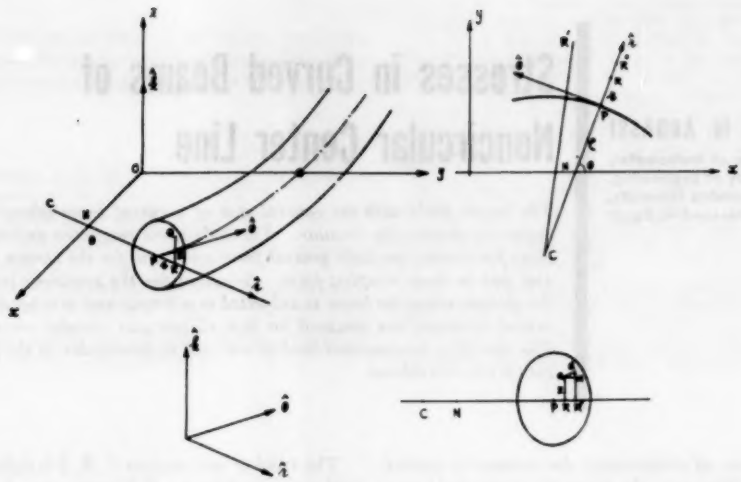

Fig. 1

Body-Stress Equations

The equations of transformations of the stresses are

$$\Theta' = \widehat{rr} + \widehat{\theta\theta} = \Theta = \widehat{xx} + \widehat{yy} \tag{8}$$

$$rr - \widehat{\theta\theta} + 2i\widehat{r\theta} = \Phi' = \Phi e^{-2i\theta} = (\widehat{xx} - \widehat{yy} + 2i\widehat{xy})e^{-2i\theta} \tag{9}$$

$$\widehat{rZ} + i\widehat{\theta Z} = \Psi' = e^{-i\theta}\Psi = (\widehat{xZ} + i\widehat{yZ})e^{-i\theta} \tag{10}$$

The body-stress equations in complex co-ordinates z, $\bar{z}$, Z are

$$\frac{\partial\Theta}{\partial\bar{z}} + \frac{\partial\Phi}{\partial z} + \frac{\partial\Psi}{\partial Z} = 0, \tag{11}$$

$$\frac{\partial\Psi}{\partial z} + \frac{\partial\overline{\Psi}}{\partial\bar{z}} + \frac{\partial\widehat{ZZ}}{\partial Z} = 0 \tag{12}$$

We have

$$2\frac{\partial}{\partial\bar{z}} = e^{i\theta}\left(\frac{\partial}{\partial r} + \frac{i}{\rho + r}\frac{\partial}{\partial\theta}\right)$$

with

$$\Theta' = \Theta, \quad \Phi' = \Phi e^{-2i\theta}, \quad \Psi' = \Psi e^{-i\theta}$$

and so the equations are

$$e^{i\theta}\left(\frac{\partial}{\partial r} + \frac{i}{\rho + r}\frac{\partial}{\partial\theta}\right)\Theta' + e^{-i\theta}\left(\frac{\partial}{\partial r} - \frac{i}{\rho + r}\frac{\partial}{\partial\theta}\right)\Phi' e^{2i\theta} + 2e^{i\theta}\frac{\partial\Psi'}{\partial Z} = 0, \tag{13}$$

$$\left[e^{-i\theta}\left(\frac{\partial}{\partial r} - \frac{i}{\rho + r}\frac{\partial}{\partial\theta}\right)\Psi' e^{i\theta} + \text{conjugate}\right] + 2\frac{\partial\widehat{ZZ}}{\partial Z} = 0 \tag{14}$$

whence

$$\left(\frac{\partial}{\partial r} + \frac{i}{\rho + r}\frac{\partial}{\partial\theta}\right)(\widehat{rr} + \widehat{\theta\theta}) + \left[\frac{\partial}{\partial r} - \frac{i}{\rho + r}\left(\frac{\partial}{\partial\theta} + 2i\right)\right](\widehat{rr} - \widehat{\theta\theta} + 2i\widehat{r\theta}) + 2\frac{\partial\Psi'}{\partial Z} = 0$$

and

$$\left[\frac{\partial}{\partial r} - \frac{i}{\rho + r}\left(\frac{\partial}{\partial\theta} + i\right)\right]\Psi' + \left[\frac{\partial}{\partial r} + \frac{i}{\rho + r}\left(\frac{\partial}{\partial\theta} - i\right)\right]\overline{\Psi}' + 2\frac{\partial\widehat{ZZ}}{\partial Z} = 0$$

Hence we have

$$\frac{\partial\widehat{rr}}{\partial r} + \frac{\widehat{rr} - \widehat{\theta\theta}}{\rho + r} + \frac{1}{\rho + r}\frac{\partial\widehat{r\theta}}{\partial\theta} + \frac{\partial\widehat{rZ}}{\partial Z} = 0, \tag{15}$$

$$\frac{1}{\rho + r}\frac{\partial\widehat{\theta\theta}}{\partial\theta} + \left(\frac{\partial}{\partial r} + \frac{2}{\rho + r}\right)\widehat{r\theta} + \frac{\partial\widehat{\theta Z}}{\partial Z} = 0, \tag{16}$$

$$\left(\frac{\partial}{\partial r} + \frac{1}{\rho + r}\right)\widehat{rZ} + \frac{1}{\rho + r}\frac{\partial\widehat{\theta Z}}{\partial\theta} + \frac{\partial\widehat{ZZ}}{\partial Z} = 0 \tag{17}$$

Compatibility Equations for Stresses

The Beltrami compatibility equations (with zero body force) are

$$(1 + \eta)\nabla^2\widehat{pq} + \frac{\partial^2}{\partial p\,\partial q}\Delta = 0 \qquad p, q, = x, y, Z \tag{18}$$

which gives the complex Beltrami equations as[2]

$$(1 + \eta)\nabla^2\Theta + 4\frac{\partial^2\Delta}{\partial z\,\partial\bar{z}} = 0, \tag{19}$$

$$(1 + \eta)\nabla^2\Phi + 4\frac{\partial^2\Delta}{\partial\bar{z}^2} = 0, \tag{20}$$

$$(1 + \eta)\nabla^2\Psi + 2\frac{\partial^2\Delta}{\partial\bar{z}\,\partial Z} = 0, \tag{21}$$

$$(1 + \eta)\nabla^2\widehat{ZZ} + \frac{\partial^2\Delta}{\partial Z^2} = 0 \tag{22}$$

while

$$\nabla^2\Phi = \nabla^2\Phi' e^{2i\theta} = e^{2i\theta}\Delta^2\Phi' \tag{23}$$

[2] A. C. Stevenson, "Some Boundary Problems of Two-Dimensional Elasticity," *Philosophical Magazine*, vol. 34, series 7, 1943, pp. 766–793.

Then

$$e^{2i\theta}\Delta^2\Phi' = \nabla^2\Phi' e^{2i\theta}$$

$$= \left[\frac{\partial^2}{\partial r^2} + \frac{1}{\rho + r}\frac{\partial}{\partial r} + \frac{\partial^2}{\partial Z^2} + \frac{1}{(\rho + r)^2}\frac{\partial^2}{\partial\theta^2} - \frac{\rho'}{(\rho + r)^3}\frac{\partial}{\partial\theta}\right]\Phi' e^{2i\theta}$$

$$= e^{2i\theta}\left[\frac{\partial^2}{\partial r^2} + \frac{1}{\rho + r}\frac{\partial}{\partial r} + \frac{\partial^2}{\partial Z^2} + \frac{1}{(\rho + r)^2}\left(\frac{\partial}{\partial\theta} + 2i\right)^2 - \frac{\rho'}{(\rho + r)^3}\left(\frac{\partial}{\partial\theta} + 2i\right)\right]\Phi' \quad (24)$$

or

$$\Delta^2\Phi' = \left[\nabla^2 + \frac{4i}{(\rho + r)^2}\frac{\partial}{\partial\theta} - \frac{4}{(\rho + r)^2} - \frac{2i\rho'}{(\rho + r)^3}\right]\Phi' \quad (25)$$

Similarly, put

$$\nabla^2\Psi = \nabla^2\Psi' e^{i\theta} = e^{i\theta}D^2\Psi' \quad (26)$$

Then

$$e^{i\theta}D^2\Psi' = e^{i\theta}\left[\frac{\partial^2}{\partial r^2} + \frac{1}{\rho + r}\frac{\partial}{\partial r} + \frac{\partial^2}{\partial Z^2} + \frac{1}{(\rho + r)^2}\left(\frac{\partial}{\partial\theta} + i\right)^2 - \frac{\rho'}{(\rho + r)^3}\left(\frac{\partial}{\partial\theta} + i\right)\right]\Psi'$$

or

$$D^2\Psi' = \left[\nabla^2 + \frac{2i}{(\rho + r)^2}\frac{\partial}{\partial\theta} - \frac{1}{(\rho + r)^2} - \frac{i\rho'}{(\rho + r)^3}\right]\Psi' \quad (27)$$

Also

$$2\frac{\partial}{\partial\bar{z}} = e^{i\theta}\mathfrak{D} = e^{i\theta}\left(\frac{\partial}{\partial r} + \frac{i}{\rho + r}\frac{\partial}{\partial\theta}\right) \quad (28)$$

So

$$4\frac{\partial^2}{\partial\bar{z}^2} = e^{i\theta}\mathfrak{D}e^{i\theta}\mathfrak{D} = e^{2i\theta}\left(\mathfrak{D} - \frac{1}{\rho + r}\right)\mathfrak{D} \quad (29)$$

So our Beltrami equations take the form

$$(1 + \eta)\nabla^2\widehat{ZZ} + \frac{\partial^2\Delta}{\partial Z^2} = 0 \quad (30)$$

$$(1 + \eta)\nabla^2\Theta' + \nabla_1^2\Delta = 0 \quad (31)$$

$$(1 + \eta)\Delta^2\Phi' + \left(\mathfrak{D}^2 - \frac{\mathfrak{D}}{\rho + r}\right)\Delta = 0 \quad (32)$$

$$(1 + \eta)D^2\Psi' + \mathfrak{D}\frac{\partial\Delta}{\partial Z} = 0 \quad (33)$$

We proceed to get the equivalent equations of the two last complex equations (32), and (33); equation (33) gives

$$(1 + \eta)\left[\nabla^2 + \frac{2i}{(\rho + r)^2}\frac{\partial}{\partial\theta} - \frac{1}{(\rho + r)^2} - \frac{i\rho'}{(\rho + r)^3}\right](\widehat{rZ} + i\widehat{\theta Z}) + \left[\frac{\partial}{\partial r} + \frac{i}{\rho + r}\frac{\partial}{\partial\theta}\right]\frac{\partial\Delta}{\partial Z} = 0 \quad (34)$$

from which we get the two compatibility equations

$$(1 + \eta)\left[\left\{\nabla^2 - \frac{1}{(\rho + r)^2}\right\}\widehat{rZ} - \left\{\frac{2}{(\rho + r)^2}\frac{\partial}{\partial\theta} - \frac{\rho'}{(\rho + r)^3}\right\}\widehat{\theta Z}\right] + \frac{\partial^2\Delta}{\partial r\partial Z} = 0 \quad (35)$$

$$(1 + \eta)\left[\left\{\nabla^2 - \frac{1}{(\rho + r)^2}\right\}\widehat{\theta Z} + \left\{\frac{2}{(\rho + r)^2}\frac{\partial}{\partial\theta} - \frac{\rho'}{(\rho + r)^3}\right\}\widehat{rZ}\right] + \frac{1}{\rho + r}\frac{\partial^2\Delta}{\partial\theta\partial Z} = 0 \quad (36)$$

Equation (32) gives

$$(1 + \eta)\left[\left\{\nabla^2 + \frac{4i}{(\rho + r)^2}\frac{\partial}{\partial\theta} - \frac{4}{(\rho + r)^2} - \frac{2i\rho'}{(\rho + r)^3}\right\}(\widehat{rr} - \widehat{\theta\theta} + 2i\widehat{r\theta}) + \left(\frac{\partial}{\partial r} + \frac{i}{\rho + r}\frac{\partial}{\partial\theta} - \frac{1}{\rho + r}\right)\left(\frac{\partial}{\partial r} + \frac{i}{\rho + r}\frac{\partial}{\partial\theta}\right)\Delta = 0 \quad (37)$$

or

$$(1 + \eta)\left[\left\{\nabla^2 + \frac{4i}{(\rho + r)^2}\frac{\partial}{\partial\theta} - \frac{4}{(\rho + r)^2} - \frac{2i\rho'}{(\rho + r)^3}\right\}(rr - \widehat{\theta\theta} + 2i\widehat{r\theta})\right] + \left[\frac{\partial^2}{\partial r^2} - \frac{2i}{(\rho + r)^2}\frac{\partial}{\partial\theta} + \frac{2i}{\rho + r}\frac{\partial^2}{\partial\theta\partial r} - \frac{1}{(\rho + r)^2}\frac{\partial^2}{\partial\theta^2} + \frac{\rho'}{(\rho + r)^3}\frac{\partial}{\partial\theta} - \frac{1}{\rho + r}\frac{\partial}{\partial r}\right]\Delta = 0 \quad (38)$$

The coefficient of i gives

$$(1 + \eta)\left[\left\{\nabla^2 - \frac{4}{(\rho + r)^3}\right\}\widehat{r\theta} + \frac{2}{(\rho + r)^2}\frac{\partial}{\partial\theta}(rr - \widehat{\theta\theta}) - \frac{\rho'}{(\rho + r)^3}(\widehat{rr} - \widehat{\theta\theta})\right] - \frac{1}{(\rho + r)^2}\frac{\partial\Delta}{\partial\theta} + \frac{1}{\rho + r}\frac{\partial^2\Delta}{\partial\theta\partial r} = 0 \quad (39)$$

The real part of the equation gives

$$(1 + \eta)\left[\left\{\nabla^2 - \frac{4}{(\rho + r)^3}\right\}(\widehat{rr} - \widehat{\theta\theta}) - 4\left\{\frac{2}{(\rho + r)^3}\frac{\partial}{\partial\theta} - \frac{\rho'}{(\rho + r)^3}\right\}\widehat{r\theta}\right] + \left\{\frac{\partial^2}{\partial r^2} - \frac{1}{(\rho + r)^2}\frac{\partial^2}{\partial\theta^2} + \frac{\rho'}{(\rho + r)^3}\frac{\partial}{\partial\theta} - \frac{1}{\rho + r}\frac{\partial}{\partial r}\right\}\Delta = 0 \quad (40)$$

Equation (31) is

$$(1 + \eta)\nabla^2(\widehat{rr} + \widehat{\theta\theta}) + \nabla_1^2\Delta = 0 \quad (41)$$

where

$$\nabla_1^2 = \frac{\partial^2}{\partial r^2} + \frac{1}{\rho + r}\frac{\partial}{\partial r} + \frac{1}{(\rho + r)^2}\frac{\partial^2}{\partial\theta^2} - \frac{\rho'}{(\rho + r)^3}\frac{\partial}{\partial\theta}$$

Adding and subtracting (40) and (41) we get the two compatibility equations

$$(1 + \eta)\left[\nabla^2\widehat{rr} - \frac{2}{(\rho + r)^3}(\widehat{rr} - \widehat{\theta\theta}) - 2\left\{\frac{2}{(\rho + r)^2}\frac{\partial}{\partial\theta} - \frac{\rho'}{(\rho + r)^3}\right\}\widehat{r\theta}\right] + \frac{\partial^2\Delta}{\partial r^2} = 0, \quad (42)$$

$$(1+\eta)\left[\nabla^2\widehat{\theta\theta}+\frac{2}{(\rho+r)^2}(\widehat{rr}-\widehat{\theta\theta})+2\left\{\frac{2}{(\rho+r)^2}\frac{\partial}{\partial\theta}-\frac{\rho'}{(\rho+r)^3}\right\}\widehat{r\theta}\right]+\left\{\frac{1}{\rho+r}\frac{\partial}{\partial r}+\frac{1}{(\rho+r)^2}\frac{\partial^2}{\partial\theta^2}-\frac{\rho'}{(\rho+r)^3}\frac{\partial}{\partial\theta}\right\}\Delta=0 \quad (43)$$

Summary

The body-stress equations and the compatibility equations for no body forces in the chosen system of curvilinear co-ordinates (r, θ, Z) are given by the following:

Body-Stress Equations

$$\left(\frac{\partial}{\partial r}+\frac{1}{\rho+r}\right)\widehat{rr}+\frac{1}{\rho+r}\frac{\partial\widehat{r\theta}}{\partial\theta}-\frac{\widehat{\theta\theta}}{\rho+r}+\frac{\partial\widehat{rZ}}{\partial Z}=0 \quad (I)$$

$$\left(\frac{\partial}{\partial r}+\frac{2}{\rho+r}\right)\widehat{r\theta}+\frac{1}{\rho+r}\frac{\partial\widehat{\theta\theta}}{\partial\theta}+\frac{\partial\widehat{\theta Z}}{\partial Z}=0 \quad (II)$$

$$\left(\frac{\partial}{\partial r}+\frac{1}{\rho+r}\right)\widehat{rZ}+\frac{1}{\rho+r}\frac{\partial\widehat{\theta Z}}{\partial\theta}+\frac{\partial\widehat{ZZ}}{\partial Z}=0 \quad (III)$$

Compatibility Equations

$$(1+\eta)\left[\nabla^2\widehat{rr}-\frac{2}{(\rho+r)^2}(\widehat{rr}-\widehat{\theta\theta})-2\left\{\frac{2}{(\rho+r)^2}\frac{\partial}{\partial\theta}-\frac{\rho'}{(\rho+r)^3}\right\}\widehat{r\theta}\right]+\frac{\partial^2\Delta}{\partial r^2}=0 \quad (IV)$$

$$(1+\eta)\left[\nabla^2\widehat{\theta\theta}+\frac{2}{(\rho+r)^2}(\widehat{rr}-\widehat{\theta\theta})+2\left\{\frac{2}{(\rho+r)^2}\frac{\partial}{\partial\theta}-\frac{\rho'}{(\rho+r)^3}\right\}\widehat{r\theta}\right]+\left\{\frac{1}{\rho+r}\frac{\partial}{\partial r}+\frac{1}{(\rho+r)^2}\frac{\partial^2}{\partial\theta^2}-\frac{\rho'}{(\rho+r)^3}\frac{\partial}{\partial\theta}\right\}\Delta=0 \quad (V)$$

$$(1+\eta)\nabla^2\widehat{ZZ}+\frac{\partial^2\Delta}{\partial Z^2}=0 \quad (VI)$$

$$(1+\eta)\left[\left\{\nabla^2-\frac{1}{(\rho+r)^2}\right\}\widehat{rZ}-\left\{\frac{2}{(\rho+r)^2}\frac{\partial}{\partial\theta}-\frac{\rho'}{(\rho+r)^3}\right\}\widehat{\theta Z}\right]+\frac{\partial^2\Delta}{\partial r\partial Z}=0 \quad (VII)$$

$$(1+\eta)\left[\left\{\nabla^2-\frac{1}{(\rho+r)^2}\right\}\widehat{\theta Z}+\left\{\frac{2}{(\rho+r)^2}\frac{\partial}{\partial\theta}-\frac{\rho'}{(\rho+r)^3}\right\}\widehat{rZ}\right]+\frac{1}{\rho+r}\frac{\partial^2\Delta}{\partial\theta\partial Z}=0 \quad (VIII)$$

$$(1+\eta)\left[\left\{\nabla^2-\frac{4}{(\rho+r)^2}\right\}\widehat{r\theta}+\frac{2}{(\rho+r)^2}\frac{\partial}{\partial\theta}(\widehat{rr}-\widehat{\theta\theta})-\frac{\rho'}{(\rho+r)^3}(\widehat{rr}-\widehat{\theta\theta})\right]-\frac{1}{(\rho+r)^2}\frac{\partial\Delta}{\partial\theta}+\frac{1}{\rho+r}\frac{\partial^2\Delta}{\partial\theta\partial r}=0 \quad (IX)$$

where

$$\Delta=\widehat{rr}+\widehat{\theta\theta}+\widehat{ZZ},$$

$$\nabla^2=\frac{\partial^2}{\partial r^2}+\frac{1}{(\rho+r)^2}\frac{\partial^2}{\partial\theta^2}+\frac{1}{\rho+r}\frac{\partial}{\partial r}-\frac{\rho'}{(\rho+r)^3}\frac{\partial}{\partial\theta}+\frac{\partial^2}{\partial Z^2}$$

At the boundary of the cross section, the stresses must satisfy the following boundary equations:

$$\frac{dZ}{ds}(\widehat{rr})-\frac{dr}{ds}(\widehat{rZ})=0, \quad (X)$$

$$\frac{dZ}{ds}(\widehat{r\theta})-\frac{dr}{ds}(\widehat{\theta Z})=0 \quad (XI)$$

$$\frac{dZ}{ds}(\widehat{rZ})-\frac{dr}{ds}(\widehat{ZZ})=0 \quad (XII)$$

Curved Beam With Applied Torque and Bending Moment Out of Its Plane of Initial Curvature

The beam is subjected at one end ($\theta = 0$) to a torque $-T\hat{j}$ and a bending moment $-M\hat{\imath}$ out of its plane of initial center line as shown in Fig. 2. Then considering the equilibrium of AP, there is a torque $T_\theta\hat{\theta}$ and a bending moment $M_\theta\hat{r}$ at P, Fig. 3, so that we have

$$-M\hat{\imath}-T\hat{j}+M_\theta\hat{r}+T_\theta\hat{\theta}=0$$

Hence

$$-M(\hat{r}\cos\theta-\hat{\theta}\sin\theta)-T(\hat{r}\sin\theta+\hat{\theta}\cos\theta)+M_\theta\hat{r}+T_\theta\hat{\theta}=0$$

whence

$$T_\theta=T\cos\theta-M\sin\theta \quad (44)$$

$$M_\theta=T\sin\theta+M\cos\theta \quad (45)$$

and,

$$\frac{dM_\theta}{d\theta}=T_\theta, \quad \frac{dT_\theta}{d\theta}=-M_\theta$$

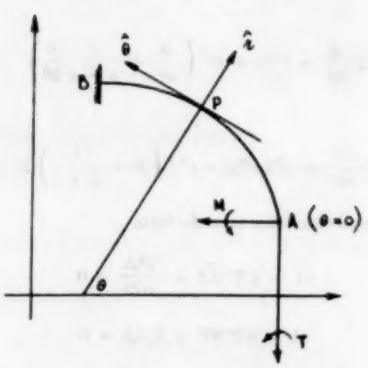

Fig. 2

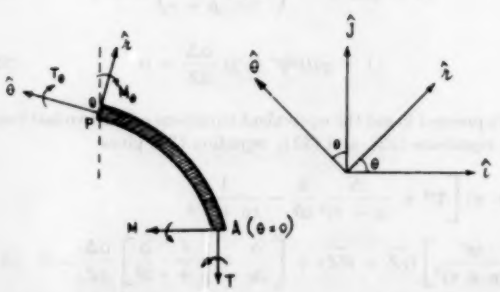

Fig. 3

We shall find the stresses by a method of successive approximations similar to that used by Göhner. When Göhner treated the case of a curved beam subjected to pure torsion, he found that two stresses only are different from zero; namely, $\widehat{r\theta}, \widehat{\theta Z}$. In the case of pure bending, four stresses are different from zero; namely, $\widehat{\theta\theta}, \widehat{rr}, \widehat{ZZ}, \widehat{rZ}$. In the foregoing case, the stresses are functions of r and Z only. In our problem, the work is more complicated since the six components of stresses are different from zero and all these stresses are functions of r, θ, and Z.

First Approximation. This approximation is indicated by suffix 0. If the beam were straight (ρ infinite), we could take the "Euler-Bernoulli" bending solution for the bending moment M_θ and the Saint-Venant torsion solution for the couple T_θ, Fig. 4.

The Euler-Bernoulli bending corresponds to $\widehat{\theta\theta}_0 = -M_\theta(Z/I)$ and all other stresses vanishing, where $I = \int Z^2 dS$ = moment of inertia of the cross section about the $\hat{r}$-axis. In the Saint-Venant torsion with the usual notation

$$T_\theta = 2\mu\tau J, \quad J = \int \chi dS$$

we have

$$\widehat{\theta Z}_0 = \frac{T_\theta}{2J}\frac{\partial\chi}{\partial r}, \quad \widehat{r\theta}_0 = -\frac{T_\theta}{2J}\frac{\partial\chi}{\partial Z}$$

We superpose these two solutions and take for our first approximation

$$\widehat{rr}_0 = \widehat{ZZ}_0 = \widehat{rZ}_0 = 0,$$

$$\widehat{\theta\theta}_0 = -M_\theta\frac{Z}{I},$$

$$\widehat{\theta Z}_0 = \frac{T_\theta}{2J}\frac{\partial\chi}{\partial r}$$

$$\widehat{r\theta}_0 = -\frac{T_\theta}{2J}\frac{\partial\chi}{\partial Z}$$

which satisfy the body-stress equations (I), (II), (III) with ρ infinite. From (XI), χ satisfies the boundary condition χ = const which can be taken zero if the cross section is simply connected as we suppose here.

Elliptic Cross Section. If the ellipse is

$$\frac{Z^2}{a^2} + \frac{r^2}{b^2} = 1,$$

we find

$$\chi = \frac{a^2b^2}{a^2+b^2}\left(1 - \frac{Z^2}{a^2} - \frac{r^2}{b^2}\right),$$

$$J = \frac{2b^2}{a^2+b^2}I$$

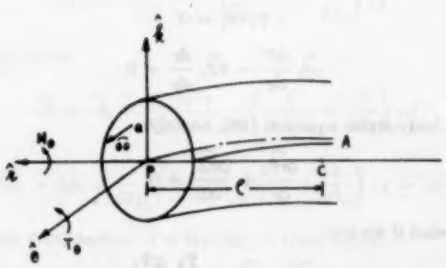

Fig. 4 Section of P looking toward A

and now,

$$\frac{\partial\chi}{\partial r} = -\frac{2a^2}{a^2+b^2}r = -\lambda r,$$

$$\frac{\partial\chi}{\partial Z} = -\frac{2b^2}{a^2+b^2}Z = -\lambda_1 Z$$

where

$$\lambda = \frac{2a^2}{a^2+b^2}, \quad \lambda_1 = \frac{2b^2}{a^2+b^2}$$

so that $J = \lambda_1 I$, and $\lambda + \lambda_1 = 2$; hence

$$\widehat{\theta Z}_0 = -\frac{T_\theta}{2I}\frac{a^2}{b^2}r,$$

$$\widehat{r\theta}_0 = \frac{T_\theta Z}{2I}$$

Circular Cross Section. If the boundary is $r^2 + Z^2 = a^2$, we find

$$\chi = {}^1/_2(a^2 - r^2 - Z^2), \quad \frac{\partial\chi}{\partial r} = -r, \quad \frac{\partial\chi}{\partial Z} = -Z$$

so that $\lambda = \lambda_1 = 1$ and therefore $J = I$; hence

$$\widehat{\theta Z}_0 = -\frac{T_\theta}{2I}r, \quad \widehat{r\theta}_0 = \frac{T_\theta}{2I}Z$$

In both elliptic and circular cross sections we have

$$\frac{\partial^2\chi}{\partial r\,\partial Z} = 0, \quad \nabla_0^2\chi = -2$$

Second Approximation. If r and Z are both small compared with ρ, then r^2/ρ^2, rZ/ρ^2, Z^2/ρ^2, and higher powers will be neglected in the body-stress equations.

In the compatibility equations, r/ρ, Z/ρ and higher powers are neglected. Denoting by suffix 1 this second approximation, the body-stress equation (I) becomes

$$\frac{\partial\widehat{rr}_1}{\partial r} + \frac{\partial\widehat{rZ}_1}{\partial Z} - \frac{\widehat{\theta\theta}_0}{\rho} - \frac{1}{\rho}\frac{\partial\widehat{r\theta}_0}{\partial\theta} = -\frac{M_\theta Z}{I\rho} - \frac{M_\theta}{2J\rho}\frac{\partial\chi}{\partial Z} \tag{46}$$

for elliptic and circular cross sections we have

$$Z = -\frac{I}{J}\frac{\partial\chi}{\partial Z},$$

so that equation (46) becomes

$$\frac{\partial\widehat{rr}_1}{\partial r} + \frac{\partial\widehat{rZ}_1}{\partial Z} = \frac{M_\theta}{2J\rho}\frac{\partial\chi}{\partial Z} \tag{47}$$

The body-stress equation (II) becomes

$$\frac{\partial\widehat{r\theta}_1}{\partial r} + \frac{\partial\widehat{\theta Z}_1}{\partial Z} = -\frac{1}{\rho}\frac{\partial\widehat{\theta\theta}_0}{\partial\theta} - \frac{2}{\rho}\widehat{r\theta}_0 = \frac{T_\theta Z}{I\rho} + \frac{T_\theta}{J\rho}\frac{\partial\chi}{\partial Z}$$

$$= \frac{T_\theta}{\rho}\left(\frac{Z}{I} + \frac{1}{J}\frac{\partial\chi}{\partial Z}\right) = 0$$

so that we have

$$\frac{\partial\widehat{r\theta}_1}{\partial r} + \frac{\partial\widehat{\theta Z}_1}{\partial Z} = 0 \tag{48}$$

Finally, the body-stress equation (III) reduces to

$$\frac{\partial r\widehat{Z}_1}{\partial r} + \frac{\partial \widehat{ZZ}_1}{\partial Z} = -\frac{1}{\rho}\widehat{rZ}_0 - \frac{1}{\rho}\frac{\partial \widehat{\theta Z}_0}{\partial \theta}$$

or

$$\frac{\partial r\widehat{Z}_1}{\partial r} + \frac{\partial \widehat{ZZ}_1}{\partial Z} = \frac{M_\theta}{2J\rho}\frac{\partial \chi}{\partial r} \tag{49}$$

The compatibility equations (IV) to (IX) become

$$(1+\eta)\nabla_0^2\widehat{rr}_1 + \frac{\partial^2\Delta_1}{\partial r^2} = 0 \tag{50}$$

$$\nabla_0^2\widehat{\theta\theta}_1 = 0 \tag{51}$$

$$(1+\eta)\nabla_0^2\widehat{ZZ}_1 + \frac{\partial^2\Delta_1}{\partial Z^2} = 0 \tag{52}$$

$$(1+\eta)\nabla_0^2 r\widehat{Z}_1 + \frac{\partial^2\Delta_1}{\partial r\partial Z} = 0 \tag{53}$$

$$(1+\eta)\left[\nabla_0^2\widehat{\theta Z}_1 + \frac{1}{\rho}\frac{\partial \widehat{\theta Z}_0}{\partial r}\right] + \frac{1}{\rho}\frac{\partial^2\widehat{\theta\theta}_0}{\partial\theta\partial Z} = 0$$

or

$$(1+\eta)\left[\nabla_0^2\widehat{\theta Z}_1 + \frac{T_\theta}{2J\rho}\frac{\partial^2\chi}{\partial r^2}\right] - \frac{T_\theta}{I\rho} = 0 \tag{54}$$

$$(1+\eta)\left[\nabla_0^2 r\widehat{\theta}_1 + \frac{1}{\rho}\frac{\partial r\widehat{\theta}_0}{\partial r}\right] + \frac{1}{\rho}\frac{\partial^2\widehat{\theta\theta}_0}{\partial\theta\partial r} = 0$$

since

$$\frac{\partial^2\widehat{\theta\theta}_0}{\partial\theta\partial r} = 0$$

we have

$$\nabla_0^2 r\widehat{\theta}_1 - \frac{T_\theta}{2J\rho}\frac{\partial^2\chi}{\partial r\partial Z} = 0$$

as already mentioned $\partial^2\chi/\partial r\partial Z = 0$ for circular and elliptic cross sections, so that we have

$$\nabla_0^2 r\widehat{\theta}_1 = 0 \tag{55}$$

From equations (47) and (49) we have

$$\frac{\partial^2\widehat{rr}_1}{\partial r^2} = \frac{\partial^2\widehat{ZZ}_1}{\partial Z^2}$$

This is satisfied if we put

$$\widehat{rr}_1 = \frac{\partial^2\Phi_1}{\partial Z^2}, \quad \widehat{ZZ}_1 = \frac{\partial^2\Phi_1}{\partial r^2}$$

Equations (47) and (49) become

$$\frac{\partial r\widehat{Z}_1}{\partial Z} = -\frac{\partial^2\Phi_1}{\partial r\partial Z^2} + \frac{M_\theta}{2J\rho}\frac{\partial\chi}{\partial Z},$$

$$\frac{\partial r\widehat{Z}_1}{\partial r} = -\frac{\partial^2\Phi_1}{\partial r^2\partial Z} + \frac{M_\theta}{2J\rho}\frac{\partial\chi}{\partial r}$$

whence

$$r\widehat{Z}_1 = -\frac{\partial^2\Phi_1}{\partial r\partial Z} + \frac{M_\theta}{2J\rho}\chi$$

Substituting the foregoing values of $\widehat{rr}_1$, $\widehat{ZZ}_1$, and $r\widehat{Z}_1$ in the boundary conditions (X) and (XII) we get

$$\frac{\partial^3\Phi_1}{dZ^2}\frac{dZ}{ds} + \frac{\partial^3\Phi_1}{\partial r\partial Z}\frac{dr}{ds} - \frac{M_\theta}{2J\rho}\chi\frac{dr}{ds} = 0,$$

$$-\left(\frac{\partial^3\Phi_1}{\partial r\partial z}\frac{dZ}{ds} + \frac{\partial^3\Phi_1}{\partial r^2}\frac{dr}{ds}\right) + \frac{M_\theta}{2J\rho}\chi\frac{dZ}{ds} = 0$$

At the boundary $\chi = 0$ and we have

$$\frac{d}{ds}\left(\frac{\partial\Phi_1}{\partial Z}\right) = 0, \quad \frac{d}{ds}\left(\frac{\partial\Phi_1}{\partial r}\right) = 0$$

Therefore $\partial\Phi_1/\partial Z$, $\partial\Phi_1/\partial r$ are constants along the boundary.

From equations (50), (52) using equation (51), we get

$$\nabla_0^2(\widehat{rr}_1 + \widehat{ZZ}_1) = 0$$

or

$$\nabla_0^4(\Phi_1) = 0$$

The unique solution for Φ_1 satisfying $\nabla_0^4(\Phi_1) = 0$ and the boundary conditions $\partial\Phi_1/\partial Z$, $\partial\Phi_1/\partial r$ are both constants along the boundary is given by

$$\Phi_1 = AZ + Br + C;$$

hence

$$\widehat{rr}_1 = 0, \quad \widehat{ZZ}_1 = 0,$$

$$r\widehat{Z}_1 = \frac{M_\theta}{2J\rho}\chi$$

so that $\Delta_1 = \widehat{\theta\theta}_1$ only.

Equations (50), (52), and (53) then reduce to

$$\frac{\partial^2\widehat{\theta\theta}_1}{\partial r^2} = 0, \quad \frac{\partial^2\widehat{\theta\theta}_1}{\partial Z^2} = 0,$$

$$\frac{\partial^2\widehat{\theta\theta}_1}{\partial r\partial Z} = -(1+\eta)\frac{M_\theta}{2J\rho}\nabla_0^2\chi$$

Since $\nabla_0^2(\chi) = -2$, wet get

$$\frac{\partial^2\widehat{\theta\theta}_1}{\partial r\partial Z} = (1+\eta)\frac{M_\theta}{J\rho}$$

so that we obtain

$$\widehat{\theta\theta}_1 = \widehat{\theta\theta}_0 + (1+\eta)\frac{M_\theta}{J\rho}rZ$$

Equations (54), (55), and the boundary condition (XI) give

$$\nabla_0^2\widehat{\theta Z}_1 = \frac{T_\theta}{I\rho(1+\eta)} - \frac{T_\theta}{2J\rho}\frac{\partial^2\chi}{\partial r^2} \tag{56}$$

$$\nabla_0^2 r\widehat{\theta}_1 = 0 \tag{57}$$

$$r\widehat{\theta}_1\frac{dZ}{ds} - \widehat{\theta Z}_1\frac{dr}{ds} = 0 \tag{58}$$

The body-stress equation (48), namely,

$$\frac{\partial r\widehat{\theta}_1}{\partial r} + \frac{\partial\widehat{\theta Z}_1}{\partial Z} = 0$$

is satisfied if we put

$$r\widehat{\theta}_1 = r\widehat{\theta}_0 - \frac{T_\theta}{2\rho}\frac{\partial\Psi_1}{\partial Z},$$

$$\widehat{\theta Z}_1 = \widehat{\theta Z}_0 + \frac{T_\theta}{2\rho}\frac{\partial \Psi_1}{\partial r}$$

Equations (56) and (57) reduce to

$$\frac{\partial}{\partial r}(\nabla_0^2 \Psi_1) = \frac{2}{I(1+\eta)} - \frac{1}{J}\frac{\partial^2 \chi}{\partial r^2}, \tag{59}$$

$$\frac{\partial}{\partial Z}(\nabla_0^2 \Psi_1) = 0 \tag{60}$$

The boundary condition (58) becomes

$$\frac{\partial \Psi_1}{\partial r}dr + \frac{\partial \Psi_1}{\partial Z}dZ = 0$$

or Ψ_1 is constant (or zero) along the boundary.

Equations (59) and (60) give

$$\nabla_0^2 \Psi_1 = \left(\frac{2}{I(1+\eta)} - \frac{1}{J}\frac{\partial^2 \chi}{\partial r^2}\right) r + C \tag{61}$$

where C is a constant.

Take $\Psi_1 = Ar\chi$, so that Ψ_1 vanishes along the boundary, we get

$$\frac{\partial^2 \Psi_1}{\partial r^2} = Ar\frac{\partial^2 \chi}{\partial r^2} + 2A\frac{\partial \chi}{\partial r},$$

$$\frac{\partial^2 \Psi_1}{\partial Z^2} = Ar\frac{\partial^2 \chi}{\partial Z^2}$$

Hence

$$\nabla_0^2 \Psi_1 = 2A\left(\frac{\partial \chi}{\partial r} - r\right)$$

For elliptic and circular cross sections

$$\frac{\partial \chi}{\partial r} = -\lambda r, \quad \frac{\partial^2 \chi}{\partial r^2} = -\lambda,$$

so that we have

$$\nabla_0^2 \Psi_1 = -2A(1+\lambda)r$$

Hence $C = 0$,

$$A = -\frac{1}{I(1+\lambda)}\left(\frac{1}{1+\eta} + \frac{\lambda}{2\lambda_1}\right)$$

whence

$$\Psi_1 = -\frac{1}{I(1+\lambda)}\left(\frac{1}{1+\eta} + \frac{\lambda}{2\lambda_1}\right) r\chi$$

and we obtain

$$\widehat{r\theta}_1 = \widehat{r\theta}_0 - \frac{\lambda_1 T_\theta}{2I\rho(1+\lambda)}\left(\frac{1}{1+\eta} + \frac{\lambda}{2\lambda_1}\right) rZ$$

$$\widehat{\theta Z}_1 = \widehat{\theta Z}_0 - \frac{T_\theta}{2I\rho(1+\lambda)}\left(\frac{1}{1+\eta} + \frac{\lambda}{2\lambda_1}\right)(\chi - \tfrac{1}{2}\lambda r^2)$$

Elliptic Cross Section. For the elliptic cross section

$$\chi = \frac{a^2 b^2}{a^2+b^2}\left(1 - \frac{Z^2}{a^2} - \frac{r^2}{b^2}\right), \quad J = \frac{2b^2}{a^2+b^2} I,$$

$$\lambda = \frac{2a^2}{a^2+b^2}, \quad \lambda_1 = \frac{2b^2}{a^2+b^2}$$

The second approximation gives the following stresses:

$$\widehat{rr}_1 = 0$$

$$\widehat{ZZ}_1 = 0$$

$$\widehat{rZ}_1 = \frac{M_\theta a^2}{4I\rho}\left(1 - \frac{Z^2}{a^2} - \frac{r^2}{b^2}\right)$$

$$\widehat{\theta\theta}_1 = -\frac{M_\theta Z}{I} + \frac{M_\theta}{2I\rho}(1+\eta)\left(1 + \frac{a^2}{b^2}\right) rZ$$

$$\widehat{r\theta}_1 = \frac{T_\theta Z}{2I} - \frac{T_\theta}{2I\rho}\frac{2b^2 + a^2(1+\eta)}{(3a^2+b^2)(1+\eta)} rZ$$

$$\widehat{\theta Z}_1 = -\frac{T_\theta}{2I}\frac{a^2}{b^2} r + \frac{T_\theta a^2}{4I\rho}\frac{2b^2 + a^2(1+\eta)}{(3a^2+b^2)(1+\eta)}\left(\frac{3r^2}{b^2} + \frac{Z^2}{a^2} - 1\right)$$

Circular Cross Section.

$$b = a, \quad \chi = \tfrac{1}{2}(a^2 - r^2 - Z^2), \quad J = I, \quad \lambda = \lambda_1 = 1$$

The second approximation gives the following stresses:

$$\widehat{rr}_1 = 0$$

$$\widehat{ZZ}_1 = 0$$

$$\widehat{rZ}_1 = \frac{M_\theta}{4I\rho}(a^2 - r^2 - Z^2)$$

$$\widehat{\theta\theta}_1 = -\frac{M_\theta Z}{I} + (1+\eta)\frac{M_\theta}{I\rho} rZ$$

$$\widehat{r\theta}_1 = \frac{T_\theta Z}{2I} - \frac{T_\theta}{8I\rho}\frac{3+\eta}{1+\eta} rZ$$

$$\widehat{\theta Z}_1 = -\frac{T_\theta r}{2I} + \frac{T_\theta}{16I\rho}\frac{3+\eta}{1+\eta}(3r^2 + Z^2 - a^2)$$

Curved Beam Subjected at One End to a Concentrated Load Perpendicular to Its Plane of Initial Curvature

Let an upward concentrated load W be applied at one end A of a curved beam perpendicular to its plane of initial curvature. Referring to Fig. 5 the bending moment M_θ and the torque T_θ at any cross section, defined by the angle θ which the normal to the center line makes with the x-axis, are given by

$$M_\theta = W \cdot AQ$$

$$T_\theta = -W \cdot QP$$

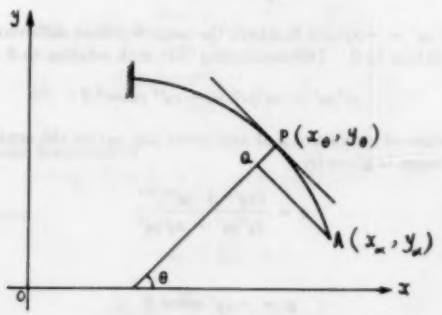

Fig. 5

The lengths AQ and PQ can be found by using elementary analytical geometry. Equation of the normal at P is

$$(y_\theta - y)\cos\theta - (x_\theta - x)\sin\theta = 0$$

Equation of tangent at P is

$$(y_\theta - y)\sin\theta + (x_\theta - x)\cos\theta = 0$$

AQ is the length of the perpendicular from A to the normal at P. If $A \equiv (x_a, y_a)$, where α is the slope of the normal at A we have

$$AQ = (y_\theta - y_a)\cos\theta - (x_\theta - x_a)\sin\theta$$

QP is the length of the perpendicular from A to the tangent at P, so that we have

$$QP = (y_\theta - y_a)\sin\theta + (x_\theta - x_a)\cos\theta$$

In Fig. 5, $x_a > x_\theta$, $y_\theta > y_a$ so that if $\theta \leq 90$ deg, AQ will be numerically positive. The origin O and the point (x_a, y_a) are in the same side with relation to the tangent at P, and O gives positive value for $(y_\theta - y)\sin\theta + (x_\theta - x)\cos\theta$; hence the expression $(y_\theta - y_a)\sin\theta + (x_\theta - x_a)\cos\theta$ is also positive, so that QP will be numerically positive and we get

$$M_\theta = W[(y_\theta - y_a)\cos\theta - (x_\theta - x_a)\sin\theta] \tag{62}$$

$$T_\theta = -W[(y_\theta - y_a)\sin\theta + (x_\theta - x_a)\cos\theta] \tag{63}$$

It is noted that

$$\frac{dT_\theta}{d\theta} = -W[(y_\theta - y_a)\cos\theta + y_\theta'\sin\theta - (x_\theta - x_a)\sin\theta + x_\theta'\cos\theta]$$

$$= -W[(y_\theta - y_a)\cos\theta - (x_\theta - x_a)\sin\theta)]$$

$$= -M_\theta$$

(since $\tan\theta = -x_\theta'/y_\theta'$)

Also

$$\frac{dM_\theta}{d\theta} = -W[(y_\theta - y_a)\sin\theta + (x_\theta - x_a)\cos\theta] + W(y_\theta'\cos\theta - x_\theta'\sin\theta)$$

$$= T_\theta + W\left(-x_\theta'\frac{\cos^2\theta}{\sin\theta} - x_\theta'\sin\theta\right)$$

$$= T_\theta - Wx_\theta'\operatorname{cosec}\theta$$

Now

$$\frac{y_\theta'}{x_\theta'} = -\cot\theta \tag{64}$$

so that $y_\theta' = -x_\theta'\cot\theta$, where the primes denote differentiation with relation to θ. Differentiating (64) with relation to θ we get

$$x_\theta''y_\theta' - x_\theta'y_\theta'' = -x_\theta'^2\operatorname{cosec}^2\theta$$

The radius of curvature ρ at any point (x_θ, y_θ) on the center line of the beam is given by

$$\rho = \frac{(x_\theta'^2 + y_\theta'^2)^{3/2}}{x_\theta''y_\theta' - x_\theta'y_\theta''}$$

hence

$$\rho = -x_\theta'\operatorname{cosec}\theta$$

so that we have

$$\frac{dM_\theta}{d\theta} = T_\theta + W\rho$$

Let

$$T_\theta^* = T_\theta + W\rho \tag{65}$$

so that

$$\frac{dT_\theta}{d\theta} = -M_\theta, \tag{66}$$

$$\frac{dM_\theta}{d\theta} = T_\theta^* = T_\theta + W\rho \tag{67}$$

T_θ can be written as

$$T_\theta = -W[(y_\theta - y_a)\sin\theta + (x_\theta - x_a)\cos\theta - \rho] - W\rho$$

hence

$$T_\theta^* = -W[(y_\theta - y_a)\sin\theta + (x_\theta - x_a)\cos\theta - \rho], \tag{68}$$

$$\frac{dT_\theta^*}{d\theta} = -M_\theta + W\rho' \tag{69}$$

We introduced the term T_θ^* so that we can use the results obtained in the previous case when the beam is subjected at one end to a torque and a bending moment out of its plane of initial curvature without unnecessary calculations.

First Approximation. Assume in the first approximation that

$$\widehat{\theta\theta}_0 = -\frac{M_\theta Z}{I}, \quad \widehat{rr}_0 = \widehat{rZ}_0 = \widehat{ZZ}_0 = 0,$$

$$\widehat{r\theta}_0 = -\frac{T_\theta}{2J}\frac{\partial\chi}{\partial Z} = -\frac{T_\theta^* - W\rho}{2J}\frac{\partial\chi}{\partial Z}$$

$$= -\frac{T_\theta^*}{2J}\frac{\partial\chi}{\partial Z} + \frac{W\rho}{2J}\frac{\partial\chi}{\partial Z}$$

$$\widehat{\theta Z}_0 = \frac{T_\theta}{2J}\frac{\partial\chi}{\partial r} = \frac{T_\theta^* - W\rho}{2J}\frac{\partial\chi}{\partial r}$$

$$= \frac{T_\theta^*}{2J}\frac{\partial\chi}{\partial r} - \frac{W\rho}{2J}\frac{\partial\chi}{\partial r}$$

where M_θ, T_θ, T_θ^* are defined by equations (62), (63), and (68).

Second Approximation. Following the same line of treatment as in the last case, it can be deduced at once that the body-stress equations (47) and (49) and the compatibility equations (50), (51), (52), and (53) remain the same but with different meaning for M_θ which is given by equation (62) so that we obtain

$$\widehat{rr}_1 = \widehat{ZZ}_1 = 0$$

$$\widehat{rZ}_1 = \frac{M_\theta}{2J\rho}\chi$$

$$\widehat{\theta\theta}_1 = -\frac{M_\theta Z}{I} + \frac{M_\theta rZ}{J\rho}(1 + \eta)$$

The body-stress equation (II) reduces to

$$\frac{\partial\widehat{r\theta}_1}{\partial r} + \frac{\partial\widehat{\theta Z}_1}{\partial Z} = -\frac{W}{J}\frac{\partial\chi}{\partial Z} \tag{70}$$

which differs from the body-stress equation (48) in the presence of the term

$$-\frac{W}{J}\frac{\partial\chi}{\partial Z}$$

The compatibility equation (VIII) reduces to

$$\nabla_0^2\widehat{\theta Z}_1 = \frac{T_\theta^*}{I\rho(1+\eta)} - \frac{T_\theta^*}{2J\rho}\frac{\partial^2\chi}{\partial r^2} + \frac{W}{2J}\frac{\partial^2\chi}{\partial r^2} \tag{71}$$

which is the same as equation (56) with the additional term

$$\frac{W}{2J}\frac{\partial^2\chi}{\partial r^2}$$

and T_θ^* as defined by (68) is written instead of T_θ in the previous case.

The compatibility equation (IX) becomes

$$\nabla_0^2(\widehat{r\theta}_1) = 0 \tag{72}$$

which is the same as equation (55).

It follows that in the case of a concentrated load W acting perpendicular to the plane of initial curvature of the beam, there will be additional shear stresses $(\widehat{r\theta})_{s1}$ and $(\widehat{\theta Z})_{s1}$ to those of the last case with T_θ^* written for T_θ, so that we have

$$\frac{\partial(\widehat{r\theta})_{s1}}{\partial r} + \frac{\partial(\widehat{\theta Z})_{s1}}{\partial Z} = -\frac{W}{J}\frac{\partial\chi}{\partial Z} \tag{73}$$

$$\nabla_0^2(\widehat{\theta Z})_{s1} = \frac{W}{2J}\frac{\partial^2\chi}{\partial r^2} \tag{74}$$

$$\nabla_0^2(\widehat{r\theta})_{s1} = 0 \tag{75}$$

together with the boundary condition

$$(\widehat{r\theta})_{s1}\frac{dZ}{ds} - (\widehat{\theta Z})_{s1}\frac{dr}{ds} = 0 \tag{76}$$

The body-stress equation (73) is satisfied if we put

$$(\widehat{r\theta})_{s1} = \frac{W\rho}{2J}\frac{\partial\chi}{\partial Z} - \frac{\partial\Psi_1}{\partial Z}$$

$$(\widehat{\theta Z})_{s1} = -\frac{W\rho}{2J}\frac{\partial\chi}{\partial r} - \frac{W}{J}\chi + \frac{\partial\Psi_1}{\partial r}$$

Equation (74) then reduces to

$$\frac{\partial}{\partial r}(\nabla_0^2\Psi_1) - \frac{W}{J}\nabla_0^2\chi = \frac{W}{2J}\frac{\partial^2\chi}{\partial r^2}$$

Since $\nabla_0^2\chi = -2$, we get

$$\frac{\partial}{\partial r}(\nabla_0^2\Psi_1) = -\frac{2W}{J} + \frac{W}{2J}\frac{\partial^2\chi}{\partial r^2}$$

Equation (75) reduces to

$$\frac{\partial}{\partial Z}(\nabla_0^2\Psi_1) = 0$$

We get

$$\nabla_0^2\Psi_1 = \left(\frac{W}{2J}\frac{\partial^2\chi}{\partial r^2} - \frac{2W}{J}\right)r$$

The boundary condition (76) gives $\Psi_1 =$ const or zero along the boundary. For elliptic or circular cross section

$$\frac{\partial\chi}{\partial r} = -\lambda r, \quad \frac{\partial^2\chi}{\partial r^2} = -\lambda, \quad J = \lambda_1 I$$

so that we have

$$\nabla_0^2\Psi_1 = -\frac{W}{2I\lambda_1}(\lambda+4)r$$

Taking $\Psi_1 = Ar\chi$, we get

$$A = \frac{W}{4I\lambda_1}\frac{\lambda+4}{\lambda+1}$$

hence

$$\Psi_1 = \frac{W}{4I\lambda_1}\frac{\lambda+4}{\lambda+1}r\chi$$

and we obtain the following stresses:

$$(\widehat{r\theta})_{s1} = -\frac{W\rho}{2I}Z + \frac{W}{4I}\frac{\lambda+4}{\lambda+1}rZ$$

$$(\widehat{\theta Z})_{s1} = \frac{W\rho}{2I}\frac{\lambda}{\lambda_1}r - \frac{W}{\lambda_1 I}\chi + \frac{W}{4\lambda_1 I}\frac{\lambda+4}{\lambda+1}(\chi - \lambda r^2)$$

Elliptic Cross Section:

$$\lambda = \frac{2a^2}{a^2+b^2}, \quad \lambda_1 = \frac{2b^2}{a^2+b^2}, \quad \chi = \frac{a^2b^2}{a^2+b^2}\left(1 - \frac{Z^2}{a^2} - \frac{r^2}{b^2}\right),$$

so that we obtain

$$(\widehat{r\theta})_{s1} = -\frac{W\rho Z}{2I} + \frac{W}{2I}\frac{3a^2+2b^2}{3a^2+b^2}rZ$$

$$(\widehat{\theta Z})_{s1} = \frac{W\rho r}{2I}\frac{a^2}{b^2} - \frac{3Wa^4}{4I}\frac{1}{3a^2+b^2}\left[1 - \frac{Z^2}{a^2} + \frac{3a^2+4b^2}{3a^2b^2}r^2\right]$$

Hence we get

$$\widehat{r\theta}_1 = \frac{T_\theta^* Z}{2I} - \frac{T_\theta^*}{2I\rho}\frac{2b^2+a^2(1+\eta)}{(1+\eta)(3a^2+b^2)}rZ - \frac{W\rho Z}{2I} + \frac{W}{2I}\frac{3a^2+2b^2}{3a^2+b^2}rZ$$

$$\widehat{\theta Z}_1 = -\frac{T_\theta^*}{2I}\frac{a^2}{b^2}r + \frac{T_\theta^* a^2}{4I\rho(3a^2+b^2)}\frac{2b^2+a^2(1+\eta)}{1+\eta}\left(\frac{3r^2}{b^2} + \frac{Z^2}{a^2} - 1\right) + \frac{W\rho r}{2I}\frac{a^2}{b^2} - \frac{3Wa^4}{4I(3a^2+b^2)}\left(1 - \frac{Z^2}{a^2} + \frac{3a^2+4b^2}{3a^2b^2}r^2\right)$$

$$\widehat{rr}_1 = \widehat{ZZ}_1 = 0$$

$$\widehat{rZ}_1 = \frac{M_\theta a^2}{4I\rho}\left(1 - \frac{r^2}{b^2} - \frac{Z^2}{a^2}\right)$$

$$\widehat{\theta\theta}_1 = -\frac{M_\theta Z}{I} + \frac{M_\theta}{2I\rho}(1+\eta)\left(1 + \frac{a^2}{b^2}\right)rZ$$

Circular Cross Section:

$$b = a, \quad \lambda = \lambda_1 = 1, \quad \chi = 1/2(a^2 - r^2 - Z^2)$$

We have

$$\widehat{rr}_1 = \widehat{ZZ}_1 = 0$$

$$\widehat{rZ}_1 = \frac{M_\theta}{4I\rho}(a^2 - r^2 - Z^2)$$

$$\widehat{\theta\theta}_1 = -\frac{M_\theta Z}{I} + \frac{M_\theta}{I\rho}(1+\eta)rZ$$

$$(\widehat{r\theta})_{01} = -\frac{W\rho}{2I}Z + {}^5/_8\frac{W}{I}rZ$$

$$(\widehat{\theta Z})_{01} = \frac{W\rho}{2I}r - {}^5/_{16}\frac{W}{I}(a^2 - Z^2 + {}^7/_5r^2)$$

$$\widehat{r\theta}_1 = \frac{T_\theta^* Z}{2I} - \frac{T_\theta^* rZ}{8I\rho}\frac{3+\eta}{1+\eta} - \frac{W\rho}{2I}Z + {}^5/_8\frac{W}{I}rZ$$

$$\widehat{\theta Z}_1 = -\frac{T_\theta^* r}{2I} - \frac{T_\theta^*}{16I\rho}\frac{3+\eta}{1+\eta}(a^2 - Z^2 - 3r^2) + \frac{W\rho}{2I}r$$

$$-\frac{3W}{16I}(a^2 - Z^2 + {}^7/_5r^2)$$

Acknowledgment

The author owes a debt of gratitude to Prof. A. C. Stevenson, University College, London, for his continuous help, suggestions, and aid in the solution of most of the problems considered here.

References

1 O. Göhner, "Schubspannungsverteilung im Querschnitt einer Schraubenfeder," *Ingenieur Archiv*, vol. 1, 1930, pp. 619–644; "Schubspannungsverteilung im Querschnitt eines gedrillten Ringstabs mit Anwendung auf Schraubenfedern," vol. 2, 1931, pp. 1–19; "Sannungsverteilung in einem an den Endquerschnitten belasteten Ringstabsektor," vol. 2, 1931, pp. 381–414; "Zur Berechnung des gebogenen oder gedrillten Ringstabs mit Kreisquerschitt und der zylindrischen Schraubenfeder," vol. 9, 1938, pp. 355–731.

2 R. Grammel, "Die Knickung von Schraubenfedern," First National Congress of Applied Mechanics, 1924, pp. 276–278; also in *Zeitschrift für argenwandte Mathematik und Mechanik*, vol. 4, 1924, pp. 384–389.

3 C. B. Biezeno and J. J. Koch, "Zeitschrift an den Herausgeber," *Zeitschrift für angewandte Mathematik und Mechanik*, vol. 5, 1925, pp. 274–280.

4 Michell, Proceedings of the London Mathematical Society, vol. 31, 1900, p. 130.

5 A. Rover, "Beanspruchung zylindrischer Schraubenfedern mit Kreisquerschnitt," *Zeitschrift des Vereines Deutscher Ingenieur*, vol. 57, 1913, pp. 1906–1911.

6 Gross and Lehr, ZVDI, 1938, p. 94.

7 Karl de Gruben, "Knicksicherheit und Tuerfederung von Druckfedern," *Zeitschrift für Vereines Deutscher Ingenieur*, vol. 86, 1942, pp. 316–317.

8 W. M. Shepherd, "On the Stresses in Close-Coiled Helical Springs," *Quarterly Journal of Mechanics and Applied Mathematics*, vol. 3, 1950, pp. 459–468.

G. HERRMANN
Associate Professor of Civil Engineering, Institute of Flight Structures, Columbia University, New York, N. Y. Mem. ASME

A. E. ARMENÀKAS
Associate Professor of Civil Engineering, Cooper Union for the Advancement of Science and Art, New York, N. Y.

Shear Buckling of Bars[1]

It is shown that a perfectly straight bar, subjected to a state of uniform shear stress, will buckle, in a manner similar to a column under compression, if the shear stress exceeds a certain critical value. The buckling equations are obtained by the Newtonian approach and also by the application of the principle of minimum potential energy. In order to provide additional insight into this buckling mechanism, a simple model is introduced and analyzed.

It is established by this investigation that a bar in a state of uniform shear stress becomes unstable for values of this stress which exceed a certain critical magnitude, and will buckle in the plane of loading in a manner analogous to a bar under compression.

The possibility of buckling as a result of uniform shear stress was recognized by the authors in an earlier investigation,[2] dealing with the influence of a general state of initial stress on the dynamic response of elastic plates. In that reference[2] the basic plate equations were derived from the general nonlinear theory of elasticity. In the present study, the buckling equations are obtained by the Newtonian approach as well as by the application of the principle of minimum potential energy. Moreover, a simple model is presented and analyzed for the purpose of providing additional insight into the buckling mechanism involved.

This case of buckling of a bar under uniform shear has little practical significance, for, in order that buckling occur in the elastic range, the bar must be extremely slender. Moreover, it is rather difficult to induce a state of uniform shear stress without impeding transverse displacements. It is therefore the mere existence of this buckling phenomenon, rather than its application, which is worthy of interest.

Formulation of Problem

A bar of constant rectangular cross section, supported by fixed hinges at its two ends, is referred to an $x - z$ Cartesian system of co-ordinates, x being the direction along the length of the bar. In order to produce a state of uniform shear stress in the bar, uniform surface shear tractions are applied along two parallel faces, Fig. 1. The assumption is made that the shear tractions are applied in such a manner so as not to impede any possible transverse displacement of the bar.

The moment condition of equilibrium requires the existence of a hinge reaction R, of magnitude

$$R = \tau ab \tag{1}$$

where a and b are the dimensions of the cross section of the bar, and τ is the magnitude of the surface traction.

It is noted that the only stress resultant acting on any cross section of the bar is a transverse shear force of magnitude R.

The problem consists of the determination of the critical value of the shear traction τ, for which it is possible to obtain an equilibrium configuration other than the straight one, shown in Fig. 1.

Equilibrium Equations

The equations of equilibrium of the buckled configuration will be obtained referring to the free-body diagram of a deformed element of original length dx, shown in Fig. 2.

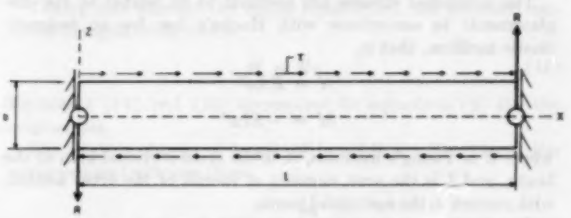

Fig. 1 Bar in a state of uniform shear

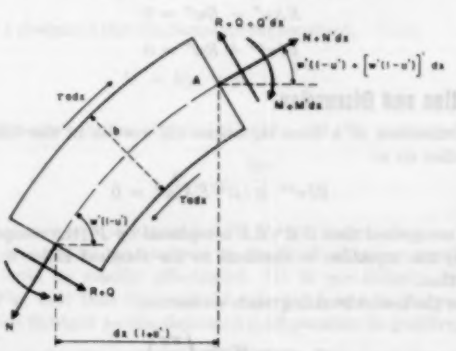

Fig. 2 Deformed bar element

[1] This investigation was supported by the United States Air Force, through the Office of Scientific Research of the Air Research and Development Command, under Contract AF 49(638)-430 with Columbia University.

[2] G. Herrmann and A. E. Armenàkas, "Vibrations and Stability of Plates Under Initial Stress," Air Force Office of Scientific Research, Technical Note 59-189, ASTIA Document 211 220, February, 1959; to be published in the Proceedings of the American Society of Civil Engineers, *Journal of the Engineering Mechanics Division*.

Contributed by the Applied Mechanics Division and presented at the Annual Meeting, Atlantic City, N. J., November 29–December 4, 1959, of The American Society of Mechanical Engineers.

Discussion of this paper should be addressed to the Secretary, ASME, 29 West 39th Street, New York, N. Y., and will be accepted until October 10, 1960, for publication at a later date. Discussion received after the closing date will be returned.

Note: Statements and opinions advanced in papers are to be understood as individual expressions of their authors and not those of the Society. Manuscript received by ASME Applied Mechanics Division, June 3, 1959. Paper No. 59—A-91.

It is assumed that the shear traction τ is applied in such a manner that the magnitude of the resultant force, acting on a given surface element, does not change after deformation. For this reason the applied shear force acting on the element is $\tau a dx$, even though this force is distributed over the area $a(1 + u')dx$ of the deformed element. Primes designate differentiation with respect to x.

The direction of the applied shear traction in the deformed position could be assumed either parallel to the undeformed axis or tangent to the elastic curve. It can be shown that, within the accuracy of the present theory, these two alternatives lead to identical results.

In addition to the stress resultants $\tau a dx$ and R, which are acting on the element before deformation, additional stress resultants N, Q, and M, Fig. 2, may be induced as a result of the deformation.

Let $u(x)$ and $w(x)$ be the components of displacement in the axial and transverse direction, respectively, of any point located on the centroidal axis of the bar. Referring to Fig. 3, an element of length dx before deformation becomes $(1 + u')\,dx$ subsequent to deformation; moreover, the angle of rotation at any point on the elastic curve is approximated by $(1 - u')w'$.

If the sum of the forces and the sum of the moments with respect to point A are set equal to zero, and if all higher-order terms involving the additional stress resultants N, Q, and M are disregarded, the following stress equations of equilibrium are obtained.

$$N' - Rw'' = 0$$
$$Q' = 0 \tag{2}$$
$$M' - Q - R(1 + u') - \tau ab = 0$$

Taking into account the initial equilibrium of the bar, as expressed by equation (1), differentiating the last of equations (2), and eliminating Q from the foregoing equations, we obtain

$$-Rw'' + N' = 0$$
$$-M'' + Ru'' = 0 \tag{3}$$

The additional stresses are assumed to be related to the displacements in accordance with Hooke's law for an isotropic elastic medium, that is,

$$N = EAu'$$
$$M = -EIw'' \tag{4}$$

where E is Young's modulus, A is the cross-sectional area of the beam, and I is the area moment of inertia of the cross section, with respect to the centroidal y-axis.

The displacement equations of equilibrium are

$$EAu'' - Rw'' = 0$$
$$EIw^{IV} + Ru'' = 0 \tag{5}$$

Solution and Discussion

Elimination of u from equations (5) results in the following equation on w:

$$EIw^{IV} + (R^2/EA)w'' = 0 \tag{6}$$

It is recognized that if R^2/EA is replaced by P (the compressive force) this equation is identical to the classical Euler buckling equation.

For the lowest buckling mode we assume

$$w = W \sin\left(\frac{\pi x}{L}\right) \tag{7}$$

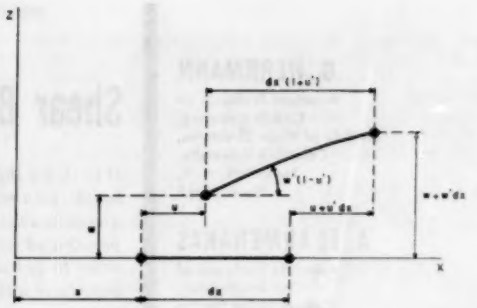

Fig. 3 Elongation and rotation of an axial element of length dx

and the critical force R_{crit} has the value

$$R_{crit} = \frac{\pi}{L}\,[(EI)\,(EA)]^{1/2} = \frac{EA\pi}{\lambda} \tag{8}$$

where λ is the slenderness ratio defined as

$$\lambda = \frac{L}{(I/A)^{1/2}}$$

It is apparent that the critical shear force is proportional to the square root of the product of the flexural stiffness EI and the compressional stiffness EA. The critical shear stress τ_{crit} is then given by

$$\tau_{crit} = \frac{E\pi}{\lambda} \tag{9}$$

For most structural material, such as metals, the elastic limit does not exceed the order of magnitude of $10^{-3}E$; therefore the smallest slenderness ratio for which buckling will take place in the elastic range, due to uniform shear, is of the order $\lambda = 10^3\pi$.

By contrast, it will be recalled that for the Euler column the critical stress is given by

$$\sigma_{crit} = \frac{E\pi^2}{\lambda^2}$$

and the smallest slenderness ratio in this case is of the order of magnitude $\lambda = 10^2$.

It is evident that only extremely slender bars will buckle, in the elastic range, when subjected to the influence of a uniform shear stress.

For certain materials, however, such as resins, the elastic limit may reach the order of magnitude of about half the value of Young's modulus. For such a material the dependence of critical stress upon the slenderness ratio, for the Euler buckling as well as the shear buckling, is shown in Fig. 4.

Energy Considerations

The buckling equations also can be derived readily on the basis of energy considerations.

The total strain energy stored in the bar during its passage from the straight to the deflected configuration, consists of two parts; namely, the strain energy of compression

$$V_C = \tfrac{1}{2}EA \int_0^L u'^2 dx \tag{10}$$

and strain energy of bending

$$V_B = \tfrac{1}{2}EI \int_0^L w''^2 dx \tag{11}$$

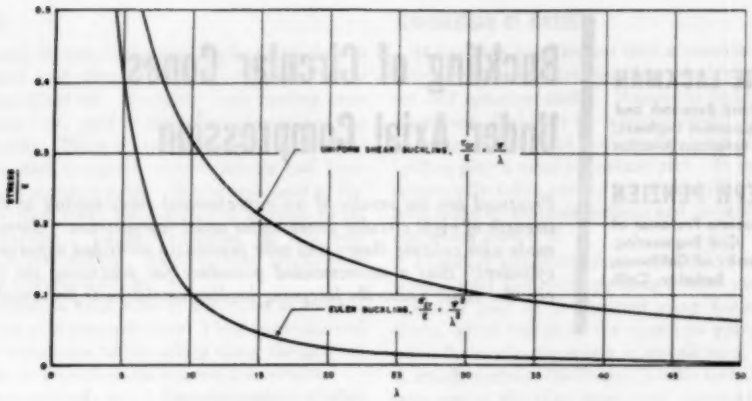

Fig. 4 Dependence of dimensionless critical stress on the slenderness ratio

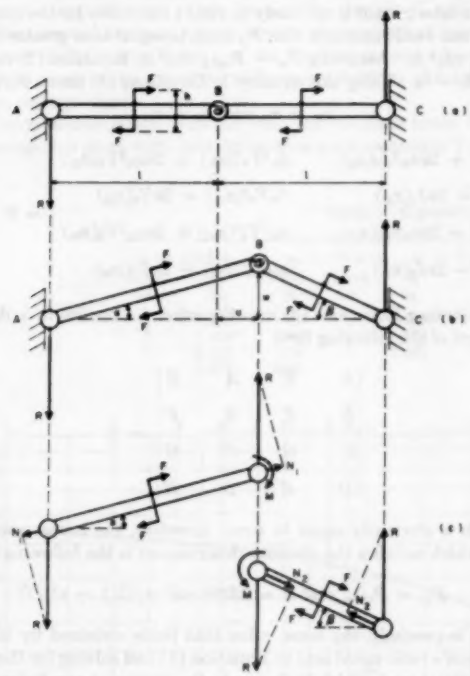

Fig. 5 Model of shear buckling

The work of external forces is conveniently evaluated by considering the moment of magnitude $\tau A = R$, per unit length of the beam, resulting from the shear traction τ. Since the angle of rotation, as seen from Fig. 3, is $w'(1 - u')$, the work of external forces is given by

$$W = -\int_0^L Rw'(1 - u')dx \tag{12}$$

The principle of minimum potential energy immediately yields the equilibrium equations (5).

A Model

In the present case, as with the classical Euler column, additional insight might be gained by considering a simple model.

The model,[1] as indicated in Fig. 5, consists of two inflexible, but compressible rods, joined together by means of a rotational spring and held at the ends by perfectly smooth, fixed hinges. Each bar is subjected to the action of a couple of magnitude Fh.

We assume that for a certain value of F an equilibrium configuration other than the straight one exists, as indicated in Fig. 5(b).

By inspection of the free-body diagram Fig. 5(c), it is apparent that the displacement w in the z-direction must be accompanied by a displacement u in the x-direction, inasmuch as the component of R in the axial direction is tension on the left bar and compression on the right one.

The relation between N_1 and R is

$$N_1 = R \sin \alpha \tag{13}$$

If $\sin \alpha$ is approximated by w/L, we have

$$N_1 = \frac{Rw}{L} \tag{14}$$

Taking into account the initial equilibrium, the moment condition of equilibrium yields

$$M = Ru \tag{15}$$

Equations (14) and (15) correspond to equations (3) for the original bar.

The relative change of length of bar AB is u/L. If c is the compressional stiffness, then

$$N_1 = \frac{cu}{L} \tag{16}$$

Let k designate the rotational spring constant. Then

$$M = k(\alpha + \beta) = \frac{2wk}{L} \tag{17}$$

Simultaneous solution of (14), (15), (16), and (17) results in

$$R_{crit} = \frac{2kc}{L} \tag{18}$$

which corresponds to expression (8) for the original bar.

For this model, an analysis on the basis of energy considerations could be readily effectuated. It is particularly evident from Fig. 5(b) that the work of external forces in the passage from the straight to the deformed configuration is positive.

[1] This model was suggested by Prof. B. A. Boley, and the authors gratefully acknowledge his interest in their work.

LESLIE LACKMAN
Structural Research and Development Engineer, North American Aviation

JOSEPH PENZIEN
Associate Professor of Civil Engineering, University of California, Berkeley, Calif.

Buckling of Circular Cones Under Axial Compression

Presented are the results of an experimental investigation to determine the buckling strength of right circular cones under axial compression. Correlation of these data is made with existing theory and with previously published experimental data on circular cylinders; thus a recommended procedure for predicting the buckling load of right circular cones under the foregoing loading condition is presented.

Theoretical Buckling Load

In a previous paper [1][1] by P. Seide, a solution to the stability problem of truncated cones loaded axisymmetrically was obtained by applying the method previously set forth by S. Timoshenko for cylinders and spheres [2]. This solution gave the following stability determinant for the buckling load:

$$\begin{vmatrix} x_{11}^3 J_3'(x_{11}) + 2\nu x_{11}^2 J_3(x_{11}) & x_{11}^3 Y_3'(x_{11}) + 2\nu x_{11}^2 Y_3(x_{11}) & x_{21}^3 J_3'(x_{21}) + 2\nu x_{21}^2 J_3(x_{21}) & x_{21}^3 Y_3'(x_{21}) + 2\nu x_{21}^2 Y_3(x_{21}) \\ x_{11} J_3'(x_{11}) - 2\nu J_3(x_{11}) & x_{11} Y_3'(x_{11}) - 2\nu Y_3(x_{11}) & x_{21} J_3'(x_{21}) - 2\nu J_3(x_{21}) & x_{21} Y_3'(x_{21}) - 2\nu Y_3(x_{21}) \\ x_{12}^3 J_3'(x_{12}) + 2\nu x_{12}^2 J_3(x_{12}) & x_{12}^3 Y_3'(x_{12}) + 2\nu x_{12}^2 Y_3(x_{12}) & x_{22}^3 J_3'(x_{22}) + 2\nu x_{22}^2 J_3(x_{22}) & x_{22}^3 Y_3'(x_{22}) + 2\nu x_{22}^2 Y_3(x_{22}) \\ x_{12} J_3'(x_{12}) - 2\nu J_3(x_{12}) & x_{12} Y_3'(x_{12}) - 2\nu Y_3(x_{12}) & x_{22} J_3'(x_{22}) - 2\nu J_3(x_{22}) & x_{22} Y_3'(x_{22}) - 2\nu Y_3(x_{22}) \end{vmatrix} = 0 \quad (1)$$

where

$$b_{1,2} = \left\{ 1 \pm \left[1 - \frac{(P_{cyl_\infty} \cos^2 \alpha)^2}{P_{cr}^2} \right]^{1/2} \right\} \quad (2)$$

$$\begin{aligned} x_{11} &= 2(b_1 s_1)^{1/2} & x_{21} &= 2(b_2 s_1)^{1/2} \\ x_{12} &= 2(b_1 s_2)^{1/2} & x_{22} &= 2(b_2 s_2)^{1/2} \end{aligned} \quad (3)$$

Seide showed that by setting Poisson's ratio equal to zero in the foregoing determinant, the lowest critical load is found to be

$$P_{cr} = P_{cyl_\infty} \cos^2 \alpha \quad (4)$$

By inspection of Equation (2) it is seen that if the value of P_{cr} is smaller than $P_{cyl_\infty} \cos^2 \alpha$, the stability determinant, Equation (1), will contain Bessel functions of complex numbers. Since such a determinant is not likely to yield a real value for the critical load, one would conclude that P_{cr} must be equal to or greater than $P_{cyl_\infty} \cos^2 \alpha$. Assuming $P_{cr} = P_{cyl_\infty} \cos^2 \alpha$, Equation (2) shows that $b_1 = b_2$. Using this equality in Equations (3) shows that

$$x_{11} = x_{21} \text{ and } x_{22} = x_{12} \quad (5)$$

Substituting Equations (5) into Equation (1) results in a determinant of the following form

$$\begin{vmatrix} A & E & A & E \\ B & F & B & F \\ C & G & C & G \\ D & H & D & H \end{vmatrix} = 0 \quad (6)$$

which is obviously equal to zero; therefore, the lowest value of P_{cr} which satisfies the stability determinant is the following:

$$P_{cr} = P_{cyl_\infty} \cos^2 \alpha = 2Et^2\pi \cos^2 \alpha / [3(1 - \nu^2)]^{1/2} \quad (7)$$

This is precisely the same value that Seide obtained by letting Poisson's ratio equal zero in Equation (1) and solving for the lowest critical load, which leads one to the erroneous conclusion that the foregoing critical load leaves out the effect of Poisson's ratio. This conclusion, however, as shown by Equation (6), is not true. Therefore it is concluded that the critical load as given by Equation (7) is the lowest critical load and that Poisson's ratio effects are properly included.

[1] Numbers in brackets designate References at end of paper.

Presented at the Summer Conference of the Applied Mechanics Division, University Park, Pa., June 20–22, 1960, of The American Society of Mechanical Engineers.

Discussion of this paper should be addressed to the Secretary, ASME, 29 West 39th Street, New York, N. Y., and will be accepted until October 10, 1960, for publication at a later date. Discussion received after the closing date will be returned.

Note: Statements and opinions advanced in papers are to be understood as individual expressions of their authors and not those of the Society. Manuscript received by ASME Applied Mechanics Division, June 18, 1959. Paper No. 60—APM-17.

Nomenclature

- C = correction factor
- D = bending stiffness per unit width of shell wall = $Et^3/12(1 - \nu^2)$
- E = Young's modulus
- P_{cr} = true axial buckling load of cone or cylinder
- P_{cyl_∞} = classical buckling load of cylinder = $2\pi Et^2/[3(1 - \nu^2)]^{1/2}$
- R = base radius of cone = $s_2 \sin \alpha$
- r = radius of cone measured in a plane normal to axis of cone; radius of cylinder
- s_1 = distance along generator from vertex to top of cone
- s_2 = distance along generator from vertex to base of cone
- t = constant wall thickness of cone or cylinder
- α = semivertex angle of cone
- ν = Poisson's ratio
- σ_{cr} = true critical stress of cone or cylinder
- σ_{cl} = classical critical stress of cone or cylinder

Experimental Results

Two sets of nickel cones having semivertex angles of 20 and 40 deg and having constant wall thickness were tested in a 60-kip Olsen Universal Testing Machine. Specially built loading caps having spherical surfaces were used to insure true loading of the cones along their generator. These cones were formed by electroplating pure nickel on steel mandrels whose surfaces had been accurately machined to a polished finish. Nickel was used as the material because of its high yield point and also because of its good electroplating qualities. Young's modulus for this material was found to be 29,000,000 psi. Different cone thicknesses were used ranging from 0.005 to 0.022 in.

Strain gages were placed on both sides of the cones at various points along the generator and circumference. These gages showed prior to buckling only membrane forces acting along the generator. Local bending due to imperfections was not measurable.

All cones buckled very suddenly into a diamond pattern similar to that which is characteristic of cylinders. Usually two rows of buckles appeared with the second row considerably less apparent than the first row next to the base. The number of individual buckles around the base circumference was somewhat uncertain because of the nonuniformity of the buckled pattern; however, in most cases there appeared to be seven buckles and in some cases perhaps eight.

The measured elastic buckling loads for the cones tested in this investigation along with their dimensions are presented in Table 1.

Correlation of Results

It has long been known that a considerable discrepancy exists between experimental and theoretical buckling loads for cylindrical and spherical shells. Numerous reasons for this discrepancy have been discussed by authors [3–6]; however, it is generally considered that local inaccuracies in shell geometry and applied loading play a most important part. In practice this discrepancy is normally taken care of by multiplying the classical theoretical load based on small deflections and no defects by an experimental correction factor, C.

Therefore for correlation purposes, it is assumed that the elastic critical load and corresponding critical stress for either cones or cylinders may be determined using Equations 8 and 9, respectively, which reduce to the equations generally used for cylinders when the semivertex angle, α, equals zero. The correction factor C, which contains the Poisson's ratio term, has been introduced to take care of the afore-mentioned discrepancy:

$$P_{cr} = 2\pi CEt^2 \cos^2 \alpha \tag{8}$$

$$\sigma_{cr} = \frac{CEt \cos \alpha}{r} \tag{9}$$

Since experimental evidence shows that the correction factor C reduces with increasing values of the ratio r/t, it would seem logi-

Table 1 Experimental buckling loads for nickel cones

Set No. 1						Set No. 2					
s_1 = 10.8 in.		s_2 = 17.2 in.		α = 20 deg		s_1 = 4.87 in.			s_2 = 7.05 in.	α = 40 deg	
Cone no.	t, in.	P_{cr}, lb	Cone no.	t, in.	P_{cr}, lb	Cone no.	t, in.	P_{cr}, lb	Cone no.	t, in.	P_{cr}, lb
1	0.005	500	5	0.0165	11500	8	0.0055	410	12	0.0115	2750
2	0.010	3400	6	0.021	17200	9	0.0055	460	13	0.015	5700
3	0.011	4250	7	0.021	21300	10	0.0095	1900	14	0.016	7570
4	0.015	8000				11	0.0100	2900	15	0.022	15300

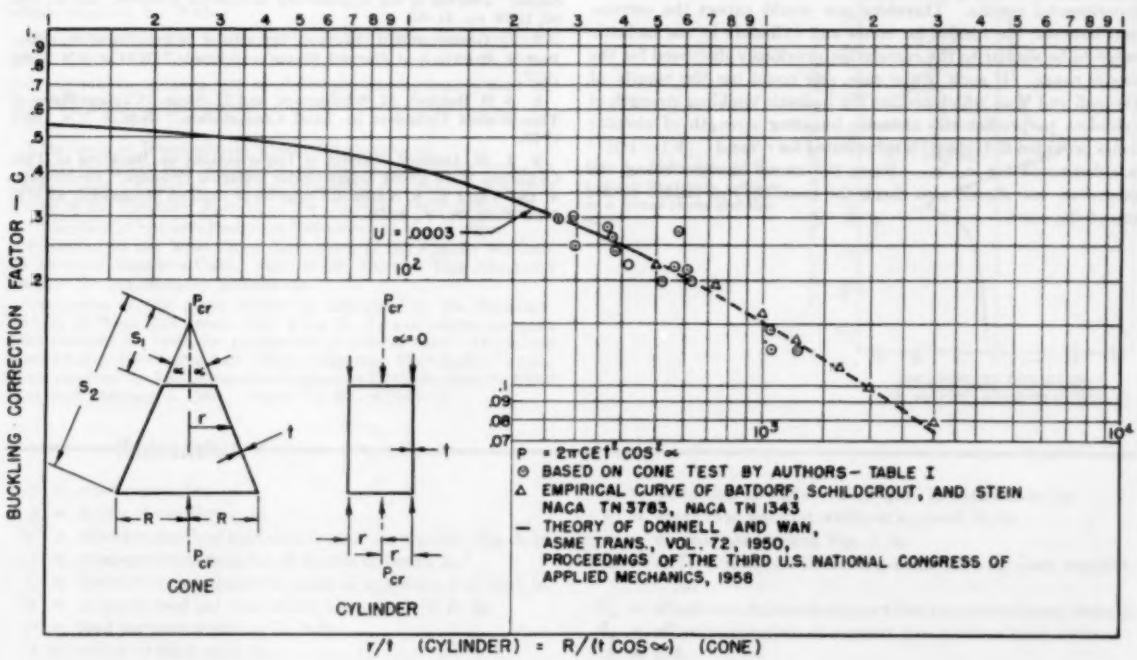
BUCKLING CORRECTION FACTOR — C
U = .0003
P = 2πCEt² COS² α
BASED ON CONE TEST BY AUTHORS— TABLE I
EMPIRICAL CURVE OF BATDORF, SCHILDCROUT, AND STEIN NACA TN 3783, NACA TN 1343
THEORY OF DONNELL AND WAN, ASME TRANS., VOL. 72, 1950, PROCEEDINGS OF THE THIRD U.S. NATIONAL CONGRESS OF APPLIED MECHANICS, 1958
CONE
CYLINDER
r/t (CYLINDER) = R/(t COS α) (CONE)

Fig. 1 Buckling correction factor C for cylinders or cones

cal to use the base radius R of the cone in determining the correction factor C to be used in Equation (8). The experimental results on cones support this reasoning as elastic buckling takes place first near the base of the cone.

The physical significance of the cos α-term in the foregoing equations is noted when one realizes that $r/\cos\alpha$ is the true radius of curvature of the cone measured normal to the generator. Since one would expect the buckling stress at a point to depend upon the true curvature at that point, the C-factor as previously obtained for cylinders as a function of r/t should be applicable to cones, provided $R/(t\cos\alpha)$ is substituted for r/t in that functional relationship.

Correlation of test data has been made by comparing the experimental correction factors for cones, as obtained using Equation (8) and the experimental critical loads shown in Table 1, with previously published correction factors for cylinders. The experimental correction factors for cones are plotted in Fig. 1 at abscissas corresponding to their respective $R/(t\cos\alpha)$-values. The correction factors for cylinders are represented by the curve in Fig. 1 which is the theoretical relationship of C versus r/t as published by Donnell and Wan [5, 9]. This relationship is based on an unevenness factor U which reflects the initial imperfections in the shell. A value of U equal to 0.0003 was selected as it is consistent with most cylinder buckling data. Comparing the cone data with this theoretical relationship shows very good agreement. Therefore the buckling load for right circular cones can be predicted with reasonable accuracy using Equation (8) and the correction-factor relationship given in Fig. 1.

It is worthy of note that the observed number of buckles around the base of the cone as previously given is also consistent with cylinder buckling data [5].

Since the elastic critical buckling stress as given by Equation (9) may be above the proportional limit of the material used, it is important to consider the case of inelastic buckling. Donnell and Wan treated this case theoretically for cylinders in a manner similar to their treatment of the elastic case, i.e., based on large deflections and imperfections, and found good agreement with experimental results. Therefore one would expect the correlation between the results for cones and cylinders in the inelastic range to be similar to the correlation previously discussed for the elastic range. If such is the case, one could use the results of Donnell and Wan which predict the inelastic buckling strength of cylinders to predict the inelastic buckling strength of circular cones provided $R/(t\cos\alpha)$ is substituted for r/t and $C\,[3(1-\nu^2)]^{1/2}$ is substituted for σ_{cr}/σ_{cl}. Since the stress changes along the generator, one should also check the possibility of failure at the top of the cone.

Conclusions

The following conclusions have been deduced from the results of this investigation:

1 The resultant elastic axial buckling load of right circular cones, loaded along their generator, can be predicted with reasonable accuracy using Equation (8) along with the corresponding correction factor given in Fig. 1.

2 The correction factor should be based on the true radius of curvature of the cone at its base rather than the true radius of curvature at mid-height.

3 The resultant elastic axial buckling load for fixed-ended, right circular cones can be predicted by the foregoing method provided the correction factor in Equation (8) is based on data for fixed-ended cylinders [7] rather than simply supported cylinders.

Acknowledgment

The authors wish to express their appreciation to the Ernest O. Lawrence Radiation Laboratory at Livermore, Calif., for furnishing the cones and testing fixtures used in this investigation.

References

1 P. Seide, "Axisymmetrical Buckling of Circular Cones Under Axial Compression," JOURNAL OF APPLIED MECHANICS, vol. 23, TRANS. ASME, vol. 78, 1956, pp. 625–628.

2 S. Timoshenko, "Theory of Elastic Stability," McGraw-Hill Book Company, Inc., New York, N. Y., 1940.

3 Th. von Karman and H. S. Tsien, "The Buckling of Thin Cylindrical Shells Under Axial Compression," *Journal of the Aeronautical Sciences*, vol. 8, 1941, pp. 303–312.

4 H. S. Tsien, "A Theory for the Buckling of Thin Shells," *Journal of the Aeronautical Sciences*, vol. 9, 1942, pp. 119–132.

5 L. H. Donnell and C. C. Wan, "Effect of Imperfections on Buckling of Thin Cylinders and Columns Under Axial Compression," JOURNAL OF APPLIED MECHANICS, vol. 17, TRANS. ASME, vol. 72, 1950, pp. 73–83.

6 G. P. R. von Willich, "The Elastic Stability of Thin Spherical Shells," *Journal of the Engineering Mechanics Division*, ASCE, vol. 85, 1959, pp. 51–65.

7 G. Gerard and H. Becker, "Handbook of Structural Stability, Part 3, Buckling of Curved Plates and Shells," NACA TN 3783, 1957.

8 S. B. Batdorf, M. Schildcrout, and M. Stein, "Critical Stress of Thin-Walled Cylinders in Axial Compression," NACA TN 1343, 1947.

9 L. H. Donnell, "Effect of Imperfections on Buckling of Thin Cylinders With Fixed Edges Under External Pressure," Proceedings of the Third U. S. National Congress of Applied Mechanics, ASME, New York, N. Y., 1958.

The Additional Deflection of a Cantilever Due to the Elasticity of the Support[2]

W. J. O'DONNELL[1]
Associate Engineer,
Westinghouse Bettis
Atomic Power Laboratory,
Pittsburgh, Pa.
Assoc. Mem. ASME

A beam is cantilevered from a semi-infinite solid with neutral axis normal to its bounding plane (two-dimensional problem). Deformation of the supporting solid allows the beam to rotate about the built-in end, producing a deflection in addition to that caused by bending and shear in the beam itself. Results of tests designed to measure this additional deflection are presented and compared with various theoretical values. Calculated deflections, based on classical bending and shear-deflection theory, are also compared with measured deflections. An experimentally verified expression for the additional deflection of a cantilever due to the elasticity of the support is given.

WHETHER or not a cantilever is machined integral with the support, there will be elastic distortions in the support which allow the cantilever to rotate at the built-in end. This rotation produces a deflection in addition to that caused by bending and shear stresses in the beam itself.

Such imperfect clamping deflections become significant relative to the greatly reduced bending deflections at small length-to-depth (x/h) ratios, Fig. 5. The object of this study is to present an experimentally verified expression for the additional deflection of a cantilever due to the elasticity of a semi-infinite support fixed at infinity.

Very little analytical work and no experimental work have been done on the problem to date. C. Weber [1],[3] F. Vogt [2], and N. Muskhelishvili [3] have made significant contributions toward an analytical solution. An exact theoretical solution has not been found. Vogt dealt principally with the case of loading over a finite section of the width t in Fig. 5. As this length of loading approaches infinity, the solution becomes identical to the plane-strain solution by Weber.

An explanation and a criticism of Weber's analytical approach are presented in this study. Muskhelishvili arrived at a different expression, making use of different assumptions which are also explained in this paper.

[1] Formerly at Westinghouse Research Laboratories.

[2] This research was conducted at the Westinghouse Research Laboratories. A portion of it was submitted as a Master of Science Thesis to the Graduate Faculty of the University of Pittsburgh.

[3] Numbers in brackets designate References at end of paper.

Presented at the West Coast Conference of the Applied Mechanics Division, Pasadena, Calif., June 27–29, 1960, of THE AMERICAN SOCIETY OF MECHANICAL ENGINEERS.

Discussion of this paper should be addressed to the Secretary, ASME, 29 West 39th Street, New York, N. Y., and will be accepted until October 10, 1960, for publication at a later date. Discussion received after the closing date will be returned. First draft of manuscript received by ASME Applied Mechanics Division, July 29, 1959; final draft, January 5, 1960. Paper No. 60—APMW-3.

Theoretical Analysis

Weber [1] assumed that a moment load M at the built-in end of a cantilever is transmitted to the support by a linear distribution of normal stresses. He then proceeded to find a stress function which satisfied all of the boundary conditions for the semi-infinite support, and developed an expression for the distortion of the loaded surface of the support, Fig. 1. The "mean" rotation θ_M of the loaded surface of the support due to a moment load M was then defined so that the work done by M acting through this mean rotation was identical with that produced by the distributed surface displacements and stresses acting over the same surface.

Taking account of differences in notation, Weber's solution for the case of plane strain is given by

$$\theta_M = \frac{(1 - \nu^2)18M}{\pi E(h')^3} \tag{1}$$

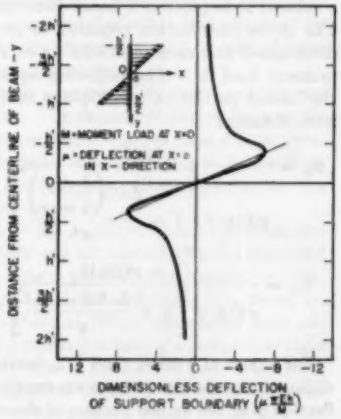
DISTANCE FROM CENTERLINE OF BEAM - y
M = MOMENT LOAD AT X=0
μ = DEFLECTION AT X=0 IN X-DIRECTION
DIMENSIONLESS DEFLECTION OF SUPPORT BOUNDARY

Fig. 1 Deflection of the support boundary subject to a linear stress distribution

Nomenclature

E = elastic modulus, psi
h = depth of cantilever, in.
h' = effective depth of load distribution on support, Fig. 5, in.
I = cross-sectional moment of inertia of beam, in.[4]
L = distance from support to point of application of load, in.
M = moment load per unit width at support, in lb/in.
P = load per unit width at L, lb/in.
r = radius of fillet radii, in.
t = width of cantilever (in Z-direction), in.
μ = deflection of surface of support in x-direction, in.
V = shear load per unit width at support, lb/in.
x, y = co-ordinate system, Fig. 5, in.
δ_x = deflection of cantilever in y-direction x in. from support, in.
θ_M = effective rotation at support due to moment load, radians
θ_S = effective rotation at support due to shear load, radians
ξ = x/h
ν = Poisson's ratio

The similarity of the equations characterizing the state of plane strain and plane stress, respectively, makes it possible to convert plane-strain solutions to plane stress and vice versa when body forces are constant and there are no variations in the z-direction. A corresponding plane-stress solution can be obtained from a plane-strain solution by substituting E for $E/(1-\nu^2)$ and ν for $\nu/(1-\nu)$. The plane-stress expression corresponding to equation (1) is given by

$$\theta_M = \frac{18M}{\pi E(h')^2} \tag{2}$$

Consider the implications of the assumption that a moment load is transmitted by a linear distribution of normal stresses at the junction of the support section and beam section. This stress distribution produces a linear distortion of the beam section which is not compatible with the distortion of the semi-infinite support at the junction as shown in Fig. 1. Hence it cannot be expected that the stress distribution remains as assumed. The fibers near $y = \pm h/2$ will take a larger load than that given by a linear stress distribution.

The most significant factor in the analytical consideration of the accuracy of this solution is the fact that the stress energy is dependent on the sum of the energies of all elements taking the load. Elements assumed to carry too much of the load are offset by those assumed to carry too little. Hence the sum of the energies is only slightly altered by assuming a stress distribution for a given equivalent load which does not correspond to the actual distribution exactly, provided this distribution is reasonably chosen.

Since the actual distribution of the stress at the junction depends on the combined effect of the support section and beam section, the method of considering the two sections separately cannot be used to obtain that distribution and the problem can only be solved for certain assumed stress distributions.

Muskhelishvili considered the mixed boundary-value problem of a semiplane loaded by an unknown stress distribution in such a manner as to produce a linear distortion over part of its surface. The stress distribution required to produce this deflection was determined and used to obtain an expression for the equivalent moment load M. The following equations for the rotation of the loaded portion of a half-plane subject to a moment load M were obtained:

$$\theta_M = \frac{16M}{\pi E(h')^2\left[1 + \dfrac{Ln^2\left(\dfrac{3-\nu}{1+\nu}\right)}{\pi^2}\right]} \quad \text{(for plane stress)} \tag{3}$$

$$\theta_M = \frac{(1-\nu^2)16M}{\pi E(h')^2\left[1 + \dfrac{Ln^2(3-4\nu)}{\pi^2}\right]} \quad \text{(for plane strain)} \tag{4}$$

For values of ν other than 1/2, horizontal shear stresses in addition to the normal stresses are required to maintain a linear deflection over the loaded portion of the support.

The rotation given by these equations when $\nu = 0.3$ is 15.7 per cent lower than that given by Weber's solution for the case of plane stress, and 14.0 per cent lower for the case of plane strain. This relatively small difference in rotation is significant because of the radically different stress distributions involved. Weber's solution assumes a linear stress distribution, whereas the stresses required to produce a linear distortion are infinite at $x = \pm h/2$. This comparison indicates that the rotation is only slightly affected by the assumed stress distribution, a point which has already been discussed.

Since the fibers near $y = \pm h/2$ take a larger load than that given by a linear stress distribution, a cubic stress distribution was considered for the present paper. For this purpose, the well-known surface displacement resulting from a concentrated load was utilized [4]. The mean rotation for a cubic stress distribution was developed by superimposing the deflections caused by a large number of concentrated loads of suitable intensities acting on short elements of the support. The result is given by equations (9) and (10) in the Conclusions of this paper. It is of interest to note that this solution is approximately equivalent to the average between the solutions given by Weber and Muskhelishvili, respectively.

The shear load at the built-in end of a cantilever also produces a rotation of the loaded area. Vogt derived an expression for the rotation due to a shear load by assuming a uniformly distributed shear stress at the support. The mean rotation was again defined so that the work input into the foundation was equivalent to that given by the distributed stresses and distortions.

The assumption of a uniform shear distribution may appear less than satisfactory since the customary beam theory gives a shear-stress distribution of parabolic shape. However, as in the case of a moment load, the distortion of the beam section will not be compatible with the distortion of the support at the junction for a parabolic shear distribution. The fibers near $y = \pm h/2$ take a larger load than that given by a parabolic distribution. Hence the assumption of a uniform shear-stress distribution appears reasonable, and although it will not give exact results, it is probably sufficiently accurate. Vogt's expression for the mean rotation caused by a shear load is given by

$$\theta_S = \frac{(1-\nu-2\nu^2)V}{Eh'} \tag{5}$$

The corresponding plane-stress expression is given by

$$\theta_S = \frac{(1-\nu)V}{Eh'} \tag{6}$$

The ratio of the mean rotation produced by a shear load to that produced by a moment load for a cantilever subject to a concentrated load at $x = L$ is given by

$$\frac{\theta_S}{\theta_M} = \frac{(1-\nu)\pi h'}{18L} \quad \text{(plane stress)} \tag{7}$$

$$\frac{\theta_S}{\theta_M} = \frac{(1-2\nu)\pi h'}{(1-\nu)18L} \quad \text{(plane strain)} \tag{8}$$

Hence the rotation due to shear is small compared to that due to bending except in the few cases where L/h' may be small.

Both shear and bending loads acting on the support also produce a mean vertical displacement of the loaded surface of the support. Since the expressions given in the conclusions of this paper are intended to give y-deflections relative to the deflected centerline of the cantilever at the built-in end, this y-deflection does not appear.

Experimental Investigation

The test specimen shown in Fig. 2 was designed symmetrically about the vertical centerline. Hence two cantilevers (A)[4] could be tested simultaneously and duplicate readings could be taken for all distortions and deflections. The center section of the test specimen was made large enough to be equivalent to a semi-infinite support with respect to the cantilevers being tested. This design was checked by measuring deflections in the support with Huggenberger extensometers. Measurable rotational deflections were confined to an area within 1 in. of the loaded surface of the support.

The larger cantilever (B) on the test specimen was used as a

[4] Letters in parentheses refer to Fig. 2.

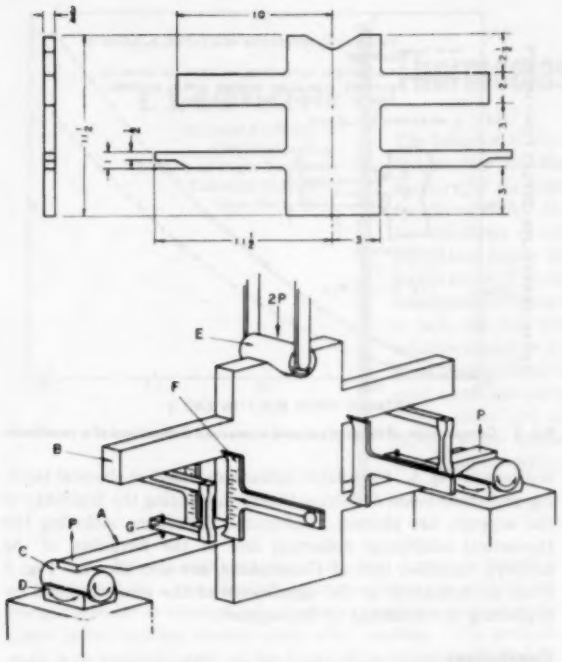

Fig. 2 Experimental setup. A—test cantilever, B—reference cantilever, C—roller of loading bolster, D—cylindrical seat of loading bolster, E—roller of support bolster, F—Huggenberger extensometer, G—clip gages

deflection-measuring reference. The specimen was designed so that the application of the load would not produce any rotation of the reference cantilevers with respect to the vertical centerline of the specimen. This design was checked experimentally by placing mirrors at the built-in end of the reference cantilevers and comparing their rotations with the rotations of mirrors at the centerline of the test specimen. The reference cantilevers did not rotate with respect to the vertical centerline of the test specimen. Hence a load applied to the specimen caused an equal y-deflection of every point on the reference cantilever with respect to the centerline of the test cantilever at the built-in end. All y-deflections were measured from the reference cantilevers. The y-deflection at $x = 0$ was subtracted from all other readings in order to obtain deflections relative to the deflected centerline of the cantilever at the built-in end.

A tensile test was run on the test-specimen material (tool steel) after heat-treating. The material was found to have an elastic modulus of 29.93×10^6 psi and a proportional limit of 110,000 psi.

Test Procedure

The deflection between the test cantilevers and the reference cantilevers was measured at x/h ratios of 0, 1/2, 1, 3/2, and 2. Deflections in the support and near the built-in end of the test cantilever were measured with Huggenberger extensometers (F). Clip gages were designed and fabricated to measure deflections at x/h ratios of 1/2, 1, and 3/2.

The clip gages were designed so that any motion between the contact points produces bending and compression stresses in the beam of the gage. These stresses vary linearly with the deflection between the contact points. The corresponding strain at the surface of the beams was picked up by A-7, SR-4 strain gages. These gages were connected through a Baldwin bridge balance switching unit to a Type N, SR-4 indicator. The smallest deflection that would produce a readable change in strain reading was of the order of 40 microin. The contact force of these gages was 0.25 lb per mil deflection. The gages are shown mounted on the test specimen in Fig. 2. The deflection at $x/h = 2$ was large enough to measure accurately with dial gages. Notice that the deflections were not measured from the centerline of the test cantilevers. Centerline deflections were obtained by subtracting the Poisson's ratio effect, i.e., $\frac{\nu P t y^2 (L - x)}{2EI}$, from measured deflections of off-centerline points. In no case did this term amount to as much as four per cent of the total deflection.

The specimen was loaded by means of a 30-ton Amsler testing machine with pendulum dynamometer and pump. The load was applied as shown in Fig. 2. The end bolsters consisted of a roller (C) mounted on a cylindrical seat (D). The roller was free to rotate, thus minimizing the frictional tensile load that might have been transmitted to the test cantilever when the specimen deformed under load. Notice that the load was applied at the neutral axis of the cantilever to eliminate the possibility of transmitting a frictional moment load. The cylindrical seat (D) was used to insure uniform loading across the cross section. The upper bolster (E), used to support the specimen, was cylindrical and free to rotate thus assuring that each test cantilever carried about one half of the total load.

Subsequent to a check of deflection versus load linearity up to maximum load, deflection readings were taken at maximum and minimum loads only.

The load-distributing effect of the fillets at the support was evaluated by taking deflection readings with fillet radii of 0.125 and 0.005 in., respectively, all other parameters being held constant. This effect was factored into the equations for the additional deflection due to rotation at the support by including the appropriate portion of the fillets in the effective depth of loading at the support h'.

Test Results

The small deflection at $x = 0$ was the most difficult to measure accurately. Four Huggenberger extensometers were used to measure this deflection simultaneously. Since readings were taken for three load cycles, the measured deflection was obtained by averaging 24 readings. The maximum deviation of any of these readings from the average was 7.7 per cent.

Accurate deflection readings were relatively easy to obtain and reproduce at all other points. The maximum deviation from the average reading at any of these points was less than 4.2 per cent. These differences resulted largely from differences in the loading, machined dimensions, and instrument locations between the two cantilevers being tested simultaneously.

The calculated deflection of the cantilever due to bending and shear stresses in the beam itself was subtracted from the measured total deflection in order to obtain the deflection caused by rotation at the support. This calculated deflection was based on classical bending-deflection theory. Shear deflections were obtained from the solution for a cantilever having a completely rigid support; i.e., a built-in end that is completely prevented from warping [5]. Had the usual shear factor of 1.2 been used, the deflections due to rotation at the support would be about 1 per cent smaller.

As previously discussed, the moment load must be transmitted to the support by a bending-stress distribution having peaks near $y = \pm h/2$ in order to make the distortion of the beam section compatible with that of the support section at the junction. Hence for the test-specimen configuration, peak bending stresses act over a Δy depth of the support which is small compared to the width of the support. The foundation offers considerable lateral (Z-direction) restraint around these areas of peak bending stress, tending to produce a plane-strain condition in the foundation. Since the stress state in the foundation is undoubtedly between plane strain and plane stress, theoretical deflections due

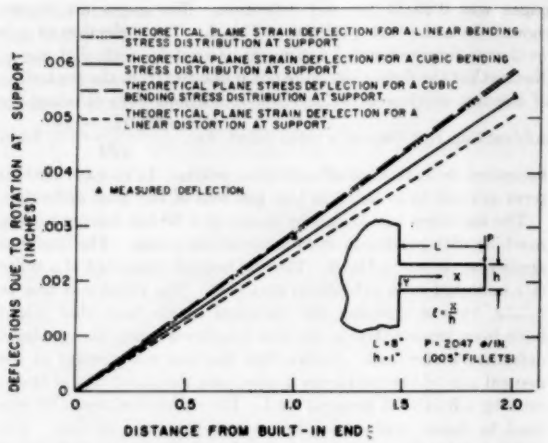
THEORETICAL PLANE STRAIN DEFLECTION FOR A LINEAR BENDING STRESS DISTRIBUTION AT SUPPORT
THEORETICAL PLANE STRAIN DEFLECTION FOR A CUBIC BENDING STRESS DISTRIBUTION AT SUPPORT
THEORETICAL PLANE STRESS DEFLECTION FOR A CUBIC BENDING STRESS DISTRIBUTION AT SUPPORT
THEORETICAL PLANE STRAIN DEFLECTION FOR A LINEAR DISTORTION AT SUPPORT
Δ MEASURED DEFLECTION
L = 8"
h = 1"
P = 2047 #/IN
(.005" FILLETS)
DEFLECTIONS DUE TO ROTATION AT SUPPORT (INCHES)
DISTANCE FROM BUILT-IN END ξ

Fig. 3 Deflection of a cantilever due to rotation at support

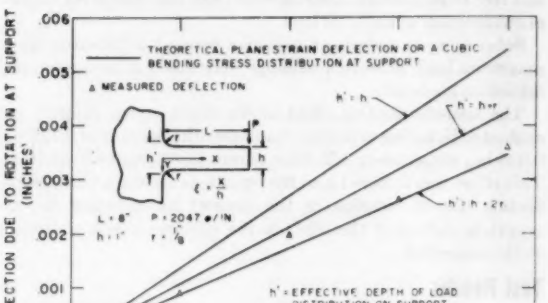
THEORETICAL PLANE STRAIN DEFLECTION FOR A CUBIC BENDING STRESS DISTRIBUTION AT SUPPORT
Δ MEASURED DEFLECTION
h' = h
h' = h + r
h' = h + 2r
L = 8"
h = 1"
P = 2047 #/IN
h' = EFFECTIVE DEPTH OF LOAD DISTRIBUTION ON SUPPORT
DEFLECTION DUE TO ROTATION AT SUPPORT (INCHES)
DISTANCE FROM BUILT-IN END

Fig. 4 Effect of fillets on deflection of a cantilever due to rotation at support

to rotation at the support are plotted in Fig. 3 for both cases (the difference being less than 10 per cent).

Theoretical deflections resulting from rotation at the support are compared with measured deflections for a cantilever having negligibly small fillets in Fig. 3. Deflections calculated on the basis of Muskhelishvili's solution were slightly smaller than measured deflections, and calculated deflections based on Weber's solution were slightly larger than measured deflections. The solution obtained for a cubic bending-stress distribution at the support proved to provide the most acceptable expression for the additional deflection due to rotation at the support, not only from an analytical point of view, but from test results as well. This solution is given by equations (9) and (10) in the Conclusions.

Theoretical deflections caused by rotation at the support are compared with measured deflections for a cantilever having fillet radii of 1/8 the beam depth in Fig. 4. The stiffening effect of increased beam thickness due to the presence of the fillets was evaluated analytically. Since this effect was found to be quite small (less than 2 per cent at $x/h = 0.5$), it was not included in the calculated bending and shear deflections. Fig. 4 indicates that the load-distributing effect of the fillets on rotation at the support can be approximated by taking $h' = h + 1.5r$. However, this method of including the effects of the fillets is only approximate, even for small fillets. A much more elaborate method and extensive tests would be required to account for relatively large fillets.

Measured total deflections are compared with calculated deflections in Fig. 5. Calculated deflections based on classical bending and shear-beam deflection theory, neglecting the flexibility of the support, are plotted. Calculated deflections including the theoretical additional deflection due to the flexibility of the support, equation (10) of Conclusions, are also shown. Fig. 5 gives an indication of the significance of the error incurred by neglecting the flexibility of the support.

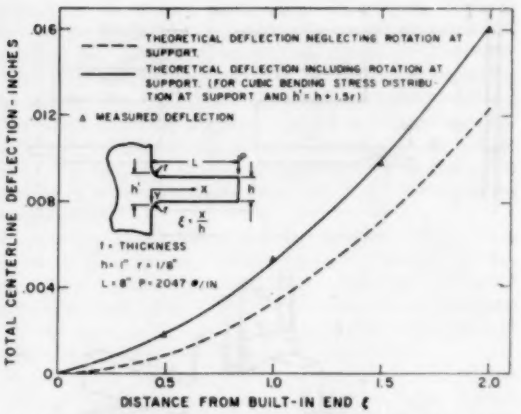
THEORETICAL DEFLECTION NEGLECTING ROTATION AT SUPPORT
THEORETICAL DEFLECTION INCLUDING ROTATION AT SUPPORT (FOR CUBIC BENDING STRESS DISTRIBUTION AT SUPPORT AND h' = h + 1.5r)
Δ MEASURED DEFLECTION
t = THICKNESS
h = 1" r = 1/8"
L = 8" P = 2047 #/IN
TOTAL CENTERLINE DEFLECTION - INCHES
DISTANCE FROM BUILT-IN END ξ

Fig. 5 Comparison of theoretical and measured deflections of a cantilever

Conclusions

The additional deflection of a cantilever due to the elasticity of the support is given by[5]

$$\delta_x = \frac{16.67\,Mx}{\pi E(h')^2} + \frac{(1-\nu)Vx}{Eh'} \quad \text{(for plane stress)} \quad (9)$$

$$\delta_x = \frac{(1-\nu^2)16.67Mx}{\pi E(h')^2} + \frac{(1-\nu-2\nu^2)Vx}{Eh'} \quad \text{(for plane strain)} \quad (10)$$

Tests indicate that the effect of the fillets can be approximated by taking $h' = h + 1.5\,r$ for $r/h \leq 1/8$. The total deflection can be obtained by adding this additional deflection to that given by classical bending and shear-deflection theory.

Acknowledgment

The author is indebted to Dr. A. M. Wahl and N. C. Small of Westinghouse Research for guidance throughout this study and to T. F. Hengstenberg of Westinghouse for instrumentation assistance.

References

1 C. Weber, "The Deflection of Loaded Gears and the Effect on Their Load Carrying Capacity," Department of Scientific and Industrial Research, Sponsored Research, Germany, Report No. 3, part 1, England, 1949.

C. Weber and K. Banaschek, "Formänderung und Profilrücknahme bei Gerad-und Schrägverszahnten Antriebstechnik," Heft 11, F. Vieweg and Sohn, Braunschweig, Germany, 1953.

2 F. Vogt, "Uber Die Berechnung der Fundamentdeformation," Avhandlinger utgil av Det Norske Videnshaps, Akademi I Oslo, I Math-Naturv., Klasse, No. 2, 1925.

3 N. I. Muskhelishvili, "Some Basic Problems of the Mathematical Theory of Elasticity," P. Noordhoff Limited, Groningen-Holland, third edition, 1953, p. 471.

4 S. Timoshenko and J. N. Goodier, "Theory of Elasticity," McGraw-Hill Book Company, Inc., New York, N. Y., second edition, 1953, p. 471.

5 S. Timoshenko, "Strength of Materials," D. Van Nostrand Company, Inc., New York, N. Y., part 1, third edition, 1955, p. 175.

[5] Relative to the deflected centerline at the built-in end.

Thermoelastic Stresses in Beams[1]

E. S. BARREKETTE
Assistant Professor of Civil Engineering, Institute of Flight Structures, Columbia University, New York, N. Y.

The behavior of elastic, free beams of arbitrary constant cross section under an arbitrary temperature distribution is investigated. An analytical method of successive approximations for the solution of linear partial differential equations is applied to the solution for thermoelastic stresses in such beams. The stresses are obtained in terms of series, the nth terms of which are of the form $\beta^n \mathfrak{L}_n(\partial^n T/\partial^n \mathfrak{X})$ where β is the ratio of the maximum linear dimension of the cross section to the length of the beam, T is the temperature, $\mathfrak{X}$ is the ratio of the axial co-ordinate to the length of the beam, and $\mathfrak{L}_n$ is a homogeneous linear integral differential operator in y and z only. When Poisson's ratio is zero, the first term of the series for the normal axial stress is identical with the solution based on a strength-of-materials analysis, and the first term of the series for the axial displacement leaves plane sections plane. The leading terms of the series provide good approximations when the temperature can be expanded in a rapidly convergent power series and in long bars ($\beta \ll 1$). The case of beams of constant circular cross section under temperatures varying only with the axial co-ordinate is examined and a numerical example is presented.

THE practical analysis of thermal stresses in beams is usually based on a one-dimensional stress-strain law and on the Bernoulli-Euler or strength-of-materials hypothesis that sections plane before heating remain plane after heating. The present work is an analysis based on the linear, three-dimensional theory of elasticity, and thus can be used to evaluate the validity of the approximate approach.

The isothermal strength-of-materials theory ordinarily agrees with experimental results[2] and predicts, in all cases, the same normal axial stresses as given by the Saint Venant bending theory for cantilever beams subjected to a bending-moment distribution which is linear with the axial co-ordinate.

The solution of the two-dimensional thermal problem was carried out by Boley [5] by means of a general step-by-step solution of the governing equations. This method was also applied to the two-dimensional isothermal problem of a loaded beam by Boley and Tolins [6].

The present work is an extension of Boley's method to the three-dimensional thermoelastic problem of beams of arbitrary constant cross section subjected to arbitrary temperature distributions. Additional details may be found in [7].

The step-by-step method is developed in general terms in the following section, and is applied in the next to a general thermoelastic stress analysis of isotropic, homogeneous, simply connected free beams. A solution for the stresses and displacements is given later for the special case of a right circular cylindrical beam subjected to temperatures varying only with the axial co-ordinate, and a numerical example is presented to illustrate the behavior of this series solution. Curves are presented to illustrate this solution to the thermoelastic problem and the accuracy of the strength-of-materials approach is discussed.

Outline of Mathematical Procedure

The solution of the problem is based on the method of reference [5] for simplifying the solution of elliptic partial differential equations defined in regions where one dimension is much larger than any of the others. This method reduces a partial differential equation in n independent variables to an infinite set of equations in $(n-1)$ independent variables. A general form of this procedure is presented here for the case of a single partial differential equation although, in what follows, it will be applied to a system of such equations.

Given an elliptic linear partial differential equation of any order n of the form

$$\sum_{j=0}^{n} D^j g(x, y, z) = f(x, y, z) \tag{1a}$$

where g is the dependent variable and

$$D^j = \sum_{r=0}^{n-j} \sum_{s=0}^{r} A_{rs}{}^{j}(y, z) \frac{\partial^{r+j}}{\partial y^{r-s} \partial z^s \partial x^j}$$

Let the solution be desired for a cylindrical region, with the generators parallel to the x-axis, defined by $z_1(y) \leqslant z \leqslant z_2(y)$, $y_1 \leqslant y \leqslant y_2$, $0 \leqslant x \leqslant L$, with boundary conditions of the form

---

[1] This work is part of a dissertation submitted by the author in partial fulfillment of the requirements for the degree of Doctor of Philosophy at Columbia University and was supported by the Wright Air Development Center. The author wishes to express his gratitude to Prof. Bruno A. Boley for his invaluable aid and advice during the course of this investigation.

[2] One explanation of the wide range of applicability of the approximate theory was given by von Karman [1][3] and Seewald [2]. They derived their results, in the isothermal case, for a two-dimensional elasticity problem by expanding the bending-moment distribution into a Taylor series along the span, and getting series expansions for the radius of curvature and for the normal axial stress. The terms of these series are proportional to successively higher derivatives of the bending moment with respect to the axial co-ordinate, and the leading term of each series is the same as that arrived at from strength-of-materials considerations. Thus if the bending-moment distribution is sufficiently smooth, i.e., if it can be represented by a rapidly converging power series, the leading term predominates in each series, and the Bernoulli-Euler hypothesis leads to good results. Donnell [3] obtained similar expansions and corrected some numerical errors in Seewald's work.

Almansi [4] developed a procedure for the problem of a cylinder under surface tractions varying as polynomials in the axial co-ordinate. Goodier [13] examined solutions of the three-dimensional isothermal case in the form of power series in β and showed that their leading terms correspond to the Saint Venant solutions.

[3] Numbers in brackets designate References at end of paper.

Presented at the Summer Conference of the Applied Mechanics Division, University Park, Pa., June 20–22, 1960, of THE AMERICAN SOCIETY OF MECHANICAL ENGINEERS.

Discussion of this paper should be addressed to the Secretary, ASME, 29 West 39th Street, New York, N. Y., and will be accepted until October 10, 1960, for publication at a later date. Discussion received after the closing date will be returned. First draft of manuscript received by ASME Applied Mechanics Division, February 27, 1959; final draft, October 28, 1959. Paper No. 60—APM-28.

$$\sum_{r=0}^{n-1}\sum_{s=0}^{r} k_{rs}(y, z)(\partial^r g/\partial y^{r-s}\partial x^s) = X_{1,2}(x, y, z) \text{ on } z = z_1, z_2 \quad (1b)$$

$$\sum_{r=0}^{n-1} k_r(y, z)(\partial^r g/\partial x^r) = G_{1,2}(y, z) \text{ on } x = 0, L \quad (1c)$$

Restatement in Terms of Infinite Series. Let

$$g = \hat{g} + \sum_{m=0}^{\infty} g_m \quad (2)$$

where $\hat{g}$ and g_m are so chosen as to satisfy the following equations:

$$\begin{aligned} D^0 g_0 &= f_0 \\ D^0 g_1 &= f_1 - D^1 g_0 \\ &\cdots \\ D^0 g_m &= f_m - \sum_{j=1}^{m} D^j g_{m-j} \qquad m \leqslant n \quad (3) \\ &\cdots \\ D^0 g_m &= f_m - \sum_{j=1}^{n} D^j g_{m-j} \qquad m \geqslant n \end{aligned}$$

$$\sum_{j=0}^{n} D^j \hat{g} = 0 \quad (4)$$

where

$$f = \sum_{m=0}^{\infty} f_m$$

The choice of the functions f_m is not unique and should be made in any manner which is convenient for the particular problem at hand. In the present problem f is a homogeneous linear function of derivatives of the temperature T, and f_m will be chosen in such a way as to contain derivatives of T with respect to x of order m only. Then it follows that g_m will contain derivatives of T with respect to x of the single order m.

If $f = \sum_{m=0}^{k} f_m$, then for $m > k$ and $m \geqslant n$ the recurrence equation

$$D^0 g_m = -\sum_{j=1}^{n} D^j g_{m-j}$$

relates g_m to g_j $(j = m - n, m - n + 1, \ldots, m - 1)$.

Clearly the expansion (2) formally satisfies equation (1a). Since no derivative with respect to x appears in their left-hand members, equations (3) are simpler to solve than equation (1a). The role of x has thus been reduced from that of an independent variable to that of a parameter. However, as a consequence, g_m cannot satisfy boundary conditions of the form of (1c), but it can be made to satisfy conditions of the following form:

$$\sum_{r=0}^{n-1}\sum_{s=0}^{r} k_{rs}(\partial^r g_0/\partial y^{r-s}\partial x^s) = X_{1,2} \quad \text{on } z = z_1, z_2 \quad (5)$$

$$\sum_{r=0}^{n-1}\sum_{s=0}^{r} k_{rs}(\partial^r g_m/\partial y^{r-s}\partial x^s) = 0 \qquad m \geqslant 1$$

Thus $\sum_{m=0}^{\infty} g_m$ formally satisfies equations of the form of (1a, b) but not of (1c). In order to complete the solution it is then necessary to determine $\hat{g}$.

Determination of $\hat{g}$. The function $\hat{g}$ must satisfy the homogeneous equation (4) with the following conditions:

$$\sum_{r=0}^{n-1}\sum_{s=0}^{r} k_{rs}(\partial^r \hat{g}/\partial y^{r-s}\partial x^s) = 0 \quad \text{on} \quad z = z_1, z_2 \quad (6a)$$

$$\sum_{r=0}^{n-1} k_r(\partial^r \hat{g}/\partial x^r) = G_{1,2} - \sum_{r=0}^{n-1}\sum_{m=0}^{\infty} k_r(\partial^r g_m/\partial x^r) \quad \text{at} \quad x = 0, \ L \quad (6b)$$

Clearly the exact determination of $\hat{g}$ is, in general, as difficult as the solution of the original problem. It is possible, however, in the case of elliptic differential equations defined in regions which have a long cylindrical shape ($h \ll L$, where h is the maximum linear dimension of the cross section) to obtain an approximate solution for $\hat{g}$ which is usually adequate. In order to obtain this approximation it is convenient to examine each end of the cylinder separately, and to do this it is necessary to classify boundary-value problems into two types, depending on whether (i) the boundary conditions can be specified arbitrarily or (ii) the boundary conditions must satisfy certain integral conditions.

An example of both these cases is provided by Laplace's equation

$$\nabla^2 \phi = 0$$

Here ϕ can be specified arbitrarily on the boundary (case i), but its normal derivative $\partial\phi/\partial n$ cannot (case ii), since the divergence theorem requires the integral of this quantity over the boundary to be zero; i.e.,

$$\int_s (\partial\phi/\partial n)ds = 0$$

With some differential equations only one case arises; for instance, for Helmholtz's equation all boundary conditions are arbitrary so that the problem is of the first type. In the case of stresses, surface tractions must satisfy conditions of equilibrium and thus the problem is of the second type.

In case (ii) it is convenient to introduce a new function $\hat{g}_a$ which satisfies the same differential equation (4) and boundary conditions on the cylindrical surface (6a) as $\hat{g}$, but satisfies average conditions on the ends as follows:

$$\int_A \sum_{r=0}^{n-1} k_r(\partial^r \hat{g}_a/\partial x^r)dA = \int_A \left[G_{1,2} - \sum_{r=0}^{n-1}\sum_{m=0}^{\infty} k_r(\partial^r g_m/\partial x^r) \right] dA \quad \text{at} \quad x = 0, L \quad (6c)$$

Thus the difference $\hat{g} - \hat{g}_a$ satisfies conditions of type (i). In problems involving simultaneous equations, as for example in the stress problem, the average conditions which the approximate functions should satisfy are of a somewhat different form from that of (6c), and each case should be examined on its own merits.

The boundary-value problems for $\hat{g}$ in the first case, and for the difference $\hat{g} - \hat{g}_a$ in the second, are end problems in which each end can be examined separately; they are in a form to which Saint Venant's principle applies.

In general, Saint Venant's principle is a property of elliptic partial differential equations [8]. Thus in the first case mentioned, if the cylinder is long and since $\hat{g}$ satisfies homogeneous condi-

tions on the cylindrical surface and nonhomogeneous ones on the ends, then $\hat{g}$ decays rapidly into the interior and is approximated by zero in the region $h < x < L - h$; i.e., away from the ends of the beam. Similarly in the second case, since $\hat{g} - \hat{g}_*$ satisfies homogeneous conditions everywhere but on the ends, then $\hat{g}_*$ adequately approximates $\hat{g}$ everywhere away from the ends. It may sometimes happen in the second case (as it does in the present problem) that the right-hand side of equation (6c) is zero; in such a case $\hat{g}_* = 0$ is a good approximation to $\hat{g}$.

Thus in all problems where Saint Venant's principle can be formulated, approximations $\hat{g}_*$ of the type described in the foregoing are usually adequate. The end problem for $\hat{g}_*$ is usually less difficult to evaluate than that for the unknown functions themselves. For example, in problems involving Laplace's equation in two dimensions, the end problem reduces to a one-dimensional one [5], and in the stress problem, as will be shown in the following section, the end problem is trivial yielding $\hat{\sigma}_{ij} = 0$. It is in general impossible to formulate a Saint Venant's principle for differential equations which are not elliptic, although under certain conditions such a principle does apply [9]. However, a Saint Venant's principle can be formulated for the heat equation [5] and for similar problems defined by parabolic differential equations. Therefore it would appear that this method would be applicable to those problems as well.

Thermal Stresses and Displacements in Beams: General Theory

The problem investigated is that of an isotropic, homogeneous, linearly elastic, long, simply connected, cylindrical beam free of body forces and surface tractions, and subjected to an arbitrary temperature distribution. Inertia effects and thermoelastic coupling are considered negligible so that time enters only as a parameter.[4] The physical properties of the material are assumed independent of the temperature and the strain and rotation tensors are assumed small.

Stresses. *Governing Differential Equations.* The components σ_{ij} of the stress tensor must satisfy the following three equations of equilibrium (7) and six equations of compatibility (8):

$$\sigma_{ij,j} = 0 \tag{7}$$

$$(1+\nu)\sigma_{ij,kk} + \sigma_{kk,ij} = -E\alpha\left[\left(\frac{1+\nu}{1-\nu}\right)T_{,kk}\,\delta_{ij} + T_{,ij}\right] \tag{8}$$

where $_{,i} = \dfrac{\partial}{\partial x_i}$ and where ν is Poisson's ratio, E the modulus of elasticity, α the coefficient of thermal expansion, T the temperature change from quiescent condition, i, j, and k can each assume any of the values 1, 2, and 3, the summation convention over a repeated index applies, and δ_{ij} is the Kronecker delta. Let

$$\sigma_{ij} = \hat{\sigma}_{ij} + \sum_{m=0}^{\infty} (IJ)_m$$

$$f_{ij} = -E\alpha\left(\frac{1+\nu}{1-\nu}\,T_{,kk}\,\delta_{ij} + T_{,ij}\right) = \sum_{m=0}^{2} f_{ijm}$$

where $\hat{\sigma}_{ij}$ and $(IJ)_m$ are functions of the Cartesian co-ordinates

[4] These effects can be neglected when a characteristic thermal time (κ/L^2) is large compared to the natural period of the lowest bending mode of vibration (see reference [10], where additional references are given).

Table 1 Equations (9)—equilibrium and compatibility equations in expanded form

$\nabla_1^2 = \dfrac{\partial^2}{\partial x^2} + \dfrac{\partial^2}{\partial y^2}$

$(KK)_m = (XX)_m + (YY)_m + (ZZ)_m$

EQUILIBRIUM EQUATIONS FROM EQS. (7)				
EQ. NO.	m = 0	m ≥ 1		
$(9a_m)$	$(YY)_{0,y} + (YZ)_{0,z} = 0$	$(YY)_{m,y} + (YZ)_{m,z} = -(YX)_{m-1,x}$		
$(9b_m)$	$(YZ)_{0,y} + (ZZ)_{0,z} = 0$	$(YZ)_{m,y} + (ZZ)_{m,z} = -(ZX)_{m-1,x}$		
$(9c_m)$	$(YX)_{0,y} + (ZX)_{0,z} = 0$	$(YX)_{m,y} + (ZX)_{m,z} = -(XX)_{m-1,x}$		
COMPATIBILITY EQUATIONS FROM EQS. (8)				
	m = 0	m = 1	m = 2	m ≥ 3
$(9d_m)$	$\nabla_1^2(XX)_0 = -\left[E\alpha/(1-\nu)\right]\nabla_1^2 T$	$\nabla_1^2(XX)_1 = 0$	$(1+\nu)\nabla_1^2(XX)_2 = -\left[(KK)_0 + (1+\nu)(XX)_0 + 2E\alpha T/(1-\nu)\right]_{,xx}$	$(1+\nu)\nabla_1^2(XX)_m = -\left[(KK)_{m-2} + (1+\nu)(XX)_{m-2}\right]_{,xx}$
$(9e_m)$	$(1+\nu)\nabla_1^2(YY)_0 + (KK)_{0,yy} = -E\alpha\left(\frac{1+\nu}{1-\nu}\nabla_1^2 T + T_{,yy}\right)$	$(1+\nu)\nabla_1^2(YY)_1 + (KK)_{1,yy} = 0$	$(1+\nu)\nabla_1^2(YY)_2 + (KK)_{2,yy} = -(1+\nu)\left[(YY)_0 + E\alpha T/(1-\nu)\right]_{,xx}$	$(1+\nu)\nabla_1^2(YY)_m + (KK)_{m,yy} = -(1+\nu)(YY)_{m-2,xx}$
$(9f_m)$	$(1+\nu)\nabla_1^2(ZZ)_0 + (KK)_{0,zz} = -E\alpha\left(\frac{1+\nu}{1-\nu}\nabla_1^2 T + T_{,zz}\right)$	$(1+\nu)\nabla_1^2(ZZ)_1 + (KK)_{1,zz} = 0$	$(1+\nu)\nabla_1^2(ZZ)_2 + (KK)_{2,zz} = -(1+\nu)\left[(ZZ)_0 + E\alpha T/(1-\nu)\right]_{,xx}$	$(1+\nu)\nabla_1^2(ZZ)_m + (KK)_{m,zz} = -(1+\nu)(ZZ)_{m-2,xx}$
$(9g_m)$	$(1+\nu)\nabla_1^2(YZ)_0 + (KK)_{0,yz} = -E\alpha T_{,yz}$	$(1+\nu)\nabla_1^2(YZ)_1 + (KK)_{1,yz} = 0$	$(1+\nu)\nabla_1^2(YZ)_2 + (KK)_{2,yz} = -(1+\nu)(YZ)_{0,xx}$	$(1+\nu)\nabla_1^2(YZ)_m + (KK)_{m,yz} = -(1+\nu)(YZ)_{m-2,xx}$
$(9h_m)$	$\nabla_1^2(ZX)_0 = 0$	$(1+\nu)\nabla_1^2(ZX)_1 = -\left[(KK)_0 + E\alpha T\right]_{,zx}$	$(1+\nu)\nabla_1^2(ZX)_2 = -(KK)_{1,zx} - (1+\nu)(ZX)_{0,xx}$	$(1+\nu)\nabla_1^2(ZX)_m = -(KK)_{m-1,zx} - (1+\nu)(ZX)_{m-2,xx}$
$(9i_m)$	$\nabla_1^2(YX)_0 = 0$	$(1+\nu)\nabla_1^2(YX)_1 = -\left[(KK)_0 + E\alpha T\right]_{,yx}$	$(1+\nu)\nabla_1^2(YX)_2 = -(KK)_{1,yx} - (1+\nu)(YX)_{0,xx}$	$(1+\nu)\nabla_1^2(YX)_m = -(KK)_{m-1,yx} - (1+\nu)(YX)_{m-2,xx}$

x, y, and z and are such that $\hat{\sigma}_{ij} = \hat{\sigma}_{ji}$ and $(IJ)_m = (JI)_m$, and where f_{ijm} contain x-derivatives of order m only, x is the axial co-ordinate and y and z (unless otherwise noted) are arbitrary co-ordinates in the plane of the cross section of the beam. Substitution of the foregoing expressions for σ_{ij} and f_{ij} into equations (7) and (8) yields, in a manner analogous to that of the preceding section, an infinite number of sets of nine equations each. A typical set is given in Table 1, equations (9). Each set contains the six unknown functions $(IJ)_m$, each of which contains derivatives of T with respect to x of the single order m. The terms $\hat{\sigma}_{ij}$ must satisfy

$$\hat{\sigma}_{ij,j} = 0$$
$$(1 + \nu)\hat{\sigma}_{ij,kk} + \hat{\sigma}_{kk,ij} = 0 \tag{10}$$

Boundary Conditions. The boundary conditions for a traction-free body are

$$n_j\sigma_{ij} = 0 \quad \text{on the surface} \quad S \tag{11}$$

where n_j are the components of the unit normal vector to the surface.

Thus the boundary conditions for $(IJ)_m$ on a cylindrical surface $z = z_1(y)$, $z_2(y)$ with generators parallel to the x-axis are

$$n_y(YJ)_m + n_z(ZJ)_m = 0, \quad J = X, Y, Z \tag{12}$$

Conditions of the form of (12) must also be satisfied by $\hat{\sigma}_{ij}$ on the cylindrical surface, but, in addition, $\hat{\sigma}_{ij}$ must satisfy conditions (13) which follow. It should be noted that, as discussed in the preceding section, in view of the fact that x appears only as a parameter in the equations defining $(IJ)_m$, no boundary conditions can be given for $(IJ)_m$ at the ends ($x = 0, L$).

$$\hat{\sigma}_{rr} = -\sum_{m=0}^{\infty}(XX)_m; \quad \hat{\sigma}_{zz} = -\sum_{m=0}^{\infty}(ZX)_m;$$
$$\hat{\sigma}_{yz} = -\sum_{m=0}^{\infty}(YX)_m \tag{13}$$

Average conditions specifying no net load, moment, or torque on the ends ($x = 0, L$) are

$$\int_A \sigma_x dA = \int_A \sigma_x y\, dA = \int_A \sigma_x z\, dA = 0 \tag{14a}$$

$$\int_A \tau_{xs} dA = \int_A \tau_{yz} dA = \int_A (\tau_{xz}y - \tau_{yz}z) dA = 0 \tag{14b}$$

and apply for all x when the cylindrical surface is traction-free; these constitute the integral conditions referred to in case (ii) of the preceding main section.

If $(XX)_m$, $(ZX)_m$, and $(YX)_m$ satisfy, for all m, equations of the form of (14) with $(IJ)_m$ replacing σ_{ij} (which in fact they do), then $\hat{\sigma}_{ij}$ must also satisfy equations of that form with $\hat{\sigma}_{ij}$ replacing σ_{ij}. Thus $\hat{\sigma}_{ija} = 0$ satisfy equations of the form of (10, 12, 14) but not of (13), and the difference $\hat{\sigma}_{ij} - \hat{\sigma}_{ija}$ gives rise to self-equilibrating tractions at the ends. By Saint Venant's principle, as indicated in the preceding section, $\hat{\sigma}_{ija} = 0$ are adequate approximations to $\hat{\sigma}_{ij}$ away from the ends of the beam.

The problem described by equations (9, 10, 12, 13) is in the desired form. Its solution is presented in the next section.

Method of Solution. The nine equations ($9a_m$, b_m, . . ., i_m) of any set $m = 1, 2, \ldots$, yield the six unknown functions $(IJ)_m$ in terms of functions of lower subscripts; i.e., $(IJ)_p$ with $p < m$, which should have been determined beforehand and may therefore be considered known. The equations of each set separate into two groups; namely, equations ($9a_m$, b_m, d_m, e_m, f_m, g_m) and ($9c_m$, h_m, i_m) of Table 1. Only $(XX)_m$, $(YY)_m$, $(ZZ)_m$, and $(YZ)_m$ appear as unknown functions in the left-hand members of the first group while only $(ZX)_m$ and $(YX)_m$ so appear in the second. The quantities with lower subscripts appearing in the right-hand sides of the equations of either group are of both types, and consequently, a coupling arises between the groups.

It should be noted that for $m \geqslant 3$ the equations maintain their form and differ only in the subscript which denotes their position in the sequence. Thus for $m \geqslant 3$ there arises a set of recurrence equations for the unknown functions $(IJ)_m$.

The details of the solution which appear in Table 2 are presented in references [7] and [11]. The principal results are as follows:

(i) The equations of the first group are similar to those of plane strain and the ones of the second to those of the Saint Venant theory of torsion and bending. The solution to these equations are expressed in terms of stress functions for which boundary-value problems are formulated. Recurrence equations for the stress functions are given in Table 2.

(ii) The terms $\hat{\sigma}_{ij}$ are approximated adequately by $\hat{\sigma}_{ija} = 0$ in the region $h < x < L - h$ of a long beam ($h \ll L$), where h is the maximum linear dimension of the cross section and L the length of the beam.

(iii) The terms $(XX)_m$, $(YY)_m$, $(ZZ)_m$, and $(YZ)_m$ are zero for m = odd and $(ZX)_m$ and $(YX)_m$ are zero for m = even.

(iv) The (nonzero) terms $(IJ)_m$ are proportional to $(h/L)^m$ and are homogeneous linear functions of $\partial^m T/\partial\xi^m$ where $\xi = x/L$ (i.e., if T is replaced by CT, with C a constant, in any of these terms, then the resultant expression is the original one multiplied by C). Thus in view of items (ii) and (iii) σ_x, σ_y, σ_z, τ_{yz} have the form

$$\sum_{m=0,\,2,\,4,\,\ldots}^{\infty}(h/L)^m\mathfrak{L}_m(\partial^m T/\partial\xi^m)$$

and τ_{xz} and τ_{xy} have the form

$$\sum_{m=1,\,3,\,5,\,\ldots}^{\infty}(h/L)^m\mathfrak{L}_m(\partial^m T/\partial\xi^m)$$

where $\mathfrak{L}_m$ are linear operators in derivatives and integrals with respect to y and z only. This is the desired form of $\mathfrak{L}_m$ and is the one which dictated the choice of the functions $(IJ)_m$ and f_{ijm}. Thus if $h/L \ll 1$ and if T can be represented by a rapidly convergent power series, then the leading terms of the series will give adequate approximations to the stresses. Note that if T is of the form

$$T = \sum_{n=0}^{N} f_n(y, z)x^n,$$

i.e., a polynomial in the spanwise direction, then the series for all the stress components terminate after $N + 1$ terms.

It is interesting to note that if T is linear in a rectangular Cartesian co-ordinate system, then $(IJ)_m = 0$ for all m, and that if $T = T(y, z)$ is harmonic then the only nonzero term is $(XX)_0$ which becomes identical with the strength-of-materials formula.

(v) The first term $(XX)_0$ in the expansion of the normal axial stress σ_x, when the y and z-axes coincide with the centroidal principal axes of the cross section is

$$(XX)_0 = E\alpha\left[-T^* + (1/A)\int_A T^* dA + (y/I_z)\int_A T^* y\, dA + (z/I_y)\int_A T^* z\, dA\right] \tag{15}$$

where

$$T^* = T - (\nu/E\alpha)\nabla_1^2\phi_0$$

I_z and I_y are moments of inertia of any cross section about the z and y-axis, respectively, and A is the area of the cross section;

Table 2 Quantities $(IJ)_m$ in terms of stress functions ϕ_m and ψ_m; boundary-value problems for ϕ_m and ψ_m

m	0	1	2	ODD $m \geq 3$	EVEN $m > 3$
$(X\,X)_m$	$-E\alpha T + \nu\nabla_1^2\phi_0 + C_{01}(x,y) + C_{02}(x,z)$	0	$\nu\nabla_1^2\phi_2 + \int_0^y (YX)_{1,x}\,dy + \int_0^z (ZX)_{1,x}\,dz$ $-(1+\nu)\int_0^y\int_0^z (YZ)_{0,xx}\,dz\,dy + C_{21}(x,y) + C_{22}(x,z)$	0	$\nu\nabla_1^2\phi_m + \int_0^y (YX)_{m-1,x}\,dy + \int_0^z (ZX)_{m-1,x}\,dz$ $-(1+\nu)\int_0^y\int_0^z (YZ)_{m-2,xx}\,dz\,dy + C_{m1}(x,y) + C_{m2}(x,z)$
$(Y\,Y)_m$	$\phi_{0,zz}$	0	$\phi_{2,zz} - \int_0^y (yx)_{1,x}\,dy$	0	$\phi_{m,zz} - \int_0^y (yx)_{m-1,x}\,dy$
$(Z\,Z)_m$	$\phi_{0,yy}$	0	$\phi_{2,yy} - \int_0^z (zx)_{1,x}\,dz$	0	$\phi_{m,yy} - \int_0^z (zx)_{m-1,x}\,dz$
$(Y\,Z)_m$	$-\phi_{0,yz}$	0	$-\phi_{2,yz}$	0	$-\phi_{m,yz}$
$(Z\,X)_m$	0	$-\psi_{1,y}$	0	$-\psi_{m,y}$	0
$(Y\,X)_m$	0	$\psi_{1,z} - \int_0^y (xx)_{0,x}\,dy$	0	$\psi_{m,z} - \int_0^y (xx)_{m-1,x}\,dy$	0
BOUNDARY VALUE PROBLEMS FOR ϕ_m AND ψ_m	$\nabla_1^4\phi_0 = -\frac{E\alpha}{1-\nu}\nabla_1^2 T$ $\phi_0 = 0$ $\frac{\partial\phi_0}{\partial n} = 0$ } ON $Z = Z_1, Z_2$	$\nabla_1^2\psi_1 = \frac{1}{1+\nu}\int_0^y [(xx)_0 + E\alpha T]_{,zz}\,dy + C_{11}(x,z)$ $= -\frac{1}{1+\nu}\int_0^z [(xx)_0 + E\alpha T]_{,yy}\,dz +$ $+\int_0^y (xx)_{0,zz}\,dy + \int_0^z (xx)_{0,yy}\,dz + C_{12}(x,y)$ $d_1(\psi_1) = dz\int_0^y (xx)_{0,z}\,dy$ ON $Z = Z_1, Z_2$	$\nabla_1^4\phi_2 = \nabla_1^2\left[\int_0^y (yx)_1\,dy + \int_0^z (zx)_1\,dz + F_{0,x}\right]_{,x}$ $d_1(\phi_{2,y}) = dy\int_0^z (zx)_{1,x}\,dz$ $d_1(\phi_{2,z}) = dz\int_0^y (yx)_{1,x}\,dy$ } ON $Z = Z_1, Z_2$	$\nabla_1^2\phi_m = \int_0^y\left[(zx)_{m-2,x} + \frac{(xx)_{m-1,z}}{1+\nu}\right]dy + C_{m1}(x,z)$ $= -\int_0^z\left[(yx)_{m-2,x} + \frac{(xx)_{m-1,y}}{1+\nu}\right]_{,x}dz +$ $+\int_0^y (xx)_{m-1,z}\,dy + \int_0^z (xx)_{m-1,y}\,dz + C_{m2}(x,y)$ $d_1(\phi_m) = dz\int_0^y (xx)_{m-1,x}\,dy$ ON $Z = Z_1, Z_2$	$\nabla_1^4\phi_m = \nabla_1^2\left[\int_0^y (yx)_{m-1}\,dy + \int_0^z (zx)_{m-1}\,dz + F_{m-2,x}\right]_{,x}$ $d_1(\phi_{m,y}) = dy\int_0^z (zx)_{m-1,x}\,dz$ $d_1(\phi_{m,z}) = dz\int_0^y (yx)_{m-1,x}\,dy$ } ON $Z = Z_1, Z_2$
C_{m1}	$b_{00}(x) + b_{01}(x)y$	$H_{0,x}\Big\|_{y=0} + \frac{\nu}{1+\nu}b_{01,x}z + C_{13}(x)$	$(1+\nu)\int_0^y\int_0^y\{-(zx)_{1,xx} + \phi_{0,yyxx}$ $-\frac{1}{1+\nu}[(xx)_0 + E\alpha T]_{,xx}\}\Big\|_{z=0} dy\,dy + b_{20}(x) + b_{21}(x)y$	$\{H_{m-1,x} + [\nu\int_0^z (yx)_{m-2}\,dz + \nu\int_0^z\int_0^z (zx)_{m-2,y}\,dz\,dz$ $-\psi_{m-2} - \nu\int_0^z\int_0^z (yz)_{m-2,x}\,dz\,dz$ $-(1-\nu)\int_0^z F_{m-2,yx}\,dz]_{,xx}\}\Big\|_{z=0} +$ $+\frac{\nu}{1+\nu}b_{(m-1)1,x}z + C_{m3}(x)$	$(1+\nu)\int_0^y\int_0^y\{-(zx)_{m-1,xx} + \phi_{m-2,yyxx}$ $-\frac{(xx)_{m-2,xx}}{1+\nu}\}\Big\|_{z=0} dy\,dy + b_{m0}(x) + b_{m1}(x)y$
C_{m2}	$d_{00}(x) + d_{01}(x)z$	$H_{0,x}\Big\|_{z=0} - \frac{\nu}{1+\nu}d_{01,x}y + C_{13}(x)$	$(1+\nu)\int_0^z\int_0^z\{-(yx)_{1,yx} + \phi_{0,zzxx}$ $-\frac{1}{1+\nu}[(xx)_0 + E\alpha T]_{,xx}\}\Big\|_{y=0} dz\,dz + d_{20}(x) + d_{21}(x)z$	$\{H_{m-1,x} - [\nu\int_0^z (zx)_{m-2}\,dy + \nu\int_0^y\int_0^y (yx)_{m-2,z}\,dy\,dy$ $+\psi_{m-2} - \nu\int_0^y\int_0^z (yz)_{m-2,x}\,dy\,dy$ $-(1-\nu)\int_0^y F_{m-2,zz}\,dy]_{,xx}\}\Big\|_{z=0}$ $-\frac{\nu}{1+\nu}d_{(m-1)1,x}y + C_{m3}(x)$	$(1+\nu)\int_0^z\int_0^z\{-(yx)_{m-1,yz} + \phi_{m-2,zzxx}$ $-\frac{(xx)_{m-2,xx}}{1+\nu}\}\Big\|_{y=0} dz\,dz + d_{m0}(x) + d_{m1}(x)z$
$\nabla_1^2 F_m$	$(x\,x)_0 - \frac{\nu}{1+\nu}\left[(k\,k)_0 + \frac{2E\alpha T}{1-\nu}\right]$	0	$(x\,x)_2 - \frac{\nu}{1+\nu}(k\,k)_2$	0	$(x\,x)_m - \frac{\nu}{1+\nu}(k\,k)_m$
h_m	$E\alpha T + (1-\nu)\nabla_1^2\phi_0$	0	$(1-\nu)\left[\nabla_1^2\phi_2 - \int_0^y (yx)_{1,x}\,dy - \int_0^z (zx)_{1,x}\,dz - F_{0,xx}\right]$	0	$(1-\nu)\left[\nabla_1^2\phi_m - \int_0^y (yx)_{m-1,x}\,dy - \int_0^z (zx)_{m-1,x}\,dz - F_{m-2,xx}\right]$

$\nabla_1^2 = \frac{\partial^2}{\partial y^2} + \frac{\partial^2}{\partial z^2}$ $\qquad d_1 = \frac{\partial}{\partial y}dy + \frac{\partial}{\partial z}dz$

F_m IS A PARTICULAR SOLUTION, H_m IS THE HARMONIC CONJUGATE OF h_m, i.e. $H_{m,y} = h_{m,z}$ $\qquad H_{m,z} = -h_{m,y}$

$a_{m0} = b_{m0} + d_{m0}$, b_{m1} AND d_{m1} ARE DETERMINED FROM: $\int_A (xx)_m\,dA = \int_A (xx)_m\,y\,dA = \int_A (xx)_m\,z\,dA = 0$

C_{m3} IS DETERMINED FROM: $\int_A [z\phi_{m,z} + y\psi_{m,y}]\,dA = \int_A z\left[\int_0^y (xx)_{m-1,x}\,dy\right]dA$

ϕ_0 is a solution of a boundary-value problem of the first type, Table 2. For $\nu = 0$, the quantity $T^* = T$ and thus the term $(XX)_0$ and the normal axial stress σ_x of the strength-of-materials theory are identical. Clearly if the beam is long and if the higher spanwise derivatives of the temperature are small then the first term $(XX)_0$ will predominate and the Bernoulli-Euler hypothesis leads to good results.

Displacements. The displacements u_i satisfy the six equations

$$u_{j,i} + u_{i,j} = 2\epsilon_{ij} = (2/E)[(1+\nu)\sigma_{ij} - (\nu\sigma_{kk} - E\alpha T)\delta_{ij}] \tag{16}$$

The displacements u, v, and w, in the directions of the x, y, and z-axes, respectively, can be expressed in series form. In the case of stresses, the terms $(IJ)_m$ contained spanwise derivatives of the temperature of the single order m. In order to maintain this correspondence between subscript and order of derivatives, the displacement series must be chosen as follows:

$$u = \hat{u} + \sum_{m=-2}^{\infty} u_m, \qquad v = \hat{v} + \sum_{m=-2}^{\infty} v_m,$$

$$w = \hat{w} + \sum_{m=-2}^{\infty} w_m$$

To these expansions rigid-body motions may of course be added. The equations which the terms of these series satisfy are obtained from equations (16) in a manner completely analogous to that used in the case of the stresses. This is done in detail in references [7] and [11], where the equations are also integrated to yield u_m, v_m, and w_m in terms of the stresses. The equations in expanded form can be grouped in such a way that only the displacements u_{m+1}, v_m, w_m appear in the group. These displacements can be determined in terms of the stresses, and this determination does not require the knowledge of any other displacement. Each group consists of six equations in three unknown functions. The manipulations involved in showing that the equations are consistent prove to be quite similar to those employed in the case of stresses. For $m \geqslant 1$ the equations in any group form a set of recurrence equations for u_m, v_m, and w_m.

If rigid-body motions are omitted, the results of such an analysis of equations (16) will be:

(i) The terms $\hat{u}$, $\hat{v}$, and $\hat{w}$ are approximately zero in the region of a long beam ($h \ll L$) where the stresses $\hat{\sigma}_{ij}$ are approximately zero; i.e., in the region $h < x < L - h$.

(ii) The terms u_m are zero for m = even, and the terms v_m and w_m are zero for m = odd.

(iii) The terms u_m, v_m, and w_m are proportional to β^m, where $\beta = h/L$, and are homogeneous linear functions of $\partial^m T/\partial\xi^m$. Thus in view of (i) and (ii) u has the form

$$\sum_{m=-1,\,1,\,3\ldots}^{\infty} \beta^m \mathfrak{L}_m(\partial^m T/\partial\xi^m)$$

and v and w have the form

$$\sum_{m=-2,\,0,\,2,\ldots}^{\infty} \beta^m \mathfrak{L}_m(\partial^m T/\partial\xi^m)$$

where $\mathfrak{L}_m$ are linear operators in derivatives and integrals with respect to y and z only.

(iv) The first term in the expansion of the axial displacement is

$$u_{-1} = \int_0^x (a_{00} + b_{01}y + d_{01}z)dx/E$$

Table 3 Quantities $(IJ)_m$, u_m, v_m, and w_m in a right circular cylinder with $T = T(x)$

m	m=ODD	0	2	4	EVEN $m \geq 4$
$\overline{(XX)}_m$	0	0	$\gamma^2\bar{T}''(-2\rho^2+1)/4(1+\nu)$	$\gamma^4\bar{T}^{IV}(3\rho^4-6\rho^2+2)/48(1+\nu)$	$\gamma^m\bar{T}^{(m)}\sum_{j=0}^{m/2} S^j_{xxm}\rho^{2j}$
$\overline{(RR)}_m$	0	0	$\gamma^2\bar{T}''\nu(-\rho^2+1)/8(1+\nu)$	$\gamma^4\bar{T}^{IV}[(5-\nu)\rho^4+3(3-\nu)\rho^2-2(2-\nu)]/192(1+\nu)$	$\gamma^m\bar{T}^{(m)}\sum_{j=0}^{m/2} S^j_{rrm}\rho^{2j}$
$\overline{(\Theta\Theta)}_m$	0	0	$\gamma^2\bar{T}''\nu(-3\rho^2+1)/8(1+\nu)$	$\gamma^4\bar{T}^{IV}[-(11-5\nu)\rho^4+3(1-3\nu)\rho^2-2(2-\nu)]/192(1+\nu)$	$\gamma^m\bar{T}^{(m)}\sum_{j=0}^{m/2} S^j_{\theta\theta m}\rho^{2j}$
$\overline{(XR)}_{m-1}$	0	0	0	$\gamma^3\bar{T}'''(\rho^3-\rho)/8(1+\nu)$	$\gamma^{m-1}\bar{T}^{(m-1)}\rho\sum_{j=0}^{(m-2)/2} S^j_{xr(m-1)}\rho^{2j}$
$\overline{(R\Theta)}_m, \overline{(\Theta X)}_m$	0	0	0	0	0
$\bar{u}_{m-1}$	0	$\frac{1}{\bar{T}_0}\int\bar{T}\,d\xi$	$\frac{\gamma}{4}\left[\bar{T}'(-2\rho^2+1)(1-\nu)+\bar{T}'(0)(\nu\rho^2-1-\nu)\right]$	$\left[\gamma^3/96(1+\nu)\right]\left\{\bar{T}'''\left[3(\rho^4-2\rho^2)(1+\nu)(2-\nu)+2(2+2\nu-\nu^2)\right]+\bar{T}'''(0)(1-\nu)(2+\nu)\right\}$	$\gamma^{m-1}\left[\bar{T}^{(m-1)}\sum_{j=0}^{m/2} U_{x(m-1)}\rho^{2j} - \bar{T}^{(m-1)}(0)\sum_{j=0}^{m/2} U_{x(m-1)}\right]$
$\bar{v}_m$	0	$\bar{T}\rho$	$\gamma^2\bar{T}''\nu\rho(\rho^2-1)/8$	$\left[\gamma^4\bar{T}^{IV}\rho/192(1+\nu)\right]\left[-(1+\nu)^2\rho^4+3(1+\nu)^2\rho^2-2(2+\nu+\nu^2)\right]$	$\gamma^m\bar{T}^{(m)}\rho\sum_{j=0}^{m/2} U_r^j{}_m\rho^{2j}$ $m \geq 2$
$\bar{w}$	0	0	0	0	0

RECURRENCE EXPRESSIONS FOR S^j_{ijm}, U^j_{im}:

$$S^j_{xxm} = \left\{\left[\nu-2j(1+\nu)\right]\left[S^{j-1}_{xx(m-2)} - \nu S^{j-1}_{rr(m-2)}\right] - \left[\nu^2+2j(1+\nu)\right]S^{j-1}_{\theta\theta(m-2)} - 4j(j-1)(1+\nu)^2 S^{j-1}_{xr(m-1)}\right\}/4j^2(1+\nu) \qquad j \geq 1$$

$$S^0_{xxm} = \sum_{j=1}^{m/2} S^j_{xxm}/(j+1)$$

$$S^j_{rrm} = \left[S^{j-1}_{xx(m-2)} - \nu S^{j-1}_{rr(m-2)} - \nu S^{j-1}_{\theta\theta(m-2)} - 4j^2(1+\nu)S^{j-1}_{xr(m-1)}\right]/8j^2(j+1)(1+\nu) \qquad j \geq 1$$

$$S^0_{rrm} = -\sum_{j=1}^{m/2} S^j_{rrm}$$

$$S^j_{\theta\theta m} = \left\{(2j+1)\left[S^{j-1}_{xx(m-2)} - \nu S^{j-1}_{rr(m-2)} - \nu S^{j-1}_{\theta\theta(m-2)}\right] + 4j^2(1+\nu)S^{j-1}_{xr(m-1)}\right\}/8j^2(j+1)(1+\nu) \qquad j \geq 1$$

$$S^0_{\theta\theta m} = S^0_{rrm}$$

$$S^j_{xr(m-1)} = -S^j_{xx(m-2)}/2(j+1)$$

$$U^j_{x(m-1)} = S^j_{xxm} - \nu S^j_{rrm} - \nu S^j_{\theta\theta m} \qquad U^j_{rm} = -\nu S^j_{xxm} - \nu S^j_{rrm} + S^j_{\theta\theta m}$$

where a_{0i}, b_{0i}, and d_{0i} are functions of x, Table 2. Thus u_{-1} leaves plane sections plane.

Right Circular Cylinder Under Temperatures Varying Only With the Axial Co-ordinate

For the right circular beam under an axisymmetric temperature distribution, the use of cylindrical co-ordinates in conjunction with the method described in section, "Outline of Mathematical Procedure," leads to ordinary differential equations in the radial co-ordinate, with the axial co-ordinate appearing only as a parameter. The development is completely analogous to that of the preceding section and is therefore not repeated.

It should be noted that this problem could be approached as a special case of the general one of the preceding main section. However, such an approach has the disadvantage that in Cartesian co-ordinates the governing differential equations are of course partial in y and z. Furthermore, a transformation to cylindrical co-ordinates, which is quite cumbersome, gives rise, despite the axisymmetric nature of the problem, to partial differential equations in the radial and tangential co-ordinates. This result is due to the fact that, because of the nonhomogeneous nature of the expanded form of the equilibrium equations, e.g., equations ($9a_2$, b_2), the stresses $(IJ)_m$ had to be defined in terms of open integrals of stresses of lower subscript, e.g., $(IJ)_2$, Table 2, as well as in terms of the usual stress functions.

The ordinary differential equations which the terms $(IJ)_m$ satisfy can be readily integrated yielding the stresses in terms of multiple integrals of the temperature with respect to the radial co-ordinate, the order of which increases with m. These integrals can be evaluated once $T(x, r)$ is known. In the special case when T is independent of r, integration leads to expressions for $(IJ)_m$ in the form $P_{ij}{}^{m}(r)(d^mT/dx^m)$ where $P_{ij}{}^{m}(r)$ are polynomials in r of degree m. These polynomials for $m = 0, 1, 2, 3, 4$, and recurrence equations for their coefficients for $m \geqslant 3$ are given in Table 3 for $T = T(x)$ in nondimensional form with

$$\xi = x/L \qquad \rho = r/a \qquad \gamma = a/L \qquad \beta = h/L$$

$$\overline{T} = T/T_i \qquad ' = \frac{d}{d\xi} \qquad \overline{T}^{(m)} = d^m\overline{T}/d\xi^m$$

$$(\overline{IJ})_m = (1 - \nu)(IJ)_m/E\alpha T_i$$

where T_i is the base temperature from which temperature increments T are measured, r the radial co-ordinate, a the radius, and x the axial co-ordinate measured along the centroidal axis of the beam.

It should be noted that for this special temperature distribution the first two terms of all series are zero and that the next terms differ from zero if $\overline{T}''' \neq 0$; i.e., if the temperature is other than linear in x. Furthermore, the elementary theory predicts zero stresses for the present case and is thus of no use in determining the actual stresses in the beam.

The displacements are linear functions of the stresses. Thus in the present case the displacements like the stresses are polynomials in the radial co-ordinate. These polynomials for u_m, v_m, and w_m are given in Table 3 in nondimensional form with

$$\bar{u}_i = u_i/\alpha T_i a$$

A detailed analysis of the axisymmetric case and a brief examination of the more general problem of a right circular cylinder under an arbitrary temperature distribution appear in reference [7].

Discussion of Numerical Results

Figs. 1–4 present the results of numerical calculations which were conducted in order to illustrate the behavior of the series solution to the thermoelastic problem.

The problem investigated was that of a free right circular, cylindrical beam insulated all around and at one end, while the other end ($x = L$) is subjected to a time-dependent heat input q which is uniformly distributed over the cross section. The beam is initially at $T = 0$. The temperature $T(x, t)$ can be obtained by a Duhamel integral of the solution for a slab which is initially at $T = 0$ and which is insulated at one face while the other is subjected to a unit step heat input [12]. The temperature in nondimensional form is as follows:

$$\overline{T} = (1/\sqrt{\pi}) \sum_{j=0}^{\infty} \int_0^{\tau} [\bar{q}(\tau - \zeta)/\sqrt{\zeta}][e^{-(2j+1-\xi)^2/4\zeta} + e^{-(2j+1+\xi)^2/4\zeta}]\, d\zeta \quad (17)$$

$$\overline{T} = \int_0^{\tau} \bar{q}\, d\tau + 2 \sum_{j=1}^{\infty} (-1)^j (\cos j\pi\xi) e^{-j^2\pi^2\eta} \int_0^{\tau} \bar{q} e^{j^2\pi^2\eta} d\tau \quad (18)$$

where

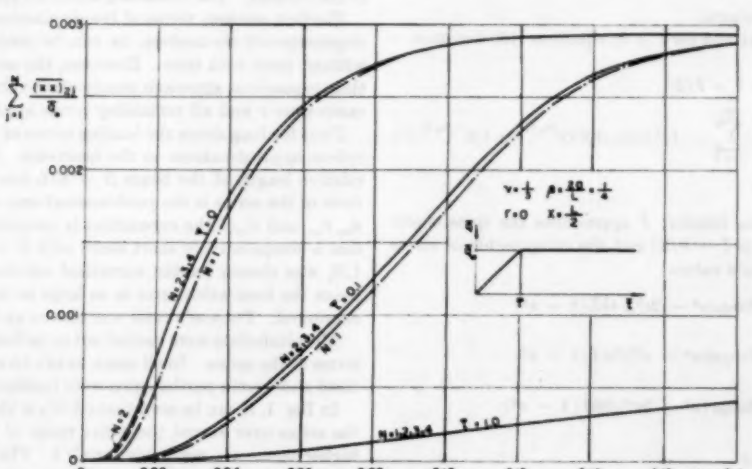

Fig. 1 Normal axial stress as a function of time; first four partial sums

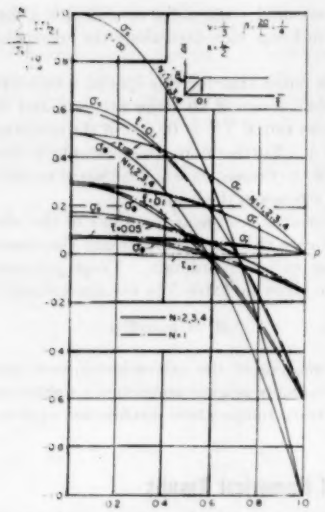

Fig. 2 Stress profiles across middle ($x = L/2$) cross section; first four partial sums

$$\bar{t} = t\kappa/L^2$$
$$\bar{q} = qL/kT_i$$
$$\kappa = k/\mu c$$

and where k is the thermal conductivity, c the specific heat, and μ the mass density. Equation (17) converges fast when $\bar{t}$ is small, and equation (18) converges fast when $\bar{t}$ is large.

Clearly the temperature is a function of time and of the axial co-ordinate only. This problem was chosen since for such a temperature distribution the strength-of-materials approach is of no use in calculating the actual stresses and a more general theory must be employed. The first term of the expansion for the normal axial stress as given by equation (15) and the strength-of-materials formula are quite similar in form and are both zero in the present problem. Thus the remaining terms in the expansion represent the actual stress.

A particular heat input was chosen, namely,

$$q(\bar{t}) = \begin{cases} q_0 \bar{t}/\bar{\tau} & 0 \leqslant \bar{t} \leqslant \bar{\tau} \\ q_0 & \bar{t} \geqslant \bar{\tau} \end{cases}$$

where q_0 and $\bar{\tau}$ are constants.

For such a heat input and for $\bar{t} \geqslant \bar{\tau}$, equation (18) becomes

$$\bar{T} = \bar{q}_0[(3\bar{x}^2 - 1)/6 + \bar{t} - \bar{\tau}/2 - (2/\pi^4\bar{\tau}) \sum_{j=1}^{\infty} (-1)^j (\cos j\pi\bar{x})(e^{j^2\pi^2\bar{\tau}} - 1)e^{-j^2\pi^2\bar{t}}/j^4]$$

where $\bar{\tau} = \tau\kappa/L^2$.

Thus as $\bar{t}$ approaches infinity, $\bar{T}$ approaches the quasi-static value $\bar{q}_0[(3\bar{x}^2 - 1)/6 + \bar{t} - \bar{\tau}/2]$ and the components of stress approach the steady-state values

$$\lim_{\bar{t}\to\infty} \sigma_x = E\alpha q_0(a^2 - 2r^2)/4kL(1 - \nu^2)$$

$$\lim_{\bar{t}\to\infty} \sigma_r = E\alpha q_0\nu(a^2 - r^2)/8kL(1 - \nu^2)$$

$$\lim_{\bar{t}\to\infty} \sigma_\theta = E\alpha q_0\nu(a^2 - 3r^2)/8kL(1 - \nu^2)$$

$$\lim_{\bar{t}\to\infty} \tau_{xr} = 0$$

$$\tau_{r\theta} = \tau_{\theta x} = 0 \text{ for all } \bar{t}$$

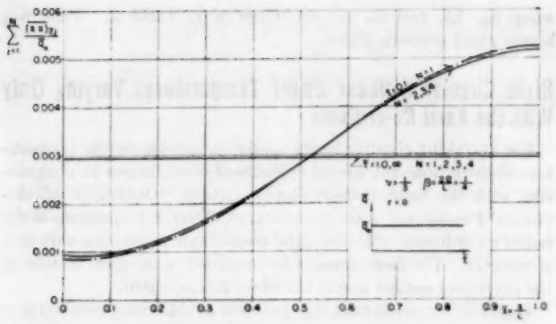

Fig. 3 Normal axial stress distribution along beam axis; first four partial sums

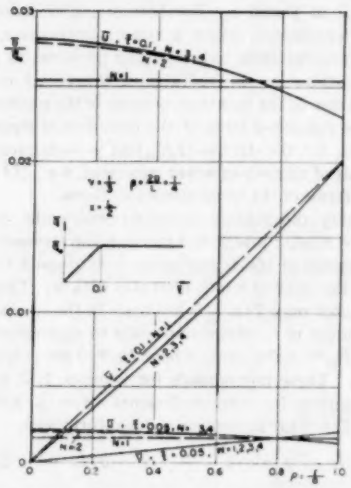

Fig. 4 Displacement profiles across middle ($x = L/2$) cross section; first four partial sums

Clearly the steady-state values of the stresses are independent of x and τ but are nevertheless functions of r. These values are the steady-state values of the first nonzero terms of the expansions of the stresses. The remaining terms all approach zero.

The first nonzero terms of the displacements and therefore the displacements themselves, as can be seen from Table 3, grow without limit with time. However, the second nonzero terms of their expansions approach steady-state values independent of the ramp-time τ and all remaining terms approach zero.

Thus for long times the leading terms of the expansions are excellent approximations to the functions. For shorter times, the relative length of the beam $\beta = h/L$ has some effect on which term of the series is the predominant one, since each term $(\bar{I}J)_m$, $\bar{u}_m$, $\bar{v}_m$, and $\bar{w}_m$ of the expansions is proportional to β^m. Therefore a comparatively short beam with $\beta = 1/4$, i.e., $\gamma = a/L = 1/8$, was chosen for the numerical calculations, since in such a beam the truncation error is as large as would ordinarily be encountered. Poisson's ratio was chosen as $\nu = 1/3$.

All calculations were carried out to include the first four nonzero terms of the series. In all cases, as can be seen from Figs. 1–4, the third and fourth partial sums were indistinguishable.

In Fig. 1, it can be seen that $(XX)_2$ is the predominant term of the series over almost the entire range of time, while $(XX)_3$ and higher terms are negligible for all $\bar{t}$. The second nonzero term $(XX)_4$ is the predominant one for very short times, but then the stresses are small and unimportant. Thus even in a relatively

short beam ($\beta = 1/4$) the first nonzero term is an adequate approximation to the stress σ_x in the interval where that stress is of any importance. In longer beams $\beta < 1/10$, the term $(XX)_4$ becomes smaller than $(XX)_2$, which thus predominates. From Fig. 2 it is also clear that even with $\beta = 1/4$, the first nonzero terms $(IJ)_2$ predominate over the entire cross section. From Fig. 3 it can be seen that the first nonzero term predominates for the entire length of the beam. Together, Figs. 1, 2, and 3 show that at steady state the stress is independent of x and τ.

Fig. 4 is a nondimensional plot of the displacement profiles across the middle cross section, corresponding to the stress profiles of Fig. 2. Again, for long beams the leading terms are adequate approximations to the actual displacements.

References

1 T. von Karman, "Ueber die Grundlagen der Balkentheorie," Abh. Aerodynam. Inst. Tech. Hochschule Aachen, vol. 7, 1927, p. 3.

2 F. Seewald, "Die Spannungen und Formaenderungen von Balken mit rechteckigem Querschnitt," Abh. Aerodynam. Inst. Tech. Hochschule Aachen, vol. 7, 1927, p. 11.

3 L. H. Donnell, "Bending of Rectangular Beams," JOURNAL OF APPLIED MECHANICS, vol. 19, TRANS. ASME, vol. 74, 1952, p. 123.

4 E. Almansi, "Sopra la deformazione dei cilindri sollecitati lateralmente," *Atti delli Reale Academia Dei Lincei*, Rendiconti, series 5, vol. 10, May 5, 1901, pp. 333–338.

5 B. A. Boley, "The Determination of Temperature, Stresses, and Deflections in Two-Dimensional Thermo-Elastic Problems," *Journal of the Aeronautical Sciences*, vol. 23, 1956, pp. 67–75.

6 B. A. Boley and I. S. Tolins, "On the Stresses and Deflections of Rectangular Beams," JOURNAL OF APPLIED MECHANICS, vol. 23, TRANS. ASME, vol. 78, 1956, pp. 339–342.

7 E. S. Barrekette, "Thermoelastic Stresses in Beams," Doctoral Dissertation, Faculty of Pure Science, Columbia University, January, 1959, LC Card No. Mic 59-2571.

8 B. A. Boley, "Some Observations on Saint Venant's Principle," Proceedings, Third U. S. National Congress of Applied Mechanics, New York, N. Y., 1958, pp. 259–264.

9 B. A. Boley, "Application of Saint Venant's Principle in Dynamical Problems," JOURNAL OF APPLIED MECHANICS, vol 22, TRANS. ASME, vol. 77, 1955, pp. 204–206. Also "On a Dynamical Saint Venant Principle," JOURNAL OF APPLIED MECHANICS, vol. 27, TRANS. ASME, vol. 81, series E, 1960, pp. 74–78.

10 B. A. Boley, "Thermal Stresses," Proceedings First Symposium on Naval Structural Mechanics, Pergamon Press, New York, N. Y., 1960.

11 E. S. Barrekette, "Thermoelastic Stresses in Beams," WADC Technical Report 59-178, ASTIA Document No. AD 213475, February, 1959.

12 H. S. Carslaw and J. C. Jaeger, "Conduction of Heat in Solids," Oxford University Press, London, England, 1947.

13 J. N. Goodier, "On the Problems of the Beam and Plate in the Theory of Elasticity," Transactions of the Royal Society of Canada, Third Series, vol. 32, sect. III, 1938, pp. 65–88.

C. C. CHANG
Professor of Fluid Mechanics,
Department of Aeronautical Engineering,
Institute of Technology,
University of Minnesota,
Minneapolis, Minn.

I. K. EBCIOGLU
Research Associate,
Department of Aeronautical Engineering,
Institute of Technology,
University of Minnesota,
Minneapolis, Minn.

Elastic Instability of Rectangular Sandwich Panel of Orthotropic Core With Different Face Thicknesses and Materials[1]

This paper treats the instability of rectangular sandwich panels with nonisotropic cores and faces of different materials or thicknesses. The simply supported panel is loaded with a uniform edge compression. The solution is expressed in terms of a major buckling coefficient, given as the ratio of the critical lateral buckling load to the critical cylindrical buckling load, which is a function of several nondimensional parameters. A single family of curves shows the buckling behavior for all parameters. The effect of a moderate temperature differential between the two faces can be approximately considered by modifying their moduli of elasticity in accordance with their temperature levels. Besides the regular panel instability, a zone of core shear instability is determined and discussed in detail. Numerical examples are presented to illustrate the application of the analysis.

RECENTLY, a great deal of theoretical effort has been devoted to buckling and bending of a homogeneous isotropic-cored sandwich panel with identical faces. Among others, Reissner's theory [1][2] with the complementary energy method and the Hoff-Eringen [3, 4] theory with the variational method should be mentioned.

The simplifying assumptions made in some of the early theories were, however, found to be inadequate to explain the behavior of aircraft sandwich structures, as indicated by the experiments of Kuenzi [14]. For example, in a sandwich panel with a honeycomb core the modulus of rigidity in the longitudinal direction of the core may be 2.5 times as much as that in the crosswise direction. Also, the ultimate shear stresses in the two directions mentioned are quite different. The assumption of the isotropic core cannot be applied without introducing appreciable error, particularly for a core weak in transverse shear.

As an added complication, the two faces may be of different thicknesses and/or materials in many applications. Furthermore, the exposed outer face of the sandwich panel may be subjected to a much higher temperature than the inner face, owing to the hot jet blast or aerodynamic heating. Such high temperature may weaken the material of the outer face, particularly by reducing its modulus of elasticity. Therefore a revision of existing theories seems necessary to take into account the practical features of sandwich structures in high-speed aircraft. In accordance with practical considerations for sandwich structures, the core will be regarded as being relatively weak under edge compression and bending, although it is favorably strong in taking transverse shear and compression. Therefore the Reissner-Hoff assumption [1, 3] of a weak core, which simplifies the analysis substantially, will be adopted as the basis of the present theory.

Regarding nonisotropic sandwich panels, Libove and Batdorf [2] considered the sandwich panel approximately as a nonisotropic thick plate and extended the classical thin-plate theory [5] to sandwich panels by introducing effective bending and shear rigidities and by including shear deflection. Their formulation regards the faces as membranes and involves a sixth-order

[1] This work is sponsored by the United States Air Force Office of Scientific Research under Contract No. AF 18(603)-112.

[2] Numbers in brackets designate References at end of paper.

Presented at the Summer Conference of the Applied Mechanics Division, University Park, Pa., June 20–22, of THE AMERICAN SOCIETY OF MECHANICAL ENGINEERS.

Discussion of this paper should be addressed to the Secretary, ASME, 29 West 39th Street, New York, N. Y., and will be accepted until October 10, 1960, for publication at a later date. Discussion received after the closing date will be returned. Manuscript received by ASME Applied Mechanics Division, April 30, 1959. Paper No. 60—APM-26.

Nomenclature

$D = \dfrac{Et^3}{12(1-\mu^2)}$ flexural rigidity

E = Young's modulus

$f = (t' + t'')/2$

G = shear modulus

$\varrho = \bar{G}_x/\bar{G}_y$ core shear rigidity ratio

$\bar{H}_y = \bar{G}_y\bar{l}$ shear stiffness

h_1, h_2 = distance from neutral plane of sandwich panel to middle of thickness of lower and upper faces, respectively

$k = N_{xy}/P_0$, edge buckling coefficient; equation (5e)

$k_1 = k - \hat{k}$ = major buckling coefficient

$\hat{k} = \dfrac{P_f}{P_0}\dfrac{(1+\beta^2)^2}{\beta^2}$, face buckling coefficient

$m = t'E'/t''E''$, ratio of extensional stiffness of lower face to that of upper one

$M_{\alpha\beta}$ = intensity of external moments applied at panel edge

n = number of half waves in direction of load

$N_{\alpha\beta}$ = loading intensity applied at panel edge

$P_f = \left(\dfrac{\pi}{L_x}\right)^2 \dfrac{E't'^3 + E''t''^3}{12(1-\mu^2)}$, sum of one fourth of buckling loads per unit width of both faces of a panel which is loaded along $y = 0$, $y = L_y$ and with $L_y \to \infty$

$P_0 = \dfrac{\pi^2\alpha^2\bar{l}^2t'E'}{(1-\mu^2)(1+m)}$, one fourth of buckling load per

(Continued on next page)

Table 1 Maxima and minima data

	Point	β	k_1	r
Minima	1	0.34881	1.94205	0.52
	2	0.41266	2.00162	0.50
	3	0.50470	2.14952	0.45
	4	0.57442	2.30504	0.40
	5	0.63565	2.46073	0.35
	6	0.69234	2.64539	0.30
	7	0.74629	2.83255	0.25
	8	0.79849	3.03335	0.20
Maxima	1′	0.25221	1.94310	0.52
	2′	0.19377	2.01331	0.50
	3′	0.11037	...	0.45
	4′	0	2.50000	0.40

partial differential equation for each variable. This approach is more applicable to sandwich with a strong core than to that with a weak one. No specific solution was given.

Following the formulation of Libove and Batdorf, Robinson [17], in 1955, obtained solutions for buckling and bending of simply supported orthotropic sandwich panels with identical faces. In recent years, a large number of reports from the Forest Products Laboratory on the same subject were published by March [6], Ericksen and March [7], Raville [10], Norris [11], and Kimel [12]. Some of their work on isotropic core has been adopted as standards for military aircraft in the United States [13]. Their approach, however, is limited to the sandwich panel with different face thicknesses but always with the same material, and is difficult to apply to two faces with different temperatures or materials.

The present work extends Hoff's theory [3] to the sandwich panel with a nonisotropic core, different face thicknesses, and different material properties. A temperature gradient across the sandwich panel may also cause a change in the material properties. Thus the theory can include indirectly the effect of a difference in temperature of the two faces. It is interesting to note that different face thicknesses and different material properties affect the major buckling coefficient simply through the parameter P_0. It is believed that the present theory takes into account the primary effect of temperature upon the major buckling coefficient. A set of numerical examples is given in Table 2 to demonstrate the practical application of the theory.

This paper contains the essential results of a lengthy report [20] by the authors.

Assumptions

1 Face Materials:

(*a*) Two faces are of different materials and thicknesses and may be under different temperatures.

(*b*) Poisson's ratios of the faces are the same.

(*c*) No local buckling of the face is allowed to occur within each core cell.

2 Core Material:

(*a*) Transverse shear rigidity of the core along the panel length may be different from that across its width, i.e., $G_x \neq G_y$

(*b*) The core material is so weak in comparison with the face materials that normal stresses and moduli of elasticity in the core can be neglected in the plane of the sandwich. Therefore the core is not considered to carry any bending moment.

(*c*) The core is not considered to carry shear stress in the plane of the panel, leaving the full share to the faces.

(*d*) The deflection due to transverse shear is considered only for the core, but not for the faces. The shear stresses in the transverse direction are uniform across the core.

(*e*) The core is strong enough to take the transverse load and handling loads.

(*f*) Nonhomogeneity of the core cells is neglected, provided that the panel is many times larger than the core cells.

3 Bond:

(*a*) All the bonds are strong enough so that under all loadings no bond failure will occur and stresses can be transmitted without discontinuity.

4 Loading:

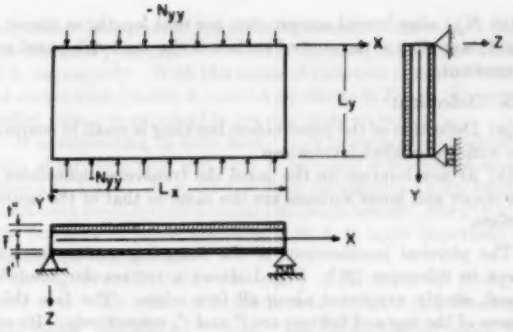

Fig. 1 Simply supported sandwich panel under edge compressions

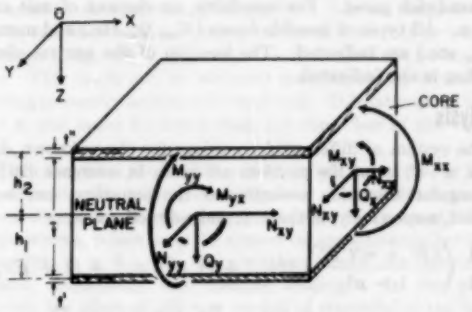

Fig. 2 Resultant forces (N_{xx}, N_{yy}, N_{xy} Q_x, Q_y) and moments (M_{xx}, M_{yy}, M_{xy}) acting on a sandwich element of unit area

Nomenclature

unit width in a sandwich panel with rigid core which is loaded along $y = 0$, $y = L_y$ and with $L_y \to \infty$

Q_α = intensity of transverse shear

$r = P_0/\hat{l}^2\bar{H}_y$, core shear stiffness parameter for sandwich plate

t = face thickness

l = core thickness

$\hat{l} = (l + f)/l$

u, v, w = face displacements in x, y, and z-directions, respectively

$\alpha = l/L_x$ core thickness ratio

$\beta = L_y/nL_x$, wave-pattern aspect ratio

$\nabla^4 = \dfrac{\partial^4}{\partial x^4} + 2\dfrac{\partial^4}{\partial x^2 \partial y^2} + \dfrac{\partial^4}{\partial y^4}$, biharmonic operator

μ = Poisson's ratio of face material

$\rho_1 = (1 + m)\hat{l}/2$

$\tau_{\alpha\beta}$ = stress tensor

Superscripts

′ lower face

″ upper face

(*a*) N_{yy}, edge lateral compression per unit length, as shown in Fig. 1, is applied at the neutral surface of the sandwich panel and is constant.

5 Deflection:

(*a*) Deflection of the panel before buckling is small in comparison with the sandwich thickness.

(*b*) At any location on the panel the transverse deflections of the upper and lower surfaces are the same as that of the neutral surface.

The physical justifications of the foregoing assumptions are given in reference [20]. Fig. 1 shows a rectangular sandwich panel, simply supported along all four edges. The face thicknesses of the top and bottom are t'' and t', respectively. Its core thickness is l. An edge compression loading, N_{yy}, is applied along two opposite edges as shown. Fig. 2 shows an element of the sandwich panel. For simplicity, an element of unit size is drawn. All types of possible forces (N_{xx}, Q_x, etc.) and moments (M_{xx}, etc.) are indicated. The location of the neutral plane in bending is also indicated.

Analysis

The system of differential equations for the unknown deflections, u', v', w, of the problem are given in reference [20]. In rectangular Cartesian co-ordinates the equations can be expressed, respectively, in the x, y, and z-directions as

$$-\frac{1}{2}\left(\frac{t'E'+m^2t''E''}{1-\mu^2}\right)[2u_{xx}'+(1-\mu)u_{yy}'+(1+\mu)v_{xy}'] + \frac{1+m}{l}\overline{H}_x\left[\frac{1+m}{l}u'+\hat{l}w_x\right]=0 \quad (1a)$$

$$-\frac{1}{2}\left(\frac{t'E'+m^2t''E''}{1-\mu^2}\right)[2v_{yy}'+(1-\mu)v_{xx}'+(1+\mu)u_{xy}'] + \frac{1+m}{l}\overline{H}_y\left[\frac{1+m}{l}v'+\hat{l}w_y\right]=0 \quad (1b)$$

$$(D'+D'')\nabla^4 w-\hat{l}\overline{H}_x\left(\frac{1+m}{l}u_x'+\hat{l}w_{xx}\right) -\hat{l}\overline{H}_y\left(\frac{1+m}{l}v_y'+\hat{l}w_{yy}\right) + N_{xx}w_{xx}+2N_{xy}w_{xy}+N_{yy}w_{yy}=0 \quad (1c)$$

For the special case considered here, $N_{xx}=N_{xy}=0$, which removes two terms from equation (1*c*). The simplified set of equations is the basis of the solution.

Boundary conditions. The boundary conditions are obtained for a simply supported panel from reference [20]. They consist of the following elastic boundary conditions:

$$u_x'+\mu v_y'=0 \qquad x=0 \text{ and } x=L_x \quad (2a)$$

$$v_y'+\mu u_x'=0 \qquad y=0 \text{ and } y=L_y \quad (2b)$$

$$u'=0 \qquad y=0 \text{ and } y=L_y \quad (2c')[3]$$

$$v'=0 \qquad x=0 \text{ and } x=L_x \quad (2c'')[3]$$

$$w_{xx}+\mu w_{yy}=0 \qquad x=0 \text{ and } x=L_x \quad (2d)$$

$$w_{yy}+\mu w_{xx}=0 \qquad y=0 \text{ and } y=L_y \quad (2e)$$

together with appropriate boundary conditions; i.e.,

$$w=0, \quad x=0, \quad x=L_x, \quad y=0, \quad \text{and } y=L_y \quad (2f)$$

Solution and buckling criterion for simply supported panel. In order to satisfy the three differential equations in equations (1), and the sixteen boundary conditions in equations (2), the solutions of u', v', and w can be taken as

$$u'=C_1\cos\frac{\pi x}{L_x}\sin\frac{n\pi y}{L_y}$$

$$v'=C_2\sin\frac{\pi x}{L_x}\cos\frac{n\pi y}{L_y} \quad (3)$$

$$w=C_3\sin\frac{\pi x}{L_x}\sin\frac{n\pi y}{L_y}$$

where C_1, C_2, and C_3 are three unknown constants to be evaluated. Substituting the foregoing assumed solutions in equation (1), we obtain three simultaneous algebraic relations for C_1, C_2, and C_3. These results can be expressed as the following matrix equation:

$$\begin{bmatrix} 2+\frac{1-\mu}{\beta^2}+\frac{2g}{r} & \frac{1+\mu}{\beta} & \pi\frac{\hat{l}^2g}{\rho_1 r}\alpha \\ \frac{1+\mu}{\beta} & \frac{2}{\beta^2}+1-\mu+\frac{2}{r} & \pi\frac{\hat{l}^2}{\rho_1 r\beta}\alpha \\ \frac{2}{\pi}\frac{g\rho_1}{r}\alpha & \frac{2}{\pi}\frac{\rho_1}{r\beta}\alpha & \left(\frac{g}{r}+\frac{1}{r\beta^2}-\frac{k_1}{\beta^2}\right)\hat{l}^2\alpha^2 \end{bmatrix}\begin{bmatrix} C_1 \\ C_2 \\ C_3 \end{bmatrix}=0 \quad (4)$$

The important physical parameters, defined in the following equations, should be explained more in detail

$$P_0=\frac{\pi^2\hat{l}^2\alpha^2}{1-\mu^2}\frac{t'E'}{1+m}, \quad (5a)$$

$$P_f=\left(\frac{\pi}{L_x}\right)^2(D'+D''), \quad (5b)$$

$$r=\frac{P_0}{\hat{l}^2\overline{H}_y}, \quad (5c)$$

$$\hat{k}=\frac{P_f}{P_0}\left(\frac{1}{\beta}+\beta\right)^2 \quad (5d)$$

$$k_1=k-\hat{k} \quad (5e)$$

P_0 in equation (5*a*) is one fourth of the buckling load per unit width for a sandwich panel with a rigid core loaded along $y=0$, $y=L_y$, and $L_y\to\infty$. P_f is the contribution of the bending rigidity of the two faces to the total buckling load N_{yy}. It is only a small fraction of N_{yy} and can be neglected except in

[3] These are Hoff's approximate boundary conditions which are introduced to replace the corresponding exact boundary conditions $u_y'+v_x'=0$, $x=0$, $x=L_x$, $y=0$, $y=L_y$, (2*c*).

the case where the core is extremely weak in transverse shear, and then P_f will share a certain portion of the load. In equation (4), P_0 is chosen as a standard to compare P_f, N_{yy}, and H_y.

Now we are to evaluate C_1, C_2, and C_3. The nontrivial solutions of C in the foregoing three homogeneous algebraic equations occur when, and only when, the square matrix in equation (4) is zero.[4]

If the geometric and material characteristics of the sandwich panel are specified, the parameters α, β, $\bar{t}$, g, ρ, and $\hat{k}$ are known constants. The only unknown is the buckling coefficient k ($=N_{yy}/P_0$). After some algebraic manipulation, k_1 can be shown from equation (4) to be

$$k_1 = \frac{(1+\beta^2 g)[(1-\mu)(1+\beta^2)^2 r + 2\beta^2(g+\beta^2)] - 2\beta^4(1-g)^2}{[(1-\mu)(1+\beta^2)^2 r + 2\beta^2(g+\beta^2)]r + \beta^2[(1-\mu)(1+\beta^2 g)r + 2\beta^2 g]} \tag{6}$$

Some physical interpretations of $\hat{k}$ and k_1 are needed. The parameter $\hat{k} = (P_f/P_0)(\beta + 1/\beta)^2$ is called the face buckling coefficient because it is essentially the ratio of the buckling load of the faces P_f to the cylindrical buckling load P_0. For the case, $r \ll 1$, $\hat{k}$ is much smaller than k_1 and can be neglected. However, for the sandwich panel with very weak core ($r \geq 1$), the omission of $\hat{k}$ may cause appreciable error and may not be justified as given in some previous works [1, 15]. The major buckling coefficient k_1 as defined in equation (6) is a function of a number of material parameters (such as g, μ, r) and geometrical parameters (such as α, β, $\bar{t}$). It is difficult to interpret directly from the equation.

To illustrate the usefulness of equation (6), Fig. 3 shows the major buckling coefficient k_1 versus the panel aspect ratio $n\beta$ for different values of the core shear rigidity parameter r. According to Kuenzi's [14] experiments, the ratio of moduli of rigidity $g = \bar{G}_x/\bar{G}_y$ for typical corrugated honeycomb core is about 2.5 if the direction of $\bar{G}_x$ is parallel to the core corrugations. If the direction of $\bar{G}_x$ is perpendicular to the core corrugations, $g = 0.4$. For expanded honeycomb core, his experiments show that for $\bar{G}_x$ parallel and perpendicular to the cell corrugations, g is 1.67 and 0.6, respectively. With this range of variation in mind, three sets of curves with $g = 2.5$, 1, and 0.4 are shown in Fig. 3. For square-celled core, g is expected to be very close to unity.

It is interesting to note that $r = 0$ corresponds physically to zero shear deflection and that k_1 becomes independent of g, as shown in Fig. 3. Also, for $r = 0$, k_1 corresponds to the buckling coefficient given by the classical thin-plate theory. For $0 < r < 1$, the influence of finite values of g on k_1 is quite important and should not be neglected.

In Fig. 3, let us follow the curve of k_1 versus $n\beta$ ($=L_y/L_x$) for $r = 0$. The value of k_1 is lowest for $n\beta = 1$ and rises higher and higher until $L_y/L_x = 1.42$. For L_y/L_x slightly larger than 1.42, the lowest value of k_1 is no longer located on the curve of $n = 1$ but lies on that of $n = 2$. Similar phenomena are well discussed in classical thin-plate theory. For the range $0 < r < 0.5$, k_1 decreases with increasing values of r, no matter what the value of L_y/L_x. As $L_y/L_x \to 0$, $k_1 \to 1/r$ in the limit for any value of g. This result can be obtained mathematically by taking a limiting process of equation (6) as $\beta \to 0$. It is interesting to note that k_1 can never be larger than $1/r$ regardless of the value of L_y/L_x.

When the faces are of different materials, no available theory can estimate the critical buckling load of a sandwich panel in practical application. For a sandwich panel with faces at different temperatures, which may be caused by aerodynamic heating or proximity to a hot jet, no available theory can predict the stresses, deflections, and collapse loadings. In the present analysis, the effect of different moduli of elasticity of the faces is included in P_0 in equation (5a). Until more exact theory is available, it is expected that the present theory can be applied to both faces of different materials and faces of different temperatures, as long as the temperature difference and the thermal warpage is small.

Equation (5c) shows that r is a function of P_0 and therefore is a function of $m = t'E'/t''E''$. In effect, the single family of curves in Fig. 3 covers all varieties of face materials and thicknesses, core properties, panel-aspect ratios, and number of half waves. This is a simple result and especially convenient for preliminary design.

In Fig. 3 the curves for different values of g ($g = 1$ — isotropic core, $g = 0.4$, and $g = 2.5$) are quite similar in general behavior. The major buckling coefficient k_1 always decreases with g.

For preliminary design, it is important to know $(k_1)_{min}$ versus r for different values of g. Therefore, the locus of $(k_1)_{min}$ versus r for $g = 2.5$, 1.0, and 0.4 of Fig. 3 are replotted in Fig. 4. It is interesting to note that for $r < 1/2$ and $g = 2.5$, the general

[4] See theorem in J. V. Uspensky, "Theory of Equations," McGraw-Hill Book Company, Inc., New York, N. Y., 1948, p. 235.

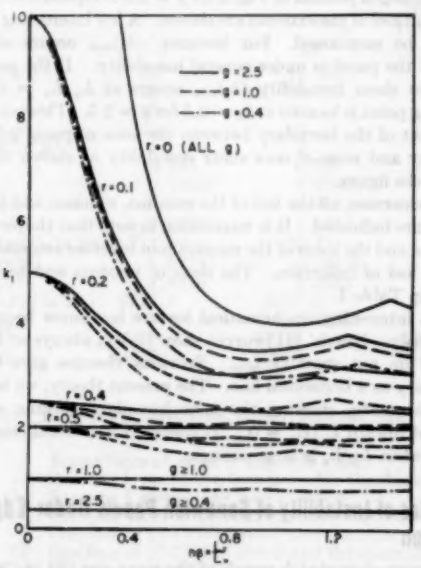

Fig. 3 Major buckling coefficients k_1 versus $n\beta(=L_y/L_x)$ at different values of $r(=P_f/\hat{t}^2H_y)$

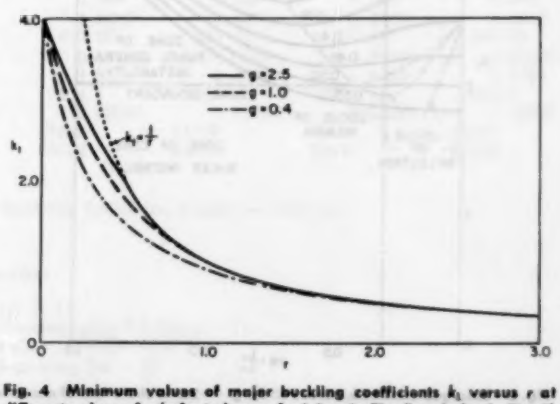

Fig. 4 Minimum values of major buckling coefficients k_1 versus r at different values of g (refer to locus of minima in Fig. 5 and also in Fig. 3)

instability of the panel occurs, while for $r > 1/2$ core shear instability occurs and $(k_1)_{min}$ coincides with the curve of $1/r$. Similar regimes occur for $g = 1.0$ and $g = 0.4$.

When the face materials are not the same, the following formulas can be used in order to determine the face stresses for a given N_{yy} as long as the panel does not buckle and has no initial curvature:

$$\tau_{yy}' = \frac{m}{1+m}\frac{N_{yy}}{t'}; \quad \tau_{yy}'' = \frac{1}{1+m}\frac{N_{yy}}{t''} \tag{7}$$

A special case. In the case of $g = 1$, equation (6) reduces to

$$k_1 = \frac{(1+\beta^2)^3}{(1+\beta^2)r+\beta^2} = \frac{\left(\frac{1}{\beta}+\beta\right)^2}{\left(1+\frac{1}{\beta^2}\right)r+1} \tag{8}$$

This is identical with the results of many investigators [1, 3, 15] except cases where the faces may be of different thicknesses and materials are now included by the definition of r.

Minimum value of k_1. In equation (6) we would like to find the minimum values of k_1 with respect to β, holding the other parameters such as g and r constant. Setting $\partial k_1/\partial\beta = 0$, we obtain the following equation in β:

$$\begin{aligned}\beta^3(1+\beta^2)\{&g[r(1-\mu)+2]^2(r+g)\beta^6\\ &+[r(1-\mu)+2]g\{[r(1-\mu)+2](r-g)\\ &\quad+2r(1-\mu)(r+1)+4r(g-1)\}\beta^4\\ &+r(1-\mu)\{[r(1-\mu)+2](3rg-r-2g)\\ &\quad+r(1-\mu)(r+1)+2r(g-1)\}\beta^2\\ &\quad+r^2(1-\mu)^2(rg-1)\} = 0\end{aligned} \tag{9}$$

It is an equation in β of tenth degree. The simplest roots are $\beta = 0$ and $\beta = \pm i$. However, by definition, $\beta = L_y/nL_x$ must be positive so the imaginary roots $\beta = \pm i$ are ruled out. The other six roots of the expression in the angular bracket are difficult to evaluate. Numerical values can be obtained for given values of g and r. In particular, when $g = 1$, equation (9) can be reduced as follows:

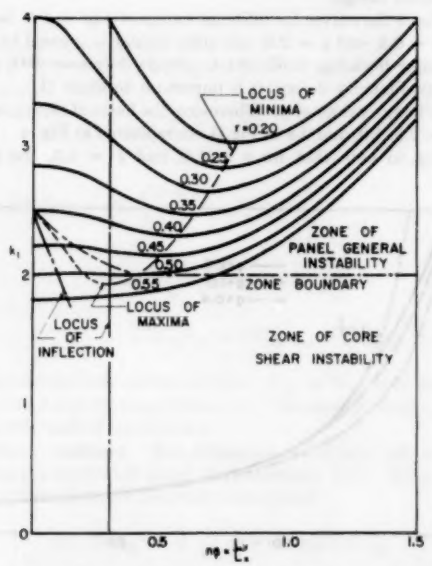

Fig. 5 Enlarged view of k_1 versus $n\beta$ for $g = 2.5$ to show loci of maxima and minima (see Fig. 3)

$$\begin{aligned}\beta^3(1+\beta^2)\{&[r(1-\mu)+2]\beta^2+r(1-\mu)\}^2[(1+r)\beta^2\\ &-(1-r)] = 0\end{aligned} \tag{10}$$

One important root which can be derived from the last bracket of equation (10) is

$$\beta = \left(\frac{1-r}{1+r}\right)^{1/2}, \quad r \le 1$$

Substituting the foregoing expression in equation (8) we have

$$(k_1)_{min} = \frac{4}{(1+r)^2}, \quad r \le 1 \tag{11a}$$

When $r \ge 1$ the root $\beta = 0$ should give a minimum value of k_1 which can be obtained easily from equation (8), i.e.,

$$(k_1)_{min} = \frac{1}{r}, \quad r \ge 1 \tag{11b}$$

Results from equations (11*a*) and (11*b*) are shown in Fig. 4. Seide and Stowell [15] [see their equations (2) and (3)] obtained these results for equal faces of the same material. In other words, the present analysis generalizes their results to faces of different thicknesses and materials, provided that r is interpreted as shown in equation (5*c*).

Features of extrema in k_1 and regions of instability. Equation (9) may need some further explanation. The root of $\beta = 0$ for finite values of L_x and L_y corresponds to $n = \infty$; i.e., an infinite number of half waves in the panel. Therefore $\beta = 0$ is not physically possible, but is an idealized case which is useful for comparison with other cases of finite values of n. Inside the angular bracket of equation (9), β always occurs in even powers and the highest one is of the sixth degree. From algebra, it can have at most three positive roots. Therefore there are four possible extrema of k_1 if $\beta = 0$ is included. However, from extensive calculation of the roots of β, two extrema, one maximum and one minimum, have been found in addition to the root $\beta = 0$, which may be a maximum or minimum of k_1 depending on the value of r.

An enlarged portion of Fig. 3 for $g = 2.5$ is reproduced in Fig. 5 where all loci of the extrema are shown. A few interesting features should be mentioned. For instance, $(k_1)_{max}$ occurs at $L_y/L_x = 0$, if the panel is under general instability. If the panel core is under shear instability $(k_1)_{min}$ occurs at $L_y/L_x = 0$. This dividing point is located at $k_1 = 2.5$ for $g = 2.5$. This is the starting point of the boundary between the zone of panel general instability and zone of core shear instability as shown in dashed line in the figure.

For clearness, all the loci of the maxima, minima, and inflection points are indicated. It is interesting to note that the locus of the maxima and the locus of the minima join together smoothly at one of the loci of inflection. The data of maxima and minima are given in Table 1.

This interesting mathematical feature has never been studied previously. Norris' [11] curves show $(k_1)_{max}$ always at $L_y/L_x = 0$, and do not show $(k_1)_{min}$. Previous theories give the zone boundary as a horizontal line. The present theory, we believe, is more accurate, showing the zone boundary turning smoothly upward toward $L_y/L_x = 0$. It checks Norris' result toward the right, when L_y/L_x is large enough.

Samples of Instability of Sandwich Panels Under Edge Compression

A group of sandwich panels of the same size (24 in. × 24 in.), the same weight (2.039 psf), and the same thickness (3/8 in.), have different face materials at different temperatures and are

illustrated as examples. The critical edge compression N_{yy} is calculated in Table 2 for seven cases. For all the cases, one face is assumed to be kept at room temperature. Except for Cases I and II, the other face is assumed to be kept always at 900 F and made always of stainless steel. Case I is a stainless-steel sandwich with identical faces both of which are at room temperature. It is the simplest case and can be used as a common standard for comparison with the other cases. For instance, N_{yy} in Case II, where one face is double the thickness of the other (i.e., $m = 2$), is 11 per cent lower than that of Case I. This indicates that N_{yy} is an optimum when $m = 1$, for both faces of the same material and thickness, and at ordinary temperature.

In Case III, one face reaches a temperature of 900 F. The modulus of elasticity drops 22 per cent. If we impose that the effect of the initial warping due to thermal expansion can be neglected in calculating N_{yy}, the present theory can be used to treat the thermal effect. If the thermal effect on $\bar{G}_x$ and $\bar{G}_y$ of the core can also be neglected, the calculation is straightforward. N_{yy} is about 12 per cent lower than that of Case I.

To remedy this situation, Case IV has more material added to the hot face so that $m = 1$ again. No improvement on N_{yy} is shown in comparison with Case III because more material is under high temperature and the load-carrying capacity decreases.

In Case V, the cold face is made of light titanium instead of stainless steel. Because of the lightness of titanium, the thickness of the hot face can be increased appreciably by keeping $m = 1$ again. It shows an unfavorable combination in comparison with Case IV as $N_{yy}/(N_{yy})_I = 82.7$ per cent.

The cold face in Case VI is made of aluminum alloy 7075-T6 which is even lighter than titanium. It is slightly better than Case V as $N_{yy}/(N_{yy})_I = 83.7$ per cent for $m = 1$. This is about 95 per cent of Case III.

In Case VII, the cold face is made of magnesium alloy, FSI-H24, which is the lightest metal considered in these calculations and $N_{yy}/(N_{yy})_I = 75.8$ per cent. It is about 86 per cent of Case III. This indicates that an all stainless-steel sandwich is better than a combination with another metal for the limited number of cases investigated. Because of a recently developed technique of manufacture, it is feasible to braze titanium-alloy face to stainless-steel core. However, if an aluminum or magnesium face is used for the cold face, a chemical bond is necessary to join such cold faces to a stainless-steel core, provided the heat conduction from the hot to the cold face is negligible.

As shown in Table 2, τ_{yy}' and τ_{yy}'' are below or close to the proportional limits of the materials used. The present elastic theory can therefore be applied.

For all the cases given, r is so small in magnitude that k_1 is within 5 per cent of that for classical thin-plate theory (i.e., $k_1 = 4$). For a better approximation, the effect of temperature on the magnitude of r should be considered and k_1 should be lower than what is shown in Table 2. We leave these calculations to the reader.

Discussions and Conclusions

1 The present theory gives some simple results:

(*a*) The implication of difference in face material, thickness, and temperature can be included analytically in the cylindrical buckling load P_0 which in turn affects the values of the shear stiffness parameter r.

(*b*) The face buckling coefficient $\hat{k}$ is usually negligible if $r \ll 1$. However, it is appreciable when $r > 1$; that is, the core is exceedingly weak.

(*c*) The major buckling coefficient k_1 can be expressed in terms of a number of useful parameters such as the panel aspect ratio $n\beta$, the core shear stiffness parameter r, the core shear rigidity ratio g, and the half-wave number n. It can be summarized in a single figure; namely, Fig. 3.

(*d*) Through the new meaning of r, all early simple results can be verified and extended to faces of different materials, thicknesses, and temperatures.

Table 2 Comparison of buckling behavior of 24-in. × 24-in. sandwich panels under edge compression

Weight $W = 2.039$ psf
Panel thickness = 3/4 in.

	I	II	III	IV	V	VI	VII
t'' (10^{-3} in.)	20	13.333	20	22.472	22.067	23.686	23.541
t' (10^{-3} in.)	20	26.667	20	17.528	34.425	52.786	84.748
E'' (10^6 psi)	30	30	23.4	23.4	23.4	23.4	23.4
E' (10^6 psi)	30	30	30	30	15	10.5	6.5
$m = t'E'/t''E''$	1	2	1.2821	1	1	1	1
$\bar{l}$ (in.)	0.335	0.335	0.335	0.335	0.31851	0.29853	0.26671
W_c/W	0.13050	0.13050	0.13050	0.13050	0.13507	0.13118	0.12498
$\bar{G}_y$ (10^6 psi)	0.069	0.069	0.069	0.069	0.069	0.069	0.069
$\beta = \bar{G}_x/\bar{G}_y$	1.6667	1.6667	1.6667	1.6667	1.6667	1.6667	1.6667
P_0 (eq. 7*a*)(lb/in.)	711.89	632.79	623.90	623.90	584.54	591.79	533.91
$r = P_0/(\bar{t}^2\bar{G}_y)$	0.02742	0.02438	0.02404	0.02404	0.02244	0.02258	0.02065
k_1 (eq. 10)	3.8336	3.8513	3.8534	3.8534	3.8627	3.8619	3.8769
$N_{yy} = k_1P_0$ (lb/in.)	2729.1	2437.1	2404.1	2404.1	2257.9	2285.4	2069.9
$N_{yy}/(N_{yy})_I$	1	0.89301	0.88093	0.88093	0.82736	0.83744	0.75847
τ_{yy}' (psi)	68227	60928	52674	53492	51160	48244	43964
τ_{yy}'' (psi)	68227	60928	67432	68579	32795	21648	12212

NOTES:

1 Core: 17-7PH stainless steel, honeycomb cell size 1/4 in., foil thickness 0.0015 in., weight = 9.533 pcf.
2 Faces:

I Equal faces of 17-7PH stainless steel.
II Same as I except one face is double the thickness of the other.
III Same as I except one face at 900 F.
IV Unequal faces of 17-7PH stainless steel, one at 900 F ($m = 1$).
V One face of 17-7PH at 900 F and the other of Republic titanium alloy RS 70 ($m = 1$).
VI One face of 17-7PH at 900 F and the other of aluminum alloy 7075-T6 ($m = 1$).
VII One face of 17-7PH at 900 F and the other of magnesium alloy ($m = 1$).

3 High-temperature properties of stainless steel and properties of titanium alloy, aluminum alloy, and magnesium alloy are obtained from NACA TN 4075, 3854, Republic titanium alloys, and Dow magnesium handbook, respectively.

2 Mathematically, the locus of maximum and minimum of k_1 with respect to $n\beta$ is determined. There are two possible regions of instability for sandwich panels under edge compression; i.e., panel general instability and panel core shear instability. The boundary between the two zones is determined and discussed in detail.

3 The theory holds for the materials of the sandwich which are in the elastic range. If the materials under loading are in the plastic range, an additional correction factor for the effective modulus of elasticity should be calculated. As the upper limit, the buckling stress of each face should never exceed the yielding stress of the material.

4 For simplicity, the Poisson ratios of the two faces are assumed to be equal. If one face is at high temperature, the Poisson ratio may reach 1/2 asymptotically in the plastic range. An additional correction should then be made. The average Poisson ratio may be used in equation (6) before such a correction factor is available. It is found that $\hat{k}$ is usually of the order of 1 per cent of k_1 for $r < 1.0$ and can be neglected. As $r \to \infty$, $k_1 \to 0$, and $k \to \hat{k}$ which is greater than zero since $\hat{k}$ is independent of r. In such a limiting case, the load-carrying capacity of the sandwich panel is due entirely to the faces.

5 It is recommended that equation (6) be used for the two faces at different temperatures, if the warpage of the panel due to the temperature difference is reasonably small. It is expected that the present theory is sufficient to meet the needs of preliminary design of sandwich panel under moderate aerodynamic heating.

6 Sometimes, if the cell size of the honeycomb or square cell is too large in comparison to the face thickness, it is possible that the face sheet may buckle locally within each cell. However, the present analysis does not assume such local buckling to occur. Additional theory is under development.

7 For the cases of g not equal to 0.4, 1.0, or 2.5, interpolation can serve the purpose for preliminary design. At present, a wide variety of parameters such as r, g, and m are being considered in calculating k_1 by means of an automatic computing machine.

8 Seven sandwich panels of the same size and weight but different materials and temperatures are used to show the application.

References

1 Eric Reissner, "Finite Deflections of Sandwich Plates," *Journal of the Aeronautical Sciences*, vol. 15, 1948, pp. 435–440.

2 Charles Libove and S. B. Batdorf, "A General Small-Deflection Theory for Flat Sandwich Plates," NACA TN 1526, 1948.

3 N. J. Hoff, "Bending and Buckling of Rectangular Sandwich Plates," NACA TN 2225, 1950.

4 A. C. Eringen, "Bending and Buckling of Rectangular Sandwich Plates," Proceedings of the First U. S. National Congress of Applied Mechanics, New York, N. Y., 1951, pp. 381–391.

5 S. Timoshenko, "Theory of Plates and Shells," McGraw-Hill Book Company, Inc., New York, N. Y., 1940.

6 H. W. March, "Effects of Shear Deformation in the Core of a Flat Rectangular Sandwich Panel. 1. Buckling Under Compressive End Load. 2. Deflection Under Uniform Transverse Load," Forest Products Laboratory Report No. 1583, 1955.

7 W. S. Ericksen and H. W. March, "Effects of Shear Deformation in the Core of a Flat Rectangular Sandwich Panel (Compressive Buckling of Sandwich Panels Having Facings of Unequal Thickness)," Forest Products Laboratory Report No. 1583-B, 1950.

8 I. S. Sokolnikoff, "Mathematical Theory of Elasticity," McGraw-Hill Book Company, Inc., New York, N. Y., 1946.

9 N. J. Hoff, "The Analysis of Structures," John Wiley & Sons, Inc., New York, N. Y., Chapman and Hill, Limited, London, England, 1956.

10 M. E. Raville, "Deflection and Stresses in a Uniformly Loaded, Simply Supported, Rectangular Sandwich Plate," Forest Products Laboratory Report No. 1847, December, 1955.

11 C. B. Norris, "Compressible Buckling Design Curves for Sandwich Panels With Isotropic Facings and Orthotropic Cores," Forest Products Laboratory Report No. 1854, February, 1956.

12 W. R. Kimel, "Elastic Buckling of a Simply Supported Rectangular Sandwich Panel Subjected to Combined Edgewise Bending and Compression," Forest Products Laboratory Report No. 1857, September, 1956, Report No. 1857-A, November, 1956.

13 ANC-23, "Sandwich Construction for Aircraft, Part II," second edition, 1955.

14 E. W. Kuenzi, "Mechanical Properties of Aluminum Honeycomb Core," Forest Products Laboratory Report No. 1849, September, 1955.

15 P. Seide and E. Q. Stowell, "Elastic and Plastic Buckling of Simply Supported Solid-Core Sandwich Plates in Compression," NACA TR No. 967, 1950.

16 S. Timoshenko, "Theory of Elastic Stability," McGraw-Hill Book Company, Inc., New York, N. Y., 1936.

17 J. R. Robinson, "The Buckling and Bending of Orthotropic Sandwich Panels With All Edges Simply Supported," *The Aeronautical Quarterly*, vol. 6, 1955, pp. 125–148.

18 P. P. Bijlaard, "Analysis of the Elastic and Plastic Stability of Sandwich Plates by the Method of Split Rigidities," *Journal of the Aeronautical Sciences*, vol. 18, part 1, May, 1951, part 2, December, 1951.

19 A. E. H. Love, "A Treatise on the Mathematical Theory of Elasticity," fourth edition, Dover Publications, Inc., New York, N. Y., 1949.

20 C. C. Chang and I. K. Ebcioglu, "Elastic Instability of Rectangular Sandwich Panel of Orthotropic Core With Different Face Thicknesses and Materials," AFOSR TN 58-221, ASTIA AD 159 122, Aeronautical Engineering Department, University of Minnesota, March, 1958.

21 C. C. Chang and B. T. Fang, "Initially Warped Sandwich Panel Under Combined Loading," submitted to *Journal Air/Space Science* for review.

Remark: Numerous other references can be found in references [4] and [9].

H. G. LANDAU
Research Associate in Mechanical Engineering; Mathematician, Heat and Mass Flow Analyzer Laboratory, Columbia University, New York, N. Y.

E. E. ZWICKY, JR.
Supervisor, Stress Analysis Engineering, Large Steam Turbine-Generator Department, General Electric Company, Schenectady, N. Y.
Mem. ASME

Transient and Residual Thermal Stresses in an Elastic-Plastic Cylinder

Equations are given for the stress rates in solid cylinders subject to transient temperature distributions, based on the assumption of an elastic, perfectly plastic material obeying a von Mises temperature-dependent yield condition. A numerical procedure for integrating the equations is developed and applied to a temperature distribution approximating a phase transformation and to a quenched cylinder. The effect of various factors on the residual stresses is noted.

Introduction

Inelastic stresses in cylinders due to transient temperature distribution are of interest because of their possible threat to the physical integrity of the part, and because they may leave residual stresses which can influence the later performance of the cylinder.

Inelastic thermal stresses in cylinders have been treated in some recent papers [1] to [5],[1] but these consider somewhat different problems from that treated here and use different methods. In [1] and [2], the methods presented are directed toward steady-state temperature distributions in hollow cylinders subjected to internal pressure. In [3] and [4], the inelastic effect is creep; i.e., viscoelasticity.

Weiner and Huddleston [5] use an elastic, perfectly plastic material model as in the present paper, but use the Tresca yield condition and do not include the temperature dependence of yield stress.

The problem considered here is that of a solid circular cylinder with an axially symmetric transient temperature distribution. The material is assumed to be elastic, perfectly plastic, and to obey a von Mises yield condition with a temperature-dependent yield stress. Elastic incompressibility, i.e., Poisson's ratio equal to one half, is not assumed, but the simplifications due to this assumption are pointed out and the effect of compressibility is noted.

The problem is formulated in the next section, and in the following section equations are derived for the stress rates in a form suitable for numerical integration. Subsequent sections outline the numerical integration procedure used, and calculated residual stresses due to a temperature distribution approximating a phase transformation are given and compared to the results of [5] and the experiments there cited. In the final section, the results of calculation on subcritical quenching of steel cylinders are given and comparisons are made noting the effects of several factors, including surface heat-transfer rate, yield stress, temperature dependence of yield stress, and compressibility.

Problem Statement

We consider a solid cylinder with radius b, of finite length and free of surface tractions. It is subjected to a known axially symmetric transient temperature distribution which does not vary along the axis, and produces a dilatation, $3\alpha T$. We consider only the part of the cylinder at sufficient distance from the end faces so that it may be assumed that planes perpendicular to the axis remain plane and perpendicular. Then the principal axes at all points of the cylinder considered will be r, θ, z.

The mean strain is then given by

$$\epsilon = {}^1/_3(\epsilon_r + \epsilon_\theta + \epsilon_z) = \alpha T + \frac{\sigma}{3K} \tag{1}$$

where σ is the mean stress

$$\sigma = {}^1/_3(\sigma_r + \sigma_\theta + \sigma_z) \tag{2}$$

and K is the elastic bulk modulus,

$$K = \frac{E}{3(1 - 2\nu)}$$

Considerable simplification is possible if it can be assumed that Poisson's ratio ν is equal to ${}^1/_2$, so that the material is elastically incompressible and volume changes are due only to the imposed temperature change. In Equation (1), this makes $1/K = 0$, eliminating the term in σ. We treat the general case with ν unrestricted, but develop the simpler equations for the incompressible case as we proceed.

Since planes perpendicular to the axis remain plane and perpendicular, the axial strain is independent of r

$$\epsilon_z = \epsilon_z(t) \tag{3}$$

The radial and tangential strains are related to the radial displacement u by

$$\epsilon_r = \frac{\partial u}{\partial r}, \qquad \epsilon_\theta = \frac{u}{r} \tag{4}$$

Each strain component may be taken as the sum of three parts; the mean strain, the deviatoric elastic strain e_i^E, and the deviatoric plastic strain e_i^P,

$$\epsilon_i = \epsilon + e_i^E + e_i^P, \qquad \text{for} \qquad i = r, \theta, z \tag{5}$$

[1] Numbers in brackets designate References at end of paper.

Presented at the Summer Conference of the Applied Mechanics Division, University Park, Pa., June 20–22, 1960, of The American Society of Mechanical Engineers.

Discussion of this paper should be addressed to the Secretary, ASME, 29 West 39th Street, New York, N. Y., and will be accepted until October 10, 1960, for publication at a later date. Discussion received after the closing date will be returned.

Note: Statements and opinions advanced in papers are to be understood as individual expressions of their authors and not those of the Society. Manuscript received by ASME Applied Mechanics Division, June 29, 1959. Paper No. 60—APM-4.

The deviatoric elastic strain rate $\dot{e}_i^E$ is related to the deviatoric stress rate $\dot{s}_i$, by the usual elastic relation

$$\dot{e}_i^E = \frac{1}{2G}\dot{s}_i, \qquad i = r, \theta, z \tag{6}$$

with

$$G = \frac{E}{2(1+\nu)},$$

the shear modulus.

There are three conditions on the stress components:

Equilibrium

$$\frac{\partial \sigma_r}{\partial r} + \frac{\sigma_r - \sigma_\theta}{r} = 0 \tag{7}$$

Zero resultant on planes perpendicular to the axis,

$$\int_0^b r\sigma_z dr = 0 \tag{8}$$

Zero radial stress at surface,

$$\sigma_r(b, t) = 0 \tag{9}$$

where b is the cylinder radius.

For the plastic stress-strain relations we use the temperature-dependent form of the von Mises yield condition for the perfectly plastic solid and the associated flow rules, as stated in general in [6]. For the cylinder the yield condition is

$$f = J_2 - k^2(T) = {}^1/_2(s_r^2 + s_\theta^2 + s_z^2) - k^2(T) \tag{10}$$

where J_2 is the second invariant of the deviatoric stress tensor, and $k(T)$ is the yield stress in simple shear at temperature T.

The flow rules associated with this yield condition are

$$\dot{e}_i^P = 0 \quad \text{if} \quad f < 0, \quad \text{or if} \quad f = 0, \quad \dot{f} < 0$$

$$\dot{e}_i^P = \mu s_i \quad \text{if} \quad f = 0, \quad \dot{f} = 0, \quad \mu = \frac{s_i \dot{e}_i^P}{2k^2(T)} \geq 0 \tag{11}$$

where

$$\dot{f} = s_i \dot{s}_i - 2k\dot{k}, \tag{12}$$

$$\dot{k} = \frac{dk}{dT}\dot{T}, \tag{13}$$

and the summation convention for repeated subscripts is used.

In thermal-stress calculations, the flow rules, Equations (11), are not convenient to use directly, because they involve the unknown stress rates, $\dot{s}_i$. The rules can be put in a more suitable, equivalent form by using the requirement of positive plastic power. We introduce $\dot{s}_i^E$ defined by

$$\dot{s}_i^E = 2G\dot{e}_i, \qquad i = r, \theta, z \tag{14}$$

which is the actual stress rate in the elastic regions and is a fictitious stress rate in the plastic regions. In terms of this stress rate, the plastic power (which is proportional to μ) is

$$s_i \dot{e}_i^P = s_i(\dot{e}_i - \dot{e}_i^E) = \frac{1}{2G}(s_i \dot{s}_i^E - s_i \dot{s}_i) \tag{15}$$

Then the flow rules can be written as follows (c.f. [6]). Introducing the function $g(r, t)$ which is zero when plastic flow occurs and equal to 1 elsewhere, the plastic strain rate is

$$\dot{e}_i^P = (1 - g(r, t))\mu s_i \qquad i = r, \theta, z \tag{16}$$

with

$$g(r, t) = 1 \quad \text{if} \quad f < 0, \quad \text{or if} \quad f = 0, \quad \dot{f}_2^E - 2k\dot{k} < 0 \tag{17}$$

$$g(r, t) = 0 \quad \text{if} \quad f = 0, \quad \dot{f}_2^E - 2k\dot{k} \geq 0$$

where

$$\dot{f}_2^E = s_i \dot{s}_i^E \tag{18}$$

From Equation (15), we also have

$$\mu = \frac{\dot{f}_2^E - 2k\dot{k}}{4Gk^2} \tag{19}$$

Stress-Rate Equations

To express the radial and tangential strains in terms of temperature and mean stress, substitute Equations (4) in (1) which gives

$$\frac{\partial}{\partial r}(ru) = r\left(-\epsilon_z + 3\alpha T + \frac{\sigma}{K}\right) \tag{20}$$

This integrates to

$$u = -{}^1/_2 r\epsilon_z + \frac{3}{r}\int_0^r \left(\alpha T + \frac{\sigma}{3K}\right) r dr \tag{21}$$

where $u(0, t) = 0$ is used, since we are considering a solid cylinder. Then from Equations (4)

$$\epsilon_r = -{}^1/_2 \epsilon_z - \frac{3}{r^2}\int_0^r \left(\alpha T + \frac{\sigma}{3K}\right) r dr + 3\left(\alpha T + \frac{\sigma}{3K}\right) \tag{22}$$

$$\epsilon_\theta = -{}^1/_2 \epsilon_z + \frac{3}{r^2}\int_0^r \left(\alpha T + \frac{\sigma}{3K}\right) r dr \tag{23}$$

Since the sum of the deviatoric stress components is zero, it is only necessary to determine two of them. In the elastically incompressible case it was found that the problem could be simplified by using as variables, s_z, and the stress difference,

$$s = s_r - s_\theta = \sigma_r - \sigma_\theta, \tag{24}$$

and the corresponding strains, ϵ_z, and

$$e = \epsilon_r - \epsilon_\theta \tag{25}$$

For the elastically compressible case, we retain s and s_z as variables and must then add the mean stress as an additional variable entering the problem.

From Equations (22) and (23)

$$e = 3\left(\alpha T + \frac{\sigma}{3K}\right) - \frac{6}{r^2}\int_0^r \left(\alpha T + \frac{\sigma}{3K}\right) r dr \tag{26}$$

The equations for the stress rates $\dot{s}$ and $\dot{s}_z$ are then, from Equations (1), (5), (6), (16)

$$\dot{s} = 2G(\dot{e} - (1 - g)\mu s) \tag{27}$$

$$\dot{s}_z = 2G\left(\dot{\epsilon}_z - \alpha\dot{T} - \frac{\dot{\sigma}}{3K} - (1 - g)\mu s_z\right) \tag{28}$$

with the term in $\dot{\sigma}$ absent in the incompressible case.

To express J_2 in the new variables, use

$$s_r = {}^1/_2(s - s_z), \qquad s_\theta = -{}^1/_2(s + s_z) \tag{29}$$

then

$$J_2 = {}^1/_4(s^2 + 3s_z^2) \tag{30}$$

The expressions for the stress components in terms of s and s_z

are obtained by using the equilibrium condition, Equation (7), and the boundary condition, Equation (9),

$$\sigma_r = \int_r^b \frac{s}{r}\,dr \tag{31}$$

Then

$$\sigma_\theta = \sigma_r - s \tag{32}$$

and

$$\sigma_z = {}^1/_2(2\sigma_r - s + 3s_z) \tag{33}$$

Also the mean stress is

$$\sigma = {}^1/_2\left[\int_r^b \frac{s}{r}\,dr - s + s_z\right] \tag{34}$$

To satisfy the zero resultant condition, Equation (8), we use Equation (33)

$$\int_0^b \sigma_z r dr = {}^1/_2 \int_0^b \left[2\int_r^b \frac{s}{r_1}\,dr_1 - s + 3s_z\right] r dr$$

Then, since

$$\int_0^b \left[\int_r^b \frac{s}{r_1}\,dr_1\right] r dr = {}^1/_2 \int_0^b sr\,dr$$

it follows that Equation (8) is equivalent to

$$\int_0^b s_z r dr = 0 \tag{35}$$

This condition is used with $\dot{s}_z$ replacing s_z, since it is assumed that Equation (35) is satisfied initially.

When compressibility is included there is a difficulty because of the fact that $\dot{\sigma}$, which is defined in terms of $\dot{s}$ and $\dot{s}_z$, occurs in the expressions for these rates, Equations (27) and (28), so that these equations do not give $\dot{s}$ and $\dot{s}_z$ explicitly. It is necessary to solve the equations simultaneously by iteration.

We first derive another expression for $\dot{\sigma}$, in terms of $\dot{T}$ and of s and s_z in the plastic regions.

Taking the time derivative of σ in Equation (34) and substituting from Equations (27) and (28)

$$\dot{\sigma} = G\left\{2\int_r^b \frac{\dot{\epsilon}}{r}\,dr - \dot{\epsilon} + \dot{\epsilon}_z - \left(\alpha\dot{T} + \frac{\dot{\sigma}}{3K}\right) - 2\int_r^b (1-g)\mu\,\frac{s}{r}\,dr + (1-g)\mu(s - s_z)\right\}$$

Now

$$2\int_r^b \frac{\dot{\epsilon}}{r}\,dr = 2\int_r^b \frac{1}{r}\left(\frac{\partial \dot{u}}{\partial r} - \frac{\dot{u}}{r}\right) dr$$

$$= 2\int_r^b \frac{\partial}{\partial r}\left(\frac{\dot{u}}{r}\right) dr = 2\left[\frac{\dot{u}(b,t)}{b} - \frac{\dot{u}}{r}\right]$$

$$= \frac{6}{b^2}\int_0^b \alpha\dot{T} r dr - \frac{6}{r^2}\int_0^r \left(\alpha\dot{T} + \frac{\dot{\sigma}}{3K}\right) r dr,$$

using Equation (21) and the fact that $\int_0^b \sigma r\,dr = 0$ which follows from the equivalence of Equations (8) and (35).

Then substituting for $\dot{\epsilon}$ from Equation (26)

$$\dot{\sigma} = G\left\{\frac{6}{b^2}\int_0^b \alpha\dot{T} r dr + \dot{\epsilon}_z - 4\left(\alpha\dot{T} + \frac{\dot{\sigma}}{3K}\right) - 2\int_r^b (1-g)\mu\,\frac{s}{r}\,dr + (1-g)\mu(s - s_z)\right\}$$

so that, expressing G and K in terms of E and ν and solving for $\dot{\sigma}$, we obtain

$$\dot{\sigma} = \frac{E}{6(1-\nu)}\left\{\frac{6}{b^2}\int_0^b \alpha\dot{T} r dr + \dot{\epsilon}_z - 4\alpha\dot{T} - 2\int_r^b (1-g)\mu\,\frac{s}{r}\,dr + (1-g)\mu(s - s_z)\right\} \tag{36}$$

This expression will be used to estimate $\dot{\sigma}$. It can be seen that in any elastic region the variation of $\dot{\sigma}$ with r depends only on $\dot{T}$.

To apply the flow rules given by Equations (16) and (17) we need to state J_2^E in terms of the new variables; this is,

$$J_2^E = s_\theta \dot{s}_\theta^E = G\{(s - s_z)(\dot{\epsilon}_r - \dot{\epsilon}) - (s + s_z)(\dot{\epsilon}_\theta - \dot{\epsilon}) + 2s_z(\dot{\epsilon}_z - \dot{\epsilon})\} = G\left\{s\dot{s} + 3s_z\left(\dot{\epsilon}_z - \alpha\dot{T} - \frac{\dot{\sigma}}{3K}\right)\right\} \tag{37}$$

Also from Equation (19)

$$\mu = \frac{1}{4k^2}\left\{s\dot{s} + 3s_z\left(\dot{\epsilon}_z - \alpha\dot{T} - \frac{\dot{\sigma}}{3K}\right) - \frac{2k\dot{k}}{G}\right\} \tag{38}$$

To obtain the axial strain rate $\dot{\epsilon}_z$, we apply the zero resultant conditions, Equation (35), to the equation for $\dot{s}_z$, Equation (28), then

$$\dot{\epsilon}_z = \frac{2}{b^2}\int_0^b [\alpha\dot{T} + (1-g)\mu s_z] r\,dr \tag{39}$$

For the compressible case, Equation (39) is used to estimate $\dot{\epsilon}_z$, using an estimated value of μ. For $1/K = 0$, this can be avoided by substituting the value of μ from Equation (38) into Equation (39) to get a relation for $\dot{\epsilon}_z$, then

$$\dot{\epsilon}_z = \frac{\int_0^b \left\{2\alpha\dot{T} + (1-g)\frac{s_z}{2k^2}\left[s\dot{s} - 3\alpha s_z\dot{T}\right] - \frac{2k\dot{k}}{G}\right\} r dr}{b^2 - {}^3/_2\int_0^b (1-g)\frac{s_z^2}{k^2}\,r dr} \tag{40}$$

for

$$1/K = 0.$$

We now have all the equations for determining the stress rates $\dot{s}$ and $\dot{s}_z$; and from them we obtain the stress components σ_r, σ_θ, and σ_z by integration with respect to time and use of Equations (31) to (33). For the elastically incompressible case the equations are particularly simple, since then $\dot{s}$ and $\dot{s}_z$ at each instant of time are determined by s, s_z, $\dot{T}$, and $k(T)$ at that time; the terms involving $\dot{\sigma}$ drop out of all the equations. The rates $\dot{s}$ and $\dot{s}_z$ are obtained from Equations (27) and (28), with $\dot{\epsilon}$ given by Equation (26) in the form

$$\dot{\epsilon} = 3\alpha\left[\dot{T} - \frac{2}{r^2}\int_0^r \dot{T} r dr\right] \tag{26a}$$

and $\dot{\epsilon}_z$ by Equation (40). The quantity μ is given by Equation (38), and $g(r, t)$ is determined from Equations (17) with J_2^E given by Equation (37). If only the residual stresses are of interest, the values of σ_r, σ_θ, and σ_z need be computed only for the final values of s and s_z.

For the compressible case, the equations for the stress rates $\dot{s}$, $\dot{s}_z$, $\dot{\sigma}$ become more complicated, since we have in addition Equation (36) for $\dot{\sigma}$, and the term in $\dot{\sigma}$ remains in the equations for $\dot{s}_z$ and also for $\dot{s}$, since it occurs in Equation (26) for $\dot{\epsilon}$. The equations must be solved simultaneously. In the numerical procedure, described in the next section, this was carried out by iteration. For this case Equation (39) was used for $\dot{\epsilon}_z$.

Numerical Computation Procedure

Computations were carried out for the phase-transformation problem treated in [5], but with the transformation taking place over an interval instead of at a point, and also for the quenched cylinder using values for the physical constants which correspond to subcritical quenching of a steel cylinder. For the phase-transformation problem, the temperature at any instant is taken as zero over the untransformed region of the cylinder, a linear increase through the interval in which the transformation is occurring, and a constant value in the transformed region. The temperature distribution of this form is assumed to move through the cylinder. For the quenching problem, the temperature was determined by solving the heat-conduction problem for the cylinder. This was done simultaneously with the stress calculation. A step-by-step procedure in time was used; that is, the temperature and stresses at all points and the location of the plastic regions at time $t + \Delta t$, are computed from the values at time, t.

The heat-conduction problem for the quenched cylinder was solved by finite differences. The following dimensionless variables were used:

$$T = \frac{T - T_0}{T_1 - T_0}, \qquad \bar{r} = \frac{r}{b}, \qquad \bar{t} = \frac{\kappa}{c\rho b^2} t,$$

$$\lambda = \frac{Hb}{\kappa}$$

where

T_1 = initial temperature
T_0 = ambient temperature
κ = thermal conductivity
c = specific heat
ρ = density
H = surface heat-transfer coefficient

The calculation was carried out for equally spaced values of $\bar{r}$ and of $\bar{t}$,

$$\bar{r} = i\Delta\bar{r}, \qquad i = 0, 1, \ldots, n, \qquad n\Delta\bar{r} = 1,$$

$$\bar{t} = j\Delta\bar{t} = \frac{j(\Delta\bar{r})^2}{2}, \qquad j = 0, 1, \ldots$$

Writing

$$T(i\Delta\bar{r}, j\Delta\bar{t}) = T_i^0, \qquad T(i\Delta\bar{r}, (j+1)\Delta\bar{t}) = T_i$$

then T was calculated from the explicit finite-difference expressions:

$$T_0 = {}^1/_2 T_0^0 + {}^1/_2 T_2^0$$

$$T_i = \frac{2i-1}{4i} T_{i-1}^0 + \frac{2i+1}{4i} T_{i+1}^0, \qquad i = 1, 2, \ldots, n-1$$

$$T_n = \frac{1}{2 + \left(\frac{2n+1}{2n^2}\right)\lambda} \left[\frac{2n-3}{4(n-1)} T_{n-2}^0 + \left(1 + \frac{2n-1}{4(n-1)}\right) T_n^0 \right]$$

For the incompressible case, the stress calculation proceeded as follows. The increments $\Delta\epsilon_i$ are calculated from Equation (26a), with a finite sum replacing the integral as in all the calculations. The increment $\Delta\epsilon_z$ is calculated from Equation (40) using values of s, s_{zi}, and g at the beginning of the interval; i.e., s_i^0, s_{zi}^0, and g_i^0 in our notation. Then trial values of s_i and s_{zi} are calculated using

$$s_i^E = s_i^0 + 2G\Delta\epsilon_i$$

and

$$s_{zi}^E = s_{zi}^0 + 2G(\Delta\epsilon_z - \alpha\Delta T_i),$$

i.e., omitting the plastic part so that we are actually using the fictitious stress rates of Equation (14). The elastic or plastic state at each point, $g_i = 1$ or 0, is then determined according to whether J_{2i}^E is less than or greater than $k^2(T_i)$ where J_{2i}^E is calculated using the trial values, s_i^E and s_{zi}^E. If $g_i = 0$, the trial values are modified by replacing them by

$$s_i = \frac{k(T_i)}{\sqrt{J_{2i}^E}} s_i^E, \qquad s_{zi} = \frac{k(T_i)}{\sqrt{J_{2i}^E}} s_{zi}^E$$

which satisfies the condition

$${}^1/_6(s_i^2 + 3s_{zi}^2) = k^2(T_i),$$

and can be seen to be equivalent to using an approximation to μ which is correct to terms of order $(\Delta t)^2$. The calculation of the μ_i is thus avoided.

If the position of the plastic regions has changed during this time step, the estimate of $\Delta\epsilon_z$ may be in error, and a correction must be applied to the s_{zi} to insure that the zero resultant condition is fulfilled. The s_i, s_{zi}, and g_i are recalculated and if the g_i have changed because of the correction, the correction process is repeated until the g_i do not change. This completes the calculation for this time step. The values of σ_r, σ_θ, and σ_z need not be calculated at each time step.

For the compressible case, the procedure is modified as follows: First μ is estimated from the previous time step using Equation (19). This is used to get approximate values of $\dot{\epsilon}_{zi}$ using Equation (39), and of $\dot{\sigma}_z$ using (36). Then s and s_z can be calculated as before except that now the computation includes $\dot{\sigma}$. Using the computed values of s and s_z, σ is computed from Equation (34) and checked with the value given by using the initial estimate of $\dot{\sigma}$. If there is agreement to within sufficient accuracy the approximate values are accepted. If not, $\dot{\sigma}$ and $\dot{\epsilon}_z$ are corrected and the calculation repeated with the corrected values until agreement is obtained.

The calculations were carried out on the IBM 704. The calculation time for a quenched cylinder was about 8 min, using $n = 20$, $\nu = 0.3$ and a piecewise linear relation for $k(T)$.

Residual Stress Due to Phase Transformation

In [5] Weiner and Huddleston determined analytically the stresses in a solid cylinder due to a phase transformation which occurs at a fixed temperature, using a discontinuous temperature distribution to approximate the effect of the phase transformation. Calculations for the same problem were made by the present method using a temperature distribution which varied linearly through an interval, as illustrated in Fig. 1 of [5]. Elastic incompressibility and constant yield stress were assumed in both sets of calculations.

It was found that the present calculations agreed fairly closely with Weiner and Huddleston's formulas especially near the surface of the cylinder, when the phase transformation interval is small; i.e., 4 per cent of the radius. However, the differences are large near the center of the cylinder, where the discontinuous distribution gave infinite stresses. The length of the transformation interval had a significant effect on the calculated stress near the cylinder center, but much less effect on the values near the surface.

Figs. 1 to 4 show some of the calculated residual-stress distributions together with comparisons with the stresses given by the Weiner and Huddleston formulas and the experimental values of

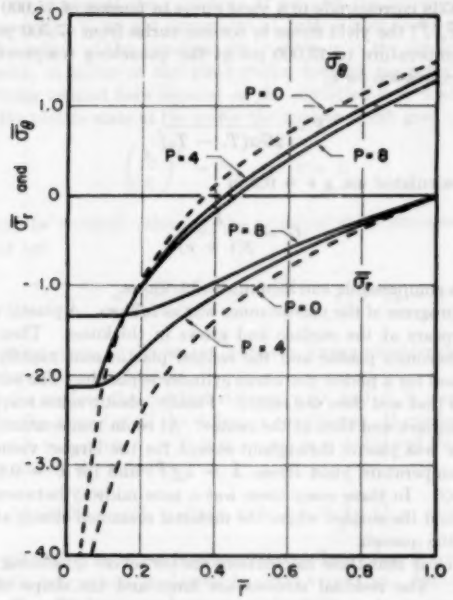

Fig. 1 Radial and tangential residual stresses after phase transformation, $\bar{k} = \sqrt{3}/2$. Values for $P = 0$ from reference [5].

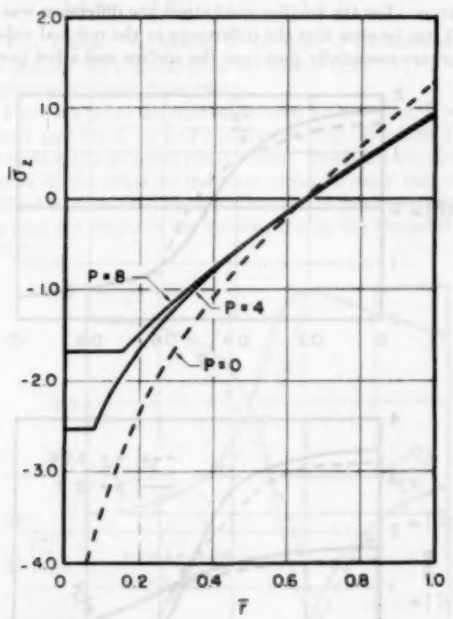

Fig. 2 Axial residual stress after phase transformation, $k = \sqrt{3}/2$. Values for $P = 0$ from reference [5].

Buhler and Scheil [7] for water-quenched solid cylinders. The notation used here differs from that in [5]. We use the dimensionless stress,

$$\bar{\sigma}_i = \frac{\sigma_i}{2G\alpha(T_1 - T_0)}, \qquad i = r, \theta, z \tag{41}$$

and

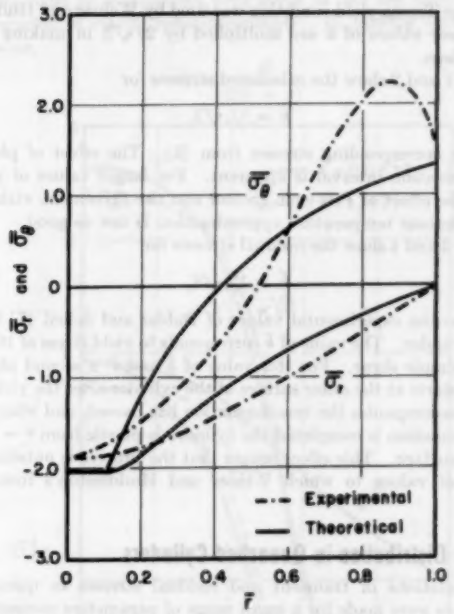

Fig. 3 Radial and tangential residual stress after phase transformation. Theoretical curve calculated with $\bar{k} = {}^3/_5\sqrt{3}$, $P = 8$. Experimental curve from reference [7].

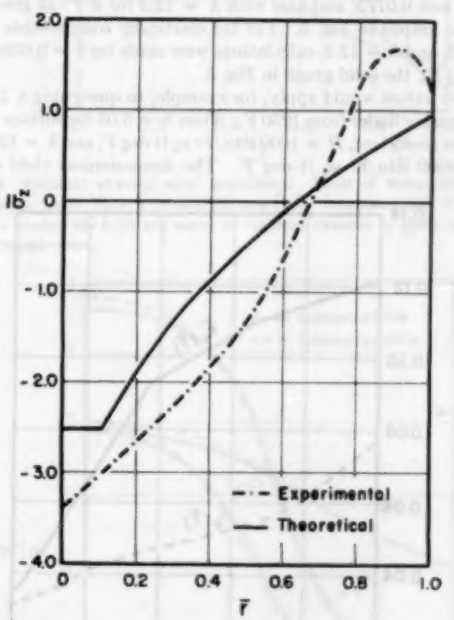

Fig. 4 Axial residual stress after phase transformation. Theoretical curve calculated with $\bar{k} = {}^3/_5\sqrt{3}$, $P = 8$. Experimental curve from reference [7].

$$\bar{k} = \frac{k}{2G\alpha(T_1 - T_0)} \tag{42}$$

where here $\alpha(T_1 - T_0)$ is the linear expansion due to the phase transformation. P is used to denote the ratio of the length of the phase-transformation interval to the cylinder radius, in per cent.

Since the Tresca yield condition was used by Weiner and Huddleston, their values of k are multiplied by $2/\sqrt{3}$ in making the comparison.

Figs. 1 and 2 show the calculated stresses for

$$\bar{k} = {}^1/_2\sqrt{3}$$

and the corresponding stresses from [5]. The effect of phase-transformation interval is apparent. For larger values of yield stress the effect of P is even greater and the agreement with the discontinuous temperature approximation is not as good.

Figs. 3 and 4 show the residual stresses for

$$\bar{k} = {}^2/_3\sqrt{3},$$

and also the experimental values of Buhler and Scheil [7] for a steel cylinder. The value of $\bar{k}$ corresponds to yield stress of 16,070 psi in simple shear. For this value of $\bar{k}$ and P a second plastic region starts at the outer surface of the cylinder after the yielding which accompanies the transformation has passed, and when the transformation is completed the cylinder is plastic from $\bar{r} = 0.66$ to the surface. This effect means that the process is outside the range of values to which Weiner and Huddleston's formulas apply.

Stress Distribution in Quenched Cylinders

Calculations of transient and residual stresses in quenched cylinders were made for a small range of parameters corresponding to subcritical water quenching of a steel cylinder a few inches in diameter. For the elastically incompressible case, calculations were made for $\lambda = 3.06$ and 12.2 for constant yield stress $\bar{k} = 0.0388$ and 0.0775, and also with $\lambda = 12.2$ for $\bar{k}(\bar{T})$ as given by the two graphs in Fig. 5. For the elastically compressible case, $\nu = 0.3$, and $\lambda = 12.2$, calculations were made for $\bar{k} = 0.0388$ and $\bar{k} = \bar{k}_a(\bar{T})$, the solid graph in Fig. 5.

These values would apply, for example, to quenching a 2.5-in-diam steel cylinder from 1250 F. Then $\lambda = 3.06$ for surface heat-transfer coefficient, $H = 1000$ Btu/hr sq ft deg F, and $\lambda = 12.2$ for $H = 4000$ Btu/hr sq ft deg F. The dimensionless yield stress $k = 0.0338$ corresponds to a yield stress in tension of 15,000 psi, and in $\bar{k}_a(\bar{T})$ the yield stress in tension varies from 47,500 psi at room temperature to 13,000 psi at the quenching temperature. In the expression for $\bar{k}$,

$$\bar{k} = \frac{k}{2G\alpha(T_1 - T_0)},$$

G was calculated using $\nu = 0.3$ in

$$G = \frac{E}{2(1 + \nu)}$$

for both compressible and incompressible cases.

The progress of the plastic zones was as follows. A plastic zone first appears at the surface and grows in thickness. Then the center becomes plastic and the central plastic zone rapidly expands and for a period the whole cylinder is plastic. The surface unloads first and then the center. Finally, plastic zones reappear at the surface and then at the center. At room temperature, the cylinder was plastic throughout except for the largest values of room-temperature yield stress, $\bar{k} = \bar{k}_a(\bar{T})$ and for $\bar{k} = 0.0775$, $\lambda = 3.06$. In these cases there was a zone midway between the center and the surface where the material remained elastic at the end of the quench.

It is clear that these calculations are for severe quenching conditions. The residual stresses are large and the shape of the stress distributions is similar for all the cases. The effect of changing λ from 3.06 to 12.2 is very small for $\bar{k} = 0.0388$ and 0.0775. The comparison is shown in Figs. 6 and 7 for the higher yield stress. For the smaller yield stress the difference was even less. It can be seen that the differences in the residual values of σ_r, σ_θ, σ_z are essentially zero near the surface and a few per cent

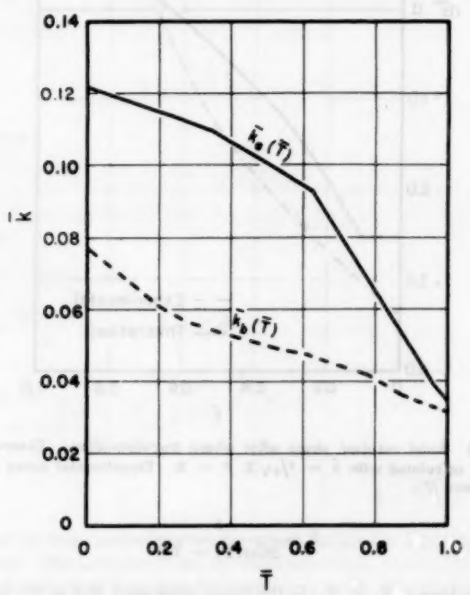

Fig. 5 Temperature dependence of yield stress, used in quenching calculations.

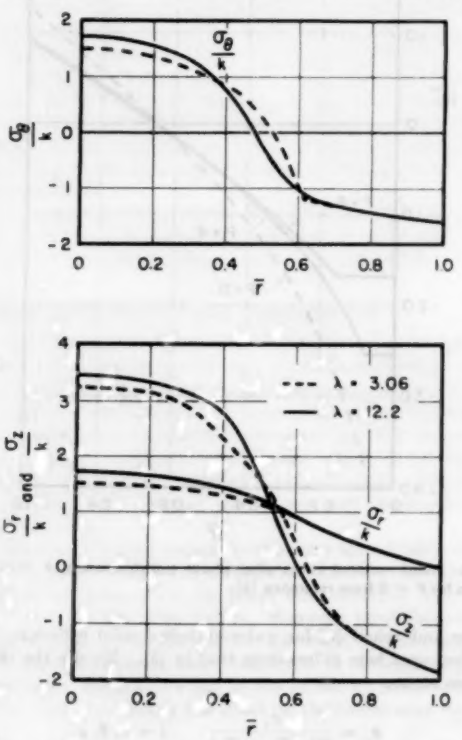

Fig. 6 Residual stresses after quenching. $\bar{k} = 0.0775$, $\lambda = 3.06$ and 12.2; incompressible material.

near the center of the cylinder. If we plot the principal shear stresses, Fig. 7, we get agreement at both center and surface.

The values of the principal shear stresses at the center of the cylinder, in terms of the yield stress, are the same for all the problems treated here because of the condition $s = 0$ at $r = 0$ and the plastic state at the end of the quench which give

$$\left(\frac{s_z}{k}\right)^2 = 3/4 \quad \text{at} \quad r = 0$$

Hence the residual values of the principal shear stresses at the center are

$$\frac{\sigma_z - \sigma_r}{2k} = -\frac{\sigma_\theta - \sigma_z}{2k} = \frac{\sqrt{3}}{2}, \qquad \sigma_r - \sigma_\theta = 0$$

The mean stress at the center, however, varies considerably with the quenching conditions.

At the surface the residual stresses, σ_θ/k and σ_r/k were very nearly the same for all the different conditions. It can be shown that at $\bar{r} = 1$, since $\sigma_r = 0$, $2(\sigma_z - \sigma_\theta) = s + 3s_z$ and this quantity satisfies the equation

$$\dot{s} + 3\dot{s}_z = 2G\left[-(1-g)\mu(s+3s_z) + 6\int_0^1 (1-g)\mu s_z \bar{r}\, d\bar{r}\right]$$

The difference, $\sigma_z - \sigma_\theta$, is zero at the surface when the cylinder is elastic everywhere, and never becomes very large. Hence when the surface is plastic, we have approximately

$$\left(\frac{\sigma_\theta}{k}\right)^2 \cong \left(\frac{\sigma_z}{k}\right)^2 = 3, \qquad \left(\frac{\sigma}{k}\right)^2 = 4/3$$

In Figs. 6 and 7, the breaks in the slope of the stress distributions indicate the boundaries of the elastic zone. For $\lambda = 12.2$, the cylinder is plastic throughout.

In Fig. 8 are given the residual stresses for $\lambda = 12.2$, $\bar{k} = 0.775$ constant and for $\bar{k} = \bar{k}_b(T)$ (shown in Fig. 5) which has the same yield stress at room temperature. Both sets are plotted as the ratio of the stress to the yield stress at room temperature. The effect is mainly an increase of about $0.2k$ in the residual mean stress near the center of the cylinder due to the temperature dependence.

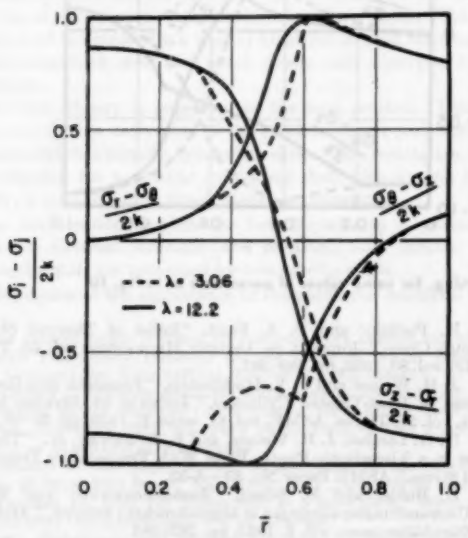

Fig. 7 Residual shear stresses after quenching. $\bar{k} = 0.0775$, $\lambda = 3.06$ and 12.2, incompressible material.

Two pairs of calculations were made to test the effect of the assumption of elastic incompressibility. In making these comparisons,

$$G = \frac{E}{2(1+\nu)}$$

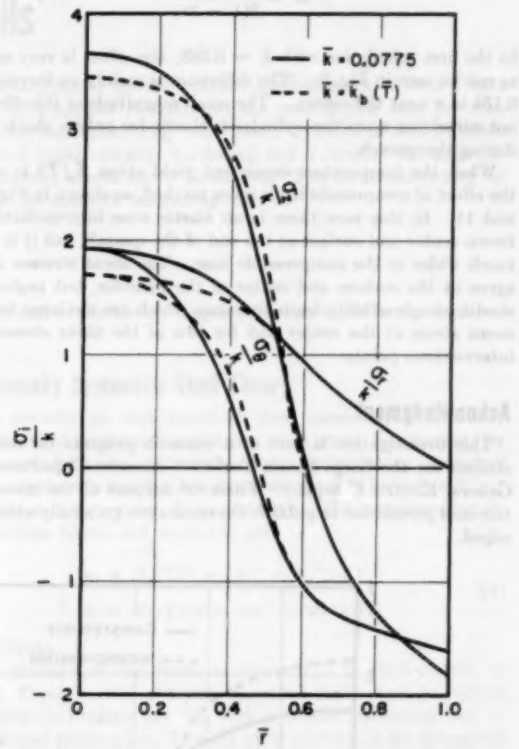

Fig. 8 Residual stresses after quenching. Effect of temperature dependence. $\lambda = 12.2$, $\bar{k} = 0.0775$ and $\bar{k}_b(\bar{T})$; incompressible material. Values plotted for $\bar{k}_b(\bar{T})$ are ratios of residual stresses to yield stress at room temperature.

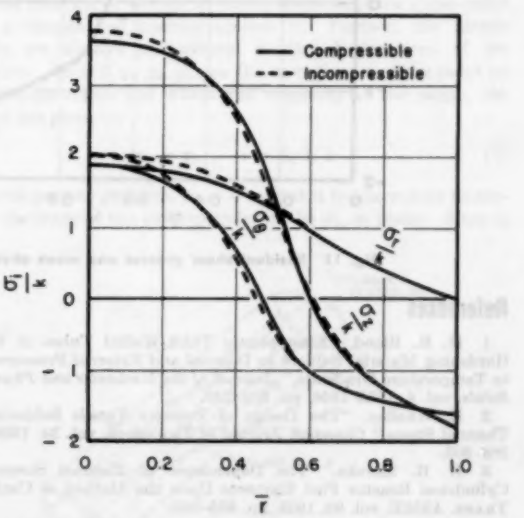

Fig. 9 Residual stresses after quenching. Effect of elastic compressibility. $\lambda = 12.2$, $\bar{k} = 0.0388$.

was calculated with the correct value, $\nu = 0.3$, although assuming elastic incompressibility amounts to taking $\nu = 1/2$ in the elastic bulk modulus

$$K = \frac{E}{3(1 - 2\nu)}$$

In the first calculation with $\bar{k} = 0.388$, the effect is very small, as can be seen in Fig. 9. The difference is mainly an increase of $0.15k$ in σ near the center. The small magnitude of the effect is not surprising since the cylinder is elastic for only a short time during the quench.

When the temperature-dependent yield stress $\bar{k}_a(\bar{T})$ is used, the effect of compressibility is more marked, as shown in Figs. 10 and 11. In this case there is an elastic zone intermediate between center and surface at the end of the quench, but it is very much wider in the compressible case. The shear stresses again agree at the surface and center of the cylinder, but neglecting elastic compressibility leads to values which are too large for the mean stress at the center and for two of the shear stresses at intermediate points.

Acknowledgment

This investigation is part of a research program on residual stresses for the Large Steam Turbine-Generator Department of General Electric Company. Financial support of the investigation and permission to publish the results are gratefully acknowledged.

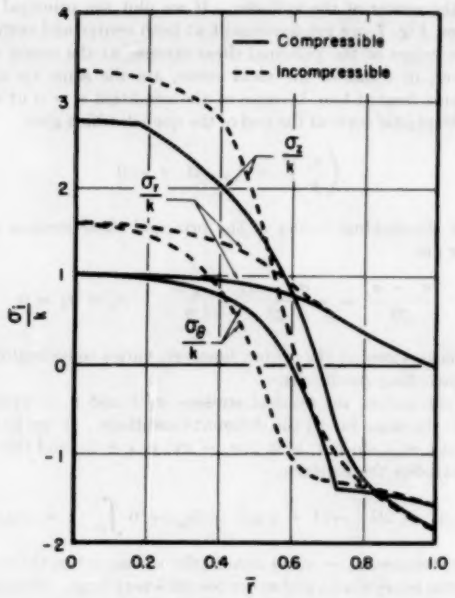

Fig. 10 Residual stresses after quenching. Effect of elastic compressibility. $\lambda = 12.2$, $\bar{k} = \bar{k}_3(\bar{T})$. Values plotted are ratios of residual stress to yield stress at room temperature.

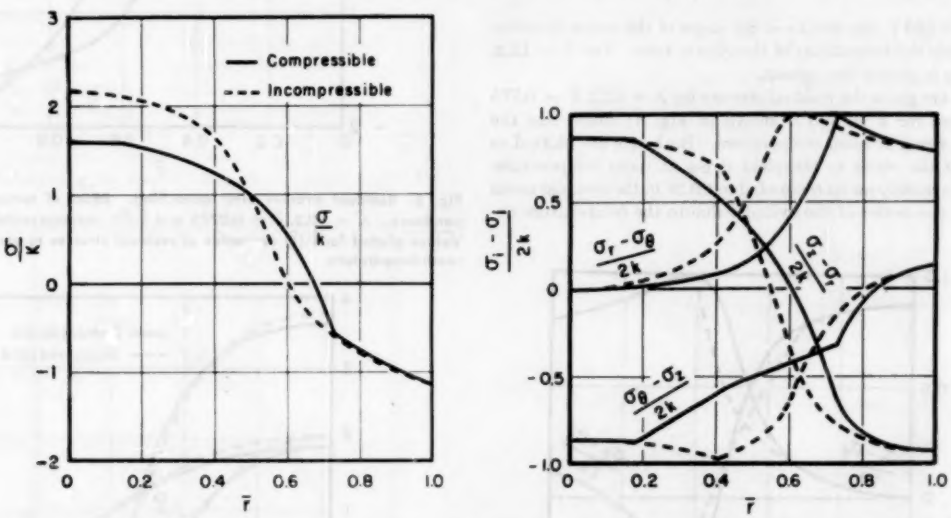

Fig. 11 Residual shear stresses and mean stress after quenching, for same values of parameters as in Fig. 10

References

1 D. R. Bland, "Elastoplastic Thick-Walled Tubes of Work-Hardening Material Subject to Internal and External Pressures and to Temperature Gradients," *Journal of the Mechanics and Physics of Solids*, vol. 4, 1955–1956, pp. 209–229.

2 E. Whalley, "The Design of Pressure Vessels Subjected to Thermal Stress," *Canadian Journal of Technology*, vol. 34, 1956, pp. 268–303.

3 K. R. Merckx, "The Dependence of Thermal Stresses in Cylindrical Reactor Fuel Elements Upon the Method of Cooling," TRANS. ASME, vol. 80, 1958, pp. 985–990.

4 H. Poritsky and F. A. Fend, "Relief of Thermal Stresses Through Creep," JOURNAL OF APPLIED MECHANICS, vol. 25, TRANS. ASME, vol. 80, 1958, pp. 589–597.

5 J. H. Weiner and J. V. Huddleston, "Transient and Residual Stresses in Heat-Treated Cylinders," JOURNAL OF APPLIED MECHANICS, vol. 26, TRANS. ASME, vol. 81, series E, 1959, pp. 31–39.

6 H. G. Landau, J. H. Weiner, and E. E. Zwicky, Jr., "Thermal Stress in a Viscoelastic-Plastic Plate With Temperature Dependent Yield Stress," ASME Paper No. 59—A-33.

7 H. Buhler and E. Scheil, "Zusammenwirken von Wärme und Umwandlungsspannungen in abgeschreckten Stählen," *Archiv für das Eisenhüttenwesen*, vol. 6, 1933, pp. 283–288.

NICHOLAS PERRONE
Associate Professor of Engineering Science, Pratt Institute, Brooklyn, N. Y. Assoc. Mem. ASME

P. G. HODGE, JR.
Professor of Mechanics, Illinois Institute of Technology, Chicago, Ill. Mem. ASME

On Strain-Hardened Circular Cylindrical Shells[1]

A consistent kinematic hardening theory termed complete hardening, based on a Tresca initial yield condition, has been applied to determine the general flow laws for rotationally symmetric shells. Representative "long" and "short" cylindrical shell problems with zero axial load are solved using complete hardening and a simpler but approximate kinematic hardening theory, termed direct hardening. The direct-hardening results compare favorably with the complete hardening ones.

Although the first paper on plastic-shell theory was published only a few years ago [1],[2] the literature is now so voluminous that it would be impracticable to give a complete bibliography. However, most of the previous papers have been concerned either with a perfectly plastic shell or with one which strain-hardens isotropically. The only exception is a paper by Onat [2] which derives the basic equations for a rotationally symmetric shell according to the Tresca yield criterion and a flow law first proposed by Prager [3]. However, the resulting nonlinear equations are so complex that there appears little hope of solving any but trivial problems.

The problem of establishing a theory of shells may be approached in one of two ways. On the one hand, certain assumptions can be made regarding the shell material and its construction and the desired relations between stress and strain resultants deduced therefrom. Alternatively, the resultants can be assumed as generalized variables and their relations postulated directly. The first method has more physical appeal; the second may offer certain simplifications.

Both methods will be demonstrated in the present paper and solutions to various problems obtained and compared. Although, for simplicity, the applications are all to circular cylindrical shells without end load, we shall present most of the theory in terms of the general rotationally symmetric shell. The approach used is simpler than that of Onat [2] in that we consider an ideal sandwich shell and hence obtain only piecewise linear equations.

The basic theory is presented in the next section. This includes a complete derivation of the yield condition and flow law for a general rotationally symmetric shell. The results are then particularized for a circular cylindrical shell without end load. Finally, a corresponding direct theory is presented.

The next section applies the two theories to a particular example. General solutions are obtained and tabular and graphical results are presented for two specific shells.

A discussion of the significance of the particular problems considered and of the theory in general is contained in the final section.

Rotationally Symmetric Shell Theory

We consider an ideal sandwich shell consisting of two very thin sheets of thickness t and tensile yield stress Y, separated by a core of thickness $2h$ which carries only shear. Principal stresses in the top and bottom sheets are denoted by $\sigma_1^+, \sigma_2^+, \sigma_3^+ = 0$ and $\sigma_1^-, \sigma_2^-, \sigma_3^- = 0$, respectively. The corresponding dimensionless forces and moments are

$$n_i = N_i/2Yt = (\sigma_i^- + \sigma_i^+)/2Y, \qquad m_i = M_i/2Yht = (\sigma_i^- - \sigma_i^+)/2Y \tag{1}$$

respectively.

The material of the sheets is assumed to be rigid-plastic, to satisfy Tresca's yield criterion of initial yield; and to harden according to Prager's law [3] with a tensile hardening rate c. In principal stress space, Tresca's yield criterion is the hexagonal cylinder shown in Fig. 1. For a rigid-plastic material, the material remains rigid unless the stress point is on the boundary of this hexagon and moving outward from it. According to Prager's law, when the material is plastic the yield cylinder translates without rotation or change of size or shape as if the stress point were a smooth ball pushing against it. Further, the plastic strains are always proportional to the displacement of the cylinder. Thus if q_1, q_2, q_3, are the co-ordinates of the point on the cylinder center line which was originally at the origin, the strains are given by

$$c\epsilon_i = q_i, \qquad i = 1, 2, 3 \tag{2}$$

In the present problem, $\sigma_3 = 0$ so that it is convenient to consider the trace of the yield cylinder in the σ_1, σ_2 plane. Since ϵ_3

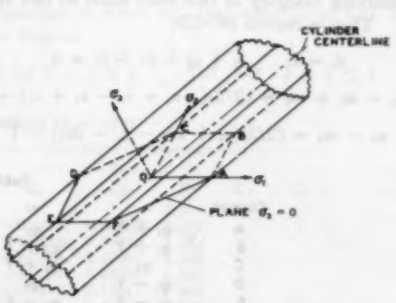

Fig. 1 Perspective of Tresca yield surface

[1] The present paper is based on research work carried out at the Brooklyn Polytechnic Institute for the Office of Naval Research under Contract No. Nonr 839(11), Project No. NR 064-416.

[2] Numbers in brackets designate References at end of paper.

Presented at the Summer Conference of the Applied Mechanics Division, University Park, Pa., June 20–22, 1960, of The American Society of Mechanical Engineers.

Discussion of this paper should be addressed to the Secretary, ASME, 29 West 39th Street, New York, N. Y., and will be accepted until October 10, 1960, for publication at a later date. Discussion received after the closing date will be returned.

Note: Statements and opinions advanced in papers are to be understood as individual expressions of their authors and not those of the Society. Manuscript received by ASME Applied Mechanics Division, December 29, 1958. Paper No. 60—APM-20.

$\neq 0$, Equations (2) no longer apply directly but must be replaced by [4]

$$q_1 = (2c/3)(2\epsilon_1 + \epsilon_2), \qquad q_2 = (2c/3)(\epsilon_1 + 2\epsilon_2) \tag{3}$$

With the point q_1, q_2 known, the stress point is the vector sum of (q_1, q_2) and a vector from the origin to a point on or in the original hexagon. In particular, if the stress point is at the corner B,

$$\sigma_1 = q_1 + Y \qquad \sigma_2 = q_2 + Y \tag{4}$$

On the other hand, on the side BC there is only one stress relation but there is an additional strain-rate normality condition:

$$\dot{\epsilon}_1 = 0 \qquad \sigma_2 = q_2 + Y \tag{5}$$

Similar results are available for all sides and vertices as shown in Table 1.

We define dimensionless extensions and curvatures of the centroidal surface of the shell by

$$e_i = (c/Y)\Lambda_i \qquad \kappa_i = (c/Y)h\mathrm{K}_i \tag{6}$$

where Λ_i and K_i are the corresponding dimensional quantities. The strains in the top and bottom surface are then

$$\epsilon_i^* = (Y/c)(e_i \mp \kappa_i) \tag{7}$$

Combination of Equations (7) and (3) then gives the relations between q_i^* and the generalized strains:

$$\begin{aligned} q_1^* &= (2/3)Y[(2e_1 + e_2) \mp (2\kappa_1 + \kappa_2)] \\ q_2^* &= (2/3)Y[(e_1 + 2e_2) \mp (\kappa_1 + 2\kappa_2)] \end{aligned} \tag{8}$$

If an element of the shell is fully plastic, both the top and bottom stress point will be on the appropriate yield hexagon. Since each hexagon has 6 sides and 6 vertices, there are 144 possible combinations of Table 1 to consider. We shall denote these regimes by inserting a hyphen between the one-or-two-letter symbol signifying the positions of the top and bottom stress points, respectively. For example, in regime *B-D* it follows from Equations (1), Table 1, and Equations (8) taken in order that

$$n_1 = (\sigma_1^- + \sigma_1^+)/2Y = (q_1^- + q_1^+)/2Y = (2/3)(2e_1 + e_2) \tag{9a}$$

Similarly, the other stress resultants are

$$n_2 = (2/3)(e_1 + 2e_2) + 1/2, \tag{9b}$$

$$m_1 = (2/3)(2\kappa_1 + \kappa_2) - 1, \tag{9c}$$

$$m_2 = (2/3)(\kappa_1 + 2\kappa_2) - 1/2 \tag{9d}$$

At a plastic regime consisting of a side and a corner, the results are slightly different. Thus in regime *BC-C*, we find

$$\begin{aligned} \dot{e}_1 = \dot{\kappa}_1, \qquad & n_1 + m_1 = (2/3)[(2e_1 + e_2) + (2\kappa_1 + \kappa_2)] \\ n_2 = (2/3)(e_1 + 2e_2) + 1, \qquad & m_2 = (2/3)(\kappa_2 + 2\kappa_1) \end{aligned} \tag{10}$$

The remaining category of two sides leads to two strain rate relations. Thus in regime *BC-CD:*

$$\begin{aligned} \dot{e}_1 = \dot{\kappa}_1 \qquad & \dot{e}_1 + \dot{e}_2 + \dot{\kappa}_1 + \dot{\kappa}_2 = 0 \\ -n_1 + n_2 - m_1 + m_2 &= (2/3)(-e_1 + e_2 - \kappa_1 + \kappa_2) + 1 \\ n_2 - m_2 &= (2/3)(e_1 + 2e_2 - \kappa_1 - 2\kappa_2) + 1 \end{aligned} \tag{11}$$

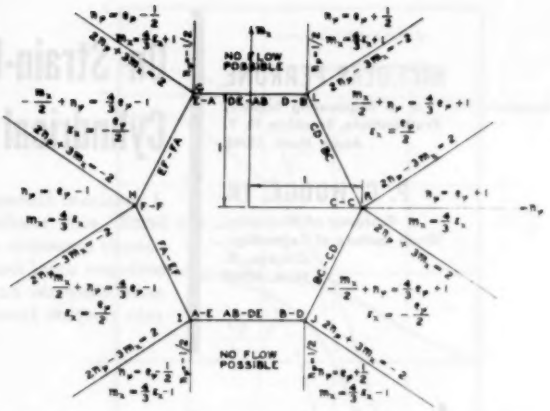

Fig. 2(a) Flow laws and dividing lines for shells with no end load-plane stress

Similar techniques may be used for the 141 other possible combinations.

The initial yield surface is easily obtained from Equations (9–11) and their counterparts by setting all strains equal to zero. Evidently it will be a hyperpolyhedron in four-dimensional stress-resultant space.

For the particular case of a circular cylindrical shell without end load

$$n_1 = n_x = 0 \tag{12a}$$

$$\kappa_2 = \kappa_\varphi = 0 \tag{12b}$$

and we can express the problem entirely in terms of $n_2 = n_\varphi$, $m_1 = m_x$, $e_2 = e_\varphi$, and $\kappa_1 = \kappa_x$. Not only does this simplify all equations, but it considerably reduces the number of equations. As shown in [5], when a strain variable is identically zero, the corresponding stress variable can be eliminated completely from the problem. Thus we need only consider those of the 144 regimes which are compatible with $\kappa_2 = 0$. As far as the initial yield surface goes, we need consider only those regimes for which Equation (12*a*) is satisfied when $q_1^* = q_2^* = 0$. In general, after plastic flow has taken place, values of q_1^* can subsist such that a different set of regimes will satisfy (12*a*) [5]. However, it can be shown [6] that in the present problem such is not the case and that all possible plastic histories will include only those regimes which initially satisfy (12*a*).

It is readily verified that only 12 regimes satisfy both of Equations (12), and that the initial yield condition is a hexagon in a space with co-ordinates n_φ and m_x. The flow laws for each regime are easily computed and the boundaries between regimes can be found by considering a stress point simultaneously in both of them. All pertinent information is shown in Fig. 2(*a*). For simplicity it has been assumed that all stress points progress regularly [7] so that the strain rates may be replaced by the strains in Table 1.

The corresponding relations via a direct approach to the shell problem are obtained by starting with the same initial yield condition in stress space and directly applying Prager's kinematic

Table 1 Plane-stress flow laws

Corner	σ_1	σ_2	Side	Strain rate	Stress-strain
A	$q_1 + Y$	q_2	*AB*	$\dot{\epsilon}_2 = 0$	$\sigma_1 = q_1 + Y$
B	$q_1 + Y$	$q_2 + Y$	*BC*	$\dot{\epsilon}_1 = 0$	$\sigma_2 = q_2 + Y$
C	q_1	$q_2 + Y$	*CD*	$\dot{\epsilon}_1 + \dot{\epsilon}_2 = 0$	$\sigma_2 - \sigma_1 = q_2 - q_1 + Y$
D	$q_1 - Y$	q_2	*DE*	$\dot{\epsilon}_2 = 0$	$\sigma_1 = q_1 - Y$
E	$q_1 - Y$	$q_2 - Y$	*EF*	$\dot{\epsilon}_1 = 0$	$\sigma_2 = q_2 - Y$
F	q_1	$q_2 - Y$	*FA*	$\dot{\epsilon}_1 + \dot{\epsilon}_2 = 0$	$\sigma_2 - \sigma_1 = q_2 - q_1 - Y$

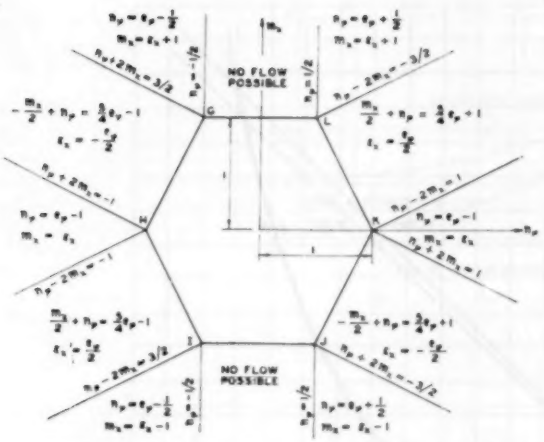

Fig. 2(b) Direct-hardening flow laws and dividing lines for shells with no end load

analogy to it. The rate of hardening is chosen to provide agreement in uniaxial tension. The flow laws shown in Fig. 2(*b*) are then obtained by a direct kinematic consideration of the figure as a rigid frame.

Example

The foregoing theories will now be used to obtain complete solutions for a simply supported cylindrical shell of length $2L$ and radius a subjected to a uniform external pressure p. We denote the inward radical displacement by w and define the following additional dimensionless quantities:

$$\xi = x/L \qquad P = pa/2Yt \qquad W = (c/Y)(w/a)$$
$$\beta^2 = L^2/2ah \qquad \theta^4 = (\mu + 3/4)\beta^4 \tag{13}$$

In terms of these quantities the equilibrium and strain-displacement relations are

$$m_x''/2\beta^2 + n_\varphi + P = 0, \qquad e_\varphi = -W, \qquad \kappa_x = -W''/2\beta^2 \tag{14}$$

where primes denote differentiation with respect to ξ.

It turns out that we will need only the three regimes G, GH, and H in the solution of this problem. The flow laws for these regimes may be combined by introducing a parameter μ which is 0 for the complete theory, Fig. 2(*a*), and 1/4 for the direct theory, Fig. 2(*b*):

$$\begin{aligned} &G\text{:}\ n_\varphi = e_\varphi - 1/2, \qquad m_x = \kappa_x(\mu + 3/4)^{-1} + 1 \\ &GH\text{:}\ n_\varphi - m_x/2 = (1 + \mu)(\mu + 3/4)^{-1} - 1, \qquad e_\varphi = 2\kappa_x \\ &H\text{:}\ n_\varphi = e_\varphi - 1, \qquad m_x = \kappa_x(\mu + 3/4)^{-1} \end{aligned} \tag{15}$$

Equations (14) are easily solved for each of the three regimes listed in (15). The complete solution for regime GH and the most general symmetric solutions for regimes G and H are as follows:

$$\left.\begin{aligned} GH\text{:}\ W &= (\mu + 3/4)(C_1 \sin \beta\xi + C_2 \cos \beta\xi) \\ n_\varphi &= C_3 \sin \beta\xi + C_4 \cos \beta\xi \\ &\quad + (\beta\xi/2)(1 + \mu)(C_2 \sin \beta\xi - C_1 \cos \beta\xi) - P \\ m_x &= 2[n_\varphi + (1 + \mu)(C_1 \sin \beta\xi) \\ &\quad + C_2 \cos \beta\xi + 1] \end{aligned}\right\} \tag{16a}$$

$$\left.\begin{aligned} G\text{:}\ W &= (\mu + 3/4)(C_5 \sin \theta\xi \sinh \theta\xi \\ &\quad + C_6 \cos \theta\xi \cosh \theta\xi) + P - 1/2 \\ n_\varphi &= -W - 1/2 \\ m_x &= (\mu + 3/4)^{1/2}(-C_5 \cos \theta\xi \cosh \theta\xi \\ &\quad + C_6 \sin \theta\xi \sinh \theta\xi + 1) \end{aligned}\right\} \tag{16b}$$

$$\left.\begin{aligned} H\text{:}\ W &= (\mu + 3/4)(C_9 \sin \theta\xi \sinh \theta\xi \\ &\quad + C_{10} \cosh \theta\xi \cos \theta\xi) + P - 1 \\ n_\varphi &= -W - 1 \\ m_x &= (\mu + 3/4)^{1/2}(-C_9 \cos \theta\xi \cosh \theta\xi \\ &\quad + C_{10} \sin \theta\xi \sinh \theta\xi) \end{aligned}\right\} \tag{16c}$$

The solution is now reduced to deciding on the proper combination of Equations (16) and evaluating the arbitrary constants from the boundary conditions. At the simply supported end,

$$W(1) = m_x(1) = 0 \tag{17a}$$

and at the center

$$W'(0) = m_x'(0) = 0 \tag{17b}$$

All physically significant quantities must be continuous at any plastic interface. In view of Equations (14) and (15) this leads to three independent conditions:

$$W, \qquad n_\varphi, \qquad m_x \text{ continuous} \tag{17c}$$

The stress profile for initial yield of a "short" cylinder, $\beta < \pi/2$ is on side GH with $\xi = 0$ at G. This suggests the profile

$$G \quad \text{for} \quad 0 \le \xi \le \rho, \qquad GH \text{ for } \rho \le \xi \le 1 \tag{18}$$

Since the continuity conditions are nonlinear in the plastic interface ρ, it is convenient to regard ρ as independent and P as dependent. Equations (17) can then be used to determine C_1, C_2, C_3, C_4, C_5, C_6, and P in Equations (16*a*, *b*) in terms of ρ. In particular, if $\rho = 0$, we obtain the load necessary for initiation of plastic flow:

$$P_0 = [1 - (1/2)\cos \beta]/(1 - \cos \beta) \tag{19}$$

Numerical results for the particular case $\beta = \pi/4$ are shown in Table 2 and Figs. 3–6. Since ρ is increasing, the assumption of regular progression is verified.

For a "long" shell, $\beta > \pi/2$, the initial stress profile is not unique. However, it turns out that subsequent flow must be according to regimes

$$H \text{ for } 0 \le \xi \le \rho, \qquad GH \quad \text{for} \quad \rho \le \xi \le 1 \tag{20}$$

Table 2 Numerical solutions to short-shell problem ($\beta = \pi/4$)

	Direct hardening ($-C_1=$)						Complete hardening ($-C_1=$)					
ρ	C_3	C_5	C_2	P	C_2	C_4	C_3	C_5	C_2	P	C_2	C_4
0				2.207						2.207		
0.12732	−1.730	−0.01833	0.002295	2.232			−2.307	−0.02117	0.002295	2.232		
0.21645	−1.780	−0.05615	0.01148	2.291			−2.375	−0.06486	0.01149	2.289		
0.30000	−1.861	−0.1150	0.03148	2.390			−2.484	−0.1329	0.03151	2.385		
0.38197	−1.983	−0.2011	0.06791	2.543			−2.648	−0.2326	0.06800	2.532		
0.50930	−2.296	−0.4168	0.1795	2.949			−3.076	−0.4830	0.1801	2.922		
0.63666	−2.888	−0.8139	0.4212	3.729			−3.885	−0.9456	0.4236	3.671		
0.76394	−4.185	−1.671	1.003	5.457	0.8317	4.487	−5.663	−1.947	1.012	5.331	0.7214	4.609

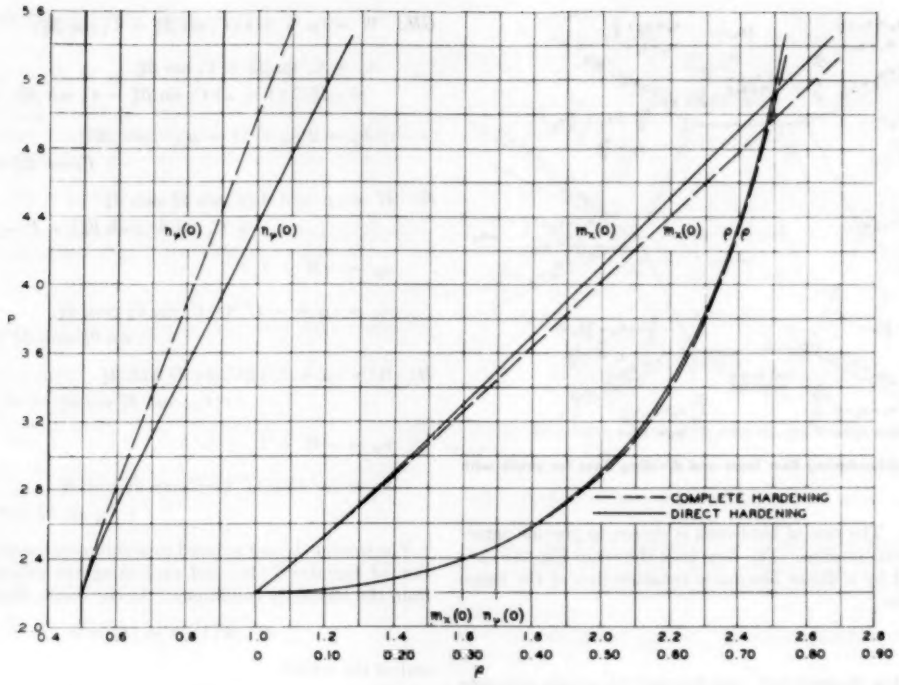

Fig. 3 Curves for short shell

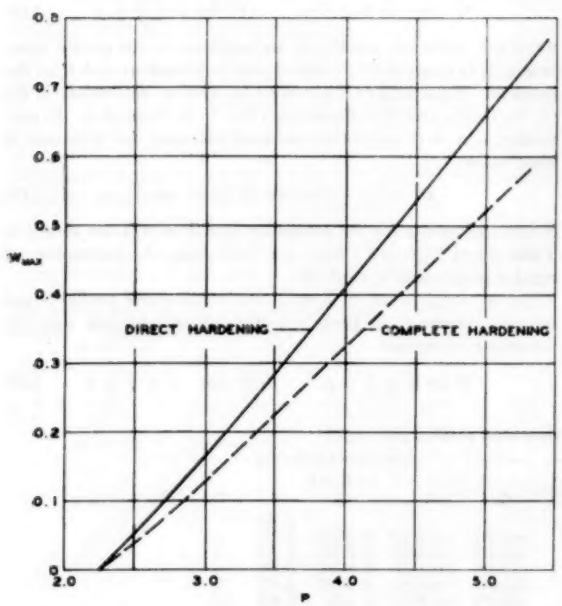

Fig. 4 Short shell—maximum deflection versus load $\beta = \pi/4$

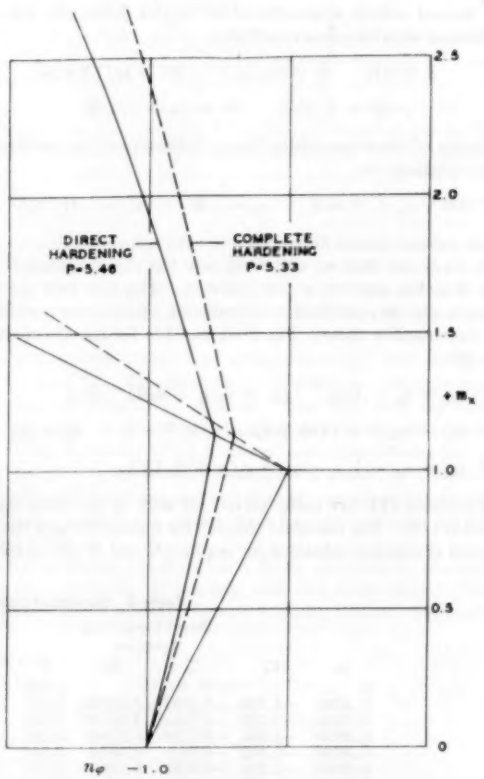

Fig. 5 Stress profiles—short shell

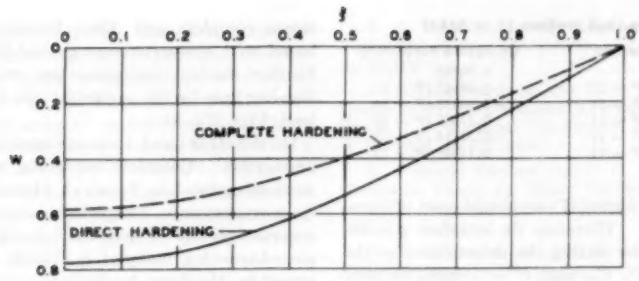

Fig. 6 Short shell—deflections $\beta = \pi/4$

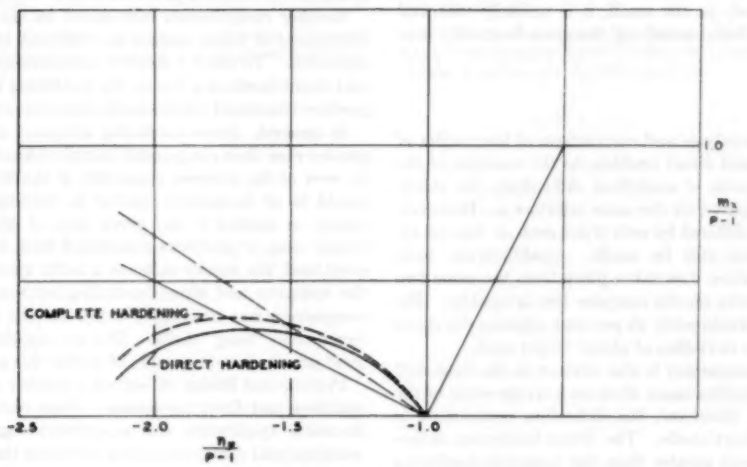

Fig. 7 Long shell—$\beta = 3/4\pi$—stress profile

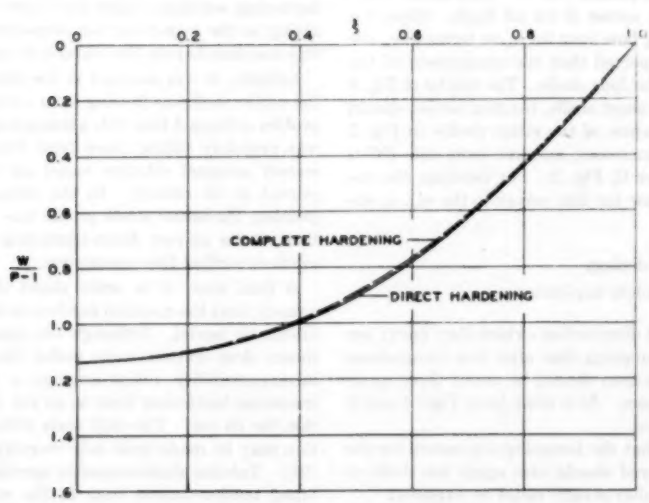

Fig. 8 Long shell—$\beta = 3/4\pi$—deflected shape

Table 3 Solution to long-shell problem ($\beta = 3/4\pi$)

Constant	Direct hardening	Complete hardening
ρ	0.69292	0.75292
$C_1 = C_2$	0.68953 (P − 1)	0.88547 (P − 1)
C_3	−0.37727 (P − 1)	−0.39678 (P − 1)
C_4	0.23936 (P − 1)	0.27535 (P − 1)
C_9	−0.13490 (P − 1)	−0.24218 (P − 1)
C_{12}	0.14043 (P − 1)	0.17981 (P − 1)

Substituting Equations (16*a*, *c*) into (17) we obtain a set of equations homogeneous in $P - 1$. Therefore the interface ρ is determined independently of P by setting the determinant of the coefficients of C_1, C_2, C_3, C_4, C_9, C_{12}, and $P - 1$ equal to zero. The remaining constants and hence the entire solution are thus linear and homogeneous in $P - 1$. Results for the particular case $\beta = 3\pi/4$ are shown in Table 3 and Figs. 7 and 8.

As shown by Boyce and Prager [10] the displacement fields obtained in the foregoing are necessarily unique but the stress rates may not be. Although velocities or displacements do not determine stress rates uniquely in the small, it is unlikely that any other solution could be found satisfying the given boundary conditions.

Conclusions

We consider first an analysis and comparison of the results of applying the complete and direct problem to the example of the preceding section. Because of analytical difficulties, the short-shell solutions were compared for the same interface ρ. However, the corresponding loads differed by only 2 per cent, so that an intelligent comparison can still be made. Qualitatively, both solutions compare well since flow takes place from the same two regimes. The quantitative results compare less favorably. The deflections differ by approximately 25 per cent whereas the stress profiles show an average deviation of about 10 per cent.

A good qualitative comparison is also evident in the long-shell solutions. The stress profiles again show an average error of the order of 10 per cent. However, the deflection comparison is much better than for short shells. The direct hardening deflections are about 3 per cent greater than the complete hardening ones.

An argument based partially on physical reasoning can be given which explains the differences in the two classes of shell solutions. For long shells, hoop-membrane action probably dominates. A rough verification of this is the approximately horizontal nature of the stress profile, Fig. 7. Also, about three quarters of the shell is at the corner H for all loads. Since the direct and complete hardening flow laws for n_φ in terms of e_φ are identical there, it is to be expected that the comparison of the two solutions should be good for long shells. The results of Fig. 8 support this conjecture. For short shells, bending action should dominate, and the vertical nature of the stress profile in Fig. 5 bears this out. As the load increases, material from side HG is continually flowing into corner G, Fig. 2. For bending, the important portion of the flow law for this corner is the m_x, κ_x expression. These are

$$m_x = \kappa_x + 1 \text{ for direct hardening,}$$
$$m_x = (4/3)\kappa_x + 1 \text{ for complete hardening}$$

For roughly the same moment distribution (which they have; see Fig. 5), it follows from the foregoing that after two integrations the complete-hardening deflections should be about three quarters of the direct-hardening ones. It is clear from Figs. 4 and 6 that this is approximately true.

It is reasonable to expect that the foregoing arguments for the long and short shells considered should also apply for shells of other dimensions, so that similar results could be expected.

From a more general viewpoint, there are many similarities between complete and direct hardening. Both approaches are based on a kinematic analogy and include a Bauschinger effect. Further marked similarities are evident in the flow laws and dividing lines for the particular case treated of shells with no axial load, Figs. 2(*a*, *b*).

On the other hand, there are many differences between the two approaches. Complete hardening refers back to a basic flow mechanism (such as Tresca's), whereas direct hardening does not. As a consequence, complete hardening probably reflects a more accurate picture of material behavior. For example, the complete-hardening material is initially isotropic and flows incompressibly; the direct-hardening material exhibits neither property. Basically, the origin of the discrepancies between both approaches is the neglect of some transverse component of frame motion. Generally, this neglected component could be expected to increase with load, so that the complete and direct-hardening results should diverge with increasing load. This conjecture is borne out in the shell problems which were solved.

Another complication introduced by the neglected transverse component of frame motion is a different hardening rate for each approach. To effect a sensible comparison between the complete and direct-hardening results the hardening rates were adjusted to produce consistent tensile-hardening properties.

In general, direct-hardening solutions can be obtained with greater ease than comparable complete-hardening solutions [5, 8]. In view of the inherent simplicity of the direct-hardening laws it would be of immediate interest to investigate their relative accuracy as applied to any given class of problems. For the particular class of problems considered here, namely, shells with no axial load, the results indicate a fairly good comparison between the complete and direct-hardening solutions. Furthermore, the comparison was noticeably better for the class of shells here referred to as "long" shells. This is a significant observation since most practical shells would fall within this group.

Perrone and Hodge [8] solved a number of plate problems with complete and direct hardening. Their results demonstrate a less favorable qualitative and quantitative agreement between the complete and direct-hardening solutions than in the present shell problems. This is probably due to the greater differences in the flow laws and dividing lines between the complete and direct-hardening problems in plates than in shells. These differences in turn are probably due to a greater reflection of three-dimensional effects in plates than in shells.

Rather than being useful only as an approximation, direct-hardening solutions might also serve the alternative purpose of aiding in the search for complete-hardening solutions. In fact, this was done here in the solution of the long-shell problem.

Initially, it was assumed in the direct-hardening solution that the entire shell was flowing from corner H. The resulting stress profiles indicated that this assumption was wrong, and that flow was probably taking place from two regimes, H and GH. A second assumed solution based on this modified flow pattern proved to be correct. In the subsequent complete-hardening problem the initial stress profile was assumed to be the same as that of the correct direct-hardening solution, and the ensuing solution verified this assumption.

A final word is in order about the basic initial postulates; namely, that the material hardens in the manner predicted by the kinematic model. Although the complete kinematic hardening theory does contain some useful idealizing ingredients such as incompressibility, initial isotropy, a Bauschinger effect, and incremental hardening there is, as yet, little experimental justification for its use. The only tests with which some slight correlation may be made were only recently performed (Naghdi, et al. [9]). Tubular aluminum-alloy specimens were subjected to combined tension-torsion tests in the strain-hardened range. The results indicated that strain-hardening proceeded roughly in the

manner predicted by the kinematic model. However, unlike the implicit assumption of the present analysis, the principal axes were constantly changing. Hence no direct correlation may be made. Evidently, tests are needed wherein the principal axes remain fixed. In the event that subsequent experiments do indicate an unsatisfactory agreement with the kinematic model, then a general linear hardening theory recently developed by Hodge [7] might find application. Kinematic hardening is contained as a special case in his general theory. Hence the solutions obtained here might still serve some purpose by pointing the way toward solution for the appropriate nonkinematic case.

References

1 D. C. Drucker, "Limit Analysis of Cylindrical Shells Under Axially Symmetric Loading," Proceedings of the First Midwestern Conference on Solid Mechanics, Urbana, Ill., 1952, Engineering Experimental Station, University of Illinois, 1953, pp. 158–163.

2 E. T. Onat, "Analysis of Shells of Revolution Composed of Work Hardening Material," *Journal of the Mechanics and Physics of Solids*, vol. 7, 1958, pp. 45–49.

3 W. Prager, "The Theory of Plasticity: A Survey of Recent Achievements," *Proceedings of The Institution of Mechanical Engineers*, vol. 169, 1955, pp. 41–57.

4 R. T. Shield and H. Ziegler, "On Prager's Hardening Rule," *Journal of Applied Mathematics and Physics (ZAMP)*, vol. 9, 1958, pp. 260–276.

5 Nicholas Perrone and P. G. Hodge, Jr., "Strain Hardening Solutions With Generalized Kinematic Models," Proceedings of the Third U. S. National Congress of Applied Mechanics, New York, N. Y., 1958, pp. 641–648.

6 Nicholas Perrone and P. G. Hodge, Jr., "Applications of a Consistent Theory for Strain Hardening Plastic Solids," PIBAL Report No. 403, Polytechnic Institute of Brooklyn, Brooklyn, N. Y., 1957.

7 P. G. Hodge, Jr., "A General Theory of Piecewise Linear Plasticity Based on Maximum Shear," *Journal of the Mechanics and Physics of Solids*, vol. 5, 1957, p. 242.

8 Nicholas Perrone and P. G. Hodge, Jr., "Strain-Hardening Solutions to Plate Problems," JOURNAL OF APPLIED MECHANICS, vol. 26, TRANS. ASME, vol. 81, series E, 1959, pp. 276–284.

9 P. M. Naghdi, F. Essenberg, and W. Koff, "An Experimental Study of Initial and Subsequent Yield Surfaces in Plasticity," JOURNAL OF APPLIED MECHANICS, vol. 25, TRANS. ASME, vol. 80, 1958, pp. 201–209.

10 W. E. Boyce and W. Prager, "On Rigid Work Hardening Solids With Singular Yield Conditions," *Journal of the Mechanics and Physics of Solids*, vol. 6, 1957, pp. 9–12.

The Elastoplastic Thick-Walled Sphere Subjected to a Radial Temperature Gradient[2]

G. R. COWPER[1]
Assistant Research Officer,
National Aeronautical Establishment,
National Research Council,
Ottawa, Canada

An exact solution is obtained for the behavior of an ideal elastoplastic hollow sphere which is thermally stressed by a slowly increasing temperature difference between the inner and outer surfaces. An approximate analysis in which elastic strains are neglected is also presented. It is shown that the approximate analysis gives the asymptotic form of the exact solution at infinitely high temperatures.

A NUMBER of papers dealing with thermal stresses in elastoplastic bodies have appeared recently. Mention may be made of the work of Wilhoit [1],[3] Bland [2], Bodner [3], and Weiner [4], who have considered thermal stresses in annuli, cylinders, flat plates, and thin spherical shells. To the list of solutions obtained by these authors, the present paper adds the example of a thermally stressed elastoplastic thick-walled hollow sphere. The thermal stresses are produced by raising, slowly and monotonically, the temperature of the inner surface of the sphere while the temperature of the outer surface is held constant. The surfaces of the sphere are free of traction, and it is assumed that the sphere is initially free of residual stress. The material of the sphere is ideally plastic, homogeneous, and isotropic, with a yield limit that is independent of hydrostatic pressure and temperature. Infinitesimal strains are assumed, and it may be confirmed *a posteriori* that this assumption is justified for an extremely wide range of temperatures. Within this framework an exact solution of the problem is found.

Since problems in plasticity are frequently simplified by neglecting all elastic strains, it is of interest to compare the exact solution with an approximate solution in which elastic strains are ignored. This is done in the final section of the paper. The comparison is especially interesting in the present case for the approximate solution contains a discontinuity which is inadmissible in the exact solution.

Governing Equations

In view of the spherical symmetry of the problem, the equilibrium and kinematic equations are

$$\frac{d\sigma_r}{dr} + \frac{2(\sigma_r - \sigma_\theta)}{r} = 0, \qquad \epsilon_r = \frac{du_r}{dr}, \qquad \epsilon_\theta = \frac{u_r}{r}$$

with the customary notation. Each component of strain is the sum of an elastic, a thermal, and a plastic part, where the elastic and thermal parts are given by the usual relations. Thus

$$\epsilon_r = \{\sigma_r - 2\nu\sigma_\theta\}/E + \alpha T + \epsilon_r^P$$

$$\epsilon_\theta = \{(1-\nu)\sigma_\theta - \nu\sigma_r\}/E + \alpha T + \epsilon_\theta^P$$

where α is the coefficient of thermal expansion, T is the temperature, and E and ν have their usual meanings. The plastic-strain components ϵ_r^P, ϵ_θ^P, must satisfy the incompressibility condition

$$\epsilon_r^P + 2\epsilon_\theta^P = 0 \tag{1}$$

On the assumption that changes in temperature take place slowly the temperature is given by the well-known steady-state distribution

$$T = T_b + \Delta T(b/r - 1)/(b/a - 1)$$

where a and b are, respectively, the radii of the inner and outer surfaces of the sphere, where T_a and T_b are the corresponding surface temperatures, and where $\Delta T = T_a - T_b$. Since the uniform part of the temperature distribution causes no thermal stress we may conveniently set $T_b = 0$. The yield condition is simply [5]

$$|\sigma_r - \sigma_\theta| \leq Y$$

where Y is the yield stress in simple tension or compression. On account of the spherical symmetry the flow rule is automatically satisfied, except possibly for sign, whenever (1) is satisfied [5]. It is assumed that the material constants E, ν, α, Y are independent of temperature.

It is now convenient to introduce nondimensional variables defined as follows:

$$q_r = \sigma_r/Y \qquad q_\theta = \sigma_\theta/Y$$

$$\zeta = r/b \qquad \beta = b/a$$

$$v = Eu_r/Y(1-\nu)b \qquad \tau = E\alpha\Delta T/Y(1-\nu)$$

$$\epsilon_r^P = E\epsilon_r^P/Y(1-\nu) \qquad \epsilon_\theta^P = E\epsilon_\theta^P/Y(1-\nu)$$

In terms of the nondimensional variables the governing equations become, after some reduction,

$$\frac{dq_r}{d\zeta} + \frac{2(q_r - q_\theta)}{\zeta} = 0 \tag{2}$$

$$|q_r - q_\theta| \leq 1 \tag{3}$$

---

[1] Formerly, Research Associate, Division of Applied Mathematics, Brown University, Providence, R. I.

[2] The results in this paper were obtained in the course of research sponsored by the Office of Naval Research under Contract Nonr-562 (20) with Brown University.

[3] Numbers in brackets designate References at end of paper.

Presented at the Summer Conference of the Applied Mechanics Division, University Park, Pa., June 20–22, 1960, of THE AMERICAN SOCIETY OF MECHANICAL ENGINEERS.

Discussion of this paper should be addressed to the Secretary, ASME, 29 West 39th Street, New York, N. Y., and will be accepted until October 10, 1960, for publication at a later date. Discussion received after the closing date will be returned.

NOTE: Statements and opinions advanced in papers are to be understood as individual expressions of their authors and not those of the Society. Manuscript received by ASME Applied Mechanics Division, July 2, 1959. Paper No. 60—APM-22.

$$\frac{dv}{d\zeta} = \frac{\tau(1/\zeta - 1)}{(\beta - 1)} + \frac{(q_r - 2\nu q_\theta)}{(1 - \nu)} + e_r^P \tag{4}$$

$$\frac{v}{\zeta} = \frac{\tau(1/\zeta - 1)}{(\beta - 1)} + \frac{(1 - \nu)q_\theta - \nu q_r}{(1 - \nu)} + e_\theta^P \tag{5}$$

$$e_r^P + 2e_\theta^P = 0 \tag{6}$$

Since the surfaces of the sphere are free of traction, the boundary conditions are $q_r = 0$ at $\zeta = \beta^{-1}$ and $\zeta = 1$.

We can anticipate the general behavior of the sphere as T_a (or τ) is raised. The inner part of the sphere, being hottest, will tend to expand more than the outer part. Hence the inner part of the sphere will press outward on the outer part, giving rise to a compressive radial stress q_r. The equilibrium of the various parts of the sphere then requires tensile hoop stresses in the outer part and compressive hoop stresses in the inner part. For sufficiently high temperatures we may expect yielding in hoop compression near the inner surface and/or yielding in hoop tension near the outer surface. The subsequent analysis will bear out this expectation.

Elastic Phase

When $\tau = 0$ the sphere is, by hypothesis, unstressed. As τ is raised the initial response is entirely elastic, and the well-known general solution [6] of the governing equations is

$$v = -\frac{(1 + \nu)A}{(1 - \nu)\zeta^2} + \frac{(1 - 2\nu)}{(1 - \nu)} B\zeta - \frac{\zeta\tau}{(\beta - 1)} + \frac{(1 + \nu)\tau}{2(1 - \nu)(\beta - 1)} \tag{7}$$

$$q_\theta = -\frac{A}{\zeta^2} + B - \frac{\tau}{2(\beta - 1)\zeta} \tag{8}$$

$$q_r = \frac{2A}{\zeta^2} + B - \frac{\tau}{(\beta - 1)\zeta} \tag{9}$$

where A and B are constants of integration. The boundary conditions $q_r(1/\beta) = q_r(1) = 0$ determine these constants as

$$A = \frac{\tau}{2(\beta^3 - 1)} \qquad B = \frac{\tau\beta(\beta + 1)}{(\beta^3 - 1)} \tag{10}$$

The elastic distribution of stress and displacement follow immediately.

The foregoing solution is valid until the stresses increase to the point where the yield condition (3) is violated. From (8), (9), and (10),

$$q_r - q_\theta = \frac{\tau}{2(\beta^3 - 1)} \left\{ \frac{3}{\zeta^3} - \frac{\beta^2 + \beta + 1}{\zeta} \right\},$$

and it is easily verified that this quantity always attains its greatest absolute value at the inner surface of the sphere. Hence yielding occurs first at the inner surface, at the temperature τ^* which is determined by the condition that $(q_r - q_\theta) = 1$ when $\zeta = 1/\beta$ and $\tau = \tau^*$. Thus

$$\tau^* = \frac{2(\beta^3 + \beta + 1)}{\beta(2\beta + 1)} \tag{11}$$

First Plastic Phase[4]

As τ is increased beyond τ^* a plastic zone spreads outward from the inner surface. Let ρ_i denote the radius of the elastic-plastic interface, and let $\eta_i = \rho_i/b$ be its nondimensional radius. Within the plastic zone the stresses are governed by the equilibrium equation (2) and the yield condition $q_r - q_\theta = 1$. These equations, together with the boundary condition $q_r(1/\beta) = 0$, immediately lead to the stress distribution

$$\left.\begin{aligned} q_r &= -2 \ln \beta\zeta \\ q_\theta &= -(1 + 2 \ln \beta\zeta) \end{aligned}\right\} \quad 1/\beta \le \zeta < \eta_i \tag{12}$$

Within the elastic zone, equations (7), (8), and (9) still apply although the constants of integration are no longer given by (10). The three unknown quantities in the elastic solution, namely, the constants of integration A and B, and the parameter η_i are fixed by the following conditions: First, $q_r = 0$ at the outer surface; next q_r is continuous at the elastic-plastic boundary; and finally, the material at the elastic-plastic boundary is just on the point of yielding. These conditions lead to the set of equations

$$2A + B - \tau/(\beta - 1) = 0$$

$$2A/\eta_i^3 + B - \tau/(\beta - 1)\eta_i = -2 \ln \beta\eta_i$$

$$3A/\eta_i^3 - \tau/2(\beta - 1)\eta_i = 1$$

from which we obtain

$$\left.\begin{aligned} A &= \frac{\eta_i^3}{(2 + \eta_i)(1 - \eta_i)} \left(1 + \frac{\ln \beta\eta_i}{1 - \eta_i}\right) \\ B &= \frac{2\eta_i(1 + \eta_i)}{(2 + \eta_i)(1 - \eta_i)} + \frac{2\eta_i(3 - \eta_i^2) \ln \beta\eta_i}{(2 + \eta_i)(1 - \eta_i)^2} \\ \tau &= 2(\beta - 1) \frac{\eta_i(1 - \eta_i^3 + 3 \ln \beta\eta_i)}{(2 + \eta_i)(1 - \eta_i)^2} \end{aligned}\right\} \tag{13}$$

Thus all parameters, including τ, which affect the stress distribution in the elastic zone are expressed in terms of the single parameter η_i. Although it would be preferable to have τ as the independent parameter, a glance at (13) clearly indicates that it is not possible to solve for η_i as an explicit function of τ.

Once A and B are known the displacement in the elastic zone follows from (7). It remains to consider displacements in the plastic zone. Elimination of e_r^P, e_θ^P, and q_θ between (2), (4), (5), and (6) yields

$$\frac{dv}{d\zeta} + \frac{2v}{\zeta} = \frac{3\tau(1/\zeta - 1)}{(\beta - 1)} + \frac{(1 - 2\nu)}{(1 - \nu)} \left(\zeta \frac{dq_r}{d\zeta} + 3q_r\right)$$

which may be integrated directly to give

$$v = \frac{\tau(3/2 - \zeta)}{(\beta - 1)} + \frac{(1 - 2\nu)\zeta q_r}{(1 - \nu)} + \frac{C}{\zeta^2} \tag{14}$$

where C is a constant of integration. Expression (14) is valid in both the elastic and plastic zones. By substituting into (14) the expressions (7) and (9) which hold in the elastic zone, we find $C = -3A$. Since A and q_r are known, (14) determines the displacement throughout the sphere.

The foregoing solution is valid until the tensile hoop stresses which exist near the outer surface cause further yielding. Let us assume that the most critical location is the outer surface, and inquire when yielding begins there. From (8), (9), and (13) we find that $(q_\theta - q_r)_{\zeta=1} = 1$ when η_i reaches the value η_i^{**} given by the equation

$$\exp\{2(1 - \eta_i^{**})^2/3\eta_i^{**}\} = \beta\eta_i^{**} \tag{15}$$

The temperature τ^{**} corresponding to η_i^{**} follows from (13) and (15),

[4] The analysis in this section follows closely the analysis of a hollow sphere under internal pressure given in [5].

$$\tau^{**} = 2(\beta - 1)\{1 + \eta_1^{**2}/(1 - \eta_1^{**})\} \tag{16}$$

We note that τ^{**} is a function of β only, the functional relationship being expressed parametrically in terms of η_1^{**} by (15) and (16).

The assumption about the most critical location for further yielding may now be checked. It can be verified that, at the temperature τ^{**}, the curve of $(q_\theta - q_r)$ versus ζ is monotone increasing in the elastic zone if, and only if, $\beta < 2e^{1/2} = 2.791$. It follows that the assumption is correct when $\beta < 2.791$. However, when $\beta > 2.791$ the curve of $(q_\theta - q_r)$ versus ζ has a maximum within the supposedly elastic zone at which point the yield condition is violated. It appears that in the latter case a second plastic zone is initiated somewhere in the interior of the elastic zone rather than at the outer surface.

Second Plastic Phase

Here we restrict ourselves to the case $\beta < 2.791$. Then as τ is increased beyond τ^{**} a second plastic zone, which began at the outer surface, spreads inward. Let the radius of the spherical boundary of the zone be ρ_2 and let $\eta_2 \equiv \rho_2/b$.

From the equilibrium equation (2), the yield condition $q_\theta - q_r = 1$, and the boundary condition $q_r(1) = 0$, the stress distribution in the second plastic zone is easily found to be

$$\left.\begin{aligned} q_r &= 2 \ln \zeta \\ q_\theta &= 1 + 2 \ln \zeta \end{aligned}\right\} \quad \eta_2 < \zeta \leq 1 \tag{17}$$

In the first plastic zone equations (12) still apply, while (8) and (9) hold in the elastic zone, although the constants of integration are now determined by the following conditions: The radial stress q_r must be continuous at $\zeta = \eta_1$ and $\zeta = \eta_2$. At $\zeta = \eta_1$ and $\zeta = \eta_2$ the material is on the point of yielding, in hoop compression and in hoop tension, respectively. These conditions lead to a set of four linear algebraic equations in the three unknowns A, B, and τ. The equations are consistent only if the determinant of the augmented matrix of coefficients vanishes, a requirement which leads to the equation

$$\ln \eta_1\eta_2 + \ln \beta = \frac{2(\eta_2/\eta_1 - 1)^2}{3\eta_2/\eta_1} \tag{18}$$

It is now convenient to introduce a parameter $\epsilon \equiv \eta_2/\eta_1 - 1$. Then, from (18) we find

$$\eta_1 = \beta^{-1/6}(1 + \epsilon)^{-1/3} \exp\{\epsilon^2/3(1 + \epsilon)\}$$

$$\eta_2 = \beta^{-1/6}(1 + \epsilon)^{1/3} \exp\{\epsilon^2/3(1 + \epsilon)\}$$

and in turn the equations for A, B, and τ can be solved to give

$$A = \frac{(1 + \epsilon)^{1/2}}{3\epsilon\beta^{1/2}} \exp\{\epsilon^2/(1 + \epsilon)\} \tag{19}$$

$$B = \frac{2(2 + 3\epsilon + 3\epsilon^2 + \epsilon^3)}{3\epsilon(1 + \epsilon)} + \ln\{(1 + \epsilon)/\beta\}$$

$$\tau = \frac{2(\beta - 1)(1 + \epsilon + \epsilon^2)}{\epsilon\beta^{1/3}(1 + \epsilon)^{1/2}} \exp\{\epsilon^2/3(1 + \epsilon)\} \tag{20}$$

Thus all quantities which appear in the formulas for stress and displacement are expressed in terms of the single parameter ϵ. The stresses in the elastic zone follow from (8) and (9), while the displacement follows from (14). The foregoing solution is valid for all temperatures greater than τ^{**}.

The growth of the plastic zones with increasing temperature is illustrated in Fig. 1. As might be expected, the sphere becomes fully plastic only for infinite temperatures. Stresses within the sphere at a number of temperatures are shown in Figs. 2 and 3. It may be noted that, as the temperature increases, the stress gradients in the elastic zone become increasingly steep, and that in the limit of infinite temperature the elastic zone degenerates to a surface of discontinuity of q_θ.

It would be an advantage to be able to eliminate the parameter ϵ between equations (19) and (20) so that the displacement

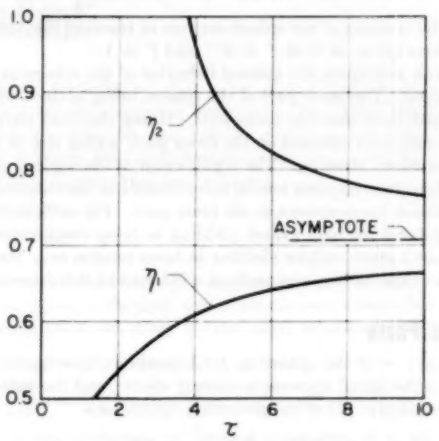

Fig. 1 Position of elastic-plastic boundaries

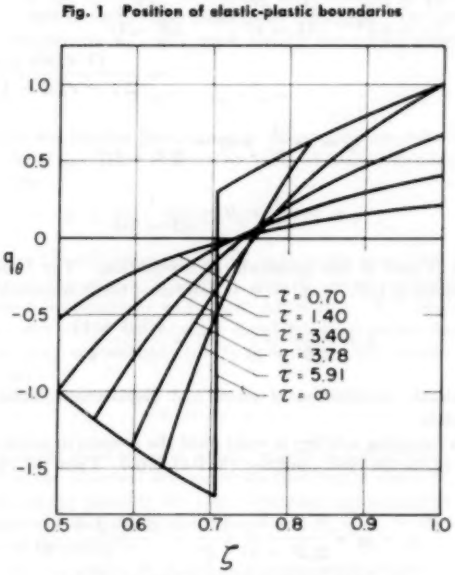

Fig. 2 Distribution of circumferential stress

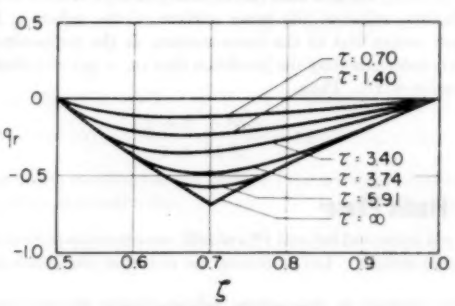

Fig. 3 Distribution of radial stress

could be expressed explicitly as a function of τ. Although this cannot be done for general τ, it can be performed approximately when ϵ is small; i.e., when τ is large. By expanding (20) in powers of ϵ and inverting the series by successive approximations, we obtain

$$\epsilon = 2(\beta - 1)/\tau\beta^{1/2} + 2(\beta - 1)^2/\tau^2\beta + 0(1/\tau^3) \quad (21)$$

By using (21) and (19) the constant $C = -3A$ may be expressed as a series of inverse powers of τ and then, from (14), the asymptotic form of the displacement is obtained,

$$v = \frac{\tau}{(\beta - 1)}\left(\tfrac{3}{2} - \zeta - \frac{1}{2\beta\zeta^2}\right) + \frac{(1 - 2\nu)\zeta q_r}{(1 - \nu)} + 0\left(\frac{1}{\tau}\right) \quad (22)$$

Similarly, we derive the expression for the width of the elastic zone,

$$\eta_2 - \eta_1 = 2(\beta - 1)/\beta\tau + 0(1/\tau^3) \quad (23)$$

Approximate Solution

Let us consider now the approximate solution in which the elastic strains are neglected. As will be seen, the neglect of elastic strains leads to considerable simplification.

When elastic strains are omitted the relations (4) and (5) reduce to

$$\frac{dv}{d\zeta} = \frac{\tau(1/\zeta - 1)}{(\beta - 1)} + e_r^P \quad (24)$$

$$\frac{v}{\zeta} = \frac{\tau(1/\zeta - 1)}{(\beta - 1)} + e_\theta^P \quad (25)$$

while the other governing equations (2), (3), and (6) remain unchanged. We note that equations (24) and (25) are incompatible with each other if the plastic strains vanish. Hence the existence of a region of zero plastic strain or of zero plastic strain rate is impossible. The entire sphere must be deforming plastically. Then clearly the sphere is divided into two zones; an inner zone within which the stresses are given by (12), and an outer zone within which the stresses are given by (17). The boundary between the two zones, determined by the condition that q_r be continuous across the boundary, is the spherical surface $\zeta = \beta^{-1/2}$. The hoop stress q_θ is discontinuous across the boundary. The foregoing stress distribution is seen to be the limit of the elastic-plastic stress distribution for infinitely high temperature.

When elastic strains are neglected, expression (14) for the displacement reduces to

$$v = \tau(\tfrac{3}{2} - \zeta)/(\beta - 1) + C/\zeta^2 \quad (26)$$

Since yielding occurs in opposite senses in the two zones of the sphere, and since the displacement and hence the strains are continuous, it follows that the plastic strain at the (fixed) boundary between the two zones must be zero. This fact enables us to determine the constant C, through the use of (25). Thus $C = -\tau/2\beta(\beta - 1)$, and hence from (26)

$$v = \frac{\tau}{(\beta - 1)}\left\{\tfrac{3}{2} - \zeta - \frac{1}{2\beta\zeta^2}\right\} \quad (27)$$

Expression (27) is the leading term of the expansion (22). The approximate analysis in which elastic strains are neglected thus yields the asymptotic limit of the exact solution for infinitely high temperatures.

A better approximation to the displacements can be obtained in the following way: We calculate the displacements from the exact stress-strain relations (4) and (5). However, to compute the elastic strains we use the approximate stress distribution given by the simplified analysis. It is easily seen that this method will lead to expression (14), it being understood that q_r in the expression denotes the radial stress given by the simplified analysis. The determination of the constant C now requires attention. Here the boundary between the two plastic zones must be regarded as an extremely thin elastic zone.[5] Recalling that $C = -3A$, we find from (8) and (9) that C is related to the stresses in the elastic region by

$$\tau/2(\beta - 1)\zeta + (q_r - q_\theta) + C/\zeta^3 = 0 \quad (28)$$

and hence

$$\frac{\tau}{2(\beta - 1)}\int\frac{d\zeta}{\zeta} + \int(q_r - q_\theta)d\zeta + C\int\frac{d\zeta}{\zeta^3} = 0 \quad (29)$$

where the integration extends over the elastic zone. If the elastic zone is thin, then

$$\int\frac{d\zeta}{\zeta} \simeq h\left\{\frac{1}{\zeta}\right\}_{\zeta=\beta^{-1/2}} = h\beta^{1/2}$$

$$\int\frac{d\zeta}{\zeta^3} \simeq h\left\{\frac{1}{\zeta^3}\right\}_{\zeta=\beta^{-1/2}} = h\beta^{3/2}$$

where h is the nondimensional width of the elastic zone. On the assumption that $(q_r - q_\theta)$ is approximately linear in the elastic zone, $\int(q_r - q_\theta)d\zeta = 0$. With these approximations, (29) yields $C = -\tau/2\beta(\beta - 1)$, and the improved approximation to the displacement is

$$v = \frac{\tau}{(\beta - 1)}\left\{\tfrac{3}{2} - \zeta - \frac{1}{2\beta\zeta^2}\right\} + \frac{(1 - 2\nu)}{(1 - \nu)}\zeta q_r \quad (30)$$

The error in (30) is $0(1/\tau)$.

An estimate of the width of the elastic zone may be obtained by considering the jumps in the terms of (28) across the elastic zone. Thus from (28)

$$[\tau/2(\beta - 1)\zeta] + [q_r - q_\theta] + [C/\zeta^3] = 0 \quad (31)$$

where the square brackets denote the change in the quantity across the elastic zone. Now $[q_r - q_\theta] = -2$, and to a first approximation

$$\left[\frac{\tau}{2(\beta - 1)\zeta}\right] \simeq \frac{h\tau}{2(\beta - 1)}\left\{\frac{d}{d\zeta}\left(\frac{1}{\zeta}\right)\right\}_{\zeta=\beta^{-1/2}} = \frac{-\beta h\tau}{2(\beta - 1)}$$

$$\left[\frac{C}{\zeta^3}\right] \simeq hC\left\{\frac{d}{d\zeta}\left(\frac{1}{\zeta^3}\right)\right\}_{\zeta=\beta^{-1/2}} = -3hC\beta^2$$

Hence, from (31),

$$h \simeq 2(\beta - 1)/\beta\tau$$

which agrees, to first order, with (23).

The approximate analysis is readily extended to the calculation of stresses in the more realistic case where the yield stress is a function of temperature. The calculation of displacements, however, becomes difficult and cumbersome owing chiefly to the fact that the boundary between the two plastic zones may move as τ varies.

Acknowledgment

The author is indebted to Prof. E. T. Onat of Brown University for much helpful advice given during the preparation of this paper.

[5] Compare the discussion in [7] or [8].

References

1 J. C. Wilhoit, Jr., "Elastic-Plastic Stresses in Rings Under Steady State Radial Temperature Variation," Proceedings of the Third U. S. National Congress of Applied Mechanics, 1958, pp. 693–700.

2 D. R. Bland, "Elastoplastic Thick-Walled Tubes of Work-Hardening Material Subjected to Internal and External Pressures and to Temperature Gradients," *Journal of the Mechanics and Physics of Solids*, vol. 4, 1956, pp. 209–229.

3 S. R. Bodner, "Elastoplastic Stress Analysis of Thin-Walled Spherical Shells Subjected to Radial Temperature Gradients," AVCO R&D Division, Lawrence, Mass. Report No. RAD-TR-2-57-25, 1957.

4 J. Weiner, "An Elastoplastic Thermal-Stress Analysis of a Free Plate," JOURNAL OF APPLIED MECHANICS, vol. 23, TRANS. ASME, vol. 78, 1956, pp. 395–402.

5 R. Hill, "The Mathematical Theory of Plasticity," Oxford University Press, London, England, first edition, 1950, pp. 97–103.

6 I. S. Sokolnikoff, "Mathematical Theory of Elasticity," McGraw-Hill Book Company, Inc., New York, N. Y., second edition, 1956, pp. 362–364.

7 W. Prager and P. G. Hodge, Jr., "Theory of Perfectly Plastic Solids," John Wiley & Sons, Inc., New York, N. Y., first edition, 1951, p. 158.

8 E. H. Lee, "On Stress Discontinuities in Plane Plastic Flow," Proceedings of the Third Symposium on Applied Mathematics, McGraw-Hill Book Company, Inc., New York, N. Y., 1950, pp. 213–228.

Rupture Instability of Plane Membranes and Solids

S. F. BORG
Professor and Head
of Civil Engineering,
Stevens Institute of Technology,
Hoboken, N. J.

A fundamentally new approach to the rupture-fracture problem is presented. Because of the particular type of dynamic phenomena being investigated, the formulation is given in terms of the conservation equations of continuum mechanics instead of in the usual elasticity-plasticity relations. The introduction of a similarity co-ordinate permits a complete closed-form solution to a particular problem of practical interest subject to certain compatibility conditions which depend upon the specific properties of the material under consideration.

Introduction

Consider a thin, uniform-thickness, infinite plane membrane subjected to a uniform edge tensile stress and hence a uniform stress field throughout. Assume the membrane is punctured by a sharp point at some interior station. In the particular formulation of the problem as presented herein, we may assume that either of two things may happen:

(*a*) The small hole and membrane remain static and in equilibrium, for all times, $t > 0$.

(*b*) The membrane will rupture catastrophically.

Whichever happens—(*a*) or (*b*)—depends upon the value of the edge stress and also the physical properties of the membrane. It will be shown that there is a possible combination of stress and material properties for which the membrane will rupture and this will represent a criterion for rupture instability of the type considered. The determination of this criterion will be discussed and we shall obtain a particular complete solution for the dynamic behavior of the membrane during this period of rupturing instability.

Because the instability is dependent upon several different parameters, it is quite likely that the solution obtained is not unique. That is, another combination of the various stress and material properties may correspond to an entirely different dynamic behavior of the rupturing membrane. However, in so far as can be determined, the solution given herein is the only one presented up to this time for the dynamic behavior of a fracturing or rupturing element. As such, it should be of interest in applied mechanics generally, and especially in connection with fatigue failures and other rupture phenomena. It also may be of interest to workers in biophysics and related fields in connection with certain cell and tissue phenomena. It is conceivable that applications may be found in celestial mechanics.

Finally, the three-dimensional analog of the symmetrical membrane also will be analyzed using the same techniques as were used for the membrane. In this case we have a solid mass subjected to a uniform tensile field throughout and the rupture criterion as well as dynamic rupturing behavior may be determined.

Presented at the Summer Conference of the Applied Mechanics Division, University Park, Pa., June 20–22, 1960, of The American Society of Mechanical Engineers.

Discussion of this paper should be addressed to the Secretary, ASME, 29 West 39th Street, New York, N. Y., and will be accepted until October 10, 1960, for publication at a later date. Discussion received after the closing date will be returned.

Note: Statements and opinions advanced in papers are to be understood as individual expressions of their authors and not those of the Society. Manuscript received by ASME Applied Mechanics Division, July 9, 1959. Paper No. 60—APM-1.

Procedure—Plane Membrane Solution

We analyze first the rupturing constant-thickness plane membrane, subjected to a particular uniform tensile edge stress, σ_o. We are interested in the behavior of this membrane starting with time $t = 0$, the instant it is punctured by a sharp point. For the dynamic phenomenon being investigated in this paper, the membrane (and solid) material may be assumed to have the properties of a border region fluid-solid or fluid-gas. Therefore the analysis may be based upon the conservation equations of continuum fluid mechanics instead of the somewhat uncertain relations of combined dynamic elasticity-plasticity action, as is usually done in analyzing fracture phenomena. However, it should be mentioned that there is an over-all compatibility equation of energy conservation in which the elastic-plastic behavior is considered—as will be shown later.

Thus the rupturing membrane must satisfy the following equations (given in the two-dimensional symmetrical polar co-ordinate form):

Mass conservation

$$\frac{\partial \rho}{\partial t} + \frac{\partial (\rho u)}{\partial r} + \frac{\rho u}{r} = 0 \tag{1}$$

Momentum conservation (Navier-Stokes equation)

$$\frac{\partial u}{\partial t} + u \frac{\partial u}{\partial r} = -\frac{1}{\rho}\frac{\partial p}{\partial r} + {}^4/_3 \nu \left(\frac{\partial^2 u}{\partial r^2} + \frac{1}{r}\frac{\partial u}{\partial r} - \frac{u}{r^2} \right) \tag{2}$$

Nomenclature

C = velocity of small disturbance in membrane or solid (velocity of sound)
p = pressure
r = radial distance co-ordinate
t = time
u = particle velocity
K = kinetic energy
P = initial strain energy of element
U = strain energy remaining in element following rupture
ξ = similarity co-ordinate
θ = angular variation
ρ = density
σ = stress, positive when tension
ν = viscosity
o = subscript, outer
i = subscript, inner

also an equation for the velocity of small disturbances (since the effect of the point rupture spreads radially and reaches a finite distance from the center of rupture),

$$C = \left(\frac{dp}{d\rho}\right)^{1/2} \tag{3}$$

In the foregoing equations, p is the negative mean value of the principal diagonal elements of the stress tensor, i.e.,

$$p = -1/3(\sigma_r + \sigma_\theta + \sigma_z) \tag{4}$$

so that for the uniform membrane stress field we have ($\sigma_r = \sigma_\theta$, $\sigma_z = 0$),

$$p = -\frac{2\sigma_r}{3} \tag{5}$$

Physically, the phenomenon may be described in the following manner (this explanation will justify the assumed boundary conditions for the foregoing mathematical formulation of the field equations):

(*A*) For $t < 0$, the entire membrane is in a uniform tensile stress state, σ_o.

(*B*) At $t = 0$, a small puncture is introduced at some interior station. We may think of this as the sudden introduction, along the arc of a small circle (the puncture point), of an equal and opposite, i.e., compressive stress, $-\sigma_o$. Hence at this inner circle we have

$$\left.\begin{aligned} \sigma_\theta &= \sigma_{\theta F} \\ \sigma_r &= 0 \\ p &= -\frac{\sigma_{\theta F}}{3} \end{aligned}\right\} \tag{6}$$

$\sigma_{\theta F}$ is the "fracture" or "tearing" stress for the material; i.e., the tensile stress which will just cause the membrane to fracture.

(*C*) for $t > 0$, conditions are as shown in Fig. 1:

(*a*) The punctured region now has a radius r_i moving with an assumed constant velocity u_i, the velocity of fracture. The stress along the circle bounding this region is $\sigma_{\theta F}$. Material density here is ρ_i. Within this circle we have a region of "dead" material, with cracks or tears or fractures as required.

(*b*) The outer-reach of the effect of the puncture is at a radius $r_o = Ct$ (where C is the velocity of small disturbances in the stressed membrane material). The *particle* velocity at radius r_o is zero, the edge stress is $+\sigma_o$, and the material density is ρ_o, the initial stressed membrane density.

(*c*) For $r_i < r < r_o$, the particle velocity, membrane density, and stress have some variable values as required by the field equations (1), (2), (3).

Because of the constant velocities of the outer and inner boundaries, and the constant stress $\sigma_{\theta F}$ at the inner boundary, an essential and fundamental simplification is involved by introducing the similarity co-ordinate

$$\xi = r/t \tag{7}$$

Since (based upon dimensional considerations) u must be linear in ξ, it follows that when

$$\frac{\nu}{t\xi^2} \ll 1$$

we may neglect the viscosity term in the Navier-Stokes equation. We will assume this is so, and we shall neglect this quantity in our subsequent analysis. Then equations (1), (2), and (3) become:

Mass conservation

$$-\xi\frac{d\rho}{d\xi} + \frac{d(\rho u)}{d\xi} + \frac{\rho u}{\xi} = 0 \tag{1a}$$

Momentum conservation

$$-\rho\xi\frac{du}{d\xi} + \rho u\frac{du}{d\xi} = -\frac{dp}{d\xi} \tag{2a}$$

State

$$C = \left(\frac{dp}{d\rho}\right)^{1/2} \tag{3}$$

Now, the phenomenon which is represented by a different map in the physical (r, t)-plane for each time t, is shown by a single field in the ξ-plane which holds for all times t, Fig. 2. Note $\xi_o = C$ is the velocity of sound of small disturbances in the stressed membrane and is the outer reach of affect. ξ_i is the velocity of the fractured boundary and hence also the fracture velocity in the membrane.

The solution to these equations which satisfies all of the physical and boundary conditions as previously given in (*A*), (*B*), and (*C*), is

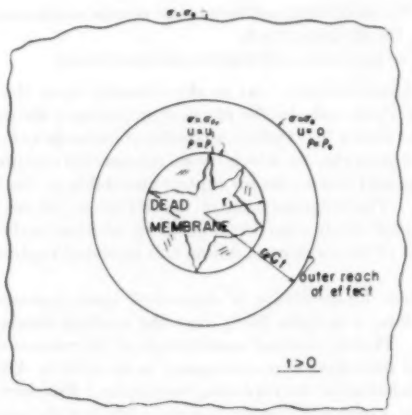

Fig. 1

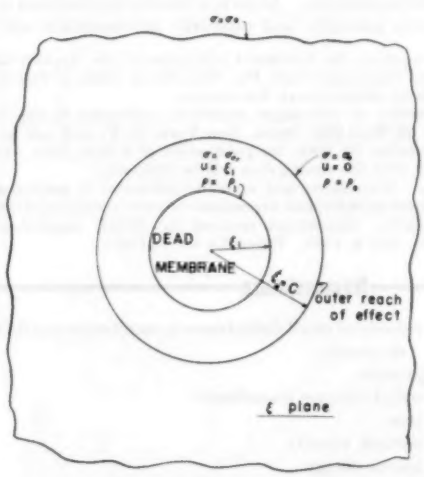

Fig. 2

$$u = \xi_o - \xi \tag{8}$$

$$\rho = \rho_o \frac{\xi_o}{\xi} \tag{9}$$

$$2\sigma_o + 3p = 6\rho_o \xi_o(\xi_o - \xi) - 3\rho_o \xi_o^2 \ln \frac{\xi_o}{\xi} \tag{10}$$

Equation (8) indicates that the velocity of the inner fracture surface is half the velocity of sound in the stressed membrane. This may be taken as the velocity of the fracture.

In this connection, it is interesting to note that Mott[1] found that the velocity of travel for a linear fatigue crack in metals is given by approximately

$$u = 0.38C \tag{11}$$

as compared to the value

$$u = 0.5C \tag{12}$$

found in the foregoing.

The solutions of Equations (8), (9), and (10) imply certain restrictions on the field quantities for the particular solution obtained:

(*a*) Because $\xi_i = \xi_o/2$, it follows that ρ_i must equal $2\rho_o$.

(*b*) Since $\sigma_{\theta F}$, the stress at the inner radius is just equal to the fracture stress for the material, from Equation (10),

$$2\sigma_o = \sigma_{\theta F} + 0.92\rho_o \xi_o^2 \tag{10a}$$

This determines the required value σ_o. From this equation it follows that

$$\sigma_{\theta F} > 0.92\rho_o \xi_o^2 \tag{10b}$$

since otherwise the membrane will fracture at points other than the inner boundary.

It seems obvious that any stress greater than σ_o as given in Equation (10*a*) (other quantities remaining the same) will also cause an instability rupture, although the complete dynamic solution will not be as given in Equations (8), (9), and (10). It is not clear what effect a change in ρ_i (other quantities remaining the same) will have on the rupture phenomenon.

It is also necessary that over-all energy conservation be maintained during the rupturing process. This is essentially a compatibility condition on any acceptable solution. To obtain this we may proceed as follows.

Let P equal the potential (strain) energy in the membrane just before it is punctured.

Let U equal the strain energy remaining in the entire membrane during rupture. This will require an assumption as to the division of p between σ_θ and σ_r. It will also depend upon the number of tears or fracture surfaces in the dead membrane.

Let K_1 equal to the kinetic energy of the portion of the membrane between r_i and r_o.

Let K_2 equal the kinetic energy of the dead membrane; i.e., the membrane for $r < r_i$.

Then over-all constancy of energy requires

$$P - U = K_1 + K_2 \tag{13}$$

In this equation P and U can be approximated for a given material of known stress-strain characteristics and for an assumed fracture configuration. Note that no restriction to elastic action is necessary. That is, the membrane may be initially stressed in the plastic range.

K_1 and K_2 can also be determined from the solution to the field equation as given in Equation (4).

[1] N. F. Mott, "Brittle Fracture of Mild Steel Plates," *Engineering* (British), vol. 164, 1947; vol. 165, 1948.

We may interpret this energy-balance equation in either of two ways:[2]

1 It may be solved (for an assumed fracture geometry) in terms of:

σ_o = critical stress
C = velocity of small disturbances
E = effective modulus of elasticity
ρ = effective density
$\sigma_{\theta F}$ = tearing stress

and a *criterion* obtained for the existence of the instability considered herein.

2 The particular instability solution obtained will occur providing the energy balance is maintained. All terms in the energy-balance expression can be approximated from the given solution for a given material except for the fracture geometry; i.e., number of tears or cracks. We may solve the equation and the solution will then give the number of cracks required for the existence of the instability in question.

The Three-Dimensional Solution

We may proceed in exactly the same way for the three-dimensional case. Now using spherical co-ordinates, and noting as before the assumption which eliminates the viscosity term from the Navier-Stokes equation, we have:

Mass conservation

$$\frac{\partial \rho}{\partial t} + \frac{\partial(\rho u)}{\partial r} + \frac{2\rho u}{r} = 0 \tag{14}$$

Momentum conservation

$$\frac{\partial u}{\partial t} + u\frac{\partial u}{\partial r} = -\frac{1}{\rho}\frac{\partial p}{\partial r} + {}^4/_3\,\nu\left(\frac{\partial^2 u}{\partial r^2} + \frac{2}{r}\frac{\partial u}{\partial r} - \frac{2u}{r^2}\right) \tag{15}$$

State

$$C = \left(\frac{dp}{d\rho}\right)^{1/2} \tag{16}$$

which become, in terms of the similarity co-ordinate, $\xi = r/t$, Equation (7):

Mass conservation

$$-\xi\frac{d\rho}{d\xi} + \frac{d(\rho u)}{d\xi} + \frac{2\rho u}{\xi} = 0 \tag{14a}$$

Momentum conservation

$$-\xi\frac{du}{d\xi} + u\frac{du}{d\xi} = -\frac{1}{\rho}\frac{dp}{d\xi} \tag{15a}$$

State

$$C = \left(\frac{dp}{d\rho}\right)^{1/2} \tag{16}$$

The solution to these which satisfies all required boundary and physical conditions is

$$u = 2(\xi_o - \xi) \tag{17}$$

[2] The over-all energy compatibility conditions involved in the two statements which follow are similar to those utilized by Griffith in his classical formulation of brittle-material crack theory and by later workers who refined the Griffith theory to include elastic and plastic effects in various approximate ways. See in this connection a paper by G. M. Boyd, "The Conditions for Unstable Rupturing of a Wide Plate," presented at the March 28, 1957, meeting of The Institution of Naval Architects in London.

$$\rho = \rho_o \left(\frac{\xi_o}{\xi}\right)^2 \tag{18}$$

$$p + \sigma_o = 2\rho_o \xi_o^2 \left[3 \ln \frac{\xi_o}{\xi} + 2\left(1 - \frac{\xi_o}{\xi}\right)\right] \tag{19}$$

which indicates that the velocity of fracture in this case is $0.67C$.

Just as for the plane membrane, an over-all energy balance must be maintained for the rupturing solid, in order for the instability to occur.

Conclusion

A physical model for a rupturing plane membrane has been developed and a particular solution has been obtained for the dynamic action of this element. Results obtained indicate that the velocity of the fracture is $0.5C$. The necessary over-all energy compatibility condition is briefly discussed.

The solution for the uniformly stressed solid indicates that the velocity of fracture is $0.67C$.

Expansion of Thick-Walled Cylinders Fabricated From Cold Bent Plates[1]

IRWIN BERMAN
Staff Engineer,
Research Division,
Foster Wheeler Corporation,
New York, N. Y.
Mem. ASME

The problem of the elastic-plastic expansion by internal pressure of thick-walled cylinders that were fabricated by cold bending initially flat plate is analyzed by the use of the principal shear theory of piecewise linear plasticity. The strain-hardening material may have been initially anisotropic and may have developed inhomogeneity and further anisotropy due to the cold bending. The numerical example which is then solved shows that, even for materials which have similar initial yield properties before bending, there are substantial differences in terms of the pressure at which initial yielding occurs in the cylinder and in terms of subsequent cylinder behavior. Those differences in cylinder behavior occur because the materials which are compared have yield surfaces which behave differently when the material is plastically strained.

THIS paper considers the stresses and deformations in inhomogeneous and anisotropic thick-walled cylinders that were made of a strain-hardening material. The stresses and deformations are caused by the application of an increasing internal pressure to the point at which the entire cylinder becomes plastic. The thick-walled cylinders were fabricated from plates which had been cold bent into the cylindrical shape. It is assumed that before they were bent the flat plates had homogeneous but anisotropic strength properties. Since a strain-hardening material is being considered, the strength properties of the plates after they are bent into the cylindrical shape may be both inhomogeneous and anisotropic. The bent plates and cylinder heads are assumed to be assembled so that the initial material properties of the cylindrical portion of the pressure vessel are the same as the final material properties of the bent plate. Therefore the cylinder analysis will include the effect of fabrication as an integral part of the results.

A short review of those portions of the theory which will be used in this paper, i.e., piecewise linear plasticity based on principal shear stresses, will be presented in the following section. In the third section, the strength properties of the plates after they are bent into the cylindrical shape are determined. The subsequent three sections present the cylinder analysis. Expressions are developed from which the stresses and strains in the cylinder may be determined in terms of various material constants. In the final section, a numerical example illustrates the importance of the results in terms of the difference in cylinder behavior for materials with similar initial yield and strain-hardening properties but different "secondary" hardening properties.

Piecewise Linear Plasticity Based on Principal Shear Stresses

The theory of piecewise linear plasticity based on principal shear stresses, hereafter called the principal shear theory, was presented as a special case of the general theory of piecewise linear plasticity by Berman and Hodge.[2] This theory may only apply to those problems of plasticity for which the principal directions of stress and strain coincide and remain fixed in each element throughout the loading process. As in the other flow theories of plasticity, the principal shear theory requires that for each material element the yield surface, flow laws, and change of yield surface with plastic flow be specified.

The criterion of initial yielding may be represented by a surface on a three-dimensional principal stress representation. If hydrostatic states of stress do not effect the yielding of a material, then the yield surface may be replaced by the yield curve in the plane of stress states for which the hydrostatic component of stress is zero. A typical initial yield curve for a material which conforms to the principal shear theory is shown in Fig. 1 as $A'B'C'D'E'F'$. The initial yield curve of Fig. 1 may also be considered as an approximation to the actual yield curve of a real material. The positions of the sides of the initial yield hexagon may be described by six linear relationships between the stresses as

$$(S_1 - S_3)/a = 1, \quad \text{side } A'B'; \tag{1}$$

$$(S_2 - S_3)/b = 1, \quad \text{side } B'C'; \tag{2}$$

$$(S_2 - S_1)/c = 1, \quad \text{side } C'D'; \tag{3}$$

$$(S_3 - S_1)/d = 1, \quad \text{side } D'E'; \tag{4}$$

$$(S_3 - S_2)/e = 1, \quad \text{side } E'F'; \tag{5}$$

$$(S_1 - S_2)/f = 1, \quad \text{side } F'A' \tag{6}$$

where S_1, S_3, and S_2 are the three principal stresses and a, b, c, d, e, and f are material constants which are required to define the position of each side of the initial yield hexagon. It should here be noted that the basic theory is only concerned with the state of stress at a point. Therefore, all material "constants" may equally well be regarded as material "variables" if they are different from point to point.

In the derivation of the flow laws, it is assumed that the rigid-plastic material is incompressible and that the plastic-strain-rate vector on a side regime of the yield polygon must be normal to that side. The flow laws for a typical side $C'D'$ may be written as

$$\dot{\varepsilon}_2 = (\dot{S}_2 - \dot{S}_1)/c, \tag{7}$$

$$\dot{\varepsilon}_1 = -\dot{\varepsilon}_2, \tag{8}$$

$$\dot{\varepsilon}_3 = 0 \tag{9}$$

[1] This paper is part of a thesis submitted by the author in partial fulfillment of the requirements for the degree of Doctor of Philosophy in Applied Mechanics at the Polytechnic Institute of Brooklyn.

Presented at the West Coast Conference of the Applied Mechanics Division, Pasadena, Calif., June 27–29, 1960, of THE AMERICAN SOCIETY OF MECHANICAL ENGINEERS.

Discussion of this paper should be addressed to the Secretary, ASME, 29 West 39th Street, New York, N. Y., and will be accepted until October 10, 1960, for publication at a later date. Discussion received after the closing date will be returned. Manuscript received by ASME Applied Mechanics Division, June 17, 1959. Paper No. 60—APMW-2.

[2] I. Berman and P. G. Hodge, Jr., "A General Theory of Piecewise Linear Plasticity for Initially Anisotropic Materials," *Arch. Mech. Stos.*, vol. 11, Nov.-Dec., 1959.

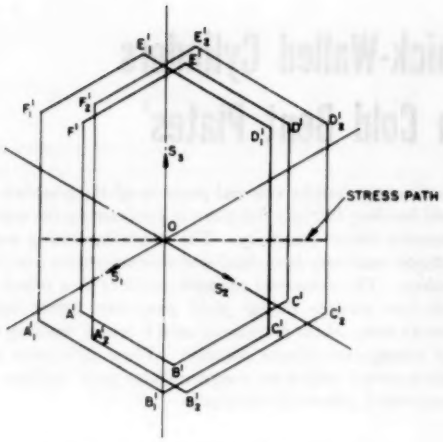

Fig. 1 Yield curves—principal shear theory

where s_1, s_2, and s_3 are the principal strains, a dot above a quantity denotes rate of change, and the capital letters A, B, C, D, E, and F are material constants called side-hardening constants. In a similar manner, the flow laws of side $F'A'$ may be expressed by equations (8) and (9) and by

$$F\dot{s}_1 = (\dot{S}_1 - \dot{S}_2)/f \tag{10}$$

Let the position on the principal stress representation shown in Fig. 1 be called the stress point. If the stress point is on a side of a yield polygon so that plastic flow and strain-hardening take place, the side moves parallel to itself along with the stress point. In addition, plastic strain-hardening on a side creates new material properties in all directions. For the principal shear theory, each remaining side moves parallel to itself at an independent constant rate. The motion of the yield curve when the stress point is acting on sides $C'D'$ and $F'A'$ is shown in Table 1.

shear theory. The cylindrical bending is caused by end couples such that at a short distance from the ends the stresses and strains are constant along each circumferential fiber. The strain in the width direction is negligible and any change in the thickness of the plate is neglected in the determination of the position of an element. Since the purpose of the plate-bending analysis is to determine the material properties of the plate after bending, and the plastic strains are large compared to the elastic strains, the material is assumed to be a rigid-plastic one. Thus, if the origin in stress space always remains within the yield curve, there is no springback of the plate and there are no residual stresses after bending.

The bending neutral axis of a circular cross section of the bent plate may be defined as the line of no change in length for an infinitesimal additional deformation. In the present simplified analysis, it is assumed that the circumferential strain is proportional to the current distance from the neutral axis. It is also assumed that the change of strain from the initial unstrained position took place continuously in the positive or negative direction. Thus the current properties are determined by the position of the neutral axis at that time.

Since the strains in the width direction are zero and the material considered is rigid-plastic, at a small axial distance from the curved edges of the bent plate, the stress in the width direction is

$$S_3 = (S_1 + S_2)/2 \tag{11}$$

where the subscripts 1, 2, and 3, as shown in Fig. 1, refer to the radial, circumferential, and width directions, respectively. The stress path for each element will be a horizontal line as shown in Fig. 1. In the following development, it is assumed that the stress path of a material element initially contacts $C'D'$ or $F'A'$ of the yield hexagon and, during metal flow, the stress point is always on side $C'D'$ or side $F'A'$ of the current yield hexagon. The inequalities which must be satisfied for this to be so will be derived later in this section.

For the portion of the plate outside of the neutral axis, while metal flow is taking place, the stress point of each element is on side $C'D'$ of the yield curve. Since the stress point contacts side

Table 1 Change of yield curve with stress point acting on sides $C'D'$ and $F'A'$

Side of stress point		$C'D'$	$F'A'$
Side motion	$A'B'$	$K_{AC}C\dot{s}_2 = (\dot{S}_1 - \dot{S}_2)/a$	$K_{aA}F\dot{s}_1 = (\dot{S}_1 - \dot{S}_2)/a$
	$B'C'$	$K_{cb}C\dot{s}_2 = (\dot{S}_2 - \dot{S}_3)/b$	$K_{BF}F\dot{s}_1 = (\dot{S}_2 - \dot{S}_3)/b$
	$C'D'$	$C\dot{s}_2 = (\dot{S}_2 - \dot{S}_1)/c$	$K_{CF}F\dot{s}_1 = (\dot{S}_2 - \dot{S}_1)/c$
	$D'E'$	$K_{dc}C\dot{s}_2 = (\dot{S}_3 - \dot{S}_1)/e$	$K_{DF}F\dot{s}_1 = (\dot{S}_3 - \dot{S}_1)/d$
	$E'F'$	$K_{EC}C\dot{s}_2 = (\dot{S}_3 - \dot{S}_2)/e$	$K_{fe}F\dot{s}_1 = (\dot{S}_3 - \dot{S}_2)/e$
	$F'A'$	$K_{FC}C\dot{s}_2 = (\dot{S}_1 - \dot{S}_2)/f$	$F\dot{s}_1 = (\dot{S}_1 - \dot{S}_2)f$

The constants K with two lower case letter subscripts are material constants and are called transition contants. They describe the ratio of the motion of the adjacent sides to that of the side on which the stress point acts. The constants K with two capital letter subscripts are material constants and are called secondary hardening constants. They describe the ratio of the motion of the remaining sides to that of the side on which the stress point acts.

Plate Bending

The material properties of the plate before bending are taken to be homogeneous but anisotropic. The plate considered is bent cold into the correct cylindrical shape with only such intermediate and final heat-treatment permitted as may be necessary to prevent brittle failure. The rate of change of the properties of an element of material is assumed to be such that the physical properties, which are present after the completion of the heat-treatment, were reached within the framework of the principal $C'D'$ from the interior of the yield curve, both the position of the stress point and the position of side $C'D'$ may be obtained from equations (3), (7), (8), and (9) and represented by

$$Cs_2 = (S_2 - S_1)/c - 1 \tag{12}$$

in terms of the strain of the element of the material.

For an element of the bent plate which is on the inside of the neutral bending axis, while metal flow is taking place, the stress point is on side $F'A'$ of the yield curve. Both the position of the stress point and the position of side $F'A'$ may be obtained from equations (6), (8), (9), and (10) and represented by

$$Fs_1 = (S_1 - S_2)/f - 1 \tag{13}$$

By the integration of the proper expression in Table 1, the position of side $C'D'$, resulting from the motion of the stress point outside of side $F'A'$, may be written as

$$K_{CF}Fs_1 = (S_2 - S_1)/c - 1 \tag{14}$$

Since the circumferential strain is proportional to the distance from the neutral axis, the circumferential strain may be expressed as

$$\epsilon_2 = r/R - 1 \tag{15}$$

where r is the radial co-ordinate measured from the current center and R is the radial distance to the neutral axis measured from the same center. Also, since the stress point of each element of the plate is on side $C'D'$ or $F'A'$ during plastic flow,

$$\epsilon_1 = -\epsilon_2 \tag{16}$$

The position of the bending neutral axis may then be determined from the equation of radial equilibrium,

$$dS_1/dr = (S_2 - S_1)/r, \tag{17}$$

the boundary conditions at the inner and outer surface, from equations (12), (13), (15) and (16), and from the continuity of the radial stress at the neutral axis. The expression from which the bending neutral axis may be obtained may then be written as

$$R[f(1 + F) \ln (R/r_i) - e(1 - C) \ln (r_o/R)] = eC(r_o - R) + fF(R - r_i) \tag{18}$$

where r_i is the inner radius and r_o the outer radius.

The foregoing analysis is predicated upon the assumption that the stress points of the elements of the plate initially contact and cause plastic flow only when they are in contact with sides $C'D'$ and $F'A'$. The conditions that are necessary for this assumption to be valid in terms of initial contact may be obtained from the equations of the initial position of the hexagon equations (1–6) and the equation of the stress path equation (11). The result may be written as

$$c < 2b, \quad c < 2d, \qquad R \leq r \leq r_o; \tag{19}$$

$$f < 2a, \quad f < 2e, \qquad r_i \leq r \leq R \tag{20}$$

After plastic flow has taken place, the conditions which are necessary in order that the stress points remain on sides $C'D'$ or $F'A'$ may be determined from the appropriate expressions in Table 1, the initial conditions, and equations (11), (15), and (16). The inequalities which must be satisfied in order that, during plastic flow, the stress points of the elements outside of the neutral axis remain in contact with side $C'D'$ may be written as

$$c(1 - C) + eCr/R < 2b(1 - K_{ab}C) + 2bK_{ab}Cr/R, \tag{21}$$

$$c(1 - C) + eCr/R < 2d(1 - K_{ad}C) + 2dK_{ad}Cr/R \tag{22}$$

The inequalities which must be satisfied in order that, during plastic flow, the stress points of the elements inside of the neutral axis remain in contact with side $F'A'$ may be written as

$$f(1 + F) - fFr/R < 2e(1 + K_{fe}F) - 2eK_{fe}Fr/R, \tag{23}$$

$$f(1 + F) - fFr/R < 2a(1 + K_{ab}F) - 2aK_{ab}Fr/R \tag{24}$$

The case of an initially isotropic, homogeneous plate will be numerically considered in the final section. Let all the yield constants be designated by c, the side-hardening constants C, and the transition constants by K'. The expression from which the neutral axis is determined may then be written as

$$\ln [(r_o/R)(r_i/R)] + C[(r_o/R) - (r_i/R)] - C \ln (r_o/r_i) = 0 \tag{25}$$

The inequalities described in equations (21), (22), (23), and (24) may all then be satisfied by the expression

$$|C(1 - r/R)(1 - 2K')| < 1 \tag{26}$$

The location of the neutral axis may be determined from equation (18) or (25). The new position of side $C'D'$ of the yield curve after the plate is bent may then be obtained. Thus the initial yield criterion for each element of the cylinder which is loaded by internal pressure is known. Let $A'B'C'D'E'F'$ of Fig. 1 represent the initial yield curve of an element of the flat plate prior to bending. A typical subsequent yield curve for an element in which the stress point acted on side $F'A'$ is shown by $A_1'B_1'C_1'D_1'E_1'F_1'$. The position of side $C_1'D_1'$ of the yield polygon may be obtained from equations (14), (15), and (16) and written as

$$S_2 - S_1 = c[1 + K_{CF}F - K_{CF}F(r/R)] \tag{27}$$

For elements of the plate which are outside of the bending neutral axis, during bending the stress point acted on side $C'D'$ of the yield curve. A typical subsequent yield curve for those material elements is shown by $A_2'B_2'C_2'D_2'E_2'F_2'$ in Fig. 1. The position of side $C_2'D_2'$ may be determined from equations (12) and (15) and written as

$$S_2 - S_1 = c(1 - C + Cr/R) \tag{28}$$

Cylinder Expansion

Since, for the partially plastic, thick-walled cylinders which are considered, the elastic strains are of the same order of magnitude as the plastic strains, both elastic and plastic strains will be accounted for. The material is assumed to be incompressible in both the elastic and plastic ranges in order to reduce the complexity of the calculations so that the important sequence of events may be followed more clearly. The problem which is solved is one for which there is negligible axial strain during the entire expansion process and for which the stress point during plastic flow always remains on side $C'D'$ of the current yield curve. The inequalities which must be satisfied so that the stress point of each element should initially contact side $C'D'$ and remain in the regime $C'D'$ during the plastic flow may be determined from Table 1 and the position of each yield polygon.

The cylinders were fabricated so that the initial yield polygon of an element is the same as its final yield polygon in the bent plate. Therefore equations (27) and (28) may be used to define the initial position of side $C'D'$ for cylinder expansion. Typical graphs of the initial position of side $C'D'$ of the yield polygon for cylinder expansion for all radial positions are shown by the solid lines in Fig. 2. Two of the curves are for a material which may harden in an isotropic manner whereas the third is for a

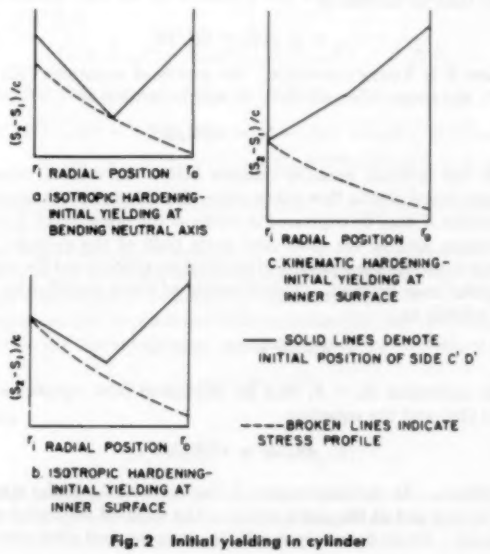
$(S_2-S_1)/c$
r_i RADIAL POSITION r_o
a. ISOTROPIC HARDENING-INITIAL YIELDING AT BENDING NEUTRAL AXIS
c. KINEMATIC HARDENING-INITIAL YIELDING AT INNER SURFACE
b. ISOTROPIC HARDENING-INITIAL YIELDING AT INNER SURFACE
—— SOLID LINES DENOTE INITIAL POSITION OF SIDE C' D'
----BROKEN LINES INDICATE STRESS PROFILE

Fig. 2 Initial yielding in cylinder

material which may harden kinematically. In isotropic hardening, subsequent yield curves are enlarged versions of the initial yield curve with the same origin. In kinematic hardening, the yield curve remains constant in size, and translates but does not rotate.

Because of negligible axial strain and complete incompressibility in both the elastic and plastic regions, the strain relationships may be written as

$$\epsilon_3 = 0, \tag{29}$$

$$\epsilon_1 + \epsilon_2 = 0 \tag{30}$$

where ϵ_1 is the radial strain, ϵ_2 the circumferential strain, and ϵ_3 the axial strain. For the small deformations that are being considered in both the elastic and the plastic portions of the cylinder, the radial and circumferential strains of an element may be expressed as

$$\epsilon_1 = du/dr, \tag{31}$$

$$\epsilon_2 = u/r, \tag{32}$$

where u is the radial displacement of an element. Equations (30), (31), and (32) may be combined and the resulting expression integrated so that the radial displacement may be expressed as

$$u = K/r \tag{33}$$

where K is an integration constant. By the use of equations (31), (32), and (33), the values of radial and tangential strain may be expressed in terms of the radial position and integration constant as

$$\epsilon_1 = -K/r^2, \tag{34}$$

$$\epsilon_2 = K/r^2 \tag{35}$$

Entire Cylinder Elastic

Under the prescribed conditions of total incompressibility, Poisson's ratio is equal to one half. For zero axial strain, the expression relating the axial strain to the stresses leads to the relationship between the stresses which may be written as

$$S_3 = (S_1 + S_2)/2 \tag{36}$$

Hooke's law, relating the circumferential strain to the stresses, may then be written as

$$\epsilon_2 = 3(S_2 - S_1)/4E \tag{37}$$

where E is Young's modulus. By means of equations (35) and (37), the stress difference $S_2 - S_1$ may be written as

$$S_2 - S_1 = 4EK/3r^2 \tag{38}$$

If the internal pressure remains below the critical value at which initial plastic flow takes place, the value of the integration constant K may be expressed in terms of the pressure, of Young's modulus, and of the inner and outer radii of the cylinder. In order to do this the equation of equilibrium which is not identically satisfied may be used. This equation of stress equilibrium may be written as

$$dS_1/dr = (S_2 - S_1)/r \tag{39}$$

The expression $S_2 - S_1$ may be eliminated from equations (38) and (39) and the equation

$$dS_1/dr = 4EK/3r^3 \tag{40}$$

obtained. At the inner radius r_i the value of the radial stress is $S_1 = -p$ and at the outer radius r_o the value of the radial stress is zero. These boundary conditions may be used after the integration indicated in equation (40) is carried out. The results are written as

$$K = (3p/2E)r_i^2/[1 - (r_i/r_o)^2] \tag{41}$$

Then, by the use of equation (40) and the outer boundary condition, the value of the radial stress may be determined as

$$S_1 = (2EK/3)[(1/r)^3 - (1/r_o)^3] \tag{42}$$

The complete stress and deformation solution may now be determined by the use of equations (33), (36), (38), (41), and (42). Thus

$$S_2 - S_1 = 2p(r_i/r)^2/[1 - (r_i/r_o)^2], \tag{43}$$

$$S_1 = -p[(r_i/r)^2 - (r_i/r_o)^2]/[1 - (r_i/r_o)^2], \tag{44}$$

$$S_2 = p[(r_i/r)^2 + (r_i/r_o)^2]/[1 - (r_i/r_o)^2], \tag{45}$$

$$S_3 = p(r_i/r_o)^2/[1 - (r_i/r_o)^2], \tag{46}$$

$$u = (3p/2E)(r_i^2/r)/[1 - (r_i/r_o)^2] \tag{47}$$

Initial Yielding

For the conditions of this problem, the stress path of each element is horizontal on the stress plane as shown in Fig. 1. When the stress point contacts side $C'D'$ of the initial yield polygon, plastic flow takes place. Three possible graphs of the initial position of side $C'D'$ are shown in Fig. 2. Also shown by dotted lines in Fig. 2 is the stress profile for the elastic cylinder when initial yielding occurs. Since this stress profile is shaped as shown in Fig. 2, initial yielding may occur only at the inner surface or at the surface of the final bending neutral axis. The elastic equation describing the stress profile equation (43) may be combined with the equation defining the position of side $C'D'$ inside the bending neutral axis equation (27). If the appropriate radii are then used, the value of the pressure at which initial yielding occurs at the bending neutral axis and at the inner surface, respectively, may be written as

$$P_{yn} = (c/2)(R/r_i)^2[1 - (r_i/r_o)^2], \tag{48}$$

$$P_{yi} = (c/2)[1 - (r_i/r_o)^2][1 + K_{CF}F - K_{CF}F(r_i/R)] \tag{49}$$

The true initial yielding will occur at the surface corresponding to the initial yield-pressure equation for which the pressure is a minimum. By the use of equations (48) and (49), if

$$[1 + K_{CF}F - K_{CF}F(r_i/R)] < (R/r_i)^2 \tag{50}$$

then initial yielding occurs at the inner surface. If

$$[1 + K_{CF}F - K_{CF}F(r_i/R)] > (R/r_i)^2 \tag{51}$$

then initial yielding occurs at the bending neutral axis. If

$$[1 + K_{CF}F - K_{CF}F(r_i/R)] = (R/r_i)^2 \tag{52}$$

then initial yielding occurs simultaneously at the inner surface and the bending neutral axis.

Elastic-Plastic Cylinder

Depending upon the effect of the previous bending-strain history on the position of side $C'D'$ of the yield polygon, under increasing internal pressure, yielding may: (*a*) start at r_i and grow outwards continuously until the entire cylinder becomes plastic; (*b*) start at r_i and grow outward, then start at R and grow both ways (the two plastic regions then expand and merge forming a single elastic-plastic boundary which grows outward until the entire cylinder becomes plastic); (*c*) start at R and grow both ways, then start at r_i and grow outward (the two plastic regions

expand and merge forming a single elastic-plastic boundary which grows outward until the entire cylinder becomes plastic); (*d*) start at R and grow both ways until the entire cylinder becomes plastic.

Only the (*a*) and (*b*) types of behavior will be discussed further in this paper since they are more likely than the others to occur in a physical problem. In order to explore the first type of behavior fully, only two cases need to be considered; namely, the case for which the position of the elastic-plastic boundary is at $r_i \leq r_y \leq R$, and the case for which the elastic-plastic boundary is at $R \leq r_y \leq r_o$, where r_y denotes the radius to the elastic-plastic boundary. The explicit stress and deformation expressions will be developed for the first type of behavior. For the second type of behavior, the case in which two plastic and two elastic regions exist side by side has to be considered in addition to the two cases considered for the first type of behavior. The results for multiple elastic-plastic regions will be discussed and tabulated.

(a) Single elastic-plastic boundary $r_i \leq r_y \leq R$. Consider the case for which the single elastic-plastic boundary lies within the limits $r_i \leq r_y \leq R$ after a pressure increase from the condition of initial yielding. At the elastic-plastic boundary, both the equation defining the initial yield condition of side $C'D'$ and the equation which determines the position of the stress point are valid. Equations (27) and (38) may be combined and the integration constant determined as

$$K = k_0(3r_y^2/2E) \tag{53}$$

where

$$2k_0 = c[1 + K_{CF}F - K_{CF}F(r_y/R)] \tag{54}$$

The complete solution for the elastic portion of the cylinder $r_y \leq r \leq r_o$ may be obtained from equations (33), (36), (38), (42), and (53) as

$$S_2 - S_1 = 2k_0(r_y/r)^2, \tag{55}$$

$$S_1 = k_0[(r_y/r)^2 - (r_y/r_0)^2], \tag{56}$$

$$S_2 = k_0[(r_y/r)^2 + (r_y/r_0)^2], \tag{57}$$

$$S_3 = k_0(r_y/r_0)^2, \tag{58}$$

$$u = k_0(3/2E)(r_y^2/r) \tag{59}$$

For the plastic portion of the cylinder, which is limited by $r_i \leq r \leq r_y$, the appropriate flow law during the period that the stress point touches side $C'D'$ of the yield hexagon is given by equation (7). The initial stress difference at each radius may be determined from side $C'D'$ of the final yield hexagon of the bent plate which is given by equation (27). Since the initial conditions must satisfy the elastic as well as the plastic expression, the initial value of the circumferential strain s_2^* may be obtained from equation (27) and from Hooke's law as shown by equation (37). The result may be written as

$$s_2^* = (3c/4E)[1 + K_{CF}F - K_{CF}F(r/R)] \tag{60}$$

The current stress difference at any radius in the plastic region may then be determined by the integration of equation (7). By the use of equations (27), (35), (53), and (60), the result may be written as

$$S_2 - S_1 = k_p + k_q(r/R) + 2k_r(r_y/r)^2 \tag{61}$$

where

$$k_p = c[1 - (3cC/4E)](1 + K_{CF}F), \tag{62}$$

$$k_q = -cK_{CF}F[1 - (3cC/4E)], \tag{63}$$

$$2k_r = (3c^2C/4E)[1 + K_{CF}F - K_{CF}F(r_y/R)] \tag{64}$$

The radial and circumferential stresses for the plastic region may then be obtained by the use of equations (39) and (61) and by the use of the inner boundary condition that at $r = r_i$, $S_1 = -p$. The axial stress may be determined by the use of equation (36). Although equation (36) was derived for the elastic region, it is also valid for the plastic region. This is so because the assumption that the stress point during plastic flow remains on side $C'D'$ means that the plastic strain in the axial direction is zero. Since the total axial strain was assumed to be zero, the elastic strain is also zero. Elastic incompressibility and Hooke's law therefore again lead to equation (36) as the expression for determining the axial stress in terms of the circumferential and radial stress. The individual stresses in the plastic region may therefore be written as

$$S_1 = -p + k_p[\ln (r/r_i)] + k_q[(r/R) - (r_i/R)] + k_r[(r_y/r_i)^2 - (r_y/r)^2], \tag{65}$$

$$S_2 = -p + k_p[1 + \ln (r/r_i)] + k_q[2(r/R) - r_i/R)] + k_r[(r_y/r_i)^2 + (r_y/r)^2], \tag{66}$$

$$S_3 = -p + k_p[(1/2) + \ln (r/r_i)] + k_q[(3r/2R) - (r_i/R)] + k_r(r_y/r_i)^2 \tag{67}$$

The value of the internal pressure which causes the elastic-plastic boundary to be at position r_y may now be calculated from equations (39), (55), and (61) and may be written as

$$p = k_0[1 - (r_y/r_o)^2] + k_p[\ln(r_y/r_i)] + k_q[(r_y/R) - (r_i/R)] + k_r[(r_y/r_i)^2 - 1] \tag{68}$$

For the first type of elastic-plastic behavior in which initial yielding starts at the inner surface and grows outward continuously, the results of this section are valid for all values of $r_i \leq r_y \leq R$. It must then be shown that yielding does not take place at the bending neutral axis before the elastic-plastic boundary reaches the bending neutral axis. Since the neutral axis was defined as the fiber which does not change in length during bending, the pertinent initial yield curve in cylinder expansion for the radius R is given by equation (3). Thus it must be shown that the stress point at the bending neutral axis, as given by the elastic expression equation (55), does not exceed the value c for all positions of the elastic-plastic boundary within the range $r_i \leq r_y \leq R$. This requirement may be satisfied by stipulating that for all values of the variable r_y/R such that $0 \leq r_y/R \leq 1$,

$$[1 + K_{CF}F - K_{CF}F(r_y/R)](r_y/R)^2 - 1 \leq 0 \tag{69}$$

Equation (69) may be written in the form

$$-K_{CF}F[(r_y/R) - 1]\{(r_y/R) - [1 + (1 + 4K_{CF}F)^{1/2}]/2K_{CF}F\} \times \{(r_y/R) - [1 - (1 + 4K_{CF}F)^{1/2}]/2K_{CF}F\} \leq 0 \tag{70}$$

from which it may be determined that, if $K_{CF}F \leq 2$, multiple regions will not form.

(b) Single elastic-plastic boundary $R \leq r_y \leq r_o$. Consider now the case in which no plastic unloading has taken place and the current single elastic-plastic boundary is within the limits $R \leq r_y \leq r_o$. If equation (28) is combined with equation (38) the resulting expression for the integration constant K may be written as

$$K = k_s(3r_y^2/2E) \tag{71}$$

where

$$2k_s = c[1 - C + C(r_y/R)] \tag{72}$$

The complete solution for the elastic portion of the cylinder, $r_y \leq r \leq r_o$, may then be determined from equations (33), (36), (38), (42), and (71), and written as

$$S_2 - S_1 = 2k_s(r_y/r)^2, \tag{73}$$

$$S_1 = -k_s[(r_y/r)^2 - (r_y/r_o)^2], \tag{74}$$

$$S_2 = k_s[(r_y/r)^2 + (r_y/r_o)^2], \tag{75}$$

$$S_3 = k_s(r_y/r_o)^2, \tag{76}$$

$$u = k_s(3/2E)(r_y^3/r) \tag{77}$$

where the deformation of equation (77) applies to the entire cylinder.

The flow law for the plastic portion of the cylinder may be expressed by equation (7). Two plastic regions are considered separately. The first is the plastic region within the limits $r_i \leq r \leq R$. For this region the stress difference $S_2 - S_1$ may be obtained from equations (27), (35), (7), (60), and (71) and written as

$$S_2 - S_1 = k_p + k_q(r/R) + 2k_i(r_y/r)^2 \tag{78}$$

where

$$2k_i = (3c^2C/4E)[1 - C + C(r_y/R)] \tag{79}$$

By the use of equations (36), (39), and (78) and the inner boundary condition that at $r = r_i$, $S_1 = -p$, the individual stresses for the plastic region $r_i \leq r \leq R$ may be written as

$$S_1 = -p + k_p[\ln(r/r_i)] + k_q[(r/R) - (r_i/R)] + k_i[(r_y/r_i)^2 - (r_y/r)^2], \tag{80}$$

$$S_2 = -p + k_p[\ln(r/r_i) + 1] + k_q[2(r/R) - (r_i/R)] + k_i[(r_y/r_i)^2 + (r_y/r)^2], \tag{81}$$

$$S_3 = -p + k_p[(1/2) + \ln(r/r_i)] + k_q[(3r/2R) - (r_i/R)] + k_i(r_y/r_i)^2 \tag{82}$$

For the remaining plastic region $R \leq r \leq r_y$, the stress difference $S_2 - S_1$ may be obtained by means of equations (28), (35), (37), (7), and (71) and written as

$$S_2 - S_1 = 2k_i(r_y/r)^2 + k_u + k_v(r/R) \tag{83}$$

where

$$k_u = c(1 - C)(1 - 3cC/4E), \tag{84}$$

$$k_v = cC(1 - 3cC/4E) \tag{85}$$

By the use of equations (36), (39), and (83) and the continuity of the radial stress at the bending neutral axis, the individual stresses for the plastic region $R \leq r \leq r_y$ may be written as

$$S_1 = -p + k_p[\ln(R/r_i)] + k_q[1 - (r_i/R)] + k_i[(r_y/r_i)^2 - (r_y/r)^2] + k_u[\ln(r/R)] + k_v[(r/R) - 1], \tag{86}$$

$$S_2 = -p + k_p[\ln(R/r_i)] + k_q[1 - (r_i/R)] + k_i[(r_y/r_i)^2 + (r_y/r)^2] + k_u[1 + \ln(r/R)] + k_v[2(r/R) - 1], \tag{87}$$

$$S_3 = -p + k_p[\ln(R/r_i)] + k_q[1 - (r_i/R)] + k_i(r_y/r_i)^2 + k_u[(1/2) + \ln(r/R)] + k_v[(3r/2R) - 1] \tag{88}$$

The relationship between the internal pressure and the current elastic-plastic boundary may be obtained from the boundary conditions and equations (39), (73), (78), and (83). The result may be expressed as

$$p = k_p[\ln(R/r_i)] + k_q[1 - (r_i/R)] + k_s[1 - (r_y/r_o)^2] + k_i[(r_y/r_i)^2 - 1] + k_u[\ln(r_y/R)] + k_v[(r_y/R) - 1] \tag{89}$$

(c) Multiple elastic-plastic boundaries. For the second type of elastic-plastic expansion, from the time that initial yielding takes place at the inner surface until the time that the elastic-plastic boundary reaches a particular value $r_i \leq r_y \leq R$, the equations of Case (*a*) are valid. Yielding then starts at the bending neutral axis and multiple elastic-plastic regions exist until the plastic regions merge. After the plastic regions merge, subsequent conditions are described by Case (*b*) until the cylinder becomes fully plastic. Thus the analysis of the case of multiple elastic-plastic boundaries will allow the complete solution for the second type of elastic-plastic expansion.

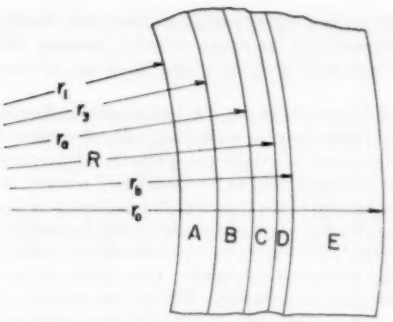

Fig. 3 Multiple elastic-plastic boundaries

The minimum value of the elastic-plastic boundary for which multiple regions exist is the minimum value of r_y for which equation (70) is not satisfied. The circumferential boundaries of the regions which will be considered are schematically shown in Fig. 3. The stresses and displacements in each region and the position of the elastic-plastic boundaries which correspond to various internal pressures may be obtained by the use of the equilibrium equation (39), the position of the stress point, the initial yield criteria, the flow law (7), the external boundary conditions, continuity of the radial stress through the thickness of the cylinder, the stress relationship (36), and the deformation expression (33). The expressions for the radial and circumferential stress in each region, together with the expressions which are used to determine the additional elastic-plastic boundaries and the internal pressure at a particular value of the inner elastic-plastic boundary r_y, are given in Table 2. These expressions will be used in the numerical example which follows.

Table 2 Expressions relating to radial and circumferential stresses

Region	Limits	Condition	Radial equation	Circumferential equation
A	$r_i \leq r \leq r_y$	Plastic	(65)	(66)
B	$r_y \leq r \leq r_a$	Elastic	(90)	(91)
C	$r_a \leq r \leq R$	Plastic	(92)	(93)
D	$R \leq r \leq r_b$	Plastic	(94)	(95)
E	$r_b \leq r \leq r_o$	Elastic	(56)	(57)

The previously undefined equations in Table 2 may be written as

$$S_1 = (S_1)_{r=r_y} + k_0[1 - (r_y/r)^2], \tag{90}$$

$$S_2 = (S_1)_{r=r_y} + k_0[1 + (r_y/r)^2], \tag{91}$$

$$S_1 = (S_1)_{r=r_a} + k_p[\ln(r/r_a)] + k_q[(r/R) - (r_a/R)] - k_r[(r_y/r)^2 - (r_y/r_a)^2], \tag{92}$$

$$S_2 = (S_1)_{r=r_a} + k_p[1 + \ln(r/r_a)] + k_q[2(r/R) - (r_a/R)] + k_r[(r_y/r)^2 + (r_y/r_a)^2], \tag{93}$$

$$S_1 = (S_1)_{r=R} + k_u(\ln(r/R)] + k_v[(r/R) - 1) - k_r[(r_y/r)^2 - (r_y/R)^2], \tag{94}$$

$$S_2 = (S_1)_{r=R} + k_u[1 + \ln(r/R)] + k_v[2(r/R) - 1] - k_r[(r_y/r)^2 + (r_y/R)^2] \tag{95}$$

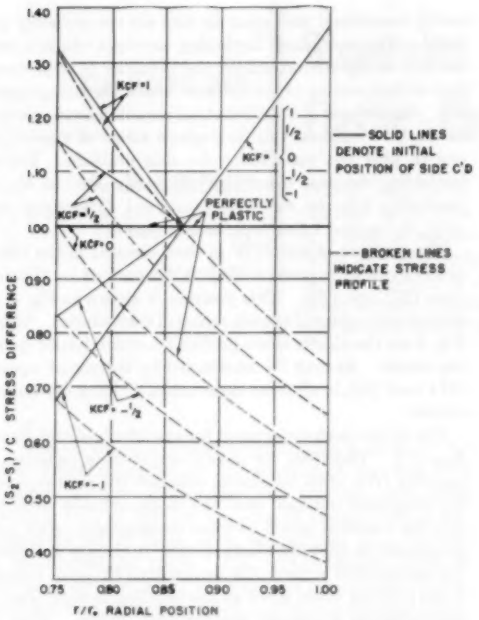

Fig. 4 Initial yielding for various values of K_{CF}

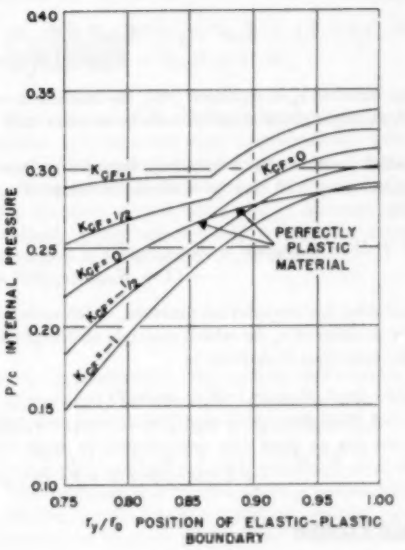

Fig. 5 Internal pressure

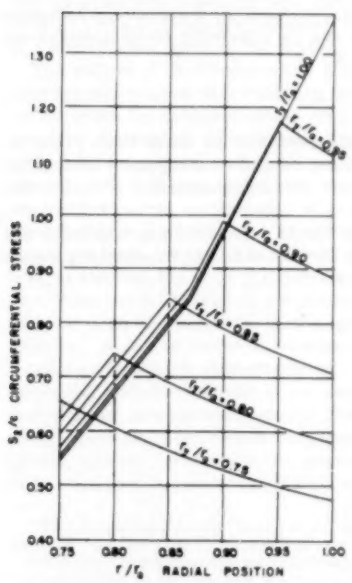

Fig. 6 Circumferential stress—$K_{CF} = -1/2$

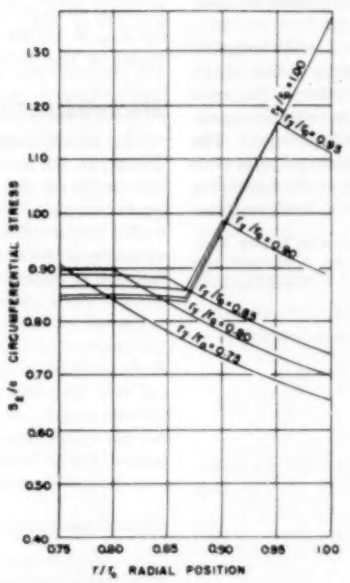

Fig. 7 Circumferential stress—$K_{CF} = 1/2$

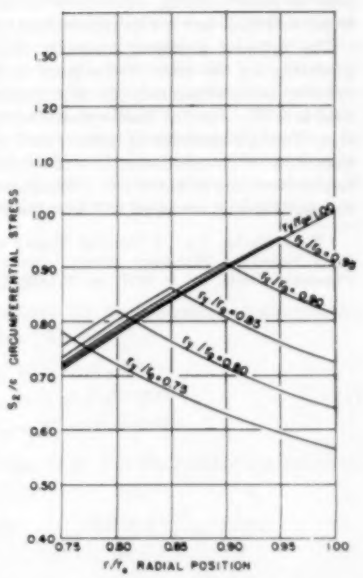

Fig. 8 Circumferential stress—perfectly plastic material

The radial position of the boundary between regions B and C is designated as r_a. It may be determined in terms of r_y by means of the expression

$$(K_{CF}F/Rr_y)r_a^2 - [(1 + K_{CF}F)/r_y - (K_{CF}F/R)]r_a - [1 + K_{CF}F - K_{CF}F(r_y/R)] = 0 \quad (96)$$

If r_a is set equal to r_y in equation (96), the maximum value of r_y for which multiple elastic-plastic boundaries exist may be determined.

The radial position of the boundary between regions D and E is designated as r_b. It may be obtained in terms of r_y from the expression

$$C(r_b/R)^2 + (1 - C)(r_b/R)^2 + K_{CF}F(r_y/R)^2 - (1 + K_{CF}F)(r_y/R)^2 = 0 \quad (97)$$

The equation for the internal pressure, which corresponds to a particular position of r_y for which multiple elastic-plastic boundaries exist, may then be written as

$$p = k_0[1 - (r_y/r_a)^2 + (r_y/r_b)^2 - (r_y/r_o)^2] + k_p[\ln(r_yR/r_ir_a)] + k_q[(r_y + R - r_i - r_a)/R] + k_r[(r_y/r_i)^2 - 1 + (r_y/r_a)^2 - (r_y/r_b)^2] + k_u[\ln(r_b/R)] + k_v[(r_b/R) - 1] \quad (98)$$

Numerical Example

Numerical calculations will now be employed to illustrate the importance of the effects of cold-bending in fabrication upon the resultant behavior of a cylinder being expanded by internal pressure. In order to keep the calculations fairly simple, in addition to its properties which are consistent with the assumptions of this paper, the material considered is isotropic and homogeneous prior to plate bending. The laws for this special case of anisotropic material were previously derived by Hodge.[3]

The cylinder geometry may be designated with complete generality by the ratio of the inner to the outer radius of the cylinder being expanded. In this numerical example the ratio used is 0.75. For the elastic-plastic material in cylinder expansion, Young's modulus is taken equal to 30,000,000 psi. The magnitude of the yield constants of the initial yield polygon prior to plate bending is 30,000 psi. The dimensionless side-hardening constants chosen are equal to 2.4 for the five strain-hardening materials considered and equal to zero for the perfectly plastic material. The secondary hardening constant which is used in this analysis is the one describing the behavior in subsequent expansion of that portion of the cylinder which was compressed in bending. Since there is a little test information available from which to choose a value of this constant, a range of values from minus one to plus one was chosen for this problem. The secondary hardening constant which has been designated as K_{CF} will independently take on the five values -1 (kinematic hardening), $-1/2$, 0, $1/2$, and 1 (isotropic hardening).

The position of side $C'D'$ of each element of the yield polygon before cylinder expansion may be determined by the use of equations (27) and (28). This position is shown in Fig. 4 for the six materials considered at each radius of the cylinder. Also plotted in Fig. 4 are the elastic stress profiles for which initial cylinder yielding occurs. As may be determined by the use of equations (50), (51), and (52), in all these cases initial yielding occurs at the inner surface.

For all the materials except the one which hardens isotropically, $K_{CF} < 2$. Therefore, for these five materials, as shown by the inequality (70), with increasing pressure the elastic-plastic boundary progresses outward until the entire cylinder becomes plastic. For the material which hardens isotropically, after yielding has progressed so that the elastic-plastic boundary is slightly beyond the initial yield surface, the inequality (70) is no longer satisfied. Thus yielding takes place at the bending neutral axis before the elastic-plastic boundary reaches that radius. With increasing pressure, the two plastic regions expand until they join. The radius at which this occurs may be obtained from equation (96). The single elastic-plastic boundary then continues outward until the entire cylinder becomes plastic.

The internal pressure corresponding to the various positions of the inner elastic-plastic boundary is shown in Fig. 5. The circumferential stress at various positions of the elastic-plastic boundary for $K_{CF} = 1/2$ and $-1/2$ and for a perfectly plastic material are shown in Figs. 6, 7, and 8.

Acknowledgments

The author takes this opportunity to thank Prof. Philip G. Hodge, Jr., for his unstinting aid and encouragement throughout the course of the author's doctoral dissertation of which this paper is a part.

The author would also like to express his appreciation to the members of the Research Division of Foster Wheeler Corporation for their co-operation.

[3] P. G. Hodge, Jr., "A General Theory of Piecewise Linear Plasticity Based on Maximum Shear," *Journal of the Mechanics and Physics of Solids*, vol. 5, 1957, pp. 242–260.

Dispersion of Flexural Waves in an Elastic, Circular Cylinder[1]

YIH-HSING PAO
Assistant Professor of Mechanics,
Cornell University, Ithaca, N. Y.

R. D. MINDLIN
Professor of Civil Engineering,
Columbia University,
New York, N. Y.
Mem. ASME

In this paper it is shown how the branches of Pochhammer's frequency equation for flexural waves in a circular cylinder may be constructed approximately with the aid of a grid of simpler curves and asymptotic equations for long and short wave lengths. With very little computation, in comparison with that required in the direct determination of the roots of Pochhammer's equation, a qualitative view is obtained of the relations between frequency, phase velocity, group velocity, and propagation constant, for any branch, as well as some information as to the shapes of the modes.

THE solutions of the linear equations of elasticity for extensional and flexural vibrations and waves in an infinitely long circular cylinder, with its surface free from traction, were given by Pochhammer [1],[2] in 1876, in the form of transcendental frequency equations which have been the subject of numerous studies in the succeeding years. The extraordinarily intricate branches of these equations give the relations between frequency, propagation constant, phase velocity, and group velocity which are required for an understanding of the physical significance of the solutions.

Recently, methods which do not require extensive numerical computation have been developed for the approximate mapping of the branches of Pochhammer's equation for extensional waves and the branches of similar equations which appear in solutions for both extensional and flexural vibrations or waves in plates [2–8]. These methods are extended, in this paper, to the case of Pochhammer's equation for flexure.

The essence of the technique of mapping has been the preliminary construction of intersecting families of simple algebraic curves which the branches cannot cross except at certain of the points of intersection. This information, along with the asymptotic behavior at long and short wave lengths, has been sufficient to permit the tracing of the branches through the grid of intersecting curves, or "bounds," in considerable detail. If the construction is performed with frequency as ordinate and propagation constant, i.e., wave number in the direction of propagation, as abscissa, the slope of the straight line connecting a point on a branch with the origin is proportional to the phase velocity and the slope of the branch itself is proportional to the group velocity. A pair of values of frequency and wave number, i.e., a point on a branch, corresponds to a mode of motion whose properties may be determined by inserting the pair into the formulas for displacement, strain, and stress. Some, and in certain cases all, of the bounds have been the branches of the frequency equation for waves in the same body with mixed, instead of traction-free, boundary conditions; one family of bounds corresponding to equivoluminal deformation, and another to rotationless dilatational deformation. Passage from mixed to traction-free boundary conditions is accompanied by coupling of the two types of deformation and leads to the complicated behavior invariably encountered with nonmixed boundary conditions. The resolution into the two types of simple deformation gives, in addition, insight into the modal composition corresponding to points on the branches both at and between intersections of bounds.

In the case of Pochhammer's equation for flexure, no such resolution is possible. Although simple bounds corresponding to equivoluminal deformation (but not to a mixed boundary-value problem) may be found, simple bounds corresponding to purely dilatational deformation are not possible. This obstacle has been surmounted, in the present study, by introducing auxiliary curves by means of which the missing bounds are constructed. Six families of curves are employed to construct the latter and the result is a second family of bounds of intricacy comparable with the branches in previous problems. Nevertheless, sufficient bounds are then available to permit the construction of the branches of Pochhammer's equation for flexure. In this paper, an analytical study of the frequency equation is summarized and an example is given of the construction of bounds and branches for Poisson's ratio 1/3 and real propagation constant.

Pochhammer's Equation

In the form given by Love [9], Pochhammer's displacements, in cylindrical co-ordinates r, θ, z, are

$$\begin{aligned} u_r &= U \cos\theta\, e^{i(\gamma z + pt)} \\ u_\theta &= V \sin\theta\, e^{i(\gamma z + pt)} \\ u_z &= W \cos\theta\, e^{i(\gamma z + pt)} \end{aligned} \tag{1}$$

where p is the circular frequency, γ is the propagation constant, and

$$\begin{aligned} U &= A\frac{\partial J_1(hr)}{\partial r} + \beta\gamma\frac{\partial J_1(\kappa r)}{\partial r} + C\frac{J_1(\kappa r)}{r} \\ V &= -A\frac{J_1(hr)}{r} - B\gamma\frac{J_1(\kappa r)}{r} - C\frac{\partial J_1(\kappa r)}{\partial r} \\ W &= iA\gamma J_1(hr) - iB\kappa^2 J_1(\kappa r) \end{aligned} \tag{2}$$

in which J_1 denotes Bessel's function of order unity and

$$\begin{aligned} h^2 &= p^2/v_1^2 - \gamma^2, \quad v_1^2 = (\lambda + 2\mu)/\rho \\ \kappa^2 &= p^2/v_2^2 - \gamma^2, \quad v_2^2 = \mu/\rho \end{aligned} \tag{3}$$

[1] This investigation was supported by the Office of Naval Research under a contract with Columbia University.

[2] Numbers in brackets designate References at end of paper.

Contributed by the Applied Mechanics Division and presented at the Annual Meeting, Atlantic City, N. J., November 29–December 4, 1959, of THE AMERICAN SOCIETY OF MECHANICAL ENGINEERS.

Discussion of this paper should be addressed to the Secretary, ASME, 29 West 39th Street, New York, N. Y., and will be accepted until October 10, 1960, for publication at a later date. Discussion received after the closing date will be returned.

NOTE: Statements and opinions advanced in papers are to be understood as individual expressions of their authors and not those of the Society. Manuscript received by ASME Applied Mechanics Division, May 13, 1959. Paper No. 59—A-84.

where λ and μ are Lamé's constants, and ρ is the density. The constant A is associated with the dilatational part of the deformation while B and C are associated with equivoluminal parts.

It is convenient to introduce dimensionless wave numbers, α, β, ζ, and frequency, Ω, in terms of the radius, a, of the cylinder and the velocity, v_2, of equivoluminal waves in an infinite medium:

$$\alpha = ha,\ \beta = \kappa a,\ \zeta = \gamma a,\ \Omega = pa/v_2 \tag{4}$$

so that (3) become

$$\alpha^2 = k^{-2}\Omega^2 - \zeta^2 \tag{5}$$

$$\beta^2 = \Omega^2 - \zeta^2 \tag{6}$$

where

$$k^2 = (\lambda + 2\mu)/\mu = 2(1 - \sigma)/(1 - 2\sigma)$$

and σ is Poisson's ratio.

Upon inserting (1) into the formulas for the components of traction across $r = a$, setting these equal to zero and eliminating the constants A, B, C, we obtain Pochhammer's frequency equation, which may be written[3]

$$J_1(\alpha)J_1^2(\beta)[f_1\mathcal{J}_\beta^2 + f_2\mathcal{J}_\alpha\mathcal{J}_\beta + f_3\mathcal{J}_\beta + f_4\mathcal{J}_\alpha + f_5] = 0 \tag{7}$$

where

$$\begin{aligned} f_1 &= 2(\beta^2 - \zeta^2)^2,\quad f_2 = 2\beta^2(5\zeta^2 + \beta^2) \\ f_3 &= \beta^4 - 10\beta^4 - 2\beta^4\zeta^2 + 2\beta^2\zeta^2 + \beta^2\zeta^4 - 4\zeta^4 \\ f_4 &= 2\beta^2(2\beta^2\zeta^2 - \beta^2 - 9\zeta^2) \\ f_5 &= \beta^2(-\beta^4 + 8\beta^2 - 2\beta^2\zeta^2 + 8\zeta^2 - \zeta^4) \end{aligned} \tag{8}$$

and

$$\mathcal{J}_x \equiv \mathcal{J}_1(x) \equiv xJ_0(x)/J_1(x) \tag{9}$$

is Onoe's function [10] of the first kind and order unity: the analog of the trigonometric cotangent. The behavior of $\mathcal{J}_1(x)$ is illustrated in Fig. 1.

In view of (5) and (6), Pochhammer's equation (7) relates the dimensionless frequency, Ω, to the dimensionless propagation constant ζ; with k, or Poisson's ratio, as a parameter. Only the squares of Ω and ζ appear in (5) and (6) so that positive and negative values are interchangeable. Negative frequencies have no physical significance but negative propagation constants are permissible and give the mirror images of the curves that are described in the sequel.

From (5) and (6) it may be seen that the plane of Ω and real positive ζ is divided into three sectors in which (7) has different behaviors according as the arguments α and β, of the transcendental functions, are real or imaginary:

Sector 1 ($0 < \Omega/\zeta < 1$): α and β imaginary
Sector 2 ($1 < \Omega/\zeta < k$): α imaginary, β real
Sector 3 ($k < \Omega/\zeta < \infty$): α and β real

In Figs. 2 and 3, the radii dividing the sectors are designated OE ($\Omega = \zeta$ or $\beta = 0$) and OD ($\Omega = k\zeta$ or $\alpha = 0$).

Calling v the phase velocity and v_g the group velocity, we have

$$v \equiv p/\gamma = v_2\Omega/\zeta,\ v_g \equiv dp/d\gamma = v_2 d\Omega/d\zeta \tag{10}$$

so that the slope of the straight line from the origin to a point in the ζ, Ω-plane satisfying (5), (6), and (7) is proportional to the phase velocity and the slope of a branch defined by (5), (6), and (7) is proportional to the group velocity, the constant of proportionality being the velocity of equivoluminal waves in an infinite medium. A point of inflection of a branch signifies a maximum or minimum of group velocity according as the change of sign is from positive to negative or vice versa as ζ increases.

[3] In determinantal form, Pochhammer's frequency equation is

$$J_1(\alpha)J_1^2(\beta)\begin{vmatrix} \zeta^2 - \beta^2 + 4 - 2\mathcal{J}_\alpha & 2\zeta(\beta^2 - 2 + 3\mathcal{J}_\beta) & 2\mathcal{J}_\beta - 4 \\ 4 - 2\mathcal{J}_\alpha & 2\zeta(\mathcal{J}_\beta - 2) & \beta^2 - 4 + 2\mathcal{J}_\beta \\ 2\zeta(\mathcal{J}_\alpha - 1) & (\beta^2 - \zeta^2)(\mathcal{J}_\beta - 1) & \zeta \end{vmatrix} = 0$$

in which the columns derive from the constants A, B, C, respectively, and the rows from the components of surface traction in the directions of r, θ, and z, respectively.

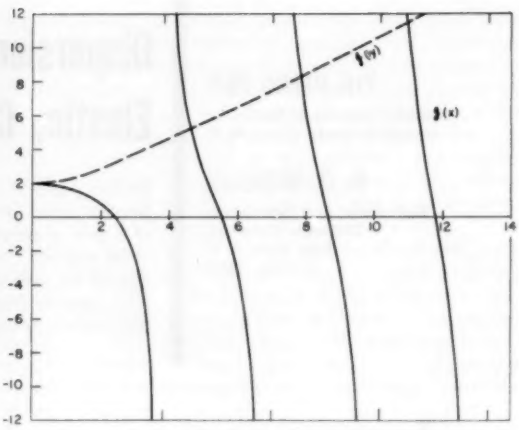

Fig. 1 Onoe's function $\mathcal{J}_1(x) = xJ_0(x)/J_1(x)$

Asymptotic Behavior at Long Wave Length

We require the ordinates, slopes, and curvatures of the branches of (7) at $\zeta = 0$, i.e., infinite wave length along the rod.

Ordinates. When $\zeta = 0$, (7) can be expressed as a product of three functions. One of the three factors is β^2, giving zero frequency as discussed in the next section. The other two factors, set equal to zero, are

$$\mathcal{J}(\beta_0) - 1 = 0 \tag{11}$$

$$2\mathcal{J}(\alpha_0) + 2\mathcal{J}(\beta_0) + \beta_0^2 - 8 = 0 \tag{12}$$

where, from (5) and (6), $\alpha_0 = \Omega/k$, $\beta_0 = \Omega$. The roots of (11) and (12) are determined readily with the aid of Onoe's tables and give the cut-off frequencies.

Corresponding to (11), A, C, and γ are zero, so that, from (2), the displacement is purely axial and equivoluminal. The roots of (11) are independent of Poisson's ratio and are almost uniformly spaced. The first seven frequencies are listed in the starred columns in Table 1 and are identified by circles along $\zeta = 0$ in Figs. 2 and 3. The associated modes of displacement have one diametral node and a number of circular nodes equal to one less than the order of the root of (11). These are the axial shear modes.

Corresponding to (12), $A/C = -J_1(\beta_0)/J_1(\alpha_0)$ and B and γ are zero, so that the motion is one of coupled dilatational and rotational plane strain in the plane of the cross section. This is an early indication of difficulties to be encountered subsequently. In the case of Pochhammer's solution for extensional waves in a rod or Rayleigh's solution [11] for both extensional and flexural waves in a plate, the analogous motion is purely dilatational. Equation (12) yields a nonuniform distribution of frequencies which varies markedly, but systematically, with Poisson's ratio, as discussed in the Appendix. The first ten frequencies, for $\sigma = 1/3$, i.e., $k = 2$, are given in Table 1 and are identified by crosses along $\zeta = 0$ in Figs. 2 and 3. Whether a mode of a given order is predominantly dilatational ($A/C > 1$) or equivoluminal ($A/C < 1$) depends on Poisson's ratio. The modes of resultant displacement have nodal points but no nodal diameters or circles. By the usual substitution of $\sigma/(1 + \sigma)$ for σ, this solution is converted to the analogous solution of Poisson's equations[4] of

[4] Reference [9], p. 497.

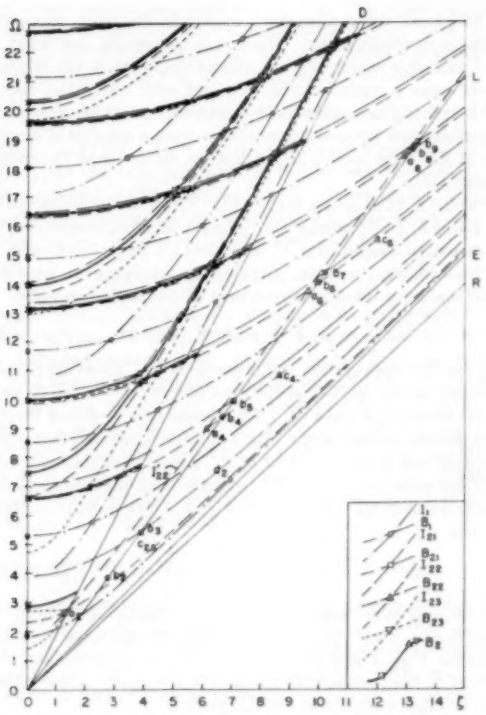

Fig. 2 Bounds, barriers, auxiliary barriers, and intersectors

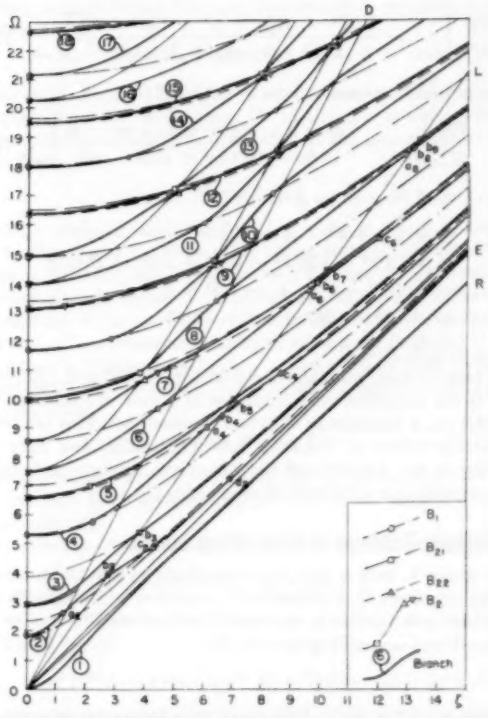

Fig. 3 Branches of Pochhammer's frequency equation traced through the grid of bounds and barriers

Table 1 Cut-off frequencies and ratios of curvatures of branches to curvatures of bounds at cut-off. Poisson's ratio = 1/3.

Branch no.	1	2*	3	4*	5	6	7*	8	9*	10	11	12*	13	14*	15	16	17*	18
Ω	0	1.84	2.86	5.33	6.55	7.48	8.53	9.97	11.70	13.14	13.91	14.86	16.35	18.02	19.50	20.26	21.16	22.67
Curv. of branch / Curv. of bound	—	3.01	1.17	0.34	0.70	0.83	1.79	1.01	0.81	0.99	0.89	1.52	1.01	0.89	1.01	0.92	1.43	1.01

* Asterisks designate axial shear modes.

extensional motion of thin plates (generalized plane stress) and then (12) is identical with the case $n = 1$ of Love's general solution for the extensional vibrations of a thin circular disk.[8]

The zero frequency in Table 1 represents the cut-off frequency of the lowest branch of (7) and also two rigid motions of the rod; one transverse translational and one rotational.

Slopes and Curvatures. As shown by Pochhammer [1], the lowest branch has the asymptotic behavior

$$\Omega = \zeta^2[(1 + \sigma)/2]^{1/2} \tag{13}$$

for $\zeta \ll 1$, so that the terminal ordinate and slope are zero and the terminal curvature is

$$d^2\Omega/d\zeta^2]_{\zeta=0} = 2[(1 + \sigma)/2]^{1/2} \tag{14}$$

To determine the slopes and curvatures of the upper branches at $\zeta = 0$, we note, first, that equation (7) may be expressed as a function of either α and β or Ω and ζ, where the two pairs of variables are related through (5) and (6). Then, calling the left-hand side of Pochhammer's equation P, we have, by the rule of differentiation of implicit functions,

$$\frac{d\Omega}{d\zeta} = -\frac{P_\zeta}{P_\Omega} = -\frac{P_\alpha\alpha_\zeta + P_\beta\beta_\zeta}{P_\alpha\alpha_\Omega + P_\beta\beta_\Omega} \tag{15}$$

[8] Reference [9], p. 498.

where a subscript designates the partial derivative with respect to that variable. Hence, from (5) and (6), if neither α nor β is zero,

$$\frac{d\Omega}{d\zeta} = \frac{k^2\zeta(\beta P_\alpha + \alpha P_\beta)}{\Omega(\beta P_\alpha + k^2\alpha P_\beta)} \tag{16}$$

so that the slope is zero at $\zeta = 0$ except if $P_\Omega = 0$; i.e., except if

$$[P_\alpha + kP_\beta]_{\zeta=0} = 0 \tag{17}$$

Again,

$$\frac{d^2\Omega}{d\zeta^2} = -\frac{1}{P_\Omega}\left[P_{\zeta\zeta} + 2P_{\zeta\Omega}\frac{d\Omega}{d\zeta} + P_{\Omega\Omega}\left(\frac{d\Omega}{d\zeta}\right)^2\right] \tag{18}$$

Now, at $\zeta = 0$, $d\Omega/d\zeta = 0$ if $P_\Omega \neq 0$; hence

$$d^2\Omega/d\zeta^2]_{\zeta=0} = -P_{\zeta\zeta}/P_\Omega]_{\zeta=0} \tag{19}$$

or, since $\alpha_\zeta = \beta_\zeta = 0$, $\alpha_{\zeta\zeta} = -\alpha^{-1}$, $\beta_{\zeta\zeta} = -\beta^{-1}$ at $\zeta = 0$,

$$\left.\frac{d^2\Omega}{d\zeta^2}\right]_{\zeta=0} = \left.\frac{k(kP_\alpha + P_\beta)}{\Omega(P_\alpha + kP_\beta)}\right]_{\zeta=0} \tag{20}$$

Upon insertion of (7) into (20), the curvatures of the branches at $\zeta = 0$ are found to be

$$\frac{d^2\Omega}{d\zeta^2}\Big]_{\zeta=0} = \frac{2(5\beta^2 - 9)\mathcal{J}_\alpha + \beta^4 - 15\beta^2 + 18}{\Omega(\beta^2 - 1)(2\mathcal{J}_\alpha + \beta^2 - 6)}\Big]_{\zeta=0} \quad (21)$$

at the cut-off frequencies given by (11) and

$$\frac{d^2\Omega}{d\zeta^2}\Big]_{\zeta=0} = \frac{(\mathcal{J}_\beta - 1)(g_1\mathcal{J}_\beta^2 + g_2\mathcal{J}_\beta + g_3) - g_4}{\Omega(\mathcal{J}_\beta - 1)(4\mathcal{J}_\beta^2 + g_5\mathcal{J}_\beta + g_6)}\Big]_{\zeta=0} \quad (22)$$

at the cut-off frequencies given by (12), where

$$\begin{aligned} g_1 &= 2(1 + k^2), \quad g_2 = 2(\beta^2k^2 - 6k^2 - 16) \\ g_3 &= (\beta^4k^2 - 12\beta^2k^2 - 40\beta^2 + 32k^2 + 184)/2 \\ g_4 &= 4(\beta^2 - 3)^2, \quad g_5 = 2(\beta^2 - 8) \\ g_6 &= (\beta^4 - 12\beta^2 + 4\alpha^2 + 32)/2 \end{aligned} \quad (23)$$

and $\alpha = \Omega/k$, $\beta = \Omega$.

It may be seen, from the denominators in (21) and (22), that (17) is the condition for coincidence of a root of (11) with one of (12); i.e., a coincidence of cut-off frequencies. This can occur at certain values of Poisson's ratio (Appendix) and then the curvatures are infinite and the slopes are nonzero and finite. The behavior is analogous to that in plates [5].

Asymptotic Behavior at Short Wave Length

In Sector 1, both α and β are imaginary so that the transcendental functions in Pochhammer's equation are nonoscillatory and there is one and only one root Ω for each real ζ. As $\zeta \to \infty$, so does Ω and the limiting form of (7) is

$$c^2[c^6 - 8c^4 + 8(3 - 2k^{-2})c^2 - 16(1 - k^{-2})] = 0 \quad (24)$$

where $c = \Omega/\zeta = v/v_2$. Equation (24) is Rayleigh's equation for the velocity of surface waves. It has one real, nonzero root corresponding to imaginary α and β. For $k = 2$, the root is $\Omega/\zeta = 0.932$ and this asymptote is shown as the line OR in Figs. 2 and 3. The displacement at large ζ is entirely analogous to that in Rayleigh's surface waves, being confined, in this case, to the neighborhood of the cylindrical surface. These results were found by Hudson [12].

In Sector 2, α is imaginary and β is real. Hence $\mathcal{J}_\beta$ is oscillatory and there is an infinity of roots for each phase velocity. When β is set equal to zero, Pochhammer's equation is satisfied identically but all the amplitudes are zero. The appropriate form of the solution, for $\beta = 0$, may be obtained by returning to equations (2) and replacing the equivoluminal parts by

$$U = iB\gamma r^2 + C, \; V = iB\gamma r^2 - C, \; W = -4Br$$

It is then found that the frequency equation is

$$\zeta(\mathcal{J}_\alpha - 2) = 0$$

Now, $\mathcal{J}_\alpha = 2$ has no roots, for imaginary α, other than $\alpha = 0$ which is inconsistent with $\beta = 0$. Hence, except at $\zeta = 0$, no branch of (7) crosses the line $\beta = 0$ (i.e., $\Omega = \zeta$ or OE in Figs. 2 and 3) so that no mode has the phase velocity v_2.

For large ζ, in Sector 2, Pochhammer's equation reduces to

$$2\mathcal{J}_\beta^2 + (\beta^2 - 4)\mathcal{J}_\beta - \beta^2 = 0$$

which yields two families of roots; namely, the roots of

$$4\mathcal{J}_\beta - 4 + \beta^2 + (16 + \beta^4)^{1/2} = 0 \quad (25a)$$

$$4\mathcal{J}_\beta - 4 + \beta^2 - (16 + \beta^4)^{1/2} = 0 \quad (25b)$$

For a given root β, (6) is approximately

$$\Omega = \zeta + \beta^2/2\zeta \quad (26)$$

for large ζ. Thus the branches in Sector 2 are asymptotic to $\Omega = \zeta$ and their distribution is determined by the roots of (25a) and (25b). All the modes, then, approach the phase and group velocity v_2 asymptotically. Since α is imaginary and large, at large ζ near this asymptote, the dilatational part of the displacement is again a surface wave, nonoscillatory along the radius; but β is real and hence the individual components of equivoluminal displacement are oscillatory along r with a number of circular nodes in the cross section depending on the order of the root of (25a) or (25b).

In Sector 3, both α and β are real. For $\alpha = 0$ (the line OD in Figs. 2 and 3) Pochhammer's equation is satisfied identically, but the associated amplitudes A, B, C are all zero. The required nontrivial solution may be obtained by returning to equations (2) and replacing the dilatational part of the displacement by

$$U = A, \; V = -A, \; W = iA\gamma r \quad (27)$$

which are the appropriate forms for $\alpha = 0$. These represent a translation of the section in the direction of x ($= r\cos\theta$) and a rotation about y ($= r\sin\theta$). The normal component of traction on the section varies linearly with x and the tangential component is uniform and in the direction of x. Along with the same equivoluminal parts as before, (27) converts Pochhammer's equation to a quadratic in $\mathcal{J}_\beta$. For $k = 2$, $\sigma = 1/3$, the quadratic has the solutions

$$4\mathcal{J}_\beta = -2 - \beta^2 \pm (\beta^4 - 12\beta^2 + 100)^{1/2} \quad (28)$$

The two families of roots, β, of (28), when substituted into (5) and (6), with $\alpha = 0$, give the points at which the branches cross $\Omega = k\zeta$ (OD in Figs. 2 and 3) and so give the frequencies and wave numbers of the modes with phase velocity equal to the velocity of dilatational waves in an infinite medium.

Bounds, Barriers, and Intersectors

A set of *bounds* of the branches of a frequency equation is defined, in this paper, as a family of curves which have the following properties:

1 Their construction requires very much less computation than that required for plotting the branches of the frequency equation directly.

2 Their co-ordinates satisfy the frequency equation only at certain points which can be determined readily.

3 They pass through a family of cut-off frequencies at $\zeta = 0$.

Curves that satisfy conditions 1 and 2, but not 3, are called *barriers*. Curves that intersect the bounds or barriers at points which satisfy the frequency equation are called *intersectors*. Branches can cross bounds or barriers only at the points of intersection of the latter with intersectors.

In the present case, one set of bounds (B_1), which terminate at the cut-off frequencies of the axial shear modes, is a family of hyperbolas and the associated intersectors (I_1) are also simple curves approximated closely by hyperbolas. The second set of bounds (B_2), which terminate at the remaining cut-off frequencies, is a family of complicated curves which are themselves constructed on a grid of three pairs of families of intersecting curves designated as *auxiliary barriers*. Two of the six families of auxiliary barriers are used subsequently as barriers of the branches.

Bounds B_1 and Intersectors I_1

Consider the equation

$$B_1 \equiv \mathcal{J}_\beta - 1 = 0 \quad (29)$$

In view of (6), (29) is the equation of a family of hyperbolas in the ζ, Ω-plane. The curves are asymptotic to $\Omega = \zeta$ (OE in Figs. 2 and 3) and pass through the cut-off frequencies of the

axial shear modes (the circles at $\zeta = 0$ in Figs. 2 and 3) as may be seen by comparison with (11). Further, when (29) is substituted in the frequency equation (7), the latter is satisfied only if $\zeta = 0$, which gives the cut-off frequencies (11), or if

$$I_1 \equiv \mathcal{J}_\alpha - 1 - (\beta^2 + \zeta^2)/2\beta^2(\beta^2 - 2) = 0 \qquad (30)$$

With (5) and (29), (30) is a family of curves whose intersections with B_1 are the only points on B_1, aside from those at $\zeta = 0$, which satisfy the frequency equation. Hence B_1 is a family of bounds and I_1 is the associated family of intersectors.

Now, for real α, (30) is approximated closely by

$$I_1 \backsimeq \mathcal{J}_\alpha - 1 = 0 \qquad (31)$$

In view of (5), (31) is a family of hyperbolas asymptotic to $\Omega = k\zeta$ (OD in Figs. 2 and 3). The intersections of the two families of hyperbolas, designated by circles in Sector 3 of Figs. 2 and 3, are, to a close approximation, points through which the branches pass, and the hyperbolas asymptotic to OE are bounds. In Sector 2, α is imaginary and (30) has only one root for each root β of (29). Thus, on each bound B_1, in Sector 2, there is one point, such as d_2 in Figs. 2 and 3, at which a branch of (7) crosses the bound. The points like d_2 on the higher bounds B_1 are far beyond the range of ζ in Figs. 2 and 3.

Bounds B_2

In previous constructions of frequency spectra by means of bounds, e.g. [3–8], the curves analogous to I_1 have also been bounds or, at least, barriers, crossed by the branches only at the intersections with B_1. Thus the branches were well determined by a grid of two intersecting families of hyperbolas. In the present case, curves such as I_1 cannot give the remaining family of cut-off frequencies (12) at $\zeta = 0$ since the cut-off modes contain coupled dilatational and equivoluminal deformation and so depend on transcendental functions of both α and β. Furthermore, two equivoluminal deformations, those associated with B and C in Equations (2), are here involved. Hence the substitution of (30) in the frequency equation (7) reduces the latter only to a quadratic in $\mathcal{J}_\beta$, instead of to (29), and the determination of the roots of the reduced equation, i.e., the determination of the points at which the branches cross I_1, involves a large amount of computation which is not worth doing since (30) does not reduce to (12) at $\zeta = 0$ in any event and so is not suitable for use as a family of bounds.

It is apparent that the additional set of bounds that is required must be a family of curves more complicated than simple hyperbolas. As a result of a study of the cofactors of Pochhammer's determinant,[3] we consider the equation

$$B_2 \equiv J_1(\alpha)J_1(\beta)[6\mathcal{J}_\alpha + 6\mathcal{J}_\beta - 24 + 3\beta^2 - \zeta^2] = 0 \qquad (32)$$

which gives the second family of cut-off frequencies (12) when $\zeta = 0$. It is shown in the following sections that the curves defined by (32) may be constructed by means of auxiliary barriers and used as the second set of bounds of Pochhammer's equation.

Auxiliary Barriers B_{21} and I_{21}. If equation (32) is expanded by multiplying through by $J_1(\alpha)$ and $J_1(\beta)$, it may be seen that if

$$B_{21} \equiv J_1(\beta) = 0 \qquad (33)$$

(32) is satisfied if and only if

$$I_{21} \equiv J_1(\alpha) = 0 \qquad (34)$$

and vice versa. In view of (5) and (6), the two families of curves (33) and (34) are hyperbolas: B_{21} asymptotic to OE and I_{21} asymptotic to OD. The only points on these two families that satisfy (32) are their intersections. Thus, B_{21} and I_{21} are auxiliary barriers of B_2. Since (34) has no roots when α is imaginary, there are no intersections in Sector 2.

Now, substitution of (33) into Pochhammer's equation reduces the latter to

$$2(\beta^2 - \zeta^2)\beta^2 J_0(\beta)J_1(\alpha) = 0 \qquad (35)$$

Since this is satisfied by $J_1(\alpha) = 0$, the intersections of I_{21} with B_{21} (except $\alpha = 0$) are roots of (7) in addition to being roots of (32). Also, from (35), (7) is satisfied at the intersections of B_{21} with

$$\beta^2 - \zeta^2 = 0 \qquad (36)$$

From (5) and (6), this is the line $\Omega = \sqrt{2}\,\zeta$ in Sector 2, marked OL in Figs. 2 and 3. Since there are no roots of (35) other than those of (34) and (36), B_{21} are not only barriers of B_2 but are also barriers of the branches of Pochhammer's equation; the branches intersecting B_{21} at and only at the intersections of B_{21} with I_{21} and OL. The former are identified by squares in Sector 3 and the latter by the squares b_3, b_4 . . . along OL in Figs. 2 and 3. From (16) it may be shown that B_{21} and the branches of (7) have the same slope

$$d\Omega/d\zeta = 1/\sqrt{2} \qquad (37)$$

at their common intersections with OL. It is shown in the last section that these intersections are points of tangency rather than crossings.

Substitution of (34) into Pochhammer's equation reduces it to

$$\alpha J_0(\alpha)J_1^2(\beta)[f_2\mathcal{J}_\beta + f_4] = 0 \qquad (38)$$

Hence, in addition to the intersections of I_{21} with B_{21}, the intersections of I_{21} with

$$f_2\mathcal{J}_\beta + f_4 = 0 \qquad (38a)$$

are also roots of (7). Equation (38a) plays the same role in (38) that (36) plays in (35); but (38a) is a family of curves whose construction requires much computation, whereas (36) is a single straight line. Hence I_{21} is not convenient for use as a family of barriers to the branches of (7) but only as a family of intersectors with B_{21}.

Bound $\zeta = \beta$. Substitution of (36) in Pochhammer's equation reduces it to

$$4\beta^4 J_1(\alpha)J_1(\beta)[1 + (1 - \mathcal{J}_\alpha)(3\mathcal{J}_\beta + \beta^2 - 5)] = 0 \qquad (39)$$

Thus, in addition to the points b_3, b_5 . . . mentioned in the preceding section, the intersections of (36) with

$$1 + (1 - \mathcal{J}_\alpha)(3\mathcal{J}_\beta + \beta^2 - 5) = 0 \qquad (40)$$

are roots of (7). These intersections are identified by the squares marked b_2, b_4 . . . along OL in Figs. 2 and 3. Since α is imaginary, (39) has no roots $J_1(\alpha) = 0$; and we have already seen that $\beta = 0$ is not a root of Pochhammer's equation. Thus line OL is a bound of (7); it is crossed by the branches at and only at the points b_3, b_5 . . . and b_2, b_4 . . . .

The modes corresponding to b_3, b_5 . . . have

$$A = 0, \qquad B = -C/\zeta$$

in equations (2), so that they are equivoluminal. They are the analogs of modes found by Lamé [13] in plates and Lamb [14] in longitudinal vibrations of circular cylinders except that, in the present case, there are no transverse sections free from traction.

Corresponding to b_2, b_4 . . . there are coupled dilatational and equivoluminal modes with

$$C = 2B\zeta = 2A(1 - \mathcal{J}_\alpha)J_1(\alpha)/J_1(\beta)$$

These have no counterparts in vibrations of plates or longitudinal vibrations of cylinders.

Auxiliary Barriers B_{22} and I_{22}. Returning to (32), we see that if

$$B_{22} \equiv 3\mathcal{J}_\beta + \beta^2 - 6 = 0 \qquad (41)$$

(32) is satisfied if and only if

$$I_{22} \equiv 6\mathcal{J}_\alpha + \beta^2 - \zeta^2 - 12 = 0 \tag{42}$$

and vice versa.[6] Hence B_{22} and I_{22} are auxiliary barriers of B_2; i.e., the curves B_2 cross B_{22} and I_{22} at and only at the intersections of B_{22} and I_{22}.

Now, if (41) is substituted in Pochhammer's equation, the resulting equation is satisfied only if $I_{22} = 0$ or if

$$I_{22}' \equiv \beta^4 - (3 + \zeta^2)\beta^2 - 3\zeta^2 = 0 \tag{43}$$

Accordingly B_{22}, in addition to being barriers of B_2, are barriers of the branches of (7), with crossings at and only at the intersections of B_{22} with I_{22} and with I_{22}'. The intersections of B_{22} and I_{22} are shown in Figs. 2 and 3 as triangles with apex up; those in Sector 2, one to each of B_{22} since α is imaginary, are the points marked $c_2, c_4 \ldots$. The intersections of B_{22} with the single curve (43) are the points marked $a_2, a_4 \ldots$.

As in the case of auxiliary barriers I_{21}, the auxiliary barriers I_{23} are found to be not well suited for use as barriers to the branches.

Auxiliary Barriers B_{23} and I_{23}. We observe that if

$$B_{23} \equiv (7\beta^2 - \zeta^2)\mathcal{J}_\beta - 16\beta^2 - \beta^2\zeta^2 + 3\beta^4 = 0 \tag{44}$$

(32) is satisfied if and only if

$$I_{23} \equiv 6(7\beta^2 - \zeta^2)\mathcal{J}_\alpha + 24\zeta^2 - 72\beta^2 + \zeta^4 - 4\zeta^2\beta^2 + 3\beta^4 = 0 \tag{45}$$

and vice versa. Hence B_{23} and I_{23} are auxiliary barriers of B_2. The motivation for their choice appears in (46) and (47). Equations (44) and (45) are not as simple to plot as are the previous curves, but enough points to construct them may be obtained without difficulty by computing their intersections with the radial lines $\beta = e\zeta$ and $\alpha = e\zeta$, respectively, for a series of values of the parameter e. The intersections of B_{23} and I_{23} are shown in Figs. 2 and 3 as triangles with apex down.

It is not necessary to investigate the possible use of B_{23} or I_{23} as barriers of the branches because sufficient curves are already available. However, it can be shown that B_{23} are in fact barriers of the branches.

Construction of Curves B_2. The auxiliary barriers B_{2j} and I_{2j}, $j = 1, 2, 3$, are shown in Fig. 2 and the curves B_2 are traced through the appropriate intersections (marked by squares and triangles) as shown enlarged in Fig. 4. The curves B_2 are shown only in Sector 3 as they are not needed in Sector 2 and do not exist in Sector 1.

Establishment of Curves B_2 as Bounds. Subject to the conditions $J_1(\alpha) \neq 0$, $J(\beta) \neq 0$, i.e., for points not on B_{21} or I_{21}, (32) may be solved, in turn, for $\mathcal{J}_\alpha$ and $\mathcal{J}_\beta$. When these expressions are substituted in Pochhammer's equation, the latter are satisfied if and only if

$$\zeta^2 B_{22} B_{23} = 0 \tag{46}$$

$$\zeta^2 I_{22} I_{23} = 0 \tag{47}$$

respectively. Hence, except for points on B_{21} or I_{21}, the branches intersect B_2 where and only where B_2 crosses B_{22}, B_{23}, I_{22}, I_{23}, and $\zeta = 0$. Now, by (41) and (42), the intersections of B_2 with B_{22} and I_{22} are common and, by (44) and (45), the intersections of B_2 with B_{23} and I_{23} are common. Accordingly, the branches cross B_2 where and only where B_2 passes through $\zeta = 0$, the intersections of B_{22} with I_{22} and the intersections of B_{23} with I_{23} — except for points on B_{21} or I_{21}. But, by (33) and (34), B_2 coincides with B_{21} or I_{21} only at the intersections of the latter two and, by (33) and (35), these intersections are roots of Pochhammer's equation. Therefore the branches cross B_2 at $\zeta = 0$ and at the intersections of B_{2j} with I_{2j}, $j = 1, 2, 3$, and at no other points. This establishes the curves B_2 as bounds.

[6] Note that the cofactors A_{31}, A_{32}, A_{33} of the elements of the third row of Pochhammer's determinant[3] are

$$A_{31} = 2\zeta\beta^2 B_{22}$$
$$3A_{32} = \beta^2 I_{22} - 2(\zeta^2 - \beta^2)B_{22}$$
$$3A_{33} = 2\zeta[\beta^2 I_{22} + (\zeta^2 - \beta^2)B_{22}]$$

and note also that $B_2 = (I_{22} + 2B_{22})J_1(\alpha)J_1(\beta)$.

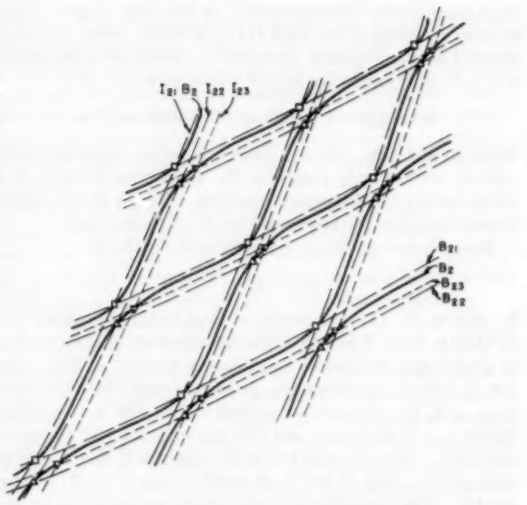

Fig. 4 Bounds B_2 traced through auxiliary barriers B_{2j} and I_{2j}

Construction of Branches

After the bounds have been drawn, as illustrated in Fig. 2 for $\sigma = 1/3$, i.e., $k = 2$, there is no further use for the auxiliary barriers B_{22}. Also, there is no further use for any of the intersectors I_1 or I_{2j}; only their intersections with their respective bounds or barriers are required for tracing the branches. Finally, the bounds B_2 are needed only in Sector 3. The remaining bounds, barriers, intersection points, and asymptotes, as well as the line OD, are shown in Fig. 3 and branches are traced through them as described later after a few preliminary remarks about asymptotic behavior.

Sequence of Branches and Bounds Near Cut-Off. Each of the branches above the first starts at a cut-off frequency, (11) or (12), where the branch coincides with a bound B_1 or B_2. The bounds have zero slopes at $\zeta = 0$, as may be ascertained by replacing P with B_1 or B_2 in (16). Whether a branch starts out above or below a bound may be determined by comparing their curvatures at $\zeta = 0$. The curvatures of the branches are given by (21) and (22) and the curvatures of the bounds may be obtained by replacing P with B_1 or B_2 in (20). Their ratios are given in Table 1 for the next seventeen modes above the first. The branch starts out above or below the bound according as the ratio is greater or less than unity.

Negative Curvature at Cut-Off. The curvatures of the bounds are always positive at $\zeta = 0$ but the curvatures of the branches may be positive or negative, depending upon Poisson's ratio and the order of the branch. As Poisson's ratio increases, the cut-off frequencies of the coupled modes increase while those of the axial shear modes remain fixed (Appendix). As the cut-off frequency of a coupled mode passes a cut-off frequency of an axial shear mode, with increasing σ, the curvatures (21) and (22) pass through infinity and change sign. The behavior is analogous to that in plates [5]. When the curvature of a branch is negative at $\zeta = 0$, the frequency drops to a minimum with increasing ζ.

In this range the phase and group velocities have opposite signs and the group velocity drops to zero at the frequency minimum [15] which is a point of intersection of a real branch with a branch corresponding to complex ζ [7]. With $\sigma = 1/3$, none of the first eighteen branches of Pochhammer's equation for flexure has a negative curvature at $\zeta = 0$ so that these phenomena do not appear in Fig. 3.

Sequence of Branches, Bounds, and Barriers at Short Wave Length. The asymptotic behavior of all the branches above the first, as $\zeta \to \infty$, is given by (25) and (26). These curves are to be compared with the barriers B_{21} and the bounds B_1, which alternate in position beginning with the root $\beta = 0$ for B_{21}, then $\beta = 1.84$ for B_1, then $\beta = 3.83$ for B_{21}, and so on. Now, the lowest root of (25) is $\beta = 0$ for (25*b*). Hence there must be a branch adjacent to $\beta = 0$; i.e., lying between OE and the lowest of bounds B_1. The next higher root of (25) and (26) is $\beta = 3.25$ for (25*a*). Hence the next branch lies between the lowest of bounds B_1 and the next barrier B_{21}. This sequence continues, with one branch between each pair of adjacent curves B_{21} and B_1, independent of the interpositions of barriers B_{22}. As β increases, the roots of (25*a*) approach the roots of $J_1(\beta) = 0$ from below and the roots of (25*b*) approach the roots of $\mathcal{J}_\beta = 1$ from below. Hence, at large ζ, the higher branches lie just below the successive curves B_{21} and B_1.

Fundamental Mode. The first branch starts at the origin as a parabola, in accordance with (13). As shown by Hudson [12], (7) has one and only one root in Sector 1 for each ζ and, as $\zeta \to \infty$, the branch approaches the phase velocity of Rayleigh surface waves (24) asymptotically. With this behavior of the branch, the phase velocity must increase monotonically, with increasing ζ, to the asymptotic velocity of surface waves and the group velocity must start at zero, increase to a maximum (at the point of inflection of the branch), and fall off asymptotically to the same velocity of surface waves. Tables of this branch have been computed by Hudson [12].

Second Branch. This starts out at the lowest cut-off frequency, $\Omega = 1.84$, of the axial shear modes, with large positive curvature ratio, as shown in Table 1, so that the branch swings sharply up above its bound B_1 and then reverses curvature in order to cross the barrier B_{22} at point a_2. The branch then continues, crossing OL at b_2, recrossing B_{22} at c_2 and, finally, crossing B_1 at d_2 so as to take its asymptotic position, with positive curvature, between B_1 and OE. In order to do this there must be a second reversal of curvature near b_2. Inspection of the resulting branch shows that, as ζ increases from zero, the phase velocity diminishes monotonically from infinity to v_2 and the group velocity starts at zero, goes through a high maximum before a_2, a shallow minimum near b_2, and then rises monotonically to v_2. Comparison can be made with computations of this branch by Abramson [16].

Third Branch. The lowest frequency, $\Omega = 2.86$, of the family of coupled cut-off modes is the starting point of the third branch. The curvature ratio is positive and slightly greater than unity so that the branch swings gradually upward away from the lowest of bounds B_2, but the branch must then reverse its curvature in order to cross OL at b_3 with the slope of the tangent to the barrier B_{21} which also crosses OL at b_3. The branch cannot cross B_{21} at b_3 because there are no points on B_{21} beyond b_3 where the branch can recross B_{21} to take its asymptotic position between B_{21} and the next lower bound B_1. Hence the branch is tangent to B_{21} at b_3 entirely from below. Since the asymptotic curvature is positive there must be another reversal of curvature near b_3. The interpretation of phase and group velocities is similar to that of the second branch, but the maximum and minimum of the group velocity are less pronounced.

Fourth Branch. Here the initial curvature ratio is positive but less than unity so that the branch hugs the underside of the second bound B_1 until it crosses B_1 at the first circled point; following which the branch turns upward toward the region where the next higher barrier B_{22} and the bound OL converge. Now, b_4 lies on OL above B_{22}, so the branch must first cross B_{22} at a_4 and then OL at b_4. Following this, the branch must recross B_{22} at c_4 and, far off to the right of the portion of the spectrum shown in Fig. 3, recross B_1 at a point d_4 so as to regain the asymptotic position between the initial bound B_1 and the next lower barrier B_{21}.

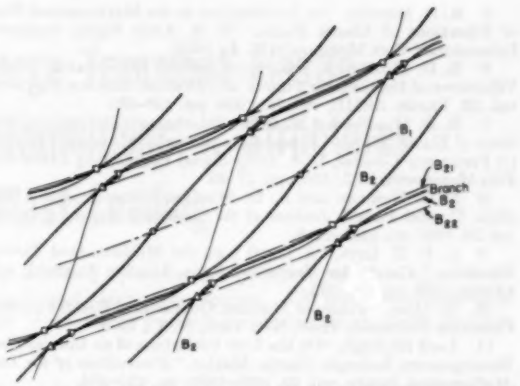

Fig. 5 Branches traced through bounds B_1 and B_2 and barriers B_{21} and B_{22} in sector 3

Higher Branches. The next two branches may be sketched in the same manner as the lower ones, but, with the seventh and eighth branches, the clusters of three intersection points of B_{2j} and I_{2j} begin to appear in Sector 3. The paths of the branches through these clusters on the barriers B_{21} and B_{22} and the bounds B_1 and B_2, at high frequencies in Sector 3, are shown in the enlarged sketch in Fig. 5. The result is the typical terrace-like structure of frequencies and phase velocities and multiple maxima and minima of group velocities of each branch. These phenomena disappear as the branch crosses OD into Sector 2. At these crossings the odd numbered branches are bounded closely above by a barrier B_{21} and below by a bound B_1. Hence the slopes of the branches are nearly the same as the slopes of B_{21}, which are all equal to $1/k$ at the intersections with OD. Thus, for the odd-numbered modes, where the phase velocity is kv_2, the velocity of dilatational waves in an infinite medium, the group velocity is approximately v_2/k which is very much less. On the other hand, the even-numbered branches behave differently. In Sector 3 adjacent to OD, the branches are squeezed against OD by the bounds B_2 immediately to the left so that the higher branches are there almost parallel to OD. However, as they cross OD, the branches must bend to the right in order to avoid the barriers B_{22} above. Hence the slopes of the branches, though high, are less than the slope of OD, i.e., for the high, even-numbered modes: where the phase velocity is the velocity of dilatational waves in an infinite medium, the group velocities are slightly less.

References

1 L. Pochhammer, "Ueber die Fortpflanzungsgeschwindigkeiten Kleiner Schwingungen in einem unbegrenzten isotropen Kreiscylinder," *Zeitschrift für Mathematik*, vol. 81, 1876, pp. 324–336.

2 A. N. Holden, "Longitudinal Modes of Elastic Waves in Isotropic Cylinders and Slabs," *Bell System Technical Journal*, vol. 30, 1951, pp. 956–969.

3 R. D. Mindlin, "Thickness-Shear and Flexural Vibrations of Crystal Plates," *Journal of Applied Physics*, vol. 22, 1951, pp. 316–323.

4 M. Onoe, "A Study of the Branches of the Velocity-Dispersion Equations of Elastic Plates and Rods," Joint Committee on Ultrasonics of the Institute of Electrical Communication Engineers and the Acoustical Society of Japan, Report, July 20, 1955.

5 R. D. Mindlin, "An Introduction to the Mathematical Theory of Vibrations of Elastic Plates," U. S. Army Signal Engineering Laboratories, Fort Monmouth, N. J., 1955.

6 R. D. Mindlin, A. Schacknow, and H. Deresiewicz, "Flexural Vibrations of Rectangular Plates," JOURNAL OF APPLIED MECHANICS, vol. 23, TRANS. ASME, vol. 78, 1956, pp. 430–436.

7 R. D. Mindlin and M. Onoe, "Mathematical Theory of Vibrations of Elastic Plates," Proceedings of the 11th Annual Symposium on Frequency Control, U. S. Army Signal Engineering Laboratories, Fort Monmouth, N. J., 1957, pp. 17–40.

8 E. G. Newman and R. D. Mindlin, "Vibrations of a Monoclinic Crystal Plate," *Journal of the Acoustical Society of America*, vol. 29, 1957, pp. 1206–1218.

9 A. E. H. Love, "A Treatise on the Mathematical Theory of Elasticity," Cambridge University Press, London, England, second edition, 1927, pp. 291–292.

10 M. Onoe, "Tables of Modified Quotients of Bessel Functions," Columbia University Press, New York, N. Y., 1958.

11 Lord Rayleigh, "On the Free Vibrations of an Infinite Plate of Homogeneous Isotropic Elastic Matter," *Proceedings of the London Mathematical Society*, vol. 20, 1888–1889, pp. 225–234.

12 G. Hudson, "Dispersion of Elastic Waves in Solid Circular Cylinders," *Physical Review*, vol. 63, 1943, pp. 46–51.

13 G. Lamé, "Lecons sur la Théorie Mathématique de l'Élasticité des Corps Solides," Gauthier-Villars, Paris, France, second edition, 1866, p. 170.

14 H. Lamb, "On Waves in an Elastic Plate," *Proceedings of the Royal Society of London*, England, series A, vol. 93, 1917, footnote on p. 122.

15 I. Tolstoy and E. Usdin, "Wave Propagation in Elastic Plates: Low and High Mode Dispersion," *Journal of the Acoustical Society of America*, vol. 29, 1957, pp. 37–42.

16 H. N. Abramson, "Flexural Waves in Elastic Beams of Circular Cross Section," *Journal of the Acoustical Society of America*, vol. 29, 1957, pp. 42–46.

APPENDIX

Variation of Cut-Off Frequencies With Poisson's Ratio

Equation (12) may be regarded as relating Ω and k and a set of barriers in the plane of k and Ω may be constructed. As suggested by the elements of Pochhammer's determinant, with $\zeta = 0$, we form the three pairs of equations

$$C_{11} \equiv J_1(\beta_0) = 0$$
$$C_{12} \equiv J_1(\alpha_0) = 0 \tag{48}$$

$$C_{21} \equiv 2\mathcal{J}(\beta_0) + \beta_0^2 - 4 = 0$$
$$C_{22} \equiv \mathcal{J}(\alpha_0) - 2 = 0 \tag{49}$$

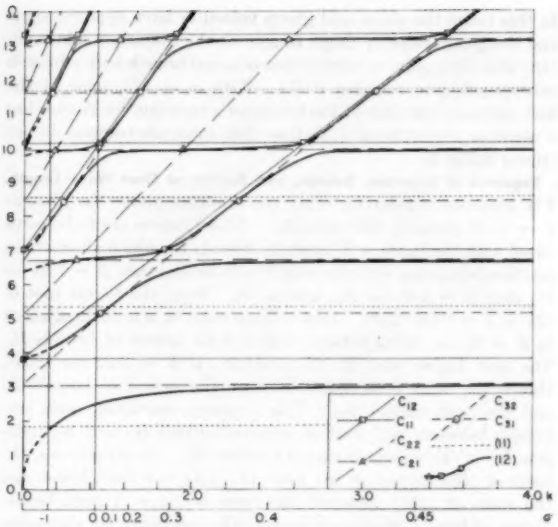

Fig. 6 Variation of cut-off frequencies with Poisson's ratio

$$C_{21} \equiv \mathcal{J}(\beta_0) - 2 = 0$$
$$C_{22} \equiv 2\mathcal{J}(\alpha_0) + \beta_0^2 - 4 = 0 \tag{50}$$

where $\beta_0 = \Omega$ and $\alpha_0 = \Omega/k$. With Ω as the ordinate and k as the abscissa, the first member of each pair is the equation of a family of horizontal lines; the second members of the first two pairs are families of inclined straight lines; and the second member of the last pair is the equation of a family of curves asymptotic to inclined straight lines. If either equation of a pair is substituted into equation (12), that equation is satisfied if and only if the other equation of the pair is satisfied. Hence the members of each pair are mutual barriers and intersectors. The branches may then be traced through the grid of lines as shown in Fig. 6. The frequencies of the axial shear modes, equation (11), are also shown in order to exhibit values of k or σ at which coincidences of cut-off frequencies occur.

Modeling of Large Transient Elastic and Plastic Deformations of Structures Subjected to Blast Loading

W. E. BAKER
Terminal Ballistics Laboratory, Ballistic Research Laboratories, Aberdeen Proving Ground, Md.
Mem. ASME

In this paper, a model law is developed for scaling of response to blast loading of structures which undergo large elastic and plastic deformations. The geometrical scaling of response predicted by this law is verified by a series of experiments on small cantilever beams.

OFTEN, in studies of the dynamic response of structures to transient loads, one wishes to measure the response of quite large structures to loading resulting from rapid release of energy from large energy sources. The very size of the structure and the magnitude of the energy release can preclude laboratory testing, or render full-scale testing prohibitively expensive and time-consuming. One must then resort to other techniques for obtaining the structural response.

As in many other branches of science, tests of suitably scaled models can be substituted for the full-scale experiments, and the response of the full-scale structures inferred from a knowledge of the model laws. Such scaling has been applied by several investigators to the problem of small-deflection elastic response of structures to dynamic loads. R. M. Hermes [1][1] developed model criteria for the elastic vibrations of beams, plates, and frames and showed by impact tests of these structural elements that the criteria were valid. H. N. Brown [2] considered modeling of the interaction between shock waves and elastic structures, using the general equations of small elastic deflections for the response of the elastic structures. However, one often wishes to predict both the large-deflection elastic response and the plastic response of large structures to transient forces. Because the model laws for the response based on small-deflection elastic equations of motion will not necessarily apply to these cases, one must generate suitable laws and confirm their validity by experiment. In this paper, the author reviews the model laws for blast loading from explosive charges and for the small-deflection elastic response of structures to such loading, discusses such laws for large-deflection elastic response and for plastic response, and presents the results of experiments conducted to confirm the modeling.

The Model Laws

Scaling of Blast Loading. The law for modeling the physical processes involved in transmission of shock waves generated in fluid media by the detonation of explosive charges or other sudden release of energy can be determined by considering the equations describing the motion of fluids. Both the equations of motion and excellent discussions of the "similarity principle," as the model law is termed, are given by Cole [3] and by Doering and Burkhardt [4] for explosive-energy sources. The similarity principle states that the pressure and other properties of a shock wave will be unchanged if the scales of length and time are changed by the same factor K as the dimensions of the explosive-loading source. The assumptions inherent in such scaling are that heat conduction and viscosity effects are negligible everywhere but in the shock fronts and that gravity effects are everywhere negligible. This modeling, also referred to as "geometrical scaling," applies equally well to the transmission of pressure pulses which do not form shocks, provided always that heat conduction and viscosity effects are negligible during the process. Such scaling has been shown by experiment to be valid for detonations of explosives in air and water over an extraordinarily large range of explosive-charge weights and distances [5, 6].

Scaling of Small-Deflection Elastic Response of Structures to Blast Loading. As was mentioned previously, the scaling law for the elastic response of structures to blast loading has been considered by H. N. Brown [2] on the basis of the general, small-deflection equations of elastic motion of solids. He demonstrates that the same geometrical scaling which governs the shock-transmission process also provides the proper modeling for structural response to the transient pressures generated during the blast process. In his analysis, the effect of gravity and strain-rate effects are assumed negligible.

Perhaps the "geometrical" modeling indicated in the foregoing can be best described by imagining the following experiment: An energy source of characteristic dimension d is initiated a distance R from an elastic structure of characteristic dimension L, producing a transient pressure loading on the structure of amplitude P and duration T, and causing the structure to respond in its natural modes of vibration with periods $\tau_1, \tau_2, \ldots \tau_n, \ldots$ and corresponding displacement amplitudes $X_1, X_2, \ldots X_n, \ldots$. Strain-time histories of response of the structure are characterized by the periods τ_n and corresponding strain amplitudes e_n. Let the entire experiment be scaled geometrically by a scale factor K, making the energy source of characteristic dimension Kd and locating the structure of characteristic dimension KL at a distance KR from the source. Then, geometrical modeling predicts that the pressure loading on the structure will be similar in form to that obtained in the first experiment, with amplitude P and duration KT; and that the structural response will also be similar in character, with the natural periods being $K\tau_1, K\tau_2, \ldots K\tau_n, \ldots$, displacement amplitudes $KX_1, KX_2, \ldots KX_n, \ldots$, and strain amplitudes $e_1, e_2, \ldots e_n, \ldots$. The blast scaling is shown graphi-

[1] Numbers in brackets designate References at end of paper.

Presented at the Summer Conference of the Applied Mechanics Division, University Park, Pa., June 20–22, 1960, of THE AMERICAN SOCIETY OF MECHANICAL ENGINEERS.

Discussion of this paper should be addressed to the Secretary, ASME, 29 West 39th Street, New York, N. Y., and will be accepted until October 10, 1960, for publication at a later date. Discussion received after the closing date will be returned.

NOTE: Statements and opinions advanced in papers are to be understood as individual expressions of their authors and not those of the Society. Manuscript received by ASME Applied Mechanics Division, July 30, 1959. Paper No. 60—APM-18.

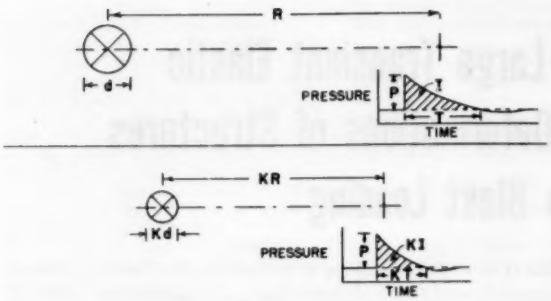

Fig. 1 Blast-wave scaling

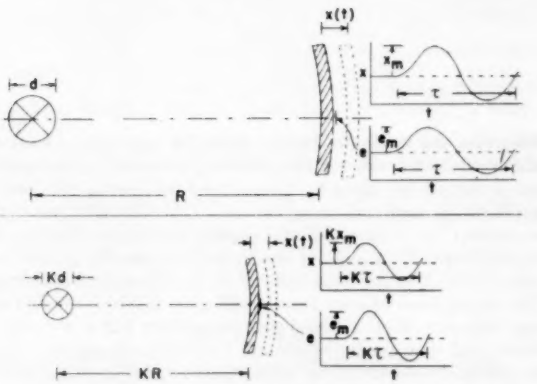

Fig. 2 Scaling of response of structure to blast wave

cally in Fig. 1 and the corresponding response scaling in Fig. 2.

Scaling of Large-Deflection Elastic Response of Structures to Blast Loading. The equations of motion of elastic solids from which Brown deduced the geometrical scaling laws are only valid for infinitesimal strains and displacements. In many cases of elastic response of structures to blast loading, the linear equations are incapable of describing the motion of the structure with any accuracy. For example, Flynn [7] has obtained solutions to the small-deflection Bernoulli-Euler beam equation for the elastic response of simply supported and cantilever beams subjected to normally incident blast loading. But, in later experiments, Locklin and Mills [8] demonstrated that neither the character nor the amplitude of the response predicted from Flynn's solutions agreed with experiment if the beams were thin enough so that large elastic deflection could occur. Some of their data are presented in Table 1. One can see that the linear theory predicts amplitudes of vibratory displacement which are considerably in error whenever the predicted displacements are an appreciable fraction of the beam length. In one extreme case, the predicted amplitude is over 10 times the measured amplitude.

The data in Table 1 indicate that any model law based on small-deflection equations will have limited usefulness unless it also can be shown to apply to large deformations and strains.

In this section, we develop a model law from the equations for large motions of both fluid and solid media by the following method of analysis:[2]

1 The complete equations of motion are presented, and the assumptions inherent in these equations are given.

2 The hypothesis of geometrical modeling of the physical process is advanced.

[2] Note that no "theory" is presented in such an analysis, in that no attempt is made to solve the equation of motion. The model law itself must be verified by experiment.

3 This hypothesis is tested by systematic substitution of scaled parameters into all of the equations of motion.

4 The hypothesis is proved by the invariance of all of the governing equations under the substitution.

Let us consider the equations governing this problem for large motions of both fluid and solid media. We will write the equations in Lagrangian co-ordinates defined by

$$x_i = a_i + u_i(a_1, a_2, a_3, t) \tag{1}$$

where the a_i are the Cartesian co-ordinates of points in the medium before deformation, u_i are the displacement components, and t is time.

In the fluid medium, the equations of motion are, except in the vicinity of shock fronts, those for an inviscid compressible fluid with negligible heat conductivity.[3]

The equations of motion are

$$\rho \frac{\partial^2 x_i}{\partial t^2} + \frac{\partial p}{\partial x_i} = 0 \tag{2}$$

where ρ is the density of the fluid and p the pressure. From conservation of mass, we obtain

$$\rho J = 0 \tag{3}$$

where

$$J = \frac{\partial(x_1, x_2, x_3)}{\partial(a_1, a_2, a_3)}$$

is the Jacobian.

From the assumptions that heat conductivity and viscosity are negligible, we obtain the energy relation

$$\frac{\partial S}{\partial t} = 0 \tag{4}$$

i.e., the entropy S does not vary with time. The fluid must also satisfy an equation of state of the form

$$p = f(\rho, S) \tag{5}$$

There is no limitation in any of the foregoing equations on displacements or magnitudes of pressure or density change.

Equations (2) through (5) are inherently nonlinear, although this is not immediately apparent from their form. If they are transposed to Eulerian form,[4] their nonlinear character becomes immediately evident.

Table 1 Comparison of measured maximum deflections of thin beams with predictions from Bernoulli-Euler beam theory

Data of Locklin and Mills [8]

Loading source	Beam thickness, in.	Maximum deflection, in. Measured	Predicted
Simply supported beams[a]			
1/16 lb Pentolite at 7.0 ft	0.025	1.9	7.4
1/8 lb Pentolite at 6.5 ft	0.051	1.1	2.8
1/8 lb Pentolite at 6.5 ft	0.125	0.36	0.35
Cantilever beams[a]			
1/25 lb Pentolite at 8.0 ft	0.025	0.40	4.6
1/16 lb Pentolite at 7.0 ft	0.051	1.9	5.8
1/8 lb Pentolite at 6.5 ft	0.125	0.84	1.70
1/8 lb Pentolite at 6.5 ft	0.250	0.36	0.44

[a] All beams were 1 in. wide and 12 in. long, cut from 6061-T6 aluminum-alloy sheet.

[3] See Courant and Friedrichs [9], pp. 13–14.

[4] See Doering and Burkhardt [4], pp. 2–4, for the equations in this form.

The description of shocks in fluids can be completed by the "jump" conditions, which relate the parameters ahead of a shock front to those behind, and by the boundary conditions at the interfaces between fluid and solid. The jump conditions are given by the following Rankine-Hugoniot equations,[6] which are obtained by considering conservation of mass, momentum, and mechanical energy of a fluid element passing through the shock front:

$$\rho_0(v_0 - V) = \rho_1(v_1 - V) \tag{6}$$

$$\rho_0(v_0 - V)^2 + p_0 = \rho_1(v_1 - V)^2 + p_1 \tag{7}$$

$$\rho_0(\tfrac{1}{2}v_0^2 + e_0)(v_0 - V) + p_0v_0 = \rho_1(\tfrac{1}{2}v_1^2 + e_1)(v_1 - V) + p_1v_1 \tag{8}$$

In these equations, V denotes shock-front velocity, v is particle velocity in direction of shock travel, and e is internal energy. Subscripts 0 and 1 refer, respectively, to regions ahead of and behind the shock.

The boundary conditions which must apply at the interface between the inviscid fluid and a solid are that the surface tractions applied to the solid must be normal to the surface (pressure forces only) and that the normal component of displacement and particle velocity must be continuous through the surface. These conditions are expressed mathematically as

$$\left.\begin{aligned} pn_i &= \sum_j n_i\sigma_{ji} \\ \bar{x}\cdot\bar{n},\ \bar{v}\cdot\bar{n} &\quad \text{continuous} \end{aligned}\right\} \tag{9}$$

Here $\bar{n}$ is a unit normal vector, and σ_{ji} a stress component in the solid. Lamb [12] shows that these conditions apply for either a moving or a stationary boundary.

The equations of motion for large deformations and large strains in an elastic, solid medium are given by Murnaghan [10] and Novozhilov [11]. The equations in Lagrangian co-ordinates are, for no body forces,

$$\sum_{j=1}^{3} \frac{\partial\sigma_{ji}}{\partial x_j} = \rho_s \frac{\partial^2 x_i}{\partial t^2} \tag{10}$$

In these equations, ρ_s is the density of the solid after deformation, and all other quantities are as defined before. These equations appear to be identical to the linear infinitesimal equations of motion. One must transpose them to Eulerian form to note their nonlinearity.

The stress-strain law corresponding to Hooke's law for infinitesimal theory[6] is

$$\sigma_{11}' = A_2 + A_1e_{11} + A_0(e_{11}^2 + \tfrac{1}{4}e_{12}^2 + \tfrac{1}{4}e_{13}^2) \tag{11}$$

for normal stresses, and

$$\sigma_{21}' = \tfrac{1}{2}\{A_1e_{12} + A_0[(e_{11} + e_{22})e_{12} + \tfrac{1}{2}e_{13}e_{23}]\} \tag{12}$$

for shear stresses. In these two equations, the e_{ij} are strain-components, σ_{ij}' are stress components referred to the dimensions of an element before deformation, and the A_i are elastic constants. Strain-rate effects are assumed negligible in this law The strain components are expressible in terms of the displacement components as[7]

$$e_{ii} = \frac{\partial u_i}{\partial a_i} + \frac{1}{2}\sum_{j=1}^{3}\left(\frac{\partial u_j}{\partial a_i}\right)^2 \tag{13}$$

$$e_{ij} = \frac{\partial u_i}{\partial a_j} + \frac{\partial u_j}{\partial a_i} + \sum_{n=1}^{3}\frac{\partial u_n}{\partial a_i}\frac{\partial u_n}{\partial a_j} \tag{14}$$

[6] See Courant and Friedrichs [9], pp. 121–124.
[6] Reference [11], p. 112.
[7] Ibid., p. 13.

The boundary conditions for the interfaces between solid and fluid have been given already. The remaining boundary conditions at the supports of the elastic structure are in the nature of constraints, requiring that certain components of displacement be zero at specified points, or that various derivatives of the displacements with respect to Eulerian co-ordinates be zero.

Let us now apply geometrical scaling to the governing equations for large motions given in the foregoing. Let $x_i' = Kx_i$, $a_i' = Ka_i$, $t' = Kt$. Displacements, velocities, and accelerations are then

$$\begin{aligned} u_i' &= Ku_i \\ v_i' &= \frac{\partial u_i'}{\partial t'} = v_i \\ \alpha_i' &= \frac{\partial^2 u_i'}{\partial t'^2} = \frac{1}{K}\alpha_i \end{aligned} \tag{15}$$

If motions in the fluid medium are to scale, equation (2) requires that

$$\rho' = \rho, \qquad p' = p \tag{16}$$

Equations (3) and (4) can be seen to be unchanged by the scaling, and equation (5) is also satisfied if the same fluid medium is used in the scaled experiment. If we note that densities and pressures are the same at corresponding points in the original and scaled experiments, and that velocities are unchanged by the scaling, we see that the Rankine-Hugoniot conditions, (6) through (8), must be unchanged. The boundary conditions (9) now specify that, in the solid body at its interfaces with the fluid, the normal stresses must be unchanged, normal displacements multiplied by K, and normal velocities unchanged.

Within the elastic body, we can see that the motions specified by (10) are unchanged if

$$\sigma_{ij}' = \sigma_{ij}, \qquad \rho_s' = \rho_s \tag{17}$$

If the elastic material is identical in both experiments, it must obey the same stress-strain law, (11) and (12). Amplitudes of strain must therefore be unchanged in the scaled experiment; i.e.,

$$e_{ij}' = e_{ij} \tag{18}$$

The relations between strain and displacement, (13) and (14), are unchanged by the scaling, because they involve only the first derivatives of displacements with respect to the space co-ordinates, which are not altered by the scaling. Lastly, the boundary conditions at restraints require that the shape of the model structure be the same as that of the original structure at corresponding scaled times.

From the foregoing analysis, we predict that the geometrical modeling which applies to the small-deflection response of elastic structures to blast loading describes the large-deflection response equally well. The same restrictions must hold; i.e., neglect of gravity effects in both fluid and solid media, neglect of heat-conduction and viscosity effects in fluid media (except in shock fronts), and neglect of strain-rate effects in solid media. Let us re-emphasize that the governing equations do not restrict amplitudes of fluid or solid motion, nor amplitudes of strain.

Scaling of Elastic-Plastic Response of Structures to Blast Loading. If one wishes to scale damage to structures from blast loading, he must investigate the scaling of the structural response for strains exceeding the elastic limit; i.e., for plastic strains. If possible, one should establish such scaling by considering the most general equations of elastic-plastic structural response. The equations of motion (10) and the associated boundary conditions generated for elastic structures apply equally well to large deflections of structures undergoing plastic deformations. However, the stress-

strain law for plastic structures differs from the elastic stress-strain law. In elastic bodies, the stress components are unique functions of the strain components, and deformations are therefore reversible. In plastic bodies, the stresses associated with increasing strains are usually different from those associated with decreasing strains, and the deformations are irreversible. One must assess the effect of the differences in the stress-strain law on scaling of response. Novozhilov[8] has shown that, when the strains are monotonically increasing in magnitude, the stress-strain laws for finite elastic deformations, given by equations (11) and (12), include Hencky's theory for elastic-plastic bodies as a special case. Therefore geometrical scaling of response to blast loading will apply to the deformation of elastic-plastic bodies while the strains are increasing in magnitude. This scaling then predicts that the limiting strain magnitudes for the initial stress-strain law are the same in the full-scale and model structures. When the strains start decreasing in magnitude, the initial stress-strain law is no longer valid. But relations of the same form as (11) and (12), with different values for the constants A_i determined by the maximum strains, will then hold. This new stress-strain law for the geometrically scaled model should be identical to that for the original structure, because the maximum strains and the physical properties which determine the A_i are identical. One can therefore conclude that the entire elastic-plastic response of a structure to blast loading should scale geometrically in the manner previously described for elastic structures and shown graphically in Figs. 1 and 2.

Experimental Procedure

To confirm the model laws discussed in the preceding section, the author performed a series of experiments on the response of slender cantilever beams to blast loading from spherical Pentolite explosive charges detonated in air. Ewing and Hanna [13] conducted for another purpose a somewhat similar series of experiments on thin aluminum-alloy beams with rectangular cross sections. They measured large-deflection elastic response for a variety of explosive-charge weights and distances, and permanent deformation for those blast loadings which were intense enough to cause plastic flow. Their experiments were modeled, using geometrical scaling, for the tests reported here.

The dimensions of the cantilever beams are given in Table 2. All beams were made from sheet aluminum, 6061T6 alloy. Beams A, B, and C are models of each other, scaled up successively by scale factor 2. Beam E is approximately a model of D, of twice the size.[9] The cantilever mounts consisted of vises made of pieces of angle iron, which were bolted to a massive steel base plate.

Table 2 Cantilever-beam dimensions

Beam	Length, in.	Width, in.	Thickness, in.
A	6	1/2	0.025
B[a]	12	1	0.051
C	24	2	0.102
D[a]	12	1	0.088
E	24	2	0.191

[a] Beams of this size were tested by Ewing and Hanna [13].

Large-Deflection, Elastic-Response Tests. For these experiments, the response of the slender beams to blast loading from spherical Pentolite explosive charges was measured by recording bending strains at stations near the beam roots. Two SR-4 resistance-wire strain gages were mounted on opposite sides of each test beam. The electrical output of each pair of gages, suitably connected in a resistance bridge, was amplified and recorded by a commercial magnetic oscillograph system having a frequency response flat from 0 to 3000 cps. High-speed motion pictures (3000 frames/sec) were taken of the response of some of the beams to the blast loading. The test arrangement is shown schematically in Fig. 3.

Strain-time histories were recorded for all of the beams in Table 2 subjected to blast waves of various intensities. Spherical Pentolite explosive charges weighing approximately[10] 1/8, 1, and 8 lb, suspended at a scaled height[11] of 2 ft/lb$^{1/3}$ above the reflector plate, were used for the experiments. The dependence of the strain-time histories on the blast loading was determined by varying the distance of each beam from the charges on successive tests. Distances were measured with an accuracy of ±0.01 ft.

Permanent-Deformation Tests. The permanent-deformation tests were carried out in a manner similar to the elastic-response tests, with the test beams merely being moved closer to the explosive charges. Permanent tip deflections of the damaged beams were recorded as a measure of the beam response. Each beam was subjected to a single blast loading, and replaced by an undamaged beam prior to the next experiment.

Results

Elastic-Response Tests. Forty-nine experiments were conducted during this phase of the tests, with the elastic response of all of the five sizes of beam being measured during almost all of the experiments. The oscillograms recorded during the experiments showed that the response of all of the beams to blast loading was characterized by two vibration frequencies. These frequencies, which represent the first two normal modes of vibration, predominated throughout the tests, with occasional higher modes being excited in small amplitude. The measured vibration frequencies agreed well with frequencies calculated from the equations which describe small-deflection elastic vibrations. A comparison of predicted[12] and measured frequencies for two typical experiments is given in Table 3. Error in measurement of frequency is estimated to be ±2 per cent.

The agreement of measured vibration frequencies with those predicted from simplified equations of motion verifies one prediction of the model law; namely, that vibration periods of model structures are changed in proportion to the linear scale factor. To complete the verification of the law for elastic response, one must compare the amplitudes of strain-time histories for experiments which are models of each other.

The test results can be divided into five groups within which

[8] Reference [11], p. 123.

[9] Note that the thickness is slightly more than doubled in this case. All beams were sheared from standard sheet stock of the thickness nearest the proper one.

[10] Actual charge weights averaged 0.121, 1.060, and 8.33 lb, respectively, with variations in individual charge weights not differing by more than 1 per cent from these means.

[11] Defined as height divided by the cube root of the explosive-charge weight.

[12] See Timoshenko [14], p. 344 for predicted vibration frequencies of cantilever beams.

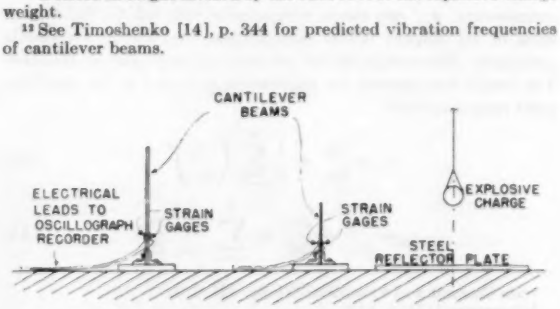

Fig. 3 Test arrangement

Table 3 Comparison of predicted and measured vibration frequencies

Beam	Mode No.	Predicted freq, cps	Meas. freq, cps	Mode No.	Predicted freq, cps	Meas. freq, cps	Mode No.	Pred. freq, cps	Meas. freq, cps
Response to blast from 1-lb explosive charge									
A	1	22.1	21.9	2	138	133.3	...	...	...
B	1	11.2	10.8	2	70.4	69.2	6	954	1000
C	1	5.61	5.45	2	35.2	33.8	6	447	467
D	1	19.3	19.1	2	121	120	6	1640	1600
E	1	10.5	10.2	2	66.0	64.3	7	1250	1200
Response to blast from 8-lb explosive charge									
A	1	22.1	21.4	2	138	135	...	...	...
B	1	11.2	10.7	2	70.4	68.2	...	...	...
C	1	5.61	5.8	2	35.2	34.5	...	...	...
D	1	19.3	19.1	2	121	120	5	1100	1100
E	1	10.5	10.1	2	66.0	64.0	...	...	...

NOTE: Dots in the Table indicate that no mode higher than the second was observed in measurable amplitude.

Table 4 Measured maximum elastic bending strains for scaled experiments

1/8-lb charge vs. Beam A		1-lb charge vs. Beam B				8-lb charge vs. Beam C			
	Max		Max		Max		Max		Max
R,[a] ft	strain × 10⁶	R, ft	strain × 10⁶	R, ft	strain × 10⁶	R, ft	strain × 10⁶	R, ft	strain × 10⁶
14.5	560	25.0	610	14.0	2280	48.0	655	26.0	2310
14.5	500	25.0	600	11.5	2910	48.0	577	24.0	2930
14.5	515	25.0	640	11.5	2330	48.0	559	21.0	4130
9.0	990	17.5	1350	11.5	2990	35.0	1310	21.0	4150
9.0	1180	17.5	1410			35.0	1370	21.0	4150
7.0	1370	17.5	1380			35.0	1430		
5.75	2910	15.0	1790			31.0	1640		
5.75	3090	15.0	1820			31.0	1600		
5.75	2800	15.0	1760			28.0	1910		
5.75	3200	14.0	2200			26.0	2310		
		14.0	1910			26.0	2260		

[a] R is the horizontal distance from a point on the ground directly beneath the explosive charge to the front face of the test beam.

the experiments should model. However, the data are too extensive to be given in full in this paper. Those for one group including the responses of Beam A to 1/8-lb charge, Beam B to 1-lb charge, and Beam C to 8-lb charge are given in Table 4. The data are also shown graphically in Fig. 4. Combined calibration and reading errors in measurement of strain amplitudes are estimated to be ±5 per cent.

The validity of the elastic-response scaling can now be determined by comparing strain amplitudes within the group at equivalent scaled distances. This comparison is made in Fig. 5. It can be seen that there is no significant difference between data within the group when scaled in this fashion, and that the response therefore scales. Although the data are not given here, the same result was obtained within all of the five model groups.

It is of interest to note that elastic tip deflections of the more slender beams observed by high-speed camera were truly large, exceeding 3/10 of the original beam lengths for many experiments. As has been mentioned before, these deformations cannot be predicted adequately by small-deflection-response theory.

Permanent-Deformation Tests. Thirty-one experiments were conducted during this phase of the tests. The data recorded during the experiments consisted merely of measurements of permanent tip deflections of the beams, measured to an accuracy of ±0.01 in. Data of Ewing and Hanna [13] were used to supplement these test results.

The model law predicts that, for properly scaled experiments, the deformed shapes of beams should be similar, and the permanent deformations should scale in proportion to the linear scale factor. Each of the pairs of beams shown in Figs. 6 through 8 were deformed during experiments which were intended to be models of each other. It can be seen that the deformed shapes are quite similar in each figure. For comparison of the test results, the measured tip deflections are grouped in the same manner as for the elastic experiments, and made nondimensional by

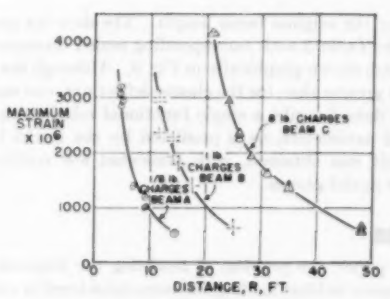

Fig. 4 Maximum bending strains for Group 2

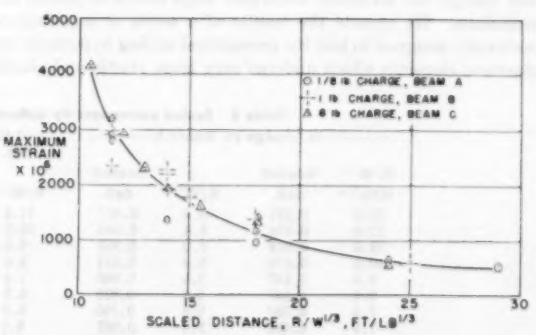

Fig. 5 Maximum bending strains versus scaled distance, Group 2

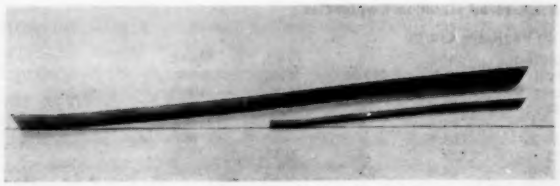

Fig. 6 Relatively small deformation of Beams B and C for same scaled blast loading

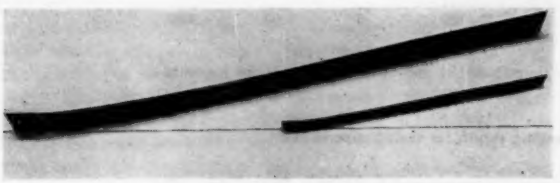

Fig. 7 Intermediate deformation of Beams D and E for same scaled blast loading

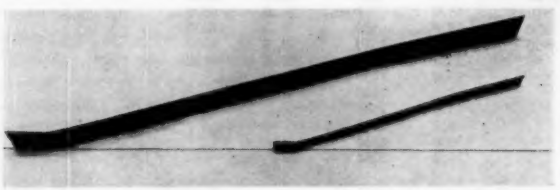

Fig. 8 Large deformation of Beams B and C for same scaled blast loading

division by the original beam length. The data for group 2 are recorded in Table 5 with corresponding scaled distances. These data are also shown graphically in Fig. 9. Although the scatter is somewhat greater than for the elastic deflections, one can see that all of the data describe a single functional relationship between the scaled parameters, as is predicted by the model law. The same result was obtained, with somewhat less scatter, for the other four model groups.

Discussion

In this paper, the problem of modeling the response of structural elements to blast loading has been considered in some detail. By studying the differential equations governing blast transmission through fluids and large-amplitude motion of structures, the author has predicted that purely geometrical modeling of a blast-loading experiment should provide proper scaling of both the transient blast loading and the transient structural response, even though the structure undergoes large elastic or plastic deformations. He reports the results of a series of experiments specifically designed to test the geometrical scaling hypothesis for structural elements which undergo very large plastic and elastic

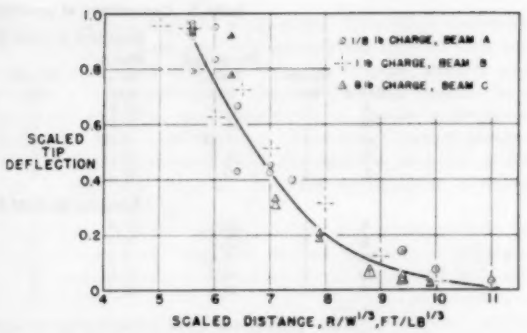

Fig. 9 Scaled cantilever tip deflections versus scaled distance, Group 2

deformations as a result of blast loading. The experimental results verify the hypothesis.

One must therefore conclude, on the basis of the analysis and experiments presented in this paper, that the same similarity principle which has been used so effectively to describe the modeling of blast waves can be used with equal facility to describe modeling of the response of structures to the transient forces generated by interaction of blast waves with structures. The principle would be expected to be invalid only if the structures were made of materials whose behavior changed markedly with change in strain rate or if "body forces," such as gravity forces, were not negligible. The scaling applies with no restrictions on amplitudes of motion or of strain amplitudes. Such problems as transverse displacement of slender beams or dynamic buckling of thin-wall shell under blast loading, where quite large deflections can occur, can then be studied by performing accurately controlled small-scale experiments and scaling the test results.

Acknowledgments

The financial support of the Division of Reactor Development, U. S. Atomic Energy Commission, for whom this work was performed, is gratefully acknowledged. The author also wishes to acknowledge the able assistance of Mr. W. O. Ewing, Jr., who performed the experiments, and of Mr. J. W. Hanna, who reduced most of the experimental data.

References

1 R. M. Hermes, "Dynamic Modeling for Stress Similitude," closing report on Office of Naval Research Contract N8 onr-523, Department of Applied Mechanics, University of Santa Clara, June, 1953.

2 H. N. Brown, "Effect of Scaling on the Interaction Between Shock Waves and Elastic Structures," Appendix I to Ballistic Research Laboratories Report No. 1011, March, 1957.

3 R. H. Cole, "Underwater Explosions," Princeton University Press, Princeton, N. J., 1948.

4 W. Doering and G. Burkhardt, "Contributions to the Theory of Detonation," translated from German as Technical Report No. F-TS-1227-1A, Wright-Patterson AFB, Dayton, Ohio, 1949.

Table 5 Scaled permanent tip deflections of cantilevers versus scaled distances

——1/8-lb. charge vs. Beam A——		—1-lb charge vs. Beam B—		—8-lb charge vs. beam C—	
$R/W^{1/3}$ ft/lb$^{1/3}$	Scaled defl.	$R/W^{1/3}$	Scaled defl.	$R/W^{1/3}$	Scaled defl.
11.0	0.035	6.4	0.427	11.0	0.010	9.9	0.020	8.8	0.074
11.0	0.038	6.4	0.665	10.0	0.037	9.9	0.024	7.9	0.202
10.0	0.078	6.0	0.950	9.0	0.122	9.4	0.029	7.9	0.185
10.0	0.070	6.0	0.833	8.0	0.315	9.4	0.030	7.1	0.318
9.4	0.137	5.6	0.940	7.0	0.514	9.4	0.046	7.1	0.305
9.4	0.147	5.6	0.920	6.5	0.728	9.4	0.030	6.3	0.860
7.4	0.397	5.6	0.790	6.0	0.622	8.8	0.057	6.3	0.781
7.4	0.401	5.6	0.965	5.5	0.945	8.8	0.068	5.6	0.926
7.0	0.428	5.6	0.965	5.0	0.954	8.8	0.074	5.6	0.949
7.0	0.455								

5 R. G. Stoner and W. Bleakney, "The Attenuation of Spherical Shock Waves in Air," *Journal of Applied Physics*, vol. 19, 1948, pp. 670–678.

6 J. Dewey and J. Sperrazza, "The Effect of Atmospheric Pressure and Temperature on Air Shock," Ballistic Research Laboratories Report No. 721, May, 1950.

7 P. D. Flynn, "Elastic Response of Simple Structures to Pulse Loading," Ballistic Research Laboratories Memorandum Report No. 525, November, 1950.

8 R. G. Locklin and S. N. Mills, Jr., "Dynamic Response of Thin Beams to Air Blast," Ballistic Research Laboratories Report No. 787, September, 1951.

9 R. Courant and K. O. Friedrichs, "Supersonic Flow and Shock Waves," Interscience Publishers, Inc., New York, N. Y., 1948.

10 F. D. Murnaghan, "Finite Deformation of an Elastic Solid," John Wiley & Sons, Inc., New York, N. Y., 1951.

11 V. V. Novozhilov, "Foundations of the Non-Linear Theory of Elasticity," translated from the first Russian edition, Graylock Press, Rochester, N. Y., 1953.

12 Horace Lamb, "Hydrodynamics," sixth edition, Dover Publications, Inc., New York, N. Y., 1945, p. 7.

13 W. O. Ewing and J. W. Hanna, "A Cantilever for Measuring Air Blast," Ballistic Research Laboratories Technical Note No. 1139, August, 1957.

14 S. Timoshenko, "Vibration Problems in Engineering," second edition, D. Van Nostrand Company, Inc., New York, N. Y., 1937.

Shock Spectra of a Nonlinear System

W. T. THOMSON[1]
Professor,
Department of Engineering,
University of California,
Los Angeles, Calif.
Mem. ASME

The peak response under pulse excitation, of a single-degree-of-freedom system with nonlinear spring approximated by two straight lines, is analytically determined. Shock spectra for the step and delta function are developed with damping as parameter. For the rectangular pulse excitation, the shock spectra for zero damping are presented with pulse duration as a parameter. For the arbitrary pulse shape, a general procedure is discussed and illustrated for the sine pulse of differing pulse duration. Generalized phase-plane plots associated with the problem are included. The shock spectra presented are applicable only when the first peak corresponds to the maximum response, thereby avoiding the questions of unloading.

THE lumped-mass system with nonlinear spring has been studied by many people. Most of these studies are for periodic excitation. The literature on the behavior of nonlinear systems excited by a pulse, however, is scarce by comparison. The work by Mindlin[2] is perhaps one of the most well known. The pulse is supplied by a drop test and for a linear or nonlinear spring the maximum deflection can be found by equating the initial potential energy to that absorbed by the spring. For a nonlinear spring, this requires a graphical integration of the area under the spring force-displacement curve. A similar procedure was used by Crede[3] with measured stiffness-displacement curve of a nonlinear isolator. Ergin[4] solves the transient-response problem of a nonlinear system by a bilinear approximation of the spring force. The slope of the first linear line is made equal to the slope at the origin and the second linear line is positioned for the minimum of the mean square error between the nonlinear spring force and the bilinear approximation. Linear solutions for each region are then matched for continuity of displacement and velocity at the intermediate point. The phase-plane method as outlined by Jacobsen[5] is perhaps the most suitable graphical procedure for the solution of the general nonlinear system.

The subject of this paper is the transient response of a single-mass system with bilinear spring and a viscous damper. The procedure adopted is that of a generalized phase plane based on equations rather than numerical evaluation. The solution is for the peak response presented in the form of a nondimensional shock spectrum.

[1] Also, Consultant, Engineering Mechanics Department, Space Technology Laboratories, Inc., Los Angeles, Calif.

[2] R. D. Mindlin, "Dynamics of Package Cushioning," *Bell System Technical Journal*, vol. 24, 1945, pp. 353–461.

[3] C. E. Crede and S. E. Young, "Theoretical and Experimental Investigation of Buckling Shock Mount," Society of Experimental Stress Analysis, vol. 5, 1948, pp. 144–153.

[4] E. I. Ergin, "Transient Response of a Nonlinear System by a Bilinear Approximation Method," JOURNAL OF APPLIED MECHANICS, vol. 23, TRANS. ASME, vol. 78, 1956, pp. 635–641.

[5] L. S. Jacobsen, "On a General Method of Solving Second-Order Ordinary Differential Equations by Phase-Plane Displacements," JOURNAL OF APPLIED MECHANICS, vol. 19, TRANS. ASME, vol. 74 1952, pp. 543–553.

Presented at the Summer Conference of the Applied Mechanics Division, University Park, Pa., June 20–22, 1960, of THE AMERICAN SOCIETY OF MECHANICAL ENGINEERS.

Discussion of this paper should be addressed to the Secretary, ASME, 29 West 39th Street, New York, N. Y., and will be accepted until October 10, 1960, for publication at a later date. Discussion received after the closing date will be returned.

NOTE: Statements and opinions advanced in papers are to be understood as individual expressions of their authors and not those of the Society. Manuscript received by ASME Applied Mechanics Division, March 2, 1959. Paper No. 60—APM-23.

The Shock-Spectra System

A shock spectrum is a plot of the maximum peak response of a linear single-degree-of-freedom oscillatory system to a specified shock excitation, as a function of the natural frequency of the oscillatory system. If the spring of the oscillatory system is nonlinear, the peak response would differ, and, although it could be plotted as a function of the natural frequency based on the initial stiffness, another factor describing the nonlinear character of the spring must be introduced. In this paper, the nonlinear character of the spring is idealized by two straight lines as shown in Fig. 1, which enables its nonlinear description to be specified by a single parameter ky_0. Many engineering materials approach this idealized spring characteristic, and a shock spectrum for such a system is desirable in estimating the response of oscillatory systems possessing such yield characteristics.

The system shown in Fig. 1 is actually a bilinear system which offers none of the difficulties of the nonlinear mathematics. The problem of determining its peak response is therefore not a formidable one provided the duration t_1 of the excitation pulse is less than the time t_0 required for the response to reach the yield value y_0. With the velocity $\dot{y}_0$ corresponding to y_0 established, the initial conditions for the second part of the problem are supplied, and the peak response can then be found. This can be done systematically in nondimensional form, where the nonlinear parameter ky_0 is incorporated in the shock spectrum. The investigation has also led to some interesting generalizations of the phase-plane plots which have not been shown before. These generalized phase-plane plots are extended to excitation pulses of any arbitrary shape.

Step-Function Excitation

Before considering pulse excitation, the problem of the step-function excitation will be considered first in order to bring out some of the pertinent features of the analysis. The differential equation of motion for the first phase of the problem, $0 < y \leq y_0$, is

$$\ddot{y} + 2\zeta\omega\dot{y} + \omega^2 y = P/M \qquad (1)$$

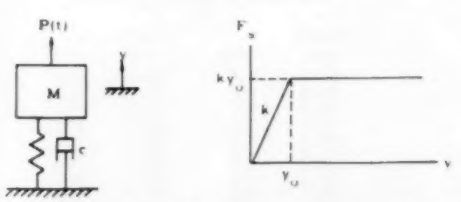

Fig. 1 Damped oscillatory system with nonlinear spring

where

$$\omega^2 = k/M$$

$$\zeta = c/c_{cr}$$

P = constant force

M = mass

To nondimensionalize the equation, we let

$$x = y/y_0$$

$$T = \omega t$$

$$\alpha = ky_0/P$$

Equation (1) now reduces to

$$\frac{d^2x}{dT^2} + 2\zeta\frac{dx}{dT} + x = \frac{1}{\alpha} \tag{2}$$

With zero initial conditions, the equations for the nondimensional displacement and velocity become

$$1 - \alpha x = \frac{e^{-\zeta T}}{(1-\zeta^2)^{1/2}}\cos\left[(1-\zeta^2)^{1/2}T - \phi\right] \tag{3}$$

$$q = \frac{e^{-\zeta T}}{(1-\zeta^2)^{1/2}}\sin(1-\zeta^2)^{1/2}T \tag{4}$$

where

$$\phi = \tan^{-1}\frac{\zeta}{(1-\zeta^2)^{1/2}}$$

$$q = \alpha\frac{dx}{dT}$$

If damping is zero, Equations (3) and (4) plot into a circle

$$(1 - \alpha x)^2 + q^2 = 1 \tag{5}$$

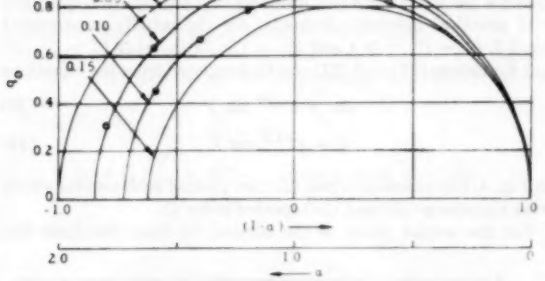

Fig. 2 Generalized phase-plane plot of equations (3) and (4)

For $\zeta \neq 0$, curves relating $(1 - \alpha x)$ to q can be obtained by choosing different values of T. The curves, including the special case for $\zeta = 0$, are shown in Fig. 2, with ζ as parameter.

Fig. 2 is used in the following manner: For any value P, and ky_0, α is known. Then for any $x \leq 1.0$, and any ζ, the corresponding nondimensional velocity q is found. Of particular interest to this problem is the value of $q = q_0$ corresponding to $x = 1$, which is the initial velocity for the second phase of the problem for $x > 1.0$.

For the second phase of the problem, the spring force ky_0 is constant and the differential equation of motion is

$$\ddot{y} + 2\zeta\omega\dot{y} + \omega^2 y_0 = \frac{P}{M} \tag{6}$$

which can be rewritten as

$$\frac{d^2x}{dT^2} + 2\zeta\frac{dx}{dT} = \frac{1}{\alpha} - 1 \tag{7}$$

The solution for the initial conditions

$$x = 1$$

$$\frac{dx}{dT} = \frac{1}{\alpha}q_0$$

where the origin of T has been shifted to T_0, is

$$x = 1 + \frac{1}{2\zeta\alpha}\left[q_0 - \left(\frac{1-\alpha}{2\zeta}\right)\right](1 - e^{-2\zeta T}) + \left(\frac{1-\alpha}{2\zeta\alpha}\right)T \tag{8}$$

$$q = \left[q_0 - \left(\frac{1-\alpha}{2\zeta}\right)\right]e^{-2\zeta T} + \frac{1-\alpha}{2\zeta} \tag{9}$$

It is clear that for $\alpha < 1$ there can be no value of T which will result in $q = 0$, the asymptotic slope at $T = \infty$ being

$$q \to \frac{1-\alpha}{2\zeta} = \frac{k\dot{y}}{\omega P} \tag{10}$$

For $\alpha > 1$, we let $q = 0$ and obtain from Equation (9) the time corresponding to the peak response

$$T_m = \frac{1}{2\zeta}\ln\left(1 - \frac{2\zeta q_0}{1-\alpha}\right) \tag{11}$$

Substituting T_m into Equation (8), the corresponding peak response becomes

$$x_m = 1 + \frac{q_0}{2\zeta\alpha} + \frac{(1-\alpha)}{4\zeta^2\alpha}\ln\left(1 + \frac{2\zeta q_0}{\alpha - 1}\right) \tag{12}$$

When $2\zeta/(\alpha - 1) \ll 1$, the expansion of $\ln(1 + \epsilon)$ results in a somewhat simplified equation

$$x_m \cong 1 + {}^1/_2\frac{q_0^2}{\alpha(\alpha-1)} - {}^2/_3\zeta\frac{q_0^3}{\alpha(\alpha-1)^2} \tag{13}$$

It can be easily verified that the first two terms of Equation (13) correspond to the undamped solution. Also, for small values of $2\zeta/(\alpha - 1)$, greater accuracy can be obtained by using Equation (13) in place of Equation (12).

A further point of interest is found with respect to Fig. 2. Although the curves for $\zeta \neq 0$ are exponentially diminishing with T, they are almost perfect circles (even for $\zeta = 0.2$) with the center shifted along the horizontal axis. To find this center, we let

$$(1 - \zeta^2)^{1/2}T = \pi$$

in which case $q = 0$ and

$$(1 - \alpha x) = e^{-\frac{\zeta\pi}{(1-\zeta^2)^{1/2}}}$$

The center of the circle is then on the horizontal axis, to the right of the origin by an amount

$$\overline{OC} = {}^1/_2\left[1 - e^{-\frac{\zeta\pi}{(1-\zeta^2)^{1/2}}}\right] \tag{14}$$

so that q and αx for the damped case can be determined with

sufficient accuracy from the new equation for the circle which is

$$(1 - \alpha x - \overline{OC})^2 + q^2 = (1 - \overline{OC})^2 \tag{15}$$

Equation (15) then enables one to determine q_0 for any α and ζ by letting $x = 1$. In Fig. 2 circles are drawn according to Equation (15) and exact values are indicated by ⊙ to show the excellence of agreement.

The shock spectrum is generally plotted in nondimensional form, with maximum dynamic response divided by the static response as ordinate, and natural period of the oscillator divided by the pulse period for the abscissa. For the step funtion, the pulse period is infinite; however, Equation (13) indicates that an ordinate proportional to x_m can be plotted as a function of α for any ζ. The ordinate desired is

$$\frac{y_m}{(P/k)} = \frac{ky_0}{P}\frac{y_m}{y_0} = \alpha x_m \tag{16}$$

The abscissa is

$$\alpha = \frac{ky_0}{P} = \frac{k}{M}\frac{My_0}{P} = \omega^2\left(\frac{My_0}{P}\right) \tag{17}$$

which is proportional to the square of the natural frequency based on initial stiffness. The curves in Fig. 3 then can be considered as a shock spectrum for the step-function excitation. The range of α possible is limited between 1 and 2. If $\alpha \leqq 1$, the exciting force is equal to or greater than the resisting force and hence the response continues to increase. If $\alpha > 2$, the peak response will occur in the linear region $y_m < y_0$ for which we have no interest in the nonlinear problem.

Although we have taken the problem of the oscillator mounted on a fixed support, the results can be extended to the case where the base is given an acceleration $-\ddot{y}_b$. With $z = y - y_b$ the differential equation of motion for the latter case is

$$\ddot{z} = 2\zeta\omega\dot{z} + \omega^2 z = -\ddot{y}_b \tag{18}$$

which indicates that the previous results are applicable by letting

$$\frac{P}{M} = -\ddot{y}_b$$

$$y = z$$

We therefore obtain new interpretations for x_m and α which are

$$x_m = \frac{z_m}{y_0} \tag{19}$$

$$\alpha = -\left(\frac{ky_0}{M\ddot{y}_b}\right) \tag{20}$$

Delta-Function Excitation

If the excitation is a delta function of impulse equal to I lb-sec, the response during the first phase of motion $0 < y \leq y_0$ is given by the equations

$$\bar{\alpha}x = \frac{e^{-\zeta T}}{(1 - \zeta^2)^{1/2}} \sin (1 - \zeta^2)^{1/2}T \tag{21}$$

$$\bar{q} = \frac{e^{-\zeta T}}{(1 - \zeta^2)^{1/2}} \cos [(1 - \zeta^2)^{1/2}T + \phi] \tag{22}$$

where

$$\phi = \tan^{-1}\frac{\zeta}{(1 - \zeta^2)^{1/2}}$$

$$\bar{\alpha} = \frac{ky_0}{I\omega}$$

$$\bar{q} = \bar{\alpha}\frac{dx}{dT}$$

These equations are somewhat similar to those of Equations (3) and (4), except that q is replaced by $\bar{\alpha}x$ and $(1 - \alpha x)$ by $\bar{q}$ with $+\phi$ instead of $-\phi$. Here we are interested only in positive values of the velocity $\bar{q}$ which indicates that only the first quadrant is of practical interest. Actually, for the usually encountered small ζ, $(1 - \zeta^2)^{1/2} \cong 1$ and $[(1 - \zeta^2)^{1/2}T + \phi] \cong (1 - \zeta^2)^{1/2}T$ and Equations (21) and (22) can be computed from the equations

$$\bar{\alpha}x = e^{-\zeta T} \sin T \tag{23}$$

$$\bar{q} = e^{-\zeta T} \cos T \tag{24}$$

In Fig. 4, Equations (21) and (22) are plotted with several values from Equations (23) and (24) spotted in by ⊙.

For the second phase of the motion, we have the force free

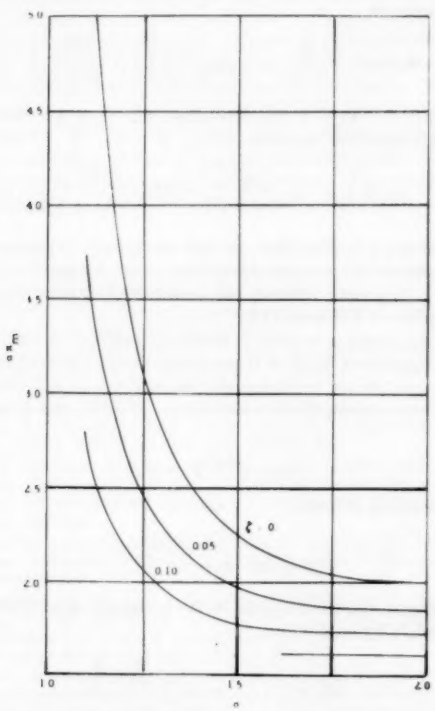

Fig. 3 Nonlinear shock spectrum for step-function excitation

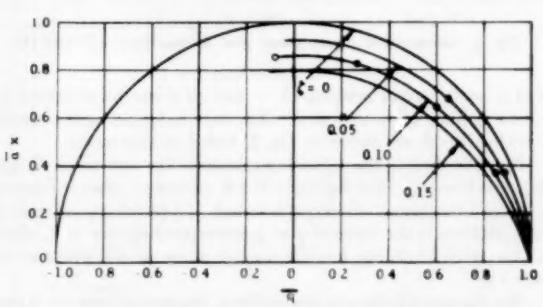

Fig. 4 Generalized phase-plane plot for delta-function excitation

condition with initial values $x = 1$ and $dx/dT = \bar{q}_0/\bar{\alpha}$. The differential equation is now

$$\frac{d^2x}{dT^2} + 2\zeta \frac{dx}{dT} = -1 \tag{25}$$

the solution of which is

$$x = 1 + \frac{1}{2\zeta}\left(\frac{\bar{q}_0}{\bar{\alpha}} + \frac{1}{2\zeta}\right)(1 - e^{-2\zeta T}) - \frac{T}{2\zeta} \tag{26}$$

where again the origin of T has been shifted to T_0. For maximum amplitude $dx/dT = 0$, or

$$T_m = \frac{1}{2\zeta} \ln\left(1 + \frac{2\zeta\bar{q}_0}{\bar{\alpha}}\right) \tag{27}$$

and Equation (26) becomes

$$x_m = 1 + \frac{1}{2\zeta}\frac{\bar{q}_0}{\bar{\alpha}} - \frac{1}{(2\zeta)^2} \ln\left(1 + \frac{2\zeta\bar{q}_0}{\bar{\alpha}}\right) \tag{28}$$

$$\cong 1 + {}^1/_2\left(\frac{\bar{q}_0}{\bar{\alpha}}\right)^2 - {}^2/_3\zeta\left(\frac{\bar{q}_0}{\bar{\alpha}}\right)^3 \tag{29}$$

The first two terms of Equation (29) are obviously the undamped solution, and the third term gives the first-order correction due to ζ, which is of sufficient accuracy for small ζ. It should be pointed out here that Equation (29) can be used for any other shape of pulsed excitation provided $\bar{q}_0/\bar{\alpha}$ is replaced by the proper velocity dx/dT and that the duration t_1 of the pulse is equal or less than T_0, the time to reach y_0.

In plotting the shock spectrum for this case, we let the ordinate be $\bar{\alpha}x_m$ and the abscissa $\bar{\alpha}$, Fig. 5. In doing so, we note that $I\omega$ has the same dimensions as P, so in effect, $\bar{\alpha}x_m$ is the ratio of the maximum response to the equivalent statical response under a load $I\omega$. The horizontal scale is

$$\bar{\alpha} = \frac{ky_0}{I\omega} = \omega\left(\frac{My_0}{I}\right)$$

so it is proportional to the natural frequency based on initial stiffness. The range of $\bar{\alpha}$ is between 0 and 1, zero corresponding to infinite value of impulse I, and $\bar{\alpha} > 1$ corresponding to the case where the peak response occurs in the linear range.

Example 1—Delta-Function Input. Given $\bar{\alpha} = ky_0/I\omega = 0.60$, and $\zeta = 0.05$, determine the maximum amplitude and the corresponding time:

From Fig. 4

$$\bar{q}_0 = \bar{\alpha}\frac{dx}{dT} = 0.72 \qquad (\bar{q}_0 = \bar{q} \text{ when } x = 1.0)$$

From Fig. 5

$$\bar{\alpha}x_m = 1.15 \qquad x_m = \frac{y_m}{y_0} = 1.92$$

From Equation 27

$$T_m = \frac{1}{2\zeta} \ln\left(1 + \frac{2\zeta\bar{q}_0}{\bar{\alpha}}\right) = 10 \ln 1.12 = 1.13$$

Rectangular Pulse

We consider one other case before considering pulses of arbitrary shape. A rectangular pulse of height P and duration $t_1 \leqslant t_0$ is assumed. In the time interval $0 < t \leqslant t_1$, the solution is identical to that of the step function, for which Equations (3) and (4) apply. At time t_1, we have

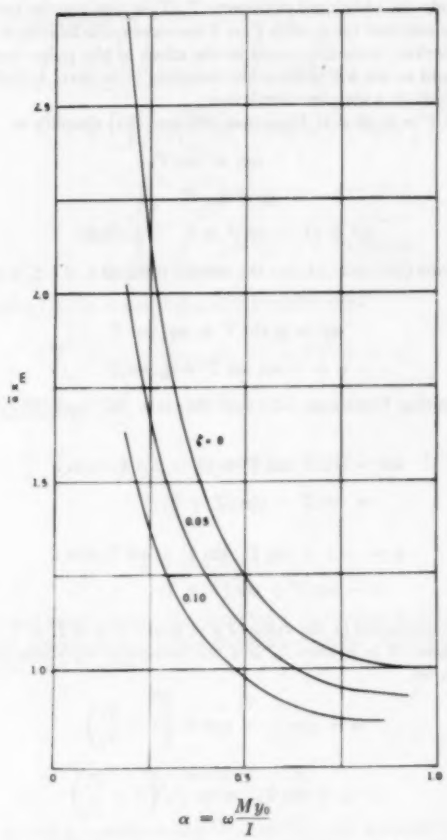

Fig. 5 Nonlinear shock spectrum for delta-function excitation

$$1 - \alpha x_1 = \frac{e^{-\zeta T_1}}{(1 - \zeta^2)^{1/2}} \cos\left[(1 - \zeta^2)^{1/2}T_1 - \phi\right] \tag{30}$$

$$q_1 = \frac{e^{-\zeta T_1}}{(1 - \zeta^2)^{1/2}} \sin (1 - \zeta^2)^{1/2}T_1 \tag{31}$$

For $t > t_1$ we have free oscillations for which the differential equation and solution, with initial conditions x_1 and $dx_1/dT = q_1/\alpha$, and origin of T shifted to T_1, are

$$\frac{d^2x}{dT^2} + 2\zeta\frac{dx}{dT} + x = 0 \tag{32}$$

$$\alpha x = \frac{e^{-\zeta T}}{(1 - \zeta^2)^{1/2}}\left\{[q_1 + \zeta\alpha x_1]\sin (1 - \zeta^2)^{1/2}T + \alpha x_1(1 - \zeta^2)^{1/2}\cos (1 - \zeta^2)^{1/2}T\right\} \tag{33}$$

$$q = \frac{-e^{-\zeta T}}{(1 - \zeta^2)^{1/2}}\left\{[\zeta q_1 + \alpha x_1]\sin (1 - \zeta^2)^{1/2}T - q_1(1 - \zeta^2)^{1/2}\cos (1 - \zeta^2)^{1/2}T\right\} \tag{34}$$

We are interested here in the value of $q = q_0$ corresponding to $x = 1$, which can be used in the equation for x_m Equation (29), which can be rewritten as

$$x_m = 1 + {}^1/_2\left(\frac{q_0}{\alpha}\right)^2 - {}^2/_3\zeta\left(\frac{q_0}{\alpha}\right)^3 \tag{29a}$$

Obviously, an additional parameter T_1/T_0 enters into the problem and the solution for q_0 with $\zeta \neq 0$ becomes quite laborious. We are, however, more interested in the effect of the pulse duration T_1/T_0 and so we will assume the damping to be zero, which then lends itself to a simpler calculation.

With $\zeta = 0$, $\phi = 0$, Equation (30) and (31) simplify to

$$1 - \alpha x_1 = \cos T_1 \tag{35}$$

$$q_1 = \sin T_1 \tag{36}$$

$$q_1^2 + (1 - \alpha x_1)^2 = 1, \qquad \text{a circle}$$

Equations (33) and (34) for the second integral $t_1 < t \leq t_0$ reduce to

$$\alpha x = q_1 \sin T + \alpha x_1 \cos T \tag{37}$$

$$q = -\alpha x_1 \sin T + q_1 \cos T \tag{38}$$

Substituting Equations (35) and (36) into (37) and (38) we obtain

$$\begin{aligned} \alpha x &= \sin T_1 \sin T + (1 - \cos T_1) \cos T \\ &= \cos T - \cos (T + T_1) \end{aligned} \tag{39}$$

$$\begin{aligned} q &= -(1 - \cos T_1) \sin T + \sin T_1 \cos T \\ &= -\sin T + \sin (T + T_1) \end{aligned} \tag{40}$$

We are interested in the value of $q = q_0$ at $t = t_0$ or $T = T_0 - T_1$. The value of x is then 1, and the foregoing equations can be written as

$$\alpha + \cos T_0 = \cos T_0 \left(1 - \frac{T_1}{T_0}\right) \tag{41}$$

$$(-q_0 + \sin T_0) = \sin T_0 \left(1 - \frac{T_1}{T_0}\right) \tag{42}$$

Equations (41) and (42) can be shown to be segments of circles for each value of T_0, as shown in Fig. 6. When $T_1/T_0 = 1$, we have the step-function solution for zero damping, which offers a starting point depending on T_0; i.e., by choosing different values of T_0, we move to different points on the large circle as starting point. Then as $T_1/T_0 < 1$ is varied, we obtain circular segments with the center at

$$\begin{aligned} \alpha_c &= -\cos T_0 \\ q_c &= \sin T_0 \end{aligned} \tag{43}$$

and radius = 1.0. The locus of the center α_c, q_c is then another circle of unit radius and center at $\alpha = 0$, $q = 0$. For T in the first quadrant, we have

$$\theta = T_0 \tag{44}$$

For T_0 in the second quadrant,

$$\theta = 180 - T_0 \tag{45}$$

The range of T_1/T_0 which have solution is then found by letting

$$T_0 \left(1 - \frac{T_1}{T_0}\right) = \theta \tag{46}$$

By substituting Equations (44) and (45) into (46), we conclude that for T_0 in the first quadrant T_1/T_0 has values along the arc ab, between 1 and zero, whereas for T_0 in the second quadrant, T_1/T_0 has values along the arc $a'b'$ between 1.0 and

$$\left(\frac{T_1}{T_0}\right)_{\min} = 2 - \frac{180}{T_0} \tag{47}$$

Thus if 10 per cent increments of T_1/T_0 are chosen, the arc ab in the first quadrant is divided into 10 intervals whereas the arc $a'b'$ in the second quadrant will have fewer 10 per cent intervals as established by Equation (47). By connecting points of equal T_1/T_0, we get solutions for the velocity q_0 corresponding to $x = 1$, for any α and T_1/T_0.

The maximum response x_m is next determined from Equation (29a) with $\zeta = 0$ and a shock spectrum αx_m versus α for any value of T_1/T_0 can be plotted. Fig. 7 is such a plot for a few values of T_1/T_0. T_0 can be found for any α and T_1/T_0 from Equation (41).

Example 2—Rectangular Pulse. Given $\alpha = ky_0/P = 0.50$ and $T_1/T_0 = 0.80$, determine maximum amplitude and the time T_0 corresponding to $x = x_m$:

From Fig. 7

$$\alpha x_m = 0.94 \qquad \therefore x_m = 1.88$$

From Equation 41

$$\cos 0.20T_0 - \cos T_0 = 0.50$$

which is satisfied by $T_0 = 61.5$ deg

If the pulse height is reduced to half with $T_1/T_0 = 0.80$, then $\alpha = 1.0$ and Fig. 7 gives

$$\alpha x_m = 1.25$$

$$x_m = 1.25$$

Equation 41 then becomes

$$\cos 0.20T_0 - \cos T_0 = 1.0$$

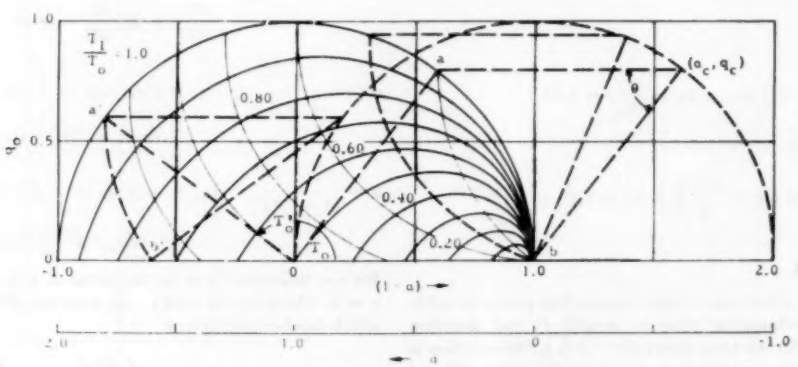

Fig. 6 Generalized phase plot for rectangular pulse

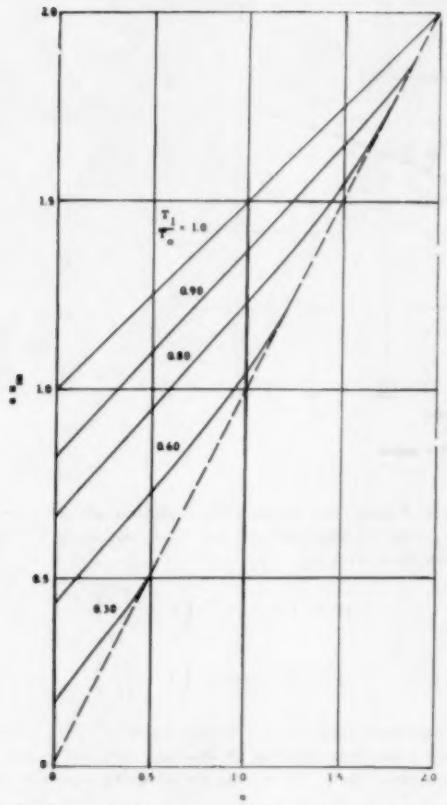

Fig. 7 Nonlinear shock spectrum for rectangular pulse with $\zeta = 0$

and $T_0 = 92$ deg

Pulse of Arbitrary Shape

We will assume as before that the pulse duration t_1 is less than the time t_0 required to reach a response y_0. The excitation $F(t)$ is normalized to

$$F(t) = P_0 f(t) \tag{48}$$

where P_0 is the maximum height of the pulse and $f(t)$ the arbitrary shape. The response at any time $t \leq t_0$ is then

$$\frac{ky}{P_0} = \frac{\omega}{(1-\zeta^2)^{1/2}} \int_0^t f(\xi) e^{-\zeta\omega(t-\xi)} \sin (1-\zeta^2)^{1/2}\omega(t-\xi) d\xi \tag{49}$$

Letting $\omega t = T$ and $\omega\xi = \beta$, this equation can be rewritten in the nondimensional form,

$$\alpha x = \frac{e^{-\zeta T}}{(1-\zeta^2)^{1/2}} \int_0^T f\left(\frac{\beta}{\omega}\right) e^{\zeta\beta} \sin (1-\zeta^2)^{1/2}(T-\beta) d\beta \tag{50}$$

For $T > T_1$, $f(\beta)$ is zero so that the foregoing integral is a constant. Letting

$$A \sin \gamma = \int_0^{T_1} f\left(\frac{\beta}{\omega}\right) e^{\zeta\beta} \sin (1-\zeta^2)^{1/2}\beta d\beta \tag{51}$$

$$A \cos \gamma = \int_0^{T_1} f\left(\frac{\beta}{\omega}\right) e^{\zeta\beta} \cos (1-\zeta^2)^{1/2}\beta d\beta \tag{52}$$

A and γ are given by

$$A = \left\{\left[\int_0^{T_1} f\left(\frac{\beta}{\omega}\right) e^{\zeta\beta} \sin (1-\zeta^2)^{1/2}\beta d\beta\right]^2 + \left[\int_0^{T_1} f\left(\frac{\beta}{\omega}\right) e^{\zeta\beta} \cos (1-\zeta^2)^{1/2}\beta d\beta\right]^2\right\}^{1/2} \tag{53}$$

$$\tan \gamma = \frac{\int_0^{T_1} f\left(\frac{\beta}{\omega}\right) e^{\zeta\beta} \sin (1-\zeta^2)^{1/2}\beta d\beta}{\int_0^{T_1} f\left(\frac{\beta}{\omega}\right) e^{\zeta\beta} \cos (1-\zeta^2)^{1/2}\beta d\beta} \tag{54}$$

Equation (50) in terms of A and γ then becomes

$$\frac{\alpha x}{A} = \frac{e^{-\zeta T}}{(1-\zeta^2)^{1/2}} \sin [(1-\zeta^2)^{1/2}T - \gamma] \tag{55}$$

Differentiating,

$$\frac{q}{A} = \frac{\alpha}{A}\frac{dx}{dT} = \frac{e^{-\zeta T}}{(1-\zeta^2)^{1/2}} \cos [(1-\zeta^2)^{1/2}T - \gamma + \phi] \tag{56}$$

where

$$\phi = \tan^{-1} \frac{\zeta}{(1-\zeta^2)^{1/2}}$$

We will again assume the damping ζ to be zero to develop an analogy similar to that of the rectangular pulse. Equations (55) and (56) then become

$$\frac{\alpha x}{A} = \sin (T - \gamma) \tag{57}$$

$$\frac{q}{A} = \sin (T - \gamma) \tag{58}$$

With x_1 and q_1 corresponding to time T_1, their substitution into Equations (37) and (38) results in

$$\frac{\alpha x}{A} = \cos (T_1 - \gamma) \sin T + \sin (T_1 - \gamma) \cos T \tag{59}$$

$$\frac{q}{A} = -\sin (T_1 - \gamma) \sin T + \cos (T_1 - \gamma) \cos T \tag{60}$$

When $T = T_0 - T_1$, $x = 1$ and $q = q_0$, so we arrive at the result

$$\frac{\alpha}{A} = \sin (T_0 - \gamma) \tag{61}$$

$$\frac{q_0}{A} = \cos (T_0 - \gamma) \tag{62}$$

These equations again represent curves similar to those in Fig. 6, and the effect of T_1/T_0 is hidden in the expressions for A and γ.

Example 3—Rectangular Pulse. For the rectangular pulse of duration t_1 and zero damping, Equations (51) and (52) give

$$A \sin \gamma = (1 - \cos T_1)$$
$$A \cos \gamma = \sin T_1$$

From these we obtain

$$\tan \gamma = \frac{1 - \cos T_1}{\sin T_1} = \tan (T_1/2) \qquad \therefore \gamma = (T_1/2)$$
$$A = 2 \sin (T_1/2)$$

Substitution of A and γ into Equations (61) and (62) results in Equations (41) and (42), given previously for the rectangular pulse.

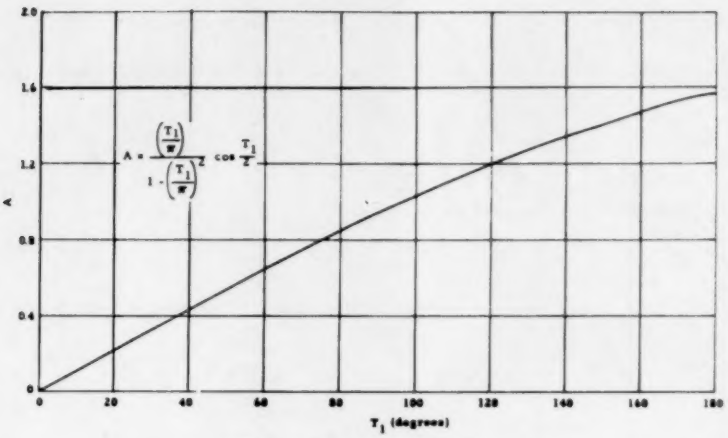

Fig. 8 Coefficient A for sine pulse

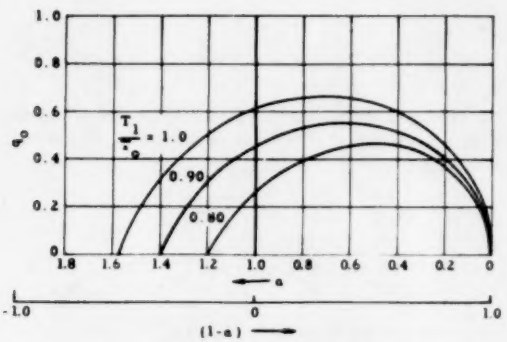

Fig. 9 Generalized phase plot for sine pulse

Example 4—Sine Pulse. For the sine pulse $P_0 \sin pt$, the excitation is zero after $pt_1 = \pi$. From Equations (51) and (52), we obtain

$$A \sin \gamma = \frac{(T_1/\pi)}{1 - (T_1/\pi)^2} \sin T_1$$

$$A \cos \gamma = \frac{(T_1/\pi)}{1 - (T_1/\pi)^2} (1 + \cos T_1)$$

The expressions for A and γ therefore become

$$A = \frac{2(T_1/\pi)}{1 - (T_1/\pi)^2} \cos (T_1/2)$$

$$\gamma = (T_1/2)$$

Values of A have been computed and plotted against $T_1 = \omega t_1$ in Fig. 8. Since A depends only on T_1, Equations (61) and (62) may now be written as

$$\alpha = A(T_1) \sin T_0 \left(1 - \frac{T_1}{2T_0}\right)$$

$$q_0 = A(T_1) \cos T_0 \left(1 - \frac{T_1}{2T_0}\right)$$

These equations indicate that for any value of T_1/T_0, a curve for q_0 versus α can be computed by choosing different values of T_0. As an example, for $T_1/T_0 = 0.90$, the foregoing equations become

$$\alpha = A(0.90T_0) \sin 0.55T_0$$

$$q_0 = A(0.90T_0) \cos 0.55T_0$$

Curves for q_0 versus α are plotted in Fig. 9 for a few values of T_1/T_0 and the general shape is somewhat similar to those for the rectangular pulse. The velocity q_0, however, is smaller because of the smaller total impulse.

It may be of interest to mention a consideration which was given in respect to this problem. Since the total impulse of a sine pulse is equal to 0.636 times the rectangular impulse of the same T_1/T_0, it was thought possible to approximate the response for the sine pulse from the curves for the rectangular pulse with T_1/T_0 reduced by 0.636. If such a procedure would result in agreement, the pulse-shape factor could be eliminated and the results could be based on the total impulse. Agreement on this basis was not obtained, however, and it appears that the influence of the pulse-shape factor cannot be eliminated, at least for large values of T_1/T_0. For small values of T_1/T_0, it is of course expected that agreement on the basis of total impulse will dominate over the pulse-shape factor.

Forced Flexural Vibrations of Sandwich Plates in Plane Strain[1]

YI-YUAN YU
Professor,
Department of Mechanical Engineering,
Polytechnic Institute of Brooklyn,
Brooklyn, N. Y.,
Mem. ASME

On the basis of the new flexural theory of elastic sandwich plates recently developed [1–3],[2] the problem of general forced flexural vibration of sandwich plates in the plane-strain case is solved. The classical method of separation of variables combined with the Mindlin-Goodman procedure [4] for treating time-dependent boundary conditions is used. As an example, the results are made use of in solving the problem of a simply supported sandwich plate in plane strain with one of the two end sections prescribed a transverse deflection varying with time.

In two recent papers [1, 2] was presented the one-dimensional plane-strain case of a new flexural theory of elastic sandwich plates, in which the transverse displacement is assumed to be uniform across the plate thickness, and the displacements in the plane of the plate are assumed to have linear variations over the thickness, with slope in the faces taken to be different from that in the core. The theory thus takes into consideration the transverse shear effects in the core and faces, the rotatory and translatory inertias of the core and faces, the flexural rigidity of the core, and the flexural and extensional rigidities of the faces. In addition, no restriction is imposed upon the magnitudes of the ratios between the thicknesses, material densities, and elastic constants of the core and faces. The theory is therefore flexible enough to be applied to any symmetrically arranged three-layered plate, including as a special case the ordinary sandwich plate that has comparatively thin but heavy and rigid faces.

On the basis of the new theory, free flexural vibrations of sandwich plates were investigated in a third paper [3]. The results indicate that, for ordinary sandwich plates, the shear effect in the faces, the rotatory inertia of the faces about their own middle planes, and the flexural rigidity of the core are negligible. Of importance are the shear effect in the core, the rotatory and translatory inertias of the core, the translatory inertia of the faces (which also has rotatory effect about the middle plane of the sandwich plate), and the joint effect of the flexural and extensional rigidities of the faces. While suppression of either the shear effect in the faces or the rotatory inertia of the faces reduces the order of the equations of motion from the sixth to fourth with respect to time, the importance of the joint effect of the face rigidities has made it impossible to reduce also the order of the equations with respect to the space co-ordinate, unless the faces of the plate are very thin and frequencies sufficiently low. As a result, the vibration analysis of finite sandwich plates, with the exception of the simply supported case, is in general complicated, and it is essential to have available a new theory of sandwich plates such as the present one. Including all the important factors, the theory was shown to be good for a very wide frequency range that is of practical interest.

[1] This research was supported by the United States Air Force under Contract AF49(638)-453 monitored by the Air Force Office of Scientific Research of the Air Research and Development Command.

[2] Numbers in brackets designate References at end of paper.

Presented at the West Coast Conference of the Applied Mechanics Division, Stanford University, Calif., September 9, 1959, of The American Society of Mechanical Engineers.

Discussion of this paper should be addressed to the Secretary, ASME, 29 West 39th Street, New York, N. Y., and will be accepted until October 10, 1960, for publication at a later date. Discussion received after the closing date will be returned.

Note: Statements and opinions advanced in papers are to be understood as individual expressions of their authors and not those of the Society. Manuscript received by ASME Applied Mechanics Division, July 7, 1959. This paper was not preprinted.

Nomenclature

w = transverse deflection of plate

ψ_1, ψ_2 = changes of slope of normal to middle plane of plate in core and faces, respectively

$D_1 = \dfrac{E_1^*}{1-\nu_1^2}\dfrac{2h_1^3}{3}$

$D_2 = \dfrac{E_2^*}{1-\nu_2^2}\dfrac{h^3-h_1^3}{3}$

$E_2 = \dfrac{E_2^*}{1-\nu_2^2}h_2$

$F_2 = \dfrac{E_2^*}{1-\nu_2^2}\dfrac{h^3-h_1^3}{2}$

$G_1 = 2\kappa\mu_1 h_1$

$G_2 = \kappa\mu_2 h_2$

E_1^*, E_2^* = Young's moduli of core and face materials, respectively

ν_1, ν_2 = Poisson's ratios of core and face materials, respectively

μ_1, μ_2 = shear moduli of core and face materials, respectively

κ = shear coefficient

h_1 = half-thickness of core

h_2 = thickness of each face

$h = h_1 + h_2$ = total half-thickness of plate

ρ_1, ρ_2 = densities of core and face materials, respectively

$p_x = (\tau_{xz})_{z=-h} + (\tau_{xz})_{z=h}$

$p_z = (\sigma_z)_{z=-h} - (\sigma_z)_{z=h}$

τ_{xz} = shear stress

σ_z = normal stress

$M_x = M_{x1} + M_{x2} + M_{x3}$

$Q_x = Q_{x1} + Q_{x2} + Q_{x3}$

M_{xi} = bending moment
Q_{xi} = shearing force
N_{xi} = membrane force
} i = 1, 2, or 3 referring to core, lower or upper face

prime = differentiation with respect to x

dot = differentiation with respect to t

Notations not listed here are defined as they first appear.

Assuming that the principal modes of free vibration are known, we shall in this fourth paper of the series solve the general forced-vibration problem of sandwich plates in plane strain. The classical method of separation of variables combined with the Mindlin-Goodman procedure [4] of dealing with time-dependent boundary conditions is used to solve the problem. In what follows, the basic equations of the new theory are first presented, in a form convenient for our present use. The orthogonality condition for the principal modes of free vibration is derived next. The formal solution of the general forced-vibration problem is then obtained. By means of the result, a specific example is finally worked out for a simply supported sandwich plate in plane strain.

Since it is sandwich plates in plane strain which are being studied, the results in this paper are also applicable to sandwich beams. In fact, it may be shown readily that the results are reducible to those for homogeneous beams of the Timoshenko type [5] as a special limiting case. The development for the sandwich is analogous to that for homogeneous beams [4, 5], but the details are necessarily somewhat more complicated, and it is of interest to see that the Mindlin-Goodman procedure can also be applied to the study of forced vibrations of sandwich structures.

Basic Equations

As in the previous papers [1–3], the face layers of the sandwich plate are identical, and the middle plane of the plate is taken to be the xy-plane. For the case of plane strain, only a unit length of the plate in the y-direction need be considered. In the z-direction, the thicknesses of the lower face, core, and upper face extend from $-h$ to $-h_1$, $-h_1$ to h_1, and h_1 to h, respectively. The thickness of the core is therefore $2h_1$, and that of each of the two faces is $h_2 = h - h_1$.

The displacement equations of motion as given in reference [1] are of the following form:

$$D_1\psi_1'' + 2D_2\psi_2'' + 2F_2h_1(\psi_1'' - \psi_2'') - G_1(\psi_1 + w') - 2G_2(\psi_2 + w') + hp_x = \rho_1(2/3)h_1^3\ddot{\psi}_1 + \rho_1(2/3)(h^3 - h_1^3)\ddot{\psi}_2 + \rho_2h_1(h^2 - h_1^2)(\ddot{\psi}_1 - \ddot{\psi}_2) \quad (1)$$

$$D_1\psi_1'' - G_1(\psi_1 + w') + 2F_2h_1\psi_2'' + 2E_2h_1^2(\psi_1'' - \psi_2'') + h_1p_x = \rho_1(2/3)h_1^3\ddot{\psi}_1 + \rho_2h_1(h^2 - h_1^2)\ddot{\psi}_2 + 2\rho_2h_1^2h_2(\ddot{\psi}_1 - \ddot{\psi}_2) \quad (2)$$

$$G_1(\psi_1' + w'') + 2G_2(\psi_2' + w'') + p_z = 2(\rho_1h_1 + \rho_2h_2)\ddot{w} \quad (3)$$

For our purpose here, Equations (1) and (2) are rearranged by first subtracting the latter from the former; thus

$$E_2h_1h_2\psi_1'' + \frac{2}{3}E_2h_2^2\psi_2'' - 2G_2(\psi_2 + w') + h_2p_x = \rho_2h_2^3\left(h_1\ddot{\psi}_1 + \frac{2}{3}h_2\ddot{\psi}_2\right) \quad (4)$$

The derivative $\ddot{\psi}_2$ is then eliminated from Equations (2) and (4) by multiplying the former by $2h_2/3$ and the latter by h_1 and subtracting; the result is

$$(2D_1 + E_2h_1^2)\psi_1'' - 2G_1(\psi_1 + w') + 6G_2(h_1/h_2)(\psi_2 + w') - h_1p_x = \left(\frac{4}{3}\rho_1h_1^3 + \rho_2h_1^2h_2\right)\ddot{\psi}_1 \quad (5)$$

Equations (3), (4), and (5) are of the desired form to be used later.

The foregoing equations of motion are subjected to the initial conditions which require the specification of the following initial plate-displacements and velocities:

$$\begin{aligned} \psi_1(x, 0) &= \psi_{10}(x) & \dot{\psi}_1(x, 0) &= \dot{\psi}_{10}(x) \\ \psi_2(x, 0) &= \psi_{20}(x) & \dot{\psi}_2(x, 0) &= \dot{\psi}_{20}(x) \\ w(x, 0) &= w_0(x) & \dot{w}(x, 0) &= \dot{w}_0(x) \end{aligned} \quad (6)$$

the right-hand sides of which represent given functions. The equations of motion are further subjected to the boundary conditions of prescribing for each section between $x = 0$ and $x = l$ one member of each of the two products $p_x(u)_{x=k}$ and $p_z(w)_{x=k}$, and prescribing for the end sections $x = 0$ and $x = l$ one member of each of the three products

$$M_x\psi_1, \quad [M_{x2} + M_{x3} - h_1(N_{x3} - N_{x2})](\psi_2 - \psi_1), \quad Q_xw$$

or, alternatively, the three products

$$[M_{x1} + h_1(N_{x3} - N_{x2})]\psi_1, \quad [M_{x2} + M_{x3} - h_1(N_{x3} - N_{x2})]\psi_2, \quad Q_xw \quad (7)$$

Since the plate stresses are related to the plate-displacements by

$$\begin{aligned} M_{x1} &= D_1\psi_1' \\ M_{x2} &= M_{x3} = F_2h_1(\psi_1' - \psi_2') + D_2\psi_2' \\ N_{x2} &= -N_{x3} = -E_2h_1(\psi_1' - \psi_2') - F_2\psi_2' \\ Q_{x1} &= G_1(\psi_1 + w') \\ Q_{x2} &= Q_{x3} = G_2(\psi_2 + w') \end{aligned}$$

the quantities mentioned in (7) may be put in the following form:

$$\begin{aligned} B_1 &= (D_1 + 2E_2h_1^2)\psi_1' + E_2h_1h_2\psi_2' && \text{or } \psi_1 && (x = 0) \\ B_2 &= (D_1 + 2E_2h_1^2)\psi_1' + E_2h_1h_2\psi_2' && \text{or } \psi_1 && (x = l) \\ B_3 &= E_2h_1h_2\psi_1' + E_2\frac{2}{3}h_2^2\psi_2' && \text{or } \psi_2 && (x = 0) \\ B_4 &= E_2h_1h_2\psi_1' + E_2\frac{2}{3}h_2^2\psi_2' && \text{or } \psi_2 && (x = l) \\ B_5 &= G_1(\psi_1 + w') + 2G_2(\psi_2 + w') && \text{or } w && (x = 0) \\ B_6 &= G_1(\psi_1 + w') + 2G_2(\psi_2 + w') && \text{or } w && (x = l) \end{aligned}$$

B_1, B_2, . . ., and B_6 being thus functions of ψ_1, ψ_2, and w. To specify the boundary conditions we may then write

$$B_i(\psi_1, \psi_2, w) = f_i(t) \qquad (i = 1, 2, \ldots, 6) \quad (8)$$

where $f_i(t)$ are prescribed functions of the time.

The method of determining the shear coefficient κ involved in G_1 and G_2 for vibration problems was described in reference [2].

Principal Modes

An infinite set of the natural frequencies ω_n and the corresponding principal modes $(\Psi_{1n}, \Psi_{2n}, W_n)$ of the sandwich plate is determined by the homogeneous equations of motion and homogeneous boundary conditions associated with Equations (3), (4), (5), and (8). In the special case of simply supported sandwich plates there is instead a triply infinite set, and the principal modes were shown to be of the following form [3] for such plates in plane strain:

$$\Psi_{1n} = a_n\cos\frac{n\pi x}{l}$$

$$\Psi_{2n} = b_n\cos\frac{n\pi x}{l} \quad (n = 1, 2, \ldots) \quad (9)$$

$$W_n = c_n\sin\frac{n\pi x}{l}$$

For each of the infinite number of values of n in Equations (9), there are three possible sets of values of $(a_n{:}b_n{:}c_n)$ defining the

mode shapes, and three corresponding frequencies. By inserting in the homogeneous equations associated with Equations (3) to (5)

$$\psi_1 = \Psi_1(x)e^{i\omega t}, \quad \psi_2 = \Psi_2(x)e^{i\omega t}, \quad w = W(x)e^{i\omega t}$$

the principal modes in the general case are found to satisfy the following equations:

$$(2D_1 + E_2h_1^2)\Psi_{1n}'' - 2G_1(\Psi_{1n} + W_n') + 6G_2(h_1/h_2)(\Psi_{2n} + W_n') = -\omega_n^2(\tfrac{4}{3}\rho_1h_1^3 + \rho_2h_1^2h_2)\Psi_{1n}$$

$$E_2h_1h_2\Psi_{1n}'' + \tfrac{2}{3}E_2h_2^2\Psi_{2n}'' - 2G_2(\Psi_{2n} + W_n') = -\omega_n^2\rho_2h_2^2(h_1\Psi_{1n} + \tfrac{3}{2}h_2\Psi_{2n}) \quad (10)$$

$$G_1(\Psi_{1n}' + W_n'') + 2G_2(\Psi_{2n}' + W_n'') = -2\omega_n^2(\rho_1h_1 + \rho_2h_2)W_n$$

The orthogonality condition of the principal modes may be derived from Equations (10), but the derivation is much simpler by starting with Clebsch's theorem [6]. For the sandwich plate in plane strain, the theorem takes the following form for any two distinct modes, here distinguished by the subscripts m and n:

$$\int_0^l\int_{-h_1}^{h_1}\rho_1(U_{1m}U_{1n} + W_{1m}W_{1n})dxdz + \int_0^l\int_{-h}^{-h_1}\rho_2(U_{2m}U_{2n} + W_{2m}W_{2n})dxdz + \int_0^l\int_{h_1}^{h}\rho_2(U_{3m}U_{3n} + W_{3m}W_{3n})dxdz = 0 \quad (\omega_m \neq \omega_n) \quad (11)$$

According to the assumed form of the displacements in the theory [1], the mode shapes in terms of the displacements and those in terms of the plate-displacements are related by the expressions

$$\begin{aligned} U_{1n} &= z\Psi_{1n} \\ U_{2n} &= -h_1(\Psi_{1n} - \Psi_{2n}) + z\Psi_{2n} \\ U_{3n} &= h_1(\Psi_{1n} - \Psi_{2n}) + z\Psi_{2n} \\ W_{1n} &= W_{2n} = W_{3n} = W_n \end{aligned}$$

and similar expressions with n replaced by m. When these expressions are substituted in Equation (11) and the integration is carried out with respect to z, we find

$$\int_0^l [(\tfrac{4}{3}\rho_1h_1 + \rho_2h_2)h_1^2\Psi_{1m}\Psi_{1n} + 3\rho_2h_2(h_1\Psi_{1m} + \tfrac{2}{3}h_2\Psi_{2m})(h_1\Psi_{1n} + \tfrac{2}{3}h_2\Psi_{2n}) + 4(\rho_1h_1 + \rho_2h_2)W_mW_n]dx = 0 \quad (\omega_m \neq \omega_n) \quad (12)$$

which is the desired condition of orthogonality. Clebsch's theorem has been used by Herrmann [7] in an analogous manner in the derivation of the orthogonality condition for a homogeneous elastic rod.

Transformation of Equations

In the manner of Mindlin and Goodman [4] we adopt the following transformation of the dependent variables in the equations of motion:

$$\begin{aligned} \psi_1(x, t) &= \phi_1(x, t) + \sum_{i=1}^{6} g_{1i}(x)f_i(t) \\ \psi_2(x, t) &= \phi_2(x, t) + \sum_{i=1}^{6} g_{2i}(x)f_i(t) \\ w(x, t) &= \phi_3(x, t) + \sum_{i=1}^{6} g_{3i}(x)f_i(t) \end{aligned} \quad (13)$$

By making these substitutions, Equations (3) to (5) become

$$\left.\begin{aligned} &(2D_1 + E_2h_1^2)\phi_1'' - 2G_1(\phi_1 + \phi_2') + 6G_2(h_1/h_2)(\phi_2 + \phi_3') + \sum_{i=1}^{6} f_i[(2D_1 + 2E_2h_1^2)g_{1i}'' - 2G_1(g_{1i} + g_{3i}') + 6G_2(h_1/h_2)(g_{2i} + g_{3i}')] - h_1p_x = (\tfrac{4}{3}\rho_1h_1^3 + \rho_2h_1^2h_2)\ddot{\phi}_1 + \sum_{i=1}^{6}\ddot{f}_i(\tfrac{4}{3}\rho_1h_1^3 + \rho_2h_1^2h_2)g_{1i} \\ &E_2h_1h_2\phi_1'' + \tfrac{2}{3}E_2h_2^2\phi_2'' - 2G_2(\phi_2 + \phi_3') + \sum_{i=1}^{6} f_i[E_2h_1h_2g_{1i}'' + \tfrac{2}{3}E_2h_2^2g_{2i}'' - 2G_2(g_{2i} + g_{3i}')] + h_2p_x = \rho_2h_2^2(h_1\ddot{\phi}_1 + \tfrac{2}{3}h_2\ddot{\phi}_2) + \sum_{i=1}^{6}\ddot{f}_i\rho_2h_2^2(h_1g_{1i} + \tfrac{2}{3}h_2g_{2i}) \\ &G_1(\phi_1' + \phi_3'') + 2G_2(\phi_2' + \phi_3'') + \sum_{i=1}^{6} f_i[G_1(g_{1i}' + g_{3i}'') + 2G_2(g_{2i}' + g_{3i}'')] + p_z = 2(\rho_1h_1 + \rho_2h_2)\ddot{\phi}_3 + \sum_{i=1}^{6}\ddot{f}_i2(\rho_1h_1 + \rho_2h_2)g_{3i} \end{aligned}\right\} \quad (14)$$

The initial conditions for ϕ_1, ϕ_2, and ϕ_3 are, on account of Equations (6),

$$\left.\begin{aligned} \phi_1(x, 0) &= \psi_{10}(x) - \sum_{i=1}^{6} g_{1i}(x)f_i(0) \\ \phi_2(x, 0) &= \psi_{20}(x) - \sum_{i=1}^{6} g_{2i}(x)f_i(0) \\ \phi_3(x, 0) &= w_0(x) - \sum_{i=1}^{6} g_{3i}(x)f_i(0) \end{aligned}\right\} \quad (15)$$

$$\left.\begin{aligned} \dot{\phi}_1(x, 0) &= \dot{\psi}_{10}(x) - \sum_{i=1}^{6} g_{1i}(x)\dot{f}_i(0) \\ \dot{\phi}_2(x, 0) &= \dot{\psi}_{20}(x) - \sum_{i=1}^{6} g_{2i}(x)\dot{f}_i(0) \\ \dot{\phi}_3(x, 0) &= \dot{w}_0(x) - \sum_{i=1}^{6} g_{3i}(x)\dot{f}_i(0) \end{aligned}\right\} \quad (16)$$

Similarly, the time-dependent boundary conditions in Equations (8), which were in terms of ψ_1, ψ_2, and w, become

$$B_i(\phi_1, \phi_2, \phi_3) + \sum_{j=1}^{6} B_i(g_{1j}, g_{2j}, g_{3j})f_j(t) = f_i(t) \quad (i = 1, 2, \ldots, 6)$$

In order that the boundary conditions on ϕ_1, ϕ_2, and ϕ_3 be homogeneous and independent of time, that is,

$$B_i(\phi_1, \phi_2, \phi_3) = 0 \qquad (i = 1, 2, \ldots, 6)$$

we must have

$$\sum_{j=1}^{6} B_i(g_{1j}, g_{2j}, g_{3j})f_j(t) = f_i(t) \qquad (i = 1, 2, \ldots, 6)$$

which may be satisfied by requiring that

$$B_i(g_{1j}, g_{2j}, g_{3j}) = \begin{cases} 0 & (i \neq j) \\ 1 & (i = j) \end{cases} \quad (i, j = 1, 2, \ldots, 6) \quad (17)$$

The functions g_{1j}, g_{2j}, and g_{3j} may then be determined according to Mindlin and Goodman's procedure.

Solution of Equations

We seek the solution of ϕ_1, ϕ_2, and ϕ_3 in the following form:

$$\left.\begin{aligned}\phi_1(x,t) &= \sum_{n=1}^{\infty} \Psi_{1n}(x)T_n(t)\\ \phi_2(x,t) &= \sum_{n=1}^{\infty} \Psi_{2n}(x)T_n(t)\\ \phi_3(x,t) &= \sum_{n=1}^{\infty} W_n(x)T_n(t)\end{aligned}\right\} \tag{18}$$

It is understood that the principal modes (Ψ_{1n}, Ψ_{2n}, W_n), assumed to be known, may actually be triply infinite in number, such as in the simply supported case, although only a single infinite series is used in each of Equations (18). Hereafter the same interpretation should be adopted whenever such similar infinite-series expansions are used. To determine $T_n(t)$, Equations (18) are first substituted in (14). Since the principal modes satisfy Equations (10), the results of substitution further become

$$\left.\begin{aligned}
&-\sum_{n=1}^{\infty} \omega_n^2\Psi_{1n}T_n + \frac{1}{{}^4/_3\rho_1h_1^3 + \rho_2h_1^2h_2}\sum_{i=1}^{6} f_i[(2D_1 + E_2h_1^2)g_{1i}'' - 2G_1(g_{1i} + g_{3i}') + 6G_2\frac{h_1}{h_2}(g_{2i} + g_{3i}')\\
&\qquad - \frac{h_1p_z}{{}^4/_3\rho_1h_1^3 + \rho_2h_1^2h_2} = \sum_{n=1}^{\infty}\Psi_{1n}\ddot{T}_n + \sum_{i=1}^{6}\bar{f}_ig_{1i}\\
&-\sum_{n=1}^{\infty} \omega_n^2(h_1\Psi_{1n} + {}^2/_3h_2\Psi_{2n})T_n + \frac{1}{\rho_2h_2^2}\sum_{i=1}^{6} f_i[E_2h_1h_2g_{1i}'' + {}^2/_3E_2h_2^2g_{2i}'' - 2G_2(g_{2i} + g_{3i}')]\\
&\qquad + \frac{h_2p_z}{\rho_2h_2^2} = \sum_{n=1}^{\infty}(h_1\Psi_{1n} + {}^2/_3h_2\Psi_{2n})\ddot{T}_n + \sum_{i=1}^{6}\bar{f}_i(h_1g_{1i} + {}^2/_3h_2g_{2i})\\
&-\sum_{n=1}^{\infty} \omega_n^2W_nT_n + \frac{1}{2(\rho_1h_1 + \rho_2h_2)}\sum_{i=1}^{6} f_i[G_i(g_{1i}' + g_{3i}'') + 2G_2(g_{2i}' + g_{3i}'')] + \frac{p_z}{2(\rho_1h_1 + \rho_2h_2)}\\
&\qquad = \sum_{n=1}^{\infty} W_n\ddot{T}_n + \sum_{i=1}^{6}\bar{f}_ig_{3i}
\end{aligned}\right\} \tag{19}$$

We proceed next to expand in series form those terms in Equations (19) which are not yet in terms of the principal modes (Ψ_{1n}, Ψ_{2n}, W_n), as follows:

$$\left.\begin{aligned}
-\frac{h_1p_z}{{}^4/_3\rho_1h_1^3 + \rho_2h_1^2h_2} &= \sum_{n=1}^{\infty} Q_n(t)\Psi_{1n}(x)\\
\frac{h_2p_z}{\rho_2h_2^2} &= \sum_{n=1}^{\infty} Q_n(t)[h_1\Psi_{1n}(x) + {}^2/_3h_2\Psi_{2n}(x)]\\
\frac{p_z}{2(\rho_1h_1 + \rho_2h_2)} &= \sum_{n=1}^{\infty} Q_n(t)W_n(x)
\end{aligned}\right\} \tag{20}$$

$$\left.\begin{aligned}
g_{1i} &= \sum_{n=1}^{\infty} G_{in}\Psi_{1n}(x)\\
h_1g_{1i} + {}^2/_3h_2g_{2i} &= \sum_{n=1}^{\infty} G_{in}[h_1\Psi_{1n}(x) + {}^2/_3h_2\Psi_{2n}(x)]\\
g_{3i} &= \sum_{n=1}^{\infty} G_{in}W_n(x)
\end{aligned}\right\} \tag{21}$$

$$\left.\begin{aligned}
&\frac{1}{{}^4/_3\rho_1h_1^3 + \rho_2h_1^2h_2}[(2D_1 + E_2h_1^2)g_{1i}'' - 2G_1(g_{1i} + g_{3i}') + 6G_2\frac{h_1}{h_2}(g_{2i} + g_{3i}')] = \sum_{n=1}^{\infty} G_{in}^*\Psi_{1n}(x)\\
&\frac{1}{\rho_2h_2^2}[E_2h_1h_2g_{1i}'' + {}^2/_3E_2h_2^2g_{2i}'' - 2G_2(g_{2i} + g_{3i}')] = \sum_{n=1}^{\infty} G_{in}^*[h_1\Psi_{1n}(x) + {}^2/_3h_2\Psi_{2n}(x)]\\
&\frac{1}{2(\rho_1h_1 + \rho_2h_2)}[G_1(g_{1i}' + g_{3i}'') + 2G_2(g_{2i} + g_{3i}'')] = \sum_{n=1}^{\infty} G_{in}^*W_n(x)
\end{aligned}\right\} \tag{22}$$

The function $Q_n(t)$ and the constants G_{in} and G_{in}^* in these equations are determined by making use of the orthogonality condition in Equation (12). Thus, multiplying the first of Equations (20) by

$$({}^4/_3\rho_1h_1^3 + \rho_2h_1^2h_2)\Psi_{1m},$$

the second by

$$3\rho_2h_2(h_1\Psi_{1m} + {}^2/_3h_2\Psi_{2m}),$$

and the third by

$$4(\rho_1h_1 + \rho_2h_2)W_m,$$

adding the results, integrating with respect to x from 0 to l, and making use of Equation (12), we obtain

$$Q_n(t) = \frac{2}{I_{nn}}\int_0^l (p_zh_1\Psi_{1n} + p_zh_2\Psi_{2n} + p_zW_n)dx \tag{23}$$

where

$$I_{nn} = \int_0^l [({}^4/_3\rho_1h_1^3 + \rho_2h_1^2h_2)\Psi_{1n}^2 + 3\rho_2h_2(h_1\Psi_{1n} + {}^2/_3h_2\Psi_{2n})^2 + 4(\rho_1h_1 + \rho_2h_2)W_n^2]dx \tag{24}$$

In entirely the same manner we find from Equations (21) and (22)

$$G_{in} = \frac{2}{I_{nn}}\int_0^l \{[{}^2/_3\rho_1h_1^3g_{1i} + \rho_2h_1h_2(2h_1g_{1i} + h_2g_{2i})]\Psi_{1n} + \rho_2h_2^2(h_1g_{1i} + {}^2/_3h_2g_{2i})\Psi_{2n} + 2(\rho_1h_1 + \rho_2h_2)g_{3i}W_n\}dx \tag{25}$$

$$G_{in}^* = \frac{2}{I_{nn}}\int_0^l \{[(D_1 + 2E_2h_1^2)g_{1i}'' + E_2h_1h_2g_{2i}'' - G_1(g_{1i} + g_{3i}')]\Psi_{1n} + [E_2h_1h_2g_{1i}'' + {}^2/_3E_2h_2^2g_{2i}'' - 2G_2(g_{2i} + g_{3i}')]\Psi_{2n} + [G_1(g_{1i}' + g_{3i}'') + 2G_2(g_{2i}' + g_{3i}'')]W_n\}dx \tag{26}$$

The series expansions in Equations (20), (21), and (22) are now substituted in Equations (19). By equating the nth terms, each of the three Equations (19) yields

$$\ddot{T}_n(t) + \omega_n^2 T_n(t) = Q_n(t) - \sum_{i=1}^{6} G_{in}\dot{f}_i(t) + \sum_{i=1}^{6} G_{in}^* f_i(t)$$

the solution of which is obviously

$$T_n(t) = A_n \cos \omega_n t + B_n \sin \omega_n t + \frac{1}{\omega_n}\int_0^t \left[Q_n(\tau) - \sum_{i=1}^{6} G_{in}\dot{f}_i(\tau) + \sum_{i=1}^{6} G_{in}^* f_i(\tau) \right] \sin \omega_n(t-\tau)d\tau \quad (27)$$

The result in Equation (27) is of the same form as the analogous expressions in references [4, 5] for homogeneous beams; however, we shall simplify it somewhat here by first introducing, by integration by parts,

$$\int_0^t \dot{f}_i(\tau) \sin \omega_n(t-\tau)d\tau = -\dot{f}_i(0) \sin \omega_n t - \omega_n f_i(0) \cos \omega_n t + \omega_n f_i(t) - \omega_n^2 \int_0^t f_i(\tau) \sin \omega_n(t-\tau)d\tau$$

Equation (27) is then written as

$$T_n(t) = \left[A_n + \sum_{i=1}^{6} G_{in} f_i(0) \right] \cos \omega_n t + \left[B_n + \frac{1}{\omega_n}\sum_{i=1}^{6} G_{in}\dot{f}_i(0) \right] \sin \omega_n t - \sum_{i=1}^{6} G_{in} f_i(t) + \frac{1}{\omega_n}\int_0^t \left[Q_n(\tau) + \sum_{i=1}^{6} (\omega_n^2 G_{in} + G_{in}^*) f_i(\tau) \right] \sin \omega_n(t-\tau)d\tau \quad (28)$$

The constants A_n and B_n are next determined by the initial displacements and velocities given in Equations (6). This is done by expanding the latter quantities in the following series form in terms of the principal modes:

$$\psi_{10}(x) = \sum_{n=1}^{\infty} C_n \Psi_{1n}$$

$$h_1\psi_{10}(x) + {}^2/_3 h_2 \psi_{20}(x) = \sum_{n=1}^{\infty} C_n(h_1\Psi_{1n} + {}^2/_3 h_2 \Psi_{2n}) \quad (29)$$

$$w_0(x) = \sum_{n=1}^{\infty} C_n W_n$$

$$\dot{\psi}_{10}(x) = \sum_{n=1}^{\infty} D_n \Psi_{1n}$$

$$h_1\dot{\psi}_{10}(x) + {}^2/_3 h_2 \dot{\psi}_{20}(x) = \sum_{n=1}^{\infty} D_n(h_1\Psi_{1n} + {}^2/_3 h_2 \Psi_{2n}) \quad (30)$$

$$\dot{w}_0(x) = \sum_{n=1}^{\infty} D_n W_n$$

The constant coefficients C_n and D_n are then determined in an entirely similar manner as $Q_n(t)$, G_{in}, and G_{in}^* were, by making use of the orthogonality condition in Equation (12). The results give

$$C_n = \frac{2}{I_{nn}}\int_0^l \{({}^2/_3\rho_1 h_1 + 2\rho_2 h_2)h_1^2\psi_{10} + \rho_2 h_1 h_2^2 \psi_{20}]\Psi_{1n} + \rho_2 h_2^2(h_1\psi_{10} + {}^2/_3 h_2\psi_{20})\Psi_{2n} + 2(\rho_1 h_1 + \rho_2 h_2)w_0 W_n]dx$$

$$D_n = \frac{2}{I_{nn}}\int_0^l \{[({}^2/_3\rho_1 h_1 + 2\rho_2 h_2)h_1^2\dot{\psi}_{10} + \rho_2 h_1 h_2^2\dot{\psi}_{20}]\Psi_{1n} + \rho_2 h_2^2(h_1\dot{\psi}_{10} + {}^2/_3 h_2\dot{\psi}_{20})\Psi_{2n} + 2(\rho_1 h_1 + \rho_2 h_2)\dot{w}_0 W_n]dx \quad (31)$$

where I_{nn} is the definite integral in Equation (24). By substituting Equations (18), (21), and (29) in (15), and equating the nth terms in each of the three Equations (15), there results

$$T_n(0) = C_n - \sum_{i=1}^{6} G_{in} f_i(0)$$

Similarly, by substituting Equations (18), (21), and (30) in (16) and equating the nth terms, each of the three Equations (16) yields

$$\dot{T}_n(0) = D_n - \sum_{i=1}^{6} G_{in}\dot{f}_i(0)$$

When these expressions of $T_n(0)$ and $\dot{T}_n(0)$ are equated to their values given by Equation (28), namely

$$T_n(0) = A_n, \qquad \dot{T}_n(0) = B_n\omega_n$$

we find

$$A_n = C_n - \sum_{i=1}^{6} G_{in} f_i(0)$$

$$B_n = \frac{1}{\omega_n}\left[D_n - \sum_{i=1}^{6} G_{in}\dot{f}_i(0) \right]$$

Equation (28) thus becomes finally

$$T_n(t) = C_n \cos \omega_n t + \frac{1}{\omega_n} D_n \sin \omega_n t - \sum_{i=1}^{6} G_{in} f_i(t) + \frac{1}{\omega_n}\int_0^t \left[Q_n(\tau) + \sum_{i=1}^{6} (\omega_n^2 G_{in} + G_{in}^*) f_i(\tau) \right] \sin \omega_n(t-\tau)d\tau \quad (32)$$

The complete solution now consists of Equations (13), (18), and (32). The functions g_{1i}, g_{2i}, and g_{3i} are determined according to Equations (17), and Q_n, G_{in}, G_{in}^*, C_n, and D_n are given by Equations (23), (25), (26), and (31).

An Example

We will now illustrate the use of the foregoing result by considering the example of a sandwich plate in plane strain, simply supported at the end sections $x = 0$ and $x = l$. The section $x = l$ is given a transverse deflection varying with time. The boundary conditions are

$$\begin{aligned} (D_1 + 2E_2h_1^2)\psi_1'(0,t) + E_2h_1h_2\psi_2'(0,t) &= 0 \\ (D_1 + 2E_2h_1^2)\psi_1'(l,t) + E_2h_1h_2\psi_2'(l,t) &= 0 \\ E_2h_1h_2\psi_1'(0,t) + E_2{}^2/_3h_2^2\psi_2'(0,t) &= 0 \\ E_2h_1h_2\psi_1'(l,t) + E_2{}^2/_3h_2^2\psi_2'(l,t) &= 0 \\ w(0,t) &= 0 \\ w(l\,t) &= f_6(t) \end{aligned} \quad (33)$$

Since $f_i(i) = 0$ $(i = 1, 2, \ldots, 5)$, we have

$$g_{1i} = g_{2i} = g_{3i} = 0 \qquad (i = 1, 2, \ldots, 5) \tag{34}$$

On the other hand, corresponding to the given function $f_6(t)$, the functions g_{16}, g_{26}, and g_{36} are determined by Equations (17), which in the present case are, on account of Equations (33),

$$\begin{aligned}
(D_1 + 2E_2h_1^2)g_{16}'(0) + E_2h_1h_2g_{26}'(0) &= 0 \\
(D_1 + 2E_2h_1^2)g_{16}'(l) + E_2h_1h_2g_{26}'(l) &= 0 \\
E_2h_1h_2g_{16}'(0) + E_2^2/_3h_2^2g_{26}'(0) &= 0 \\
E_2h_1h_2g_{16}'(l) + E_2^2/_3h_2^2g_{26}'(l) &= 0 \\
g_{36}(0) &= 0 \\
g_{36}(l) &= 1
\end{aligned}$$

These conditions are satisfied by having

$$g_{16}(x) = g_{26}(x) = 0, \qquad g_{36}(x) = x/l \tag{35}$$

Substituting Equations (34) and (35) together with the principal modes given in Equations (9) for simply supported plates into Equations (25) and (26), we find

$$\begin{aligned}
G_{in}^* &= 0 \qquad (i = 1, 2, \ldots, 6) \\
G_{in} &= 0 \qquad (i = 1, 2, \ldots, 5)
\end{aligned}$$

$$\begin{aligned}
G_{6n} = 8(-1)^{n+1}(\rho_1h_1 + \rho_2h_2)c_n/n\pi[(^4/_3\rho_1h_1^3 + \rho_2h_1^2h_2)a_n^2 \\
+ 3\rho_2h_2(h_1a_n + {}^2/_3h_2b_n)^2 + 4(\rho_1h_1 + \rho_2h_2)c_n^2]
\end{aligned}$$

Since $p_x = p_z = 0$, Equations (23) yields $Q_n = 0$. For simplicity, assume all initial displacements and velocities to be zero, and we have $C_n = D_n = 0$ according to Equations (31). Equation (32) therefore becomes

$$T_n(t) = G_{6n}\omega_n \int_0^t f_6(\tau) \sin \omega_n(t - \tau)d\tau - G_{6n}f_6(t) \tag{36}$$

As a special case of the example let us take

$$f_6(t) = K \sin \omega t$$

Equation (36) then yields

$$T_n(t) = KG_{6n}\frac{\omega^2}{\omega^2 - \omega_n^2}\left(\frac{\omega_n}{\omega}\sin \omega_n t - \sin \omega t\right)$$

The displacement w, for instance, is, according to Equations (13) and (18),

$$\begin{aligned}
w(x, t) = \sum_{n=1}^{\infty} c_n \sin \frac{n\pi x}{l} KG_{6n}\frac{\omega^2}{\omega^2 - \omega_n^2}\left(\frac{\omega_n}{\omega}\sin \omega_n t\right. \\
\left. - \sin \omega t\right) + \frac{x}{l}K \sin \omega t
\end{aligned} \tag{37}$$

It is easily verified that

$$w(0, t) = 0,\ w(l, t) = K \sin \omega t = f_6(t)$$

$$w(x, 0) = 0, \qquad \dot{w}(x, 0) = K\omega\left[-\sum_{n=1}^{\infty} G_{6n}c_n \sin \frac{n\pi x}{l} + \frac{x}{l}\right] = 0$$

The bracket in the last equation is zero because the summation is precisely the series expansion of the function x/l. The boundary and initial conditions are thus all satisfied.

References

1 Yi-Yuan Yu, "A New Theory of Elastic Sandwich Plates—One-Dimensional Case," JOURNAL OF APPLIED MECHANICS, vol. 26, TRANS. ASME, vol. 81, series E, 1959, pp. 415–421.

2 Yi-Yuan Yu, "Simple Thickness-Shear Modes of Vibration of Infinite Sandwich Plates," JOURNAL OF APPLIED MECHANICS, vol. 26, TRANS. ASME, vol. 81, 1959, series E, pp. 679–681.

3 Yi-Yuan Yu, "Flexural Vibrations of Elastic Sandwich Plates," *Journal of Aero/Space Sciences*, vol. 27, 1960, pp. 272–282.

4 R. D. Mindlin and L. E. Goodman, "Beam Vibrations With Time-Dependent Boundary Conditions," JOURNAL OF APPLIED MECHANICS, vol. 17, TRANS. ASME, vol. 72, 1950, pp. 377–380.

5 G. HERRMANN, "Forced Motions of Timoshenko Beams," JOURNAL OF APPLIED MECHANICS, vol. 22, TRANS. ASME, vol. 77, 1955, pp. 53–56.

6 A. E. H. Love, "A Treatise on the Mathematical Theory of Elasticity," Dover Publications, New York, N. Y., 1944, p. 180.

7 G. Herrmann, "Forced Motions of Elastic Rods," JOURNAL OF APPLIED MECHANICS, vol. 21, TRANS. ASME, vol. 76, 1954, pp. 221–224.

D. C. GAZIS
Research Laboratories,
General Motors Corporation,
Warren, Mich.
Assoc. Mem. ASME

R. D. MINDLIN
Professor of Civil Engineering,
Columbia University, New York, N. Y.
Mem. ASME

Extensional Vibrations and Waves in a Circular Disk and a Semi-Infinite Plate[1]

A set of approximate equations of extensional motion of elastic plates is solved for the case of axially symmetric vibrations of a circular disk and the results are compared with experiments performed by E. A. G. Shaw. Special attention is given to a new mode of vibration, discovered by Shaw, in which the deformation is predominantly at the edge of the disk. It is shown how this mode arises from the complex conjugate roots of the frequency equation of an infinite plate. The properties of the edge-mode are examined in detail in a study of the reflection of straight-crested extensional waves at the edge of a semi-infinite plate.

Introduction

In a previous paper [1][2] a derivation was given of approximate, two-dimensional equations of extensional motion, of an elastic plate, which take into account the effect of coupling between extensional, symmetric thickness-stretch, and symmetric thickness-shear deformations. These equations result from retaining the zero-order, first-order, and second-order terms of an expansion of the displacements in a series of Legendre polynomials of the thickness co-ordinate and they are referred to in the sequel as "second-order equations."

As pointed out in reference [1], a number of important properties of the frequency spectrum contained in the exact theory [2, 3] of extensional motion of an infinite plate are reproduced by the second-order equations, whereas they do not appear in the zero-order approximation [4, 5] or in a first-order approximation [6]. Among these properties is a pair of segments, of the second and third branches, with complex conjugate wave-numbers, Fig. 1. Complex wave-numbers signify modes whose shapes are given by products of trigonometric and exponential functions in Cartesian co-ordinates and by functions of similar behavior in other co-ordinate systems. These mode-shapes are physically unacceptable in the case of free vibrations of an infinite plate but they are important in transients or when other boundaries, in addition to the free faces, are introduced. In this paper it is shown how the modes associated with complex wave-numbers account for edge vibrations observed experimentally by Shaw [7] in circular disks of barium titanate which were excited in axially symmetric, extensional motion.

Shaw observed coupling of the extensional modes with an unusual mode whose amplitude was large near the circular boundary of the disk and decreased rapidly toward the center. The coupling occurred at a frequency essentially independent of the radius of the plate and far below the lowest frequency associated with real wave-numbers of the second and third branches for the infinite plate. The latter circumstance implies that the usual thickness-stretch and thickness-shear modes cannot account for the observed coupling inasmuch as, for a linearly elastic material, a mode of the infinite plate has overtones in a finite plate but no subtones and hence its influence on the frequency spectrum at frequencies far below its frequency range is not appreciable. Shaw expressed the opinion that some other type of motion was in resonance with the radial extensional motion. A type of motion that has the proper frequency range and mode-shape is one corresponding to complex portions of the frequency spectrum, which were not studied until later [8, 9]. One may expect that an investigation of the extensional vibrations of circular plates within the framework of the general, linear theory of elasticity will provide a theoretical explanation of the phenomenon observed by Shaw. However, such an investigation would be encumbered by a doubly infinite series expression for each mode because each of the infinity of modes in the three-dimensional solution for an infinite plate gives rise to an infinity of modes in the presence of the additional free boundary. Now, the second-order equations contain complex branches analogous to those of the three-dimensional theory and only three modes of the infinite plate are introduced in an axially symmetric problem. Thus the approximate equations have the requisite qualitative properties

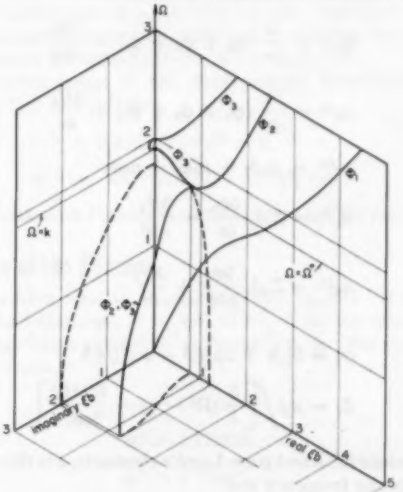

Fig. 1 The three branches of the frequency spectrum (frequency versus propagation constant) of an infinite plate according to the second-order equations. Dashed lines are projections of complex segment on co-ordinate planes.

[1] This investigation was supported, in part, by the Office of Naval Research under a contract with Columbia University.

[2] Numbers in brackets designate References at end of paper.

Presented at the Summer Conference of the Applied Mechanics Division, University Park, Pa., June 20–22, 1960, of The American Society of Mechanical Engineers.

Discussion of this paper should be addressed to the Secretary, ASME, 29 West 39th Street, New York, N. Y., and will be accepted until October 10, 1960, for publication at a later date. Discussion received after the closing date will be returned.

Note: Statements and opinions advanced in papers are to be understood as individual expressions of their authors and not those of the Society. Manuscript received by ASME Applied Mechanics Division, April 30, 1959. Paper No. 60—APM-3.

and are considerably simpler in form. Accordingly, they have been employed in this paper in an attempt to obtain an insight into the phenomena which take place at the frequency of the edge vibrations.

A characteristic equation appropriate to the circular disk was obtained within the framework of the second-order theory and evaluated numerically by means of an IBM 704 digital computer. The results of this investigation may be summarized as follows: The second-order equations include the edge vibrations but their frequencies are somewhat lower than the experimental values obtained by Shaw. The discrepancy is probably due to the fact that, although the second-order equations provide a very good approximation of the real and imaginary segments of the first three branches of the three-dimensional theory, the approximation of the complex segments is only fair. However, the theoretical results of the second-order equations are in very good qualitative agreement with the experimental results, in so far as the edge vibrations are concerned, and they are in excellent quantitative agreement over the remainder of the spectrum from zero frequency up to frequencies considerably higher than the thickness frequencies.

It is found that the edge mode, at a free edge, cannot be composed of contributions from the two complex segments alone but always involves the extensional deformation associated with the real, lowest branch. Thus the edge vibration is always linked with the usual type of extensional vibration in the interior of the plate. This situation and the detailed behavior in the neighborhood of the edge-resonance are investigated, in the last section of the paper, by means of a study of the reflection of a sinusoidal train of straight-crested extensional waves at a free, straight edge at normal incidence.

Frequency Equation for a Circular Disk

We refer the plate to cylindrical co-ordinates r, θ, and x_2 with the faces at $x_2 = \pm b$. It is required to obtain the axially symmetric, extensional modes of vibration of a plate bounded by the free faces and by a free, cylindrical surface $r = a$. The plate-displacements $u_r^{(0)}$, $u_\theta^{(0)}$, $u_2^{(1)}$, $u_r^{(2)}$, and $u_\theta^{(2)}$, as defined in reference [1],[3] are expressed in terms of three potential functions ϕ_i, $i = 1, 2, 3$, and two potential functions H_0 and H_2, all of them harmonic functions of time, according to

$$
\begin{aligned}
u_r^{(0)} &= \frac{\partial}{\partial r}(\phi_1 + \phi_2 + \phi_3) - \frac{\partial H_0}{r\partial\theta} \\
u_\theta^{(0)} &= \frac{\partial}{r\partial\theta}(\phi_1 + \phi_2 + \phi_3) + \frac{\partial H_0}{\partial r} \\
u_2^{(1)} &= \alpha_1\phi_1 + \alpha_2\phi_2 + \alpha_3\phi_3 \\
u_r^{(2)} &= \Sigma_i\beta_i\frac{\partial\phi_i}{\partial r} - \frac{\partial H_2}{r\partial\theta} \\
u_\theta^{(2)} &= \Sigma_i\beta_i\frac{\partial\phi_i}{r\partial\theta} + \frac{\partial H_2}{\partial r}
\end{aligned}
\tag{1}
$$

where

$$
\begin{aligned}
\alpha_i &= b[(\lambda + 2\mu)\xi_i^2 - \rho\omega^2]/\kappa_1\lambda \\
\beta_i &= \alpha_i b \Big/ \left[\frac{3}{4}(\Omega^2 - 4) - \frac{E'b^2\xi_i^2}{5\mu\kappa_2^2}\right]
\end{aligned}
\tag{2}
$$

In Equations (2) λ and μ are Lamé's constants, ρ is the density, ω is the circular frequency and

$$
E' = 4\mu(\lambda + \mu)/(\lambda + 2\mu), \qquad \Omega = \omega/\omega_s \tag{3}
$$

[3] The second-order equations are given in invariant form in the last section of reference [1].

where

$$
\omega_s = (\pi/2b)(\mu/\rho)^{1/2} \tag{4}
$$

In addition, the κ_s ($s = 1$ to 4) are the correction coefficients of the second-order theory and the ξ_i ($i = 1, 2, 3$) are the three roots of the cubic equation

$$
\begin{vmatrix} a_{11} & a_{12} & 0 \\ a_{12} & a_{22} & a_{23} \\ 0 & a_{23} & a_{33} \end{vmatrix} = 0 \tag{5}
$$

where

$$
\begin{aligned}
a_{11} &= k^2z^2 - \Omega^2 \\
a_{22} &= \kappa_2^2z^2/3 + 4\kappa_1^2k^2/\pi^2 - \kappa_3^2\Omega^2/3 \\
a_{33} &= E'z^2/5\mu + 12\kappa_2^2/\pi^2 - \kappa_4^2\Omega^2/5 \\
a_{12} &= 2\kappa_1(k^2 - 2)z/\pi \\
a_{23} &= -2\kappa_2^2z/\pi
\end{aligned}
$$

and

$$
z = 2\xi b/\pi, \qquad k^2 = 2(1 - \nu)/(1 - 2\nu) \tag{6}
$$

with ν denoting Poisson's ratio.

For axially symmetric motion, the potentials H_0 and H_2 are set equal to zero. The remaining potentials satisfy the Helmholtz equations

$$
(\nabla^2 + \xi_i^2)\phi_i = 0 \tag{7}
$$

which become, in axially symmetric, cylindrical co-ordinates,

$$
\left(\frac{d^2}{dr^2} + \frac{1}{r}\frac{d}{dr} + \xi_i^2\right)\phi_i = 0 \tag{8}
$$

The general solution of Equation (8) is given in terms of Bessel functions by

$$
\phi_i = A_iJ_0(\xi_ir) + B_iY_0(\xi_ir) \tag{9}
$$

where, in the absence of singularities at the origin, the B_i are taken equal to zero.

The plate-strains, in the axially symmetric case, are expressed in terms of the potential functions ϕ_i by means of the invariant equations of reference [1] as follows:

$$
\begin{aligned}
\epsilon_{rr}^{(0)} &= \Sigma_i\phi_i'' \\
\epsilon_{\theta\theta}^{(0)} &= r^{-1}\Sigma_i\phi_i' \\
\epsilon_{22}^{(0)} &= b^{-1}\Sigma_i\alpha_i\phi_i \\
\epsilon_{r2}^{(1)} &= \frac{1}{2}\Sigma_i(\alpha_i + 3b^{-1}\beta_i)\phi_i' \\
\epsilon_{rr}^{(2)} &= \Sigma_i\beta_i\phi_i'' \\
\epsilon_{\theta\theta}^{(2)} &= r^{-1}\Sigma_i\beta_i\phi_i' \\
\epsilon_{r\theta}^{(0)} &= \epsilon_{\theta 2}^{(0)} = \epsilon_{r\theta}^{(2)} = \epsilon_{\theta 2}^{(2)} = 0
\end{aligned}
\tag{10}
$$

where primes denote differentiation with respect to r. Similarly, the components of plate-traction acting across the cylindrical surfaces $r = \text{const}$ are

$$
\begin{aligned}
\tau_{rr}^{(0)} &= 2\Sigma_i[(\lambda + 2\mu)\phi_i'' + \lambda(b^{-1}\kappa_3\alpha_i\phi_i + r^{-1}\phi_i')] \\
\tau_{r2}^{(1)} &= (2\mu\kappa_2^2/3)\Sigma_i(\alpha_i + 3b^{-1}\beta_i)\phi_i' \\
\tau_{rr}^{(2)} &= (2E'/5)\Sigma_i(\beta_i\phi_i'' + \nu r^{-1}\beta_i\phi_i')
\end{aligned}
\tag{11}
$$

Using the solution (9) for ϕ_i, one obtains, on $r = a$,

$$\tau_{rr}^{(0)} = C_1\Sigma_i A_i T_{1i}$$
$$\tau_{rz}^{(1)} = C_2\Sigma_i A_i T_{2i} \tag{12}$$
$$\tau_{rr}^{(2)} = C_2\Sigma_i A_i T_{3i}$$

where

$$T_{1i} = \zeta_i J_1(\zeta_i) - (k^2\gamma^2/2)J_0(\zeta_i)$$
$$T_{2i} = \left[1 - \frac{15\kappa_2^2(1-\nu)R^2}{2(\zeta_i^2 - \delta^2)}\right]\zeta_i(\zeta_i^2 - \gamma^2)J_1(\zeta_i)$$
$$T_{3i} = \frac{\zeta_i^2 - \gamma^2}{\zeta_i^2 - \delta^2}\zeta_i[(1-\nu)J_1(\zeta_i) - \zeta_i J_0(\zeta_i)] \tag{13}$$
$$R = a/b, \quad \zeta_i = \xi_i a = R\xi_i b$$
$$\gamma^2 = (\pi R\Omega/2k)^2, \quad \delta^2 = (1/8)\pi^2\kappa_4^2 R^2(1-\nu)(\Omega^2 - 4)$$
$$C_1 = \frac{4\mu}{a^2}, \quad C_2 = -\frac{2\mu(\lambda + 2\mu)\kappa_2^2}{3\lambda\kappa_1 R a^2} = \frac{C_3}{3R}$$

The problem of computing the natural frequencies of a given circular plate is now formulated in the usual manner. The boundary conditions, in the absence of external forces, are

$$\tau_{rr}^{(0)} = \tau_{rz}^{(1)} = \tau_{rr}^{(2)} = 0 \tag{14}$$

on $r = a$ and a nontrivial solution is obtained if the determinant of the matrix of the coefficients of the A_i in Equations (12) is zero; i.e.,

$$|T_{ij}| = 0, \quad i, j = 1, 2, 3 \tag{15}$$

The determinantal equation (15) may be evaluated as follows: A given value of Poisson's ratio ν fixes the correction coefficients κ_s ($s = 1$ to 4) as explained in reference [1]. From the cubic equation (5), the three values of $\xi_i b$ are computed for an assumed value of the frequency ratio Ω. Equation (15) is thereby reduced to a transcendental equation on $R\ (= a/b)$. The roots R for the chosen Ω are then computed by an iteration technique as explained in the following section.

For low frequencies and long wave-lengths ($\Omega \ll 1$, $z \ll 1$) Equations (5) and (15) reduce to

$$\Omega = (2\xi_1 a/\pi R)[2/(1-\nu)]^{1/2} \tag{16}$$

$$\xi_1 a J_0(\xi_1 a) = (1-\nu)J_1(\xi_1 a) \tag{17}$$

respectively. These coincide with Poisson's solution [4, 10].

Numerical Solution of the Frequency Equation

A table of values of Ω and R satisfying (5) and (15) was computed by means of an IBM 704 digital computer using an "interval halving" iteration technique.

For a fixed value of Ω the determinant of Equation (15) is a function of R alone. The value of this determinant is computed at a prescribed starting point R_1 and at intervals of a specified ΔR thereafter up to and including a prescribed end point R_2. A change of sign of the determinant across an interval ΔR indicates a root in that interval. The interval is then halved and the direction of "scanning" is reversed; the process is repeated until a root is obtained within a prescribed accuracy. Additional roots are obtained by re-entering successively into the iteration subroutine, with a new starting point just beyond the last root obtained, until the entire region $R_1 \leqslant R \leqslant R_2$ is covered or until a prescribed number of roots is obtained.[4] The present computations were carried out for a maximum of eleven roots in the region $0 \leqslant \Omega \leqslant 3.0$ and $0 \leqslant R \leqslant 20$. The allowable "relative error" (i.e., the error divided by the root) was 10^{-4}.

The evaluation of the determinant in (15) is simplified by the fact that it is an even analytic function of the ζ_i. The nature of the ζ_i or, equivalently, the roots z_i of the cubic equation (5), for different ranges of Ω is seen in Fig. 1.[5] For $\Omega < \Omega^*$ one of the three z_i is real and the other two are complex conjugate; for $\Omega^* < \Omega < k$ and $\Omega > 2$ all three are real; and for $k < \Omega < 2$ two are real and one is pure imaginary. It may be ascertained that for $\Omega > \Omega^*$, where the z_i are either real or imaginary, the determinant is always real. For $\Omega < \Omega^*$, if z_3 is the complex conjugate of z_2, i.e., $z_3 = \bar{z}_2$ in the usual notation, then the terms of the third column of the determinant in (15) are the complex conjugates of the terms of the second column; i.e.,

$$T_{j3} = \bar{T}_{j2} = \Re_{j2} - i\,\Im_{j2} \tag{18}$$

where $\Re_{j2}$ and $\Im_{j2}$ are the real and imaginary parts, respectively, of T_{j2}. Hence adding and subtracting the two columns, one obtains

$$|T_{kj}| = -4i\begin{vmatrix} T_{11} & \Re_{12} & \Im_{12} \\ T_{21} & \Re_{22} & \Im_{22} \\ T_{31} & \Re_{32} & \Im_{32} \end{vmatrix} \tag{19}$$

i.e.; the characteristic determinant is pure imaginary. The determinant on the right-hand side of Equation (19) was employed, in the computations, in the region $\Omega < \Omega^*$. For very low frequencies, the roots of Equation (17), the asymptotic form of the frequency equation, may be obtained conveniently through the use of Onoe's tables [11].

The variation of the mode-shapes with frequency was also investigated numerically by computing the displacement fields of a number of modes of vibration at a few selected points of the spectrum. For a given root of the frequency equation (15), the two amplitude ratios A_2/A_1 and A_3/A_1 were determined by using two of the three compatible boundary conditions (14). These ratios were inserted in Equations (9) and (1) and the displacements $u_r^{(0)}$, $u_z^{(1)}$, and $u_r^{(2)}$ were computed for twenty points along the radius of the plate. The displacements were then normalized with respect to the maximum value of displacement-component appearing in the particular mode. It should be remarked that for $\Omega < \Omega^*$ the two amplitude ratios corresponding to the complex conjugate wave-numbers z_i are also complex conjugate. Their real and imaginary parts were computed by utilizing the reduced determinant of the right-hand side of Equation (19).

The limiting forms of the displacements corresponding to Equations (16) and (17) are

$$u_r^{(0)} = AJ_1(\xi_1 r), \quad u_r^{(2)} = 0$$
$$u_z^{(1)} = -A[\nu\xi_1 a/\kappa_1(1-\nu)R]J_0(\xi_1 r) \tag{20}$$

These coincide with Poisson's solution except for the factor κ_1.

Discussion of the Results

The frequency ratio $\Omega = \omega/\omega_s$ is plotted against the ratio of radius to half-thickness, $R = a/b$, in Fig. 2 for the first eleven modes using Shaw's value 0.31 for Poisson's ratio. For this value of Poisson's ratio,

$$\kappa_1^2 = 0.634835$$
$$\kappa_2^2 = 1.175035$$
$$\kappa_3^2 = 0.771867$$
$$\kappa_4^2 = 1.785839$$

[4] The role of Ω and R may be reversed in the coded program to obtain roots Ω for a constant R.

[5] See also reference [1] for a detailed discussion of the frequency spectrum of the second-order theory.

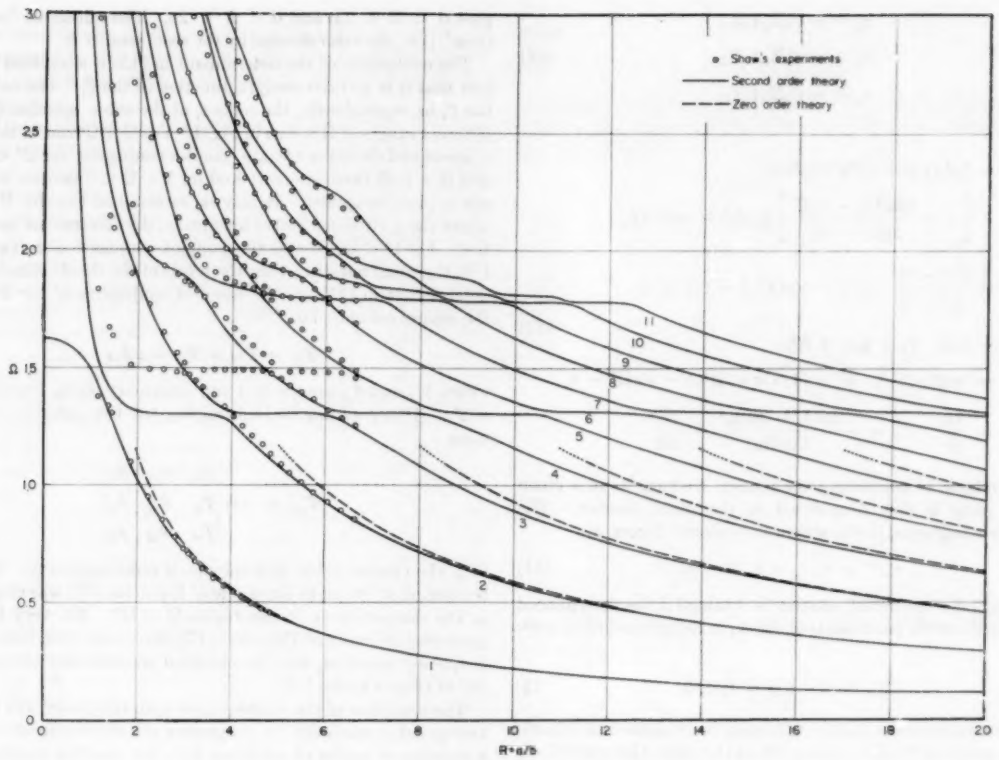

Fig. 2 Frequency spectrum of a circular disk

$$k = 1.905670$$

$$\Omega^* = 1.760744$$

In Fig. 2 are also plotted Shaw's experimental results. In order to convert Shaw's frequencies to the ordinate Ω, it is necessary to know the shear-wave velocity, $v_2 = (\mu/\rho)^{1/2}$, in barium titanate. Shaw's value of $v_2 = 2755$ m/sec, which is based on his measurements and an average of four approximate solutions by Aggarwal and Shaw, was not used. Instead, v_2 was determined from Shaw's experimental results in the neighborhood of the frequency of a family of exact solutions given by Lamb.[6] These are equivoluminal modes with circular frequency and diameter-thickness ratios

$$\omega = (\pi/b)(\mu/2\rho)^{1/2}, \quad a/b = 2\gamma_m/\pi \tag{21}$$

where the γ_m are the roots of

$$J_1'(\gamma_m) = 0, \quad \text{i.e.,} \quad \gamma_m = 1.841, 5.331, 8.536, \ldots \tag{22}$$

hence

$$a/b = 1.172, 3.394, 5.434, \ldots \tag{23}$$

If f is the frequency, Shaw's ordinate for these modes is

$$2fb = (\mu/2\rho)^{1/2} \tag{24}$$

Shaw's frequencies for the first mode near $a/b = 1.172$ are at an extreme of his range of measurements and do not appear to be reliable[7]; but the second and third roots (23) both occur at $2fb =$ 1900 m/sec. Hence

$$v_2 = (\mu/\rho)^{1/2} = 2690 \text{ m/sec} \tag{25}$$

A comparison of the experimental frequencies with the theoretical results of the second-order theory, in Fig. 2, reveals very good general agreement, except that the theoretical frequency of the edge modes ($\Omega \backsimeq 1.31$) is lower than the experimental value ($\Omega \backsimeq 1.47$) by about 12 per cent. An investigation was made of the possibility that the discrepancy might be due to exceptional sensitivity to Poisson's ratio. However, the result was negative. In the range $0.25 \lesssim \nu \lesssim 0.40$, the frequencies of the edge modes were found to remain in the interval $1.30 < \Omega_e < 1.35$. Computations were also made with a variety of values of the correction coefficients κ_2, obtained by matching the exact and approximate frequency spectra of an infinite plate at points other than those at infinite wave-length; but no improvement was obtained. Another source of error in the approximate theory is that the boundary conditions involve stress-resultants and stress-couples rather than tractions at all points across the thickness of the plate. However, this raises, rather than lowers, the frequency. The most likely cause of the discrepancy seems to be that, although the second-order theory provides a good approximation of the real and imaginary segments of the first three branches of the frequency spectrum of an infinite plate as given by the exact theory, it provides only a fair reproduction of the associated complex segments; and it appears that the details of the complex segments become important in the neighborhood of the frequency of the edge modes.

As the frequency diminishes, both the experimental and mathematical results approach Poisson's, as given by Equations (16) and (17) and shown by dashed lines in Fig. 2. As the frequency increases above Ω_e, the typical terrace-like structure of the high-frequency spectrum of plates begins to develop at a frequency

[6] Footnote on p. 122 of reference [3].

[7] All of the equivoluminal modes should have the same frequency and, as $R \to 0$, the frequency of the first mode of the disk should approach the frequency of the first longitudinal mode of a thin rod of length $2b$; i.e., $2fb = [(1 + \nu)\mu/2\rho]^{1/2}$.

whose asymptotic value, as $R \to \infty$ is $\Omega \backsimeq 1.76$ in both Shaw's experiments and the second-order theory. As observed by Shaw, this is the frequency minimum Ω^* rather than the cut-off frequency of the lowest, symmetric thickness-mode which, in the present case of $\nu < 1/3$, is the thickness-stretch mode with frequency given by $\Omega = k \backsimeq 1.9$. Accordingly, there is an important difference, in this aspect of high-frequency spectra, between extensional and flexural vibrations of plates. In the latter, the asymptotic frequency of the lowest terrace-like structure is always the cut-off frequency ($\Omega = 1$) of the lowest, antisymmetric thickness-shear mode. This is because the second branch for the infinite plate never has a real minimum other than at cut-off ($\xi b = 0$) in the case of flexure [8]. The axially symmetric flexural vibrations of a circular disk are discussed in reference [12].

Returning, now, to frequencies in the neighborhood of Ω_e, computations based on the second-order theory show that the displacements do, in fact, conform with Shaw's observations. In Fig. 3 are plotted the computed values of the displacement functions for the third mode of the disk for three frequencies: one just below the frequency Ω_e of the edge vibration, one at and one just above this frequency. Immediately above and below Ω_e the displacements are distributed across the plate in much the same manner as in Poisson's solution, Equations (20), except that the radial displacement $u_r^{(0)}$ is considerably suppressed and there is a thickness-shear displacement $u_r^{(2)}$ of about the same amplitude. As Ω approaches Ω_e, coupling with the edge mode takes place which, at $\Omega = \Omega_e$ results in large amplitudes of edge vibrations characterized by displacements which include a component large near the edge and rapidly decaying toward the center of the plate. It should be noted that, as the frequency passes from below to above Ω_e, the number of nodal circles for each mode is reduced by one. Thus each mode attains above Ω_e a mode-shape similar to the mode-shape of the next lower mode for $\Omega < \Omega_e$.

The character of the quasi-exponential decay of the displacements at $\Omega = \Omega_e$ is essentially independent of the radius at the "plateau" of edge vibrations. This is shown in Fig. 4 where the theoretical value of the normalized displacement $u_2^{(1)}$ is plotted against r'/b, where r' is the radial distance from the edge of the plate, for two values of R (3.0 and 5.0). These two values of R correspond to points on the plateaus at Ω_e on the branches of the second and third modes, respectively. It is seen that the first nodal circle from the edge occurs at a distance of r'/b approximately equal to 0.75, essentially the same in both cases. This substantiates Shaw's concluding remark that edge vibrations should be expected to occur also for circular disks with very large ratios of radius to thickness, inasmuch as the character of the edge vibrations is essentially independent of this ratio.

There are additional interesting properties of the edge mode which are exposed more readily in the problem of reflection considered in the next section.

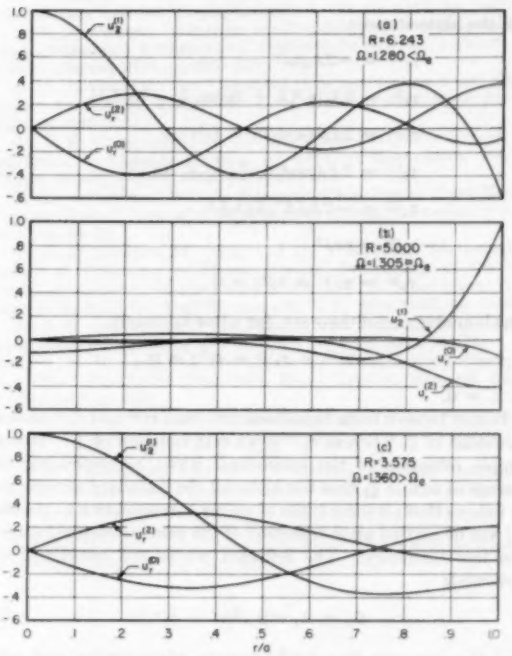

Fig. 3 Distributions of radial ($u_r^{(0)}$), thickness-stretch ($u_2^{(0)}$), and thickness-shear ($u_r^{(2)}$) displacements at frequencies in the neighborhood of frequency of edge-mode

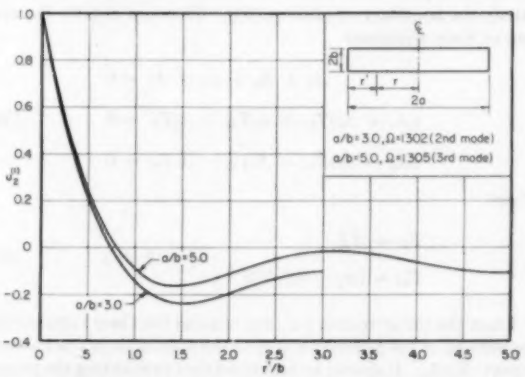

Fig. 4 Distribution of thickness-stretch displacements in two edge-modes

Reflection at the Free Edge of a Semi-Infinite Plate

Consider a semi-infinite plate bounded by the free faces $x_2 = \pm b$ and a free edge at $x_1 = 0$ and extending to infinity in the direction x_1 increasing. Assume that a sinusoidal extensional wave of a normalized frequency $\Omega < \Omega^*$ is continuously generated at $x_1 = \infty$ and propagated toward $x_1 = 0$. Referring to the invariant field equations of reference [1] one may ascertain that the sinusoidal wave is associated with the dilatational potential ϕ_1 corresponding to the real root z_1 of the cubic equation (5). The potential

$$\phi_1 = A_0 \exp\,[i(\omega t + \xi_1 x_1)] \tag{26}$$

satisfies the wave equation and generates the desired type of extensional wave. The associated displacement field is

$$\begin{aligned} u_1^{(0)} &= A_0 \xi_1 i \exp\,[i(\omega t + \xi_1 x_1)] \\ u_2^{(1)} &= A_0 \alpha_1 \exp\,[i(\omega t + \xi_1 x_1)] \\ u_1^{(2)} &= A_0 \beta_1 \xi_1 i \exp\,[i(\omega t + \xi_1 x_1)] \\ u_3^{(0)} &= u_2^{(2)} = 0 \end{aligned} \tag{27}$$

where α_1 and β_1 are given by Equations (2). Omitting exponentials in the sequel, one obtains the plate-strains

$$\begin{aligned} \epsilon_1^{(0)} &= -A_0 \xi_1^2 \\ \epsilon_2^{(0)} &= A_0 \alpha_1 / b \\ \epsilon_1^{(2)} &= -A_0 \beta_1 \xi_1^2 \\ \epsilon_3^{(1)} &= A_0 i \xi (\alpha_1 + 3\beta_1 / b) \\ \epsilon_3^{(0)} &= \epsilon_\circ^{(0)} = \epsilon_4^{(1)} = \epsilon_3^{(2)} = \epsilon_3^{(3)} = 0 \end{aligned} \tag{28}$$

and the plate-stresses

$$\begin{aligned}
\tau_1^{(0)} &= -2A_0\rho\omega^2 \\
\tau_2^{(0)} &= 2A_0[\kappa_1^2(\lambda + 2\mu)\alpha_1/b - \lambda\kappa_1\xi_1^2] \\
\tau_3^{(0)} &= 2A_0\lambda(\kappa_1\alpha_1/b - \xi_1^2) \\
\tau_6^{(1)} &= 2A_0(\mu\kappa_2^2/3)i\xi_1(\alpha_1 + 3\beta_1/b) \\
\tau_1^{(2)} &= -2A_0(E'/5)\beta_1\xi_1^2 \\
\tau_2^{(2)} &= \nu\tau_1^{(2)} \\
\tau_5^{(0)} &= \tau_4^{(1)} = \tau_3^{(2)} = 0
\end{aligned} \tag{29}$$

The boundary conditions are, for a free boundary,

$$\tau_1^{(0)} = \tau_1^{(2)} = \tau_6^{(1)} = 0 \tag{30}$$

at $x_1 = 0$.

It may be seen from Equations (29) that $\tau_1^{(0)}$ and $\tau_1^{(2)}$ are even functions of ξ_1 whereas $\tau_6^{(1)}$ is an odd function of ξ_1. Hence a simple reflection of the extensional wave, corresponding to a change of sign of ξ_1 does not make all the boundary stresses zero. It follows that all three types of waves corresponding to the three ϕ_j will be excited upon reflection of the pure extensional wave at the free boundary. The reflected waves are associated with potentials

$$\phi_j = A_j \exp\,[i(\omega t - \xi_j x_1)] \tag{31}$$

and the corresponding displacements, plate-strains, and plate-stresses may be derived from Equations (27), (28), and (29) by substituting $-\xi_j$ for ξ_1. The boundary stresses due to the incident wave plus the stress due to the three reflected waves must satisfy the boundary conditions (30). Thus one obtains the system of three equations

$$\begin{aligned}
A_0 + A_1 + A_2 + A_3 &= 0 \\
(A_0 + A_1)T_{21} + A_2T_{22} + A_3T_{23} &= 0 \\
(A_0 - A_1)T_{31} - A_2T_{32} - A_3T_{33} &= 0
\end{aligned} \tag{32}$$

where

$$\left.\begin{aligned}
T_{2j} &= \beta_j\xi_j^2 \\
T_{3j} &= (\alpha_j + 3\beta_j/b)\xi_j^2
\end{aligned}\right\} \quad j = 1, 2, 3. \tag{33}$$

From the linear system (32) one obtains the three ratios of the amplitudes of the reflected waves to the amplitude of the incident wave: A_j/A_0. It should be remarked that in selecting the proper sign for the complex wave numbers one should bear in mind that in order to be physically acceptable they should correspond to functions decreasing for increasing x_1. It is seen that the two complex wave-numbers which should be entered in Equations (31) are

$$\left.\begin{aligned}
\xi_2 &= c - id \\
\xi_3 &= -c - id
\end{aligned}\right\} \quad c, d > 0 \tag{34}$$

Thus in addition to a reflected pure extensional wave, one obtains two "complex-waves" corresponding to motion localized near the free edge of the plate.

An investigation of the expressions for the A_j/A_0 leads to the following conclusions: For $\Omega < \Omega^*$ the three amplitude ratios are always complex, and their moduli satisfy the relations

$$|A_1/A_0| = 1, \quad |A_2/A_0| = |A_3/A_0| = |A_c/A_0| \quad \text{(say)} \tag{35}$$

The complex value of A_1/A_0 implies that the reflected pure extensional wave has a phase lag η with respect to the incident wave, given by

$$\tan\,\eta = -\mathfrak{I}_1/\mathfrak{R}_1, \qquad -\pi \leqslant \eta \leqslant \pi \tag{36}$$

where $\mathfrak{R}_1$ and $\mathfrak{I}_1$ are the real and imaginary parts of the ratio A_1/A_0.

The phase of the reflected extensional wave and the magnitude of the amplitude A_c/A_0 of the complex waves were computed numerically on the IBM 704 for Ω in the neighborhood of the frequency of edge vibrations. It was found that for $\Omega \ll \Omega_e$ the amplitude $|A_c/A_0|$ is small and the phase difference between the incident and reflected extensional waves is nearly π. As Ω approaches Ω_e, $|A_c/A_0|$ increases very rapidly until, for $\Omega = \Omega_e \approx 1.314$, it reaches a maximum value of approximately 7.7, Fig. 5. At the same time the phase difference diminishes until it reaches the value 0 for $\Omega = \Omega_e$ as also shown in Fig.5. If Ω is increased beyond Ω_e, the amplitude $|A_c/A_0|$ decreases rapidly to very small values and the phase difference changes sign and increases rapidly from 0 to nearly π. In addition to $|A_c/A_0|$, Fig. 5 contains plots of $\mathfrak{R}_1$ and $\mathfrak{I}_1$ versus Ω.

Fig. 5 illustrates the details of the phenomena involved in the edge vibrations. This type of motion is in resonance with the pure extensional type of motion at a distinct frequency which the second-order theory gives as approximately equal to 1.314 ω_e for $\nu = 0.31$. Shaw's experiments indicate that this frequency of resonance is slightly higher, namely, in the neighborhood of 1.47 ω_e. In any case, at this frequency level a pure extensional wave gives rise to a large amplitude of edge-vibrational motion upon reflection at a free boundary, after a normal incidence. By analogy, in the case of a circular disk which has been discussed in the main part of this paper, one may visualize the edge vibrations as continuously generated, at the frequency of resonance, by reflection of extensional circular-crested waves at the free circular boundary.

An important feature, observable in Fig. 5, is that the ampli-

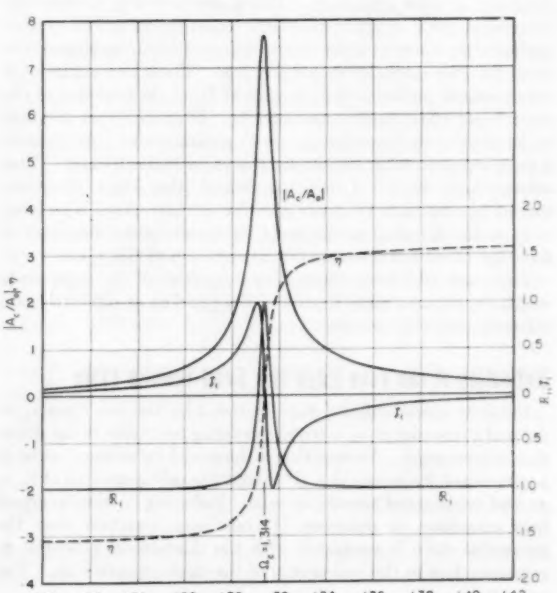

Fig. 5 Ratio ($|A_c/A_0|$) of amplitude of edge-vibration to amplitude of incident wave in the neighborhood of frequency of edge-mode. Also shown are the real ($\mathfrak{R}_1$) and imaginary ($\mathfrak{I}_1$) parts of the ratio (A_1/A_0) of amplitudes of incident and reflected waves and their phase difference (η).

tude ratio $|A_e/A_s|$ passes through a finite maximum and never reaches infinity. This means that the large edge-deformation is always coupled with a nondecaying extensional deformation of the usual kind. Consider, for example, a transient disturbance at the edge, initiated either by external excitation at the edge or by an incident wave from the interior of the plate. If this disturbance contains energy at frequency Ω_e, an edge-vibration will be induced. However, the edge-deformation is always coupled with extensional deformation and hence the energy that is temporarily trapped at the edge will gradually leak into the interior of the plate as an extensional wave traveling with the phase and group velocities corresponding to frequency Ω_e of the extensional mode (ϕ_1). The group velocity (v_2 times the slope of the branch in Fig. 1) at Ω_e is less than the group velocities of extensional waves at lower frequencies and hence the trailing wave generated by the edge mode will be outdistanced by the main reflected transient. These phenomena have been observed by J. Oliver [13] in experiments with rods.

References

1 R. D. Mindlin and M. A. Medick, "Extensional Vibrations of Elastic Plates," JOURNAL OF APPLIED MECHANICS, vol. 26, TRANS. ASME, vol. 81, series E, 1959, pp. 561–569.

2 Lord Rayleigh, "On the Free Vibrations of an Infinite Plate of Homogeneous Isotropic Elastic Matter," *Proceedings of the London Mathematical Society*, vol. 20, 1889, pp. 225–234.

3 H. Lamb, "On Waves in an Elastic Plate," *Proceedings of The Royal Society*, London, England, series A, vol. 93, 1917, pp. 114–128.

4 S. D. Poisson, "Mémoire sur l'équilibre et le mouvement des corps élastiques," *Mémoires de l'Académie des Sciences*, series 2, vol. 8, Paris, France, 1829, pp. 357–370.

5 A. L. Cauchy, "Sur l'équilibre et le mouvement d'une plaque solide," *Exercices de Mathématique*, vol. 3, Bure Frères, Paris, France, 1828, pp. 328–355.

6 T. R. Kane and R. D. Mindlin, "High-Frequency Extensional Vibrations of Plates," JOURNAL OF APPLIED MECHANICS, vol. 23, TRANS. ASME, vol. 78, 1956, pp. A-277-283.

7 E. A. G. Shaw, "On the Resonant Vibrations of Thick Barium Titanate Disks," *Journal of the Acoustical Society of America*, vol. 28, 1956, pp. 38–50.

8 R. D. Mindlin, M. Onoe, and M. A. Medick, "Mathematical Theory of Vibrations of Elastic Plates," Proceedings of the 11th Annual Symposium on Frequency Control, U. S. Army Signal Engineering Laboratories, Fort Monmouth, N. J., May 1957, pp. 1–38.

9 J. W. C. Sherwood, "Propagation in an Infinite Plate," *Journal of the Acoustical Society of America*, vol. 30, 1958, pp. 979–984.

10 A. E. H. Love, "A Treatise on the Mathematical Theory of Elasticity," Cambridge University Press, London, England, fourth edition, 1927, p. 498.

11 M. Onoe, "Tables of Modified Quotients of Bessel Functions of the First Kind for Real and Imaginary Arguments," Columbia University Press, New York, N. Y., 1958.

12 H. Deresiewicz and R. D. Mindlin, "Axially Symmetric Flexural Vibrations of a Circular Disk," JOURNAL OF APPLIED MECHANICS, vol. 22, TRANS. ASME, vol. 77, 1955, pp. 86–88.

13 J. Oliver, "Elastic Wave Dispersion in a Cylindrical Rod by a Wide-Band Short-Duration Pulse Technique," *Journal of the Acoustical Society of America*, vol. 29, 1957, pp. 189–194.

HSU LO
Professor of Aeronautical Engineering, Purdue University, Lafayette, Indiana

J. E. GOLDBERG
Professor of Structural Engineering, Purdue University

J. L. BOGDANOFF
Professor of Engineering Science, Purdue University
Mem. ASME

Effect of Small Hub-Radius Change on Bending Frequencies of a Rotating Beam

By the method of perturbation, a simple relation is formulated for the determination of the change of bending frequencies of a rotating beam due to a small change of hub radius. The first-order solution shows that a frequency parameter γ is a linear function of the hub-radius change and the constant of proportionality is readily obtainable from known parameters. The frequency ω itself can also be represented by a linear function of the hub-radius change. This confirms the results previously obtained by Boyce by repeated solutions of the differential equations for a particular beam. Higher-order solutions are also established and shown to be convergent within the limitation imposed on the amount of the hub-radius change allowable.

Given an untwisted beam mounted on a hub of radius R, rotating at a constant speed Ω, as shown in Fig. 1. The beam is allowed to vibrate flexurally in a plane making an angle $[(\pi/2) - \beta]$ with the plane of rotation. The bending frequencies $\omega^{(i)}$ and the modal shapes $V^{(i)}$, $i = 1, 2, 3 \ldots$, can be determined from the solution of the following differential equation[1] with the proper boundary conditions:

$$\frac{d^2}{dx^2}\left[EI\frac{d^2V}{dx^2}\right] - \frac{d}{dx}\left[N\frac{dV}{dx}\right] - m(\omega^2 + \Omega^2\sin^2\beta)\,V = 0 \quad (1)$$

where

$$N = \Omega^2\int_x^L (R + x)m\,dx \quad (2)$$

Here x is the axial distance along the beam measured from the root where the beam is attached to the hub, EI is the bending stiffness, m is the mass per unit length along the beam, and L is the length of the beam from root to tip.

The following question often confronts a designer: "Is there a simple way to estimate the change in frequencies due to a small change in hub radius without repeating the lengthy solution of equation (1)?" The first clue to the answer to the question came from Boyce,[2] who considered the specific case of a uniform beam vibrating in a plane perpendicular to the plane of rotation ($\beta = 0$). By assigning various values to the hub radius and by repeated solutions of equation (1), Boyce demonstrated that, as long as the hub radius is small, the bending frequency ω is nearly a linear function of hub radius. In the present paper the problem is approached in a more general manner with fewer restrictions on the system considered.

The Basic Equations

Equation (1) is rewritten in the following nondimensional form:

$$[\overline{EI}V'']'' - \alpha^2[\overline{N}V']' - \gamma^2\overline{m}V = 0 \quad (3)$$

where

$$\overline{N} = \int_{\bar{x}}^1 (\bar{R} + \bar{x})\overline{m}\,d\bar{x} \quad (4)$$

In these equations the following nondimensional notation is used:

$$\begin{aligned} \overline{EI} &= EI/(EI)_0 \\ \overline{m} &= m/m_0 \\ \bar{R} &= R/L \\ \bar{x} &= x/L \end{aligned} \quad (5)$$

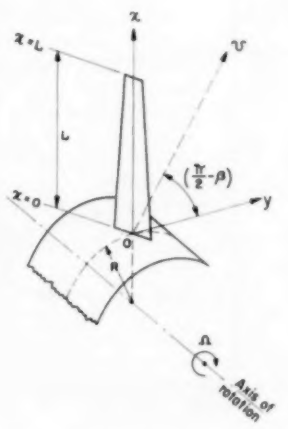

Fig. 1 The system under consideration

[1] The derivation of this equation can be found from the following paper: Hsu Lo and J. L. Renbarger, "Bending Vibrations of a Rotating Beam," Proceedings of the First U. S. National Congress of Applied Mechanics, New York, N. Y., 1952.

[2] W. E. Boyce, "Effect of Hub Radius on the Vibrations of a Uniform Bar," Journal of Applied Mechanics, vol. 23, *Trans. ASME*, vol. 78, 1956, pp. 287–290.

Presented at the West Coast Conference of the Applied Mechanics Division, Pasadena, Calif., June 27–29, 1960, of The American Society of Mechanical Engineers.

Discussion of this paper should be addressed to the Secretary, ASME, 29 West 39th Street, New York, N. Y., and will be accepted until October 10, 1960, for publication at a later date. Discussion received after the closing date will be returned. First draft of manuscript received by ASME Applied Mechanics Division January 13, 1958; final draft received December 29, 1959. Paper No. 60—APMW-5.

$$\alpha^2 = (\Omega^2 m_0 L^4)/(EI)_0$$

$$\gamma^2 = m_0 L^4(\omega^2 + \Omega^2 \sin^2\beta)/(EI)_0 \qquad (5)\ \textit{cont.}$$

where the prime system refers to differentiation with respect to $\bar{x}$ and the subscript 0 refers to quantities at root section ($\bar{x} = 0$). For beams clamped at the root the boundary conditions can be written as:

$$\begin{aligned} &\text{At}\quad \bar{x} = 0, \qquad V = V' = 0 \\ &\text{At}\quad \bar{x} = 1, \qquad V'' = [EIV'']' = 0 \end{aligned} \qquad (6)$$

When there is a small change in the hub radius from R to $R_1 = R + \Delta R$, while all the other conditions are maintained, equations (3) and (4) become

$$[\bar{E}\bar{I}V_1'']'' - \alpha^2[\bar{N}_1 V_1']' - \gamma_1^2 \bar{m} V_1 = 0 \qquad (7)$$

$$\bar{N}_1 = \int_{\bar{x}}^1 (\bar{R}_1 + \bar{x})\bar{m}d\bar{x} \qquad (8)$$

where

$$\bar{R}_1 = \bar{R} + \delta \qquad (9)$$

$$\delta = \Delta R/L \qquad (10)$$

$$\gamma_1^2 = m_0 L^4(\omega_1^2 + \Omega^2 \sin^2\beta)/(EI)_0 \qquad (11)$$

Here ω_1 and V_1 are the new bending frequency and mode corresponding to the new hub radius R_1. The boundary conditions are not affected by the change of the hub radius. They remain the same form as given by equation (6) except V is replaced by V_1.

When equation (3) is multiplied by V_1 and integrated from root to tip, one has

$$\int_0^1 \bar{E}\bar{I}V''V_1''d\bar{x} + \alpha^2 \int_0^1 \bar{N}V'V_1'd\bar{x} - \gamma^2 \int_0^1 \bar{m}VV_1 d\bar{x} = 0 \qquad (12)$$

where the following identities have been used:

$$\int_0^1 V_1[\bar{E}\bar{I}V'']''d\bar{x} = \int_0^1 \bar{E}\bar{I}V''V_1''d\bar{x}$$

$$\int_0^1 V_1[\bar{N}V']'d\bar{x} = \int_0^1 \bar{N}V'V_1'd\bar{x}$$

These identical relations can be verified by integrating by parts and by making use of the boundary conditions. Similarly, when equation (7) is multiplied by V and integrated from root to tip, one has

$$\int_0^1 \bar{E}\bar{I}V''V_1''d\bar{x} + \alpha^2 \int_0^1 \bar{N}_1 V'V_1'd\bar{x} - \gamma_1^2 \int_0^1 \bar{m}VV_1 d\bar{x} = 0 \qquad (13)$$

Subtracting equation (12) from (13) gives

$$\alpha^2 \int_0^1 (\bar{N}_1 - \bar{N})V'V_1'd\bar{x} - (\gamma_1^2 - \gamma^2)\int_0^1 \bar{m}VV_1 d\bar{x} = 0 \qquad (14)$$

Substituting equations (4), (8), (9), and (11) into (14) yields

$$\alpha^2 \delta K_1 - (\gamma_1^2 - \gamma^2)K_2 = 0 \qquad (15)$$

where

$$\begin{aligned} K_1 &= \int_0^1 \left(\int_{\bar{x}}^1 \bar{m}\, d\bar{x}\right) V'V_1'd\bar{x} \\ K_2 &= \int_0^1 \bar{m}\, VV_1 d\bar{x} \end{aligned} \qquad (16)$$

Equation (15) forms the base for the operations which follow.

Perturbation

When the change of the hub radius, ΔR, is small such that $\delta \ll 1$, one may write the new frequency parameter γ_1 in terms of a power series of δ. Thus

$$\gamma_1 = \gamma \sum_{n=0}^{\infty} a_n \delta^n \qquad (17)$$

where the parameters a_n are to be determined by the method of perturbation. Substituting equation (17) into (15) gives

$$\alpha^2 \delta K_1 - \gamma^2 \left[\left(\sum_{n=0}^{\infty} a_n \delta^n\right)^2 - 1\right] K_2 = 0$$

When this equation is expanded into a series with ascending powers of δ, one has

$$\begin{aligned} &\delta^{(0)}\{-\gamma^2(a_0^2 - 1)\} + \delta\{\alpha^2 K_1 - \gamma^2(2a_0a_1)K_2\} \\ &\quad + \delta^2\{-\gamma^2(2a_0a_2 + a_1^2)\}K_2 + \cdots\cdots\cdots = 0 \end{aligned} \qquad (18)$$

By setting the coefficient of the $\delta^{(0)}$-term equal to zero, one obtains

$$a_0 = \pm 1 \qquad (19)$$

The plus sign has to be used in order to satisfy the condition that at $\delta = 0$, $\gamma_1 = \gamma$. By equating the coefficient of δ-term to zero, one has

$$a_1 = \alpha^2 K_1/2\gamma^2 K_2 \qquad (20)$$

If all the terms containing the second and higher powers of δ are neglected, one has the first-order solution

$$\gamma_1 = \gamma(1 + a_1\delta) \qquad (21)$$

This gives a linear relation between the frequency parameter γ_1 and δ, with the slope of the linear relation given as a_1. To calculate a_1 from equation (20), one needs to know the new bending modal shape V_1 which cannot be determined without a repeated solution of the differential equation. An approximate solution for a_1 can be obtained, however, if we concede that, for small changes of the hub radius, the change of the modal shape is small and can be neglected. Furthermore, equation (20) is similar to Rayleigh's formulation and one expects that the error in replacing V_1 by V may be greatly reduced during the integrating process. One may thus obtain an approximate value of a_1 from the following equation

$$a_1 = \frac{\alpha^2}{\gamma^2} \frac{\int_0^1 \left(\int_{\bar{x}}^1 \bar{m}d\bar{x}\right)(V')^2 d\bar{x}}{2\int_0^1 \bar{m}(V)^2 d\bar{x}} \qquad (22)$$

where the right-hand side involves only known parameters.

By substituting equations (5) and (11) into (21) and solving for ω_1, one obtains the relation between the new frequency ω_1 and the parameter δ as shown in the following:

$$\omega_1 = [(\omega^2 + \Omega^2 \sin^2\beta)(1 + a_1\delta)^2 - \Omega^2 \sin^2\beta]^{1/2} \qquad (23)$$

This relation can be linearized by expanding into a series and discarding the higher-order terms of δ. The result is

$$\omega_1 = \omega\left(1 + a_1 \frac{\omega^2 + \Omega^2 \sin^2\beta}{\omega^2}\,\delta\right) \qquad (24$$

For the particular case $\beta = 0$, this is reduced to

$$\omega_1 = \omega(1 + a_1\delta) \qquad (25)$$

which confirms the results previously obtained by Boyce.

Higher-Order Solutions

Higher-order solutions can be obtained by following the same procedure outlined. Setting the coefficient of the δ^n-terms, $n = 0, 1, 2, 3 \ldots$ of equation (18) to zero separately, one obtains the following set of equations:

$$\begin{aligned}
&0 \text{ order} && a_0^2 - 1 = 0 \\
&1\text{st order} && \alpha^2 K_1 - \gamma^2(2a_0a_1)K_2 = 0 \\
&2\text{nd order} && 2a_0a_2 + a_1^2 = 0 \\
&3\text{rd order} && 2a_0a_3 + 2a_1a_2 = 0 \\
&4\text{th order} && 2a_0a_4 + 2a_1a_3 + a_2^2 = 0 \\
&n\text{th order} && \sum_{j=0}^{n} a_j a_{n-j} = 0
\end{aligned} \tag{26}$$

The parameters a_n can be calculated successively from equation (26). The first five parameters are

$$a_0 = 1, \quad a_1 = \alpha^2 K_1/2\gamma^2 K_2, \quad a_2 = -a_1^2/2, \quad a_3 = a_1^3/2, \quad a_4 = -5a_1^4/8$$

It follows that the $\gamma_1 - \delta$ relation can be expressed as:

$$\begin{cases}
\text{1st order:} & \gamma_1 = \gamma(1 + a_1\delta) \\
\text{2nd order:} & \gamma_1 = \gamma(1 + a_1\delta - a_1^2\delta^2/2) \\
\text{3rd order:} & \gamma_1 = \gamma(1 + a_1\delta - a_1^2\delta^2/2 + a_1^3\delta^3/2) \\
\text{4th order:} & \gamma_1 = \gamma(1 + a_1\delta - a_1\delta^2/2 + a_1^3\delta^3/2 - 5a_1^4\delta^4/8)
\end{cases} \tag{27}$$

Convergence

The remaining problem is that of establishing the convergence of the infinite series

$$\gamma_1 = \gamma \sum_{n=0}^{\infty} a_n\delta^n$$

and determining its radius of convergence. This problem can be treated by means of the following considerations: Let

$$g(\delta) = \sum_{n=0}^{\infty} a_n\delta^n$$

Equation (17) becomes

$$\gamma_1 = \beta g(\delta) \tag{28}$$

Substituting this relation into equation (15) gives

$$\alpha^2\delta K_1 - \gamma^2[g^2(\delta) - 1]K_2 = 0$$

whereas

$$g(\delta) = \left(\frac{\alpha^2\delta K_1 + \gamma^2 K_2}{\gamma^2 K_2}\right)^{1/2}$$

When equation (20) is substituted into the preceding equation, the latter becomes

$$g(\delta) = (1 + 2a_1\delta)^{1/2} \tag{29}$$

The infinite series

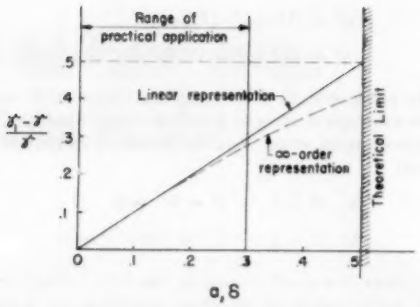

Fig. 2 Comparison between first-order and infinite-order solution

$$\sum_{n=0}^{\infty} a_n\delta^n$$

converges to the sum given by (29). The radius of convergence is

$$|2a_1\delta < 1|$$

or

$$|\delta| < \frac{1}{2a_1} \qquad a_1 > 0 \tag{30}$$

One may also recognize directly from the set of equations (26) that the infinite series

$$\sum_{n=0}^{\infty} a_n\delta^n$$

is the binomial expansion of the expression $(1 + 2a_1\delta)^{1/2}$.

It may be noted here that the process of proving the convergence of the series actually constitutes a direct solution of the problem without using the perturbation method. The presentation of the perturbation method is retained in this paper because of its logical use in obtaining the first-order solution and because of the possibility of its extension to more complicated rotating systems.

Concluding Remarks

It has been proved that, for the system under consideration, a small change ΔR of the hub radius R, other conditions remaining the same, will cause a change $\Delta\gamma$ in the frequency parameter γ, whereas $\Delta\gamma$ is nearly proportional to δ. The constant of proportionality ($a_1\gamma$) can be determined approximately from known parameters by the use of equation (22). The frequency ω_1 itself can also be represented as a linear function of δ. This conclusion is valid for beams with variable EI and m along the beam, and can be shown to be true for a variety of boundary conditions other than the clamped cantilever beam used in this paper. A limitation on δ is given by equation (30).

Higher-order representations of the γ_1-δ relation are also obtained as given by equations (27). Because of the approximation used in equation (23) for the calculation of a_1, the use of higher-order representation is deemed unnecessary. A chart is provided as shown in Fig. 2 to show the comparison between the linear and the infinite-order representation.

Forced Lateral Vibration of a Uniform Cantilever Beam With Internal and External Damping[1]

HO CHONG LEE
Department of Mechanical Engineering, Rensselaer Polytechnic Institute, Troy, N. Y.

The steady-state response problem of a uniform beam with a sinusoidal shaking force at the base is studied for the case where the beam material is the general linear substance represented by a model having an additional spring element in parallel with the Maxwell elements. In the analysis, the stress-strain relationship is applied only to the longitudinal strain of the beam, leaving the shear stress-strain relation to be that of a perfectly elastic material. The exact solution with a numerical example is given for one case where the shear and rotatory inertia effects are neglected. This result is compared with the solution obtained by a tabular method. The results of both methods are in excellent agreement.

THE general linear substance, as designated by Jaeger [2],[2] is represented by models shown in Fig. 1. Models (*a*) and (*b*) are mechanically equivalent [3]. Model (*a*) will be adopted in the following analysis. The stress-strain relationship for this model is given as

$$\sigma + \alpha \frac{d\sigma}{dt} = \beta\epsilon + \gamma \frac{d\epsilon}{dt}$$

where

$$\alpha = \frac{c}{k}$$

$$\beta = E$$

$$\gamma = \frac{E + k}{k} c$$

Let $y(x, t)$ be the lateral displacement of a section of the beam measured positively downward at time t and at the position x

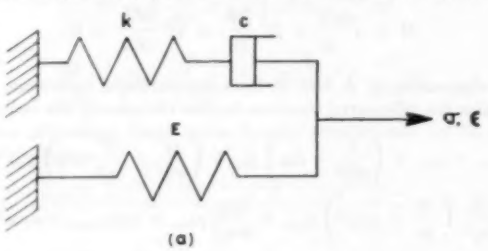

Fig. 1 Models of general linear substance

[1] From a thesis submitted in partial fulfillment of the requirements for the degree of Master of Mechanical Engineering in the Department of Mechanical Engineering, Rensselaer Polytechnic Institute, Troy, New York, May, 1959.

[2] Numbers in brackets designate References at end of paper.

Presented at the Summer Conference of the Applied Mechanics Division, University Park, Pa., June 20–22, 1960, of THE AMERICAN SOCIETY OF MECHANICAL ENGINEERS.

Discussion of this paper should be addressed to the Secretary, ASME, 29 West 39th Street, New York, N. Y., and will be accepted until October 10, 1960, for publication at a later date. Discussion received after the closing date will be returned.

NOTE: Statements and opinions advanced in papers are to be understood as individual expressions of their authors and not those of the Society. Manuscript received by ASME Applied Mechanics Division, May 28, 1959. Paper No. 60—APM-15.

Nomenclature

Y = lateral displacement at any section x, in.
M = bending moment at any section x, in-lb
Q = shearing force at any section x, lb
ρ = mass density of beam (constant), lb-sec^2 in.$^{-4}$
ρ_r = ρ, used to indicate rotatory inertia terms
A = cross-sectional area of beam, sq in.
I = area moment of inertia of beam cross section (constant), (in.^{4})
ψ = angle of tilt of beam cross section, radians
γ' = angle of shear at neutral axis, radians
k' = numerical factor depending on shape of beam cross section, (constant), (dimensionless)
G = shear modulus, psi
η = external damping factor (constant), lb-sec/in.^{2}
ϵ = longitudinal unit strain in beam material, in/in
σ = unit stress, psi
c = internal damping factor (constant), lb-sec/in^2
E = first spring constant, psi
k = second spring constant, psi

(Continued on next page)

which is measured positively to the right along the neutral axis before deformation of the beam. Fig. 2 shows the free-body diagram with such a co-ordinate system. Then, the following equations are obtained from Newton's laws and from "Strength of Materials" as explained by Timoshenko [5],

$$\rho A \frac{\partial^2 y}{\partial t^2} = \frac{\partial Q}{\partial x} - \eta \frac{\partial y}{\partial t} \tag{1}$$

$$\rho_r I \frac{\partial^2 \psi}{\partial t^2} = Q - \frac{\partial M}{\partial x} \tag{2}$$

$$\frac{\partial y}{\partial x} = \psi + \gamma' \tag{3}$$

$$Q = k'\gamma' AG = k'AG\left(\frac{\partial y}{\partial x} - \psi\right) \tag{4}$$

$$\epsilon = -z \frac{\partial \psi}{\partial x} \tag{5}$$

$$M = \int_A \sigma z dA \tag{6}$$

$$\sigma + \alpha \frac{\partial \sigma}{\partial t} = \beta\epsilon + \gamma \frac{\partial \epsilon}{\partial t} \tag{7}$$

The combination of equations (5), (6), and (7) gives

$$M + \alpha \frac{\partial M}{\partial t} + \beta I \frac{\partial \psi}{\partial x} + \gamma I \frac{\partial^2 \psi}{\partial t \partial x} = 0 \tag{8}$$

By eliminating Q, ψ, and M from the foregoing equations, one obtains the differential equation for free vibration of the beam:

$$y_{xxxx} + \kappa_1 y_{tt} + \left(\frac{1}{a^2 b^2} + \kappa_1\kappa_2\right) y_{tt} + \left(\frac{\kappa_2}{a^2 b^2} + \frac{b^2}{a_r^2}\kappa_1\kappa_5\right) y_{tttt} + \frac{\kappa_5}{a_r^2}\left(\frac{1}{a^2} + \kappa_1\kappa_2 b^2\right) y_{tttt} + \frac{\kappa_2\kappa_5}{a^2 a_r^2} y_{tttttt} + \kappa_2\kappa_3 y_{xxxxtt} - \kappa_1\kappa_5 b^2 y_{xxtt} - \left(\frac{1}{a_r^2} + \frac{\kappa_5}{a^2} + \kappa_1\kappa_2\kappa_3\kappa_5 b^2\right) y_{xxtttt} - \frac{\kappa_2}{a_r^2}(1 + \kappa_3\kappa_5) y_{xxtttt} = 0 \tag{9}$$

where subscripts indicate the partial derivatives with respect to the corresponding variables, respectively, and a, b, κ_1, κ_2, κ_3, and κ_5 are constants defined in the Nomenclature. The rotatory inertia terms are also distinguished by subscript r for later use. The same differential equation can be obtained by the variational method (see footnote 1).

For forced vibration, the base of the beam is assumed to be sinusoidally shaken in the following analysis. Two co-ordinate systems, one Newtonian (y, x) and one moving co-ordinate system (Y, x), are used. Let the vertical axis of both co-ordinate systems coincide as shown in Fig. 3. Then the lateral displacement in the Newtonian sense is

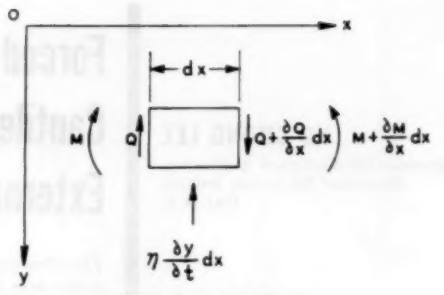

Fig. 2 Free-body diagram

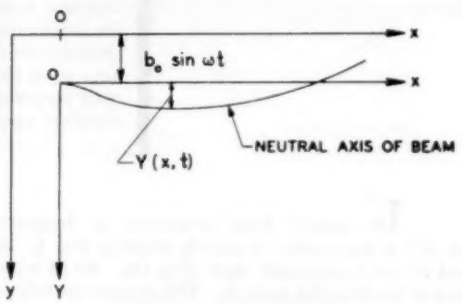

Fig. 3 Co-ordinate systems

$$y(x, t) = Y(x, t) + b_0 \sin \omega t \tag{10}$$

where b_0 is the maximum displacement of the moving co-ordinate system and ω is the phase velocity of the driving force. In the new co-ordinate system, the same procedure as used before can be followed to obtain a differential equation for the forced vibration. This, however, is equivalent to substituting equation (10) into equation (9) which gives

$$Y_{xxxx} + \kappa_1 Y_{tt} + \left(\frac{1}{a^2 b^2} + \kappa_1\kappa_2\right) Y_{tt} + \left(\frac{\kappa_2}{a^2 b^2} + \frac{b^2}{a_r^2}\kappa_1\kappa_5\right) Y_{tttt} + \frac{\kappa_5}{a_r^2}\left(\frac{1}{a^2} + \kappa_1\kappa_2 b^2\right) Y_{tttt} + \frac{\kappa_2\kappa_5}{a^2 a_r^2} Y_{tttttt} + \kappa_2\kappa_3 Y_{xxxxtt} - \kappa_1\kappa_5 b^2 Y_{xxtt} - \left(\frac{1}{a_r^2} + \frac{\kappa_5}{a^2} + \kappa_1\kappa_2\kappa_3\kappa_5 b^2\right) Y_{xxtttt} - \frac{\kappa_2}{a_r^2}(1 + \kappa_3\kappa_5) Y_{xxtttt} = \left[-\kappa_1 + \left(\frac{\kappa_2}{a^2 b^2} + \frac{b^2}{a_r^2}\kappa_1\kappa_5\right)\omega^2 - \frac{\kappa_2\kappa_5}{a^2 a_r^2}\omega^4\right] b_0\omega \cos \omega t + \left[\frac{1}{a^2 b^2} + \kappa_1\kappa_5 - \frac{\kappa_5}{a_r^2}\left(\frac{1}{a^2} + \kappa_1\kappa_2 b^2\right)\omega^2\right] b_0\omega^2 \sin \omega t \tag{11}$$

Nomenclature

z = normal distance from neutral surface to any elemental strip in cross section of beam, in.
L = length of beam (constant), in.
u = spatial distribution of cosine component, in.
v = spatial distribution of sine component, in.
P = cosine component of bending moment, in-lb
T = sine component of bending moment, in-lb
p, q = argument factors for spatial distribution of vibration, in.$^{-1}$
a_0, b_0 = vibration amplitudes of base, in.
ω = phase velocity of driving force, rad/sec
ω_1 = first natural frequency of undamped beam, rad/sec
t = time, sec
i = $\sqrt{-1}$
α = c/k
β = E
γ = $c(k + E)/k$
a^2 = E/ρ
a_r^2 = $E/\rho_r = a^2$
b^2 = I/A
κ_1 = η/EI
κ_2 = c/k
κ_3 = $1 + (k/E)$
κ_4 = k/E
κ_5 = $E/k'G$

The solution of the steady-state response takes the form,

$$Y(x, t) = u(x) \cos \omega t + v(x) \sin \omega t \tag{12}$$

Here $u(x)$ and $v(x)$ are the spatial distributions of the cosine and sine components, respectively, of the motion, and ω is the phase velocity of the driving force. Substituting equation (12) into equation (11) and letting the coefficients of $\cos \omega t$ and $\sin \omega t$ individually be zero, one obtains

$$u^{(4)} + Bu^{(2)} + Cu + Dv^{(4)} + Ev^{(2)} + Fv = -Fb_0 \tag{13}$$

$$-Du^{(4)} - Eu^{(2)} - Fu + v^{(4)} + Bv^{(2)} + Cv = -Cb_0 \tag{14}$$

where parenthesized superscripts indicate the order of derivatives with respect to x, and

$$B = \left(\frac{1}{a_r^2} + \frac{\kappa_5}{a^2} + \kappa_1\kappa_2\kappa_3\kappa_5 b^2\right)\omega^2$$

$$C = -\left(\frac{1}{a^2b^2} + \kappa_1\kappa_2\right)\omega^2 + \frac{\kappa_5}{a_r^2}\left(\frac{1}{a^2} + \kappa_1\kappa_2 b^2\right)\omega^4$$

$$D = \kappa_2\kappa_5\omega$$

$$E = -\kappa_1 b^2\kappa_5\omega + \frac{\kappa_2}{a_r^2}(1 + \kappa_3\kappa_5)\omega^2$$

$$F = \kappa_1\omega - \left(\frac{\kappa_2}{a^2b^2} + \frac{b^2}{a_r^2}\kappa_1\kappa_5\right)\omega^3 + \frac{\kappa_2\kappa_5}{a^2a_r^2}\omega^5$$

After successive differentiation, v can be eliminated from equations (13) and (14), giving

$$P'u^{(8)} + 2Q'u^{(6)} + (2R' + W')u^{(4)} + 2X'u^{(2)} + Z'u = 0 \tag{15}$$

where

$$P' = 1 + D^2,$$
$$Q' = B + DE,$$
$$R' = C + DF,$$
$$W' = B^2 + E^2,$$
$$X' = BC + EF,$$
$$Z' = C^2 + F^2$$

Similarly,

$$P'v^{(8)} + 2Q'v^{(6)} + (2R' + W')v^{(4)} + 2X'v^{(2)} + Z'v = -Z'b_0 \tag{16}$$

Equations (15) and (16) are eighth-order ordinary differential equations. When the numerical values of all the parameters are given, the general solution is obtained by finding eight roots from the characteristic equation which is biquartic since the differential equation contains only even-order derivatives. The general solutions, $u(x)$ and $v(x)$, therefore, will have eight constants each and a total of sixteen arbitrary constants. However, equations (13) and (14) furnish the required relations between the arbitrary constants of $u(x)$ and $v(x)$, so that eight arbitrary constants remain. These eight constants are determined by the use of proper boundary conditions for a specific problem. To demonstrate the procedure, a more detailed solution is given in the following sections for a simpler case without shear and rotatory inertia effects.

Case Without Shear and Rotatory Inertia Effects

For this case $1/a_r^2 = \kappa_5 = 0$, and the differential equation (11) reduces to

$$Y_{xxxx} + \kappa_1 Y_{tt} + \left(\frac{1}{a^2b^2} + \kappa_1\kappa_2\right)Y_{tt} + \frac{\kappa_2}{a^2b^2}Y_{ttt} + \kappa_2\kappa_3 Y_{xxtt} = \left(-\kappa_1 + \frac{\kappa_2}{a^2b^2}\omega^2\right)b_0\omega\cos\omega t + \left(\frac{1}{a^2b^2} + \kappa_1\kappa_2\right)b_0\omega^2\sin\omega t \tag{17}$$

This equation now becomes

$$u^{(4)} - \left(\frac{1}{a^2b^2} + \kappa_1\kappa_2\right)\omega^2 u + \kappa_2\kappa_3\omega v^{(4)} + \left(\kappa_1\omega - \frac{\kappa_2}{a^2b^2}\omega^3\right)v = -\left(\kappa_1\omega - \frac{\kappa_2}{a^2b^2}\omega^3\right)b_0 \tag{18}$$

$$-\kappa_2\kappa_3\omega u^{(4)} - \left(\kappa_1\omega - \frac{\kappa_2}{a^2b^2}\omega^3\right)u + v^{(4)} - \left(\frac{1}{a^2b^2} + \kappa_1\kappa_2\right)\omega^2 v = \left(\frac{1}{a^2b^2} + \kappa_1\kappa_2\right)\omega^2 b_0 \tag{19}$$

$$A'u^{(8)} + 2(B' - C')u^{(4)} + D'u = 0 \tag{20}$$

$$A'v^{(8)} + 2(B' - C')v^{(4)} + D'v = -D'b_0 \tag{21}$$

where

$$A' = 1 + \kappa_2^2\kappa_3^2\omega^2$$
$$B' = \kappa_1\kappa_2\kappa_3\omega^2$$
$$C' = \left(\frac{1}{a^2b^2} + \kappa_1\kappa_3\right)\omega^2 + \frac{\kappa_2^2\kappa_3}{a^2b^2}\omega^4$$
$$D' = \kappa_1^2\omega^2 + \left(\frac{1}{a^4b^4} + \kappa_1^2\kappa_2^2\right)\omega^4 + \frac{\kappa_2^2}{a^4b^4}\omega^6$$

If the differential operator be denoted symbolically by $\mathfrak{D}$, one readily obtains

$$\mathfrak{D}^4 = \frac{-B' + C' \pm [(B' - C')^2 - A'D']^{1/2}}{A'} = \alpha_1 \pm i\beta_1$$

where α_1 and β_1 are found to be

$$\alpha_1 = \frac{\dfrac{1 + \kappa_2^2\kappa_3\omega^2}{a^2b^2} - \kappa_1\kappa_2\kappa_4}{1 + \kappa_2^2\kappa_3^2\omega^2}\omega^2 \tag{22}$$

$$\beta_1 = \frac{\dfrac{\kappa_2\kappa_4}{a^2b^2}\omega^2 + \kappa_1(1 + \kappa_2^2\kappa_3\omega^2)}{1 + \kappa_2^2\kappa_3^2\omega^2}\omega \tag{23}$$

so that

$$\mathfrak{D} = \{\pm(q \pm ip), \quad \pm i(q \pm ip)\}$$

where

$$q = \sqrt{1/2\left[\sqrt[4]{\alpha_1^2 + \beta_1^2} + \sqrt{1/2\,(\sqrt{\alpha_1^2 + \beta_1^2} + \alpha_1)}\right]} \tag{24}$$

$$p = \sqrt{1/2\left[\sqrt[4]{\alpha_1^2 + \beta_1^2} - \sqrt{1/2\,(\sqrt{\alpha_1^2 + \beta_1^2} + \alpha_1)}\right]} \tag{25}$$

Using equations (18), (19), (24), and (25) to obtain the required relations between the arbitrary constants of $u(x)$ and $v(x)$, one finds the general solution to be

$$u(x) = C_1\cosh qx\cos px + C_2\sinh qx\cos px + C_3\sinh qx\sin px + C_4\cosh qx\sin px + C_5\cos qx\cosh px + C_6\sin qx\cosh px + C_7\sin qx\sinh px + C_8\cos qx\sinh px \tag{26}$$

$$v(x) = -C_3 \cosh qx \cos px - C_4 \sinh qx \cos px + C_1 \sinh qx \sin px + C_2 \cosh qx \sin px + C_7 \cos qx \cosh px - C_8 \sin qx \cosh px - C_5 \sin qx \sinh px + C_6 \cos qx \sinh px - b_0 \quad (27)$$

It is interesting to note that equations (26) and (27) can be obtained directly from the solution for the undamped case by the use of complex inertia and modulus. The differential equation and the general solution, respectively, for the undamped vibration are

$$\frac{d^4y}{dx^4} - r^4y = r^4\delta_0 \quad (28)$$

$$y(x) = C_1 \sin rx + C_2 \sinh rx + C_3 \cos rx + C_4 \cosh rx - \delta_0 \quad (29)$$

where $r^4 = \rho A\omega^2/EI$, and δ_0 is the amplitude at the base. The solution for the damped case, equation (12), can be expressed as

$$Y(x, t) = u(x) \cos \omega t + v(x) \sin \omega t = \mathrm{Re}\{\Phi(x)e^{-i\omega t}\}$$

where Re represents the real part and $\Phi(x) = u(x) + iv(x)$. Hence, if a complex solution is assumed, one finds the differential equation to be

$$\frac{d^4\Phi}{dx^4} - (KZ)\Phi = KZ(ib_0) \quad (30)$$

where $KZ = \alpha_1 + i\beta_1$ as given by equations (22) and (23). The comparison of equations (28) and (30) leads to the solution of $r^4 = \alpha_1 + i\beta_1$ which gives

$$r = \{\pm(q + ip); \quad +i(q + ip)\} \quad (31)$$

Therefore one replaces r in equation (29) by the complex roots of equation (31), δ_0 by $a_0 + ib_0$ (here $a_0 = 0$), and the C by complex constants to obtain

$$\Phi(x) = y_1 + y_2 + y_3 + y_4 = u(x) + iv(x)$$

where $u(x)$ and $v(x)$ have the same form as the general solution, equations (26) and (27). Here KZ is the product of the complex inertia and the complex flexibility, equivalent to $\rho A\omega^2/EI$ in the undamped case, and gives the four roots of equation (31). This method, therefore, requires only the determination of the complex flexibility which can be found independently by deriving the moment equation $M = Y_{xx}/Z$ and using the operator $d/dt = -i\omega$. For the general linear substance, the complex flexibility is found to be

$$Z = \frac{1 + \kappa_2^2\kappa_3\omega^2 + i\kappa_2\kappa_4\omega}{EI(1 + \kappa_2^2\kappa_3^2\omega^2)} \quad (32)$$

Since the complex inertia $K = (\rho A\omega^2 + i\eta\omega)$, the product KZ becomes $\alpha_1 + i\beta_1$ which immediately gives the four roots.

If the solution for a cantilever beam is to be obtained, one finds the required boundary conditions to be

$$Y(0, t) = u(0) \cos \omega t + v(0) \sin \omega t = 0 \quad (33)$$

$$\frac{\partial Y(0, t)}{\partial x} = u^{(1)}(0) \cos \omega t + v^{(1)}(0) \sin \omega t = 0 \quad (34)$$

$$M(L, t) = P(L) \cos \omega t + T(L) \sin \omega t = 0 \quad (35)$$

$$Q(L, t) = P^{(1)}(L) \cos \omega t + T^{(1)}(L) \sin \omega t = 0 \quad (36)$$

where P and T are cosine and sine components of the bending moment, respectively. Equations (33) and (34) give

$$C_5 = -C_1, \quad C_7 = C_3 + b_0, \quad C_8 = -C_4 \text{ and } C_6 = -C_2 \quad (37)$$

Substitution of equations (12), (35), and (36) into equation (8), in which $\psi = Y_x$ for this case, gives

$$u^{(2)}(L) + \frac{\kappa_2\kappa_4\omega}{1 + \kappa_2^2\kappa_3\omega^2} v^{(2)}(L) = 0 \quad (38)$$

$$-\frac{\kappa_2\kappa_4\omega}{1 + \kappa_2^2\kappa_3\omega^2} u^{(2)}(L) + v^{(2)}(L) = 0 \quad (39)$$

$$u^{(3)}(L) + \frac{\kappa_2\kappa_4\omega}{1 + \kappa_2^2\kappa_3\omega^2} v^{(3)}(L) = 0 \quad (40)$$

$$-\frac{\kappa_2\kappa_4\omega}{1 + \kappa_2^2\kappa_3\omega^2} u^{(3)}(L) + v^{(3)}(L) = 0 \quad (41)$$

The remaining four constants will be determined from the foregoing equations.

Numerical Example

For the purpose of illustrating the theory, parameters are arbitrarily chosen as follows:

$\rho = 0.733 \times 10^{-3}$ lb-sec^2/in^4; $L = 12$ in.;

$A = {}^1/_2$ in. $\times$ 1 in. $= {}^1/_2$ in.^{2}; $\omega = 360$ rad/sec; $\frac{\omega}{\omega_1} = 0.505$

$E = 30 \times 10^6$ psi; $k = 15 \times 10^6$ psi; $c = 25 \times 10^2$ lb-sec/in^2;

$\eta = 0.05$ lb-sec/in^2; $b_0 = 1$ in.

$I = 0.0104$ in^4; $\frac{1}{a^2b^2} = 1.1724 \times 10^{-8}$;

$\kappa_1 = 1.599 \times 10^{-7}$; $\kappa_2 = 1.6667 \times 10^{-3}$;

$\kappa_3 = 1.5$; $\kappa_4 = 0.5$;

$\alpha_1 = 1.1973633 \times 10^{-4}$; $\beta_1 = 0.741765198 \times 10^{-4}$;

$q = 0.107895$; $p = 0.015057$; $\frac{\kappa_2\kappa_4\omega}{1 + \kappa_2^2\kappa_3\omega^2} = 0.1948$

Equations (38) to (41) with equations (26), (27), and (37) give the following simultaneous equations:

$$2.645863C_1 + 3.136476C_2 + 0.381374C_3 + 0.754939C_4 = 0.182013$$

$$0.381374C_1 + 0.754939C_2 - 2.645863C_3 - 3.136476C_4 = 0.351706$$

$$0.789310C_1 + 2.797340C_2 + 0.588840C_3 + 0.809870C_4 = 0.34897$$

$$0.588840C_1 + 0.809870C_2 - 0.789310C_3 - 2.797340C_4 = -1.24057$$

from which one obtains

$C_1 = -0.20969391$; $C_2 = 0.17854227$; $C_3 = -0.97198960$; $C_4 = 0.72529153$

With the foregoing constants known, $u(x)$, $v(x)$, $P(x)$, $T(x)$, $P^{(1)}(x)$, and $T^{(1)}(x)$ are calculated and plotted in Figs. 4 and 5. In Fig. 5, these values for the undamped case, where $u = P = P^{(1)} = 0$, are plotted for comparison.

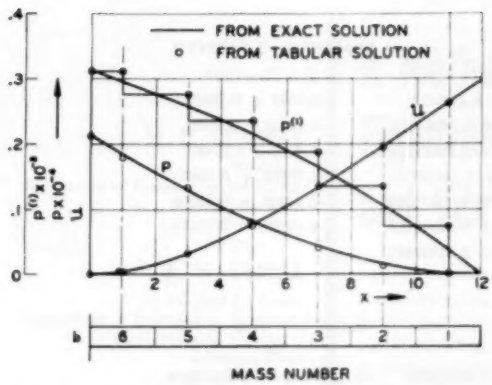

Fig. 4 Displacement, moment, and shear distribution of cosine component

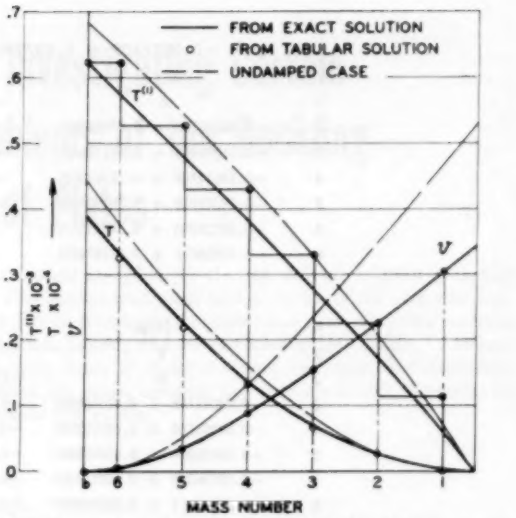

Fig. 5 Displacement, moment, and shear distribution of sine component

Tabular Method. The foregoing exact solution was checked with the tabular method, developed by Myklestad [4]. In his scheme $m_{n+1}\omega^2$ is replaced by

$$(m_{n+1}\omega^2 + i\omega\kappa'_{n+1}),$$

where

$$\kappa'_{n+1} = \eta \cdot l_{n+1},$$

and y_{n+1} is replaced by

$$(y_{n+1} + a_0 + ib_0),$$

where $a_0 + ib_0$ describes the motion of the base of a beam. Instead of the flexibility $1/EI$, one has to find the complex flexibility Z, which for the general linear substance is

$$Z = \frac{(1 + \kappa_2{}^2\kappa_3\omega^2) + i\kappa_3\kappa_4\omega}{EI(1 + \kappa_3{}^2\kappa_3{}^2\omega^2)}$$

The parameters of the previous section were adapted to the tabular method by dividing the length of the beam into six equal intervals. Then following Myklestad's notations, one finds in addition to the quantities given in previous sections,

$$l_1 = l_2 = \ldots = l_5 = 2 \text{ in.}; \; l_6 = 1 \text{ in.}$$

$$m_n = 0.733 \times 10^{-3} \text{ lb sec}^2/\text{in}$$

$$m_n\omega^2 = 95 \text{ lb/in}, \quad n = 1, 2, \ldots . 6$$

$$\omega\kappa_n{}' = \omega\eta l_n = 36 \text{ lb/in}, \quad n = 1, 2, \ldots . 6$$

$$Z = (2.72178 + 0.530217i)10^{-6}$$

$$V_{M_n} = Zl_n = (5.44356 + 1.060434i)10^{-6}, \quad n = 1, 2, \ldots . 5$$

$$V_{M_6} = Zl_6 = (2.712178 + 0.53217i)10^{-6}$$

Table 1

n	1 $\frac{m\omega^2 + i\omega K'}{10^6}$	2 $g_\phi = (2) + I(3) + U_M(4) + U_P(5)$ for $(n-1)$	3 $h_\phi = (3) + V_M(4) + V_P(5)$ for $(n-1)$	4 $H_\phi \times 10^{-6} = (4) + I(5)$ for $(n-1)$	5 $G_\phi \times 10^{-6} = (5)_{n-1} + (1)(2)$
1	0.000095 + 0.000036i	0	1	0	0
2	0.000095 + 0.000036I	2	1	0	0.0001900 + 0.00007200i
3	0.000095 + 0.000036i	4.00063862 + 0.00039561i	1.00095793 + 0.00059342i	0.0003800 + 0.00014400i	0.00057005 + 0.00021606i
4	0.000095 + 0.000036i	6.00638630 + 0.00395638i	1.00574774 + 0.00356089i	0.00152009 + 0.00057612i	0.00114051 + 0.00043267i
5	0.000095 + 0.000036i	8.02937864 + 0.01820271i	1.01916115 + 0.01187367i	0.00380114 + 0.00144145i	0.00190265 + 0.00072345i
6	0.000095 + 0.000036i	10.09325729 + 0.05779804i	1.04791418 + 0.02970691i	0.00760641 + 0.00288836i	0.00285943 + 0.00109230i
b	0.000000 + 0.00000	11.15195782 + 0.09420040i	1.07068747 + 0.04384600i	0.01046583 + 0.00398066i	0.00285943 + 0.00109230i

n	6 $g = (6) + I(7) + U_M(8) + U_P(9)$ for $(n-1)$	7 $h = (7) + V_M(8) + V_P(9)$ for $(n-1)$	8 $H \times 10^{-6} = (8) + I(9)$ for $(n-1)$	9 $G \times 10^{-6} = (9)_{n-1} + (1)[(6) + a_0 + b_0 i]$
1	y_1	0	0	$(0.00009500 + 0.00003600i)y_1$ $-0.00003600 + 0.00009500i$
2	$(1.00031931 + 0.00019781i)y_1$ $- 0.00019781 + 0.00031931i$	$(0.00047896 + 0.00029671i)y_1$ $- 0.00029671 + 0.00047896i$	$(0.00019000 + 0.00007200i)y_1$ $- 0.00007200 + 0.00019000i$	$(0.00019002 + 0.00007203i)y_1$ $-0.00007203 + 0.00019002i$
3	$(1.00287384 + 0.00178038i)y_1$ $- 0.00178038 + 0.00287384i$	$(0.00239491 + 0.00148373i)y_1$ $- 0.001483735 + 0.00239491i$	$(0.00057005 + 0.00021606i)y_1$ $- 0.00021606 + 0.00057005i$	$(0.00028523 + 0.00010830i)y_1$ $- 0.00010830 + 0.00028523i$
4	$(1.01149617 + 0.00712317i)y_1$ $- 0.00712317 + 0.1149617i$	$(0.00670670 + 0.00415639i)y_1$ $- 0.00415639 + 0.00670670i$	$(0.00114051 + 0.00043267i)y_1$ $-0.00043267 + 0.00114051i$	$(0.00038107 + 0.00014539i)y_1$ $-0.00014539 + 0.00038107i$
5	$(1.03193933 + 0.01979766i)y_1$ $- 0.01979766 + 0.03193933i$	$(0.01437651 + 0.00891662i)y_1$ $-0.00891662 + 0.01437651i$	$(0.00190265 + 0.00072345i)y_1$ $- 0.00072345 + 0.00190265i$	$(0.00047839 + 0.00018442i)y_1$ $-0.00018442 + 0.00047839i$
6	$(1.07188806 + 0.04459418i)y_1$ $- 0.04459418 + 0.07188806i$	$(0.02637508 + 0.01638363i)y_1$ $-0.01638363 + 0.02637508i$	$(0.00285942 + 0.00109230i)y_1$ $- 0.00109230 + 0.00285942i$	$(0.00057861 + 0.00022725i)y_1$ $-0.00022725 + 0.00057861i$
b	$(1.10210733 + 0.06337658i)y_1$ $- 0.06337658 + 0.10210733i$	$(0.03430583 + 0.02133540i)y_1$ $-0.02133540 + 0.03430583i$	$(0.00343804 + 0.00131955i)y_1$ $- 0.00131955 + 0.00343804i$	$(0.00057861 + 0.00022725i)y_1$ $-0.00022725 + 0.00057861i$

Table 2

$\phi = -0.0327309 + 0.0379268i$ $\quad y_1 = -0.2594949 + 0.3032494i$

n	(2)	(6)	$y = (6) - (2)\phi$
1	0	−0.1688296 + 0.2740212i	−0.2595 + 0.30325i
2	−0.06546180 + 0.07585360i	−0.25983322 + 0.30361624i	−0.19437 + 0.2278i
3	−0.13095950 + 0.15171847i	−0.26256092 + 0.30654174i	−0.1316 + 0.1548i
4	−0.19674448 + 0.22767352i	−0.27176136 + 0.31638335i	−0.07502 + 0.0887i
5	−0.26349916 + 0.30393285i	−0.29358429 + 0.33973692i	−0.03008 + 0.03580i
6	−0.33255350 + 0.38091317i	−0.33626682 + 0.38536551i	−0.00371 + 0.00445i
b	−0.36858634 + 0.41987481i	−0.36858672 + 0.41987481i	0

Table 3

n	$(4)\phi$	(8)	$M_n(10^{-6}) = (4)\phi - (8)$
1	0	0	0
2	0	−0.00014313 + 0.00022894i	−0.00014313 − 0.00022894i
3	−0.00001789 + 0.00000970i	−0.00042951 + 0.00068685i	−0.00041162 − 0.00067715i
4	−0.00007160 + 0.00003879i	−0.00085990 + 0.00137409i	−0.00078830 − 0.00133530i
5	−0.00010934 + 0.00009698i	−0.00143657 + 0.00229190i	−0.00132723 − 0.00219492i
6	−0.00036029 + 0.00019600i	−0.00216554 + 0.00344309i	−0.00180525 − 0.00324709i
b	−0.00049353 + 0.00026665i	−0.00261185 + 0.00413820i	−0.00211832 − 0.00387155i

Table 4

n	$(5)\phi$	(9)	$S(10^{-6}) = (9) - (5)\phi$
1	0	−0.00007157 + 0.00011447i	−0.00007157 + 0.00011447i
2	−0.00000895 + 0.00000485i	−0.00014318 + 0.00022895i	−0.00013423 + 0.00022410i
3	−0.00002685 + 0.00001455i	−0.00021516 + 0.00034363i	−0.00018831 + 0.00032908i
4	−0.00005374 + 0.00002910i	−0.00028837 + 0.00045890i	−0.00023463 + 0.00042980i
5	−0.00008972 + 0.00004848i	−0.00036449 + 0.00057560i	−0.00027477 + 0.00052712i
6	−0.00013502 + 0.00007270i	−0.00044631 + 0.00069510i	−0.00031129 + 0.00062240i
b	−0.00013502 + 0.00007270i	−0.00044631 + 0.00069510i	−0.00031129 + 0.00062240i

$$V_{Fn} = U_{Mn} = \frac{Zl_n^2}{2} = (5.44356 + 1.060434i)10^{-6}, \quad n = 1, 2, \ldots . 5$$

$$V_{Fb} = U_{Mb} = \frac{Zl_b^2}{2} = (1.36089 + 0.265109i)10^{-6}$$

$$U_{Fn} = \frac{Zl_n^3}{6} = (3.62904 + 0.706956i)10^{-6}, \quad n = 1, 2, \ldots . 5$$

$$U_{Fb} = \frac{Zl_b^3}{6} = (0.45363 + 0.088369i)10^{-6}$$

Initial values at the free end of the beam are given as:

$$g_{\phi_1} = H_{\phi_1} = G_{\phi_1} = h_1 = H_1 = 0; \quad h_{\phi_1} = 1; \quad g_1 = y_1$$

$$G_1 = (m_1\omega^2 + i\omega\kappa_1')(y_1 + ib_0)$$

The first calculation appears in Table 1. At the base $\alpha_b = y_b = 0$, which gives

$$\phi = \frac{h_b}{h_{\phi b}} = \frac{g_b}{g_{\phi b}}$$

so that

$$y_1 = -0.259495 + 0.303249i$$

$$\phi = -0.032731 + 0.037927i$$

These initial values make it possible to complete the table. The complete solution appears in Tables 2, 3, and 4 and the results are plotted in Figs. 4 and 5 for comparison with the results obtained from the exact solution.

Acknowledgment

The author wishes to express his thanks to Prof. K. E. Bisshopp, Head of the Mechanical Engineering Department, Rensselaer Polytechnic Institute, for suggesting the problem and indicating methods for obtaining the solutions.

References

1 K. E. Bisshopp, "Forced Torsional Vibration of Systems With Distributed Mass and Internal and External Damping," JOURNAL OF APPLIED MECHANICS, vol. 26, TRANS. ASME, series E, vol. 81, 1959, pp. 8–12.

2 J. C. Jaeger, "Elasticity, Fracture and Flow," John Wiley & Sons, Inc., New York, N. Y., 1956.

3 H. Kolsky, "Stress Waves in Solids," Oxford University Press, London, England, 1953.

4 N. O. Myklestad, "Fundamentals of Vibration Analysis," McGraw-Hill Book Company, Inc., New York, N. Y., 1956.

5 S. Timoshenko, "Vibration Problems in Engineering," Third Edition, D. Van Nostrand Company, Inc., New York, N. Y., 1955.

Supplementary References

6 H. Holzer, "Biegungschwingungen mit Berücksichtingung der Stabmasse und der äusseren und inneren Dämpfung," *Zeitschrift für angewandte Mathematik und Mechanik*, vol. 8, 1928, pp. 272–283.

7 K. Muto, "Biegungschwingungen mit Berücksichtigung der Stabmasse und der äusseren und inneren Dämpfung," *Zeitschrift für angewandte Mathematik und Mechanik*, vol. 10, 1930, pp. 346–353.

8 N. O. Myklestad, "The Concept of Complex Damping," JOURNAL OF APPLIED MECHANICS, vol. 19, TRANS. ASME, vol. 74, 1952, pp. 284–286.

9 N. O. Myklestad, "Analysis of Forced Vibration of Beams," JOURNAL OF APPLIED MECHANICS, vol. 20, TRANS. ASME, vol. 75, 1953, pp. 53–56.

10 K. Suyehiro, "Damped Transversal Vibration of Prismatic Bars," Earthquake Research Institute, Bulletin No. 6, March, 1929, pp. 63–70.

A Method for Investigating Certain Eigenvalue Problems of the Buckling and Vibration of Plates

H. D. CONWAY
Professor,
Department of Engineering Mechanics,
Cornell University,
Ithaca, N. Y.

A. W. LEISSA
Assistant Professor,
Department of Engineering Mechanics,
The Ohio State University,
Columbus, Ohio
Assoc. Mem. ASME

In a recent investigation,[1] a method was given for the approximate solution of certain boundary-value problems. This method lends itself well to the use of the electronic digital computer and is extended here to investigate the eigenvalue problems of the buckling under two-dimensional hydrostatic loading and the vibration of thin plates. The two-dimensional hydrostatic buckling loads of clamped square and equilateral-triangular plates are found by this method, the values agreeing well with the results obtainable by other methods where these results are known.

When solving boundary-value problems, a series solution to the differential equation may be written, but it is frequently impossible to meet the required conditions at all points on the boundary. To overcome this difficulty, the boundary conditions may be met only at discrete points, retaining sufficient terms in the series solution to meet the conditions at these points. The greater the number of points chosen, the greater in general will be the accuracy of the results, and the value of the electronic digital computer in solving the resulting simultaneous equations is immediately apparent.

The foregoing approach has been successful in the approximate solution of a number of boundary-value problems,[1] and will be extended here to the solution of certain eigenvalue problems of plates. It will be illustrated by the problem of the buckling of clamped plates in a state of two-dimensional hydrostatic stress. Application of the boundary conditions then leads to a determinant, the roots of which give the buckling load. The method for investigating the vibrations of plates also will be indicated.

Analysis

From the small-deflection theory of plates, the Lagrange differential equation to be solved is, with the usual notation

$$D\nabla^4 w = q. \tag{1}$$

For a plate in a state of two-dimensional uniform compressive stress P/h acting in its plane where h is the plate thickness, we write $q = -P\nabla^2 w$ for buckling and obtain

$$\nabla^2(\nabla^2 + k^2)w = 0, \quad k^2 = P/D. \tag{2}$$

Considering solutions in the polar co-ordinate form $w = F(r)\cos n\theta$ the differential equation in $F(r)$ is obtained yielding the solution

$$w = \sum_{n=0}^{\infty} [A_n J_n(kr) + B_n Y_n(kr) + C_n(kr)^n + D_n(kr)^{-n}] \cos n\theta, \tag{3}$$

where J_n and Y_n are Bessel functions of the first and second kinds, respectively.

This is the equation commonly used for the analysis of the buckling loads of a circular plate in its various modes with nodal circles and diameters. However, it will be utilized here for obtaining the buckling loads of clamped plates having arbitrary boundaries. It will first be illustrated by the problem of the clamped square plate because this is relatively simple, has been the subject of a considerable number of investigations, and close bounds on the value of the buckling load P are well known. It therefore provides a good example for testing the present method.

Fig. 1 shows the clamped square of side $2a$ together with the loading and co-ordinate system adopted. Because of the axes of symmetry of the plate, the values of the integers n in equation (3) must be multiples of four. Retaining only six terms in equation (3), and omitting $Y_n(kr)$ and $(kr)^{-n}$, because they become singular at the center of a solid plate, we write with a slight change of notation,

$$w = AJ_0(kr) + B + CJ_4(kr)\cos 4\theta + D(kr)^4 \cos 4\theta + EJ_8(kr)\cos 8\theta + F(kr)^8 \cos 8\theta \tag{4}$$

The boundary conditions of zero deflection and radial slope are

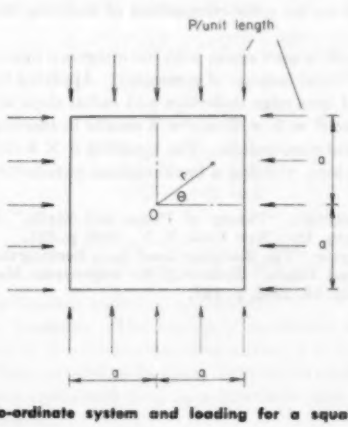

Fig. 1 Co-ordinate system and loading for a square plate

[1] H. D. Conway, "The Approximate Solution of Certain Boundary-Value Problems," accepted for publication in the JOURNAL OF APPLIED MECHANICS. See also J. Barta, "Über die näherungsweise Lösung einiger zweidimensionaler Elastizitätsaufgaben," *ZAMM*, vol. 17, 1937, p. 184.

Presented at the Summer Conference of the Applied Mechanics Division, University Park, Pa., June 20–22, 1960, of THE AMERICAN SOCIETY OF MECHANICAL ENGINEERS.

Discussion of this paper should be addressed to the Secretary, ASME, 29 West 39th Street, New York, N. Y., and will be accepted until October 10, 1960, for publication at a later date. Discussion received after the closing date will be returned. Manuscript received by ASME Applied Mechanics Division, August 18, 1959. Paper No. 60—APM-25.

satisfied along the clamped edges, the particular edge points being chosen at $\theta = 0$, $\pi/8$ and $\pi/4$ for their obvious simplification of equation (4). By symmetry, this results in meeting these conditions at a total of 16 points around the boundary. Substituting the six boundary conditions into equation (4) yields the following set of homogeneous equations, written in matrix form as

$$\begin{bmatrix} J_0(ka) & 1 & J_4(ka) & (ka)^4 & J_8(ka) & (ka)^8 \\ J_0'(ka) & 0 & J_4'(ka) & 4(ka)^3 & J_8'(ka) & 8(ka)^7 \\ J_0(ka\sec\pi/8) & 1 & 0 & 0 & -J_8(ka\sec\pi/8) & -(ka\sec\pi/8)^8 \\ J_0'(ka\sec\pi/8) & 0 & 0 & 0 & -J_8'(ka\sec\pi/8) & -(8ka)^7(\sec\pi/8)^8 \\ J_0(\sqrt{2}\,ka) & 1 & -J_4(\sqrt{2}\,ka) & -4(ka)^4 & J_8(\sqrt{2}\,ka) & 16(ka)^8 \\ J_0'(\sqrt{2}\,ka) & 0 & -J_4'(\sqrt{2}\,ka) & -16(ka)^3 & J_8'(\sqrt{2}\,ka) & 128(ka)^7 \end{bmatrix} \begin{bmatrix} A \\ B \\ C \\ D \\ E \\ F \end{bmatrix} = \begin{bmatrix} 0 \\ 0 \\ 0 \\ 0 \\ 0 \\ 0 \end{bmatrix} \tag{5}$$

where the primes indicate differentiation with respect to the argument, kr.

For a nontrivial solution of equations (5), the determinant for the coefficient matrix is set equal to zero, and roots of ka must be determined to give the desired nullity. The implicit form requires an iterative type of solution to converge to the answer. By desk calculator, this is a laborious process, but use of the IBM 704 digital computer only requires approximately 16 millisec per iteration.

The result obtained for this example is a value of the buckling-load parameter ka equal to 3.622. This compares favorably with the corresponding upper bound of 3.626 reported by Timoshenko[2] using a Rayleigh-Ritz method and the lower bound of 3.616 obtained by Taylor.[3]

It is of interest to examine also the result obtained by meeting the boundary conditions of the plate only at its mid-points and corners. This is obtained by considering the first four terms of equation (4), which results in deleting the third and fourth rows and fifth and sixth columns of the coefficient matrix in equation (5). The value of the buckling-load parameter ka obtained in this case is 3.69, which represents a deviation of only approximately 2 per cent from the foregoing results.

As a further example, the corresponding problem of the buckling of a clamped equilateral triangular plate will be considered. This problem is chosen partly because, to the authors' knowledge, no solution for it has thus far been presented. In particular, the equilateral triangle shown in Fig. 2 of side $\sqrt{6}\,a$ is chosen, for it is circumscribed by the same circle as the square of side $2a$ and therefore allows for some comparison of buckling loads between the two.

Equation (3) is used again, with the integers n now appearing as multiples of three because of symmetry. Applying the boundary conditions of zero edge deflection and radial slope at points corresponding to $\theta = 0$, $\pi/6$, and $\pi/3$ results in meeting the conditions at 12 external points. The resulting 6×6 determinant is set equal to zero, yielding a buckling-load parameter ka, of 5.08. Similarly, meeting the conditions at only the six corner and edge mid-points results in a value of 4.90.

It is interesting to note that reducing the number of boundary points gives different effects in the two examples. In the case of the triangle, the removal of the quarter points resulted in a lower buckling load; however, for the square it increased the value.

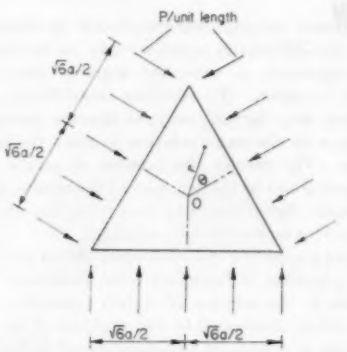

Fig. 2 Co-ordinate system and loading for an equilateral-triangular plate

It can be seen that the foregoing method of analysis represents a powerful tool for obtaining buckling loads of plates of arbitrary shape under this loading, particularly when high-speed computational equipment is available. A similar procedure may be used to determine the vibration modes and frequencies for plates of arbitrary shape, by satisfying the differential equation of motion exactly and applying the desired boundary conditions at discrete edge points. For this problem, the solution of the differential equation for a solid plate is

$$F = \sum_{n=0}^{\infty} [A_n J_n(kr) + B_n I_n(kr)] \cos n\theta \tag{6}$$

where the deflections are given by

$$w = F(r, \theta)e^{i\omega t}, \qquad k^4 = \omega^2 \rho h/D.$$

where ρ is the density and ω the circular frequency.

Acknowledgment

The paper was written during the tenure of a visiting professorship by one of the authors (H. D. Conway), at the Ohio State University, and his sincere thanks are expressed for the opportunity thus afforded.

[2] S. Timoshenko, "Theory of Plates and Shells," McGraw-Hill Book Company, Inc., New York, N. Y., 1940, p. 321.

[3] G. I. Taylor, "The Buckling Load for a Rectangular Plate With Four Clamped Edges," *Zeitschrift für angewandte Mathematik und Mechanik*, vol. 13, 1933, p. 147.

Dynamical Response of an Elastic Half-Space to Tangential Surface Loadings[1]

CHI-CHANG CHAO[2]
Assistant Professor,
Department of Aeronautical Engineering,
Stanford University,
Stanford, Calif.

Exact and closed-form solutions are obtained for both tangential and vertical surface displacements of a homogeneous isotropic elastic half-space due to the application, at a point on the surface, of a concentrated force tangential to the plane boundary and varying with time as the Heaviside unit function. Similar expressions for the displacements in the interior of the body along a line directly below the applied force are derived. Solutions are obtained by a semi-inverse method with the aid of Laplace and Hankel transforms. The reciprocal relation in the static case, between tangential displacement due to a vertical force and vertical displacement due to a tangential force, is preserved in the dynamic case.

THE dynamic response of an elastic half-space under the action of a time-dependent concentrated force has attracted the interest of many applied scientists [1].[3] Owing to the complexities of the mathematics involved, all of the literature concerning this kind of problem has been confined to axial symmetrical or two-dimensional cases, where the concentrated force is acting perpendicular to its plane boundary (or a line source acts on it).

The present investigation considers the response of an elastic half-space to tangential surface loadings, and therefore cannot use the simplifications which accompany axial symmetry. In this paper, surface displacements and displacements directly below the applied force, which varies with time as the Heaviside unit function, are obtained in closed form with the aid of integral transform techniques and a semi-inverse method.

Formulation of the Boundary-Value Problem

Governing Differential Equations. For an isotropic elastic body, the displacement $\mathbf{u}$, in the absence of prescribed body forces, satisfies the equation:

$$(\lambda + \mu)\nabla\nabla\cdot\mathbf{u} + \mu\nabla^2\mathbf{u} - \rho\ddot{\mathbf{u}} = 0 \tag{1}$$

where $\dot{\mathbf{u}} = \partial\mathbf{u}/\partial t$, λ and μ are Lamb's elastic moduli, and ρ is the mass density of the body. The stress tensor $\mathbf{d}$ is related to the displacement by:

$$\mathbf{d} = \lambda\nabla\cdot\mathbf{u}\mathbf{I} + \mu(\nabla\mathbf{u} + \mathbf{u}\nabla) \tag{2}$$

The vector $\mathbf{u}$ can be expressed in terms of a dilatational scalar potential φ and an equivoluminal vector potential $\mathbf{g}$ according to

$$\mathbf{u} = \nabla\varphi + \Delta\times\mathbf{g} \tag{3}$$

with

$$\nabla\cdot\mathbf{g} = 0 \tag{4}$$

Then equation (1) will be satisfied if φ and $\mathbf{g}$ are solutions of the following set of wave equations

$$a^2\nabla^2\varphi - \ddot{\varphi} = 0 \tag{5}$$

$$b^2\nabla^2\mathbf{g} - \ddot{\mathbf{g}} = 0 \tag{6}$$

where

$$a^2 = (\lambda + 2\mu)/\rho;\ b^2 = \mu/\rho \tag{6a}$$

Let

$$\Phi = L[\varphi] = \int_0^\infty e^{-pt}\varphi dt,\quad G = L[\mathbf{g}],$$
$$\mathbf{U} = L[\mathbf{u}]\quad\text{and}\quad \Sigma = L(\mathbf{d})$$

denote the Laplace transforms of φ, $\mathbf{g}$, $\mathbf{u}$ and $\mathbf{d}$, respectively. Then, if the medium is initially at rest, the Laplace transforms of equations (2), (3), (4), (5), and (6) are

$$\Sigma = \lambda\nabla\cdot\mathbf{U}\mathbf{I} + \mu(\nabla\mathbf{U} + \mathbf{U}\nabla) \tag{7}$$

$$\mathbf{U} = \nabla\Phi + \nabla\times\mathbf{G} \tag{8}$$

$$\nabla\cdot\mathbf{G} = 0 \tag{9}$$

$$\nabla^2\Phi - h^2\Phi = 0 \tag{10}$$

$$\nabla^2\mathbf{G} - k^2\mathbf{G} = 0 \tag{11}$$

where

$$h = p/a,\qquad k = p/b \tag{11a}$$

and p is the Laplace transform parameter.

Boundary Conditions. The boundary conditions on the elastic half-space $z \geq 0$ with traction-free surface $z = 0$, when a concentrated force parallel to its plane boundary is applied inside the medium and varies with time as a Heaviside unit function, will now be taken up.

---

[1] The results presented in this paper are based on a dissertation submitted in partial fulfillment of the requirements for the degree of Doctor of Philosophy, in the Faculty of Pure Science, Columbia University. The investigation was sponsored by the Office of Naval Research. The author is indebted to Prof. Bruno A. Boley, his thesis adviser, for the criticism and advice received.

[2] Formerly Research Assistant, Institute of Flight Structure, Columbia University, New York, N. Y.

[3] Numbers in brackets designate References at end of paper. Reference [1] contains a detailed review of the literature.

Presented at the Summer Conference of the Applied Mechanics Division, University Park, Pa., June 20–22, 1960, of THE AMERICAN SOCIETY OF MECHANICAL ENGINEERS.

Discussion of this paper should be addressed to the Secretary, ASME, 29 West 39th Street, New York, N. Y., and will be accepted until October 10, 1960, for publication at a later date. Discussion received after the closing date will be returned. Manuscript received by ASME Applied Mechanics Division, June 17, 1958; final draft received, August 18, 1959. Paper No. 60—APM-29.

Consider an infinite elastic medium, initially at rest acted upon by a concentrated force at $(0, \theta_0, C)$, parallel to the x-axis ($\theta = 0$), of magnitude F and varying with time as a Heaviside unit function. The displacements, denoted here as $\mathbf{U}_{01}$, can be easily obtained from the Stokes-Love solution for the infinite medium [2, 3, 4]. The Laplace transforms of the displacement components given by that solution in cylindrical co-ordinate system are:

$$U_{01r} = \frac{F\cos\theta}{4\pi\rho p^2}\left[\frac{\partial^2}{\partial r^2}\left(\frac{e^{-hR_1} - e^{-kR_1}}{R_1}\right) + k^2\frac{e^{-kR_1}}{R_1}\right]$$

$$U_{01\theta} = -\frac{F\sin\theta}{4\pi\rho p^2}\left[\frac{1}{r}\frac{\partial}{\partial r}\left(\frac{e^{-hR_1} - e^{-kR_1}}{R_1}\right) + k^2\frac{e^{-kR_1}}{R_1}\right] \quad (12)$$

$$U_{01z} = \frac{F\cos\theta}{4\pi\rho p^2}\frac{\partial^2}{\partial r\,\partial z}\left(\frac{e^{-hR_1} - e^{-kR_1}}{R_1}\right)$$

where

$$R_1 = r^2 + (z - c)^2 \quad (12a)$$

If now a force equal but opposite to the foregoing acts at $(0, \theta_0, -c)$, then the response of the medium to this force will be denoted by

$$\mathbf{U}_{02} = -\mathbf{U}_{01}(0, \theta_0, -c;\ r, \theta, z, p) \quad (12b)$$

The Laplace transforms of the tractions on the plane $z = 0$ caused by these two forces are easily found to be

$$\Sigma_{zr} = -\frac{\mu F\cos\theta}{2\pi\rho p^2}\frac{\partial}{\partial c}\left[2\frac{\partial^2}{\partial r^2}\left(\frac{e^{-hR} - e^{-kR}}{R} + k^2\frac{e^{-kR}}{R}\right)\right]$$

$$\Sigma_{z\theta} = \frac{\mu F\sin\theta}{2\pi\rho p^2}\frac{\partial}{\partial r}\left[\frac{2}{r}\frac{\partial}{\partial c}\left(\frac{e^{-hR} - e^{-kR}}{R}\right) + k^2\frac{e^{-kR}}{R}\right] \quad (13)$$

$$\Sigma_{zz} = 0$$

where

$$R^2 = r^2 + c^2 \quad (13a)$$

If $\mathbf{U}$ is a displacement function for the medium $z > 0$ which produces equal and opposite tractions to those of equation (13) on the $z = 0$ plane, then $\mathbf{U}_{01} + \mathbf{U}_{02} + \mathbf{U}$ will be the displacements of an elastic half-space with traction-free boundaries and acted upon by a concentrated force of magnitude F at $(0, \theta_0, c)$, parallel to its plane boundary and varying with time as Heaviside unit function. It is therefore the Laplace transform of the desired solution.

Since $\mathbf{U}_{01}$ and $\mathbf{U}_{02}$ are known from equation (12) it is now necessary to determine $\mathbf{U}$ to complete the solution. In other words, we are seeking the solutions to equations (9), (10) and (11) under boundary conditions which, from equations (7), (8) and (13), assume the following form:

$$\mu\left[2\frac{\partial^2\Phi}{\partial r\,\partial z} + \frac{\partial^2 G_\theta}{\partial r^2} + \frac{1}{r}\frac{\partial G_\theta}{\partial r} - \frac{G_\theta}{r^2} - \frac{\partial^2 G_\theta}{\partial z^2} + \frac{\partial}{\partial\theta}\left(\frac{1}{r}\frac{\partial G_z}{\partial z} - \frac{1}{r}\frac{\partial G_r}{\partial r} + \frac{G_r}{r^2}\right)\right]_{z=0}$$

$$= \frac{F\mu}{\pi\rho p^2}\cos\theta\frac{\partial}{\partial c}\left[\frac{\partial^2}{\partial r^2}\left(\frac{e^{-hR} - e^{-kR}}{R}\right) + \frac{k^2}{2}\frac{e^{-kR}}{R}\right] \quad (14)$$

$$\mu\left[\frac{\partial^2 G_r}{\partial z^2} - \frac{1}{r^2}\frac{\partial^2 G_r}{\partial\theta^2} - \frac{\partial^2 G_z}{\partial r\,\partial z} + \frac{\partial}{\partial\theta}\left(\frac{2}{r}\frac{\partial\Phi}{\partial z} + \frac{1}{r}\frac{\partial G_\theta}{\partial r} + \frac{G_\theta}{r^2}\right)\right]_{z=0}$$

$$= -\frac{F\mu}{\pi\rho p^2}\sin\theta\frac{\partial}{\partial c}\left[\frac{1}{r}\frac{\partial}{\partial r}\left(\frac{e^{-hR} - e^{-kR}}{R}\right) + \frac{k^2}{2}\frac{e^{-kR}}{R}\right] \quad (15)$$

$$\left[\lambda h^2\Phi + 2\mu\left(\frac{\partial^2\Phi}{\partial z^2} + \frac{\partial^2 G_\theta}{\partial r\,\partial z} + \frac{1}{r}\frac{\partial G_\theta}{\partial z} - \frac{1}{r}\frac{\partial^2 G_r}{\partial\theta\,\partial z}\right)\right]_{z=0} = 0 \quad (16)$$

Method of Solution

From the foregoing formulation, it is seen that the θ-variations in the boundary conditions appear in the form of either cosine or sine functions. Further observations of the boundary conditions of equations (14) and (15) show that linear combinations of the quantities Φ, G_θ, $\partial G_z/\partial\theta$, $\partial G_r/\partial\theta$ are proportional to $\cos\theta$ and linear combinations of the quantities G_r, $\partial^2 G_r/\partial\theta^2$, G_z, $\partial\Phi/\partial\theta$, $\partial G_\theta/\partial\theta$ are proportional to $\sin\theta$ on $z = 0$ plane. This suggests that the solution may be taken in the following form:

$$\begin{aligned}
\Phi(r, \theta, z, p) &= Q(r, z, p)\cos\theta \\
G_\theta(r, \theta, z, p) &= H_\theta(r, z, p)\cos\theta \\
&= 1/2[H_1(r, z, p) - H_2(r, z, p)]\cos\theta \\
G_r(r, \theta, z, p) &= H_r(r, z, p)\sin\theta \\
&= 1/2[H_1(r, z, p) + H_2(r, z, p)]\sin\theta \\
G_z(r, \theta, z, p) &= H_z(r, z, p)\sin\theta
\end{aligned} \quad (17)$$

By substituting equations (17) into equations (8), (9), (10), (11), (14), (15) and (16), with some manipulations[4] to maneuver the differential equations and boundary conditions in such a way that further simplification by Hankel transform can be performed, we have a set of new equations to describe our boundary-value problem in terms of Q and H in the following manner.

Three equations defining the displacements of the medium:

$$U_r = \left[\frac{\partial Q}{\partial r} + \frac{H_z}{r} - {}^1/_2\frac{\partial(H_1 - H_2)}{\partial z}\right]\cos\theta = U_1\cos\theta \quad (18)$$

$$U_\theta = \left[-\frac{Q}{r} + \frac{\partial(H_1 + H_2)}{\partial z} - \frac{\partial H_z}{\partial r}\right]\sin\theta = U_2\sin\theta \quad (19)$$

$$U_z = \left[{}^1/_2\frac{\partial(H_1 - H_2)}{\partial r} - \frac{H_2}{r} + \frac{\partial Q}{\partial z}\right]\cos\theta = U_3\cos\theta \quad (20)$$

Three boundary conditions on the plane $z = 0$:

$$\left\{\lambda h^2 Q + \mu\left[2\frac{\partial^2 Q}{\partial z^2} + \frac{\partial^2 H_1}{\partial r\,\partial z} - \frac{1}{r}\frac{\partial^2}{\partial r\,\partial z}(r^2 H_2)\right]\right\}_{z=0} = 0 \quad (21)$$

$$\left\{\frac{2}{r}\frac{\partial^2}{\partial r\,\partial z}(rQ + rH_z) + \left(\frac{\partial^2}{\partial r^2} + \frac{1}{r}\frac{\partial}{\partial r}\right)H_1 - \frac{\partial^2 H_1}{\partial z^2}\right\}_{z=0} = \frac{F}{\pi\rho p^2}\frac{\partial}{\partial c}\left[\left(\frac{\partial^2}{\partial r^2} + \frac{1}{r}\frac{\partial}{\partial r}\right)\left(\frac{e^{-hR} - e^{-kR}}{R}\right) + k^2\frac{e^{-kR}}{R}\right] \quad (22)$$

$$\left\{r\frac{\partial}{\partial r}\left[\frac{1}{r}\left(2\frac{\partial Q}{\partial z} + \frac{\partial H_1}{\partial r}\right)\right] + \frac{\partial^2 H_2}{\partial z^2}\right\}_{z=0} = \frac{F}{\pi\rho p^2}\frac{\partial}{\partial c}\left[r\frac{\partial}{\partial r}\left(\frac{1}{r}\frac{\partial}{\partial r}\right)\left(\frac{e^{-hR} - e^{-kR}}{R}\right)\right] \quad (23)$$

One constraint condition between H_1, H_2, and H_z:

[4] See reference [1] for detailed algebraic manipulations.

$$\frac{1}{r^2}\frac{\partial}{\partial r}(r^2H_2) + \frac{\partial H_1}{\partial r} + 2\frac{\partial H_z}{\partial z} = 0 \tag{24}$$

Four governing differential equations to be satisfied by Q, H_1, H_2, and H_z:

$$\frac{\partial^2 H_1}{\partial r^2} + \frac{1}{r}\frac{\partial H_1}{\partial r} + \frac{\partial^2 H_1}{\partial z^2} - k^2 H_1 = 0 \tag{25}$$

$$\frac{\partial^2 H_2}{\partial r^2} + \frac{1}{r}\frac{\partial H_2}{\partial r} - \frac{4H_2}{r^2} + \frac{\partial^2 H_2}{\partial z^2} - k^2 H_2 = 0 \tag{26}$$

$$\frac{\partial^2 H_z}{\partial r^2} + \frac{1}{r}\frac{\partial H_z}{\partial r} - \frac{H_z}{r^2} + \frac{\partial^2 H_z}{\partial z^2} - k^2 H_z = 0 \tag{27}$$

$$\frac{\partial^2 Q}{\partial r^2} + \frac{1}{r}\frac{\partial Q}{\partial r} - \frac{Q}{r^2} + \frac{\partial^2 Q}{\partial z^2} - h^2 Q = 0 \tag{28}$$

Now take the Hankel transform [4] of the zeroth order for equations (22), (25), of the first order of equations (21), (24), (27), (28), and of second order for equations (23), (26). With the notation

$$\begin{aligned}
\int_0^\infty rQJ_1(r\xi)dr &= \psi(\xi, z, p)\\
\int_0^\infty rH_1J_0(r\xi)dr &= \zeta(\xi, z, p)\\
\int_0^\infty rH_2J_2(r\xi)dr &= \eta(\xi, z, p)\\
\int_0^\infty rH_zJ_1(r\xi)dr &= \chi(\xi, z, p)
\end{aligned} \tag{29}$$

and making the usual assumption that the functions behave properly at zero and infinity, we finally have[5]

$$\begin{aligned}
\frac{d^2\psi}{dz^2} - (\xi^2 + h^2)\psi &= 0\\
\frac{d^2\zeta}{dz^2} - (\xi^2 + k^2)\zeta &= 0\\
\frac{d^2\eta}{dz^2} - (\xi^2 + k^2)\eta &= 0\\
\frac{d^2\chi}{dz^2} - (\xi^2 + k^2)\chi &= 0
\end{aligned} \tag{30}$$

$$\left.\begin{aligned}
&\xi\eta - \xi\zeta + 2\frac{d\chi}{dz} = 0\\
&\left[\lambda h^2\psi + \mu\left(2\frac{d^2\psi}{dz^2} - \xi\frac{d\zeta}{dz} - \xi\frac{d\eta}{dz}\right)\right]_{z=0} = 0\\
&\left[2\xi\frac{d}{dz}(\psi + \chi) - \xi^2\zeta - \frac{d^2\zeta}{dz^2}\right]_{z=0}\\
&\qquad = \frac{F}{\pi\rho p^2}\left[\xi^2 e^{-(\xi^2+h^2)^{1/2}c} - (\xi^2 + k^2)e^{-(\xi^2+k^2)^{1/2}c}\right]\\
&\left[-2\xi\frac{d\psi}{dz} + \xi^2\zeta + \frac{d^2\eta}{dz^2}\right]_{z=0}\\
&\qquad = -\frac{F}{\pi\rho p^2}\xi^2\left[e^{-(\xi^2+h^2)^{1/2}c} - e^{-(\xi^2+k^2)^{1/2}c}\right]
\end{aligned}\right\} \tag{31}$$

The general solutions to the set of equations (30) are

$$\begin{aligned}
\psi &= Ae^{-(\xi^2+h^2)^{1/2}z} + A_1e^{(\xi^2+h^2)^{1/2}z}\\
\zeta &= Be^{-(\xi^2+k^2)^{1/2}z} + B_1e^{(\xi^2+k^2)^{1/2}z}\\
\eta &= Ce^{-(\xi^2+k^2)^{1/2}z} + C_1e^{(\xi^2+k^2)^{1/2}z}\\
\chi &= De^{-(\xi^2+k^2)^{1/2}z} + D_1e^{(\xi^2+k^2)^{1/2}z}
\end{aligned} \tag{32}$$

where the coefficients A, B, C, and so on, are arbitrary functions of ξ and p. It is seen that, if the solutions are to remain finite at infinity, the arbitrary functions A_1, B_1, C_1, and D_1 must be zero. Therefore substitution of equations (32) with $A_1 = B_1 = C_1 = D_1 = 0$ into equations (31) yields the solutions of ψ, ζ, η, χ as:

$$\psi = \frac{Fe^{-(\xi^2+h^2)^{1/2}z}}{\pi\rho p^2 M}\xi(\xi^2 + k^2)^{1/2}[2\xi^2 e^{-(\xi^2+h^2)^{1/2}c} - (2\xi^2 + k^2)e^{-(\xi^2+k^2)^{1/2}c}]$$

$$\zeta = \frac{Fe^{-(\xi^2+k^2)^{1/2}z}}{\pi\rho p^2 M}\{[(2\xi^2 + k^2)^2 - 2\xi^2(\xi^2 + h^2)^{1/2}(\xi^2 + k^2)^{1/2}]e^{-(\xi^2+h^2)^{1/2}c} - (2\xi^2 + k^2)\xi^2 e^{-(\xi^2+k^2)^{1/2}c}\} \tag{33}$$

$$\eta = \frac{Fe^{-(\xi^2+k^2)^{1/2}z}}{\pi\rho p^2 M}[-(2\xi^2 + k^2)\xi^2 e^{-(\xi^2+h^2)^{1/2}c} + 2\xi^2(\xi^2 + h^2)^{1/2}(\xi^2 + k^2)^{1/2}e^{-(\xi^2+k^2)^{1/2}c}]$$

$$\chi = -\frac{F}{2\pi\rho p^2}\frac{\xi}{(\xi^2 + k^2)^{1/2}}e^{-(\xi^2+k^2)^{1/2}(z+c)}$$

where

$$M = (2\xi^2 + k^2)^2 - 4\xi^2(\xi^2 + h^2)^{1/2}(\xi^2 + k^2)^{1/2} \tag{34}$$

The next step consists of the inversion of the Hankel and Laplace transforms. The first is set up formally here; the latter is taken up in the next section.

From equations (29) and the well-known Hankel inversion formula; we have

$$Q(r, z, p) = \int_0^\infty \xi\psi J_1(\xi r)d\xi \tag{35}$$

$$H_1(r, z, p) = \int_0^\infty \xi\zeta J_1(\xi r)d\xi \tag{36}$$

$$H_2(r, z, p) = \int_0^\infty \xi\eta J_2(\xi r)d\xi \tag{37}$$

$$H_z(r, z, p) = \int_0^\infty \xi\chi J_1(\xi r)d\xi \tag{38}$$

Use of equations (35) to (38) as well as (18), (19) and (20), with the aid of equation (24), gives

$$U_1 + U_3 = -\int_0^\infty [\xi^2(\psi - \chi) + \xi(\xi^2 + k^2)^{1/2}\eta]J_2(\xi r)d\xi \tag{39}$$

$$U_1 - U_3 = \int_0^\infty [\xi^2(\psi + \chi) + \xi(\xi^2 + k^2)^{1/2}\zeta]J_0(\xi r)d\xi \tag{40}$$

$$U_2 = -\int_0^\infty [\xi^2\zeta + \xi(\xi^2 + h^2)^{1/2}\psi + \xi(\xi^2 + k^2)^{1/2}\chi]J_1(\xi r)d\xi \tag{41}$$

Equations (18), (19), (20), (39), (40), and (41) define the displacement function $\mathbf{U}$; together with $\mathbf{U}_{01}$ and $\mathbf{U}_{02}$, which were defined in equations (12) and (12a), they constitute the Laplace transform of the solution for the case of the force at $(0, \theta_0, c)$ parallel to the plane boundary of an elastic half-space.

The foregoing analysis has been purely formal. It may be

[5] See Appendix for formulas used in this derivation.

verified, however, by direct substitution that the solutions satisfy the Laplace transform of equation (1) and the boundary conditions defined earlier in this paper. Furthermore, it can be easily proved that the transform of equation (1) has a unique solution under the type of boundary conditions which arise here; the proof is almost identical with the usual proof of uniqueness of solution in the theory of elasticity and therefore is omitted here. From Lerch's theorem [5], it is known that to a given Laplace-transform function there corresponds (except possibly at points of a set of zero measure, i.e., within the difference of a null function) a unique inverse; hence the inverse of the equations cited will give the desired solution in the physical co-ordinates.

Inverse Transformation

The inverse Laplace transformations of equations (39), (40), and (41) are extremely complicated and in general will not yield solutions in closed form. As an example, in an analogous problem which represents the case of a vertical force inside the half-space, even the surface displacements (i.e., the solution at $z = 0$) were expressed [6] in terms of ten complex integrals which can be evaluated numerically only with the aid of electronic computers. Therefore, in this paper, only two special cases of equations (39) to (41) will be inverted; namely,

1 $z = c = 0$; i.e., the surface displacements corresponding to a tangential force acting at a point on the surface.

2 $r = c = 0$; i.e., the displacements along the z-axis directly below an applied tangential force which acts at a point (the origin) on the surface.

Solutions to these two cases can be expressed in closed form. Furthermore, in order to simplify the calculations, λ is assumed to be equal to μ (corresponding Poisson's ratio = 1/4); it is, however, clear that this restriction is in no way essential to the development presented.

Case I $z = c = 0$. Equations (39) to (41) may be written explicitly in the following forms after some algebraic manipulations:

$$U_1 + U_2 = \frac{F}{64\pi\mu b}\int_0^\infty \xi^3 \frac{20\xi^4 + 32\xi^2k^2 + 9k^4 - 12(\xi^2 + k^2)^{3/2}(\xi^2 + h^2)^{1/2}}{k(\xi^2 + k^2)^{1/2}\left(\xi^2 + \frac{k^2}{4}\right)(\xi^2 + \beta^2k^2)(\xi^2 + \gamma^2k^2)} J_2(\xi r)d\xi \quad (42)$$

$$U_1 - U_2 = \frac{F}{64\pi\mu b}\int_0^\infty \xi \frac{44\xi^6 + 80\xi^4k^2 + 39\xi^2k^4 + 6k^6 + 12\xi^2(\xi^2 + k^2)^{5/2}(\xi^2 + h^2)^{1/2}}{k(\xi^2 + k^2)^{1/2}\left(\xi^2 + \frac{k^2}{4}\right)(\xi^2 + \beta^2k^2)(\xi^2 + \gamma^2k^2)} \quad (43)$$

$$\cdot [J_0(\xi r)d\xi]$$

$$U_3 = \frac{F}{64\pi\mu b}\int_0^\infty \xi^2 \frac{6(2\xi^2 + k^2)(\xi^2 + k^2)^{1/2}(\xi^2 + h^2)^{1/2} - 4\xi^4 - 10\xi^2k^2 - 3k^4}{k\left(\xi^2 + \frac{k^2}{4}\right)(\xi^2 + \beta^2k^2)(\xi^2 + \gamma^2k^2)} \quad (44)$$

$$\cdot [J_1(\xi r)d\xi]$$

where

$$\beta^2 = (3 - \sqrt{3})/4 \quad \text{and} \quad \gamma^2 = (3 + \sqrt{3})/4 \quad (44a)$$

It can be seen that, except for the Bessel functions, the integrands of equations (42) to (44) are homogeneous in ξ and k in such a manner that, should a change of variables

$$\xi = kz = \frac{pz}{b} \quad (45)$$

be made, the integrals of equations (42) to (44) will take the form

$$W = \int_0^\infty f_1(z) J_\mu\left(\frac{prz}{b}\right) dz \quad (46)$$

Clearly this can be rewritten as

$$W = \int_0^\infty f(z) J_\mu\left(\frac{prz}{b}\right) dz + A\int_0^\infty J_\mu\left(\frac{prz}{b}\right) dz \quad (47)$$

where $f(z)$ is observed to be real when z is real and the constant A is chosen so that

$$\lim_{z\to\infty} f(z) = 0 \quad \text{as} \quad 0\left(\frac{1}{z^2}\right) \quad (47a)$$

The second integral of equation (47), denoted here as W_0, can be immediately integrated as

$$W_0 = A\int_0^\infty J_\mu\left(\frac{prz}{b}\right) dz = \frac{Ab}{pr} \quad (48)$$

and its inverse Laplace transform is simply

$$L^{-1}(W_0) = w_0 = \frac{Ab}{r} \quad (49)$$

The first integral, denoted here as W_1, can be written as[6]

$$W_1 = (R \text{ or } I)\int_0^\infty f(z)\int_0^1 g(y)e^{ipryz/b}(1 - y^2)^{-1/2}\, dydz \quad (50)$$

Now, change the order of integration and extend z to the complex z-plane. It is seen that each of the functions $f(z)$ has four branch points situated at

$$z = \pm i; \qquad z = \pm i/\sqrt{3} \quad (50a)$$

and two simple poles[7] at

$$z = \pm\gamma i \quad (50b)$$

Branch cuts are now made as indicated in Fig. 1 such that $f(z)$ will be single-valued and analytic on the z-plane in agreement with the previous choice of signs made implicitly in choosing the constants A_1, B_1, C_1, and D_1 equal to zero in equation (32), where the positive signs were chosen for the quantities $(\xi^2 + h^2)^{1/2}$ and $(\xi^2 + k^2)^{1/2}$. The path of integration in equation (50) was along the real axis; it may be replaced by integration along the imaginary axis as shown in Fig. 1, since by virtue of equation (47a) and of Jordon's lemma, integration along the infinite arc gives no contribution. Furthermore, it can be observed that integration along the semicircular arcs around two branch points in this path

[6] See Appendix for the integral expressions of Bessel function used here.

[7] From examination of the denominator of equations (42), (43), and (44), it would appear that additional poles occur at $z = \pm\beta i$, $\pm i/2$. With the branch cut in Fig. 1, it can, however, be shown that the numerator is also zero at these points in such a manner that no poles arise.

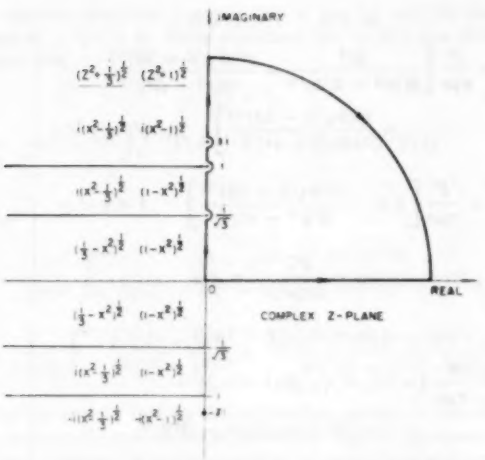

Fig. 1 Quantities indicated are values of $(Z^2+1)^{1/2}$ and $(Z^2+1/3)^{1/2}$ on various positions of the imaginary axis. Paths of integration for equation (50)

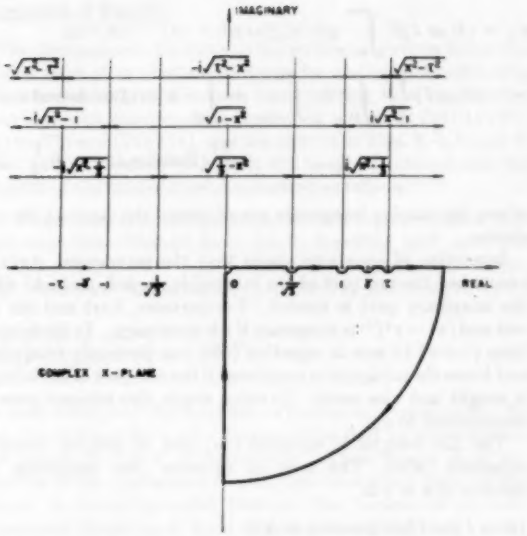

Fig. 2 Quantities indicated are values of $(1/3 - x^2)^{1/2}$, $(1 - x^2)^{1/2}$ and $(x^2 - \tau^2)^{1/2}$ on various positions of the real axis. Paths of integration for equation (58)

also tends to zero as the two semicircles shrink to the branch points. Therefore equation (50) becomes

$$W_1 = (R \text{ or } I)\left\{P\int_0^1 g(y)(1-y^2)^{-1/2}\int_0^\infty f(ix)e^{-pyx/b}idxdy + \pi i\int_0^\infty \phi(y)(1-y^2)^{-1/2}\,\mathrm{Res}\,(\gamma i)e^{-p\gamma y/b}dy\right\} = W_{11}+W_{10} \quad (51)$$

where P stands for the principal value of the integral which follows and $f(ix)$ is the value of $f(x)$ along the altered path (the imaginary axis) taken in accordance with the branch cuts. The residue at the pole at $z = \gamma i$ is

$$\mathrm{Res}\,(\gamma i) = [(z-\gamma i)f(z)]_{z=\gamma i} \quad (51a)$$

The second integral of equation (51), denoted there as W_{10} can be transformed by letting:

$$r\gamma y/b = s \quad (52)$$

then we have

$$W_{10} = (R \text{ or } I)\pi i\,\mathrm{Res}\,(\gamma i)\int_0^{r\gamma/b} e^{-ps}g\left(\frac{bs}{r\gamma}\right)\left(1-\frac{b^2s^2}{r^2\gamma^2}\right)^{-1/2}\frac{b}{\gamma^2}\,ds \quad (53)$$

It may be observed that the integrand of equation (53) is of the same form as that of Laplace transformation; one may therefore immediately perform the inverse Laplace transformation of W_{10}, with the result:

$$L^{-1}(W_{10}) = w_{10} = \left\{\begin{array}{ll}(R \text{ or } I)\pi bi\,\mathrm{Res}\,(\gamma i)g(\tau/r)(\gamma^2-r^2)^{-1/2}/r & \tau<\gamma \\ 0 & \tau>\gamma\end{array}\right\} \quad (54)$$

where

$$\tau = bl/r \quad (54a)$$

There remains to be inverted the first integral of equation (51); namely, W_{11}. For this integral, let, as before,

$$ryx/b = s \quad (55)$$

then

$$W_{11} = (R \text{ or } I)P\int_0^1 g(y)(1-y^2)^{-1/2}\int_0^\infty f(ibs/ry)e^{-ps}(ib/ry)dsdy \quad (56)$$

$$= (R \text{ or } I)P\int_0^\infty e^{-ps}\int_0^1 g(y)(1-y^2)^{-1/2}f(ibs/ry)(ib/ry)dyds$$

The inversion can now once again be immediately performed; it gives

$$w_{11} = L^{-1}(W_{11}) = (R \text{ or } I)P\int_0^1 g(y)(1-y^2)^{-1/2}f(i\tau/y)(ib/ry)dy \quad (57)$$

or, more conveniently,

$$w_{11} = (R \text{ or } I)P\int_\tau^\infty g(\tau/x)f(ix)(x^2-\tau^2)^{-1/2}(ib/r)dx \quad (57a)$$

Equation (57a) can be integrated for all three cases of $f(z)$ corresponding to equations (42), (43), and (44). However, it is inconvenient to deal with the infinite integrals of the type appearing in equation (57a); it will be found that for the case of equations (43) and (44) it is possible to replace the infinite integral by one over a finite range. This transformation can be performed when (and these conditions are satisfied for the foregoing cases) the integrand of equation (57a) has either no pole or a simple pole at the origin, and furthermore, on the real axis and the imaginary axis near the origin (if it is a simple pole), the integrand is real or imaginary, respectively, when the use of the imaginary or real part is indicated in front of the integral.

If the foregoing requirements are fulfilled, then the integration variable x is again extended into the complex plane and branch cuts are made as indicated in Fig. 2 (which is consistent with the previous branch cuts of Fig. 1 and with the choice of positive sign for $(1-y^2)^{-1/2}$ in equation (50). As there are no singularities on the lower half of this complex plane, the closed contour integral of Fig. 2 is zero. Hence,

$$w_{11} = (R \text{ or } I)P \int_{\tau}^{\infty} g(\tau/x)(f(ix)x^2 - \tau^2)^{-1/2}(ib/r)dx$$

$$= -(R \text{ or } I)\left\{P \int_0^{\tau} + \int_{-i\infty}^{0} + \int_{C_R} + \pi i\,(\text{Residues at } x = \gamma) + \frac{\pi i}{2}\,(\text{Residue at } x = 0)\right\} \quad (58)$$

where the missing integrands are of course the same as the one shown.

Inspection of equations shows that the polynomial $g(\tau/x)$ is even when the real part of the integral is needed, and odd when the imaginary part is needed. Furthermore, $f(ix)$ and idx are real and $(x^2 - \tau^2)^{1/2}$ is imaginary if x is imaginary. In the interval from $(-i\infty)$ to zero in equation (58), x is obviously imaginary, and hence the integrand is imaginary if the real part of the integral is sought and vice versa. In other words, this integral gives no contribution to w_{11}.

The last integral in equation (58) goes to zero by virtue of equations (47*a*). The term in equation (58) containing the residues at $x = \gamma$ is

$$(R \text{ or } I)[\pi i\,(\text{Residue at } x = \gamma)]$$

$$= (R \text{ or } I)\left[\pi i \text{ Res } (\gamma i)g\left(\frac{\tau}{\gamma}\right)(\gamma^2 - \tau^2)^{-1/2}\left(\frac{b}{r}\right)\right] \quad (58a)$$

The last term is

$$(R \text{ or } I)\left[\frac{\pi i}{2}\,(\text{Residue at } x = 0)\right]$$

$$= (R \text{ or } I)\left[-\left(\frac{\pi b}{2r}\right)xg\left(\frac{\tau}{x}\right)f(ix)(x^2 - \tau^2)^{-1/2}\right]_{x=0} \quad (58b)$$

and its value is finite because of the previous restrictions at this point.

The final result for the integral w_{11} may then be written as

$$w_{11} = w_{110} + w_{111} + w_{112} \quad (58c)$$

where

$$w_{110} = -(R \text{ or } I)\int_0^{\tau} g(\tau/x)f(ix)(x^2 - \tau^2)^{-1/2}(ib/r)dx \quad (59)$$

$$w_{111} = -(R \text{ or } I)[\pi i \text{ Res } (\gamma i)g(\tau/\gamma)(\gamma^2 - \tau^2)^{-1/2}(b/r)] \quad (60)$$

$$w_{112} = -(R \text{ or } I)[-(\pi bi/2\tau r)T(0)] \quad (61)$$

and

$$T(x) = xg(\tau/x)f(ix) \quad (61a)$$

It may be well at this point to recapitulate our results thus far. It is desired to invert the expressions given by equations (42) to (44). With the change of variables of equation (45) and with the subsequent alterations in the various paths of integration and manipulations described in equations (46) through (61) the results may be summarized symbolically as

$$u_1 + u_2 = w_0 + w_{10} + w_{11} \quad (62)$$

$$u_1 - u_2 = w_0 + w_{10} + w_{110} + w_{111} + w_{112} \quad (63)$$

$$u_3 = w_0 + w_{10} + w_{110} + w_{111} + w_{112} \quad (64)$$

where the functions w_0, w_{10}, w_{11}, w_{110}, w_{111}, and w_{112} are given by equations (49) (54), (57), (59), (60), and (61), respectively. Of course these functions are calculated using the appropriate expression for $f(z)$ in each case.

The detailed calculation of the foregoing quantities are carried out elsewhere and therefore omitted here. The final results for the case $z = c = 0$ are:

$$\left.\begin{aligned} u_1 &= 0 \qquad \tau < 1/\sqrt{3} \\ u_1 &= \frac{F}{\pi\mu r}\left[\frac{9\tau^3}{8(3\tau^2 - 3/4)^{1/2}} - \frac{\tau^3(6\sqrt{3} + 10)^{1/2}}{16(\tau^2 - \beta^2)^{1/2}} - \frac{\tau^3(6\sqrt{3} - 10)^{1/2}}{16(\gamma^2 - \tau^2)^{1/2}}\right] \qquad 1/\sqrt{3} < \tau < 1 \\ u_1 &= \frac{F}{\pi\mu r}\left[1/2 - \frac{\tau^3(6\sqrt{3} - 10)^{1/2}}{8(\gamma^2 - \tau^2)^{1/2}}\right] \qquad 1 < \tau < \gamma \\ u_1 &= \frac{F}{2\pi\mu r} \qquad \gamma < \tau \end{aligned}\right\} \quad (65)$$

$$\left.\begin{aligned} u_2 &= 0 \qquad \tau < 1\sqrt{3} \\ u_2 &= \frac{F}{\pi\mu r}\left\{-\tfrac{3}{16} + \tfrac{3}{8}\,[3(\tau^2 - \tfrac{1}{4})]^{1/2} - \tfrac{1}{16}[(10 + 6\sqrt{3})(\tau^2 - \beta^2)]^{1/2} + \tfrac{1}{16}[(6\sqrt{3} - 10)(\gamma^2 - \tau^2)]^{1/2}\right\} \qquad \frac{1}{\sqrt{3}} < \tau < 1 \\ u_2 &= \frac{F}{\pi\mu r}\left\{-\tfrac{3}{8} + \tfrac{1}{8}\,[(6\sqrt{3} - 10)(\gamma^2 - \tau^2)]^{1/2}\right\} \qquad 1 < \tau < \gamma \\ u_2 &= -\frac{3F}{8\pi\mu r} \qquad \gamma < \tau \end{aligned}\right\} \quad (66)$$

and

$$\left.\begin{aligned} u_3 &= 0 \qquad \tau < \frac{1}{\sqrt{3}} \\ u_3 &= \frac{\sqrt{6}F\tau}{32\pi^2\mu r}\left\{6K(m) - 18\Pi(8m^2, m) - (4\sqrt{3} - 6)\Pi[-(12\sqrt{3} - 20)m^2, m] + (4\sqrt{3} + 6)\Pi[(12\sqrt{3} + 20)m^2, m]\right\} \qquad \frac{1}{\sqrt{3}} < \tau < 1 \\ u_3 &= \frac{\sqrt{6}nF\tau}{32\pi^2\mu r}\left\{6K(n) - 18\Pi(8, n) - (4\sqrt{3} - 6)\Pi[-(12\sqrt{3} - 20), n] + (4\sqrt{3} + 6)\Pi[(12\sqrt{3} + 20), n]\right\} \qquad 1 < \tau < \gamma \\ u_3 &= \frac{\sqrt{6}nF\tau}{32\pi^2\mu r}\left\{6K(n) - 18\Pi(8, n) - (4\sqrt{3} - 6)\Pi\,[-(12\sqrt{3} - 20), n] + (4\sqrt{3} + 6)\Pi[(12\sqrt{3} + 20), n]\right\} + \frac{F\tau}{8\pi\mu r(\tau^2 - \gamma^2)^{1/2}} \qquad \gamma < \tau \end{aligned}\right\} \quad (67)$$

where

$$m = \frac{3\tau^2 - 1}{2} \quad (67a)$$

$$n = \frac{1}{m} \quad (67b)$$

$$K(x) = \int_0^{\pi/2} \frac{d\theta}{(1 - x^2\sin^2\theta)^{1/2}} \quad (67c)$$

$$\Pi(y, x) = \int_0^{\pi/2} \frac{d\theta}{(1 + y\sin^2\theta)(1 - x^2\sin^2\theta)^{1/2}} \quad (67d)$$

are complete elliptical integrals (10) of the 1st and 3rd kinds.

Case 2 $r = c = 0$. From equations (39) to (41), one obtains for this case

$$U_3 = 0 \tag{68}$$

$$U_1 = -U_2 = {}^1/_2 \int_0^\infty [\xi^2(\psi + \chi) + \xi(\xi^2 + k^2)^{1/2}\zeta]d\xi = I_3 + I_4 \tag{69}$$

where

$$I_3 = -\frac{F}{2\pi\mu b} \int_0^\infty \frac{(\xi^2 + k^2)^{1/2}\xi z_0 - (\xi^2+k^2)^{1/2}z}{k[(2\xi^2 + k^2)^2 - 4\xi^2(\xi^2 + k^2)^{1/2}(\xi^2 + k^2)^{1/2}]}\, d\xi$$

$$I_4 = \frac{F}{4\pi\mu b} \int_0^\infty \left\{ \frac{\xi(\xi^2 + 2k^2)}{k^2(\xi^2 + k^2)^{1/2}} + \frac{4\xi^2(\xi^2 + k^2)(\xi^2 + k^2)^{1/2} - 2\xi^2(2\xi^2 + k^2)(\xi^2 + k^2)^{1/2}}{k^3[(2\xi^2 + k^2)^2 - 4\xi^2(\xi^2 + k^2)^{1/2}(\xi^2 + k^2)^{1/2}]} \right\} [e^{-(\xi^2+k^2)^{1/2}z} d\xi]$$

It may be noticed that no Bessel function appears in this case, and therefore the inversion is much simpler than the previous one. It is only necessary to perform a change of variables in such a way that the integrals of equation (69) take the form of the definition of Laplace transform; then the inversion can be carried out immediately by inspection. Let then

$$\begin{aligned} \xi &= k(s_1^2 - 1/3)^{1/2} = k\left[\left(\frac{bs}{z}\right)^2 - 1/3\right]^{1/2} \quad \text{for} \quad I_3 \\ \xi &= k(s_1^2 - 1)^{1/2} = k\left[\left(\frac{bs}{z}\right)^2 - 1\right]^{1/2} \quad \text{for} \quad I_4 \end{aligned} \tag{70}$$

Thus

$$I_3 = -\frac{F}{2\pi\mu z} \int_{z/b\sqrt{3}}^\infty \frac{s_1(s_1^2 - {}^1/_2)(s_1^2 + {}^2/_3)^{1/2}}{(2s_1^2 + {}^1/_3)^2 - 4s_1(s_1^2 - {}^1/_2)(s_1^2 + {}^2/_3)^{1/2}} e^{-rs}ds \tag{71}$$

$$I_4 = \frac{F}{4\pi\mu z} \int_{z/b}^\infty \left\{ (s_1^2 + 1) + \frac{2s_1(s_1^2 - 1)[2s_1^2(s_1^2 - {}^2/_3) - (2s_1^2 - 1)s_1]}{(2s_1^2 - 1)^2 - 4s_1(s_1^2 - 1)(s_1^2 - {}^2/_3)^{1/2}} \right\} e^{-rs}ds \tag{72}$$

The inverse Laplace transform of these two integrals can be observed immediately and the final results are

$$\left.\begin{aligned} u_3 &= -u_3 = 0 \qquad \tau_1 < 1\sqrt{3} \\ u_1 &= -u_2 \\ &= -\frac{F}{2\pi\mu z} \frac{\tau_1(\tau_1^2 - {}^1/_2)(\tau_1^2 + {}^2/_3)^{1/2}}{(2\tau_1^2 + {}^1/_3)^2 - 4\tau_1(\tau_1^2 - {}^1/_2)(\tau_1^2 + {}^2/_3)^{1/2}} \\ &\qquad \frac{1}{\sqrt{3}} < \tau_1 < 1 \\ u_1 &= -u_3 = \frac{F}{4\pi\mu z} \left\{ (\tau_1^2 + 1) \right. \\ &\quad - \frac{2\tau_1(\tau_1^2 - {}^1/_2)(\tau_1^2 + {}^2/_3)^{1/2}}{(2\tau_1^2 + {}^1/_3)^2 - 4\tau_1(\tau_1^2 - {}^1/_2)(\tau_1^2 + {}^2/_3)^{1/2}} \\ &\quad \left. + \frac{2\tau_1^2(\tau_1^2 - 1)[2\tau_1(\tau_1^2 - {}^2/_3)^{1/2} - (2\tau_1^2 - 1)]}{(2\tau_1^2 - 1)^2 - 4\tau_1(\tau_1^2 - 1)(\tau_1^2 - {}^2/_3)^{1/2}} \right\} \qquad 1 < \tau \end{aligned}\right\} \tag{73}$$

where

$$\tau_1 = \frac{bt}{z} \tag{73a}$$

and

$$u_3 = 0 \tag{74}$$

Discussion of Results

The displacement functions at the surface or directly below the applied force of an elastic half space due to the application of a concentrated tangential surface force varying with time as the Heaviside unit function were present in equations (18) to (20), (65) to (67) and (73), (74), and are plotted in Figs. 3, 4, 5, and 6. A few general remarks concerning the foregoing solution and the behavior of the medium are summarized as follows:

1 Inspections of equations (65) to (67) and Figs. 3 to 5 show that there exist three distinct wave fronts, traveling with velocities $a = [(\lambda + 2\mu)/\rho]^{1/2}$, $b = [\mu/\rho]^{1/2}$, and b/γ, respectively. Physically, these three waves may be identified as the pressure wave, the shear wave, and the Rayleigh surface wave, respectively. In Figs. 3 to 5, these three wave fronts are marked by three arrows with letters P, S, and R, respectively. These figures show the variation of the displacements with time at any one point on the surface; it should be noted, however, that because of the nondimensional character of the variables plotted, the same curves are valid for all values of r.

Before the arrival of the pressure wave, the medium was completely at rest. At the arrival of the P-wave the velocities experience a sudden jump. The arrival of the S-wave is marked by a finite jump in u_θ; however, for displacements u_r and u_z it is marked only by discontinuities in the corresponding velocity components The arrival of the R-wave is marked by infinite discontinuity in u_r and u_z, while for u_θ, only a discontinuity in velocity occurs.

In the neighborhood of R-wave front, the major portion of the displacement is u_r and u_θ is proportional to

$$\frac{1}{r(r^2 - \gamma^2)^{1/2}} = \frac{1}{r[(\tau - \gamma)(\tau + \gamma)]^{1/2}} = \frac{1}{[\gamma(\tau + \gamma)]^{1/2}} \frac{1}{\sqrt{rr_R}} \tag{75}$$

where

$$|r_R| = |r - (bt/\gamma)| \tag{75a}$$

is the distance from the R-wave front. It is thus seen that these displacement components vary as $(1/rr_R)^{1/2}$ in the neighborhood of the wave front of the surface waves. Thus at large distances from the applied force, only small u_θ displacement occurs, while the other components still assume very large values when the surface wave arrives.

For large times the solution of course approaches the results of the static solution [7]. For the u_r and u_θ displacement components in fact the steady-state values are assumed immediately after the departure of the R-wave, and remain constant thereafter. The u_z-component, on the other hand, approaches the static value asymptotically with r.

2 Equations (18) to (20) show that u_r and u_γ are proportional to $\cos\theta$, and that u_θ is proportional to $\sin\theta$. Thus in directions perpendicular to that of the applied force (i.e., $\theta = \pm\pi/2$) u_θ is

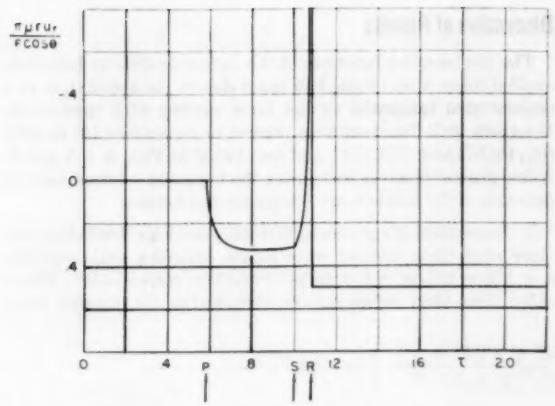

Fig. 3 U_r-components of displacement on the $Z = 0$ surface versus nondimensional time $\tau = bt/r$

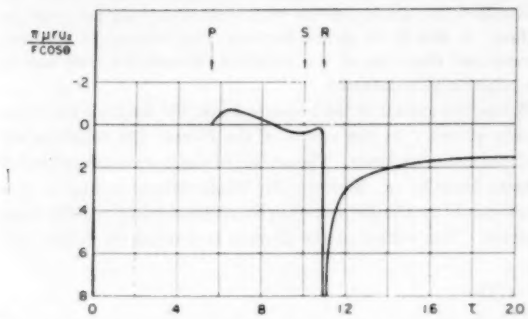

Fig. 5 U_r-components of displacement in the $Z = 0$ surface versus nondimensional time $\tau = bt/r$

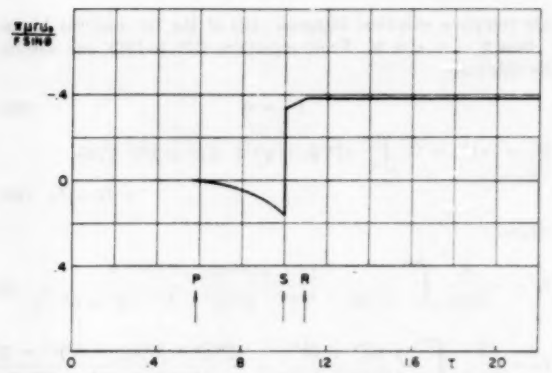

Fig. 4 U_θ-components of displacement on the $Z = 0$ surface versus nondimensional time $\tau = bt/r$

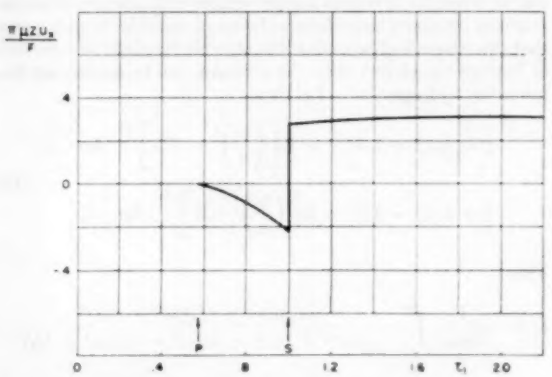

Fig. 6 U_z-components of displacement along the Z-axis versus nondimensional time $\tau_1 = bt/Z$

the only nonzero component; therefore along these lines no strong surface waves are felt and the response of the medium decays very rapidly with distance at all times. This result perhaps gives a partial explanation of the fact that in seismograph recordings of some earthquakes, the Rayleigh surface wave is notably absent.

3 In the steady-state solution, it can be observed that on the surface of the elastic half space, the quantity $[u_r/F \cos\theta]$, corresponding to a tangential force on the surface, is equal to the quantity $[u_r/F]$, corresponding to a vertical force on the surface. Such a reciprocal relation is seen to be preserved for all time for the dynamic case by comparing the quantity $[u_r/F \cos\theta]$ of this paper to the corresponding quantity $[u_r/F]$ of reference [8].

4 The nonzero displacement component directly below the applied force is $u_z = u_r \cos\theta - u_\theta \sin\theta$; it is plotted in Fig. 6. It is seen that only two wave fronts are present in this case; namely, those corresponding to a pressure wave and a shear wave. At the shear-wave front, a finite jump of magnitude $(F/2\pi\mu z)$ occurs; thereafter the displacement approaches the static value asymptotically with τ_1.

5 In reference [8] the integral theorem

$$\int_0^\infty J_0(k\,r\,x)xm(x)dx = -\left(\frac{2}{\pi}\right) I \int_0^\infty K_0(k\,r\,u)im(iu)du \quad (76)$$

is used in connection with the inverse Laplace transformation. For the case of inverting the quantity $(U_1 + U_2)$ of this paper, this theorem does not seem applicable since the Bessel function of order two is involved. However, for the quantities $(U_1 - U_2)$ and U_3 use of this theorem will lead to exactly the same results as obtained here. In so far as the author is aware, however, this theorem was proved only by a numerical check at two specific points in reference [9], which is the work cited in reference [8] in this connection. Therefore it seems that the inverse-transformation procedure given in the present paper is more general than that of reference [8]; furthermore, the work presented here may serve as the basis of an analytical proof of the integral theorem in question.

References

1 Chi-Chang Chao, "Dynamical Response of an Elastic Half-Space to Tangential Surface Loadings," Technical Report No. 11, Nonr-266 (20), Columbia University, New York, N. Y., 1958.

2 G. G. Stokes, "On the Dynamical Theory of Diffraction," 1849, *Transactions of the Cambridge Philosophical Society*, vol. 9, 1856, pp. 1–62.

3 A. E. H. Love, "The Propagation of Wave-Motion in an Isotropic Elastic Solid Medium," *Proceedings of the London Mathematical Society*, vol. 1, 1904, pp. 291–344.

4 I. N. Sneddon, "Fourier Transforms," first edition, McGraw-Hill Book Company, Inc., New York, N. Y., 1951.

5 H. S. Carslow and J. C. Jaeger, "Operational Methods in Applied Mathematics," second edition, Oxford University Press, 1947.

6 C. L. Pekeris and Hanna Lifson, "Motion of the Surface of a Uniform Elastic Half-Space Produced by a Buried Pulse," *Journal of the Acoustical Society of America*, vol. 29, 1957, pp. 1233–1238.

7 V. Cerruti, "Ricerche Intorno all'Equilibrio dei Corpi Elastici Isotropi," Accademia Nazionale dei Lincei, *Mem. fis. mat.*, Roma, 1882.

8 C. L. Pekeris, "The Seismic Surface Pulse," *Proceedings of the National Academy of Sciences*, vol. 41, 1955, pp. 469–480.

9 H. Bateman and C. L. Pekeris, "Transmission of Light From a

Point Source in a Medium Bounded by Diffusely Reflecting Parallel Plane Surfaces," *Journal of the Optical Society of America*, vol. 35, 1945, pp. 651–657.

10 N. W. McLachlan, "Bessel Functions for Engineers," second edition, Oxford University Press, 1955.

APPENDIX

Following are some integral equalities which are used for deriving equations (30) and (31). These formulas can be obtained easily by the properties of Bessel function and the usual assumption that the integrand behaves properly at zero and infinity as in reference [4]:

$$\int_0^\infty r\left(\frac{\partial^2}{\partial r^2}+\frac{1}{r}\frac{\partial}{\partial r}-\frac{\gamma}{r^2}\right)F(r)J_\gamma(\xi r)dr = -\xi^2\int_0^\infty rF(r)J_\gamma(\xi r)dr \quad (77)$$

$$\int_0^\infty r\left[\frac{\partial}{\partial r}F(r)\right]J_1(\xi r)dr = -\xi\int_0^\infty rF(r)J_0(\xi r)dr \quad (78)$$

$$\int_0^\infty \frac{1}{r}\frac{\partial}{\partial r}(r^2F)J_1(\xi r)dr = \xi\int_0^\infty rFJ_2(\xi r)dr \quad (79)$$

$$\int_0^\infty r^2\frac{\partial}{\partial r}\left(\frac{F}{r}\right)J_2(\xi r)dr = -\xi\int_0^\infty rFJ_1(\xi r)dr \quad (80)$$

$$\int_0^\infty \frac{\partial}{\partial r}(rF)J_0(\xi r)dr = \xi\int_0^\infty rFJ_1(\xi r)dr \quad (81)$$

The integral expressions of Bessel function to be used in equation (50) is:

$$J_\gamma(x) = \frac{2\left(\frac{x}{2}\right)^\gamma}{\Gamma(1/2)\Gamma(\gamma+1/2)}\int_0^1 (1-y^2)^{\gamma-1/2}\cos xy\,dy \quad (82)$$

and in particular, by using the technique of integration by parts,[8] equation (82) can be expressed in the form

$$J_\gamma(x) = (R \text{ or } I)\left\{\int_0^1 g(y)e^{ixy}(1-y^2)^{-1/2}dy\right\} \quad (83)$$

where R and I indicate, respectively, the real and imaginary parts of the quantity following; the real part in equation (83) is used if γ is even, and the imaginary if γ is odd. Then for $\gamma = 0, 1, 2$, one may write

$$J_0(x) = R\left\{\frac{2}{\pi}\int_0^1 e^{ixy}(1-y^2)^{-1/2}dy\right\}, \quad g(y) = \frac{2}{\pi} \quad (84)$$

$$J_1(x) = I\left\{\frac{2}{\pi}\int_0^1 ye^{ixy}(1-y^2)^{-1/2}dy\right\}, \quad g(y) = \frac{2y}{\pi} \quad (85)$$

$$J_2(x) = R\left\{\frac{2}{\pi}\int_0^1 (1-2y^2)e^{ixy}(1-y^2)^{-1/2}dy\right\}, \quad g(y) = \frac{2}{\pi}(1-2y^2) \quad (86)$$

[8] The number of required integrations by parts is γ, which is here assumed to be an integer.

K. KLOTTER
Professor of Engineering Mechanics,
Stanford University,
Stanford, Calif.
Mem. ASME

E. KREYSZIG
Professor of Mathematics,
Ohio State University,
Columbus, Ohio

On a Special Class of Self-Sustained Oscillations[1]

This paper deals with the "modified van der Pol differential equations" $\ddot{q} - (\text{sgn } \dot{q})(\delta/2)\dot{q}^2 h(q) + \kappa^2 f(q) = 0$, *where* $h(q)$ *and* $f(q)$ *are suitable functions. It is shown that there exists a unique limit cycle. For the limit amplitude both lower and upper bounds are established in the case of unrestricted values* δ. *For small values* δ *the limit amplitude can be calculated immediately.*

Introduction—Systems Treated

THE classical example of a system exhibiting self-sustained oscillations is the one described by the differential equation

$$\ddot{q} - \delta\dot{q}(1 - \alpha^2 q^2) + \kappa^2 q = 0, \tag{1}$$

known as the "van der Pol differential equation." This differential equation cannot be solved in closed form. Properties of its solutions have been studied extensively, however, by various means and from different points of view. Sparked by a paper by Levinson and Smith [1][2] dealing with

$$\ddot{q} + g(q, \dot{q})\dot{q} + f(q) = 0, \tag{2}$$

a theory for this rather general class of differential equations was developed [2]. Because the assumptions made in that theory in regard to the coefficients of the differential equation are rather weak (in order to keep the conclusions general), no very specific results can be expected from it. Hence it seems desirable to investigate special classes of differential equations, describing self-sustained oscillations, which can be treated more fully; preferably differential equations for which closed-form solutions, at least for the first integral, can be provided, if only in form of quadratures.

One of the authors [3] has drawn attention to two such differential equations, which may be called "modified" or "associated" van der Pol equations. They are

$$\ddot{q} - (\text{sgn } \dot{q})(\kappa^2 s)(1 - \beta^2\dot{q}^2) + \kappa^2 f(q) = 0 \tag{3}$$

and

$$\ddot{q} - (\text{sgn } \dot{q})(\delta/2)\dot{q}^2(1 - \alpha^2 q^2) + \kappa^2 f(q) = 0 \tag{4}$$

Equation (3) has been treated by the authors in a recent paper [4], and Equation (4) in an earlier one [5]. The present paper will be concerned with a generalized form of (4), namely

$$\ddot{q} - (\text{sgn } \dot{q})(\delta/2)\dot{q}^2 h(q) + \kappa^2 f(q) = 0, \tag{5}$$

with $\delta > 0$. Assumptions on $h(q)$ and $f(q)$ will be stated in the section, "Assumptions on Functions. . ."

The second term in (5) governs the energy input and output. In a way familiar from the discussion of the van der Pol Equation (1), it can be shown that the oscillations obeying Equation (5) also tend toward a stationary regime, a limit cycle. To determine the details of that limit cycle is the main objective of the present study. For example, upper and lower bounds for the limit amplitude will be derived in later sections. Also, in the final section, we shall apply our results to Equation (4), which is a special case of Equation (5).

Physically, Equation (5) may describe electrical oscillations in a circuit containing active elements, or it may describe mechanical oscillations. In the former case, q may denote a voltage or a current; in the latter a displacement or a velocity. Here we will use "mechanical language" for interpreting the phenomena, and we will speak of q as a displacement.

Transformation of Equation (5)

If we introduce the dependent variable $V = \dot{q}^2$ and use q as the independent variable, Equation (5) reduces to a first-order linear equation for $V(q)$,

$$\frac{dV}{dq} - (\text{sgn } \dot{q})\delta h(q)V = -2\kappa^2 f(q) \tag{6}$$

For $\dot{q} < 0$ this equation takes the form

$$\frac{dV}{dq} + \delta\, h(q)V = -2\kappa^2 f(2) \tag{7a}$$

The oscillation that starts from a displacement $q = Q_1 > 0$ with zero velocity is governed by (7a). When the oscillating system reaches the next extreme displacement, denoted by Q_2, the velocity changes direction and the subsequent part of the oscillation will be described by

$$\frac{dV}{dq} - \delta h(q)V = -2\kappa^2 f(q), \tag{7b}$$

until the following extreme displacement Q_3 is reached, and so on.

If we split both functions, $f(q)$ and $h(q)$, into an even part (subscript e) and an odd part (subscript o),

$$f = f_e + f_o, \qquad h = h_e + h_o,$$

and introduce the new variable

$$\tilde{q} = \begin{cases} q & \text{for} \quad \dot{q} < 0 \\ -q & \text{for} \quad \dot{q} > 0 \end{cases} \tag{8}$$

---

[1] The results presented in this paper were obtained in the course of a study supported by a grant from the National Science Foundation.

[2] Numbers in brackets designate References at end of paper.

Presented at the West Coast Conference of the Applied Mechanics Division, Stanford, Calif., September 9, 1959, of THE AMERICAN SOCIETY OF MECHANICAL ENGINEERS.

Discussion of this paper should be addressed to the Secretary, ASME, 29 West 39th Street, New York, N. Y., and will be accepted until October 10, 1960, for publication at a later date. Discussion received after the closing date will be returned.

NOTE: Statements and opinions advanced in papers are to be understood as individual expressions of their authors and not those of the Society. Manuscript received by ASME Applied Mechanics Division, June 18, 1959. This paper was not preprinted.

the motions in the two directions are described by

$$\frac{dV}{d\tilde{q}} + \delta[h_+(\tilde{q}) + h_-(\tilde{q})]V = -2\kappa^2[f_+(\tilde{q}) + f_-(\tilde{q})] \quad \text{for} \quad \dot{q} < 0$$
$$\frac{dV}{d\tilde{q}} + \delta[h_+(\tilde{q}) - h_-(\tilde{q})]V = -2\kappa^2[f_+(\tilde{q}) - f_-(\tilde{q})] \quad \text{for} \quad \dot{q} > 0 \tag{9}$$

respectively. If in particular $h(q)$ is even and $f(q)$ is odd, the two forms of (9) are identical; writing q again for $\tilde{q}$ we have

$$\frac{dV}{dq} + \delta h(q)V = -2\kappa^2 f(q) \tag{9a}$$

Assumptions on Functions $(h)q$ and $(f)q$

Physically, $h(q)$ governs the energy exchange during the oscillation, $f(q)$ is proportional to the restoring force. We shall occasionally refer to these functions as the "energy function" and the "restoring function."

It is clear that the various oscillations governed by Equation (5) may have almost no properties in common if we subject the functions $h(q)$ and $f(q)$ only to such conditions under which unique solutions exist for every choice of initial values. Here, however, we are primarily interested in self-sustained oscillations; hence, we will impose conditions on $h(q)$ and $f(q)$ which single out self-sustained oscillations from all the types of solutions which may otherwise occur. The conditions will be chosen with regard to practical importance. This means we will avoid unnecessary generality which would yield more complicated formulas without adding new ideas to the discussion. We also will omit cases which are meaningless from the physical point of view. It will become clear that some of the restrictions imposed here could be lessened if this should prove desirable.

First, we will take advantage of the simplifications offered by requiring $f(q)$ to be an odd function and $h(q)$ to be an even function.

For the reasons mentioned we will also require:

(i) The function $f(q)$ to represent a restoring force proper; that is, a force that tends to decrease the absolute value of the displacement q.

(ii) The function $h(q)$ to be such that for small displacements q energy is fed into the system, while for large absolute values of the displacement energy is drained from it.

These requirements will form conditions on the behavior of $h(q)$ in the vicinity of the origin and on the growth of both $f(q)$ and $h(q)$ for large absolute values of q.

Hence we decide to require:

1 $f(q)$ to be an odd polynomial satisfying

$$f(q) > 0 \quad \text{for} \quad q > 0 \tag{10}$$

2 $h(q)$ to be an even polynomial of a type that there exists a positive number a such that

$$h(q) > 0 \quad \text{for} \quad |q| < a$$
$$h(q) < 0 \quad \text{for} \quad |q| > a \tag{11}$$

We will prove that under these assumptions there exists a unique limit cycle whose positive and negative maximum displacements have the same absolute value. Instead of "maximum displacement" we will use the term "amplitude" forthwith. The amplitude of the limit cycle will be termed limit amplitude and will be denoted by $Q^*(>0)$.

The Amplitude Relationship

Equation (9a) has the general solution

$$V(q) = -\frac{2\kappa^2}{s(q)}\,[k(q) + \bar{C}] \tag{12}$$

where

$$k(q) = \int_0^q s(x)f(x)dx$$
$$s(q) = e^{j(q)}$$
$$j(q) = \delta \int_0^q h(x)dx, \tag{13}$$

and $\bar{C}$ denotes the constant of integration.

If the oscillation starts from $q = Q_1 > 0$ with initial velocity $\dot{q} = 0$, the special solution is

$$V(q) = \frac{2\kappa^2}{s(q)}\,[k(Q_1) - k(q)] \tag{14}$$

This function describes the motion as long as the differential equation (9a) is valid; that is, until $V(q)$ vanishes for the first time after the start. Hence the equation

$$k(Q_2) = k(Q_1) \tag{15a}$$

determines the second amplitude $Q_2 \neq Q_1$, the equation

$$k(Q_3) = k(Q_2) \tag{15b}$$

the third, $Q_3 \neq Q_2$, and so forth. We shall find that $Q_2 < 0$, $Q_3 > 0$, etc. Equations (15) will be called the amplitude relationship.

Properties of the Amplitudes

We start by proving two propositions:

(*A*) $k(q)$ is bounded as $q \to \infty$
(*B*) $k(q) \to \infty$ as $q \to -\infty$

Because of our earlier assumptions in regard to the functions $f(q)$ and $h(q)$, we may represent $f(q)$ in the form

$$f(q) = \sum_{k=0}^{n} c_k q^{2k+1} \qquad \text{with } c_n > 0; \tag{16}$$

and $h(q)$ in the form

$$h(q) = \sum_{k=0}^{m} a_k q^{2k} \qquad \text{with } m \geq 1 \text{ and } a_m < 0 \tag{17}$$

From (17) it follows that there exists a value $q = c > 0$ such that

$$h(q) < -q \text{ for all } q > c, \tag{18}$$

(Fig. 1 shows a special and very simple example.) Hence there exists a number C such that

$$k(c) = C + \int_0^c e^{-z} f(x)\,dx \tag{19a}$$

and for $q > c$

$$k(q) < C + \int_0^q e^{-z} f(x)\,dx \tag{19b}$$

Therefore, because of (16) we obtain the result

$$\lim_{q\to\infty} k(q) < C + \lim_{q\to\infty} \int_0^q e^{-z} f(x)dx = C + \sum_{k=0}^{n} c_k \Gamma(2k+2) < \infty; \tag{20}$$

this proves proposition (*A*).

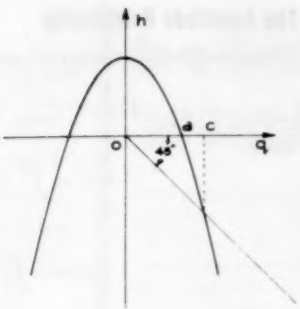

Fig. 1 Example of function $h(q)$

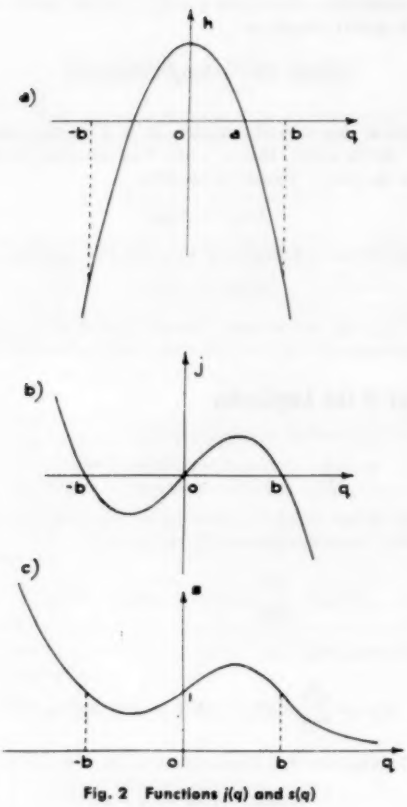

Fig. 2 Functions $j(q)$ and $s(q)$

Because of our assumptions on the function $h(q)$ there exists a unique number $q = b > 0$, as the zero of the function $j(q)$ of (13) (see Fig. 2 which refers to the example of Fig. 1), and we have

$$\begin{aligned} j(q) < 0, \quad s(q) < 1 \quad \text{for } -b < q < 0 \\ j(q) > 0, \quad s(q) > 1 \quad \text{for } q < -b \end{aligned} \tag{21}$$

From these properties of $s(q)$ it follows that there exists a number $D > 0$, such that

$$k(-b) = \int_0^{-b} f(x)dx - D$$

and (22)

$$k(-q) > \int_0^{-q} f(x)dx - D \quad \text{for } -q < -b$$

Hence, because of (16)

$$\lim_{q \to \infty} k(-q) = \infty; \tag{23}$$

this proves proposition (B).

Since

$$\begin{aligned} s(q) > 1 \quad \text{for} \quad 0 < q < b \\ s(q) < 1 \quad \text{for} \quad -b < q < 0 \end{aligned} \tag{24}$$

and since $f(q)$ is odd and satisfies (10), we have

$$k(q) > k(-q) \quad \text{for} \quad 0 < q \leqq b \tag{25}$$

Because $k(q)$ remains bounded for $q \to \infty$ whereas $k(-q) \to \infty$ for $q \to \infty$, there exists a number $q = \eta > b$ such that

$$k(q) < k(-q) \quad \text{for} \quad q \geqq \eta \tag{26}$$

Using the theorem by Weierstrass on zeros of real functions which are continuous in a closed interval we find from (25) and (26) that the equation

$$k(q) = k(-q) \tag{27}$$

has at least one solution in the interval $b \leqq q \leqq \eta$. Because $s(q) > 0$ and in view of (16) we find that $k(q)$ is a monotone function of q for $0 \leqq q$ as well as for $q \leqq 0$. From these facts we obtain the following intermediate results:

1 If the oscillations start from rest at any positive amplitude $Q_1 \leqq b$, the sequence of the absolute values of the subsequent amplitudes $Q_2, Q_3 \ldots$ increases in monotone fashion and tends to a limit $q = Q_*{}^*$.

2 If the oscillations start from rest at amplitudes $Q_1 \geqq \eta$, the afore-mentioned sequence decreases in monotone fashion and tends to a limit $q = Q_1{}^* \geqq Q_*{}^*$.

That is, every such solution has a limit cycle. In the next section we shall show that this is true for any value of the starting amplitude Q_1 and that consequently there exists exactly one limit cycle.

Existence and Uniqueness of Limit Amplitude Q^*

By definition of the limit cycle the limit amplitude $Q^* > 0$ satisfies the equation

$$k(Q^*) = k(-Q^*) \tag{28}$$

From the considerations in the preceding section we know that this equation has at least one solution in the interval S given by $b \leqq q \leqq \eta$, where b is the zero of the function $j(q)$, Fig. 2, and η is sufficiently large. Furthermore, all solutions of (28), are located in that interval. Now, we shall be able to show that (28) has exactly one solution.

Suppose that (28) has more than one solution. Let $q = q_1$ and $q = q_2$ be any two of these. Clearly, both q_1 and q_2 are situated in S. Then, we have

$$k(q_1) = k(-q_1) \quad \text{and} \quad k(q_2) = k(-q_2);$$

or (29)

$$\int_{q_1}^{q_2} s(x)f(x)dx - \int_{-q_1}^{-q_2} s(x)f(x)dx = 0$$

Since $h(x)$ is even, $j(x)$ is odd; furthermore $f(x)$ is odd. Hence

$$k(-q) = \int_0^q e^{-j(x)} f(x)dx \tag{30}$$

Equation (30) tells that (29) is equivalent to

$$\int_{q_1}^{q_2} \sinh\,[j(x)]f(x)dx = 0 \tag{31}$$

Since $j(x) < 0$ in the interval S and since $f(x)$ satisfies (10), the whole integrand in (31) does not change sign. Hence $q_1 = q_2$ is the only solution of (31) in S.

We may sum up our results as follows:

Let $f(q)$ be an odd polynomial satisfying (10), and let $h(q)$ be an even polynomial satisfying (11). Then for every choice of starting amplitude $q = Q$ the Equation (5) describes self-sustained oscillations which tend to a unique limit cycle. The sequence of the absolute values of the amplitudes $Q_1, Q_2, Q_3 \ldots$ is monotone.

Furthermore, for the amplitudes $Q_1, Q_2 \ldots$ and $\hat{Q}_1, \hat{Q}_2 \ldots$ of two different oscillations of the same system, starting from rest at $Q_1 > 0$ and $\hat{Q}_1 > Q_1$, respectively, we find

$$|\hat{Q}_i| > |Q_i| \qquad i = 2, 3, \ldots \tag{32}$$

Bounds for Limit Amplitude Q^*

A lower bound for the limit amplitude $Q^* > 0$ is obtained immediately from (21), Fig. 3:

$$Q^* > b \tag{33}$$

This bound cannot be improved without using special properties of $f(q)$ and $h(q)$ beyond the general assumptions made in regard to these functions. If we would specify such additional properties of $f(q)$ and $h(q)$, we might obtain better lower bounds by a procedure similar to that by which upper bounds will be derived in the following section.

Since Q^* is defined as the positive zero of a function represented by an integral, it is obvious that lower as well as upper bounds for Q^* can be derived by using familiar procedures of numerical integration. These lead to bounds of any desired degree of accuracy. Another way for obtaining bounds is to consider comparison problems. Although this method may not yield results of the same degree of accuracy, it has the considerable advantage that its steps can be interpreted physically. We shall, therefore, proceed with this method.

Let $H(q)$ denote a piecewise continuous function such that

$$h(q) < H(q) \quad \text{for} \quad -\infty < q < \infty \tag{34a}$$

holds and that the integral

$$J(q) = \delta \int_0^q H(x)dx \tag{34b}$$

exists for all finite values of $|q|$. Then there is

$$\begin{aligned} J(q) &> j(q) \quad \text{for} \quad q > 0 \\ J(q) &< j(q) \quad \text{for} \quad q < 0 \end{aligned} \tag{34c}$$

We use the notation

$$K(q) = \int_0^q e^{J(x)} f(x)dx \tag{35a}$$

Since $f(q)$ is odd we obtain from (10) and (34c)

$$K(q) > k(q) \quad \text{and} \quad K(-q) < k(-q) \qquad \text{for} \quad q > 0 \tag{35b}$$

Hence, if the equation

$$K(q) = K(-q) \tag{36}$$

has solutions $q = U > 0$, the smallest of these solutions U is an upper bound for Q^*, Fig. 4. Equation (36) has at least one solution $q \neq 0$ if, and only if, the relation $K(q) < K(-q)$ holds for some value $q > 0$. This follows from (25), (35b), and the continuity of $K(q)$. In particular, if we choose a function $H(q)$ which satisfies (34a) and conditions of the type (11), say

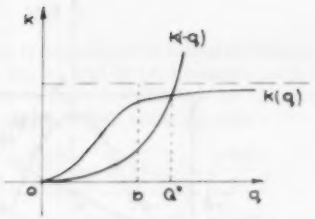

Fig. 3 Functions $k(q)$ and $k(-q)$

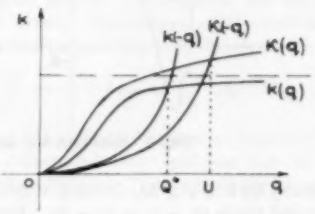

Fig. 4 Functions $k(q)$ and $K(q)$

$$\begin{aligned} H(q) &> 0 \quad \text{for} \quad |q| < a^* \\ H(q) &< 0 \quad \text{for} \quad |q| > a^* \end{aligned} \tag{37}$$

where $a^* > a$, then (36) has exactly one solution. In that case our approach amounts to replacing the given problem by a simpler comparison problem with a larger limit amplitude.

In the following section we shall consider this procedure in more detail.

Methods of Determining Upper Bounds for Limit Amplitude

The computational importance of the method, outlined in the preceding section, for deriving upper bounds of Q^* lies in the fact that we may choose functions $H(q)$ in such a way that $K(q)$, defined by (35a) and (34b), can be expressed by elementary or tabulated higher transcendental functions, whereas, in general, no such representations for $k(q)$ exist.

Let us follow up this idea. First we shall prove the following statement:

For every polynomial $h(q)$ satisfying (11), a function $H(q)$ can be chosen so that the Equation (36) contains a finite number of elementary transcendentals and has exactly one solution, which, then, is an upper bound U for Q^*.

Indeed, for every function $h(q)$ satisfying (11) there exist positive numbers A_1 and $\bar{a}$ such that the function (see Fig. 5)

$$H_1(q) = \begin{cases} +A_1 & \text{for} \quad |q| \leqq \bar{a} \\ -A_1 & \text{for} \quad |q| > \bar{a} \end{cases} \tag{38}$$

satisfies (34a). From this, we obtain

$$J(q) = \begin{cases} -\delta A_1(q + 2\bar{a}) & \text{for} \quad q \leqq -\bar{a} \\ \delta A_1 q & \text{for} \quad |q| \leqq \bar{a} \\ -\delta A_1(q - 2\bar{a}) & \text{for} \quad q \geqq \bar{a} \end{cases} \tag{39}$$

Since $H_1(q)$ is even and $f(q)$ is odd we find from (35a)

$$K(q) - K(-q) = 2 \int_0^q \sinh [J(x)] f(x)dx \tag{40a}$$

For the following we shall abbreviate the right-hand side by $2\Delta(q)$, hence

$$\Delta(q) = \int_0^q \sinh [J(x)] f(x)dx \tag{40b}$$

Because of (10) and (39) the function $\Delta(q)$ increases in a mono-

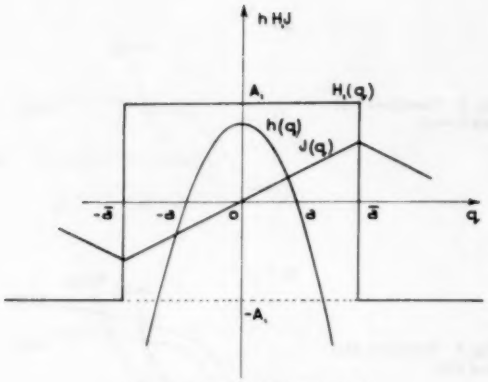

Fig. 5 Functions $h(q)$ and $H_1(q)$

tone way for $0 \leqq q \leqq 2\bar{a}$. From $q = 2\bar{a}$ it decreases in a monotone way and tends to $-\infty$ as $q \to \infty$. Hence $\Delta(q)$ has exactly one positive zero and therefore (36) one solution $q > 0$. Furthermore, because $f(q)$ is a polynomial, it is obvious from (39) that (36) involves only a finite number of exponentials and polynomials.

An example will be discussed in the last section.

We proceed to deriving more accurate upper bounds for Q^* by choosing other types of functions H, suitable to serve in (34*a*). The bounds will be obtained from equations involving higher transcendentals. The new functions are

$$H_2(q) = A_2 - 2B_2|q|, \quad \text{with} \quad A_2 > 0, \quad B_2 > 0 \tag{41}$$

They are even functions and suitable for every even polynomial $h(q)$ satisfying (11). In other words: There exist constants A_2 and B_2 such that (41) satisfies (34*a*). From (41) we find

$$J(q) = \delta(A_2 q - B_2 q^2) \quad \text{for} \quad q \geqq 0,$$

and from (40*b*) we obtain

$$\Delta(q) = \int_0^q \sinh\,(\delta A_2 x - \delta B_2 x^2) f(x)dx \quad (q \geqq 0)$$

This equation leads to the estimates

$$\Delta(q) < \sinh \delta A_2 q \int_0^q \cosh\,\delta B_2 x^2 f(x) - \int_0^q \sinh\,\delta B_2 x^2 f(x)dx \quad (q > 0)$$

After inserting (16) for $f(q)$ and setting $\delta B_2 x^2 = z$, the resulting integrals can be integrated by parts. In this manner the expression on the right-hand side of the foregoing formula can be expressed by elementary functions and Fresnel integrals for purely imaginary argument. For evaluating these integrals, tables are given in [6] and [7], or else tables of the incomplete gamma functions for real arguments can be used. We do not discuss the procedure in detail but turn to a third choice for H which will prove more convenient.

This third choice for $H(q)$ is

$$H_3(q) = A_3 - 3B_3 q^2, \quad A_3 > 0, \quad B_3 > 0 \tag{42}$$

Equation (42) means to say that there exist constants $A_3 > 0$, and $B_3 > 0$ such that (42) satisfies (34*a*) for all values of q. From (42) we obtain

$$J(q) = \delta q[A_3 - B_3 q^2] \tag{42a}$$

We define a new function

$$N(q) = e^{\delta A_3 q} \int_0^q e^{-\delta B_3 x^3} f(x)dx$$

From (36*a*) we find

$$K(q) < N(q), \quad K(-q) > N(-q); \quad q > 0 \tag{43}$$

Since the function $H_3(q)$, defined by (42), satisfies a condition of the type (37) the equation $K(q) = K(-q)$ has exactly one solution $q > 0$, as follows from the proof of uniqueness in an earlier section.

Now we are going to prove that the equation

$$N(q) = N(-q) \tag{44}$$

has a solution $q > 0$; this solution, hence, is an upper bound for the limit amplitude Q^*. Clearly, $N(q) > N(-q)$ for sufficiently small values of $q > 0$, as follows from (35*b*) and (25). Since $N(q)$ is continuous it suffices to show that there are values of $q > 0$ for which $N(q) < N(-q)$, or equivalently $N(-q) - N(q) > 0$.

From (16) we see that there exists a positive number $q = \tau$ such that $f(q) > 3A_3\delta$ for all $q > \tau$. For $q > \sigma \equiv +(3A_3/B_3)^{1/2}$ we have $B_3 q^3 > 3A_3 q$. Now, let ζ be the larger one of the two values σ, τ. Then, we find

$$N(-q) - N(q) = e^{-\delta A_3 q} \int_0^q e^{\delta B_3 x^3} f(x)dx - e^{\delta A_3 q} \int_0^q e^{-\delta B_3 x^3} f(x)dx$$

$$> e^{-\delta A_3 q}[e^{\delta A_3 \zeta} N(-\zeta) + e^{3\delta A_3 q} - e^{-3\delta A_3 \zeta}] - e^{\delta A_3 q} \int_0^q f(x)dx \quad (q > 0)$$

From this it follows that for sufficiently large $q > 0$

$$N(-q) - N(q) > 0$$

$N(q)$ can be expressed in terms of the incomplete gamma function

$$P(m;x) = \int_0^x e^{-y} y^{m-1} dy$$

Putting $\delta B_3 x^3 = z$ we find

$$N(\pm q) = (1/3)(\delta B_3)^{-1/3} e^{\pm \delta A_3 q} \int_0^{\pm \delta B_3 q^3} e^{-z} f\left[\left(\frac{z}{\delta b}\right)^{1/3}\right] z^{1/3} dz;$$

inserting (16) into this, Equation (44) takes the form

$$e^{\delta A_3 q} P_n(\delta B_3 q^3) = P_n(-\delta B_3 q^3) \tag{45}$$

where

$$P_n(x) = \sum_{k=0}^{n} \frac{c_k}{(\delta B_3)^{2(k+1)/3}} P[2(k+1)/3; x]$$

In many cases the relation (45) can be simplified. For instance, if all the coefficients of $f(q)$ in the representation (16) are positive, a function $L(q) > N(q)$ (for $q > 0$) is obtained by replacing the incomplete gamma functions in the expression for $N(q)$ by the corresponding (complete) gamma functions. Furthermore, in this case a function $M(q) < N(-q)$ (for $q > 0$) can be obtained by using the techniques shown in [5] and [8]. Clearly, if the equation $M(-q) - L(q) = 0$ has a solution $q > 0$, this is an upper bound for the solution $q > 0$ of Equation (44).

Small Oscillations

Equations (15) express the amplitude relationship. We may insert the MacLaurin series of $k(q)$ into (15). If, and as long as, the values $|q|$ stay small, we may approximate the series by one of its partial sums consisting of a small number of terms.

From (13) and (17) we find for $s(q)$ the expression

$$s(q) = \sum_{\lambda=0}^{\infty} \frac{1}{\lambda!}\left[\delta \sum_{k=0}^{m} \frac{a_k q^{2k+1}}{2k+1}\right]^{\lambda}$$
$$= 1 + \delta a_0 q + \frac{\delta^2 a_0^2}{2} q^2 + \delta\left(\frac{\delta^2}{6} a_0^3 + \frac{a_1}{3}\right) q^3 + \ldots \quad (46)$$

and for $k(q)$ [cf. (13)] by integrating term by term

$$k(q) = q^2\left[\frac{c_0}{2} + \frac{\delta a_0 c_0}{3} q + \frac{1}{4}\left(c_1 + \frac{\delta^2 a_0^2 c_0}{2}\right) q^2 + \ldots\right] \quad (47)$$

If $k_p(q)$ denotes the function given by the terms in (47) which are written explicitly, the zero $q = q_0 (\neq Q_1)$ of the equation

$$k_p(q) - k_p(Q_1) = 0 \quad (48)$$

is an approximate value for the amplitude Q_2.

For determining that zero, any one of the customary methods may be used. By applying Newton's method and using the value $q_1 = -Q_1$ as a first approximation q_1 for Q_2, we obtain the second approximation q_2 in the form

$$q_2 = -Q_1 - 2Q_1^2 \frac{(1/3)\delta a_0 c_0 + (1/3)\delta\left(a_0 c_1 + \frac{a_1 c_0}{3} + \frac{\delta^2}{6} a_0^3 c_0\right) Q_1^2}{c_0 - \delta a_0 c_0 Q_1 + \left(c_1 + \frac{\delta^2}{2} a_0^2 c_0\right) Q_1^2}$$

If the limit amplitude falls into the range of validity of the expression, a similar method can be used for determining an approximate value for it. Whether or not a manageable number of terms will yield a satisfactory approximation will depend entirely on the coefficients in the representations (16) and (17).

Examples

We will illustrate our methods and results by an example. As such we use a polynomial for $h(q)$ of smallest degree compatible with (11); namely,

$$h(q) = 1 - \alpha^2 q^2; \quad \alpha > 0 \quad (49)$$

By doing so Equation (5) reduces to Equation (4). This equation has been investigated earlier [5].

The quantities a from (11), b from the section "Properties of the Amplitudes," assume values

$$a = \frac{1}{\alpha}, \qquad b = \frac{+\sqrt{3}}{\alpha} \quad (50)$$

Hence from (33) we obtain as a lower bound for the limit amplitude

$$Q^* > +\sqrt{3}/\alpha \quad (50a)$$

It is worth noting that this bound is independent of both δ and the function $f(q)$.

Upper bounds for the limit amplitude Q^* can be obtained as described in the section, "Methods of Determining Upper Bounds. . . ." We may choose

$$H_1(q) = \begin{cases} 1 & |q| \leq \bar{a} \\ -1 & |q| > \bar{a} \end{cases} \quad (51)$$

where $\bar{a} = +\sqrt{2}/\alpha$. This function H_1 is of form (38) and satisfies (34a). The function $f(q)$ we take as linear, $f(q) = q$. The equation $\Delta(q) = 0$, with $\Delta(q)$ from (40) yields

$$x \cosh(2\lambda - x) + \sinh(2\lambda - x) = 2\lambda \cosh \lambda \quad (52)$$

with $\lambda = \delta\bar{a}$ and $x = \delta q$. Its single root x constitutes an upper bound for the dimensionless limit amplitude δQ^*. For example, if $\lambda = 1$ we find from (52) $\delta Q^* < 4.1$.

A more accurate upper bound may be obtained as follows: For the sake of simplicity, we let $h(q)$ of (49) coincide with $H_3(q)$ given by (42); this leads to $A_3 = 1$, and $3B_3 = \alpha^2$. With these values and for $f(q) = q$, Equation (45) takes the form

$$3^{1/6}\Gamma^2 q P\left(\tfrac{2}{3}; \frac{\alpha^2\delta q^3}{3}\right) = P\left(\tfrac{2}{3}; -\frac{\alpha^2\delta q^3}{3}\right) \quad (53)$$

For obtaining an approximate solution of this equation we may replace P on the left-hand side by $\Gamma(2/3)$; this will increase slightly the value of the bound. The integral on the right-hand side (denoting the dimensionless quantity $\alpha^2\delta q^3$ by r^3)

$$P(\tfrac{2}{3}; -r^3) = \int_0^{-r^3} e^{-x} x^{-1/3}\, dx = \int_0^{r^3} e^x x^{-1/3} dx \quad (54)$$

may be calculated by first determining its value for a small $\bar{q} > 0$ (using the MacLaurin series) and then applying one of the formulas for numerical integration. Thus we obtain an upper bound

$$\delta Q^* < 2.9 \quad (55)$$

The exact value is $\delta Q^* = 2.2$ (taken from [5] where it was obtained by numerical integration).

As has been mentioned previously, more accurate bounds can be obtained by applying procedures of numerical integration to the integral

$$\int_0^q \sinh\,[j(x)]f(x)dx$$

whose positive zero defines Q^*.

Small Values of δ in Equation (5)

It should be kept in mind that up to this point we have not restricted the value of the coefficient δ in Equation (5); this means the amount of energy exchanged during a cycle can be either large or small. All previous results pertain to that general case. If, however, that coefficient δ happens to be small, very simple results follow. For the limiting case of $\delta q \ll 1$ the amplitude Q^* of the limit cycle can be calculated by using the standard procedure known as the Kryloff-Bogoliuboff method [9].

That method leads to the following statements: If the solution of the differential equation

$$\ddot{q} + \kappa^2 q + \epsilon\kappa^2 k(q, \dot{q}) = 0, \qquad \epsilon \ll 1 \quad (56)$$

is assumed in the form

$$q = Q(t) \sin\,[\kappa t + \theta(t)] \quad (57)$$

the functions $Q(t)$ and $\theta(t)$ are determined by the two first-order differential equations

$$\dot{Q} = -\frac{1}{2\pi}\epsilon\kappa \int_0^{2\pi} k(Q \sin x, \kappa Q \cos x) \cos x\, dx \quad (58a)$$

and

$$\delta Q = +\frac{1}{2\pi}\epsilon\kappa \int_0^{2\pi} k(Q \sin x, \kappa Q \cos x) \sin x\, dx \quad (58b)$$

Applying (58) to Equation (5) with $\delta q \ll 1$, we find

$$\dot{Q} = \frac{1}{2\pi}\frac{\delta\kappa}{2} Q^2 \int_0^{2\pi} |\cos x|^3 h(Q \sin x) dx \quad (59a)$$

and

$$\dot{\theta} = 0 \quad (59b)$$

The limit cycle amplitude Q^* follows from the condition $\dot{Q} = 0$, hence from

$$\int_0^{2\pi} |\cos x|^3 \, h(Q^* \sin x) dx = 0 \qquad (60)$$

This condition is independent of both δ and κ.

We list the results for a few examples. The function

$h = 1 - \alpha^2 q^2$ leads to $\alpha^2 Q^{*2} = 5$ or $\alpha Q^* = \sqrt{5} = 2.24$

$h = 1 - \alpha^4 q^4$ $\alpha^4 Q^{*4} = 35/3$ $\alpha Q^* = \sqrt[4]{35/3} = 1.84$

$h = 1 - \alpha^6 q^6$ $\alpha^6 Q^{*6} = 21$ $\alpha Q^* = \sqrt[6]{21} = 1.66$

$h = 1 - \alpha^{2k} q^{2k}$ $(\alpha Q^*)^{2k} =$

$$\frac{\phi_2}{\phi_2 - \left(\frac{k}{1}\right)\phi_4 + \left(\frac{k}{2}\right)\phi_6 - + \ldots \phi_{2k+2}} \qquad (61)$$

where (for n even)

$$\phi_n = \frac{4}{\pi}\int_0^{\pi/2} \cos^{n+1} x \, dx = \frac{n}{n+1}\cdot\frac{n-2}{n-1}\cdot\ldots\cdot\frac{2}{3}\cdot\frac{4}{\pi}$$

is a function frequently encountered in connection with the Kryloff-Bogoliuboff method or the Ritz method, see [10] and [11].

It would be possible to write down explicitly the results for the general form (17) of function $h(q)$. We refrain from giving the result in general terms and content ourselves with the three-term example

$$h(q) = 1 + a_1 q^2 + a_2 q^4 \qquad \text{with} \qquad a_2 < 0 \qquad (62)$$

After introducing (62) into (60) we find Q^{*2} from the quadratic equation

$$(Q^{*2})^2 - {}^7/_3 \frac{a_1}{|a_2|} Q^{*2} - {}^{35}/_3 \frac{1}{|a_2|} = 0 \qquad (63)$$

For the special case $h = 1 + q^2 - q^4$ this would lead to $Q^{*2} = 4.79$.

References

1 N. Levinson and O. Smith, "A General Equation for Relaxation Oscillations," *Duke Mathematical Journal*, vol. 9, 1942, pp. 382–403.

2 See, e.g., E. A. Coddington and N. Levinson, "Theory of Ordinary Differential Equations," McGraw-Hill Book Company, Inc., New York, N. Y., 1955.

3 K. Klotter, "Free Oscillations of Systems Having Quadratic Damping and Arbitrary Restoring Forces," JOURNAL OF APPLIED MECHANICS, vol. 22, TRANS. ASME, vol. 77, 1955, pp. 493–499.

4 K. Klotter and E. Kreyszig, "Oscillations Governed by a Modified van der Pol Equation," *Quarterly of Applied Mathematics*, to be published.

5 K. Klotter and E. Kreyszig, "Über eine besondere Klasse selbsterregter Schwingungen," *Ingenieur-Archiv*, vol. 25, 1957, pp. 389–403.

6 E. Kreyszig, "Über den allgemeinen Intergralsinus $Si(z, a)$," *Acta Mathematica*, vol. 85, 1951, pp. 117–181.

7 E. Kreyszig, "Der allgemeine Integralcosinus $Ci(z, a)$," *Acta Mathematica*, vol. 89, 1953, pp. 107–131.

8 H. Schubart, "Über die Grenzamplitude einer Klasse selbsterregter Schwingungen," *Ingenieur-Archiv*, vol. 27, 1959, pp. 66–72.

9 N. Kryloff and N. Bogoliuboff, edited by S. Lefschetz, "Nonlinear Mechanics," Princeton University Press, Princeton, N. J., 1949.

10 K. Klotter, "The Attenuation of Damped Free Vibrations," *Proceedings*, Second U. S. National Congress of Applied Mechanics, ASME, 1954, pp. 85–93.

11 K. Klotter, "Nonlinear Vibrations Problems Treated by the Averaging Method of W. Ritz," *Proceedings*, First U. S. National Congress of Applied Mechanics, ASME, 1951, pp. 125–131.

T. K. CAUGHEY
Associate Professor
of Applied Mechanics,
California Institute of Technology,
Pasadena, Calif.

Random Excitation of a Loaded Nonlinear String

This paper is devoted to the study of a chain of particles connected by a massless elastic string subjected to random excitation. It is shown that, as a result of the additional stress induced by the stretching of the string, the mean squared deflection of every particle is reduced compared with that for the equivalent linear problem.

THE linearized problem of the oscillations of a light string loaded at equal intervals was first discussed by Bernoulli [1][1] and later in more detail by Lagrange [2]. In their treatment, the tension in the string was assumed to remain constant; however, even for small deflections the tension in the string increases, giving rise to nonlinear effects. These nonlinear effects have been studied by several authors [3–7] in the case of the continuous mass distribution. The purpose of this paper is to analyze these nonlinear effects in the case of a loaded string subject to random excitation.

Formulation

Consider an elastic string of length L, clamped at its ends, and carrying N equally spaced particles of mass m. The nomenclature used is as follows:

u_i = transverse deflection of ith mass particle
T_0 = initial tension in string
m = mass of each particle
$m\beta$ = viscous damping coefficient on each mass
A = cross-sectional area of string
E = elastic modulus of string
L = length of string
$\Delta L = L/N + 1$
$mf_i(t)$ = force acting on ith mass particle

If the deflections and slopes are considered to be moderately small (consistent with the string remaining elastic), the equation of motion of the ith mass particle is

$$m\left(\frac{d^2u_i}{dt^2} + \beta\frac{du_i}{dt}\right) = \left[T_0 + \frac{EA}{2L\,\Delta L}\cdot\sum_{j=1}^{N+1}(u_j - u_{j-1})^2\right]\left[\frac{ui_{+1} + ui_{-1} - 2ui}{\Delta L}\right] + mf_i(t) \quad (1)$$

Subject to the boundary conditions:

$$u_0(t) = u_{N+1}(t) = 0 \quad (2)$$

In the analysis which follows, it will be assumed that $f_i(t)$ is a stationary, randomly varying, Gaussian variable with the following cross correlation:

$$\overline{f_i(t)f_j(t+\tau)} = \langle f_i(t)f_j(t+\tau)\rangle_{ave} = 2D\delta_{ij}\delta(\tau) \quad (3)$$

where

$$\left.\begin{aligned}\delta_{ij} &= 0 \quad i \neq j\\ &= 1 \quad i = j\end{aligned}\right\} \text{ is Kronecker's delta}$$

It will be observed that equation (1) is quasi-linear; although nonlinear in the time variable, it is linear in the space variable; hence the eigenmodes for (1) will be the same as for the linearized problem obtained by setting $A = 0$ in (1). Expressing u_i and f_i in terms of the eigenfunctions for the linearized problem, let

$$\left.\begin{aligned}u_i &= \sum_{k=1}^{N} A_k(t)\sin\frac{k\pi i}{N+1}\\ f_i &= \sum_{k=1}^{N} B_k(t)\sin\frac{k\pi i}{N+1}\end{aligned}\right\} \quad (4)$$

Consider the terms in the square bracket in (1):

$$\left[\ \right] = T_0 + \frac{EA}{2L\,\Delta L}\sum_{j=1}^{N+1}(u_j - u_{j-1})^2 \quad (5)$$

Substituting (4) into (5),

$$\left[\ \right] = T_0 + \frac{EA}{2L\,\Delta L}\sum_{j=1}^{N+1}\left(\sum_{k=1}^{N} 2A_k\sin\frac{k\pi}{2(N+1)}\cos\frac{k\pi(2j-1)}{2(N+1)}\right)^2 \quad (6)$$

$$= T_0 + \frac{2EA}{L\,\Delta L}\sum_{j=1}^{N+1}\sum_{r,s=1}^{N} A_rA_s\sin\frac{r\pi}{2(N+1)}\sin\frac{s\pi}{2(N+1)}\cos\frac{r\pi(2j-1)}{2(N+1)}\cos\frac{s\pi(2j-1)}{2(N+1)} \quad (7)$$

Interchanging the order of summation in (7):

$$\left[\ \right] = T_0 + \frac{2EA}{L\,\Delta L}\sum_{r,s=1}^{N} A_rA_s\sin\frac{r\pi}{2(N+1)}\sin\frac{s\pi}{2(N+1)}\sum_{j=1}^{N+1}\cos\frac{r\pi(2j-1)}{2(N+1)}\cos\frac{s\pi(2j-1)}{2(N+1)} \quad (8)$$

[1] Numbers in brackets designate References at end of paper.

Presented at the West Coast Conference of the Applied Mechanics Division, Pasadena, Calif., June 27–29, 1960, of THE AMERICAN SOCIETY OF MECHANICAL ENGINEERS.

Discussion of this paper should be addressed to the Secretary, ASME, 29 West 39th Street, New York, N. Y., and will be accepted until October 10, 1960, for publication at a later date. Discussion received after the closing date will be returned.

NOTE: Statements and opinions advanced in papers are to be understood as individual expressions of their authors and not those of the Society. Manuscript received by ASME Applied Mechanics Division, August 3, 1959. Paper No. 60—APMW-1.

Now

$$\sum_{j=1}^{N+1} \cos \frac{r\pi(2j-1)}{2(N+1)} \cos \frac{s\pi(2j-1)}{2(N+1)} = 0 \qquad r \neq s$$
$$= \frac{N+1}{2} \qquad r = s \tag{9}$$

(see Hildebrand, reference [8]). Hence,

$$\left[\ \right] = \left[T_0 + \frac{EA(N+1)\Delta L}{L(\Delta L)^2} \sum_{r=1}^{N} A_r^2 \sin^2 \frac{r\pi}{2(N+1)}\right] \tag{10}$$

Now $(N+1)\Delta L = L$. Let

$$\alpha = \frac{EA}{T_0(\Delta L)^2} \tag{11}$$

Hence,

$$\left[\ \right] = T_0\left[1 + \alpha \sum_{r=1}^{N} A_r^2 \sin^2 \frac{r\pi}{2(N+1)}\right] \tag{12}$$

Substitute (4) into (1) and make use of (12):

$$\sum_{k=1}^{N} m(\ddot{A}_k + \beta \dot{A}_k) \sin \frac{k\pi i}{N+1} = mf_i(t) + \frac{2T_0}{\Delta L}\left[1 + \alpha \sum_{r=1}^{N} A_r^2 \sin^2 \frac{\pi r}{2(N+1)}\right] \sum_{k=1}^{N} A_k \sin \frac{k\pi i}{N+1}\left(\cos \frac{k\pi}{N-1} - 1\right) \tag{13}$$

Dividing through by m and setting:

$$\omega_k^2 = \frac{4T_0}{m\,\Delta L} \sin^2 \frac{k\pi}{2(N+1)} \tag{14}$$

Equation (13) becomes:

$$\sum_{k=1}^{N} \left\{\ddot{A}_k + \beta \dot{A}_k + \omega_k^2\left[1 + \alpha' \sum_{r=1}^{N} A_r^2 \omega_r^2\right] A_k\right\} \sin \frac{k\pi i}{N+1} = f_i(t) \tag{15}$$

where

$$\alpha' = \frac{mAE}{4T_0^2 \Delta L} \tag{16}$$

Multiply both sides of (15) by $\sin l\pi i/(N+1)$ and sum on i from 1 to N. Now the eigenfunctions of the linearized problem have the following orthogonality properties:

$$\sum_{i=1}^{N} \sin \frac{l\pi i}{(N+1)} \sin \frac{k\pi i}{(N+1)} = 0 \qquad l \neq k$$
$$= \frac{N+1}{2}, \qquad l = k \tag{17}$$

(see Hildebrand, reference [8]).

Making use of the orthogonality conditions (17), equation (15) reduces to

$$\ddot{A}_l + \beta \dot{A}_l + \omega_l^2\left[1 + \alpha' \sum_{r=1}^{N} A_r^2 \omega_r^2\right] A_l = \frac{2}{N+1} \sum_{i=1}^{N} f_i(t) \sin \frac{l\pi i}{N+1} = B_l(t) \tag{18}$$
$$l = 1, 2, \ldots N$$

where

$$B_l(t) = \frac{2}{N+1} \sum_{i=1}^{N} f_i(t) \sin \frac{l\pi i}{N+1} \tag{19}$$

Before proceeding to the solution of equations (18), it is necessary to calculate the correlation between the various B_l and, in particular, to calculate the autocorrelation of the B_l, for if this is known, it is a simple matter to calculate the power spectrum of the B_l.

Cross Correlation Between $B_l(t)$ and $B_k(t)$

The cross correlation between $B_l(t)$ and $B_k(t)$ is defined as:

$$R_{lk}(\tau) = \overline{B_l(t)B_k(t+\tau)} = \langle B_l(t)B_k(t+\tau)\rangle_{avg} \tag{20}$$

The bar superscript denotes the time average, while the notation $\langle\ \rangle_{avg}$ indicates the ensemble or stochastic average. For a stationary process the time average and the ensemble average are the same.

Using (19), equation (20) becomes:

$$R_{lk}(\tau) = \left(\frac{2}{N+1}\right)^2 \left\langle \sum_{i,j=1}^{N} f_i(t)f_j(t+\tau) \sin \frac{l\pi i}{(N+1)} \sin \frac{k\pi j}{(N+1)} \right\rangle_{avg} \tag{21}$$

Now, from (3),

$$\overline{f_i(t)f_j(t+\tau)} = 2D\delta_{ij}\delta(\tau)$$

Hence,

$$R_{lk}(\tau) = \left(\frac{2}{N+1}\right)^2 \sum_{i,j=1}^{N} 2D\delta_{ij}\delta(\tau) \sin \frac{l\pi i}{(N+1)} \sin \frac{k\pi j}{(N+1)} \tag{22}$$

$$= 2D\left(\frac{2}{N+1}\right)^2 \delta(\tau) \sum_{i=1}^{N} \sin \frac{l\pi i}{(N+1)} \sin \frac{k\pi i}{(N+1)} \tag{23}$$

Using the orthogonality relationship (17),

$$R_{lk}(\tau) = \frac{4D}{(N+1)}\,\delta(\tau)\delta_{lk} \tag{24}$$

Thus there is no cross correlation between the B_l, and the autocorrelation of the B_l is given by

$$R_{ll}(\tau) = \frac{4D}{N+1}\,\delta(\tau) \tag{25}$$

The power spectrum $b_l(\omega)$ of $B_l(t)$ is therefore given by

$$b_l(\omega) = 4\int_0^\infty R_{ll}(\tau) \cos \omega\tau d\tau = \frac{8D}{(N+1)} \Big/ \text{cycle} \tag{26}$$

Method of Solving Equations (18)

As there exists no technique for solving equations (18) exactly, approximate techniques must be used. A method which has been used successfully in the past for nonlinear differential equations with deterministic inputs is the method of equivalent linearization [9, 10]. In this method the original nonlinear differential equation is replaced by a quasi-linear differential equation in such a way that the error (sometimes called the equation

deficiency), in so doing, is made as small as possible. The work of Klotter [10] shows that there is a very close parallel between the method of equivalent linearization and the Ritz-Galerkin method for solving linear equations. It will now be shown that by a slight modification of the technique, the method of equivalent linearization may be used to solve equations (18).

Rewriting equation (18) in the form

$$\ddot{A}_l + B\dot{A}_l + \omega_l^2 K_l A_l + \epsilon(A_1, A_2, \ldots A_N) = B_l(t) \quad (27)$$

where

$$\omega_l^2 K_l A_l + \epsilon(A_1, A_2, \ldots A_N) = \omega_l^2 \left[1 + \alpha' \sum_{r=1}^{N} A_r^2 \omega_r^2\right] A_l$$

If in (27), $\epsilon(A_1, A_2, \ldots A_N)$ is neglected, (27) is linear and can be solved readily. The smaller $\epsilon(A_1, A_2, \ldots A_N)$ is, the smaller the error in neglecting it. The logical choice of K_l is, therefore, that value of K_l which minimizes $\epsilon(A_1, A_2, \ldots A_N)$.

The choice of minimization procedure is somewhat arbitrary, but by analogy with the Ritz-Galerkin method, and for mathematical expediency, it is desirable to use the minimization of the mean squared error

$$\overline{\epsilon^2} = \frac{1}{2T} \int_{-T}^{T} (\omega_l^2)^2 \left\{\left[1 + \alpha' \sum_{r=1}^{N} \omega_r^2 A_r^2\right] A_l - K_l A_l\right\}^2 dt \quad (28)$$

If the process is an ergodic one, then equation (28) may be replaced by the stochastic average. Further, since the B_l are uncorrelated,

$$\therefore \overline{\epsilon^2} = \int_{-\infty\ N\text{-fold}}^{\infty} \int_{-\infty}^{\infty} [\omega_l^2]^2 \left\{\left[1 + \alpha' \sum_{r=1}^{N} A_r^2 \omega_r^2\right] A_l - K_l A_l\right\}^2 \prod_{i=1}^{N} \{p(A_i) dA_i\} \quad (29)$$

where $p(A_i)$ is the first probability density function of A_i; i.e., $p(A_i)dA_i$ is the probability that A_i lies in the range A_i to $A_i + dA_i$. If in (27) $\epsilon(A_1, A_2, \ldots A_N)$ is neglected, A_l is Gaussian, since B_l is Gaussian. Thus,

$$p(A_i) = \frac{1}{(2\pi)^{1/2}\sigma_i} \exp(-A_i^2/2\sigma_i^2) \quad (30)$$

$$\sigma_i^2 = \overline{A_i^2}$$

Minimizing $\overline{\epsilon^2}$ with respect to K_l:

$$K_l = \left[\int_{-\infty\ N\text{-fold}}^{\infty} \int_{-\infty}^{\infty} A^2 \prod_{i=1}^{N} \{p(A_i) dA_i\}\right]^{-1} \int_{-\infty\ N\text{-fold}}^{\infty} \int_{-\infty}^{\infty} \left[1 + \alpha' \sum_{r=1}^{N} \omega_r^2 A_r^2\right] A_l^2 \prod_{i=1}^{N} \{p(A_i) dA_i\} \quad (31)$$

Evaluating the integrals, using (30)

$$K_l = 1 + \alpha' \left[\sum_{r=1}^{N} \omega_r^2 \sigma_r^2 + 2\omega_l^2 \sigma_l^2\right] \quad (32)$$

If in equation (27) $\epsilon(\ldots)$ is neglected, then

$$\ddot{A}_l + \beta \dot{A}_l + \omega_l^2 K_l A_l = B_l(t) \quad (33)$$

The power spectrum a_l of A_l is therefore given by

$$a_l(\omega) = b_l(\omega) \{[\omega_l^2 K_l - \omega^2]^2 + [\omega\beta]^2\}^{-1} \quad (34)$$

where

$$b_l(\omega) = \frac{8D}{(N+1)} \Big/ \text{cycle}$$

The mean squared value of A_l is readily computed from (34). Thus,

$$\sigma_l^2 = \overline{A_l^2} = \int_0^{\infty} a_l(\omega) d\omega \quad (35a)$$

$$= \frac{2D}{(N+1)} \frac{1}{\beta \omega_l^2 K_l} \quad (35b)$$

Let

$$\frac{2D}{(N+1)\beta} = \mu \quad (36)$$

Then (36) becomes

$$\omega_l^2 \sigma_l^2 K_l = \mu \quad (37)$$

Substituting for K_l from (32),

$$\omega_l^2 \sigma_l^2 \left\{1 + \alpha' \left[\sum_{r=1}^{N} \omega_r^2 \sigma_r^2 + 2\omega_l^2 \sigma_l^2\right]\right\} = \mu \quad (38)$$

Let

$$\alpha' \sum_{r=1}^{N} \omega_r^2 \sigma_r^2 = S \quad (39)$$

Therefore equation (38) may be written

$$\alpha' \omega_l^2 \sigma_l^2 \{1 + S + 2\alpha' \omega_l^2 \sigma_l^2\} = \mu\alpha' \quad (40)$$

Solving for $\alpha' \omega_l^2 \sigma_l^2$,

$$\alpha' \omega_l^2 \sigma_l^2 = \frac{-(1+S) \pm [(1+S)^2 + 8\mu\alpha']^{1/2}}{4} \quad (41)$$

The negative radical may be eliminated, since $\alpha' \omega_l^2 \sigma_l^2$ is positive. Thus,

$$\alpha' \omega_l^2 \sigma_l^2 = \frac{-(1+S) + [(1+S)^2 + 8\mu\alpha']^{1/2}}{4} \quad (42)$$

Summing (42) on l from 1 to N,

$$S = \alpha' \sum_{r=1}^{N} \omega_r^2 \sigma_r^2 = \frac{N}{4} \{-(1+S) + [(1+S)^2 + 8\mu\alpha']^{1/2}\} \quad (43)$$

Rearranging terms and squaring

$$\left[1 + \left(1 + \frac{4}{N}\right) S\right]^2 = (1+S)^2 + 8\mu\alpha' \quad (44)$$

Solving for S, and retaining the positive square root:

$$S = \{-1 + [1 + 4(N+2)\mu\alpha']^{1/2}\} \left[2\left(1 + \frac{2}{N}\right)\right]^{-1} \quad (45)$$

Substituting (45) into (42), σ_l^2 may be calculated. It will be observed from (42) that $\omega_l^2 \sigma_l^2$ is independent of l, hence there is the same strain energy in each mode.

Calculation of Mean Square Deflection $\overline{U_i^2}$

Using equation (4),

$$\overline{U_i^2} = \langle U_i^2 \rangle_{avg} = \left\langle \left[\sum_{k=1}^{N} A_k \sin \frac{k\pi i}{N+1} \right]^2 \right\rangle_{avg} \tag{46}$$

$$= \sum_{l,k=1}^{N} \langle A_l A_k \rangle_{avg} \sin \frac{k\pi i}{N+1} \sin \frac{l\pi i}{N+1} \tag{47}$$

Owing to the particular cross-correlation function (3), the A_i are uncorrelated. Therefore

$$\overline{U_i^2} = \sum_{k=1}^{N} \sigma_k^2 \sin^2 \frac{k\pi i}{N+1} \tag{48}$$

Using equation (42),

$$\overline{U_i^2} = \frac{-(1+S) + [(1+S)^2 + 8\mu\alpha']^{1/2}}{4\alpha'} \sum_{k=1}^{N} \frac{1}{\omega_k^2} \sin^2 \frac{k\pi i}{N+1} \tag{49}$$

In the linearized problem obtained by setting $\alpha' = 0$ in (15),

$$\overline{U_{i,0}^2} = \mu \sum_{k=1}^{N} \frac{1}{\omega_k^2} \sin^2 \frac{k\pi i}{N+1} \tag{50}$$

Thus

$$\frac{\overline{U_i^2}}{\overline{U_{i,0}^2}} = \frac{-(1+S) + [(1+S)^2 + 8\mu\alpha']^{1/2}}{4\alpha'} \tag{51}$$

Now

$$\begin{aligned} [(1+S)^2 + 8\mu\alpha']^{1/2} &< [(1+S)^2 + 8\mu\alpha'(1+S) + (4\mu\alpha')^2]^{1/2} \\ &< [(1+S+4\mu\alpha')^2]^{1/2} \\ &< (1+S+4\mu\alpha') \end{aligned} \tag{52}$$

Therefore

$$\frac{\overline{U_i^2}}{\overline{U_{i,0}^2}} < \frac{-(1+S) + (1+S+4\mu\alpha')}{4\mu\alpha'} < 1 \tag{53}$$

Thus the mean squared deflection of every particle is always less than the mean squared deflection in the equivalent linear string.

Conclusions

From the foregoing analysis, it is clearly seen that the effect of the nonlinearity in the problem is to reduce the mean squared deflection of every particle compared with the corresponding quantity in the equivalent linear problem.

References

1 Johann Bernoulli, Petrop Comm., t III, 1728, p. 13. Also, Collected Works, vol. III, p. 198.

2 J. L. Lagrange, "Mécanique analytique," nouvelle edition, Paris, Courcier, pp. 1811–1815.

3 G. F. Carrier, "On the Non-Linear Vibration Problem of the Elastic String," *Quarterly of Applied Mathematics*, vol. 3, 1945, pp. 157–165.

4 G. F. Carrier, "A Note on the Vibrating String," *Quarterly of Applied Mathematics*, vol. 7, 1949, pp. 97–101.

5 E. W. Lee, "Non-Linear Forced Vibrations of a Stretched String," *British Journal of Applied Physics*, vol. 8, 1957, pp. 411–413.

6 T. K. Caughey, unpublished Caltech Report No. 85, 1956.

7 T. K. Caughey, "Response of a Nonlinear String to Random Loading," JOURNAL OF APPLIED MECHANICS, vol. 26, TRANS. ASME, series E, vol. 81, 1959, pp. 341–344.

8 F. B. Hildebrand, "Methods of Applied Mathematics," Prentice-Hall, Inc., New York, N. Y., 1952, chapter 3.

9 N. Minorsky, "Non-Linear Mechanics," Edwards, Ann Arbor, Mich., 1947.

10 K. Klotter, "An Extension of the Conventional Concept of the Describing Function," *Proceedings*, Symposium on Non-Linear Circuit Analysis, vol. 6, 1956, p. 151.

K. KLOTTER
Professor,
Division of Engineering Mechanics,
Stanford University, Stanford, Calif.
Mem. ASME

P. R. COBB
Assistant Professor of Engineering Science,
Arizona State University,
Tempe, Ariz.
Assoc. Mem. ASME

On the Use of Nonsinusoidal Approximating Functions for Nonlinear Oscillation Problems[1]

When treating nonlinear oscillation problems by the Ritz-Galerkin method the approximating function is conventionally chosen as a sinusoid or a polynomial of sinusoids with their amplitudes as the open parameters. In this paper the advantages are pointed out that may be gained from choosing a nonsinusoidal approximating function that contains additional parameters related to the shape of the function.

The "Parabolic" Approximation

THE Ritz-Galerkin method (or Ritz averaging method) [1][2] has been found to be a useful tool for solving boundary-value problems [2]. Also, it has been applied successfully to nonlinear oscillation problems [3, 4]. Conventionally, the function $\tilde{q}(t)$, approximating the actual solution $q(t)$, is chosen as a polynomial composed of the products of the open parameters and the co-ordinate functions (mostly trigonometric functions),

$$\tilde{q} = \sum_{k=1}^{n} C_k \psi_k(t) \tag{1a}$$

specifically

$$\tilde{q} = Q_1 \sin \omega t + Q_2 \sin 2\omega t + \ldots + Q_n \sin n\omega t. \tag{1b}$$

The accuracy of the results, in general, increases with the number of terms used; hence it is possible to improve on the results by simply taking additional terms in (1). However, adding more terms greatly increases the computational work, especially in nonlinear problems. It is possible that a considerable advantage can be gained by using more "flexible" approximating functions $\psi_k^*(t)$, individually capable of describing more closely the actual q-t relationship.

If, as is frequently the case, the curve representing the q-t relationship for a half cycle is symmetric about its mid-point, the quarter period, only one quarter of the curve need be described by the approximating function $\tilde{q}(t)$. In the remaining parts of the period the curve can be described by its symmetry properties. Thus nonperiodic approximating functions may be used.

In this paper we propose to show the advantages gained by using the parabolic function

$$\tilde{q} = Q\psi^*(t) = \frac{Q}{\alpha - 1}(\alpha\tau - \tau^\alpha) \tag{2}$$

as an approximating function. τ denotes a de-dimensionalized time

$$\tau = \frac{t}{T/4} = \frac{2\omega t}{\pi}$$

going from 0 to 1 during a quarter of the period T. The function

$$\psi^*(t) = \frac{\alpha\tau - \tau^\alpha}{\alpha - 1}$$

[1] Partial results of work supported by a grant from the National Science Foundation to Stanford University.

[2] Numbers in brackets designate References at end of paper.

Presented at the West Coast Conference of the Applied Mechanics Division, Stanford, Calif., September 9, 1959, of THE AMERICAN SOCIETY OF MECHANICAL ENGINEERS.

Discussion of this paper should be addressed to the Secretary, ASME, 29 West 39th Street, New York, N. Y., and will be accepted until October 10, 1960, for publication at a later date. Discussion received after the closing date will be returned.

NOTE: Statements and opinions advanced in papers are to be understood as individual expressions of their authors and not those of the Society. Manuscript received by ASME Applied Mechanics Division, April 30, 1959. This paper was not preprinted.

Nomenclature

$E[q] = 0$ = differential equation in $q(t)$
F = functional
I = integral of F
P = maximum value of forcing function
Q = unknown parameter
T = period of oscillation ($T = 2\pi/\omega$)
$f(q)$ = known function of q
p = known parameter in the forcing function
q = dependent variable
$\tilde{q}$ = approximating function
$r(\alpha)$, $\bar{r}(\alpha)$ = known functions of α (reference Table 1)
$s = p/\kappa^2$
t = time
$u_n(\alpha)$, $\bar{u}_n(\alpha)$ = known functions of α and n (reference Table 1)
$v(\alpha, \beta)$, $\bar{v}(\alpha, \beta)$ = known functions of α and β (reference Table 1)
α = unknown parameter
β = known constant
γ = unknown parameter
$\eta^2 = (\omega/\kappa)^2$
κ^2 = known parameter in differential equation
$\lambda(n)$ = function of n defined by equation (16)
μ = dimensional constant
$\xi^2 = (\pi\kappa/2\omega)^2$
$\sigma(n)$ = known function of n
τ = de-dimensionalized time ($\tau = 2\omega t/\pi$)
$\varphi(n)$ = function of n defined in reference [3]
$\chi(n)$ = function of n defined in reference [3]
$\psi(t)$ = co-ordinate function
ω = circular frequency
$(\dot{})$ = differentiation with respect to time t
$(\,)'$ = differentiation with respect to de-dimentionalized time τ

has the properties (primes denoting derivatives with respect to τ)

$$\psi^*(0) = 0 \qquad \psi^*(1) = 1 \qquad \psi^{*\prime}(1) = 0; \tag{3a}$$

$$\tilde{q}(0) = 0 \qquad \tilde{q}(1) = Q \qquad \tilde{q}'(1) = 0 \tag{3b}$$

Q is a conventional, coefficient-type parameter (representing an "amplitude"); α, however, is not; it determines the shape of the curve. The plot of the function $\psi^*(\alpha, \tau)$ is shown in Fig. 1 for parameter values $\alpha \to 0$, $\alpha = 2$, $\alpha = 4$, $\alpha \to \infty$. As α approaches zero the function $\psi^*(\alpha, \tau) \to 1$ and the graph of the function is a horizontal line from $\tau = 0$ to $\tau = 1$. As α approaches infinity $\psi^*(\alpha, \tau) \to \tau$, a straight line from 0, 0 to 1, 1. Thus $\psi^*(\alpha, \tau)$ assumes a shape bounded by the triangle (0, 0), (0, 1), and (1, 1).

Not infrequently the problem arises as to which of the parabolas, described by the values of the "shape parameter" α, will best represent a sinusoid. One way of determining the value α for such a best approximation is to require that the areas under the two curves, the sinusoid and the parabola, be equal:

$$\int_0^1 \sin \frac{\pi\tau}{2}\, d\tau = \int_0^1 \frac{\alpha\tau - \tau^\alpha}{\alpha - 1}\, d\tau \tag{4}$$

From (4) we find $\alpha = 2.70$. If an integer value of α is desired, the value closest to 2.7, namely, $\alpha = 3$, would be the appropriate one. In a later section use will be made of these particular values.

The Ritz-Galerkin Procedure for Generalized Functions

For problems where the integral I, which is to be given a stationary value, can be expressed as

$$I = \int_{t_1}^{t_2} F(q, \dot{q}, t)dt, \tag{5}$$

the use of the conventional type approximating functions (1a) leads to the conditions [3]

$$\frac{\partial I}{\partial C_k} = \int_{t_1}^{t_2} E[\tilde{q}]\psi_k(t)dt + \left[\frac{\partial F}{\partial \dot{\tilde{q}}}\ \psi_k(t)\right]_{t_1}^{t_2} = 0; \tag{6}$$

a set of n-equations for the n open parameters C_k. $E[q] = 0$ is the differential equation of the system under discussion. If the limits t_1 and t_2 and the co-ordinate functions are chosen so that

$$\left[\frac{\partial F}{\partial \dot{\tilde{q}}}\ \psi_k(t)\right]_{t_1}^{t_2} = 0$$

equations (6) simplify to

$$\int_{t_1}^{t_2} E(\tilde{q})\psi_k(t)dt = 0, \qquad k = 1, 2, \ldots, n. \tag{7}$$

Equations (7) are the Ritz-Galerkin equations for the conventional type of approximating functions (1a).

If more general (nonconventional type) approximating functions, e.g. (2), are used, the Ritz-Galerkin procedure takes a somewhat different form. For

$$\tilde{q} = \sum_{i=1}^{m} \tilde{q}_i(\gamma_{i1}, \gamma_{i2}, \ldots, \gamma_{in}, t) \tag{8}$$

(where m is the number of terms and n is the number of parameters per term) the Ritz conditions are:

$$\frac{\partial I}{\partial \gamma_{ik}} = \int_{t_1}^{t_2} E[\tilde{q}]\,\frac{\partial \tilde{q}}{\partial \gamma_{ik}}\, dt + \left[\frac{\partial F}{\partial \dot{\tilde{q}}}\,\frac{\partial \tilde{q}}{\partial \gamma_{ik}}\right]_{t_1}^{t_2} = 0; \tag{9}$$

$$i = 1, 2, \ldots, m; \qquad k = 1, 2, \ldots, n$$

There are as many such conditions as there are open parameters.

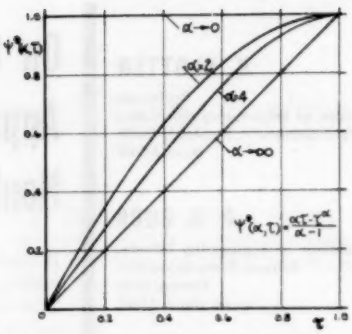

Fig. 1 Flexible approximating function $\psi^*(\alpha, \tau)$

It is seen that (9) reduces to (6) for the choice (1a) of approximating function.

For the parabolic approximation (2) conditions (9) become

$$\int_{t_1}^{t_2} E[\tilde{q}]\,\frac{\partial \tilde{q}}{\partial Q}\, dt + \left[\frac{\partial F}{\partial \dot{\tilde{q}}}\,\frac{\partial \tilde{q}}{\partial Q}\right]_{t_1}^{t_2} = 0 \tag{10a}$$

$$\int_{t_1}^{t_2} E[\tilde{q}]\,\frac{\partial \tilde{q}}{\partial \alpha}\, dt + \left[\frac{\partial F}{\partial \dot{\tilde{q}}}\,\frac{\partial \tilde{q}}{\partial \alpha}\right]_{t_1}^{t_2} = 0 \tag{10b}$$

t_1 or τ_1 can be chosen to be zero

$$\left(\frac{\partial \tilde{q}}{\partial Q} = \frac{\partial \tilde{q}}{\partial \alpha} = 0 \quad \text{at} \quad \tau_1 = 0\right)$$

and t_2 can be chosen equal to $T/4$, $\tau_2 = 1$. For $\tau_2 = 1$ it can be shown quite generally that $\partial F/\partial \dot{\tilde{q}} = 0$ for all differential equations of the form

$$\ddot{q} + \kappa^2 f(q) = 0. \tag{11}$$

By these appropriate choices of limits of integration and approximating function, equations (10a) and (10b) reduce to

$$\int_0^1 E[\tilde{q}]\psi^*(\tau)d\tau = 0 \quad \text{and} \quad \int_0^1 E[\tilde{q}]\,\frac{\partial q}{\partial \alpha}\, d\tau = 0. \tag{12}$$

These are the two conditions for Q and α.

Free Oscillations, Special Restoring Forces

In order to be able to compare the results of the parabolic approximation (2) with exact or approximate results from other sources, we shall apply the parabolic approximation (2) to free oscillations, described by the differential equation

$$\ddot{q} + \kappa^2 f(q) = 0, \tag{13}$$

for systems having

$$(a)\ \ f(q) = \mu^{n-1}q^n; \qquad (b)\ \ f(q) = \sum_n \mu^{n-1}q^n.$$

(a) $f(q) = \mu^{n-1}q^n$. Here (if de-dimensionalized with respect to time) the differential equation (13) becomes

$$q'' + \xi^2\mu^{n-1}q^n = 0 \quad \text{with} \quad \xi^2 = \frac{\pi^2\kappa^2}{4\omega^2}$$

If (2) is chosen as the approximating function, the Ritz conditions (12) yield

$$-r(\alpha) + \xi^2\mu^{n-1}Q^{n-1}u_n(\alpha) = 0 \tag{14a}$$

$$-\bar{r}(\alpha) + \xi^2\mu^{n-1}Q^{n-1}\bar{u}_n(\alpha) = 0. \tag{14b}$$

Table 1 Values of $r(\alpha)$, $\bar{r}(\alpha)$, $u_n(\alpha)$, $\bar{u}_n(\alpha)$, $v(\alpha,\beta)$, and $\bar{v}(\alpha,\beta)$

$$r(\alpha) = \alpha\left[1 - \frac{1}{2\alpha - 1}\right]$$

$$\bar{r}(\alpha) = \alpha\left[\frac{(\alpha - 1)}{(2\alpha - 1)^2} - \frac{1}{\alpha} + \frac{1}{2\alpha - 1}\right]$$

$$u_1(\alpha) = \frac{1}{(\alpha - 1)}\left[\frac{\alpha^3}{3} - \frac{2\alpha}{\alpha + 2} + \frac{1}{2\alpha + 1}\right]$$

$$\bar{u}_1(\alpha) = \frac{1}{(\alpha - 1)}\left[\frac{\alpha}{\alpha + 2} - \frac{1}{2\alpha + 1} - \frac{\alpha}{3} + \frac{1}{\alpha + 2} + \frac{\alpha(\alpha - 1)}{(\alpha + 2)^2} - \frac{(\alpha - 1)}{(2\alpha + 1)^2}\right]$$

$$u_2(\alpha) = \frac{1}{(\alpha - 1)^2}\left[\frac{\alpha^3}{4} - \frac{3\alpha^2}{(\alpha + 3)} + \frac{3\alpha}{2(\alpha + 1)} - \frac{1}{(3\alpha + 1)}\right]$$

$$\bar{u}_2(\alpha) = \frac{1}{(\alpha - 1)^2}\left[\frac{\alpha^2}{(\alpha + 3)} - \frac{\alpha}{(\alpha + 1)} + \frac{1}{(3\alpha + 1)} - \frac{\alpha^3}{4} + \frac{2\alpha}{(\alpha + 3)} - \frac{1}{2(\alpha + 1)} + \frac{\alpha^2(\alpha - 1)}{(\alpha + 3)^2} - \frac{\alpha(\alpha - 1)}{2(\alpha + 1)^2} + \frac{(\alpha - 1)}{(3\alpha + 1)^2}\right]$$

$$u_3(\alpha) = \frac{1}{(\alpha - 1)^3}\left[\frac{\alpha^4}{5} - \frac{4\alpha^3}{(\alpha + 4)} + \frac{6\alpha^2}{(2\alpha + 3)} - \frac{4\alpha}{(3\alpha + 2)} + \frac{1}{(4\alpha + 1)}\right]$$

$$\bar{u}_3(\alpha) = \frac{1}{(\alpha - 1)^3}\left[\frac{\alpha^3}{(\alpha + 4)} - \frac{3\alpha^2}{(2\alpha + 3)} + \frac{3\alpha}{(3\alpha + 2)} - \frac{1}{(4\alpha + 1)} - \frac{\alpha^3}{5} + \frac{3\alpha^2}{(\alpha + 4)} - \frac{3\alpha}{(2\alpha + 3)} + \frac{1}{(3\alpha + 2)} + \frac{\alpha^2(\alpha - 1)}{(\alpha + 4)^2} - \frac{3\alpha^2(\alpha - 1)}{(2\alpha + 3)^2} + \frac{3\alpha(\alpha - 1)}{(3\alpha + 2)^2} - \frac{(\alpha - 1)}{(4\alpha + 1)^2}\right]$$

$$v(\alpha, \beta) = \frac{1}{(\beta - 1)}\left[\frac{\beta\alpha}{3} - \frac{\beta}{(\alpha + 2)} - \frac{\alpha}{(\beta + 2)} + \frac{1}{(\alpha + \beta + 1)}\right]$$

$$\bar{v}(\alpha, \beta) = \frac{1}{(\beta - 1)}\left[\frac{\beta(\alpha - 1)}{(\alpha + 2)^2} - \frac{\beta}{3} + \frac{\beta}{(\alpha + 2)} - \frac{(\alpha - 1)}{(\alpha + \beta + 1)^2} + \frac{1}{(\beta + 2)} - \frac{1}{(\alpha + \beta + 1)}\right]$$

These two equations for the two unknowns Q and α involve certain functions of α and n; $r(\alpha)$, $\bar{r}(\alpha)$, $u_n(\alpha)$, and $\bar{u}_n(\alpha)$. These functions are listed in Table 1 for $n = 1, 2$, and 3.

Using the ratio $\eta^2 = (\omega/\kappa)^2$, we may express the results (14*a*) and (14*b*) in the forms

$$\eta^2 = \mu^{n-1}Q^{n-1}\frac{\pi^2}{4}\frac{u_n(\alpha)}{r(\alpha)} \tag{15a}$$

and

$$\eta^2 = \mu^{n-1}Q^{n-1}\frac{\pi^2}{4}\frac{\bar{u}_n(\alpha)}{\bar{r}(\alpha)}. \tag{15b}$$

For a given n the equations (15*a*) and (15*b*) must be identical; the fractions can be equated and a value of α determined. Table 2 gives values of α for $n = 0, 1, 2, 3, \ldots 7$. (Remember that the value of α determines the shape of the $\tilde{q}$-t curve.) With the values of α established for the various values of n, equations (15*a*) and (15*b*) can be expressed as

$$\eta^2 = \lambda(n)\mu^{n-1}Q^{n-1} \tag{16}$$

and values of $\lambda(n)$ can be computed (Table 2 for $n = 1, 2, 3, \ldots 7$).

(*b*) $f(q) = \sum_n \mu^{n-1}q^n$. If the restoring force is represented by a polynomial of the displacement, the differential equation becomes (with τ as the independent variable)

Table 2 Values of α and $\lambda(n)$ as a function of n

n	α	$\lambda(n)$
0	2	1.234
1	2.70	1.000
2	3.41	0.834
3	4.11	0.713
4	4.82	0.622
5	5.52	0.551
6	6.23	0.494
7	6.94	0.448

α: See equation (2).
$\lambda(n)$: See equation (16).

$$q'' + \xi^2 \sum_n \mu^{n-1}q^n = 0$$

If the approximating function (2) is used and the limits of integration are taken as $\tau_1 = 0$ and $\tau_2 = 1$, the two Ritz conditions (12) for the determination of Q and α lead to

$$-r(\alpha) + \xi^2 \sum_n \mu^{n-1}Q^{n-1}u_n(\alpha) = 0 \tag{17a}$$

$$-\bar{r}(\alpha) + \xi^2 \sum_n \mu^{n-1}Q^{n-1}\bar{u}_n(\alpha) = 0. \tag{17b}$$

These equations correspond to (14*a*) and (14*b*).

As an example of the "polynomial" system we consider

$$q'' + \xi^2(q + \mu^2 q^3) = 0$$

For this case equations (17*a*) and (17*b*) become

$$\eta^2 = \frac{\pi^2}{4}\frac{u_1(\alpha)}{r(\alpha)} + \mu^2Q^2\frac{\pi^2}{4}\frac{u_3(\alpha)}{r(\alpha)}; \tag{18a}$$

$$\eta^2 = \frac{\pi^2}{4}\frac{\bar{u}_1(\alpha)}{\bar{r}(\alpha)} + \mu^2Q^2\frac{\pi^2}{4}\frac{\bar{u}_3(\alpha)}{\bar{r}(\alpha)}. \tag{18b}$$

These two equations relate the quantities η^2, Q, and α. If any one of the three is known, the $\eta^2 - Q$ relationship and the $\tilde{q}$-t curve can be determined.

As the maximum displacement Q becomes smaller and smaller we find from equations (18*a*) and (18*b*)

$$\eta^2 = \frac{\pi^2}{4}\frac{u_1(\alpha)}{r(\alpha)} \quad \text{and} \quad \eta^2 = \frac{\pi^2}{4}\frac{\bar{u}_1(\alpha)}{\bar{r}(\alpha)}.$$

This result pertains to the linear system where $\lambda(1) = 1.0$ and $\alpha = 2.70$ (best approximation of a sine function). When the maximum displacement becomes larger and larger the effect of the first term of (18*a*) and (18*b*) becomes negligible, the limiting condition can be written as

$$\eta^2 = \frac{\pi^2}{4}\frac{u_3(\alpha)}{r(\alpha)}\mu^2Q^2 \quad \text{and} \quad \eta^2 = \frac{\pi^2}{4}\frac{\bar{u}_3(\alpha)}{\bar{r}(\alpha)}\mu^2Q^2.$$

This can be shown to be the same $\eta^2 - Q$ relationship as for a pure cubic spring [$\lambda(3) = 0.713$ and $\alpha = 4.11$].

From the foregoing consideration of limiting cases it has been shown that, depending on the maximum displacement Q, α has values between 2.70 and 4.11 and the $\eta^2 - Q$ relationship is such that η^2 approaches unity as the maximum displacement Q becomes small and that it approaches $0.713\,\mu^2Q^2$ as Q becomes large.

Comparison With Results Available

The comparison to be made here will be restricted to the simplest case, $f(q) = \mu^{n-1}q^n$, because it does not involve extensive calculations and still yields representative results. Comparison will be made between (*A*) the exact solution, (*B*) the conven-

Table 3 Values of the coefficients $\chi(n)$, $\varphi(n)$, and $\lambda(n)$ and the percentage errors

n	$\chi(n)$	$\varphi(n)$	$\lambda(n)$	Per cent error in $\varphi(n)$	Per cent error in $\lambda(n)$
0	1.234	1.273	1.234	3.2	0
1	1.000	1.000	1.000	0	0.0
2	0.837	0.849	0.834	1.4	−0.4
3	0.719	0.750	0.713	4.4	−0.8
4	0.628	0.679	0.622	8.1	−1.0
5	0.558	0.625	0.551	12.1	−1.3
6	0.501	0.582	0.494	16.1	−1.4
7	0.455	0.547	0.448	20.1	−1.5

Per cent in $\varphi(n) = \left[\frac{\varphi(n)}{\chi(n)} - 1\right] 100$

Per cent error in $\lambda(n) = \left[\frac{\lambda(n)}{\chi(n)} - 1\right] 100$

tional, one-term sinusoidal approximation, (C) the nonsinusoidal parabolic approximation as presented in the foregoing, and (D) the conventional, two-term sinusoidal approximation. The results of the first three methods (A), (B), (C) can be expressed as

$$\eta^2 = \sigma(n)\mu^{n-1}Q^{n-1}, \tag{19}$$

where $\sigma(n)$ depends on the method of solution used. $\sigma(n)$ represents $\chi(n)$ for the exact method (A) of solution [3], $\phi(n)$ for the one-term sine-function approximation (B) [3], and $\lambda(n)$ for the parabolic-function approximation (C). Form (19) of the $\eta^2 - Q$ relationship is inherent in the Ritz method when a one-term approximation is used. For values of $n = 0, 1, 2, \ldots 7$ the values of the coefficients $\chi(n)$, $\phi(n)$, and $\lambda(n)$ are listed in Table 3. Also listed are the "percentage errors"

$$\left[\frac{\sigma(n)}{\chi(n)} - 1\right] 100$$

for the two approximate solutions (B) and (C). (Because the quantity Q appears in the same power for the three methods of solution considered, the error is independent of Q and depends on n only.) By comparing the values of $\chi(n)$, $\phi(n)$, and $\lambda(n)$ we see that the methods (B) and (C) approximate the solutions quite well for small values of n. For $n = 3$ the sinusoidal approximation (B) is within 4.4 per cent of the exact result (A) and the parabolic approximation (C) is within 0.8 per cent. Furthermore, it can be shown that the two-term sinusoidal approximation (D) is within 0.27 per cent of the exact result. However, when n is large, e.g., $n = 7$, the sinusoidal approximation (B) slips to 20 per cent error while the parabolic function approximation (C) stays within 1.5 per cent of the exact answer. For the two-term sinusoidal approximation the error becomes 2.6 per cent.

It might seem unfair to compare the one-term, one-parameter sinusoidal approximation with the one-term, two-parameter parabolic approximation. It is readily admitted that the parabolic approximation involves more work than that required for the one-term sinusoid. However, it is equally unfair to compare the "parabola" to a two-term, sinusoidal approximation. Not only does the two-term sinusoid involve integrating products of sine functions, but also the resulting $\eta^2 - Q$ relationships are determined by lengthy, nonlinear algebraic equations. The parabolic approximation, on the other hand, involves integrating powers of α and solving a high-order polynomial in α. Therefore a fair comparison weighing closeness of results againts efforts expended is rather difficult to make.

Figs. 2 and 3 are plots of q versus τ and approximating error versus time for $n = 3$ using the results of the three methods (A, B, C) under consideration. They clearly show the superiority of the parabolic over the one-term sinusoidal approximation. The high degree of accuracy of the parabolic approximation is due to its ability to better represent the shape of the q-t relationship. The one-term sinusoidal assumption is compelled to approximate the actual curve by an adjustment in the maximum value only.

For the case where $f(q)$ is a polynomial, a comparison has been carried out for limiting cases of $f(q) = q + \mu^2 q^3$. The details are omitted here; they may be found in [5]. It will suffice to say that the comparison yields a graph quite similar, both qualitatively and quantitatively, to Fig. 3.

Forced Oscillations

In regard to forced oscillations, results have been obtained for the two sample systems

$$\ddot{q} + \kappa^2 q = \frac{\pm p}{\beta - 1}(\beta\tau - \tau^\beta) \tag{20a}$$

and

$$\ddot{q} + \kappa^2 \sum_n \mu^{n-1} q^n = \frac{\pm p}{\beta - 1}(\beta\tau - \tau^\beta), \tag{20b}$$

with $\beta = 3$.

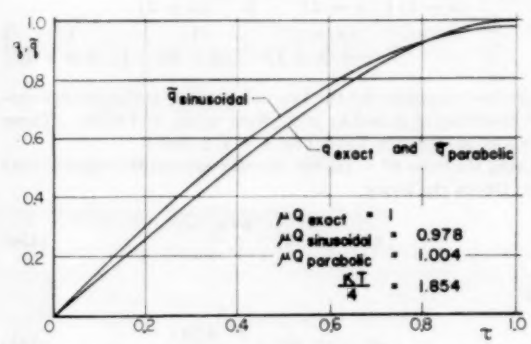

Fig. 2 Displacement-time curves for system $\ddot{q} + \kappa^2\mu^2 q^3 = 0$

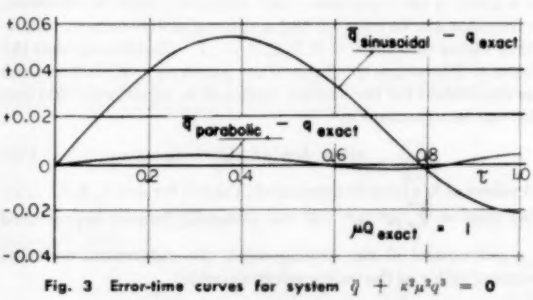

Fig. 3 Error-time curves for system $\ddot{q} + \kappa^2\mu^2 q^3 = 0$

A parabolic forcing function has been chosen instead of the customary sine function. In the realm of nonlinear differential equations the advantages of the sinusoidal forcing function disappear. Therefore, use of such a parabolic forcing function is not unreasonable. The choice of $\beta = 3$ was completely arbitrary, but 3 happens to be the nearest integer to the best value ($\beta = 2.70$) for a parabolic approximation of a sine function with the same quarter period.

Comparisons with the conventional Ritz results have been carried out for certain limiting cases of (20*a*) and (20*b*). They too will be found in [5]. Their results again indicate the advantages gained by the use of a parabolic approximation.

References

1 W. Ritz, "Über eine neue Methode zur Lösung gewisser Variations probleme der mathematischen Physik," *Crelles Journal für die reine und angewandte Mathematik*, vol. 135, 1909, pp. 1–61.

2 I. S. Sokolnikoff, "Mathematical Theory of Elasticity," McGraw-Hill Book Company, Inc., New York, N. Y., 1956, pp. 404–411.

3 K. Klotter, "Nonlinear Vibration Problems Treated by the Averaging Method of W. Ritz," Proceedings, First U. S. National Congress of Applied Mechanics, New York, N. Y., 1952, pp. 125–131.

4 K. Klotter, "Steady-State Vibrations in Systems Having Arbitrary Restoring and Arbitrary Damping Forces," Proceedings of the Symposium on Nonlinear Circuit Analysis, New York, N. Y., 1953, pp. 234–258.

5 K. Klotter and P. R. Cobb, "Nonlinear Vibration Problems Treated by Extensions of the Ritz Averaging Method," Technical Report 109, Division of Engineering Mechanics, Stanford University, Stanford, Calif., 1957. (Report available from Division of Engineering Mechanics, Stanford University.)

Journal of APPLIED MECHANICS

Brief Notes

On the recommendation of the Executive Committee of the ASME Applied Mechanics Division, it was decided to initiate a section devoted to brief notes on technical matters in mechanics. These notes must not be longer than 750 words (about 2½ double-spaced typewritten pages, including figures) and will be subject to the usual review procedure prior to publication. After approval such notes will be published as soon as possible, normally in the next issue of the Journal. The notes should be submitted to the Technical Editors of the Journal of Applied Mechanics.

Stress-Displacement Relations for Shell Membranes in Oblique Co-Ordinates

G. D. GALLETLY[1]

In this note the relations between the internal forces in a shell membrane and the corresponding deformations are derived for shells with oblique rectilinear planforms. The derivation is an extension of that previously given for rectangular planforms.

Introduction

The membrane equations of equilibrium for thin elastic shells in either orthogonal or oblique rectilinear co-ordinate systems are well known. The corresponding stress-displacement relations are not quite so well known, having been derived quite recently for orthogonal rectilinear co-ordinates by both Reissner [1][2] and Flügge and Geyling [2]. To the author's knowledge, the corresponding stress-displacement relationships for oblique rectilinear co-ordinates have not been derived. Since the use of shells with oblique rectilinear planforms is by no means unheard of, there seemed to be some merit in determining the stress-displacement relations for these shells. This objective is the purpose of the present Note. To make the presentation self-contained the equilibrium equations are also recorded, although they are not derived.

Mathematical Preliminaries[3]

An element of the shell under discussion, together with its projection on the xy-plane, is shown in Fig. 1. The angle between the x and y-axis will be denoted by 2ϕ and the z-axis will be taken perpendicular to the xy-plane (i.e., vertically downward).

Unit vectors along the x, y, and z-axes will be denoted by $\mathbf{a}$, $\mathbf{b}$, and $\mathbf{c}$. These vectors satisfy the following relations:[4]

$$\mathbf{a}\cdot\mathbf{b} = \cos 2\phi, \qquad \mathbf{b}\cdot\mathbf{c} = \mathbf{c}\cdot\mathbf{a} = 0 \tag{1}$$

$$\mathbf{a}\times\mathbf{b} = \mathbf{c}\sin 2\phi$$

$$\left.\begin{aligned}\mathbf{b}\times\mathbf{c} &= \mathbf{a}\csc 2\phi - \mathbf{b}\cot 2\phi\\ \mathbf{c}\times\mathbf{a} &= \mathbf{b}\csc 2\phi - \mathbf{a}\cot 2\phi)\end{aligned}\right\} \tag{2}$$

The radius vector to the point A on the middle surface of the shell is

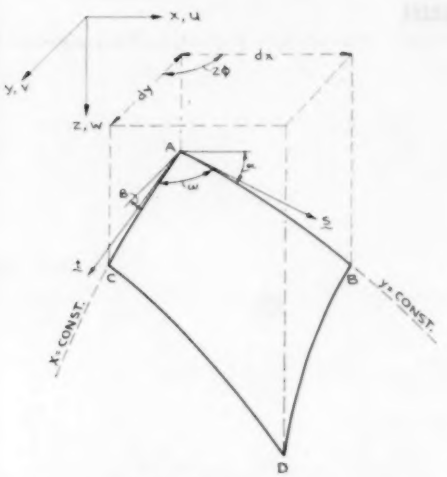

Fig. 1 Shell element and its projection on the xy-plane

$$\mathbf{r} = x\mathbf{a} + y\mathbf{b} + z\mathbf{c} \tag{3}$$

and the two vectors $\mathbf{s}$ and $\mathbf{t}$, tangent to the surface, are

$$\left.\begin{aligned}\mathbf{s} &= \partial\mathbf{r}/\partial x = \mathbf{a} + z_x\mathbf{c}\\ \mathbf{t} &= \partial\mathbf{r}/\partial y = \mathbf{b} + z_y\mathbf{c}\end{aligned}\right\} \tag{4}$$

where the subscripts x and y denote, as usual, partial differentiation with respect to those variables. The lengths of $\mathbf{s}$ and $\mathbf{t}$ are

$$\left.\begin{aligned}s &= |\mathbf{s}\cdot\mathbf{s}|^{1/2} = (1 + z_x^2)^{1/2}\\ t &= |\mathbf{t}\cdot\mathbf{t}|^{1/2} = (1 + z_y^2)^{1/2}\end{aligned}\right\} \tag{5}$$

A vector normal to the surface is obtained from

$$\mathbf{n} = \mathbf{s}\times\mathbf{t} \tag{6}$$

From Equations (2) and (4) one finds

$$\mathbf{n} = -\frac{1}{\sin 2\phi}(z_x - z_y\cos 2\phi)\mathbf{a} - \frac{1}{\sin 2\phi}(z_y - z_x\cos 2\phi)\mathbf{b} + \sin 2\phi\,\mathbf{c} \tag{7}$$

The length of $\mathbf{n}$ is found from $n = |\mathbf{n}\cdot\mathbf{n}|^{1/2}$, utilizing Equation (1). This gives

$$n = \sin 2\phi\,\sqrt{\Omega} \tag{8}$$

where

$$\Omega = 1 + \csc^2 2\phi(z_x^2 + z_y^2 - 2z_xz_y\cos 2\phi) \tag{9}$$

Thus the unit inward normal vector to the surface at the point

[1] Shell Development Company, Emeryville, Calif.

[2] Numbers in brackets indicate References at end of Note.

[3] The relations in this section follow directly from simple vector analysis.

[4] The usual vector notation is employed.

Discussion of papers in Brief Notes should be addressed to the Secretary, ASME, 29 West 39th Street, New York, N. Y., and will be accepted until October 10, 1960, for publication at a later date. Discussion received after the closing date will be returned.

Manuscript received by ASME Applied Mechanics Division, February 15, 1960.

x, y, z has the following direction cosines with the co-ordinate axes:

$$\left.\begin{aligned} l &= -\Omega^{-1/2}(z_x - z_y \cos 2\phi)\csc^2 2\phi \\ m &= -\Omega^{-1/2}(z_y - z_x \cos 2\phi)\csc^2 2\phi \\ n &= \Omega^{-1/2} \end{aligned}\right\} \tag{10}$$

These relations are useful when considering loadings other than purely vertical.

The angle ω between the two tangent vectors $\mathbf{s}$ and $\mathbf{t}$ is obtained from

$$\mathbf{s}\cdot\mathbf{t} = st\cos\omega \tag{11}$$

Thus

$$\cos\omega = \frac{\cos 2\phi + z_x z_y}{(1 + z_x^2)^{1/2}(1 + z_y^2)^{1/2}} \tag{12}$$

and

$$\sin\omega = \frac{\Omega^{1/2}\sin 2\phi}{(1 + z_x^2)^{1/2}(1 + z_y^2)^{1/2}} \tag{13}$$

The element of surface area dA is given by $dA = st\sin\omega\,dx\,dy$. Thus from Equations (5) and (13)

$$dA = \Omega^{1/2}\sin 2\phi\,dx\,dy \tag{14}$$

Equations of Equilibrium

The forces per unit length acting on the shell element will be denoted by N_x, N_y, and N_{xy}.[5]

As usual, their horizontal components per unit horizontal length of the x and y-axes will be designated by $\overline{N}_x\left(= N_x\frac{\cos\alpha}{\cos\beta}\right)$, $\overline{N}_y\left(= N_y\frac{\cos\beta}{\cos\alpha}\right)$ and $\overline{N}_{xy}(= N_{xy})$.[6] The components of the external load, in the x, y, and z-direction, per unit projected area ($dx\,dy = 1$), will be denoted by p_x, p_y, and p_z.

As is known, the equations of equilibrium assume the form

$$\left.\begin{aligned} &\frac{\partial\overline{N}_x}{\partial x} + \frac{\partial\overline{N}_{xy}}{\partial y} + p_x\sin 2\phi = 0 \\ &\frac{\partial\overline{N}_y}{\partial y} + \frac{\partial\overline{N}_{xy}}{\partial x} + p_y\sin 2\phi = 0 \\ &\frac{\partial}{\partial x}(\overline{N}_x z_x + \overline{N}_{xy}z_y) + \frac{\partial}{\partial y}(\overline{N}_y z_y + \overline{N}_{xy}z_x) \\ &\qquad + p_z\sin 2\phi = 0 \end{aligned}\right\} \tag{15}$$

The introduction of the Airy stress function F defined by

$$\left.\begin{aligned} \overline{N}_x &= F_{yy} - \sin 2\phi\int p_x dx \\ \overline{N}_y &= F_{xx} - \sin 2\phi\int p_y dy \\ \overline{N}_{xy} &= -F_{xy} \end{aligned}\right\} \tag{16}$$

satisfies the first two equations of Equations (15) identically and reduces the third to

$$z_{xx}F_{yy} - 2z_{xy}F_{xy} + z_{yy}F_{yy} = p \tag{17}$$

where p is given by

$$p = \sin 2\phi(-p_z + z_x p_x + z_y p_y + z_{xx}\int p_x dx + z_{yy}\int p_y dy) \tag{18}$$

[5] The subscript x and y on the quantities N or ϵ indicates direction and not partial differentiation.

[6] N_x, N_y, $\overline{N}_x$, $\overline{N}_y$ include both normal and shearing stresses as the parametric curves are not orthogonal. $N_{xy} = N_{xy}$ represent shear stresses only.

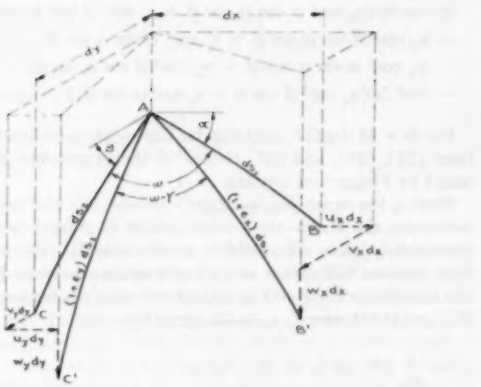

Fig. 2 Displacement components and the strains ϵ_x, ϵ_y, γ

Stress-Displacement Relations

Instead of employing Reissner's variational theorem, the stress-displacement relations will be determined herein in the traditional manner (cf. [2]). The middle-surface displacement components along the co-ordinate axes x, y, z will be denoted by u, v, and w, and a positive shear strain γ of the shell element will be defined as a decrease of the angle ω in the first quadrant of the x, y-system (see Fig. 2). The original and final lengths of the sides of the element are then

$$\left.\begin{aligned} \mathbf{AB} &= \mathbf{a}\,dx + \mathbf{c}\,dx\tan\alpha \\ \mathbf{AB}' &= \mathbf{a}(1 + u_x)dx + \mathbf{b}\,v_x dx + \mathbf{c}(\tan\alpha + w_x)dx \end{aligned}\right\} \tag{19}$$

$$\left.\begin{aligned} \mathbf{AC} &= \mathbf{b}\,dy + \mathbf{c}\,dy\tan\beta \\ \mathbf{AC}' &= \mathbf{a}\,u_y dy + \mathbf{b}(1 + v_y)dy + \mathbf{c}(\tan\beta + w_y)dy \end{aligned}\right\} \tag{20}$$

Defining extensional strain in the usual engineering manner; i.e.

$$\epsilon = \frac{\text{Final length} - \text{original length}}{\text{Original length}} \tag{21}$$

then from Equations (19) and (20) and using the relation [from Equations (1) and (3)]

$$r^2 = |\mathbf{r}\cdot\mathbf{r}| = x^2 + y^2 + z^2 + 2xy\cos 2\phi \tag{22}$$

one obtains, to the first order in u_x, and so forth:

$$\epsilon_x = (u_x + v_x\cos 2\phi)\cos^2\alpha + w_x\sin\alpha\cos\alpha \tag{23}$$

$$\epsilon_y = (v_y + u_y\cos 2\phi)\cos^2\beta + w_y\sin\beta\cos\beta \tag{24}$$

The shear strain γ is found from the relation

$$\mathbf{AC}'\cdot\mathbf{AB}' = (AC')(AB')\cos(\omega - \gamma) = (1 + \epsilon_x)(1 + \epsilon_y)dx\,dy\cos(\omega - \gamma) \doteq \cos\alpha\cos\beta \tag{25}$$

From Equations (19) and (20) there also follows

$$\mathbf{AC}'\cdot\mathbf{AB}' = dx\,dy[(1 + u_x)u_y + (1 + v_y)v_x + v_x u_y + (\tan\alpha + w_x)(\tan\beta + w_y) + (1 + u_x)(1 + v_y)\cos 2\phi] \tag{26}$$

Equating the relations (25) and (26), utilizing Equations (23) and (24), setting $\cos\gamma = 1$, $\sin\gamma = \gamma$, and retaining only terms of the first power of one of the derivatives of u, v, w, one finds:

$$\gamma = \frac{1}{\sin\omega}[(u_y\cos\alpha\cos\beta - u_x\cos^2\alpha\sin\alpha\sin\beta + v_x\cos\alpha\cos\beta - v_y\cos^2\beta\sin\alpha\sin\beta + w_x\cos^2\alpha\sin\beta + w_y\cos^2\beta\sin\alpha)$$

$$+ \cos 2\phi(u_x \sin^2 \alpha \cos \alpha \cos \beta + v_y \sin^2 \beta \cos \alpha \cos \beta$$
$$- u_y \cos^2 \beta \sin \alpha \sin \beta - v_x \cos^2 \alpha \sin \alpha \sin \beta$$
$$- w_x \cos^2 \alpha \sin \alpha \cos \beta - w_y \cos^2 \beta \cos \alpha \sin \beta)$$
$$- \cos^2 2\phi(u_y \cos^2 \beta \cos \alpha + v_x \cos^2 \alpha \cos \beta)] \quad (27)$$

For $\phi = 45$ deg (i.e., rectangular Cartesian co-ordinates) Equations (23), (24), and (27) reduce to the expressions previously found by Flügge and Geyling.

Having the strain-displacement relations, it is now necessary to determine the stress-strain relationships in oblique co-ordinates. Fortunately, these are available in reference [2]. The differential shell element will appear as a parallelogram in a plane tangent to the middle surface (see Fig. 3) and the relations between N_x, N_y, N_{xy} and the strains ϵ_x, ϵ_y, γ are given by

$$\epsilon_x = \frac{1}{Eh} [N_x \csc \omega + 2N_{xy} \cot \omega + N_y \sin \omega(\cot^2 \omega - \nu)] \quad (28)$$

$$\epsilon_y = \frac{1}{Eh} [N_y \csc \omega + 2N_{xy} \cot \omega + N_x \sin \omega(\cot^2 \omega - \nu)] \quad (29)$$

$$\gamma = \frac{(1 + \nu)}{Eh} [N_x \cos \omega + 2N_{xy} + N_y \cos \omega] \quad (30)$$

where h is the shell thickness and ν is Poisson's ratio.

The stress-displacement relations in oblique rectilinear co-ordinates are then obtained by equating the expressions (23) and (28), (24) and (29), (27) and (30). This step will not be carried out here, although there is obviously no difficulty in so doing. Instead, attention will be restricted to shallow shells, for which the stress-displacement relations are much less complicated. (A shell is defined as shallow if z_x^2, z_y^2, z_{xy} can be neglected in comparison to unity. Reissner [1] suggests that if z_x, $z_y \leq 1/5$ then shallow-shell theory should be accurate enough for practical purposes.)

For shallow shells, one has therefore:

$$\left.\begin{aligned} \cos \alpha &= \cos \beta = 1 \\ \sin \alpha &= \tan \alpha = z_x \\ \sin \beta &= \tan \beta = z_y \\ \cos \omega &= \cos 2\phi \therefore \omega = 2\phi \end{aligned}\right\} \quad (31)$$

Utilizing the approximations (31) in Equations (23), (24), and (27), substituting the resulting expressions in Equations (28), (29), and (30), neglecting the quadratic terms of the slope components z_x and z_y, and setting

$$\bar{N}_x = N_x, \quad \bar{N}_y = N_y, \quad \bar{N}_{xy} = N_{xy}$$

one obtains

$$(u_x + v_x \cos 2\phi + w_x z_x) = \frac{\csc 2\phi}{Eh} [\bar{N}_x + 2\bar{N}_{xy} \cos 2\phi + \bar{N}_y(\cos^2 2\phi - \nu \sin^2 2\phi)] \quad (32)$$

$$(v_y + u_y \cos 2\phi + w_y z_y) = \frac{\csc 2\phi}{Eh} [\bar{N}_y + 2\bar{N}_{xy} \cos 2\phi + \bar{N}_x(\cos^2 2\phi - \nu \sin^2 2\phi)] \quad (33)$$

$$[(u_y + v_x) \sin^2 2\phi + (w_x z_y + w_y z_x) - (w_x z_x + w_y z_y) \cos 2\phi] = \frac{(1 + \nu) \sin 2\phi}{Eh} [\bar{N}_x(\cos 2\phi + 2\bar{N}_{xy} + \bar{N}_y \cos 2\phi)] \quad (34)$$

Equations (32) to (34) are the stress-displacement relations in oblique rectilinear co-ordinates according to linear shallow-shell membrane theory. For $\phi = 45$ deg they reduce to those given previously by Reissner.

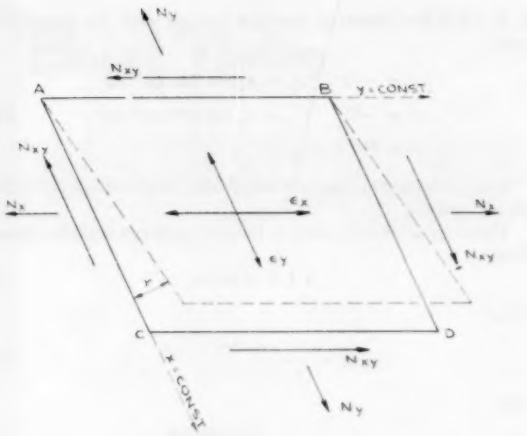

Fig. 3 Projection of shell element onto plane tangent to the middle surface

Final Note

It is not clear whether the membrane deformations, in either rectangular or oblique co-ordinates, adequately portray the deformation picture for shells of negative Gaussian curvature (e.g., hyperbolic paraboloids). In connection with this, see reference [2]. It is also of interest to note that Vlasov [3] states that membrane theory cannot be applied to such shells.

The author is indebted to the reviewer of this note for drawing his attention to references [4] and [5]. Unfortunately, the author has been unable to obtain a copy of [4]. In [5], Rüdiger derives two second-order partial differential equations for shells with oblique rectilinear planforms using the tensorial formulation of differential geometry. One of these equations is in terms of displacements, the other in terms of a stress function. This latter is equivalent to Equation (18) of this Note.

References

1 E. Reissner, "On Some Aspects of the Theory of Thin Elastic Shells," *Journal of the Boston Society of Civil Engineers*, vol. 42, 1955, pp. 100–133.

2 W. Flügge and F. Geyling, "A General Theory of Deformations of Membrane Shells," Proceedings, Ninth International Congress of Applied Mechanics, vol. 6, 1957, pp. 250–262.

3 V. Z. Vlasov, "Cylindrical Shells and New Ways of Developing Thin-Walled Spatial Systems in Structural Mechanics," Proceedings, Second Symposium on Concrete Shell Roof Construction, 1958, pp. 121–146 (see item 7 on p. 146).

4 A. Beles and M. Mihailescu, "Equilibrium Equations in Oblique Co-ordinates for Shells of Constant Thickness," *Applied Mechanics Reviews*, vol. 11, 1958, Rev. No. 4430.

5 D. Rüdiger, "Spannungen und Verschiebungen der krummen Flächen mit schiefem Grundriss," *Ingenieur-Archiv*, vol. 9, 1955, p. 265.

A Note on the Stability Problem of Shallow Translational Shells

KRISTOFFER APELAND[1]

REISSNER's procedure for determining buckling loads, origi-

[1] Civil Engineer (Norway), University of California, Berkeley, Calif. Appointment supported by the International Cooperation Administration under the Visiting Research Scientists Program administered by the National Academy of Sciences of the United States of America.

Manuscript received by ASME Applied Mechanics Division, January 29, 1960.

nally applied to hyperbolic paraboloid shells of equal and opposite principal curvatures in reference [1],[2] will be generalized to the case of any shallow translational surface. The explicit solutions obtained are based on Marguerre's equations [2] which have been suitably amended by inclusion of a curvature parameter.

1 Basic differential equations

We consider a class of shallow translational shells, the middle surface of which is defined by

$$z(x, y) = \frac{1}{2} k_2(\gamma x^2 - y^2) \quad \text{where} \quad \gamma = \frac{k_1}{k_2}. \tag{1}$$

Introduction of (1) into Marguerre's nonlinear bending equations yields

$$\begin{aligned} \nabla^4 F &= Eh[k_2(w_{,xx} - \gamma w_{,yy}) + (w_{,xy})^2 - w_{,xx} w_{,yy}] \\ &\quad + (\int q_x dx)_{,yy} + (\int q_y dy)_{,xx} - \nu(q_{x,x} + q_{y,y}) \\ D\nabla^4 w &= q_z - k_2(F_{,xx} - \gamma F_{,yy}) + w_{,xx}F_{,yy} + w_{,yy}F_{,xx} \\ &\quad - 2w_{,xy}F_{,xy} - [(\gamma k_2 x + w_{,x})(\int q_x dx)]_{,x} \\ &\quad - [(-k_2 y + w_{,y})(\int q_y dy)]_{,y} \end{aligned} \tag{2}$$

where w is the transverse displacement component, and the Airy stress function $F(x, y)$ is defined by:

$$N_{xx} = F_{,yy} - \int q_x dx, \quad N_{yy} = F_{,xx} - \int q_y dy, \quad N_{xy} = -F_{,xy}. \tag{3}$$

All symbols used have the usual meaning of the theory of shells. We note that the middle surface of the shell is an elliptic paraboloid, cylinder, or a hyperbolic paraboloid according to $\gamma < 0$, $\gamma = 0$, or $\gamma > 0$. For load in the z-direction only, (2) can be specialized as follows.

Nonlinear bending theory

$$\begin{aligned} \nabla^4 F - Eh[k_2(w_{,xx} - \gamma w_{,yy}) + (w_{,xy})^2 - w_{,xx}w_{,yy}] &= 0 \\ D\nabla^4 w + k_2(F_{,xx} - \gamma F_{,yy}) - w_{,xx}F_{,yy} + 2w_{,xy}F_{,xy} & \\ - w_{,yy}F_{,xx} &= q_z. \end{aligned} \tag{4}$$

Linear bending theory

$$\begin{aligned} \nabla^4 F - Ehk_2(w_{,xx} - \gamma w_{,yy}) &= 0, \\ D\nabla^4 w + k_2(F_{,xx} - \gamma F_{,yy}) &= q_z. \end{aligned} \tag{5}$$

Nonlinear membrane theory

$$\begin{aligned} \nabla^4 F - Eh[k_2(w_{,xx} - \gamma w_{,yy}) + (w_{,xy})^2 - w_{,xx}w_{,yy}] &= 0, \\ (k_2 - w_{,yy})F_{,xx} - (\gamma k_2 + w_{,xx})F_{,yy} + 2w_{,xy}F_{,xy} &= q_z. \end{aligned} \tag{6}$$

Linear membrane theory

$$k_2(F_{,xx} - \gamma F_{,yy}) = q_z. \tag{7}$$

2 Solution of a particular boundary-value problem

For constant uniform load on the shell the linear membrane theory equation (7) has a solution of the following form:

$$F = \frac{q_z}{2k_2(1 + \gamma^2)}(x^2 - \gamma y^2), \qquad w = 0. \tag{8}$$

By inspection it may be seen that the expressions (8) also satisfy the equations (4). Therefore for any translational shell the linear membrane theory solutions (8) are also a solution of the boundary-value problem of the more complete nonlinear bending theory, i.e., the particular case when the boundary conditions are directly satisfied by the solution. For a rectangular shell bounded by lines $x = (0, a)$ and $y = (0, b)$, solution (8) satisfies the following boundary conditions:

$$\left.\begin{aligned} w &= 0 \\ M_{xx} &= 0 \\ N_{xy} &= 0 \\ N_{xx} &= -\gamma q_z/k_2(1 + \gamma^2) \end{aligned}\right\} \text{at } x = 0, a, \quad \text{and}$$

$$\left.\begin{aligned} w &= 0 \\ M_{yy} &= 0 \\ N_{yx} &= 0 \\ N_{yy} &= q_z/k_2(1 + \gamma^2) \end{aligned}\right\} \text{at } y = 0, b \tag{9}$$

These boundary conditions are seldom encountered in practice. However, we are interested in the solution (8) mainly as a basis for investigating effects which are not influenced significantly by the boundary conditions. Hence the foregoing solution may serve as a basis for the study of a wider range of problems. The range of applicability of the foregoing solution will be studied (see section 4). Although not explicitly stated in reference [1], the boundary conditions (9) were implied in Reissner's derivation of the buckling load for hyperbolic paraboloid shells.

3 A stability problem approach for uniformly loaded shells

Following Reissner [1] we investigate the solution (8) of the boundary-value problem given by the differential equations (4) and the boundary conditions (9). To determine if other solutions of the problem are possible, we add incremental functions to the solutions (8) for w and F.

$$F = \frac{q_z}{2k_2(1 + \gamma^2)}(x^2 - \gamma y^2) + \Phi, \quad w = 0 + w. \tag{10}$$

Introducing (10) into the differential equations (4) and retaining only the linear terms results in the following equations:

$$\begin{aligned} \nabla^4 \Phi - Ehk_2(w_{,xx} - \gamma w_{,yy}) &= 0 \\ D\nabla^4 w + k_2(\Phi_{,xx} - \gamma \Phi_{,yy}) & \\ + \frac{q_z}{k_2(1 + \gamma^2)}(\gamma w_{,xx} - w_{,yy}) &= 0. \end{aligned} \tag{11}$$

Equations (11) are satisfied by a solution of the following form:

$$\begin{aligned} w &= A \sin(\alpha x) \sin(\beta y) \\ \Phi &= B \sin(\alpha x) \sin(\beta y) \end{aligned} \tag{12}$$

where A and B are constants, and α and β are defined by

$$\alpha = \frac{m\pi}{a}, \quad \beta = \frac{n\pi}{b}. \tag{12a}$$

Introduction of the expressions (12) into the equations (11) gives the following equations for the unknown coefficients A and B:

$$\begin{aligned} Ehk_2(\alpha^2 - \gamma\beta^2)A + (\alpha^2 + \beta^2)^2 B &= 0 \\ \left[D(\alpha^2 + \beta^2)^2 - (\gamma\alpha^2 - \beta^2)\frac{q_z}{k_2(1 + \gamma^2)}\right]A & \\ - k_2(\alpha^2 - \gamma\beta^2)B &= 0. \end{aligned} \tag{13}$$

The determinant of the system (13) must vanish for nontrivial solutions. From this condition the admissible values of a uniform load $q_z = -p_0$ are given by the expression:

$$\frac{p_0}{k_2(1 + \gamma^2)} = D\frac{(\alpha^2 + \beta^2)^2}{\beta^2 - \gamma\alpha^2} + Ehk_2^2\frac{(\alpha^2 - \gamma\beta^2)^2}{(\beta^2 - \gamma\alpha^2)(\alpha^2 + \beta^2)^2}. \tag{14}$$

Equation (14) gives the admissible values of the load p_0 for any shallow translational shells. Special cases are as follows:

[2] Numbers in brackets indicate References at end of Note.

(a) Hyperbolic paraboloid shell having equal and opposite principal curvatures ($\gamma = 1$):

$$\frac{p_0}{2k_2} = D\frac{(\alpha^2+\beta^2)^2}{\beta^2-\alpha^2} + Ehk_2^2\frac{\beta^2-\alpha^2}{(\alpha^2+\beta^2)^2} \tag{15}$$

which except for notation is identical to the formula presented by Reissner [1].

(b) Rotational paraboloid shell ($\gamma = -1$):

$$\frac{p_0}{2k_2} = D(\alpha^2+\beta^2) + Ehk_2^2\frac{1}{\alpha^2+\beta^2}. \tag{16}$$

Replacing k_2 in the expression (16) by $1/R$ we find an approximate formula for shallow spherical shells, viz.:

$$p_0 = \frac{Eh}{R}\left[\frac{h^2(\alpha^2+\beta^2)}{6(1-\nu^2)} + \frac{2}{R^2(\alpha^2+\beta^2)}\right], \tag{17}$$

which is a well-known formula from the classical buckling theory of spherical shells; see, for example, Girkmann [3], Equation no. (1310b).

Parabolic cylindrical shells

($\gamma = 0$):

$$\frac{p_0}{k_2} = D\frac{(\alpha^2+\beta^2)^2}{\beta^2} + Ehk_2^2\frac{\alpha^4}{\beta^2(\alpha^2+\beta^2)^2}. \tag{18}$$

Replacing k_2 in the expression (18) by $1/R$, we find an approximate formula for shallow circular cylindrical shells, viz.:

$$p_0 = \frac{Eh}{R}\left[\frac{h^2(\alpha^2+\beta^2)^2}{12(1-\nu^2)\beta^2} + \frac{\alpha^4}{R^2(\alpha^2+\beta^2)^2\beta^2}\right]. \tag{19}$$

For very long cylindrical shells we may set $\alpha \approx 0$. The formulas (18) and (19) then reduce to buckling formulas for vaults, including snap-through buckling. See, for example, Timoshenko [4].

4 Discussion

It should be emphasized that the procedure used in developing the buckling formula has the same limitations as the classical stability theory approach. Moreover, it is limited by the shallowness restrictions, that is, the assumptions that $(z_{,x})^2$, $(z_{,y})^2$, and $(z_{,x}z_{,y})$ are negligible in comparison with unity. This limitation on the application of the shallow-shell theory is discussed by Reissner [1], who states as a general rule that shallow-shell theory will be more than sufficiently accurate as long as $(z_{,x})$, $(z_{,y}) \leq 1/8$ and often accurate enough for practical purposes as long as $(z_{,x})$, $(z_{,y}) \leq 1/2$.

As was pointed out in section 2, we will determine when the derived formulas will have physical significance other than for the particular boundary conditions (9). It can be seen by inspection that the second term on the right of Equation (14) expresses the coupling of the Φ-effect to the w-effect. This term increases the possible values of the load p_0 for a given set of values of α and β. If we consider the special case when the second term is zero, we find that the smallest possible value of p_0 is obtained for $\alpha = 0$, that is, for infinitely long buckling length in x-direction. We introduce the half wave lengths l_x and l_y defined by the equations

$$\alpha = \frac{\pi}{l_x}, \quad \beta = \frac{\pi}{l_y}. \tag{20}$$

As was pointed out by Reissner [1], a finite value of the buckling length l_x will only modify the solution but will not change its character. We therefore study the simple case $\alpha = 0$. Then the Equation (14) reduces to

$$\frac{p_0}{k_2(1+\gamma^2)} = D\frac{\pi^2}{l_y^2} + Ehk_2^2\gamma^2\frac{l_y^2}{\pi^2}. \tag{21}$$

From Equation (21) we obtain the following value of the buckling length l_y which makes p_0 smallest, i.e.,

$$l_y = \frac{\pi}{\sqrt[4]{12(1-\nu^2)}}\cdot\sqrt{\frac{h}{\gamma k_2}} = \frac{\pi}{4\sqrt[4]{3(1-\gamma^2)}}\cdot a\cdot\sqrt{\frac{h}{c_1}}, \tag{22}$$

where

$$\gamma k_2 = k_1 = \frac{8c_1}{a^2} \tag{22a}$$

and c_1 is the rise of the shell over the length a in the x-direction. If we set the length a equal to the width b, we see that for sufficiently small values of h/c_1 the half wave length l_y is appreciably smaller than the width of the shell. This means that, when $h/c_1 \ll 1$, a large number of nodes will be formed. Therefore, when $h/c \ll 1$, the effect of the boundary conditions on the solution tends to become insignificant and consequently (14) gives the possible values of the load p_0 for any boundary conditions on such a shell.

If we identify the half wave length l_x with the finite length a of the cylindrical shell, we may write Equation (18) in the following form:

$$\frac{p_0}{k_2} = Ehk_2^2\frac{b^2}{\pi^2}\left[\frac{\pi^4}{768(1-\nu^2)}\left(\frac{b}{a}\right)^4\left(\frac{h}{c}\right)^2\frac{\left[1+\left(n\frac{a}{b}\right)^2\right]^2}{n^2} + \frac{1}{n^2\left[1+\left(n\frac{a}{b}\right)^2\right]^2}\right] \tag{23}$$

By inspection it can be seen from Equation (23) that, for $h/c \ll 1$, the first term on the right will be negligible in comparison with the second term as long as n is a small number. Therefore the smallest value of p_0 will occur for large n values, which means that for cylindrical shells of ordinary side length ratios the criterion for application of (14) is also $h/c \ll 1$.

However, we see from expression (18) that for $\alpha = 0$, that is, for the infinitely long cylindrical shell, we obtain the buckling formula for the shallow vault, including snap-through. This special case is therefore limited to the boundary conditions (9).

References

1 E. Reissner, "On Some Aspects of the Theory of Thin Elastic Shells," *J. Boston Society of Civil Engineers*, 1955, pp. 100–133.

2 K. Marguerre, "Zur Theorie der Gekrümmten Platte Grosser Formänderung," Proceedings of Fifth International Congress of Applied Mechanics, 1938, pp. 93–101.

3 K. Girkmann, "Flächentragwerke," Springer Verlag, Wien, 1954.

4 S. Timoshenko, "Theory of Elastic Stability," McGraw-Hill Book Co., Inc., New York, N. Y., 1936.

Transient Response of Linear Viscoelastic Plates[1]

G. E. MASE[2]

THE governing equation for the dynamic response of linear viscoelastic plates based upon small deflection theory has been given by Biot.[3] This equation, developed from the associated elastic plate equation by means of the principle of correspondence relating equations in the two fields, is taken here in the form

$$B_1\nabla^4 w(x, y, t) + \rho h p^2 w(x, y, t) = f(x, y, t) \qquad (1)$$

in which

w = the deflection of the middle surface of the plate
ρ = the plate density
h = the plate thickness (assumed constant)
f = the plate loading per unit area
B_1 = a linear differential time operator
p = the operator $\dfrac{\partial}{\partial t}$

In the notation of the Biot reference,[3] the operator B_1 is given as

$$B_1 = \frac{h^3 Q(3KP + Q)}{3P(3KP + 4Q)} \qquad (2)$$

for a plate material which responds elastically under hydrostatic pressure. Here K is the bulk modulus of the material, and P and Q are linear operators of the form

$$P = \sum_{n=0}^{E} a_n \frac{\partial^n}{\partial t^n}, \qquad Q = \sum_{n=0}^{F} b_n \frac{\partial^n}{\partial t^n}$$

From this it is evident that B_1 may be written

$$B_1 = \frac{R(p)}{S(p)} \qquad (3)$$

in which $R(p)$ and $S(p)$ are polynomials in the operator p.

If Equation (1) is subjected to a Laplace transformation with respect to time, it is observed that the resulting transformed equation has the same form as the equation governing the static deflection of an elastic plate of the same shape, resting upon an elastic foundation and having essentially the same boundary conditions. Thus Equation (1) becomes upon transformation (bars denote transforms of unbarred terms),

$$\frac{R(s)}{S(s)}\nabla^4 \bar{w}(x, y, s) + \rho h s^2 \bar{w}(x, y, s) = \bar{f}(x, y, s) \qquad (4)$$

for a plate which is initially at rest in its undeflected position. Rearranging, this may be written

$$\nabla^4 \bar{w} = \frac{S(s)}{R(s)}\bar{f} - \frac{\rho h s^2 S(s)}{R(s)}\bar{w} \qquad (5)$$

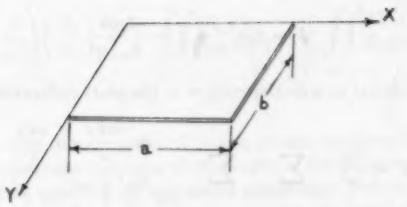

Fig. 1 Rectangular plate

which is observed to have the exact form in the space variables of the elastic foundation plate equation (see Timoshenko[4]). Therefore, using the literature of known solutions to the static elastic equation, transformed solutions of the dynamic viscoelastic solutions are obtained and these inverted directly by the usual operational procedures to give the desired result.

As an example, consider a simply supported rectangular plate of the dimensions shown in Fig. 1 assumed to be made of a Kelvin type material which is designated by

$$P = 1$$
$$Q = 2G + 2\eta p$$

where G is the shear modulus, and η the coefficient of viscosity. Let a uniformly distributed load of intensity f_0 be suddenly applied at time $t = 0$. Then

$$f(x, y, t) = f_0 U(t)$$

in which $U(t)$ is the unit step function. Equation (5) for this case becomes

$$\nabla^4 \bar{w} = \frac{f_0}{\frac{h^3}{3}(G + \eta s)s} - \frac{\rho h s^2 \bar{w}}{\frac{h^3}{3}(G + \eta s)s} \qquad (6)$$

the solution of which (see Timoshenko[4]) is given as

$$\bar{w} = \frac{16 f_0}{\pi^2}\sum_{m=1,3,5}^{\infty}\sum_{n=1,3,5}^{\infty}\frac{\sin\dfrac{m\pi x}{a}\sin\dfrac{n\pi y}{b}}{mns\,(2GA_{mn} + 2\eta A_{mn}s + \rho h s^2)} \qquad (7)$$

in which

$$A_{mn} = \frac{\pi^4 h^3}{6}\left(\frac{m^2}{a^2} + \frac{n^2}{b^2}\right)^2$$

Formal termwise Laplace inversion of this series gives

$$w(x, y, t) = \frac{8 f_0}{G\pi^2}\sum_{m=1,3,5}^{\infty}\sum_{n=1,3,5}^{\infty}\frac{1}{mn\,A_{mn}}\left\{1 + \left(\frac{1}{1 - \dfrac{A_{mn}\eta^2}{2\rho h G}}\right)^{1/2} e^{-\frac{\eta A_{mn}}{\rho h}t}\sin\left(\sqrt{\frac{2GA_{mn}}{\rho h} - \frac{A_{mn}^2\eta^2}{\rho^2 h^2}}\,t - \psi\right)\right\}\sin\frac{m\pi x}{a}\sin\frac{n\pi y}{b} \qquad (8)$$

[1] The results presented herein were obtained in the course of research sponsored by the Division of Engineering Research, Michigan State University, East Lansing, Mich.

[2] Associate Professor of Applied Mechanics, Michigan State University, East Lansing, Mich.

[3] M. A. Biot, "Dynamics of Viscoelastic Anisotropic Media," Proceedings of the Second Midwestern Conference on Solid Mechanics, Purdue University, September, 1955, p. 94.

Manuscript received by ASME Applied Mechanics Division, October 15, 1959.

[4] S. Timoshenko, "Theory of Plates and Shells," McGraw-Hill Book Company, Inc., New York, N. Y., 1940, pp. 248 and 249.

[5] Ibid., p. 252.

where $$\psi = \tan^{-1}\sqrt{1 - \frac{2gph}{A_{mn}\eta^2}}$$

It is of interest to note that as $t \to \infty$ the plate deflection becomes

$$w = \frac{16f_0}{\pi^2}\sum_{m=1,3,5,}^{\infty}\sum_{n=1,3,5}^{\infty}\frac{\sin\frac{m\pi x}{a}\sin\frac{n\pi y}{b}}{mn\,\frac{Gh^3}{3}\left(\frac{m^2}{a^2}+\frac{n^2}{b^2}\right)^2}$$

Thus the transient response in this case is a decaying sine vibration about the terminal elastic deflection position.

A Note on the Hydrodynamic Pocket Bearing

C. F. KETTLEBOROUGH[1]

Using relaxation methods, accurate solutions are presented for the hydrodynamic pocket bearing. These are compared with an approximate solution. It is found that the latter gives quite accurate results with a considerable decrease in time and effort.

Nomenclature

A = width of bearing
b^* = side land width
B^* = length of pumping land
C_F = friction function
C_W = load function
$C_f = C_F/C_W = fL/h_1$
d^* = end land width
E^* = length of pocket
f = coefficient of friction
F = friction force
G^* = width of pocket
h_1 = outlet film thickness
h_2 = film thickness over pumping land
k = film ratio h_2/h_1
L = length of bearing in direction of motion
p = pressure
P = nondimensional pressure $\left(p = \frac{6\mu UL}{h_1^2}P\right)$
P_p = pocket pressure
U = velocity of moving surface
w^* = effective pocket perimeter = $(2E + G)$
W = total load
x, z = co-ordinates
X, Z = nondimensional co-ordinates
μ = viscosity of oil

Introduction

The hydrodynamic pocket thrust bearing was first discussed by Wilcock [1].[2] Further results, using the electrolytic tank, were reported by Kettleborough [2]; in the discussion to this paper, Wilcock improves on his approximate solution but points out that his computations and those obtained by the electrolytic tank differed considerably. In order to check the relative accuracy of the results, the governing equations have been solved by relaxation methods.

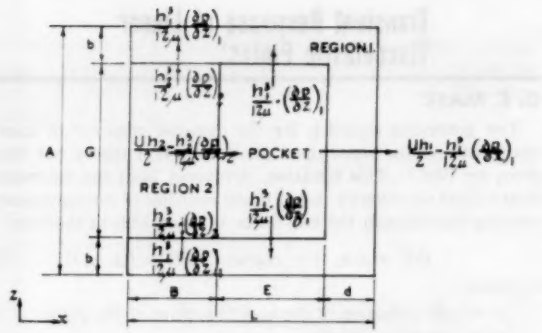

Fig. 1 Plan view of pocket bearing, showing components of oil flow per unit length

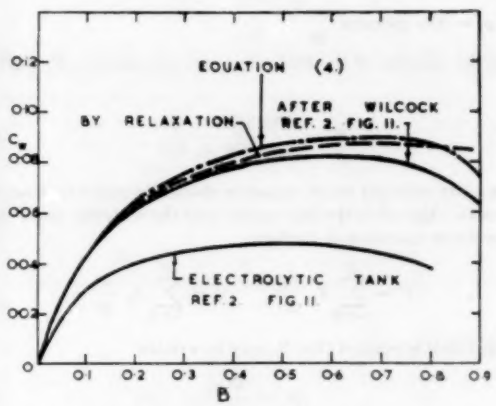

Fig. 2 Load function for different lengths of pumping land

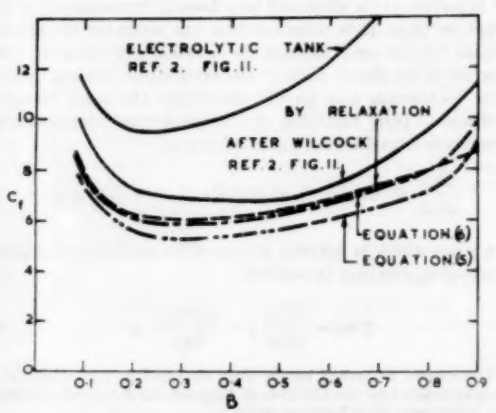

Fig. 3 Friction function for different lengths of pumping land

Theory

Because the oil-film boundaries are parallel surfaces, Reynolds equation reduces to Laplace's equation. Thus over each parallel section the pressure distribution is given by $\nabla^2 p = 0$ with the boundary conditions that p is zero (relative to atmosphere)

[1] Professor of Mechanical Engineering, University of Auckland, New Zealand.

[2] Numbers in brackets indicate References at end of Note.

* These symbols are illustrated in Fig. 1. They are all nondimensional in terms of length L.

Manuscript received by ASME Applied Mechanics Division, July 17, 1959.

around the edges of the bearing and the continuity equation for the pocket (see Fig. 1) which is

$$\int^G \left\{ \frac{Uh_2}{2} - \frac{h_2^3}{12\mu}\left(\frac{\partial p}{\partial x}\right)_2 \right\} dz = \int^G \left\{ \frac{Uh_1}{2} - \frac{h_1^3}{12\mu}\left(\frac{\partial p}{\partial x}\right)_1 \right\} dz + 2\int^E \frac{h_1^3}{12\mu} \cdot \left(\frac{\partial p}{\partial z}\right)_1 dx \quad (1)$$

Using the substitutions defined in the Nomenclature this equation takes the nondimensional form

$$\int^G \left\{ k^2 \left(\frac{\partial P}{\partial X}\right)_2 - \left(\frac{\partial P}{\partial X}\right)_1 \right\} dZ + 2\int^E \left(\frac{\partial P}{\partial Z}\right)_1 \cdot dX = G(k-1) \quad (2)$$

The equation for the pressure distribution is

$$\nabla^2 p = 0 \quad (3)$$

For a given pad geometry equation (3) is solved by relaxation techniques in a similar manner to that described in reference [3]. In applying the continuity equation (2), the slopes are determined by finite difference formulas at the edge of the pocket along each mesh line and the integration carried out numerically.

Knowing the nondimensional pressure parameter, the operating characteristics are

$$C_W = \left(\frac{W}{\mu U}\right)\left(\frac{h_1^2}{L^2}\right) = 6\int_0^1 \int_0^{A/L} P \, dX \, dZ$$

$$C_F = \left(\frac{F}{\mu U}\right)\left(\frac{h_1}{L^2}\right) = -\iint_{\text{Region 1}} dX\,dZ - \frac{1}{k}\iint_{\text{Region 2}} dX\,dZ - 3(k-1)\int^G P_p \cdot dZ$$

For $k = 1.88$, $b = d = 0.1$, $G = 0.8$, results are given in Figs. 2 and 3 to show the influence of the length of the pumping land.

Wilcock's approximate solution is modified so that (a) the end land width d is not necessarily equal to the side land width; (b) the effective pocket perimeter w equals $(2E + G)$; (c) corrections are made to Wilcock's equations (29) (reference [2], p. 542).

The operating characteristics are

$$C_W = \left(\frac{W}{\mu U}\right)\left(\frac{h_1^2}{L^2}\right) = \frac{6d(k-1)G \cdot b}{\alpha(Gb + 2Ed + k^3KGdb \cdot Ctnh\ KB)} \quad (4)$$

$$C_F = \left(\frac{F}{\mu U}\right)\left(\frac{h_1}{L^2}\right) = \left(\frac{GB}{k} + 2b + Gd\right) \quad (5)$$

where

$$\frac{1}{\alpha} = \left(\frac{G+b}{K}\right)\left\{ ctnh\ KB - csch\ KB + K\left(E + \frac{d}{2}\right)\right\}$$

and

$$K = \left(\frac{2}{k^4 bG}\right)^{1/2}$$

Computations have been made using these formulas and are

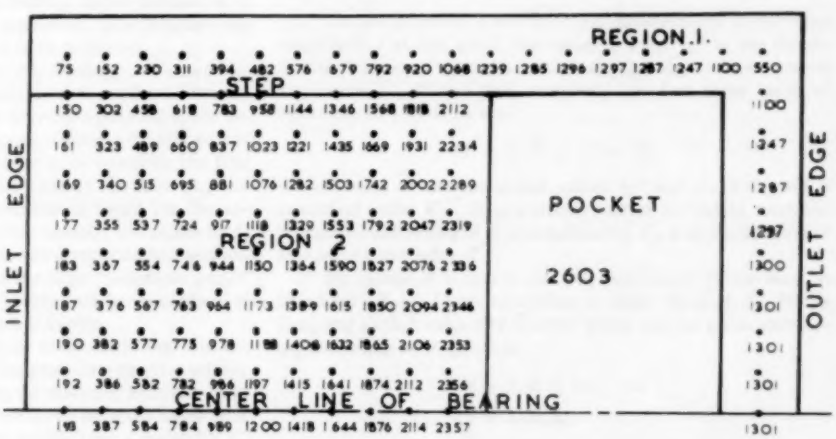

Fig. 4 Nondimensional pressure distribution for pocket bearing

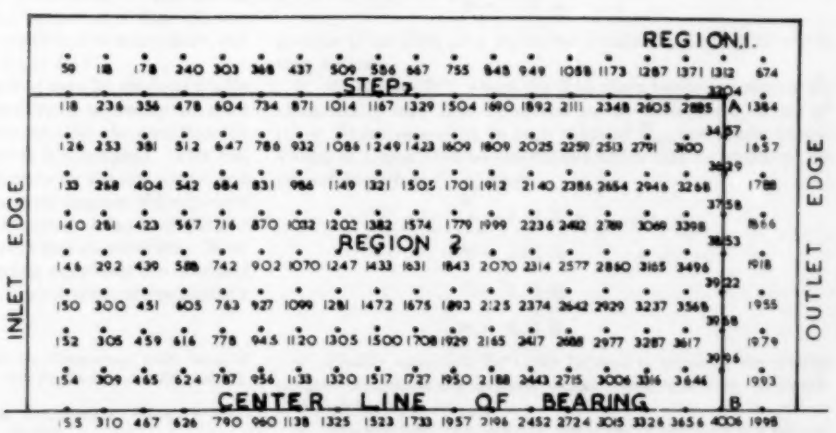

Fig. 5 Nondimensional pressure distribution for bearing without pocket

also presented in Figs. 2 and 3 together with other curves given in Fig. 11 (reference [2]). From these graphs it is clearly evident that Wilcock's simplified approach yields relatively accurate figures. The C_f curve is closer to the relaxed curve when the third component of friction force is considered, i.e., the component due to the oil film pressure:

$$C_F = \left(\frac{F}{\mu U}\right)\left(\frac{h_1}{L^2}\right) = \left\{\frac{GB}{K} + (2b + Gd) + \frac{G}{2}(k-1)\cdot\alpha\cdot C_W\right\} \quad (6)$$

Figs. 4 and 5 show two typical pressure parameter distributions and indicates to what extent the approximate solution is at error. The main assumptions for the latter are: (*a*) The pressure does not vary in the *z*-direction across region 2; (*b*) the pressure falls linearly from the pocket across region 1; (*c*) in the case of Fig. 5 the pressure is constant along that portion of the step labeled AB.

Conclusions

Wilcock's approximate solution for this bearing configuration yields accurate results when compared with the relaxed solutions; at the same time the difference in time required to reach operating figures bears no comparison. As the electrolytic tank figures are no longer available for analysis, it is impossible to ascertain the source of error.

Some trial solutions using a resistance network analog give results of a similar magnitude to those obtained by relaxation.

References

1 D. F. Wilcock, "The Hydrodynamic Pocket Bearing," TRANS. ASME, vol. 77, 1955, pp. 311–319.

2 C. F. Kettleborough, "The Hydrodynamic Pocket Thrust Bearing," *Proceedings, I. Mech. E.*, vol. 170, 1956, p. 535.

3 C. F. Kettleborough, "The Stepped Thrust Bearing—A Solution by Relaxation Methods," JOURNAL OF APPLIED MECHANICS, vol. 21, TRANS. ASME, vol. 76, 1954, p. 19.

NOTE: In checking over the proofs, a numerical error was detected. Referring to Fig. 2 and using equation (4), the value of C_W is actually 0.0825 and not 0.0721 when $B = 0.9$. As $C_f = C_F/C_W$, this affects the corresponding points in Fig. 3. With $B = 0.9$ the value of C_f derived using equations (5) and (6) should be 8.06 and 9.00, respectively. The over-all effect is to show that Wilcock's analysis gives good results over the full range.

Journal of APPLIED MECHANICS

Discussion

Analysis of a Nonlinear Mechanical System With Three Degrees of Freedom[1]

F. R. ARNOLD.[2] The author's interesting application of the Duffing method to the study of this steady-state behavior of nonlinear systems having three degrees of freedom leads to some interesting points for discussion. These concern the relation of the solutions presented by the author to solutions obtainable by other methods, the physical significance of the approximations, the number of solutions or behavior modes to be expected corresponding to each disturbance frequency, and finally a procedure for manipulating the necessary algebraic equations in a manner which avoids graphical constructions in the determination of amplitude values.

Equations (5) as presented by the author are exactly the same as those obtained by a so-called Fourier-series approach of his reference [2] or by the Ritz averaging method of his reference [6]. The only differences are in procedure for obtaining the equations and the apparent significance of their solutions. By the Duffing and the Fourier approach, terms involving higher harmonics of the disturbance frequency must be neglected. The Ritz averaging method does not yield any terms to be neglected.

Although the philosophy behind the Duffing or Fourier approach is such that there is some hope of correspondence between the approximate solutions and the quite complicated exact behavior of a physical system, the approximate solutions so obtained will be exactly the same as those to be found by the Ritz averaging method. We may, therefore, attach the same physical significance to the values of the coefficients found for the approximating functions of equations (4); namely, the values of A, B, and C will be those which make the approximate solutions come as close as possible to satisfying the same "minimum principle" as the exact solutions must precisely satisfy—regardless of whether or not the minimum principle is known.

From an examination of the response diagrams in Fig. 3 of the paper, as well as the description of the procedure used for solving equations (6), it is believed that several modes of behavior have not been detected. It is observed that if one assigns a value to A in equation (6*d*) for the purpose of establishing a value for K, there will generally be two additional values for A that will also yield the same K. These other values will lead to many more, but definitely corresponding, values for B and for C.

In order that much more information may be made available as a result of the algebraic manipulations necessary to solve equations (5) or (6), it is recommended that the equations be made dimensionless before the solution is attempted. This will simultaneously lead to simpler coefficients for the unknowns, and a single curve on a corresponding response diagram will represent solutions for an infinity of physical systems. As an example of a dimensionless result obtained by operating on equations (5) of the author, the following corresponding equations are obtained if, for convenience, the symbol μ^2 is used in place of the author's μ:

$$-\eta^2\bar{A} + \bar{A} + \bar{A}^3 - \bar{m}_2\eta^2\bar{B} - \bar{m}_3\eta^2\bar{C} = \bar{s} \qquad (5a')$$

$$-\eta^2\bar{A} + \bar{A} + \bar{A}^3 - \bar{m}_2\eta^2\bar{B} - \bar{k}_2(\bar{C} - \bar{B}) - \bar{k}_3\bar{\mu}_2^2(\bar{C} - \bar{B})^3 = 0 \qquad (5b')$$

$$-\eta^2\bar{A} + \bar{A} + \bar{A}^3 - \bar{k}_2(\bar{B} - \bar{A}) - \bar{k}_3\bar{\mu}_2^2(\bar{B} - \bar{A})^3 = 0 \qquad (5c')$$

where

$$\eta^2 = \omega^2/(k_1/m_1); \quad \bar{m}_2 = m_2/m_1; \quad \bar{m}_3 = m_3/m_1$$

$$\bar{k}_2 = k_2/k_1; \quad \bar{k}_3 = k_3/k_1$$

$$\bar{A} = (3/4)^{1/3}\mu_1 A; \quad \bar{B} = (3/4)^{1/3}\mu_1 B; \quad \bar{C} = (3/4)^{1/3}\mu_1 C$$

$$\bar{s} = (3/4)^{1/3}\mu_1(F_0/k_1); \quad \mu_2^2 = (\mu_2/\mu_1)^2 = \mu_2/\mu_{1\text{author}}$$

$$\bar{\mu}_2^2 = (\mu_2/\mu_1)^2 = \mu_2/\mu_{1\text{author}}$$

It will be noted that signs of $\bar{\mu}^2$ terms change for softening spring nonlinearity; also that the first three terms in each of equations (5′) constitute a dimensionless form of the author's K which will be designated $\bar{K}$ in the following prescription for solution which avoids the need for any graphical approximations; all calculations will result in usable data:

1 Do not prescribe a value for the dimensionless disturbance magnitude $\bar{s}$ at this point, but assign a value η_i^2 to the dimensionless frequency η^2, and a numerical value $\bar{A}_{i1}$ to dimensionless amplitude $\bar{A}$. If one then represents the first three terms of equations (5′) by $\bar{K}$ so that

$$(1 - \eta^2)\bar{A} + \bar{A}^3 = \bar{K},$$

the insertion of the numerical values η_i^2 and $\bar{A}_{i1}$ will yield a numerical value $\bar{K}_i$. It is a simple matter to find at most the two additional values of $\bar{A}$, symbolized by $\bar{A}_{i2}$ and $\bar{A}_{i3}$ that would also satisfy the value $\bar{K}_i$.

2 By means of equation (5*c*′), at most three values may be found for $(\bar{B} - \bar{A})$ corresponding to each value at $\bar{A}_{ij}$ in the foregoing so that values for $\bar{B}$ result which may be given identifying subscripts as B_{ijk}, where

$$i = 1, 2, 3, 4, \ldots n,$$

$$j = 1, 2, 3,$$

$$k = 1, 2, 3,$$

in order to tie them properly to the $\bar{A}$-values and the η^2 to which they belong.

3 Equation (5*b*′), where the first three terms are simply $\bar{K}_i$ numerically, may now be solved for at most three values of $(\bar{C} - \bar{B})$ corresponding to each value of $\bar{B}_{ijk}$ previously found. Values of $\bar{C}$ may thus be determined which may be identified by subscripts such as C_{ijkm}, where

$$i = 1, 2, 3, 4, \ldots . n,$$

$$j = 1, 2, 3,$$

$$k = 1, 2, 3,$$

$$m = 1, 2, 3.$$

4 Finally, equation (5*a*′) may be used to solve for the dimensionless disturbance-amplitude values which also may be identified by subscripts as $\bar{s}_{ijkm}$.

5 The resulting data may be displayed in the form of response

[1] By S. A. Hovanessian, published in the December, 1959, issue of the JOURNAL OF APPLIED MECHANICS, vol. 26, TRANS. ASME, vol. 81, series E, pp. 546–548.

[2] Associate Professor of Mechanical Engineering, Stanford University, Stanford, Calif. Assoc. Mem. ASME.

diagrams where $\bar{A}$, $\bar{B}$, and $\bar{C}$ are plotted against $\bar{s}$ for constant values of η^2. Such a diagram differs from that usually employed for one and two-degree-of-freedom systems, but may be replotted in the form of conventional amplitude versus frequency for constant-disturbance amplitude if desired, as probably would be preferred.

For the specific examples chosen to be illustrated by the author, the dimensionless equations (5′) have very simple coefficients and their solutions could be simply applied to all physical systems having similar mass or spring-characteristic ratios regardless of the absolute values involved. Solutions obtained by hand can be quite straightforward but involve tremendous amounts of work so that any device which adds to increasing the range of applicability of a type solution is very worth while.

Of particular interest would be the free-vibration behavior and conditions for which forced oscillations of one or the other of the masses are small.

Effect of Shear Deformations on the Bending of Rectangular Plates[1]

ENRICO VOLTERRA.[2] Equations which are very similar to those obtained by E. Reissner [1, 2, 3],[3] in his theory of bending of thin elastic plates (by taking into account the transverse-shear deformation of the plate and by an application of Castigliano's theorem of minimum energy), and which equations were used by the authors of the paper under discussion, can be derived directly by applying the second approximation of the method of internal constraints to the static problem of bending of rectangular plates.

Let the components of the elastic displacement in the X, Y, and Z-directions of the rectangular plate of sides a and b, shown in Figs. 1(a) and 1(b), be:

$$\left.\begin{aligned} u(x, y, z) &= z\mu_x(x, y) \\ v(x, y, z) &= z\mu_y(x, y) \\ w(x, y, z) &= \nu_z(x, y) + \frac{z^2}{2} f(x, y) \end{aligned}\right\} \tag{1}$$

The normal stress σ_z is given by:

$$\sigma_z = \lambda z \left[\frac{\partial \mu_x}{\partial x} + \frac{\partial \mu_y}{\partial y} + f\right] + 2Gzf \tag{2}$$

where λ (Lamé's constant) and G (modulus of rigidity) are connected to Young's modulus E and to Poisson's ratio ν of the material of the plate by the well-known relationships:

$$\lambda = \frac{\nu E}{(1 + \nu)(1 - 2\nu)}; \quad G = \frac{E}{2(1 + \nu)}$$

By satisfying the requirement that $\sigma_z = 0$, the following relationship for the unknown function $f(x, y)$ is obtained from equation (2):

$$f(x, y) = -\frac{\nu}{(1 - \nu)}\left[\frac{\partial \mu_x(x, y)}{\partial x} + \frac{\partial \mu_y(x, y)}{\partial y}\right] \tag{3}$$

The terms containing second-order powers z^2 in the expressions for the components of strain will be neglected in comparison with linear terms. In view of the foregoing assumptions and in view of equation (3) the components of strain are given by the following expressions:

$$\left.\begin{aligned} \epsilon_x &= z\frac{\partial \mu_x}{\partial x} & \gamma_{xy} &= z\left(\frac{\partial \mu_x}{\partial y} + \frac{\partial \mu_y}{\partial x}\right) \\ \epsilon_y &= z\frac{\partial \mu_y}{\partial y} & \gamma_{yz} &= \mu_y + \frac{\partial v_z}{\partial y} \\ \epsilon_z &= -\frac{\nu}{(1 - \nu)} z\left(\frac{\partial \mu_x}{\partial x} + \frac{\partial \mu_y}{\partial y}\right) & \gamma_{xz} &= \mu_x + \frac{\partial v_z}{\partial x} \\ e &= \frac{1 - 2\nu}{1 - \nu} z\left(\frac{\partial \mu_x}{\partial x} + \frac{\partial \mu_y}{\partial y}\right) \end{aligned}\right\} \tag{4}$$

The potential energy of the plate U is given by the expression:

$$u = \int_V \left[\frac{\lambda}{2} e^2 + G(\epsilon_x^2 + \epsilon_y^2 + \epsilon_z^2) + \frac{G}{2}(\gamma_{xy}^2 + K\gamma_{yz}^2 + K\gamma_{xz}^2)\right] dxdydz \tag{5}$$

In equation (5) V is the volume of the plate. The factor K is introduced into equation (5) to take into account the nonlinear distribution of shear stresses over the cross section of the plate. It has the same significance as the well-known Timoshenko shear coefficient, and in this specific case should be [4] $K = 1/1.2 = 0.833$.

By substituting into equation (5) equations (4), by integrating with respect to z, and calling $I = \int_{-H/2}^{H/2} z^2 1dz = \frac{H^3}{12}$ where H is the constant thickness of the plate and A the area of the surface of the plate, the following expression for the potential energy of the plate is obtained:

$$\begin{aligned} U = \int_A \Bigg\{ & \frac{E}{2(1 - \nu^2)}\left[I\left(\frac{\partial \mu_x}{\partial x}\right)^2 + I\left(\frac{\partial \mu_y}{\partial y}\right)^2\right] \\ & + \frac{\nu E}{(1 - \nu^2)} I \frac{\partial \mu_x}{\partial x}\frac{\partial \mu_y}{\partial y} \\ & + \frac{E}{4(1 + \nu)}\left[I\left(\frac{\partial \mu_x}{\partial y}\right)^2 + I\left(\frac{\partial \mu_y}{\partial x}\right)^2 + 2I\frac{\partial \mu_x}{\partial y}\frac{\partial \mu_y}{\partial x}\right. \\ & + KH(\mu y)^2 + KH\left(\frac{\partial \nu_z}{\partial y}\right)^2 + 2KH\mu_y\frac{\partial \nu_z}{\partial y} + KH(\mu_x)^2 \\ & \left. + KH\left(\frac{\partial \nu_z}{\partial x}\right)^2 + 2KH\mu_x\frac{\partial \nu_z}{\partial x}\right]\Bigg\} dxdy \end{aligned}$$

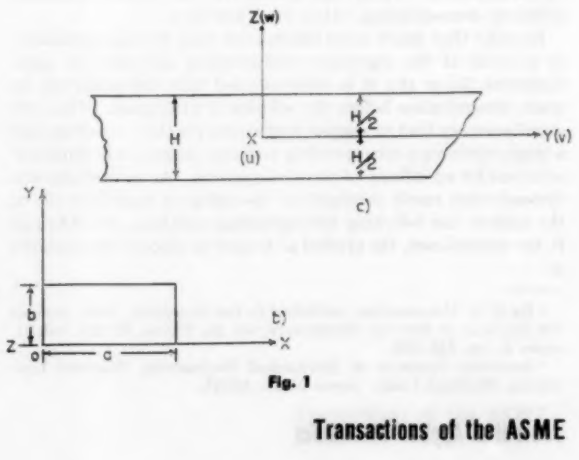

Fig. 1

[1] By V. L. Salerno and M. A. Goldberg, published in the March, 1960, issue of the JOURNAL OF APPLIED MECHANICS, vol. 27, TRANS. ASME, vol. 82, series E, pp. 54–58.

[2] Professor of Engineering Mechanics, The University of Texas, Austin, Texas. Mem. ASME.

[3] Numbers in brackets indicate References at end of discussion.

In the following the function w_z which represents the vertical displacement of the middle surface of the plate will be indicated by the letter w_0.

The condition of internal equilibrium of the plate is furnished by the Principle of Virtual Displacements [5]. In fact, by expressing that the variation of the elastic potential is equal to the work of the external forces, and since the work done by the external distributed force $p(x, y)$ acting on the middle surface of the plate in a virtual displacement δw_0 is given by the following expression:

$$\delta L = \int_A p(x, y)\delta w_0 dx dy$$

then the equations of equilibrium:

$$\left.\begin{aligned} &D\frac{\partial^2\mu_x}{\partial x^2} + \frac{1+\nu}{2}D\frac{\partial^2\mu_y}{\partial x\partial y} + \frac{1-\nu}{2}D\frac{\partial^2\mu_x}{\partial y^2} - \frac{EHK}{2(1+\nu)}\frac{\partial w_0}{\partial x} - \frac{EHK}{2(1+\nu)}\mu_x = 0 \\ &D\frac{\partial^2\mu_y}{\partial y^2} + \frac{1+\nu}{2}D\frac{\partial^2\mu_x}{\partial x\partial y} + \frac{1-\nu}{2}D\frac{\partial^2\mu_y}{\partial x^2} - \frac{EHK}{2(1+\nu)}\frac{\partial w_0}{\partial y} - \frac{EHK}{2(1+\nu)}\mu_y = 0 \\ &\frac{EHK}{2(1+\nu)}\Delta w_0 + \frac{EHK}{2(1+\nu)}\left(\frac{\partial\mu_x}{\partial x} + \frac{\partial\mu_y}{\partial y}\right) = -p(x, y) \end{aligned}\right\} \quad (6)$$

and the boundary conditions:

$$\left.\begin{aligned} &\text{at } x = \begin{cases}=0\\=a\end{cases} \text{ for } 0 \le x \le b; \quad \text{at } y = \begin{cases}=0\\=b\end{cases} \text{ for } 0 \le x \le a \\ &D\left(\frac{\partial\mu_x}{\partial x} + \nu\frac{\partial\mu_y}{\partial y}\right)\delta\mu_x = 0 \quad \frac{1-\nu}{2}D\left(\frac{\partial\mu_y}{\partial x} + \frac{\partial\mu_x}{\partial y}\right)\delta\mu_x = 0 \\ &\frac{1-\nu}{2}D\left(\frac{\partial\mu_x}{\partial y} + \frac{\partial\mu_y}{\partial x}\right)\delta\mu_y = 0 \quad D\left(\frac{\partial\mu_y}{\partial y} + \nu\frac{\partial\mu_x}{\partial x}\right)\delta\mu_y = 0 \\ &\frac{EHK}{2(1+\nu)}\left(\frac{\partial w_0}{\partial x} + \mu_x\right)\delta w_0 = 0 \quad \frac{EHK}{2(1+\nu)}\left(\frac{\partial w_0}{\partial y} + \mu_y\right)\delta w_0 = 0 \end{aligned}\right\} \quad (7)$$

are obtained.

In equations (6) and (7) $D = \dfrac{EH^3}{12(1-\nu^2)}$ and $\Delta = \left(\dfrac{\partial^2}{\partial x^2} + \dfrac{\partial^2}{\partial y^2}\right)$ is Laplace's two-dimensional operator.

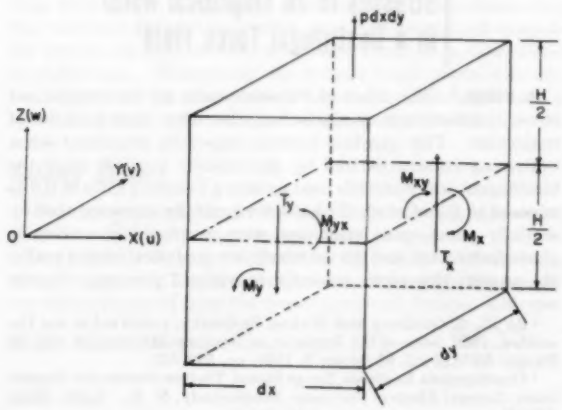

Fig. 2

The shear forces T_x and T_y, the bending moments M_x and M_y, and the twisting moments M_{xy} and M_{yx} per unit length of the plate (see Fig. 2) are defined by the following expressions:

$$\left.\begin{aligned} T_x &= \int_{-H/2}^{H/2}\tau_{xz}\,1\,dz = \int_{-H/2}^{H/2}GK\gamma_{xz}\,1\,dz \\ &= \frac{EKH}{2(1+\nu)}\left(\frac{\partial w_0}{\partial x} + \mu_x\right) \\ T_y &= \int_{-H/2}^{H/2}\tau_{yz}\,1\,dz = \int_{-H/2}^{H/2}GK\gamma_{yz}\,1\,dz \\ &= \frac{EKH}{2(1+\nu)}\left(\frac{\partial w_0}{\partial y} + \mu_y\right) \end{aligned}\right\} \quad (8)$$

$$\left.\begin{aligned} M_x &= \int_{-H/2}^{H/2}\sigma_x z\,1\,dz = D\left(\frac{\partial\mu_x}{\partial x} + \nu\frac{\partial\mu_y}{\partial y}\right) \\ M_y &= \int_{-H/2}^{H/2}\sigma_y z\,1\,dz = D\left(\frac{\partial\mu_y}{\partial y} + \nu\frac{\partial\mu_x}{\partial x}\right) \end{aligned}\right\} \quad (9)$$

$$M_{xy} = M_{yx} = \int_{-H/2}^{H/2}\tau_{xy}z\,1\,dz = \int_{-H/2}^{H/2}G\gamma_{xy}\,1z\,dz = \frac{1-\nu}{2}D\left(\frac{\partial\mu_x}{\partial y} + \frac{\partial\mu_y}{\partial x}\right) \quad (10)$$

In view of equations (8), (9), and (10), equations (6) can be written:

$$\left.\begin{aligned} &\frac{\partial M_x}{\partial x} + \frac{\partial M_{yx}}{\partial y} = T_x \\ &\frac{\partial M_{yx}}{\partial x} + \frac{\partial M_y}{\partial y} = T_y \\ &\frac{\partial T_x}{\partial x} + \frac{\partial T_y}{\partial y} = -p \end{aligned}\right\} \quad (11)$$

By differentiating the first of equations (6) with respect to x, the second with respect to y, and then by adding them together, the following equation is obtained:

$$\left[D\Delta - \frac{EHK}{2(1+\nu)}\right]\left(\frac{\partial\mu_x}{\partial x} + \frac{\partial\mu_y}{\partial y}\right) = \frac{EHK}{2(1+\nu)}\Delta w_0 \quad (12)$$

By eliminating the term $\left(\dfrac{\partial\mu_x}{\partial x} + \dfrac{\partial\mu_y}{\partial y}\right)$ between equation (12) and the last of equations (6), the following equation is obtained:

$$D\Delta\Delta w_0 = \left[1 - \frac{H^2}{6(1-\nu)K}\Delta\right]p(x, y) \quad (13)$$

From equations (8) and (9) the following equation is obtained:

$$M_x - \frac{H^2}{6K}\frac{\partial T_x}{\partial x} - \frac{\nu H^2}{6(1-\nu)K}\left(\frac{\partial T_x}{\partial x} + \frac{\partial T_y}{\partial y}\right) = -D\left(\frac{\partial^2 w_0}{\partial x^2} + \nu\frac{\partial^2 w_0}{\partial y^2}\right)$$

and in view of the last of equations (11) one obtains:

$$M_x - \frac{H^2}{6K}\frac{\partial T_x}{\partial x} + \frac{\nu H^2}{6(1-\nu)K}p = -D\left(\frac{\partial^2 w_0}{\partial x^2} + \nu\frac{\partial^2 w_0}{\partial y^2}\right) \quad (14)$$

In the same way for M_y one obtains:

$$M_y - \frac{H^2}{6K}\frac{\partial T_y}{\partial y} + \frac{\nu H^2}{6(1-\nu)K}p = -D\left(\frac{\partial^2 w_0}{\partial y^2} + \nu\frac{\partial^2 w_0}{\partial x^2}\right) \quad (15)$$

By combining equations (8) and (10) one obtains:

$$M_{xy} = M_{yx} = \frac{1-\nu}{2}D\left(\frac{\partial \mu_x}{\partial y} + \frac{\partial \mu_y}{\partial x}\right)$$

$$= \frac{H^2}{12K}\left(\frac{\partial T_x}{\partial y} + \frac{\partial T_y}{\partial x}\right) - \frac{EH^3}{12(1+\nu)}\frac{\partial^2 w_0}{\partial x \partial y}$$

and finally:

$$M_{xy} - \frac{H^2}{12K}\left(\frac{\partial T_x}{\partial y} + \frac{\partial T_y}{\partial x}\right) = -(1-\nu)D\frac{\partial^2 w_0}{\partial x \partial y} \quad (16)$$

By substituting in the first of equations (11) the values given by equations (14) and (16) for M_x and M_y, and in view of the last of equations (11), one obtains:

$$T_x - \frac{H^2}{12K}\Delta T_x + \frac{H^2}{12(1-\nu)K}\frac{\partial p}{\partial x} = -D\frac{\partial}{\partial x}\Delta w_0 \quad (17)$$

In the same way for T_y one obtains:

$$T_y - \frac{H^2}{12K}\Delta T_y + \frac{H^2}{12(1-\nu)K}\frac{\partial p}{\partial y} = -D\frac{\partial}{\partial y}\Delta w_0 \quad (18)$$

In the case of a very thin plate $H \to 0$, and the foregoing equations reduce to the following:

$$D\Delta\Delta w_0 = p(x, y) \quad (13')$$

$$M_x = -D\left(\frac{\partial^2 w_0}{\partial x^2} + \nu\frac{\partial^2 w_0}{\partial y^2}\right) \quad (14')$$

$$M_y = -D\left(\frac{\partial^2 w_0}{\partial y^2} + \nu\frac{\partial^2 w_0}{\partial x^2}\right) \quad (15')$$

$$M_{xy} = -(1-\nu)D\frac{\partial^2 w_0}{\partial x \partial y} \quad (16')$$

$$T_x = -D\frac{\partial}{\partial x}\Delta w_0 \quad (17')$$

$$T_y = -D\frac{\partial}{\partial y}\Delta w_0 \quad (18')$$

of the classical theory.

The corresponding equations of Reissner's theory are:

$$D\Delta\Delta w_0 = \left(1 - \frac{H^2}{10}\frac{2-\nu}{1-\nu}\Delta\right)p(x, y) \quad (13'')$$

$$M_x - \frac{H^2}{5}\frac{\partial T_x}{\partial x} - \frac{H^2}{10}\frac{\nu}{(1-\nu)}p = -D\left(\frac{\partial^2 w_0}{\partial x^2} + \nu\frac{\partial^2 w_0}{\partial y^2}\right) \quad (14'')$$

$$M_y - \frac{H^2}{5}\frac{\partial T_y}{\partial y} - \frac{H^2}{10}\frac{\nu}{1-\nu}p = -D\left(\frac{\partial^2 w_0}{\partial y^2} + \nu\frac{\partial^2 w_0}{\partial x^2}\right) \quad (15'')$$

$$M_{xy} - \frac{H^2}{10}\left(\frac{\partial T_x}{\partial y} + \frac{\partial T_y}{\partial x}\right) = -(1-\nu)D\frac{\partial^2 w_0}{\partial x \partial y} \quad (16'')$$

$$T_x - \frac{H^2}{10}\Delta T_x + \frac{H^2}{10(1-\nu)}\frac{\partial p}{\partial x} = -D\frac{\partial}{\partial x}\Delta w_0 \quad (17'')$$

$$T_y - \frac{H^2}{10}\Delta T_y + \frac{H^2}{10(1-\nu)}\frac{\partial p}{\partial y} = -D\frac{\partial}{\partial y}\Delta w_0 \quad (18'')$$

E. Reissner, in his theory of bending of thin elastic plates, starts from appropriate and rational assumptions regarding the variation of stresses across the thickness of the plate, i.e., the bending stresses vary linearly while the transverse shear stresses vary parabolically, and the normal stress σ_z is different from zero. Making use of Castigliano's theorem of minimum energy to introduce the conditions of compatibility in the analysis, he reaches equations which, although more accurate, are extremely close to the ones which are derived in the present discussion by applying the second approximation of the method of internal constraints. The application of both theories to problems of plates subjected to uniformly distributed loads, such as the ones considered by the authors of the paper under discussion, leads to almost the same numerical results.

NOTE: The material presented in this discussion is based on an investigation which is being conducted under the sponsorship of The National Science Foundation, Washington, D. C., and is presented with the permission of The National Science Foundation.

References

1 E. Reissner, "On the Theory of Bending of Elastic Plates," *Journal of Mathematics and Physics*, vol. 23, 1944, p. 184.

2 E. Reissner, "The Effect of Transverse Shear Deformation on the Bending of Elastic Plates," JOURNAL OF APPLIED MECHANICS, vol. 12, TRANS. ASME, vol. 67, 1945, pp. A-69 to A-77.

3 E. Reissner, "On Bending of Elastic Plates," *Quarterly of Applied Mathematics*, vol. 5, 1947, p. 55.

4 L. Bolle, "Contribution au problème linèaire de flexion d'une plaque élastique," *Bulletin Technique de la Suisse Romande*, Oct. 11 and 25, 1947, pp. 281 and 293.

5 G. Kirchhoff, Vorlesungen über Mathematische Physik, Mechanik, 1877, p. 450.

6 S. Timoshenko and S. Woinowsky-Krieger, "Theory of Plates and Shells," McGraw-Hill Book Co., Inc., New York, N. Y., 1959, p. 88.

Authors' Closure

The authors wish to thank Dr. Volterra for his presentation of the plate equations by an approximation of the method of internal constraints.

Since Dr. Volterra indicates that his equations are extremely close to the more accurate ones of E. Reissner, and since the application of both theories to problems of plates sustaining uniformly distributed loads leads to almost identical numerical results, the authors believe that Dr. Volterra's contribution does not affect the results obtained by them in their recent paper.

Stresses in an Ellipsoidal Rotor in a Centrifugal Force Field[1]

A. RUBIO.[2] The effect of Poisson's ratio on the stresses and stress distribution in an elastic body has often been a matter of conjecture. This question becomes especially important when evaluating stresses secured by photoelastic methods since the birefringent test materials used possess a Poisson's ratio of 0.5 as opposed to 0.3 of steel. It has been generally supposed that essentially plane stress structures were portrayed accurately in photoelastic work and the extremely few analytical results available support this view, generally to within 7 per cent. For the

[1] By M. A. Goldberg and Michael Sadowsky, published in the December, 1959, issue of the JOURNAL OF APPLIED MECHANICS, vol. 26, TRANS. ASME, vol. 81, series E, 1959, pp. 549–552.

[2] Development Engineer, Large Steam Turbine-Generator Department, General Electric Company, Schenectady, N. Y. Assoc. Mem. ASME.

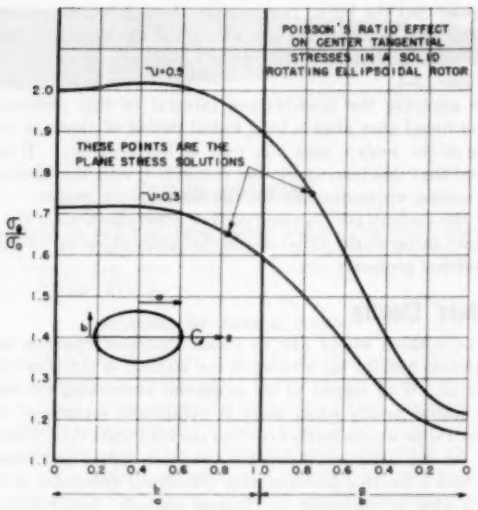

Fig. 1

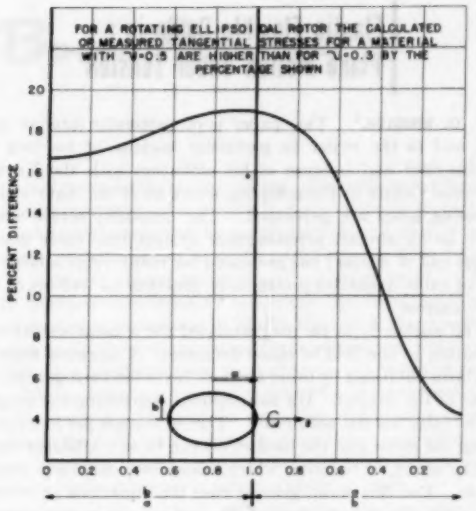
FOR A ROTATING ELLIPSOIDAL ROTOR THE CALCULATED
OR MEASURED TANGENTIAL STRESSES FOR A MATERIAL
WITH ν=0.5 ARE HIGHER THAN FOR ν=0.3 BY THE
PERCENTAGE SHOWN
PERCENT DIFFERENCE

Fig. 2

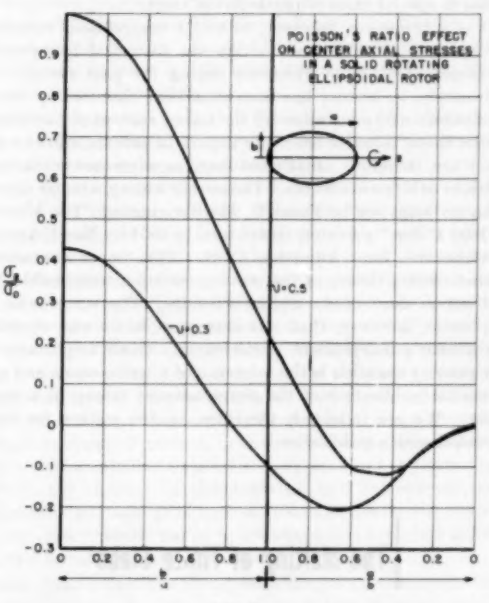

Fig. 3

three-dimensional object, even fewer analytical cases are available and these become very important because of the advances in frozen-stress techniques in photoelasticity.

The excellent analytical work on a solid rotating ellipsoidal rotor presented by the authors provides another opportunity for testing of our thoughts on the role of Poisson's ratio. Professor Sadowsky forwarded the original stress equations used to secure the curves in his paper. From these, the tangential and axial stresses at the center of a rotating ellipsoid were calculated for $\nu = 0.5$. The comparisons are shown in the curves, Figs. 1–3 of this discussion, for various values of one of the shape parameters. The first curve shows the center axial stresses and how these follow very closely at ratios of a/b between 0 and 0.4 and diverge drastically outside this range. The axial stresses can get as high as 25 per cent of the tangential stress for $\nu = 0.3$, and as high as 50 per cent for $\nu = 0.5$.

The second curve shows the difference between the tangential stresses at various shape ratios with Poisson's ratio at 0.3 and 0.5. The variation of this difference with shape is shown on the third curve. The variation between the curves at the two plane-stress conditions, located as points on the second curve, is $\sigma_{\phi(0.5)}/\sigma_{\phi(0.3)} = 1.061$, which is exactly what the usual plane-stress theory predicts. However, as the third curve shows, medium to long models show a difference of about 1.18. This means that the correction for photoelastically ($\nu = 0.5$) determined tangential stresses for medium to long bodies is about three times those normally used. Fortunately, the stresses found photoelastically are higher than the stresses for a material (such as steel) with a $\nu = 0.3$ so that conservative stresses are being quoted.

Authors' Closure

The authors thank Mr. A. Rubio for his interesting comments; these have definite bearing on photoelastic anlaysis.

One point should be re-emphasized: the exact plane stress solutions, evaluated in the equatorial plane, are numerically equal to the values obtained from the two-dimensional theory. This can be seen from the field equations. When $\left(\frac{b}{a}\right)^2 = \frac{4\nu(1+\nu)}{(1-\nu)(3+\nu)}$,

$$\sigma_r = \left\{\frac{(3+\nu)}{8}(b^2 - r^2) - \frac{\nu(1+\nu)}{2(1-\nu)}z^2\right\}\rho\omega^2$$

$$\sigma_\phi = \left\{\frac{1}{8}\left[(3+\nu)b^2 - (1+3\nu)r^2\right] - \frac{\nu(1+\nu)}{2(1-\nu)}z^2\right\}\rho\omega^2$$

$$\sigma_z = \tau_{r\phi} = \tau_{\phi z} = \tau_{rz} = 0$$

With $z = 0$, the foregoing reduces to the usual two-dimensiona results.[3]

[3] S. Timoshenko and J. N. Goodier, "Theory of Elasticity," McGraw-Hill Book Co., Inc., second edition, 1951, p. 71.

Elastic Flexible Cable in Plane Motion Under Tension[1]

F. O. RINGLEB.[2] This paper is of particular interest in general and to the writer in particular because of his own work in this field and because of his affiliation with the Naval Air Material Center in Philadelphia, where all of the Navy's aircraft arresting gears are developed. The unusually severe use of a cable in an aircraft arresting-gear system (the cable manufacturers call it misuse) has presented for many years a large number of cable-dynamics problems of practical as well as of scientific interest.

The author is to be congratulated for a most valuable contribution to the field of cable dynamics. Compared with what has been published by other authors, his is the most general treatment of the subject. His assumptions concerning the properties of the cable are not restricting. The cable mass per foot can vary along the cable, and the local stress can be any arbitrary function of the strain, a function which, moreover, can vary along the cable. For this most general case the equations of motion of the cable are totally hyperbolic and can be solved using the method of characteristics as the author shows in general and discusses in special cases of particular interest.

It is appropriate, however, to add a few remarks concerning the position of this paper within the historical framework of development of cable dynamics during the past decade. Unfortunately, its history has been somewhat obscured by security regulations, and even more by the recent custom of the industry to distribute valuable scientific papers in private editions only, which are, therefore, usually not listed as references in other publications or reference works. The author was apparently unaware of an investigation by Frank E. Marble, entitled "The Motion of a Finite Cable," privately distributed in 1954 by North American Instruments, Inc., Altadena, Calif. This paper contains the characteristics theory of the moving cable in considerable detail and covers most of the author's results. The writer wishes to emphasize, however, that this statement in no way diminishes the author's independent performance. More important than any priority question is the existence of a well-written and easily accessible publication of the characteristics theory of a moving cable. We are indebted, therefore, to the author for having provided such a publication.

The Melting of Finite Slabs[1]

E. M. SPARROW.[2] The authors are to be commended for their continuing efforts in generalizing the heat-balance integral to increase its utility. In the present paper, as well as in its predecessor, attention is focused on a plane geometry. It would be desirable to know something about the utility of the heat-balance integral in another geometry. For example, one might apply the method to the transient heat flow in an infinitely extended solid through which there passes an infinitely long cylindrical hole. Suppose that the initial temperature throughout the material is T_i, and then at $t = 0$, the temperature at the surface of the hole is raised to a level T_s. The "exact" solution is given by Jakob[3] in Table 13-4.

In applying the heat-balance integral to this problem, the writer found that after a brief initial period of time the predictions of the surface heat flux were of low accuracy. It is suspected that this inaccuracy was connected with the choice of a polynomial approximation for the temperature profile.

If the authors are planning further generalizations of the heat-balance integral, the writer would encourage them to consider the cylindrical geometry.

Authors' Closure

The authors would like to thank Professor Sparrow for his comments and for his interest in the method of the heat balance integral. With regard to his suspicions concerning the use of a polynomial profile when there is cylindrical symmetry, at the present time we can neither confirm nor invalidate this. Nevertheless, we can point out a paper by van der Velden and Schaffers[4] in which a freezing problem with cylindrical symmetry is solved using what is essentially an integral method. Logarithmic profiles were assumed by analogy with the cylindrically symmetrical problem without freezing, and the results, according to the authors, differ by only a few per cent from more exact results. This example does not rule out the possibility that a polynomial profile would work just as well, and it would be interesting to know more of the details of the problem Professor Sparrow worked out and for which he obtained low accuracy.

A Theory of Lubrication With Turbulent Flow and Its Application to Slider Bearings[1]

EDWARD SAIBEL.[2] In the paper by Y. T. Chou and the writer, referred to by the author as reference [5], only fully developed turbulence is treated; consequently, there is no direct connection between the pressure distribution and viscosity. This being the case we draw no such conclusion as is attributed to us in the last paragraph of the present paper, nor do we think such a conclusion can be drawn from our work.

Author's Closure

To clarify the misunderstanding, the following statement from the last paragraph of the paper [5] by Dr. Chou and Prof. Saibel is quoted: "It is clear that the turbulence increases the pressure distribution and the load-carrying capacity of slider-bearing lubrication. However, the power loss also increases." On the other hand, the author's analysis shows that the pressure distribution and load-carrying capacity of a slider bearing with turbulent flow can be either larger or smaller than the corresponding laminar lubrication depending on the choice of the lubricant. Hence the author concludes, "This differs from the conclusion of Chou and Saibel [5]."

---

[1] By Wen-Hsiung Li, published in the December, 1959, issue of the JOURNAL OF APPLIED MECHANICS, vol. 26, TRANS. ASME, vol. 81, series E, pp. 587–593.

[2] Woodbury Heights, N. J.

[1] By T. R. Goodman and J. J. Shea, published in the March, 1960, issue of the JOURNAL OF APPLIED MECHANICS, vol. 27, TRANS. ASME, vol. 82, series E, pp. 16–24.

[2] Professor of Mechanical Engineering, University of Minnesota, Minneapolis, Minn. Assoc. Mem. ASME.

[3] Max Jakob, "Heat Transfer," vol. 1, John Wiley & Sons, Inc., New York, N. Y., 1949, p. 267.

[4] H. A. van der Velden and W. J. Schaffers, "Das Berechnen der notwendigen Kalteleistung beim Abteufen von Gefrierschachten," *Glückauf*, vol. 20, 95th year, 1959, pp. 1237–1244.

[1] By L. N. Tao, published in the March, 1960, issue of the JOURNAL OF APPLIED MECHANICS, vol. 27, TRANS. ASME, vol. 82, series E, pp. 1–4.

[2] Department of Mechanics, Rensselaer Polytechnic Institute, Troy, N. Y. Mem. ASME.

Servomechanisms

Servomechanisms and Regulating System Design. Volume 1, Second Edition. By Harold Chestnut and Robert W. Mayer. John Wiley & Sons, Inc., New York, N. Y., 1959. Cloth, 6 × 9½ in., xvii and 680 pp. $11.75.

REVIEWED BY JOHN R. WARD[1]

This book is so well known that little need be said here to describe its contents and philosophy. In this second edition sections on root loci and analog computers have been added, and some reorganization and extension have taken place in the sections relating to Bode plots and error coefficients—the latter with an unfortunate typographical omission of a complete line of text.

The authors have aimed at a wide and comprehensive coverage of the technology of lumped parameter linear systems at a rather elementary level. In fact, the reviewer cannot but feel that the chapters on complex numbers and on the classical solution of linear differential equations are largely redundant and could either have been omitted entirely or relegated to a short appendix. It is also felt that the introduction of the root-locus method should have made possible a rather tighter integration of the allied concepts of transient and sinusoidal response in terms of the poles and zeros of the transfer functions. There is, however, little doubt that this text will be as popular as the previous edition, in view of its wide and now updated coverage.

Thermodynamics

An Introduction to the Physical Theories of Equilibrium Thermostatics and Irreversible Thermodynamics. By Herbert B. Callen. John Wiley & Sons, Inc., New York, N. Y., 1960. Cloth, 5⅞ × 9 in., xvi and 376 pp. $8.

REVIEWED BY J. KESTIN[2]

The flow of new text and reference books on thermodynamics continues without interruption, testifying to the elusive subtlety of the subject and the prevalent dissatisfaction with those already available. However, the present book does not belong to the category in which the author provides yet one more permutation on the theme of a course of x credit-hours during y semesters. Its appearance constitutes that rare event, a fresh concept of the whole basis of the subject, arrived at after a sustained and successful intellectual effort.

Professor Callen has adopted in his book what he calls the postulational approach conceived by his former teacher, Professor Laszlo Tisza of the Massachusetts Institute of Technology. In doing so, he drives to their logical conclusion some of the ideas first incorporated in E. A. Guggenheim's "Thermodynamics" (North Holland, 1957). The postulational approach leads to a direct and logically simple development of fundamentals and endows them with a quality which can only be described by the nonscientific word—elegance. Nevertheless, this kind of approach is not without its shortcomings. The inherent difficulty in adopting a postulational approach is, first, to choose postulates which, as the author says "can be made plausible and instinctive," and, second, to demonstrate that the postulates are truly "justified by *a posteriori* success rather than by *a priori* proof." The reviewer, perhaps unconsciously influenced by the classical and nonetheless elegant expositions of M. Planck and A. Sommerfeld, prefers the methods of formulating (and suitably generalizing) easily derivable principles from properly selected critical experiments. This is largely a matter of scientific temperament and taste. The second aspect, the *a posteriori* justification of the postulates, in the reviewer's opinion, has not been given adequate weight in the book, and one gains the impression that a nonspecialist student is expected to take too much on trust.

To quote one of the author's own examples, the postulational presentation of thermodynamics is analogous to the study of nonrelativistic mechanics conceived as a derivation of the consequences of Lagrange's or Hamilton's formulations, rather than on the basis of Newton's laws. The former results in great generality and elegance but the latter keeps the student in much closer touch with physical reality.

The book begins with a study of Basic Concepts and Postulates (Chap. 1) during which, as is proper, it is discovered that the science is based on more postulates than the four "laws" of thermodynamics (zeroth, first, second, and third). Although the postulates are phrased in terms of macroscopic concepts, the microscopic point of view is skillfully woven into the canvas. But this intimate intertwining of the two points of view, without the full statistical apparatus, begs many questions and is very hard on the nonspecialist reader. Once again, the reviewer's instinct would cause him to prefer a clear-cut distinction and a separate study of the two approaches in the traditional manner.

The reviewer wishes to criticize somewhat the author's formulation of Postulate II (the Second Law). Although suitably circumscribed in a preceding section, the statement is apt to be misleading if read out of context, in that insufficient stress is put on the fact that it applies to adiabatically enclosed systems only. Similarly, the choice of a dimensionless unit for entropy, perfectly correct in itself, puts a good deal of strain on the student who may later concentrate on applications and may find himself compelled to use dimensional analysis.

Chaps. 2 and 3 continue the exposition with a penetrating study of the Conditions of Equilibrium and Some Formal Relationships, including the Euler equation and the Gibbs-Duhem relation, but not the Maxwell Relations which receive a chapter all to themselves (Chap. 7).

In Chap. 4 (Processes and Thermodynamic Engines) a distinction is made between quasi-static and reversible processes, the need for which is not clear to the reviewer. A quasi-static process is defined as a succession of equilibrium states (a *reversible* process in the usual terminology), but it is not made clear to the reader that, in general, a quasi-static process involves the exchange of heat with the surroundings. A reversible process is defined as one for which the entropy increase vanishes. It is clear that the distinction, to use conventional language, is a matter of choice of system and depends on whether the transfer of heat from the sources to the system is reversible or not. Again, the reviewer feels that for a nonspecialist reader and for one who studies the subject because of its applicability to real processes, the distinc-

[1] Professor, Division of Engineering, Brown University, Providence, R. I.

[2] Professor, Division of Engineering, Brown University, Providence, R. I.

tion is not a useful one. It has some merit only if it is decided to analyze all processes in terms of closed systems confined within adiabatic walls.

Chap. 5 on Alternative Formulations and Legendre Transformations and Chap. 6 on the Extremum Principle in the Legendre Transformed Representations are beautifully written and impart to the reader a real sense of perspective and a deep understanding of the equivalence of alternative formal schemes in thermodynamics. Chaps. 8 and 9 constitute masterful expositions of stability and phase transitions and include a general formulation of the Le Chatelier-Braun principle. Chaps. 9 and 10 conclude the treatment of fundamentals and complete Part I of the book. They deal with the Third Law (Chap. 9) in a convincing way and provide a summary of principles (Chap. 10).

Parts II and III (Chaps. 12 to 17) deal with Representative Applications (II) and Fluctuations and Irreversible Thermodynamics (III). Together they occupy less than half of the book and are necessarily sketchy. They analyze selected topics in an authoritative way and the reviewer regrets that they are so short —particularly Chap. 16 on Irreversible Thermodynamics, a subject of which the author is a recognized master. The science of Thermodynamics, or, as the author prefers, of thermostatics, is applicable to so many and varied phenomena, ranging from very low temperature physics to internal-combustion engines through thermoelasticity, chemical, electrochemical, and magnetic phenomena, that every author is forced to make an "agonizing appraisal" and concentrate on topics for which he has a particular liking or whose importance he regards as overwhelming. This aspect is, perhaps, the one most responsible for the long string of books on the subject. The present, all too short, treatise stands out as a unique example of rare mastery. No serious thermodynamicist will omit to accord it pride of place on the shelves of his library and to devote a good deal of time to its careful study.

Photoelasticity

Einfuhrung in die Spannungsoptik. By Albrecht Kuske. Wissenschaftliche Verlagsgesellschaft MBH, Stuttgart, Germany, 1959. Cloth, 9½ × 7 in., xi and 220 pp., illus. 38 DM.

REVIEWED BY ROSCOE GUERNSEY, JR.[3]

ACCORDING to the preface, it is the intent of this book to stimulate increased application of photoelasticity to practical problems. Emphasis is therefore placed on surveying the types of problems that can now be solved, and the more recent methods available for their solution.

The early chapters are devoted to an exposition of the fundamentals of stress analysis in two and three dimensions, and the optical principles employed in photoelasticity. The optical behavior of polariscope and model is explained by means of the so-called *j*-circle method developed by Dr. Kuske. This graphical procedure for analyzing transmitted polarized light will probably be unfamiliar to most American readers. Two chapters are devoted to a description of photoelastic apparatus and a rather complete survey of the properties of available photoelastic plastics.

The last six chapters cover the application of photoelasticity to a variety of two and three-dimensional problems. Among the topics treated are conventional two-dimensional methods with an extensive treatment of singular points; solution of plate problems by means of the two-sheet method and the superposition method; the stress freezing method of three-dimensional analysis using conventional stress patterns and also convergent light patterns; solution of three-dimensional problems with transmitted light and the *j*-circle procedure; and brief introductions to scattered light methods and dynamic problems.

In each case, the theory of the method is explained, and procedures for determining interior stresses as well as boundary stresses are covered in some detail. Illustrations of the application of these methods to practical problems are given by means of examples taken from Dr. Kuske's work over the past 20 years. For the most part, the illustrations are treated qualitatively, relatively few quantitative results being given.

American readers may be most interested in the treatment given to the study of plates and shells. The discussions of scattered light and dynamic problems are too short to be of much value. The remainder of the book covers material which is rather well known.

[3] General Electric Company, Schenectady, N. Y.

Flames

Flames, Their Structure, Radiation and Temperature. Second Revised Edition. By A. G. Gaydon and H. G. Wolfhard. The Macmillan Company, New York, N. Y., 1960. Cloth, 8½ × 5½ in., xiii and 383 pp. $14.

REVIEWED BY S. S. PENNER[4]

THIS second edition constitutes a somewhat revised and slightly enlarged version of the text that first appeared six years ago. Some of the more recent literature is covered through addition of about 200 new references. The chapter arrangement in the second edition is as follows: Chap. I (6 pp.): qualitative introductory remarks concerning flames; II (34 pp.): premixed flames; III (15 pp.): flow patterns and flame shapes; IV (27 pp.): measurement of burning velocities; V (45 pp.): mechanism of flame propagation; VI (27 pp.): diffusion flames; VII (14 pp.): unstable flames; VIII (35 pp.): solid carbon in flames; IX (24 pp.): radiation processes in flames; X (22 pp.): flame temperature measurements by use of the spectrum-line reversal method; XI (27 pp.): other methods for measuring flame temperatures; XII (19 pp.): calculation of flame temperatures; XIII (21 pp.): ionization in flames; XIV (27 pp.): combustion processes of rocket-type fuels; XV (5 pp.): recent progress on some flame problems.

Reference to the spatial distribution shows, for example, that roughly one third of the total volume of the book deals specifically with temperature measurements and radiation studies, whereas less than 8 per cent of the available space is devoted to a discussion of diffusion flames. These figures may serve to underscore the fact that books tend to reflect the tastes and preferences of authors rather than the topical material that is of most vital importance to the "average" reader. This type of individual topical selection is present not only in the broad outlines of the text and in the quoted references, but it is also carried over into the analytic treatment of specific topics. The informed reader may perhaps question the authors' judgment in presenting in 1960 lengthy discussions of thermal and diffusion "theories" of laminar flame propagation and, at the same time, dismissing the more complete and necessarily more complex analytical work as "beyond the scope of this book."

The book of Gaydon and Wolfhard constitutes a useful, intuitive first introduction to combustion phenomena. The discussion is not encyclopedic and the description of physical phenomena tends to be oversimplified. Nevertheless, the viewpoint of the authors should be stimulating to laymen and informed readers alike since it represents one of the classical approaches to combustion phenomena.

[4] Professor of Jet Propulsion, Division of Engineering, California Institute of Technology, Pasadena, Calif.

Turbulence

Turbulence. By J. O. Hinze. McGraw-Hill Book Company, Inc., New York, N. Y., 1959. Cloth, 9 × 6 in., lx and 586 pp. $15.

REVIEWED BY M. S. UBEROI[5]

PHYSICAL properties of turbulence, statistical averages, and techniques used to measure them are described in the first two chapters. Hot-wire anemometry is fully discussed. The next two chapters deal with the kinematics and dynamics of isotropic turbulence, isotropic scalar fields, pressure fluctuations, and anisotropic turbulence. The last three chapters are devoted to transport processes in turbulent flows, free shear flows (jet and wakes), and wall shear flows (channel flows and boundary layers). Any statistical theory consists of two parts. The first is devoted to defining suitable averages which invariably exceed the number of equations relating them. In the second part one complements the equations by assuming certain relations among the average quantities so that the determinate set of equations can be solved. The main difficulty is in finding these relations guided by experimental facts or intuition. Some have confused statistical formalism with real progress in turbulence. The author avoids this pitfall to a large extent.

Throughout the book, basic concepts are clearly explained and analysis compared with latest experimental results. The author includes older inexact but irreplaceable mixture length theories of shear flows which have fallen into contempt with some of the elite. A fairly complete set of references is given at the end of each chapter. The book is of real interest to workers in the field of turbulent flows, heat transfer, and diffusion.

Combustion

Design and Performance of Gas Turbine Power Plants. W. R. Hawthorne and W. T. Olson, Editors. Princeton University Press, Princeton, N. J., 1960. Cloth, 9½ × 6 in., xiii and 563 pp., illus. $15.

REVIEWED BY A. G. SMITH[6]

VOLUME XI of the Princeton "High Speed Aerodynamics and Jet Propulsion," the book under review, is a very useful volume saddled with a slightly misleading title. The book deals with only a part of the field implied by its title, and the Editor's preface shows that vol. X, "Aerodynamics of Turbines and Compressors," is intended as a "companion piece." Readers will possibly want to survey parts of vol. XII as well, before they feel that they have covered "Design and Performance of Gas Turbine Power Plants."

The present volume devotes 342 of its 563 pages to Combustion. The book is laid out in 4 "parts." 1—Introduction, 4 pages; 2—Combustion chamber design, 342 pages; 3—Mechanical and metallurgical aspects, 107 pages; 4—turbine powerplants, 90 pages.

Nine authors have contributed "sections" to part 2, treating "Requirements and Processes" (Peter Lloyd); "Experimental Techniques" (Hoyt C. Hottel and Glen C. Williams); "Fuel Injection" (Alec Radcliffe); "Flame Stabilization" (J. Howard Childs); "Mixing Processes" (Charles C. Graves and Wilfred E. Scull); "Fuels for Aircraft Gas Turbine Engines" (Louis C. Gibbons); and "Combustion Chamber Development" (Walter T. Olson).

This part of the book cannot fail to be valuable to combustion engineers and research workers. The 398 cited references, with few exceptions, date up to 1956, which is about as late as can be expected for an authoritative book with a large number of contributors.

Part 3 has two sections: "Mechanics of Materials for Gas Turbine Applications" (Egon Orowan and C. Richard Soderberg), and "Flutter Problems in Gas Turbines" (Jan R. Schnittger). The first of these sections provides both a conventional introduction to basic dislocation ideas, which cannot be said to do justice to modern thought on the application of the theory to creep and fatigue, and also a review of the engineering formulation which, though of some value, omits reference to the important cases of varying stress and temperature. The Flutter section is a useful survey of work up to about 1957, and the author has made the best of the unenviable task of explaining the diverse and intractable phenomena of blade flutter. As the author prudently predicted, important contributions have been made since he concluded his survey.

Part 4 has a single section titled "Performance" by Dennis H. Mallinson and Sidney J. Moyes. After a treatment of the thermodynamics of the compressor-combustor-turbine "gas generator" on a semiperfect gas basis, the section proceeds to an exposition of the complex interactions of intake, compressor, combustor, turbine, and propelling nozzle in producing the equilibrium running condition. Engines up to "double-compound" complexity are considered.

The book as a whole is very useful and obviously an essential acquisition to any library with "gas turbine" customers.

Gas Dynamics

Handbook of Supersonic Aerodynamics, Section 16, Mechanics of Rarefied Gases. By S. A. Schaaf and L. Talbot. Aerodynamics Handbook Staff of The Johns Hopkins University, Baltimore, Md., 1959.

REVIEWED BY G. N. PATTERSON[7]

THIS section of the new edition of the Handbook of Supersonic Aerodynamics has been prepared by two authors whose outstanding contributions to the subject of rarefied gas dynamics make them well qualified to prepare a review. The subject is introduced by a quantitative description of the flow regimes and a discussion of the present state of our knowledge of the interaction of gas molecules with surfaces in so far as the requirements of the aerodynamicist are concerned. Emphasis is naturally placed on free-molecule flow for which an extensive literature now exists. The authors then proceed with a consideration of slip flow, the regime of moderate rarefaction, leaving out the little-understood transition region. The article is well illustrated with curves showing such data as aerodynamic forces and heat transfer for simple geometrical shapes in both free-molecule and slip flow.

It is possible that some empirical data from the transition regime might have been included. However, the authors do provide references to research in near-free-molecule flow, a recent development of considerable importance to the designer.

No mention is made of the important subject of free-molecule probes. It is likely that this subject has been left to other sections of the Handbook although it properly forms part of the theory of free-molecule flow and should be of considerable interest to designers. This criticism is relatively minor, however, and does not detract from the excellence of this section of the Handbook.

[5] Professor, Department of Aeronautical and Astronautical Engineering, The University of Michigan, Ann Arbor, Mich.

[6] Professor of Aircraft Propulsion, The College of Aeronautics, Cranfield, Bletchley, Bucks, England.

[7] Director, Institute of Aerophysics, University of Toronto, Toronto, Canada.

Cylindrical Shells

Calcolo delle Volte Cilindriche Circolari Sottili. Prepared by the Istituto Nazionale per le Applicazioni del Calcolo. Edizioni Cremonese, Rome, Italy, 1960. Cloth, $5^3/_4 \times 73.4$ in., xvii and 322 pp., illus. Lire 3500.

REVIEWED BY M. G. SALVADORI[1]

UNDER the direction of G. Krall, the Italian National Computing Laboratory of M. Picone has prepared the most complete set of tables for the evaluation of membrane and bending stresses in thin cylindrical shells with circular cross section available to date. This book has the same purpose as the Manual of Engineering Practice No. 31 of ASCE, Design of Cylindrical Concrete Shell Roofs, but differs in the type of tables presented and in the kind of information given both qualitatively and quantitatively.

The Italian manual gives the complete derivation of the formulas used in the tabulations, which consider a rather general type of loading of which the dead load, the snow load, the wind load, and the hydrostatic pressure load are particular cases. Only two types of shells are considered: long shells with $a/L = 0.36$ and $h/L = 0.0025$ (type I), and short shells with $a/L = 2.7$ and $h/L = 0.0081$ (type II). The bending solutions are obtained by means of one or two terms of the corresponding Fourier expansions. The eighth-order differential equation used is Flügge's equation. Its solution is obtained by the iterational approach of A. A. Jakobsen. The solution procedures and the evaluation of the characteristic roots are thoroughly discussed.

Tables for all the stress resultants, the displacements, and the cross-sectional rotation are given essentially for the dead load and include the membrane and the bending resultants. The dead load equivalent to a snow load is indicated to avoid unnecessary duplication of tables. The classical antisymmetrical wind load is considered for type I shells of small opening angle. The stress resultants are computed and tabulated for the following longitudinal boundary conditions: 1 Simple support without longitudinal displacement; 2 Fixed boundary; 3 Simple support with longitudinal displacement permitted; 4 Free boundary; 5 Two equal shells in contact; 6 Two shells in contact, one with 90, the other with 60-deg openings; 7 Single shells with boundary beam; 8 Equal adjoining shells with boundary beams. The values of the main stress resultants for these conditions are also tabulated for increments of 5 degrees of the colatitude, for opening angles of 90 and 60 degrees for the dead load, for opening angles of 45 degrees for dead load and wind, and of 25 degrees for a shell with boundary beam under dead load.

Tables for the evaluation of stress resultants (under other boundary conditions and other values of the opening angles) at any point in the shell are also given which greatly facilitate the computations. Bending stresses at transverse boundaries are considered; the corresponding fourth-order equation is set up and solved and the corresponding solutions tabulated. Tables for the evaluation of stresses in complete cylinders (tanks) are given for $a/h = 5$, 10, 15, and 20.

Poisson's ratio is assumed equal to zero throughout, the equations are set up without assuming that the twisting moments on longitudinal and transverse sections are identical (but proved to be such numerically), and all the tabulated coefficients are given with 6 decimal figures.

This book is the result of the collaboration between a great design engineer and a group of powerful applied mathematicians for a period of over 7 years. It may be considered both a treatise on cylindrical thin shell theory and the most complete manual on cylindrical shells available to the design engineer today.

[1] Professor, Department of Civil Engineering and Engineering Mechanics, Columbia University, New York, N. Y.

Preliminary Announcement

The field of Experimental Mechanics will be covered by two international conferences during the week of October 29–November 3, 1961.

An **International Symposium on Photoelasticity** will be held on October 20–31 at the Illinois Institute of Technology, Chicago, Ill. Manuscripts should be sent to

Dr. Paul D. Flynn, Secretary
International Symposium on Photoelasticity
Illinois Institute of Technology
Chicago 16, Ill.

An **International Congress on Experimental Mechanics** will be held on November 1–3 in New York City. Manuscripts should be sent to

Dr. Roscoe Guernsey, Jr., Chairman
Publications Committee, SESA
General Engineering Laboratory
General Electric Company
Schenectady 5, N. Y.

Papers for these conferences should be submitted before January 31, 1961

Journal of APPLIED MECHANICS

Information for Authors

• Manuscripts should be submitted in final form to the Technical Editors. Each manuscript must be accompanied by a statement that it has not been published elsewhere nor has it been submitted for publication elsewhere. A paper which would occupy more than five pages of the Journal may be returned to the author for abridgment.

• The author should state his business connection, the title of his position, and his mailing address. A short abstract (50 to 100 words) should be included on the first page immediately preceding the introductory paragraph of the paper.

• Three copies of the manuscript are required. One of these must be a carefully prepared printer's copy, typed in double spacing, on one side of the page only, with wide margins, on $8^1/_2$ by 11-in. opaque white paper. Mimeographed manuscripts, if prepared with exceptional care, can be accepted provided they are completely edited.

• As far as possible, all mathematical expressions should be typewritten. Greek letters and other symbols not available on the typewriter should be carefully inserted in ink. Care should be taken to distinguish between capital and lowercase letters, between zero (0) and the letter (*O*), between the numeral (1) and the letter (*l*), etc. A letter representing a vector cannot be printed with an arrow above or below it. The letter should be underscored with a single wavy line, wherever it appears in the text, to designate boldface type. A list of symbols carefully marked for the use of the editor (thus: κ, Greek l.c. kappa), if it has not been included in the body of the paper, should accompany the manuscript on a separate page.

• Before preparing a manuscript the author should study printed articles in the Journal, with special attention to the form and style of mathematical expressions, tables, footnotes, references, and abstract. Numbers that identify mathematical expressions should be enclosed in parentheses. Numbers that identify references at the end of the paper should be enclosed in brackets. Care should be taken to arrange all tables and mathematical expressions in such a way that they will fit into a single column when set in type. Equations that might extend beyond the width of one column (fractions that should not be broken or long expressions enclosed in parentheses) should be rephrased to go on two or more lines within column width. Fractional powers are preferred to root signs and should always be used in more elaborate formulas. The solidus should be used instead of the horizontal line for fractions wherever possible.

• A normal paper should not exceed five pages in the Journal. It is about 6000 words or twenty to twenty-five double-spaced typewritten pages inclusive of drawings. A Brief Note should not exceed 750 words or about one column in the Journal inclusive of drawings.

• Originals and two copies of figures must accompany the manuscript. Line drawings should not be larger than $8^1/_2 \times 11$ inches and should be planned for reduction to column width. Lettering should be large enough to be clearly legible when the illustration is reduced. The originals of line drawings must be in India ink on white or pale blue tracing paper or tracing cloth. Photographs of equipment or test specimens must be glossy prints and should be used sparingly. Captions for figures should be typed double-spaced and included as the last page of the manuscript. The figure number and author's name should be written in the margin or on the back of each illustration.

• Titles of papers should be brief.

• Authors can obtain copies of the ASME Manual MS-4, "An ASME Paper," from the Technical Editors and are urged to do so before drafting their papers in final form.

• Papers published in the Journal of Applied Mechanics must be presented at a Meeting, either in person or by title. Scheduling of papers is in the hands of the Secretary of the Applied Mechanics Division. Authors should indicate their preference in this respect to the Technical Editors when submitting a paper.

• An author is entitled to 25 preprints free of charge (in the case of two authors, 15 each; three or more authors, 10 each). Larger quantities of preprints or reprints can be ordered from Editorial Department, The American Society of Mechanical Engineers, 29 West 39th Street, New York 18, N. Y. Quotations will be sent on request.

ASME Publications Committee

Please address all communications to:

Technical Editors

Journal of Applied Mechanics, ASME

Division of Engineering

Brown University

Providence 12, R. I.

NOW IN ONE VOLUME

The technical papers, design data, and brief notes on technical matters in mechanics listed at the right.

Originally published in the 1959 issues of the

Journal of Applied Mechanics

they have now been brought together in

SECTION 3

of the

1959 ASME TRANSACTIONS

PUBLISHED

IN SECTION 1 are the eighty papers and discussions of the 1959 Journals of Engineering for Power and Industry.

IN SECTION 2, the hundred and twelve papers and discussions contained in the 1959 Journals of Basic Engineering and Heat Transfer.

PRICES

For each section.....$16.00
($8.00 to ASME members)

For the three sections.....$38.00
($19.00 to ASME members)

Public and engineering college libraries may purchase these sections at members' prices.

THE AMERICAN SOCIETY OF MECHANICAL ENGINEERS

29 W. 39th St., N. Y. 18, N. Y.

Experimental Surface-Wave Method for Recording Force-Time Curves.
Forced Torsional Vibration of Systems With Distributed Mass and Damping.
Frequencies of a Flexible Circular Plate and Light Elastic Half-Space.
Analytical Design of Disk Cams by Independent Position Equations.
Stress Distribution and Plastic Deformation in Rotating Cylinders.
Transient and Residual Stresses in Heat-Treated Cylinders.
The Nonlinear Bending of Thin Rods.
Stresses and Deflections in Circular Plate Loaded Over a Segment.
Transverse Flexure of a Thin Plate Containing Two Circular Holes.
Limit Analysis of Symmetrically Loaded Thin Shells of Revolution.
On Influence Coefficients and Nonlinearity for Thin Shells of Revolution.
A Theorem of Maximum Strain Energy.
Plastic Stress-Strain Relationships—Effect of Loading Path and History.
A Stress-Strain Relation for Hexagonal Close-Packed Array of Spheres.
A Mathematical Model of the Stress-Strain Diagram and Hysteresis Loop.
A Definition of Stable Inelastic Material.
Retarded Flow of Bingham Materials.
An Experiment on Compressible-Flow Perturbations.
Transient Film Condensation.
Effect of Turbulence on Slider-Bearing Lubrication.
Theory of Flight of the Sounding Rocket.
On Supersonic Wind Tunnels With Low Free-Stream Disturbances.
Velocity and Temperature Fluctuation Measurements in a Turbulent Boundary Layer.
Density Variation Effects in Stepped-Thrust Bearings.
Response of a Nonlinear String to Random Loading.
Response to Van Der Pol's Oscillator to Random Excitation.
A Perturbation Solution of the Equations of Motion of a Gyroscope
Vibration of Beam-Mass Systems With Time-Dependent Boundary Conditions.
Dynamic Loading Tests of an Aircraft-Type Beam.
Viscous Damping in Flexural Vibrations of Bars.
Natural Modes and Their Stability in Two-Degree-of-Freedom Systems.
On Finite Bending of Pressurized Tubes.
Instability and Folding Deformation of a Viscoelastic Medium in Compression.
Stress Distribution in Semi-Infinite Strip Subjected to Concentrated Load.
Postbuckling Behavior of Rectangular Plates With Small Initial Curvature.
New Theory of Elastic Sandwich Plates—One-Dimensional Case.
On Invariant Perforation in an Infinite Strip.
Thermal Stresses in Moderately Thick Elastic Plates.
Analysis of Plane Stress in Polar Co-ordinates.
The Stress Function of a Radial Strain.
Determination of Safe Loads of Beams Subjected to Twisting and Bending Moments.
Effect of a Nonisothermal Free Stream on Boundary-Layer Heat Transfer.
Visual Studies of the Wall Layers in the Turbulent Boundary Layer.
Unsteady Laminar Boundary Layers Over an Arbitrary Cylinder.
On Journal Bearings of Finite Length With Variable Viscosity.
Analysis of Complex Kinematic Chains With Influence Coefficients.
A Theory of Oil Whip.
On Critical Speeds of a Shaft Supported by a Ball Bearing.
Root-Locus Analysis of Structural Coupling in Control Systems.
Normal Vibrations of Uniform Plate Carrying Any Number of Finite Masses.
Transients in Simple Undamped Oscillators Under Inertial Disturbances.
On Laterally Loaded Semicircular Plate With Clamped Edges.
Direct Determination of Stresses in Plane Elasticity Problems.
Stresses in a Stretched Slab Having a Spherical Cavity.
Influence Coefficients for Edge-Loaded Short, Thin, Conical Frustrums.
Upper and Lower Bounds for Special Eigenvalues.
Analysis of a Compression Test of a Model of a Granular Medium.
A Reassessment of Deformation Theories of Plasticity.
Collapse Loads of Rings and Flanges Under Uniform Twisting Moment.
Creep of Thick-Walled Tubes Under Internal Pressure.
Strain-Hardening Solutions to Plate Problems.
Determination of Creep Deflection of a Rivet in Double Shear.
Boundary-Layer Solution for a Flow in a Diverging Passage Having a Swirl Component
Slow Rotatory Motion of a Circular Disk About One of Its Diameters in a Viscous Fluid.
Thermal Stresses Owing to a Hot Spot in a Rectangular Strip.
Impact and Moving Loads on a Slightly Curved Elastic Half Space.
Stability of Forced Oscillations With Nonlinear Second-Order Terms.
On Inertia Effects in a Transient Thermoelastic Problem.
Coupled Torsional and Longitudinal Vibrations of a Thin Bar.
Production of Rotation in a Confined Liquid Through Translational Motion of the Boundaries.
Nonlinear Creep Deformations of Columns of Rectangular Cross Section.
Forced Vibrations of a Circular Plate.
On the Propagation of Shock Waves in a Nonhomogeneous Elastic Medium.
The Frequency of Flexural Vibration of Rectangular Orthotropic Plates With Clamped or Supported Edges.
Axially Symmetric Extensional Vibrations of a Circular Disk With a Concentric Hole.
Analysis of a Nonlinear Mechanical System With Three Degrees of Freedom.
Stresses in an Ellipsoidal Rotor in a Centrifugal Force Field.
Carrying Capacity of Elastic-Plastic Shells With Various End Conditions.
Extensional Vibrations of Elastic Plates.
Triaxial Tension at the Head of a Rapidly Running Crack in a Plate.
Viscous Flow Through Tubes of Multiple Connected Cross Sections.
On the Accuracy of Some Shell Solutions.
The Drag on Spheres and Cylinders in a Stream of Dust-Laden Air.
Elastic Flexible Cable in Plane Motion Under Tension.
Incremental Stress-Strain Law Applied to Work-Hardening Plastic Materials.
On the Plastic Flow of Coulomb Solids Beyond Original Failure.
The Free Vibrations of Grillages.
Piping Flexibility Analysis by Stiffness Matrix.
A Photoelastic Approach to Transient Stress Problems Employing Low-Modulus Materials.
Rupture Characteristics of Safety Diaphragms.
Bending of Isosceles Right Triangular Plates.
Developments in the Application of the Grid Method to Dynamic Problems.
The Solution of Elastic Stability Problems With the Electric Analog Computer.
Symmetric Vortex Separation on Circular Cylinders and Cones.
Thermoelastic Problem for a Transversely Isotropic Hollow Sphere Embedded in an Elastic Medium.
Transient Analysis of Stress-Wave Penetration in Plates.
Transverse Flexure of a Semi-Infinite Thin Plate Containing an Infinite Row of Circular Holes.
Fundamental Frequency of a Thin, Flat Circular Plate Simply Supported Along a Circle of Arbitrary Radius.

DESIGN DATA AND METHODS

Stress-Concentration Factors for T-Heads.
The Frequency of Vibration of Rectangular Isotropic Plates.
Factors of Stress Concentration Due to Elliptical Fillets.

BRIEF NOTES

Buoyancy Effects in Forced-Convention Flow. Thermally Induced Twists in Thin Plates. Deflections and Vibrations of Clamped Sectorial Plates. Thermal Distributions Without Thermal Stresses. Thin-Walled Cylinders Under Torsion and Pressure. Transient Heat Transfer for Flow in Ducts. Upper and Lower Bounds for Stiffness of Plates. Cross-Section Distortion and the Timoshenko Beam Equation. Analysis of Paraboloidal Shells. Natural Frequencies of Two Nonlinear Systems. Response of a Slab to Impact. Thermal Stresses in Long Cylindrical Shells. Dynamic Characteristics of Undamped Vibration Systems. Large Deflections of a Clamped Elliptical Plate. Thermal Stresses at Spherical Cavities. Deflection of a Thick Ring in Diametral Compression. The Biot-Willis Coefficients for a Sandstone. Circular Plates on Elastic Foundation. Frequencies of Vibration of Stiffened Plates. Design of a π Network for Heat-Flow Analog. Stress Distribution in a Square Tube. Creep of Elastic Belt on a Pulley. Modification of Rayleigh's Principle for Calculating Beam Frequencies. Yield Point Load of an Annular Plate. Analysis of Indeterminate Structures by Displacement Method. Internal Damping of Thermal Origin in Thin Wires. Lateral Buckling of Tapered Narrow Beam. Stresses in Infinite Wedges Tapered in Width and Thickness. Minimization of Spring Torque. Steady-State Response of Linear Vibration Systems. Further Understanding of Shakedown Theorems. Series Solution for Ellipsoidal Shells.